AD-A238 424

UMENTATION PAGE

Form Approved
OMB No 0704-0188

2. Report Date.	3. Report Type and Dates Covered.
October 1989	Final

4. Title and Subtitle.

Forecasters Handbook for the Arctic

5. Funding Numbers.

Program Element No	63704N
Project No	X1596
Task No	--
Accession No.	DN658753

6. Author(s).

Dr. Frank S. Sechrist, Robert W. Fett, Dennis C. Perryman

7. Performing Organization Name(s) and Address(es).

Naval Environmental Prediction Research Facility
Monterey, CA 93943-5006

8. Performing Organization Report Number.

Technical Report
TR 89-12

9. Sponsoring/Monitoring Agency Name(s) and Address(es).

Space and Naval Warfare Systems Command (PMW-141)
Washington, DC 20363-5100

10. Sponsoring/Monitoring Agency Report Number.

11. Supplementary Notes.

Contributing authors: Ronald J. Miller, Rolf H. Langland, LT Dennis R. Miller, USN

12a. Distribution/Availability Statement.

Approved for public release; distribution is unlimited.

12b. Distribution Code.

13. Abstract (*Maximum 200 words*).

Weather and ice conditions for the Arctic seas—Beaufort Sea, Greenland Sea, Norwegian Sea, Barents Sea, Kara Sea, Laptev Sea, East Siberian Sea, Sea of Okhotsk, Baffin Bay, and Davis Strait—and major land forms and islands are described. This work is a complete revision of the 1962 version and contains quick-reference material for operational forecasters as well as background material to enhance further understanding of Arctic phenomena. Satellite imagery case studies are included, and an entire section is devoted to polar low development. The appendices provide monthly maps for average air temperatures, mean surface pressures, and mean 700-mb heights for the Arctic region. Inversion statistics and seasonal ice movement patterns are also included.

14. Subject Terms.

Arctic Ocean	Greenland
Alaska	U.S.S.R.
Canada	Arctic weather

15. Number of Pages.
364

16. Price Code.

17. Security Classification of Report.	18. Security Classification of This Page.	19. Security Classification of Abstract.	20. Limitation of Abstract.
UNCLASSIFIED	UNCLASSIFIED	UNCLASSIFIED	Same as report

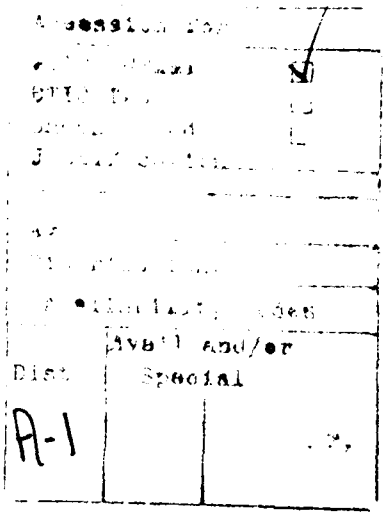

Contents

THIS PAGE INTENTIONALLY LEFT BLANK

FOREWORD

The Forecasters Handbook for the Arctic is one of a series of regional forecaster handbooks produced by the Naval Environmental Prediction Research Facility (NEPRF). This publication has been developed in response to Commander, Naval Oceanography Command requirement PACMET 87-16, validated by the Chief of Naval Operations (OP-096).

The primary objective of this publication is to provide fleet forecasters and Naval operational decisionmakers with a comprehensive reference on environmental conditions in the Arctic. Included are several satellite pictures that provide reference images for various seasonal phenomena and specific examples of satellite imagery interpretation.

This handbook should be regarded as a flexible document, capable of being updated and revised as applicable. Fleet users are urged to submit comments and suggested changes that can be incorporated into the handbook to increase its usefulness.

THIS PAGE INTENTIONALLY LEFT BLANK

RECORD OF CHANGES

CHANGE NUMBER	DATE OF CHANGE	DATE ENTERED	PAGE NUMBER	ENTERED BY

THIS PAGE INTENTIONALLY LEFT BLANK

1. GENERAL INTRODUCTION

1.1 Objective

The Arctic region has gained importance in recent years due to the discovery of large oil reserves and the potential of other vital resources in the area. Any confrontation with other nations in the Arctic is likely to take place under adverse conditions in a hostile and not well-known environment. The need for an updated version of the Arctic Forecast Guide is readily apparent.

The original objective was to revise the Arctic Forecast Guide, written in 1962. Considering the amount of research carried out in the polar regions since then, however, the decision was made to conduct a major rewrite. The objective, therefore, became one of producing a useful, up-to-date handbook that would provide a reference for the operational forecaster and still contain background material that could be studied to enhance further understanding of Arctic phenomena. Several good references are available on various specific phenomena of the Arctic (aircraft icing, icebergs, etc.), and to include lengthy sections on all phenomena in this guide is unrealistic. A good statistical reference for the Alaska region is the *Climatic Atlas* produced by the National Climatic Center (Asheville, North Carolina) and the Arctic Environmental Information and Data Center (University of Alaska, Fairbanks, Alaska). The reader is directed to the reference section for further reading if desired.

1.2 Approach

Using the 1962 version as a basis, certain sections of that publication were targeted for expansion while new sections were to be added. Because of the usefulness of satellite imagery in weather forecasting today, an entire section is dedicated to weather satellite case studies. A good climatological database is difficult to find and maintain in data sparse areas, the Arctic being a prime example. Due to investment in an Arctic Buoy program by the United States, Canada, and other international partners over the past several years, however, it has been possible to create an improved climatology of mean monthly surface pressures and temperatures over the icecap. These data are included in the handbook. Also, the decision was made to include sections on refractivity, polar lows, and numerical models, all of which are new to the 1990 version.

1.3 Organization and Contents

To provide the reader with an understanding of the physical environment of the Arctic, a chapter on physical characteristics is presented early. This chapter includes submarine topography, major landforms and islands, Arctic ice and currents and tides. Several locator maps are included to help the reader's geographic orientation. The chapter on Arctic climatology includes subsections on major causal factors and individual elements. The section on polar lows presents general polar low patterns, plus five case studies supported by weather charts and satellite pictures. The chapter on refractivity has a subsection describing the Integrated Refractive Effects Prediction System (IREPS) and IREPS products. The section on numerical models touches on the basics of atmospheric models and discusses the pitfalls of relying solely on their outputs. The reference section contains five dozen references; only three of the documents were published before 1962, and half were published since 1985. For easy referral, a glossary of ice terms and monthly maps of air temperature and surface pressure are included in the appendices section. For a complete review of what is included in this handbook, the reader is referred to the table of contents.

Weather charts included in the text are operational charts produced by the Fleet Numerical Oceanography Center. Station plots may be difficult to read; however, the intent, in general, is to show the large-scale analysis. When necessary, amplification of smaller scale phenomena is included in the text.

Draft copies of this handbook were given to several reviewers. Where feasible, their comments and suggestions have been incorporated into the final version. The reviewers' assistance in completing this handbook is greatly appreciated.

2. PHYSICAL CHARACTERISTICS OF THE ARCTIC

Since the time of the ancient Greeks, scholars have been intrigued by the similarities and the differences between the Earth's north and south polar regions. While both are cold and have abundant ice, when stripped of water and ice they possess striking dissimilarities. In the south appears a huge continent with an area of nearly 5 million sq mi (14 million sq km). But in the north just the opposite occurs, the huge Arctic Ocean Basin with an area nearly as great. This section provides an opportunity to examine the physical characteristics of the high north.

2.1 Submarine Topography of the Arctic Basin

Figure 2-1 shows the bathymetry of the Arctic Ocean. It illustrates a number of features that determine the nature of the ice distribution and circulation. The prominent *Lomonosov Ridge* splits the region into two major subbasins: the Eurasian and Amerasian. It stretches from the Laptev Sea to Ellesmere Island. The Eurasian Basin is bounded to the south by Greenland, Spitsbergen, and the Taimyr Peninsula. It extends to a maximum depth in excess of 13,780 ft (4,200 m). Large amounts of water can obviously be exchanged between this basin and the Atlantic Ocean by way of the Greenland and Norwegian Seas. The water from the Arctic Ocean is cold and fresher while the North Atlantic Current provides warmer and more saline water to mix in the basin. Note that the continental shelf surrounding the Eurasian Basin is very narrow, averaging only 23 to 58 mi (37–93 km).

In contrast, the other Arctic Ocean basin, the Amerasian, has a very broad continental shelf, up to 342 mi (550 km) across. The Amerasian Basin has an average depth of 12,960 ft (3,750 m) and extends from Ellesmere Island to the East Siberian Sea. It includes the Canadian Basin (Beaufort Sea), which is connected with the Pacific Ocean by the narrow (40 mi or 64 km) and shallow (148 ft or 45 m) Bering Strait.

The marginal seas, which make up the edges of the Arctic Ocean over the continental shelf, occupy 35 percent of the entire ocean area but account for only 2 percent of the volume (large areal extent but relatively shallow), indicating great water depth in the two major basins. Most of the rivers supplying the Arctic Ocean flow into the shallow seas and make the ocean fresher in spring and subject it to more evaporation because of the

Figure 2-1. Bathymetry of the Arctic Ocean (Sater et al., 1971).

depth-to-exposed-area ratio. Through the Bering Strait only near-surface water flows into the Arctic Ocean. In this area the Arctic Ocean has Pacific Ocean characteristics.

Furthermore, the large canyons leading into the Arctic have an influence on the nature of the water. These act as pathways for egress of water from warmer oceans into the shallow Arctic seas and mixing can alter the state of water and ice.

As noted before, the Arctic Ocean is almost completely landlocked with the exception of a small number of restricted openings, generally of small depth, which act more as sills than as open passages for the circulation of the water. Some examples are the Bering Strait,

the Nares Strait (9 mi or 15 km wide, 820 ft or 250 m deep) between Ellesmere Island and Greenland, and the numerous narrow channels throughout North America. The only large communication pathway is the Fram Strait at the top of the North Atlantic Ocean between Spitsbergen and Greenland, where a deep trench (deeper than 6,562 ft or 2,000 m for more than 155 mi or 250 km) allows warm Atlantic waters to flow freely into the Arctic Basin. Simultaneously, a powerful surface countercurrent of drifting ice and cold water comes out of the polar sea, paralleled by an important deep overflow of Arctic waters that cascades over sills into the North Atlantic on both sides of Iceland. On the eastern side, despite the presence of a large unrestricted passage, the shallow continental platform of the Barents Sea prevents a large exchange with the North Atlantic; this particular inflow plays only a secondary role.

The overall transfer through the Fram Strait is enormous, representing more than 35 million cu ft (7 million cu m) per second. It brings into the Arctic Ocean huge amounts of warm, saline water, which, sinking to middepths, drive permanent transpolar currents and contribute to giving to the whole Arctic Basin a role of heat radiator in the heart of the northern cold territories. This powerful Atlantic inflow, however, coming from the direction of offshore America and western Europe, threatens to become a source of possible pollution.

Finally, the geometry of the Arctic Ocean provokes the convergence of the circumpolar runoffs coming from adjacent continents: from Siberia and North America powerful rivers carry hundreds of megatons of fresh water into the Arctic Basin. At the present rate, the Yenisei, Ob, Lena, Kolyma, and Mackenzie Rivers, draining a continental area of more than 4 million sq mi (10 million sq km), have a runoff equivalent to five times the Mississippi River and almost half the Amazon. This fresh water, spreading at the surface of the heavier saline marine water, prevents normal convection and reduces vertical mixing; thus it seriously impedes biological development, a situation that is quite contrary to that of the Antarctic Ocean. Runoff brings also a great mass of natural sediments, as well as organic material and undesirable chemicals from midlatitude fallout on the drainage basins of circumpolar rivers. Those pollutants tend to remain in the surface freshwater; they are distributed all around the Arctic Basin by the "Transpolar Drift" from northern Siberia to the Fram Strait, and relayed by the Pacific Gyre north of North America, so that all circum-Arctic countries receive their share.

2.2 The Arctic Seas

The Arctic Ocean is the world's smallest ocean with an area of 5 million sq mi (14 million sq km). Relatively little is known about the Arctic Ocean because of its limited access by ships and its isolation from population centers. Open water areas of the Arctic consist primarily of leads and polynyi that figure significantly in the Arctic heat budget. These openings are characterized by water vapor evaporation to the air at a rate two orders of magnitude greater than evaporation from ice. Tides vary over the Arctic Ocean from as much as an inch or two (2–5 cm) in the Beaufort Sea to as much as 40 ft ($\approx$ 12 m) in some embayments of the Canadian Archipelago (Lopez, 1986).

Arctic Ocean water consists of three different water masses. The surface layer, *Arctic water*, is generally near the freezing point but relatively dilute with salinities around

28–32 parts per thousand (ppt). Below about 165 ft (50 m) the salinity increases rapidly with depth (Fig. 2-2). Because temperature has less effect on density than salinity in cold Arctic water, however, the vertical profiles of salinity and density are virtually parallel.

Immediately below the Arctic water is the *Atlantic layer* ranging from a depth of 650 to 3,000 ft (200–900 m). This layer has temperatures near freezing, often reaching 37 °F (3 °C). The salinity in this layer is quite uniform at near 35 ppt. This layer is a major heat source within the Arctic Ocean.

Finally, the *bottom water* makes up the deepest layer. Temperature and salinity are both quite uniform in this layer at about 31 °F (−0.5 °C) and 34.95 ppt. It constitutes nearly 60 percent of the water volume in the Arctic Basin.

The following subsection discusses the salient features of each of the major Arctic seas. Boundaries of the various seas are shown in Fig. 2-3.

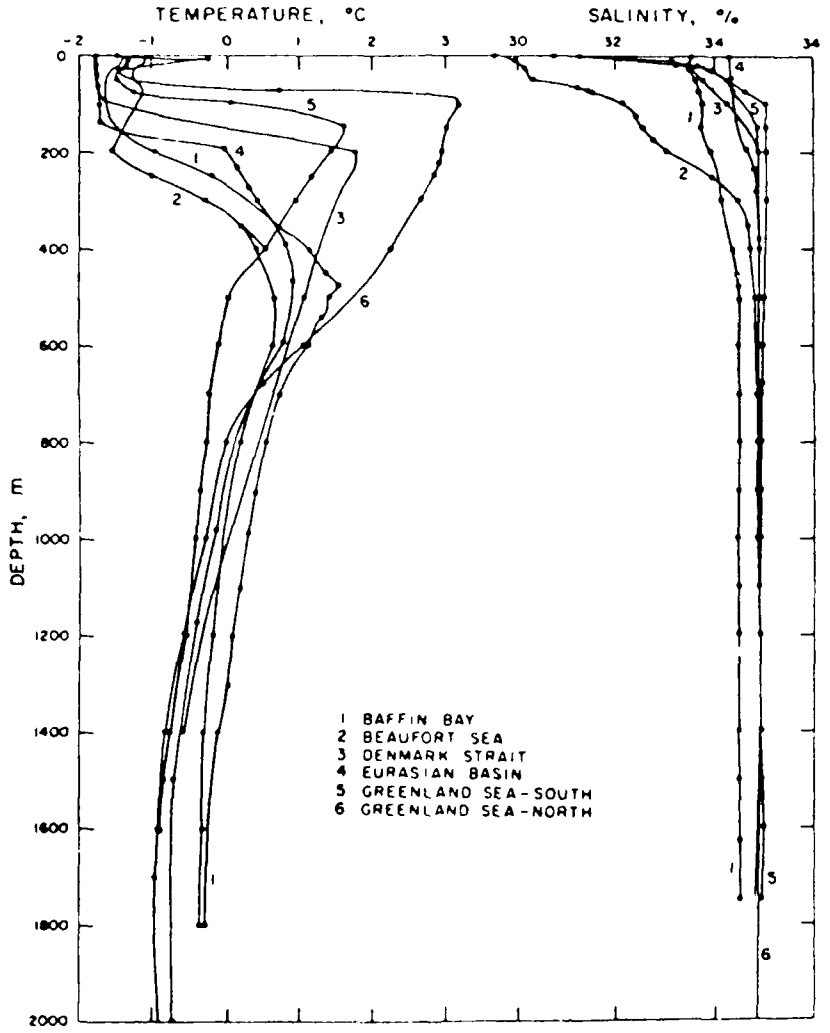

Figure 2-2. Vertical Profiles of Temperature and Salinity at Six Arctic Locations (Welsh et al., 1986).

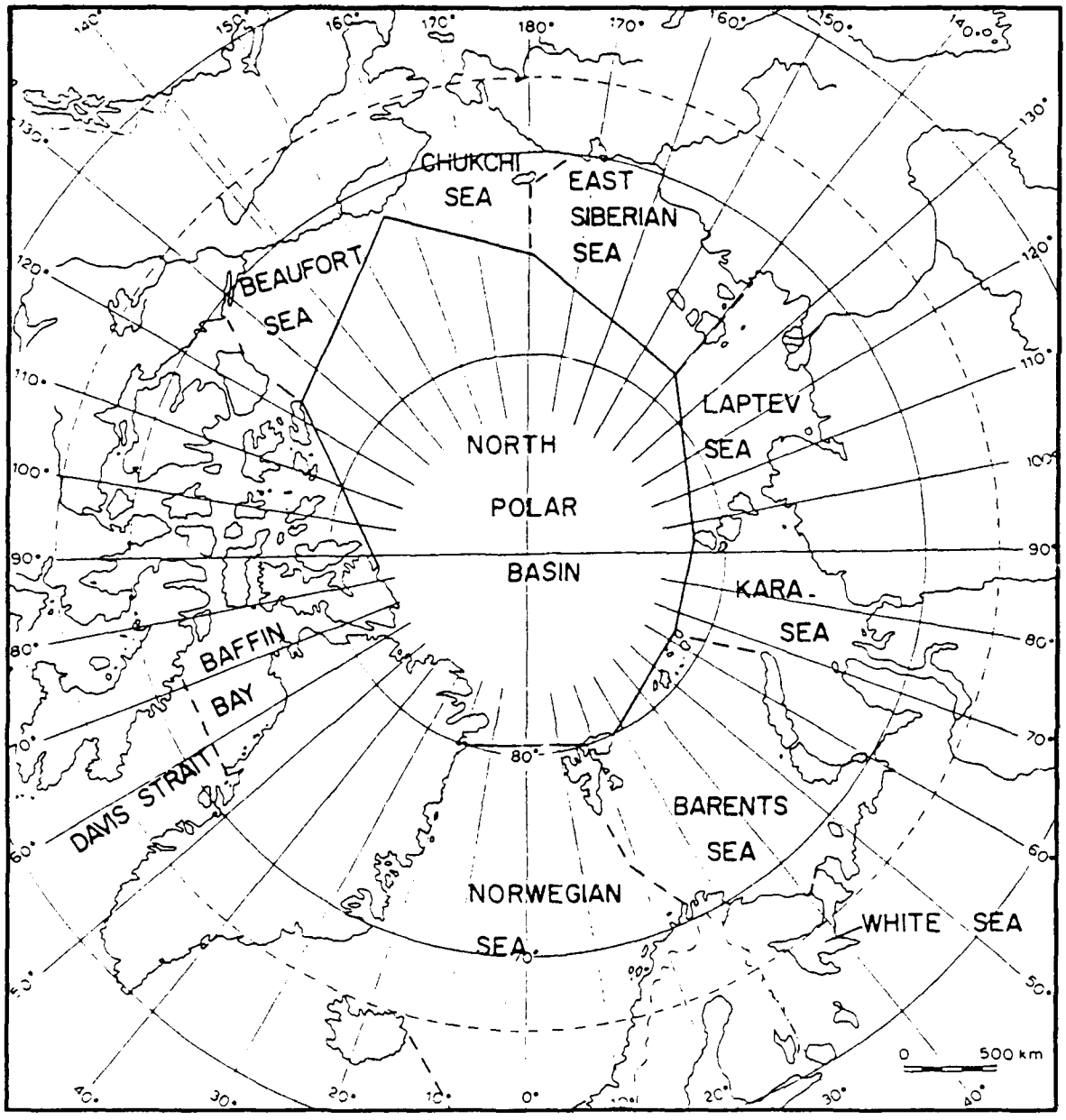

Figure 2-3. The Arctic Seas (Orvig, 1970).

Note (applicable to subsections 2.21 through 2.2.10):

(1) Quoted wind speeds and wave heights are climatological values. *Maximum* winds usually occur with synoptic storm systems or with polar lows and are known to exceed 60 kt (30 m/s).

(2) Reference is made to polar and subarctic climates. In general, polar climate refers to the air temperature being less than 50 °F (10 °C) in the warmest months, whereas in a subarctic climate the temperature in the warmest months is above 50 °F (10 °C).

(3) Extensive use was made of the material included in *A Compendium of Arctic Environmental Information* (Welsh, 1986). This book is very useful for those working in the Arctic.

2.2.1 Beaufort Sea

The Beaufort Sea's surface Arctic water is about 330 ft (100 m) thick and is the coldest of all the water masses. Furthermore, it is the only layer that undergoes significant seasonal changes in temperature and salinity. These changes are in response to the freezing and thawing of the pack ice, plus the freezing and thawing of rivers in coastal areas.

The Atlantic layer in the case of the Beaufort Sea is overlain by Pacific water, which enters through the Bering Strait. The Pacific water is, of course, relatively warmer than the other layers.

The circulation of the Beaufort Sea is dominated by the clockwise Beaufort Gyre that covers the entire Canadian and Beaufort Deeps. The currents flow at a rate of 1–2 n mi/day (2–4 km/day) but may be highly variable along coasts and may even reverse direction depending on local surface winds and/or synoptic pattern winds.

The sea ice of the Beaufort Sea is packed up against the Canadian and Alaskan coasts due to the gyre. Thus, navigation and observations are restricted in all seasons except late summer. Seas are normally less than 3 ft (1 m) due to the extensive ice cover but may reach 5 ft (1.5 m) for brief periods in late summer. They can reach 20 ft (6 m) in fall and spring with severe storm events.

The climate of the Beaufort Sea can be summarized as follows: Summer temperatures range from −15 °F to 54 °F (−26 °C to −12 °C); in winter the range is −35 °F to 1 °F (−37 °C to −17 °C). The record low temperature is −72 °F (−58 °C), and the temperature may be less than −25 °F (−31.5 °C) 85 days/year. Winds may exceed 21 kt (11 m/s) 55 days/year.

2.2.2 Baffin Bay and Davis Strait

Baffin Bay at its maximum depth reaches 6,600 ft (2,012 m), making it one of the deeper bodies of Arctic water. In this region the cold Arctic waters mix with the warmer Atlantic Ocean. Thus, the variations in surface characteristics are great in their response to seasonal and migratory storm conditions. The surface water temperatures can range from 30 °F (−1 °C) to as high as 41 °F (5 °C) and salinities are in the low thirties parts per thousand. Unlike the Beaufort Sea, the waters in Baffin Bay circulate counterclockwise. The West Greenland Current transports the warm Atlantic water along the eastern boundary of the Bay (Fig. 2-4). By the time this current reaches the northern extremes of the Bay it has cooled but is still warmer and more saline than the Arctic water it meets there. At this northernmost point it converges with the Canadian Current. The resultant mixing significantly affects weather and sea conditions. Here the Canadian Current begins to transport water southward along the east coast of Baffin Island. This Canadian Current carries southward much sea ice and icebergs. South of the Davis Strait the Canadian Current is joined by the warmer waters of an extension of the East Greenland Current to form the Labrador Current.

These currents are responsible for the contrast of ice conditions between the eastern and western sides of Davis Strait. The warm West Greenland Current keeps the eastern part of the Strait virtually ice free the year round as far north as 70 °N. Conversely, the cold south-flowing Canadian Current keeps the western portion of the Strait filled with

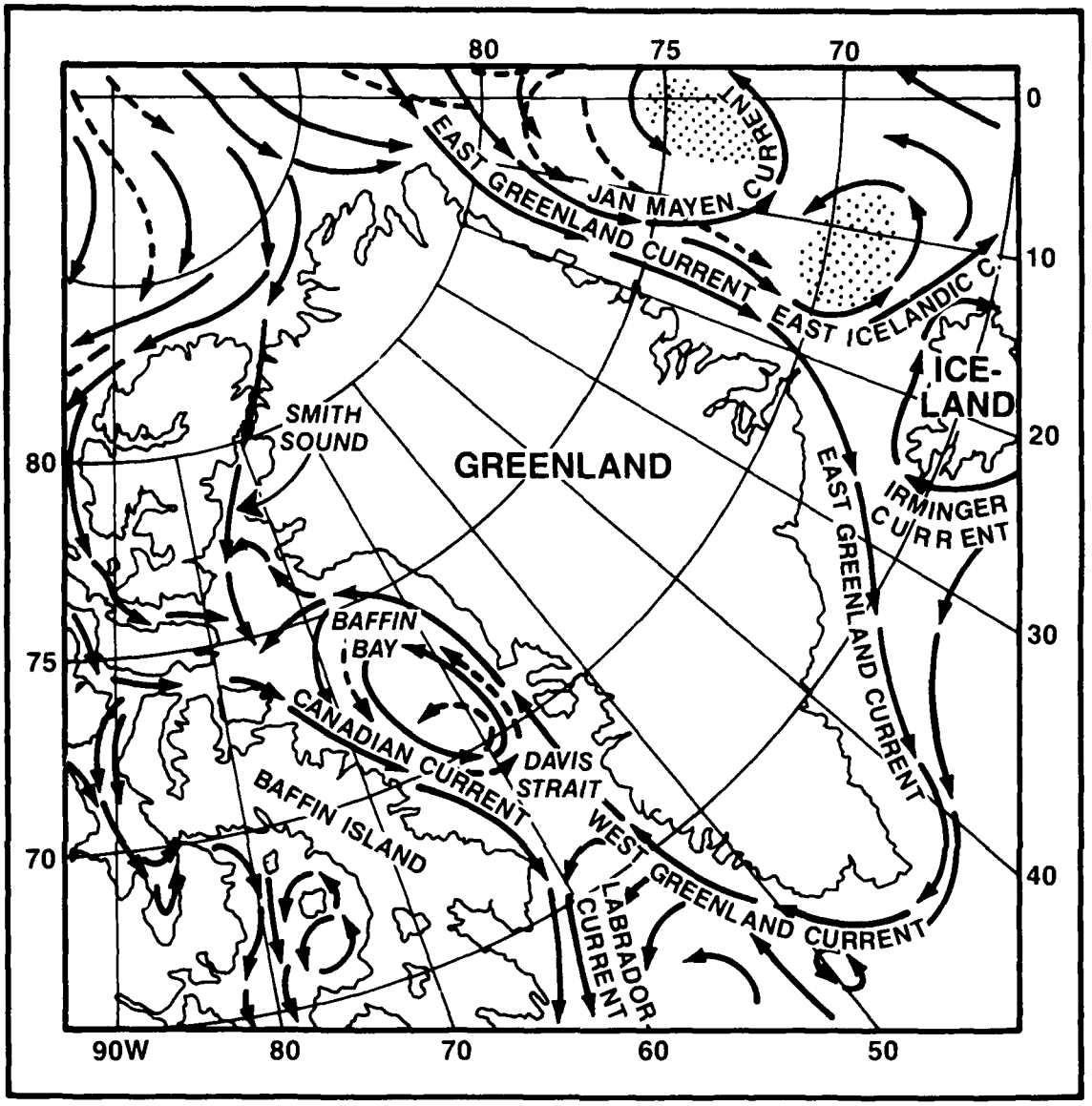

Figure 2-4. Greenland and Davis Strait Ocean Currents (adapted from Welsh et al., 1986).

ice throughout the year. The prevailing northerly winds in the area help to maintain a large patch of open water in Smith Sound (northern Baffin Bay), commonly referred to as *North water.*

The climate of the Baffin Bay area is sub-Arctic in the south and polar in the north, with coldest temperatures in the north and along the coast of Canada. High winds are common along the Greenland coast often due to katabatic (a wind blowing down an incline) flow off the icecap. These winds can rise quickly and often reach 65 kt (32 m/s). Fog is responsible for visibilities below 1.2 mi (2 km) 80 days/year. Winter temperatures range between −63 °F and 10 °F (−53 °C and −12 °C); in summer the range is between 10 °F and 50 °F (−12 °C and 10 °C). The lowest recorded temperature was −76 °F (−60 °C). Typical winds are northwesterly in winter and easterly in summer.

2.2.3 Greenland Sea

The large Greenland Basin reaches a maximum depth of 15,900 ft (4,846 m); the mean depth is 4,738 ft (1,444 m). The two basins of this sea contain deep water with a temperature of 30 °F (−1 °C) and salinity of 34.92 ppt. The Atlantic water above the deep water comes from the Irminger Current and is warm (>46 °F (8 °C) and saline (>35 ppt). To the south, vertical mixing of Atlantic water and Arctic water in winter results in a homogeneous water mass in the upper layers. This water is warmer, less saline, and called North Icelandic winter water.

The principal current in the Greenland Sea is the East Greenland Current (Fig. 2-5). Locally, this current can reach speeds of 0.5 to 1.0 kt (25–50 cm/sec) just south of the Denmark Strait. A cyclonic gyre is located north of Jan Mayen between the Greenland Current and a branch of the Norwegian Current flowing west of Svalbard. This Greenland Gyre dominates the Greenland Basin.

Sea ice occupies the entire sea but is minimal in September. The Greenland Sea normally contains a large amount of old ice that comes from the Arctic Ocean. Icebergs from the east coast of Greenland are also common.

The climate of the Greenland Sea area is polar. Visibility is less than 1.25 mi (2 km) for about 20 days/year in the north and 30 days/year in the south. Summer is the foggiest season. In the north, the record low temperature is −60 °F (−51 °C); in the south −29 °F (−34 °C). Winds can exceed 21 kt (11 m/s) 26 days/year in the north and 74 days/year in the south. Correspondingly, the sea state is much greater in the south.

2.2.4 Norwegian Sea

The Norwegian Sea is made up of North Atlantic water and Norwegian Deep water. The latter is formed in winter near Jan Mayen Island in the western part of the sea. The North Atlantic Current provides the warm, saline Atlantic water to the Norwegian Sea and helps to keep it ice free throughout the year.

The Norwegian Gyre is cyclonic and in the center of this sea. It moves water southeastward north of Iceland. The climate of the Norwegian Sea area is sub-Arctic. Precipitation is rather extensive here because the sea lies in the midst of major storm tracks. This fact also explains the generally rough seas. Visibility is less than 1.25 mi (2 km) for about 160 days/year due to low cloudiness and fog.

Winter temperatures range from 30 °F to 39 °F (−1 °C to 4 °C); in summer the range is 30 °F to 50 °F (−1 °C to 10 °C). The lowest recorded temperature is 10 °F (−12 °C), which is considerably warmer than the other sea areas examined so far.

2.2.5 Barents Sea

Barents Sea lies entirely over the continental shelf and therefore is quite shallow. Its mean depth is only 750 ft (230 m). Small tongues of Atlantic water enter the Barents Sea from the Arctic Basin at depths of 490 to 655 ft (150–200 m) through the deep straits between the islands.

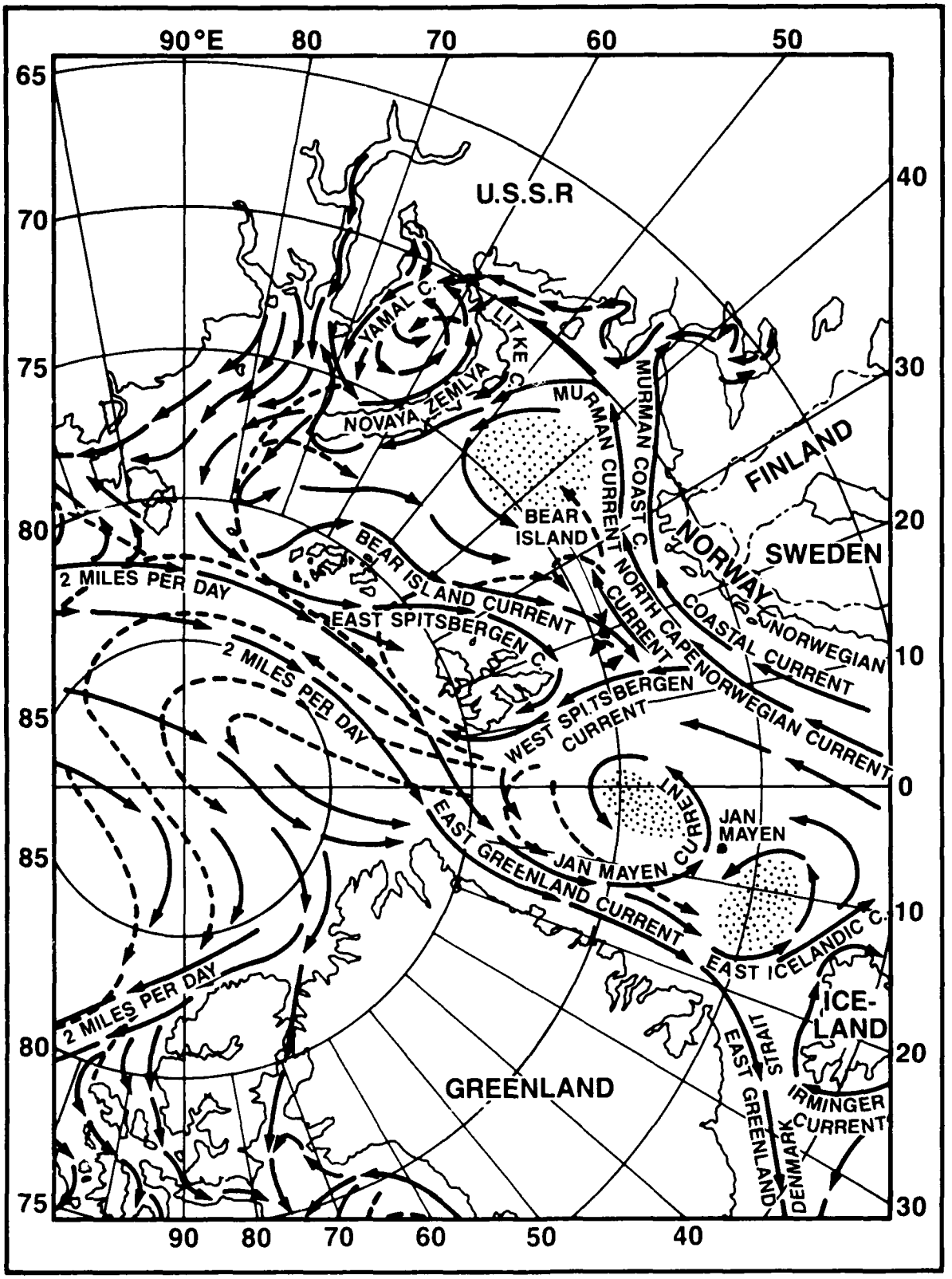

Figure 2-5. East Greenland to U.S.S.R. Ocean Currents (adapted from Welsh et al., 1986).

The circulation of the Barents Seas is counterclockwise with the Norwegian Coastal Current and Norwegian Atlantic Current merging to form the warm and saline North Cape Current. Bear Island is the site of the mixing of several currents. The cold Arctic water in the Bear Island Current mixes with the warm, saline Atlantic water and establishes a frontal zone in the vicinity of the island.

Sea ice is rare in the southwestern portion of the Barents Sea. In April, however, the sea can be 75 percent ice covered. Ice buildup is least in September and in some years, during September, the entire sea has been ice free. The large expanses of open water in the Barents Sea make the ice susceptible to wide variations in location.

The Barents Sea, being on the storm track, has wide weather variations and is a highly unstable region of the Arctic. Coupled with the open nature of the sea ice, the active wind regimes associated with the storms make for rough seas and high waves. Visibility is restricted to less than 1.25 mi (2 km) about 90 days each year. The winter temperatures range between −26 °F to 5 °F (−32 °C to −15 °C); in summer the range is from 32 °F to 45 °F (0 °C to 7 °C). The record low temperature is −60 °F (−51 °C), and the temperature may be less than −25 °F (−31.5 °C) 70 days/year. Winds may exceed 21 kt (11 m/s) 34 days/year. Half the year, seas may exceed 5 ft (1.5 m).

2.2.6 Kara Sea

Like the Barents Sea, the shallow Kara Sea lies entirely on the continental shelf, has a mean depth of 387 ft (118 m) and a maximum depth of 2,035 ft (620 m). Due to the fresh water supplied by the Ob and Yenisei Rivers, the salinity of the surface water is low, from about 7 to 20 ppt. This fresh water supply sets up a northward-moving current along the coast of Taimyr. In the southwest of the sea this current sets up a counterclockwise eddy.

Ice conditions are highly variable in the Kara Sea, but ice is apt to be heavy either in the northwest or in the southwest. Small icebergs are found north of Novaya Zemlya and Severnaya Zemlya (Fig. 2-6). Here the ice may be 5- to 10-ft (1.5- to 3-m) thick in winter, and large hummocks appear to heights of 30 ft (9 m). These "stamukhi" tend to be grounded, which limits movement of the ice pack (see Ice Glossary, Appendix A). East winds drive much ice between the islands, making the straits there impassable.

The climate of the Kara Sea is polar. Precipitation is less than 4 in (10 cm) per year. Visibilities are generally poor, less than 1.25 mi (2 km) about 130 days/year.

Wintertime temperature ranges from −20 °F to 25 °F (−29 °C to −4 °C); in summer it is more like 10 °F to 45 °F (−12 °C to 7 °C). The lowest recorded temperature is −54 °F (−48 °C), and the temperature can be below −25 °F (−31.5 °C) 30 days/year. Winds tend to be southerly in winter, northerly in summer. These winds exceed 21 kt (11 m/s) 70 days/year. The light winds and extensive pack ice allow seas in excess of 3 ft (1 m) only rarely.

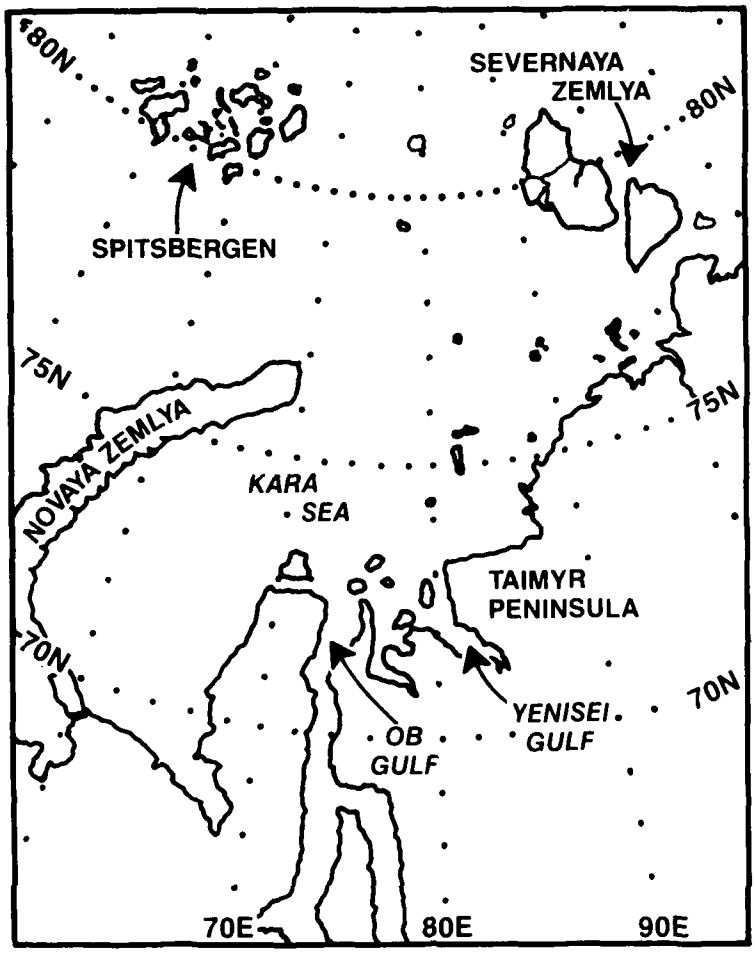

Figure 2-6. Kara Sea Region.

2.2.7 Laptev Sea

Sixty-four percent of the Laptev Sea is less than 328 ft (100 m) deep. Characteristics of the Laptev Sea are, therefore, highly dependent on seasonal ice cover and storminess. The surface water has relatively low salinities and varies, as does the temperature, with distance from the coast. Near the coast temperatures are up and salinities down.

The circulation in the Laptev Sea is counterclockwise, splitting at the Lena Delta (Fig. 2-7). One part moves north to the Arctic Drift, and the other part flows into the East Siberian Sea, east of the New Siberian Islands.

The climate of the Laptev Sea is definitely polar. The precipitation is light, and the year round sea ice precludes high seas. Visibility is less than 1.25 mi (2 km) for 75 days/year due to fog in the summer and blowing snow during the winter months. Winter temperature range is −29 °F to 1 °F (−34 °C to −17 °C); in summer, 10 °F to 45 °F (−12 °C to 7 °C). The record low temperature is −54 °F (−48 °C), and the temperature may be less than −25 °F (−31.5 °C) 60 days/year. Winds are highly variable from southeast to northwest, and winds can exceed 21 kt (11 m/s) 50 days/year.

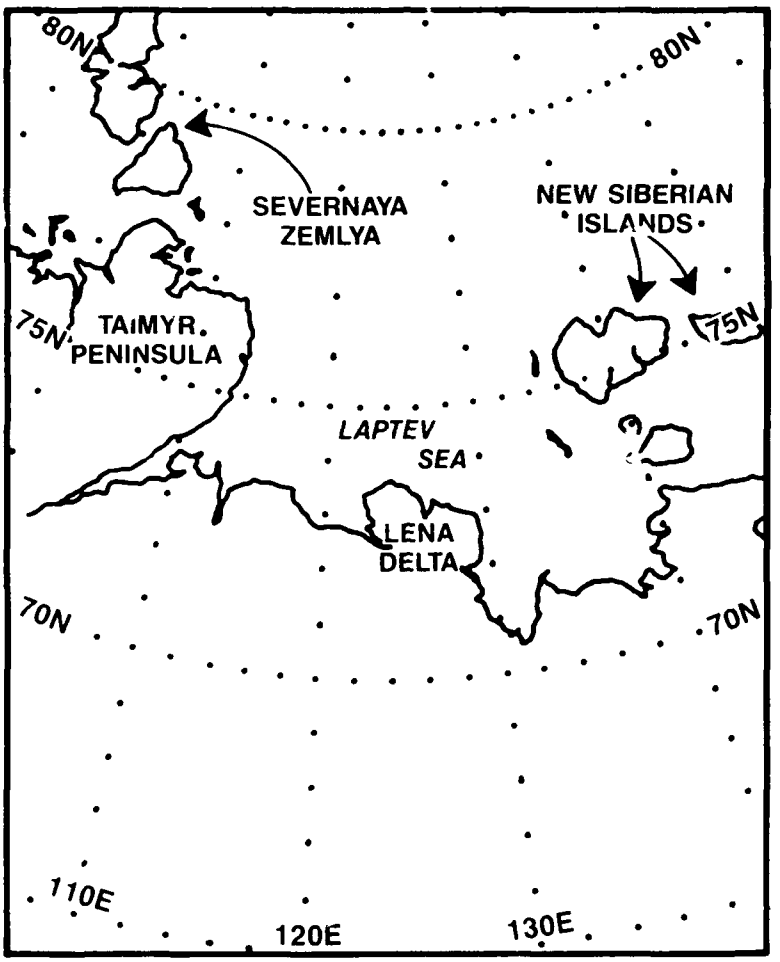

Figure 2-7. Laptev Sea Region.

2.2.8 East Siberian Sea

One of the shallowest of the Arctic seas, the East Siberian Sea depths range from 33 ft to 60 ft (10–20 m) in the western and central regions of the sea to 98 ft to 131 ft (30–40 m) in the east. Not unlike the Laptev Sea, the East Siberian Sea's water characteristics depend largely on ice conditions and river runoff. The eastern part of the sea is usually colder and more saline. Even so, salinities can be as low as 10–15 ppt and increase to 30 ppt near the edge of the ice. At the ice edge, temperatures are usually near 32 °F (0 °C) and increase to as much as 42 °F to 44 °F (6 °C to 7 °C) in late summer near the mouths of the rivers with a south wind blowing.

River outflows tend to give a counterclockwise circulation to the waters of the East Siberian Sea. The sea is characterized, however, by a very heavy ice cover and small icebergs from nearby islands. When the polar anticyclone weakens, thus widening the cyclonic water circulation, an increase occurs in pack ice from higher latitudes into the sea. The navigation season is 6 to 8 weeks in the east and 8 to 10 weeks in the west.

The East Siberian Sea has a polar cli. .ate. Winter temperatures range from −35 °F to 5 °F (−37 °C to −15 °C); in summer the range is 10 °F to 45 °F (−12 °C to 7 °C).

The record low temperature is −54 °F (−48 °C). Meanwhile, the winds are predominately east and northeast in summer and west to southwest in autumn. The northwesterlies can be quite strong, reaching 39 kt to 49 kt (20–25 m/s), and hence may generate 13 ft to 16 ft (4–5 m) waves. Winds can exceed 21 kt (11 m/s) 23 days/year. Visibility is restricted to less than 1.25 mi (2 km) for 90 days/year.

2.2.9 Chukchi Se

The Chukchi Sea is that portion of the Arctic Ocean lying immediately north of the Bering Strait (Fig. 2-8). Its area is 225,000 sq mi (582,000 sq km). It is everywhere underlain by the continental shelf. Depths for the most part are between 35 and 213 ft (65 m). Two submarine canyons cross the shelf. Barrow Canyon extends northeast from about 80 mi (150 km) west of Point Barrow to terminate into the Beaufort Sea north of Point Barrow. Herald Canyon is situated northward along 175 °W, from 70 °N to the edge of the continental shelf.

The circulation in the Chukchi Sea is broadly cyclonic. Warm water enters through the eastern side of the Bering Strait throughout the year. In July and August the surface

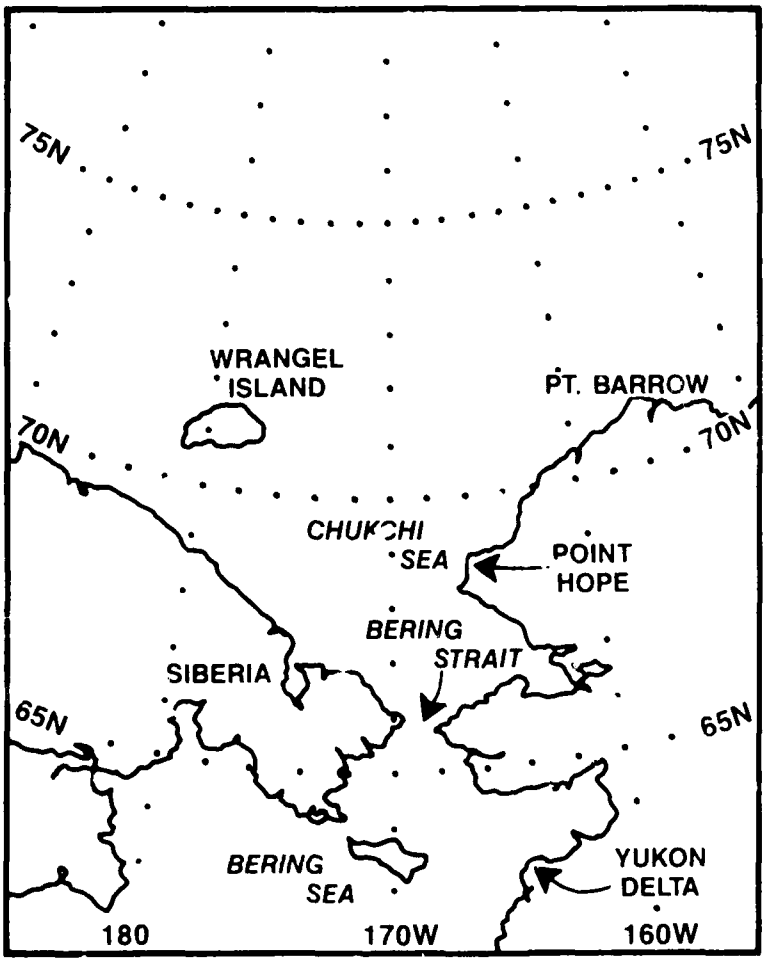

Figure 2-8. Chukchi Sea Region.

temperature of this stream may be 50 °F (10 °C), with salinity less than 30 ppt due to the runoff from the Yukon River south of the Bering Strait. The current divides near Point Hope. One portion continues northeastward toward Point Barrow where it turns westward and joins the general Arctic Basin circulation. The other portion branches northwestward from Point Hope to pass north of Wrangel Island. A cold current sets southeastward from the East Bering Sea along the Siberian coast toward the Bering Strait. It usually turns north before reaching the Strait, but exceptionally may flow southward through the Strait on its western side.

The cold flow of water along the Siberian coast toward the Bering Strait contrasts with the warmer, more saline water to the east. August surface temperatures in this flow range from about 32 °F (0 °C) at the western edge of the Chukchi Sea to 43 °F (6 °C) off Mys Dezhneva. Salinity is low, less than 29 ppt, and sometimes much lower, due to discharge from the Siberian rivers.

2.2.10 Sea of Okhotsk

The Sea of Okhotsk is located where the continent of Asia is separated from the Pacific Ocean by the Kuril Islands and the Kamchatka Peninsula (Fig. 2-9). Depths in the Sea

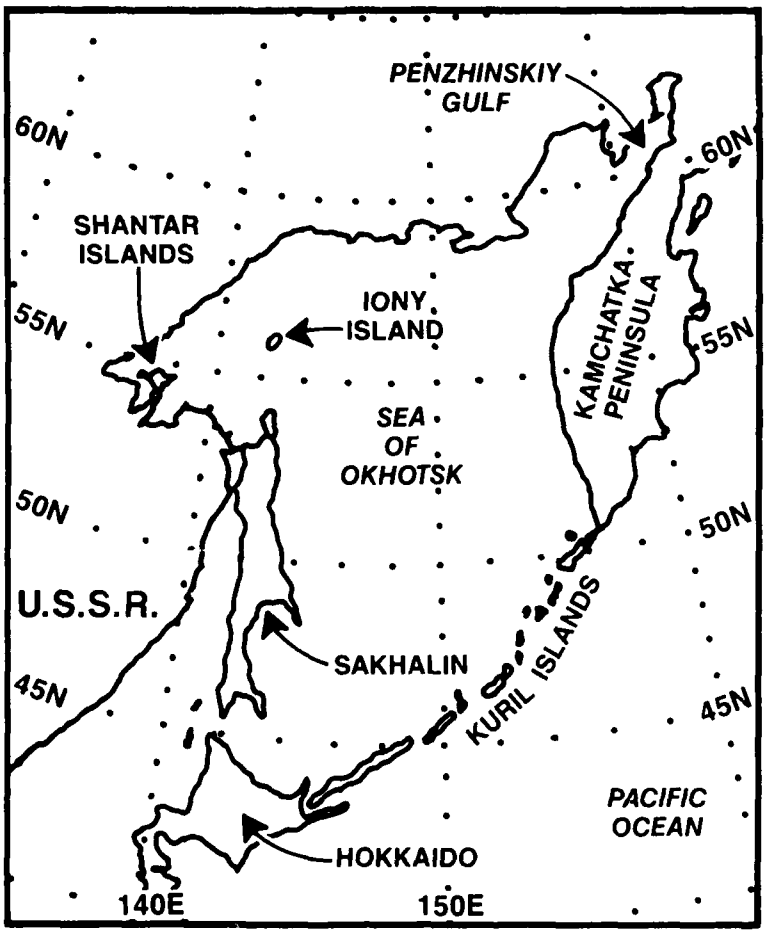

Figure 2-9. Sea of Okhotsk Region.

of Okhotsk range from a shelf under 600 ft (183 m) in the north to over 10,800 ft (3,292 m) near the Kuril arc, but here the slope between the two is gradual except off the east coast of Sakhalin, where it is fairly steep.

The general circulation in the Sea of Okhotsk is cyclonic and runs strongest 20 to 40 mi (30–60 km) offshore. A complex pattern of currents has been reported from the middle of the sea. The current moves north along western Kamchatka at 0.5 kt (25 cm/sec); in other sectors velocities up to 1 kt (50 cm/sec) are recorded. The Sea of Okhotsk has one unusual feature that affects both the ice conditions and the climate: the patches of substantially colder water (34 °F to 43 °F or 1 °C to 6 °C) that are located at the entrance of Penzhinskiy Gulf in the northeast, off Iony Island, and between the Shantar Islands and northern Sakhalin. These cold spots mark upwellings of colder, deeper water, the cause of which is still in doubt. They are associated with continuous dense fogs in the summer and concentrations of ice in the winter. The exchange of water with the Pacific Ocean is not great, due to the shallow depths (1,558 ft or 475 m) of the channels between the Kuril Islands. Pacific waters normally enter through the northeastern channels and Okhotsk water leaves by the southwestern channels.

2.3 Major Islands and Other Land Forms

2.3.1 Alaska and the Aleutian Islands

A primary characteristic of this region of the Arctic is the mountainous terrain. The Aleutians extend for more than a thousand miles from the Alaskan Peninsula to Attu Island (Fig. 2-10). Unimak is the easternmost island, and it is the largest of the 150 islands—about 65 mi (106 km) long and 25 mi (40 km) wide. The islands are, in some instances, glaciated and volcanic. Though treeless they support fairly luxurious growths of grass and willow and alder shrubs. They are noted for periods of extensive fog and sometimes gusty winds, called williwaws. The island area is known best as the birthplace of the Aleutian Low. The islands experience highly variable weather due to the frequent cyclonic storms in the area. Sea currents are swift around the islands and fog is frequent. On Unalaska Island, Dutch Harbor has a mean temperature of 32 °F (0 °C) in January and 51 °F (10.5 °C) in July, which is representative of most of the towns. Precipitation varies between 50 to 70 in (127–178 cm) annually.

The mainland of Alaska is meteorologically significant because of the Brooks Range, a range of mountains extending west to east in the northern quarter of Alaska. The area from these peaks to the north Alaskan coast is known as the *North Slope*. In subsequent chapters, the role of all these features that affect Arctic weather will be explored.

2.3.2 Canadian Arctic Archipelago

The many islands of the archipelago form a triangle with apexes at 61 °N in the east, 67 °N in the west, and the northern tip of Ellesmere Island at 83 ° 30 ′ N (Fig. 2-11). Islands lying north of 74 °N are called the Queen Elizabeth Islands. Most of these islands are glaciated and mountainous, with remnant icecaps on Ellesmere, Axel Heiberg, Devon, and Bylot Islands.

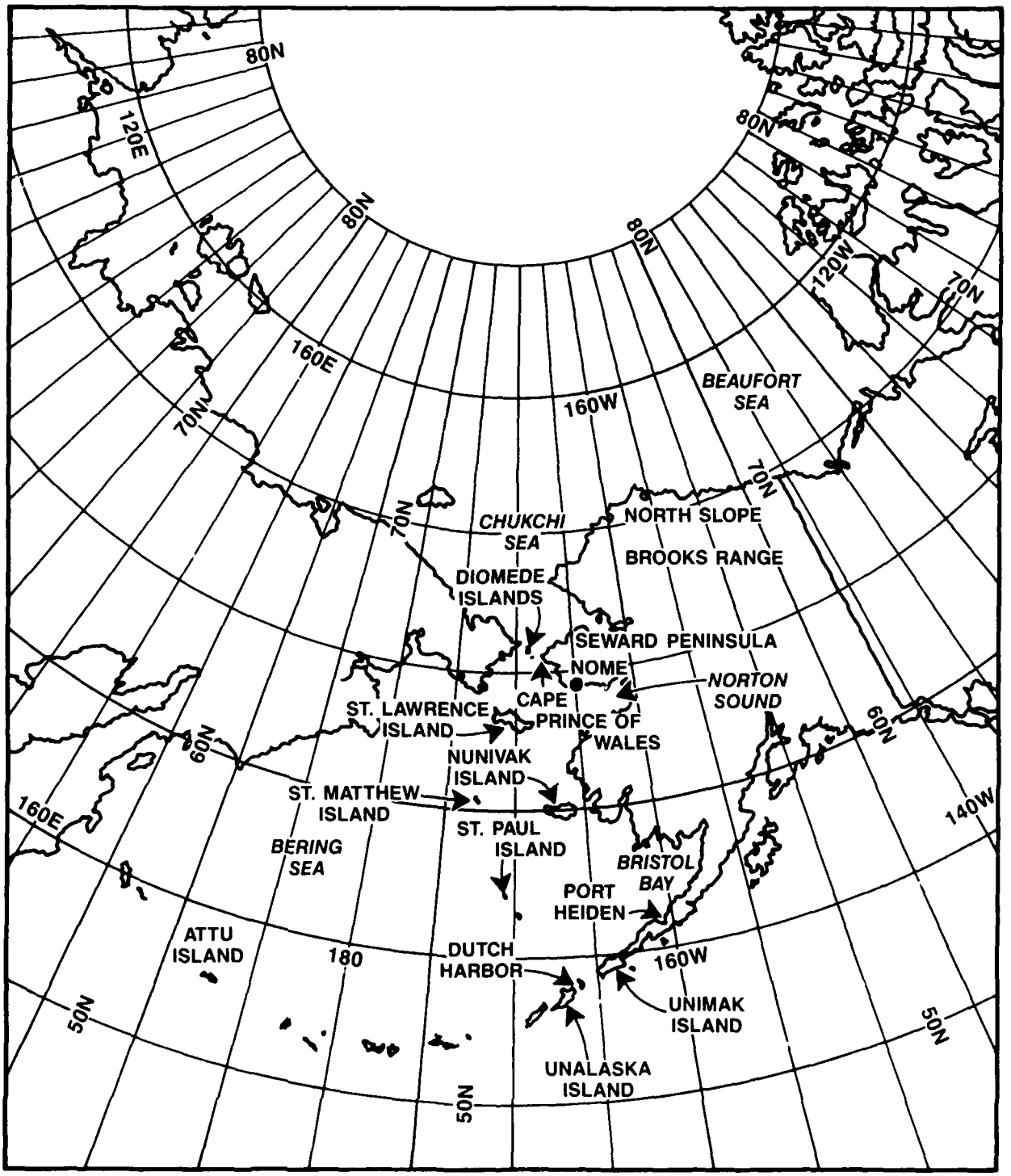

Figure 2-10. Alaska and the Aleutian Islands.

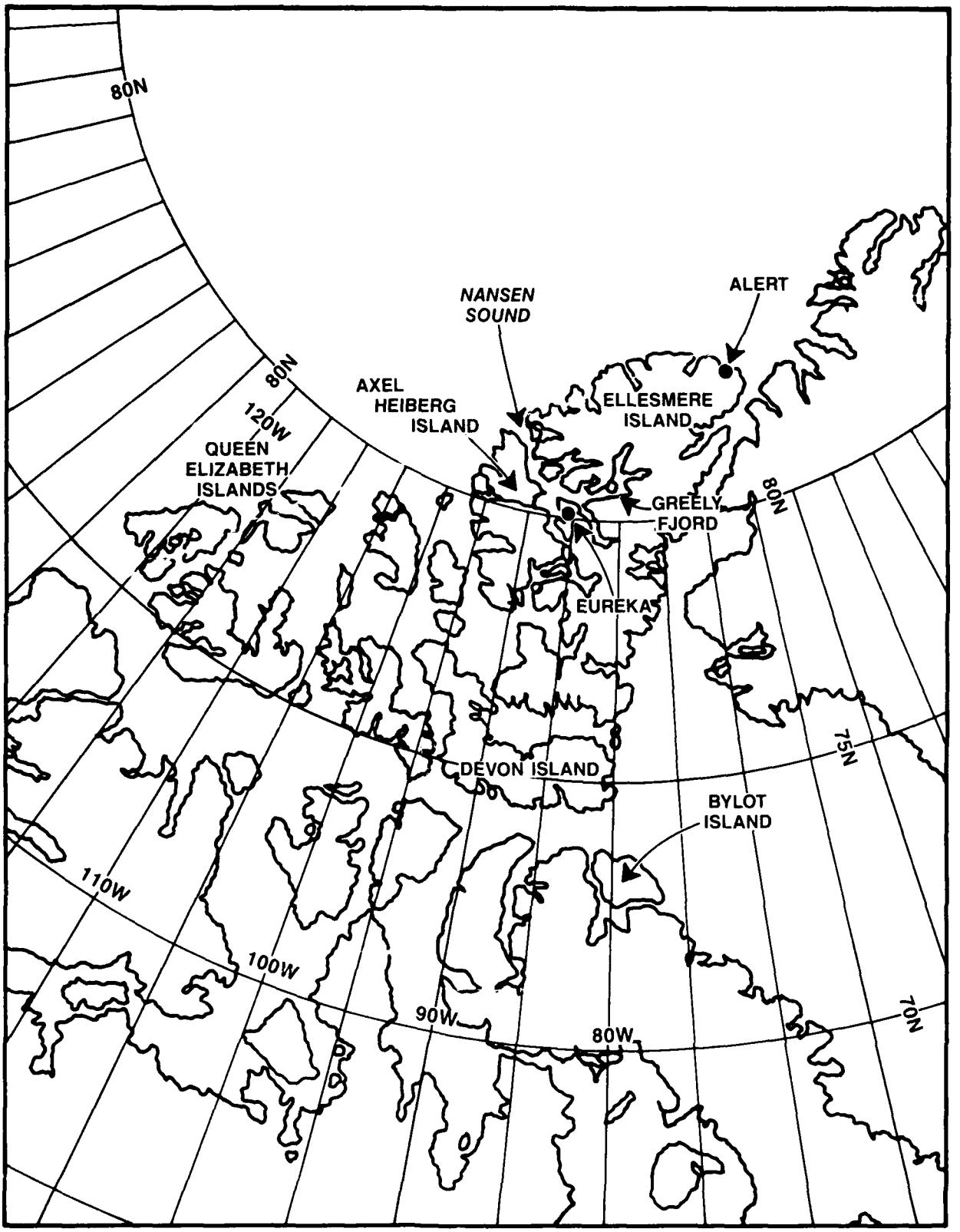

Figure 2-11. Canadian Archipelago Region.

The climate here is sub-Arctic in the south and polar in the north, as winters are long and cold with mean temperatures between −30 °F to −20 °F (−35 °C to −29 °C). February is the coldest month with temperatures dropping usually to between −35 °F and −40 °F (−37 °C and −40 °C). The record low temperature is −63 °F (−53 °C). The warmest areas are those exposed to the open waters of the Davis Strait in summer. July mean temperatures range between 40 °F and 50 °F (4.5 °C and 0 °C), with most stations reaching 60 °F (15.5 °C) sometime during the summer.

Precipitation is relatively light over the entire archipelago and rarely does it exceed 10 in (25 cm) annually. About half of the precipitation falls in the form of snow, which is likely in any month of the year.

2.3.3 Ellesmere Island

Ellesmere Island is the third largest and most northern island in the Canadian Archipelago. It is part of Canada's Northwest Territories (NWT). Weather stations were established on the island's southwest side at Eureka in 1947 and at Alert in the northeast in 1950.

Ellesmere Island is mountainous and has several icecaps. Numerous fjords indent the entire coast, but the most impressive one is the 200 mi (320 km) long Nansen Sound-Greely Fjord on the west coast. Northeast of this fjord are the plateau and lowlands. A rather unique ice shelf is found along the north coast, and the south and east coasts have open water only briefly in late summer.

The climate is cool and damp with temperatures rarely rising above 40 °F (4 °C). Short spells of warm weather can occur in the interior, however, where temperatures may reach 60 °F to 70 °F (15 °C to 20 °C).

2.3.4 Baffin Island

Baffin Island is about 1,000 mi (1,600 km) long and up to 500 mi (800 km) wide. The area of this fifth largest island in the world, which lies in the Canadian Archipelago, is 183,810 sq mi (476,068 sq km).

The island is mountainous in the east where some glaciers and icecaps reach elevations in excess of 8,000 ft (2,400 m). Cumberland Sound and Frobisher Bay are the better known of the many bays and fjords fringing the Baffin Island coast. The west-central coast is lowland and the northern and southern areas are generally plateaus. Airports are located at Frobisher and Cape Dyer. Other landing strips are situated at Nanisivik, Pond Inlet, Clyde River and Broughton Island.

2.3.5 Greenland

The world's largest island, Greenland, is covered by a sheet of ice spread over 80 percent of its area of 700,000 sq mi (1,820,000 sq km). This ice sheet is the source of most of the North Atlantic's icebergs. In profile, the ice sheet forms three broad domes, the highest of which is more than 10,000 ft (3,048 m). The ice thickness alone is probably in excess of 7,000 ft (2,134 m). Tongues of ice extend from this huge sheet to the coast. Greenland's

northern tip at Cape Morris Jessup (83° 39′N) (Fig. 2-12) is the farthest northland of the Northern Hemisphere. It is 1,600 mi (2,575 km) from here to the southernmost point at Cape Farewell (59° 46′N). The width at the widest point is just under 700 mi (1,126 km). The ice sheet is absent in three main areas: in the southwest, where the inland ice is separated by 100 mi (161 km) from Davis Strait; north of Scoresby Sound in the east; and in Peary Land in the north.

Temperatures on the icecap range from −49 °F to 27 °F (−45 °C to −3 °C) throughout the year. The great elevation of the ice gives rise to spectacular katabatic winds all along the Greenland coast. This subject will be discussed further in subsequent sections. On the west coast, mean temperatures range rather uniformly from 18 °F (−8 °C) in February at Ivigtut in the southwest, to −20 °F (−28 °C) at Smith Sound in the northwest. Summertime temperatures are more uniform, 50 °F (10 °C) in the south and 35 °F to 40 °F (1 °C to 5 °C) in the north.

Figure 2-12. Baffin Island and Greenland.

Precipitation varies from 46 in (117 cm) of snow at Ivigtut in the south to 10 in (25 cm) north of 69°N. Except for portions of the southeast coast, the entire island is ice locked in winter and fog is prevalent, especially near the broken ice. Fog or stratus will form over the marginal ice zone with on-ice wind flow.

2.3.6 Svalbard (Spitsbergen)

Svalbard is an Arctic archipelago made up of a main group of large islands known as Spitsbergen, Bear Island, Hope Island, and some smaller islands (Fig. 2-13). The Spitsbergen Archipelago consists of West Spitsbergen, Prince Charles Foreland, Northeast Land, Barents Island, and Edge Island and has a total area of 23,700 sq mi (62,370 sq km). The entire Svalbard landmass is only slightly larger at 24,000 sq mi (63,158 sq km), and it contains several volcanic cones and hot springs.

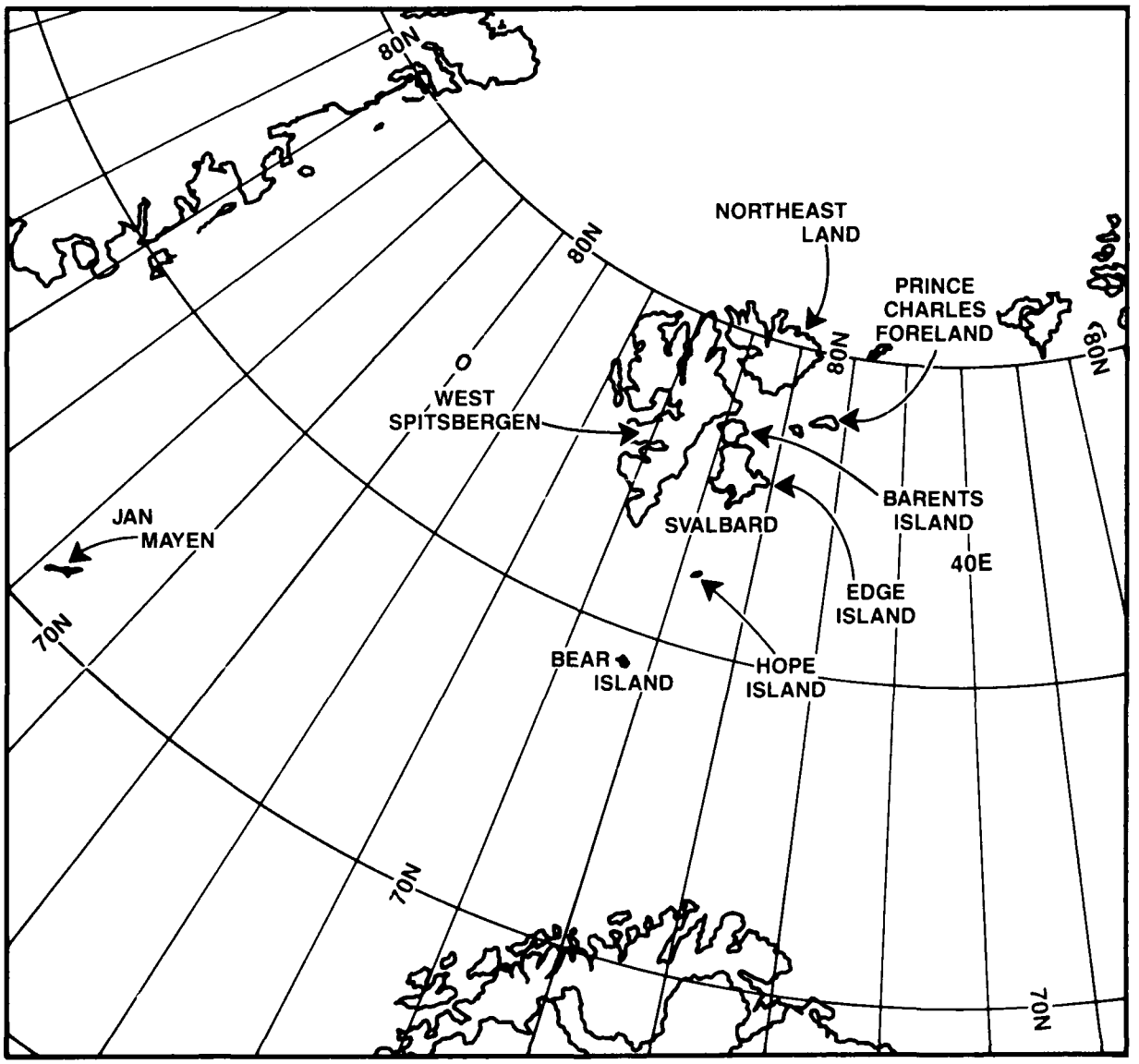

Figure 2-13. Svalbard Archipelago.

The Arctic climate here is stormy and rather mild in the west but much colder and quieter in the east. The islands are extensively glaciated (90 percent) but some peaks do penetrate the snowfields in the west and many of the valleys here are ice free.

2.3.7 Novaya Zemlya

Novaya Zemlya is also an archipelago consisting of two main islands and a number of smaller ones situated off the coast of European U.S.S.R. (Fig. 2-14). The total area of these islands is about 31,382 sq mi (81,593 sq km). The two main islands form a crescent shape and are separated by the Strait of Matochkin Shar. The Karskiye Vorota separates the archipelago from Vaigach Island to the southeast.

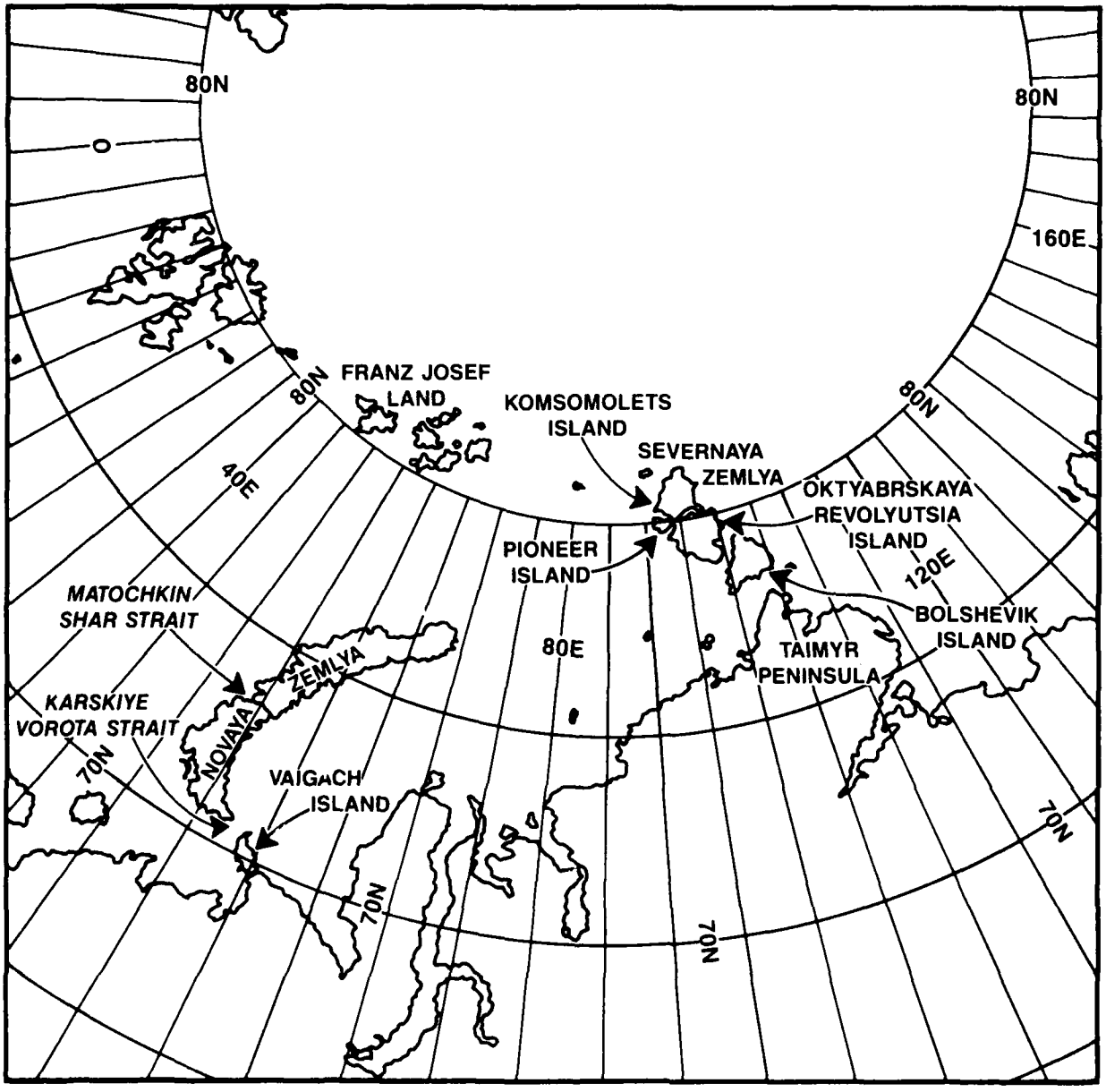

Figure 2-14. Novaya Zemlya, Severnaya Zemlya, and Franz Josef Land.

Novaya Zemlya is mountainous, being an extension of the Urals. The highest peak is on the southern portion of the island and reaches an elevation of 5,217 ft (1,590 m). The main northern island, having high terrain, is largely ice covered along a glacial ridge while the southern half is ice free, like an Arctic desert.

Average temperatures range from −7.6 °F (−22 °C) in January to 43.5 °F (6 °C) in July. Precipitation varies from 6 to 9 in (15–23 cm) annually.

2.3.8 Severnaya Zemlya

This island is an archipelago of the U.S.S.R. in the Arctic Ocean. Its name means "northern land." Separating the Kara and Laptev Seas, it lies north of the Taimyr Peninsula (see Fig. 2-5) and is part of the Russian Republic. Slightly less than half of its area of 14,300 sq mi (37,000 sq km) is ice covered. The four main islands are Komsomolets, Pioneer, Oktyabrskaya Revolyutsia, and Bolshevik.

2.3.9 Franz Joseph Land

This Arctic archipelago belongs to the U.S.S.R. and lies east of Svalbard and north of Novaya Zemlya (Fig. 2-14). It is made up of about 100 islands that lie between 80 °N and 82 °N, and 43 °E and 65 °E. The islands are similar in appearance and have glaciers and icecaps over the thousand-foot-high landmasses. Perhaps as much as 90 percent of their area is covered by ice; the smaller islands are completely buried in ice.

2.3.10 Jan Mayen

Jan Mayen is a bleak and desolate Arctic island between Greenland and northern Norway at about 71 °N 8 °W (Figs. 2-13 and 2-15). It is 33 mi (53 km) long and 10 mi (16 km) wide at its greatest breadth. Jan Mayen is of volcanic origin and has two major peaks: Beerenberg (7,470 ft or 2,277 m) in the northeast and Rudolftoppen (2,525 ft or 769 m) 25 mi (40 km) away to the southwest. The two peaks are joined by a ridge that is at all points at least 656 ft (200 m) in elevation.

Glaciers on the islands are fully developed, and the climate is cold and foggy. It is named for a Dutch whaler captain named Jan Jacobsz May. Its Norwegian weather station has been in operation since 1921. It is home to a NATO airport.

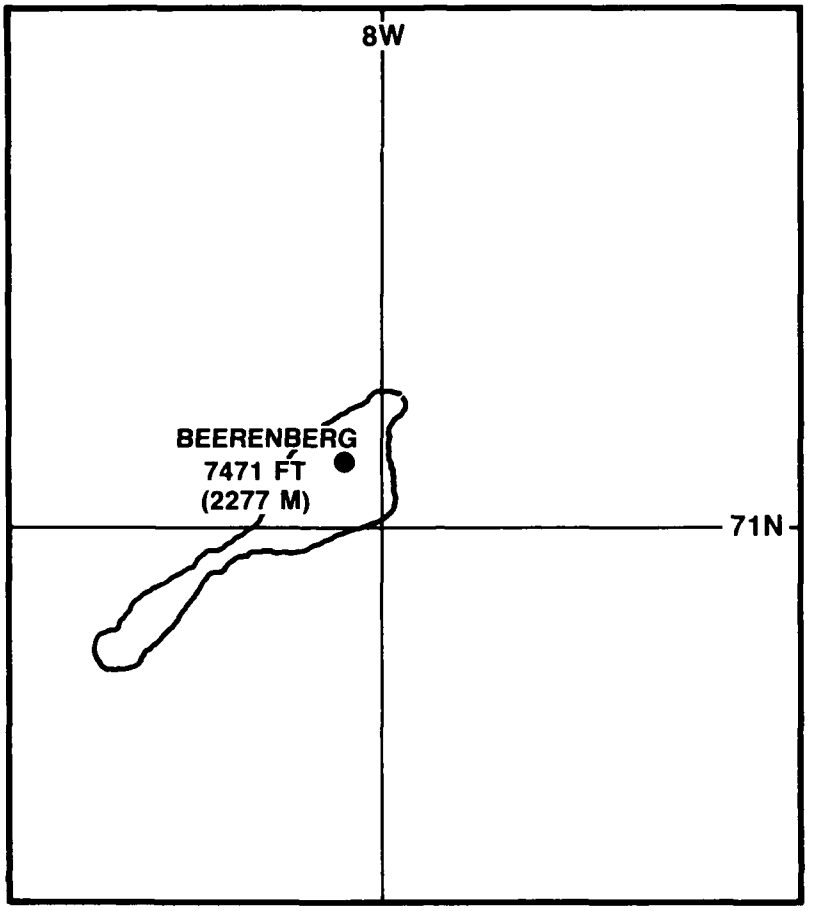

Figure 2-15. Jan Mayen.

2.4 The Arctic Ice

2.4.1 Ice Coverage Characteristics

The ice that covers the Arctic Ocean is constantly on the move in response to wind and ocean currents. Its response to the seasons is dramatic: the average area of ice coverage can shrink from 4.7 million sq mi (11.7 million sq km) in late winter to half that size in late summer. Figure 2-16 shows the average annual maximum and minimum ice limits in the Arctic and sub-Arctic regions. The area between these two limits is known as the *Marginal Sea Ice Zone.* (Hence, the acronym *MIZEX* for the marginal ice zone experiments conducted in the 1980s.)

In some areas near the edges of the ice sheet, waves and swells can also affect the ice motion. Variable stresses such as tensile, shear, and compressive are constantly at work to cause ice floes to separate and produce open water lanes (LEADS) or open water "lakes" (POLYNYI). In contrast, floe collisions may cause the ice to pile up in huge HUMMOCKS or RIDGES that may reach 33 ft (10 m) in height above water and 164 ft (50 m) below. When occurring near shorefast ice, the collisions create chaotic zones of rubble, hummocks, and pressure ridges that collectively become known as a FLAW.

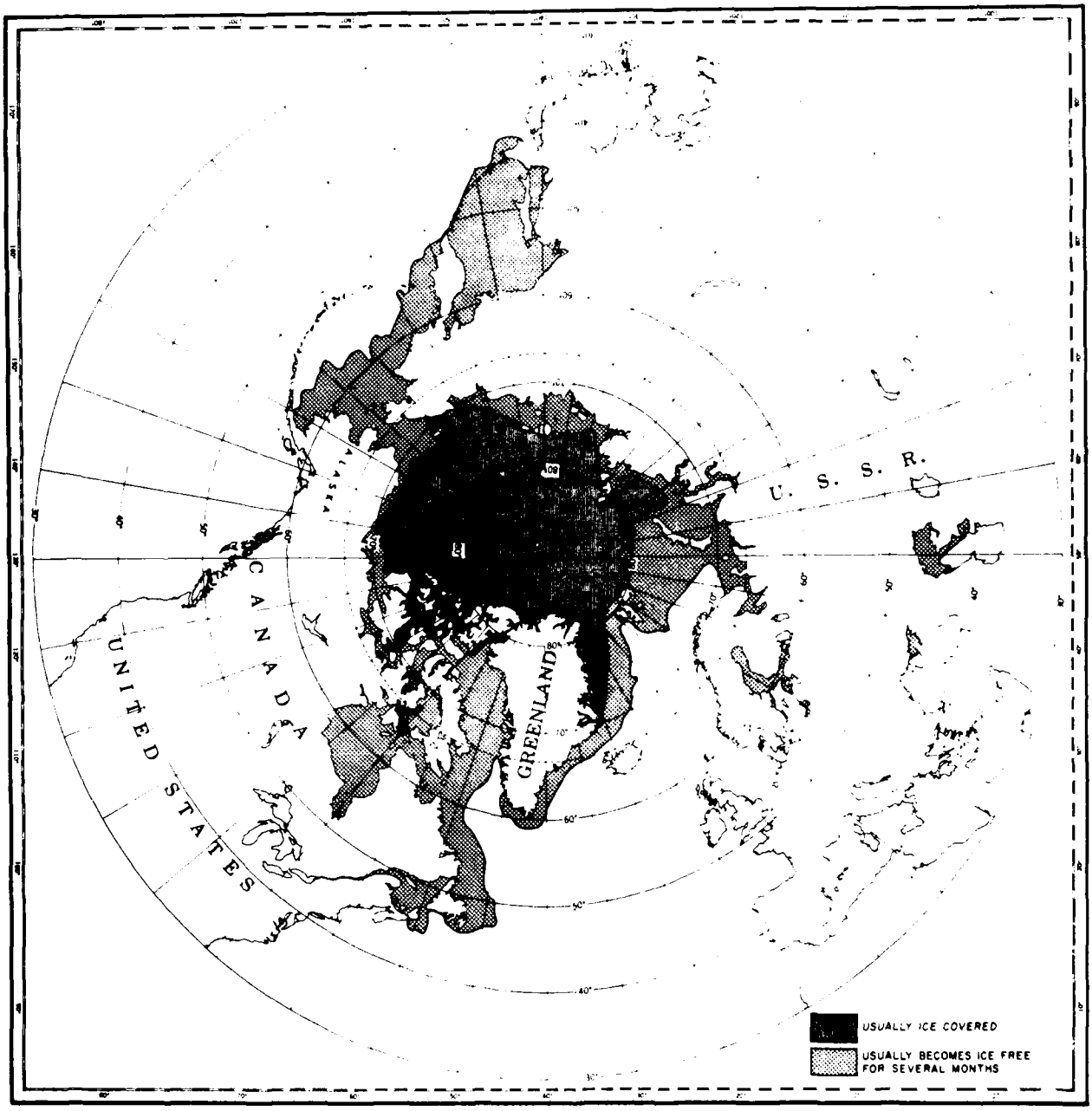

Figure 2-16. Average Annual Maximum and Minimum Ice Coverage (Sater et al., 1971).

2.4.2 Development of Sea Ice

SEA ICE forms differently from lake ice. Because the maximum density of lake water occurs at 39 °F (4 °C), it expands on falling below that temperature, has less density, and therefore rises. Hence, the bulk of the lake remains at 39 °F as ice formation takes place on the surface. After that, additional ice forms on the bottom of the ice surface.

Sea ice does not achieve its maximum density, or start freezing, until it is cooled to 28.6 °F (−2 °C). In its initial stages, the crystalline structure of sea ice incorporates brine and is not solid. It will, therefore, bend under a load before it fractures, while newly formed freshwater ice, brittle and also more transparent, will fracture suddenly, like a windowpane. Because of its elasticity, even sea ice 4 in (10 cm) thick is unsafe to walk on, while freshwater ice only half as thick will support a human being.

In the absence of any wind or strong current, sea ice first appears on the surface as an oily film of crystals. This FRAZIL ICE thickens to a kind of gray slush called GREASE ICE, which then thickens vertically to form an elastic layer of ice crystals an inch (2–3 cm) or so thick called NILAS. Young nilas bends like watered silk over a light ocean swell and is nearly transparent (i.e., dark like the water). When it is about 4 in (10 cm) thick, nilas begins to turn gray and is called YOUNG ICE, or GRAY ICE. When gray ice finally becomes opaque it is called FIRST-YEAR ICE. And in these later stages it thickens more slowly.

Although sea water has a salinity in the vicinity of 35 ppt, ice grown from sea water seldom has a salinity greater than one-third or one-fourth this value. Frazil ice crystals are nearly pure water. When a mass of frazil crystals congeal to form nilas, however, they entrap pockets of sea water between them, some of which have an elevated salt content caused by the expulsion of salts during the freezing of the frazil crystals. Ice older than one melt season has a much lower salinity than first-year ice. The reasons for this are not well known. Nevertheless, the result is that OLD ICE is remarkably "fresh", with salinities varying around 2 ppt.

By spring, first-year ice might be 4 to 6 ft (1–2 m) thick. If it does not melt completely during the summer, it becomes SECOND-YEAR ICE in the fall, tinted blue and much harder. Brine in the upper layers has drained out during the summer and fresh ice crystals have filled the drained areas. Second-year ice continues to thicken, until it stabilizes after a few years at about 10 to 12 ft (3–4 m). If it remains unmelted through a second summer, it is simply called MULTIYEAR ICE, or polar PACK ICE, to distinguish it from first and second year pack ice.

The albedo of ice strongly depends on its age and thickness. Frazil or new ice up to 2 in (5 cm) thick has a very low albedo and actually appears dark against a water surface. LIGHT NILAS, measuring 2 to 4 inches (5–10 cm) in thickness, has a low albedo and appears dark gray. Young ice between 2 and 4 in has a moderate albedo and appears grayish. First-year ice with thickness greater than 12 in (30 cm) has a relatively high albedo of reflected *visible* light and appears very light gray against SNOW-COVERED ICE. Albedos in the infrared are different and will be discussed elsewhere.

2.4.3 Ice of Land Origin

Ice that has been formed on land as a result of the compaction of snow into GLACIERS is frequently found in certain regions of the Arctic. In these regions, the glaciers flow to the sea and form ice shelves. The ice shelves calve off ICEBERGS or ICE ISLANDS. Because of their large mass and unusual strength, icebergs are a hazard to navigation. Figure 2-17 provides size comparisons for ice of land origin. Ice that remains fixed to the coast is known as FAST ICE.

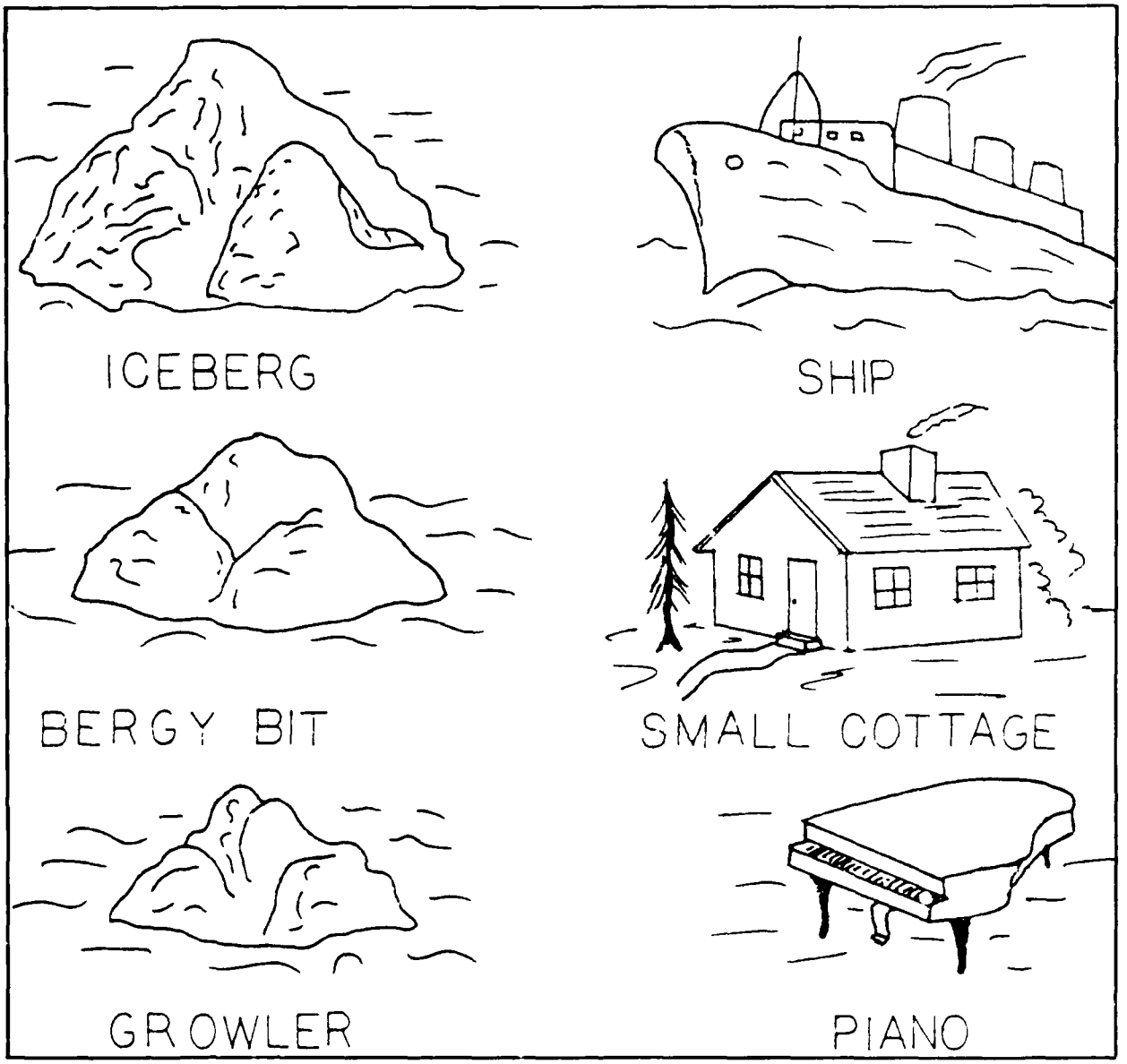

Figure 2-17. Comparison of Ice Sizes.

2.4.4 Ice Islands

Large sections of land ice (up to nearly 200 ft [60 m] thick and 20 mi [30 km] wide), called ice islands, occasionally break away from the northern edge of the Ellesmere Island ice shelf to join the moving pack ice. These ice islands float slowly in an erratic, large, clockwise circle around the North American side of the Arctic Ocean in the Beaufort (Pacific) Gyre. Eventually they disintegrate or exit into the Greenland Sea via the East Greenland Drift. Some have been recognizable for as long as 30 years. Almost as extensive as ice islands but much thicker are tabular icebergs, which break off whole from the foot of a tidewater glacier. With a volume of 40 to 50 cu mi (165–210 cu km), they are the largest objects afloat in the Northern Hemisphere.

2.4.5 Icebergs

Icebergs, which are much smaller than ice islands, break off the seaward ends of glaciers in Greenland, Northeastern Canada, Svalbard, and the Soviet Arctic. The primary source of icebergs, however, is the Greenland ice sheet, which has a maximum thickness of 10,827 ft (3,300 m) and annually calves about 314,400 cu yds (240 cu km) of ice into the surrounding seas. Because of the geographically limited distribution of iceberg sources, icebergs are not a serious problem in the North Pacific, the Bering Sea, or any part of the central Arctic Ocean.

Estimates of icebergs calved annually by the Greenland ice sheet vary from 20,000 to 34,000, with most being produced by the west coast of Greenland glaciers. Although these statistics are numerically impressive, they do not provide the volumetric or mass information needed to estimate the noise effects on naval operations or threats to navigation.

The iceberg drift pattern is such that icebergs formed along the east coast usually drift around the southern tip of Greenland and then move north, joining those icebergs calved from west coast glaciers. This drift continues northward up to Baffin Bay, where the icebergs swing around and start moving south along the coasts of Baffin Island, Labrador, and Newfoundland. They finally reach the Grand Banks and ultimately melt in the North Atlantic. Icebergs make or are the sources of distinctive noise in the Arctic, especially in the potential choke point areas of the eastern Arctic.

2.5 Distribution of the Arctic Ice

In large part, the limits of the Arctic ice cover is determined by the bordering land-masses. The greatest variation in ice cover occurs in the marginal seas of the Chukchi and Bering Seas and Sea of Okhotsk on the Pacific side, and in the Greenland and Norwegian Seas and Baffin Bay on the Atlantic side.

The Arctic ice edge climatology charts for April (Fig. 2-18) and for October (Fig. 2-19) were constructed by graphically compositing the maximum and minimum ice edge extremes from eleven years (1972–82) of the Joint Ice Center's operational eastern and western Arctic ice analyses centered closest to the fifteenth of the month.

During the spring (March–April) the sea ice makes its deepest penetration southward. In the fall (September–October) the extent of the ice is at its minimum. Climate and ocean currents play the largest roles in determining the extent of the ice in any season. For example, the warm Atlantic Current continuously transports heat into the Norwegian Sea. Thus, the open water is indented poleward during all seasons in the eastern Atlantic sector. A comparison of fall and spring charts shows that the ice edge remains in the Svalbard region throughout the year. In the Barents Sea, where the effects of the Atlantic Current are less pronounced, the ice edge location is more variable.

As noted in the climatology charts, sea ice distribution can vary considerably from season to season and from area to area throughout the marginal Arctic seas. These changing conditions have a tremendous effect on the weather conditions in the Arctic as well as the military's ability to operate in these areas. The successful Arctic forecaster must be knowledgeable about the changing sea ice conditions and their effects on Arctic operations. The following detailed descriptions of sea ice conditions in the Arctic Ocean and adjoining seas will assist in gaining that knowledge. The terminology used to describe these sea ice conditions is in accordance with the World Meteorological Organization's (WMO) Sea Ice Nomenclature, WMO-No. 259, TP 145, which is included as Appendix A.

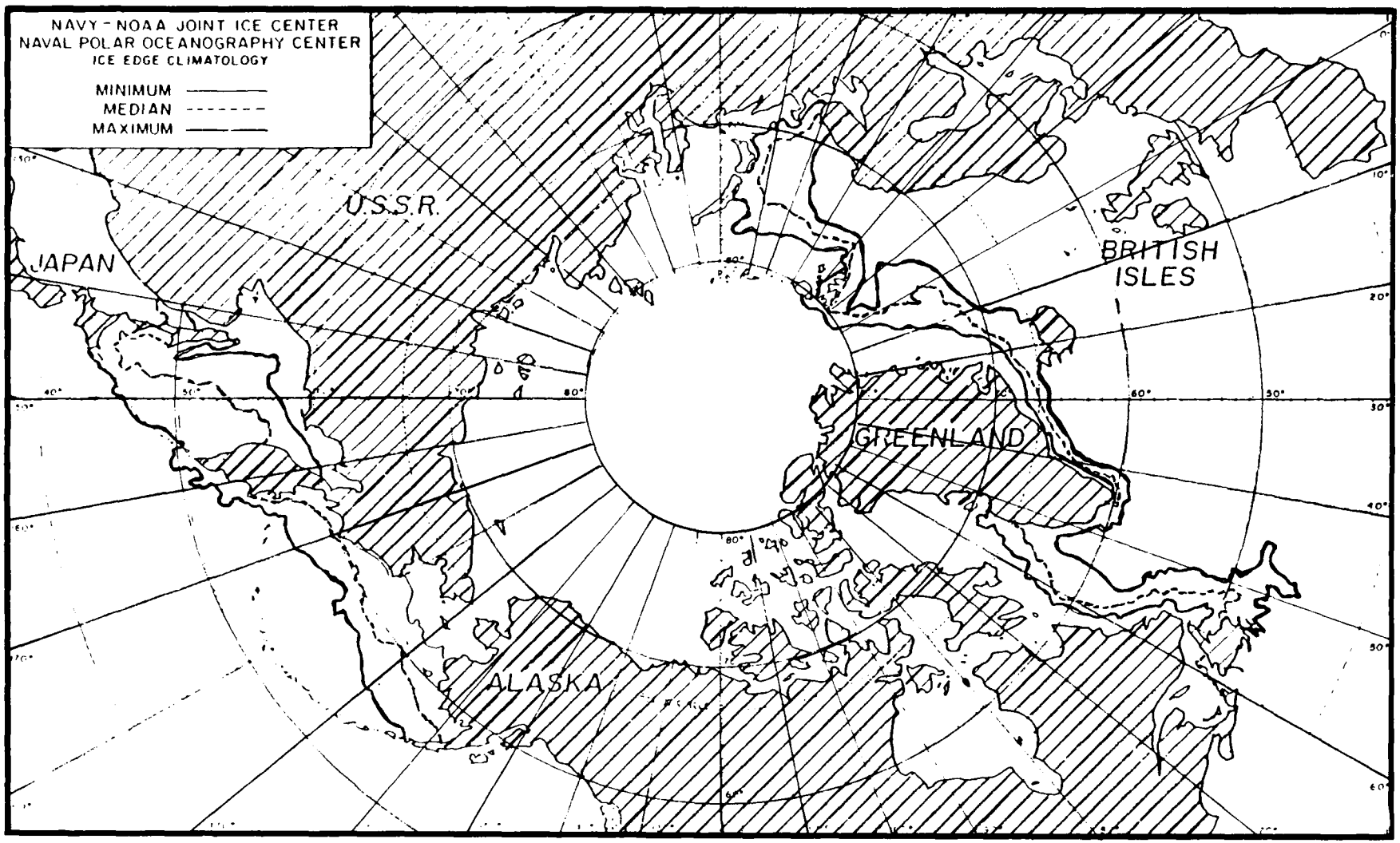

Figure 2-18. Statistical Ice Edges in the Northern Hemisphere (April) (Stringer et al., 1984).

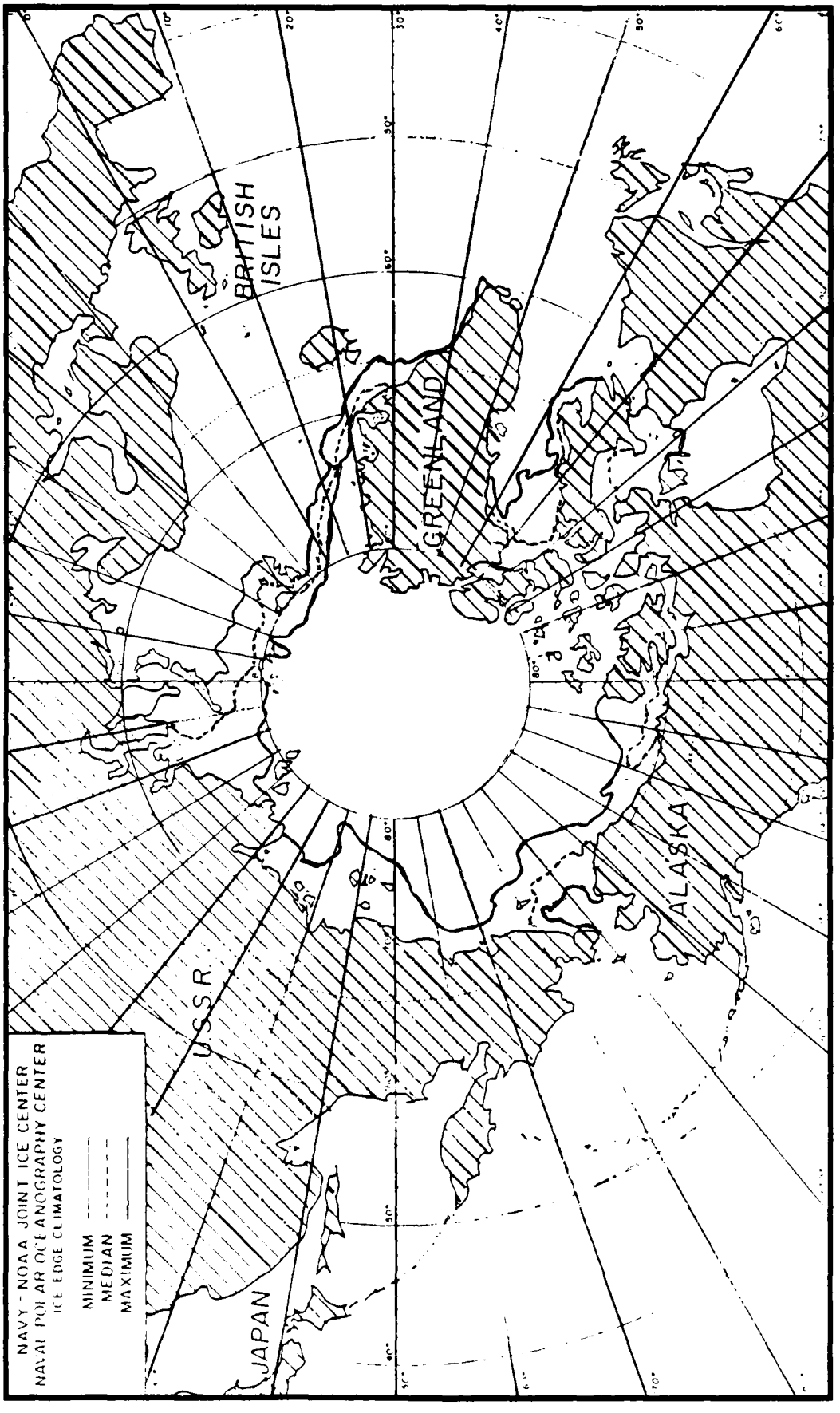

Figure 2-19. Statistical Ice Edges in the Northern Hemisphere (October) (Stringer et al., 1984).

2.5.1 General Ice Distribution in the Arctic Basin

The Arctic pack is a floating conglomeration of pieces of sea ice of all sizes, from huge masses many miles in diameter to small pieces not much larger than a normal office desk. In the winter, the whole Arctic Basin is covered by an elastic ice sheet in which many short narrow leads, cracks, and fractures are opened and closed by the stress of winds and currents and the effects of continual expansion and contraction of the ice itself. At any given time, even in the dead of winter, significant amounts of open water in the Arctic Basin can be found, but the water openings that do form are covered rapidly by new ice growth.

Within the Arctic Basin the freezeup starts in mid-September, and by mid-November the freezeup is complete throughout the Arctic Basin. Due to the prevailing northerly and northeasterly winds in the fall and winter months, the ice pack starts to close in on the shores of Alaska and the U.S.S.R. On the Alaskan coast the ice pack often moves onto the coast about mid-September but may retreat northward again off the coast. But by mid-October it is hard on the coast and stays throughout the winter. Islands off the coast of the U.S.S.R. (Novaya Zemlya, Severnaya Zemlya, and the New Siberian Islands) act as a barrier to the advancing polar ice pack and allow the areas to the south of the islands to remain ice free for a longer period of time than along the Alaskan coast. By mid-November, however, the U.S.S.R. coastal seas are covered by ice for the winter.

Ice breakup in the Arctic Basin does not occur as such. The summer melt starts in June and by mid-August is at its maximum. In midsummer as much as 5 percent of the Arctic Basin may become ice free as the first-year ice melts and the basin becomes dominated by multiyear and second-year ice. Vast amounts of puddling and many thaw holes become apparent as the first-year ice decays and eventually melts, leaving many cracks and leads throughout the Arctic Basin. Along the fringe or southern portion of the Arctic Basin are areas where the major ice melt and decay takes place and consequently, where ship navigation becomes possible. The summer melt of ice begins west of Point Barrow, Alaska with the northerly transport of warm water through the Bering Strait. At the same time, the land warms and relatively warm water begins to flow from the rivers. These warming waters act as melting agents that help open large shore leads along the coasts of Alaska and the U.S.S.R.

In midwinter the Arctic Basin is covered by some type of ice 99 percent of the time. As the wind and ocean currents move the ice pack, leads and cracks open in the pack and new ice forms rapidly in these openings. As the ice pack moves, the ice bangs and bumps together causing ridges of ice, called pressure ridges. Continual pressure on the ice from the prevailing north to northeasterly winter winds causes extremely large pressure ridges to develop for many miles along the coastal areas of Alaska and the U.S.S.R.

The currents of the Arctic Ocean form what is called the Arctic Gyre, which has a anticyclonic flow around the Arctic Basin. The Arctic Gyre slowly carries the ice pack in a anticyclonic whirl around the basin. So slowly, in fact, that it takes 15 to 20 years or longer for a piece of ice to complete this trip. As the ice rotates, some is expelled through the Bering Strait, Canadian Archipelago, and the East Greenland Sea. Ninety-five percent of the multiyear ice that is expelled from the Arctic Basin is through the East Greenland Sea. This ice slowly drifts southward, breaks up, and melts.

2.5.2 Ice Distribution in the Seas Bordering Alaska

Gulf of Alaska

Ice distribution in the Gulf of Alaska is limited to the formation of winter ice in the sheltered harbors and coastal indentations from mid-December to mid-April. The warm Alaska current keeps the area to the south of the Aleutian Island chain and the mainland free of ice in the unconfined areas.

Bering Sea

The Bering Sea is covered with vast expanses of winter ice. This ice is much thinner and weaker, however, than the ice formed in Baffin Bay and Davis Strait at equal latitudes. In fact, in the southern parts of the Bering Sea, the ice remains predominantly medium-winter thickness throughout the winter. Even the ice in the northern Bering Sea is seldom more than about 3 ft (1 m) thick. Several factors account for this characteristic: (1) the greater expanse and depth of the water, (2) the predominantly stronger winds, and (3) the warmer north setting currents.

The freezeup begins with fast ice formation along the Seward Peninsula (refer to Fig. 2-10) in early November. By the end of November, the pack ice normally extends south to about 60 °N, while fast ice can be found in the coastal indentations and bays as far south as Bristol Bay.

The maximum extent of the ice occurs in April. At this time the ice boundary normally extends from the coast at Port Heiden to St. Paul Island, and then to the west. South of about 60 °N the ice pack normally consists of BELTS and PATCHES drifting in random patterns. North of 60 °N a more or less continuous pack of heavy ice forms. The fast ice generally extends from 5 to 10 mi (10–20 km) offshore, being more extensive and heavier in Norton Sound and along the north coasts of Nunivak and St. Lawrence Islands. Areas of perennial open water (or at most thinner areas of young ice) exist in the vicinities of 63 °N 167 °W, 63 °N 174 °W, 64 °N 171 °W, and between Nunivak Island and the mainland.

The ice characteristics vary greatly north and south of 60 °N. To the north, the area is dominated by thick winter ice in the form of large, vast floes that are quite heavily ridged and virtually totally snow covered. South of 60 °N the ice is predominantly medium-winter thickness in small- to medium-sized FLOES, with rafting the predominant topographical feature.

Usually, extensive CRACKS and small leads will exist between the vicinities of Cape Prince of Wales and the Diomede Islands. The area where the Bering Sea meets the Chukchi Sea is one of conflicting currents. Most of the ocean currents in the Bering Sea set to the north. Due to these warm currents, and because total melt occurs annually in the Bering Sea, polar ice does not occur in this sea. Occasional pieces of ice will be seen that have the appearance of thick polar ice. These pieces, actually FLOEBERGS caused by the piling up of thin elastic and very weak ice caused by tidal and wind action, occur especially around the south coast of St. Matthew Island, the northeast coast of St. Lawrence Island, and the vicinity of the fast-ice edge at Nome.

The breakup process in the Bering Sea is quite rapid and is due almost entirely to warming temperatures and warm currents. The ice pack normally recedes to the north of St. Matthew Island by May, to the north of St. Lawrence Island by June, and to the north

of the Bering Strait by July. The fast ice along the coast usually disintegrates even more rapidly due to the more rapid warmup of adjacent land and the contribution of river runoff. This rapid disintegration results in the frequent appearance of leads along the coast as the breakup process begins.

Bristol Bay

Bristol Bay is open to shipping from early May to late November. During the winter, this area contains a narrow band of fast ice along the shore with belts and patches up to about seven-eighths concentration in the central bay. In the spring, disintegration occurs along the shore due to fresh water runoff, and along the seaward edge due to warming currents.

Norton Sound

Norton Sound is open to shipping from early June to mid-November. During the winter, the inner sound is covered with fast ice and the outer sound is covered by heavy winter ice formations. The latter is extremely difficult to penetrate due to heavy ridging. In the spring, the inner sound usually opens earlier than the outer sound.

Chukchi and Beaufort Sea

The ice conditions in both these seas are complex and are complicated by the erratic movement of the polar pack. The Beaufort Sea is affected more by this phenomenon than the Chukchi Sea.

In late October, the freezeup cycle begins. At this time the polar pack begins to move down the continental coasts under the influence of the predominantly seasonal northerly winds. At the same time, the bays and inlets along the coast begin to freeze over with fast ice. Throughout the year the Arctic pack is subject to moving against the coast. Toward the end of the shipping season in September, the shipping lanes are closed more and more frequently, and by late October or early November, the ice is on the coast to stay.

Winter ice in the Chukchi Sea is subject to considerable breakup due to the pressure of the wind, currents, and tides. Ice forms first in areas such as Kotzebue Sound in October (Fig. 2-20). By the first of November, the sound is completely covered except for scattered shore leads that open from time to time.

The breakup occurs in June, with scattered leads opening along the coastline from Cape Lisburne to Point Barrow. At about the same time, a lead commences to form at the mouth of the MacKenzie River. The leads gradually extend toward each other as the ice weakens and melts. Finally, the winter fast ice disintegrates and the Arctic pack recedes to the north. Usually, a lead can be navigated to Point Barrow by early July. By late July, the entire Alaskan coast is usually navigable, although it is subject to sudden closing due to shifts in the Arctic pack. The lead increases in width in August, the best month for navigation in this area. The lead varies in width from 3 to 5 n mi (5–10 km) to as much as 50 n mi (90 km) wide along the coast from Point Barrow to Barter Island. From Barter Island east to MacKenzie Bay, the lead widens considerably due to the influx of warm fresh water from the MacKenzie River. An area of year round open water normally exists in the Beaufort Sea, southwest of Banks Island, due to the abrasive action of the moving Arctic pack against the fast ice of the coast.

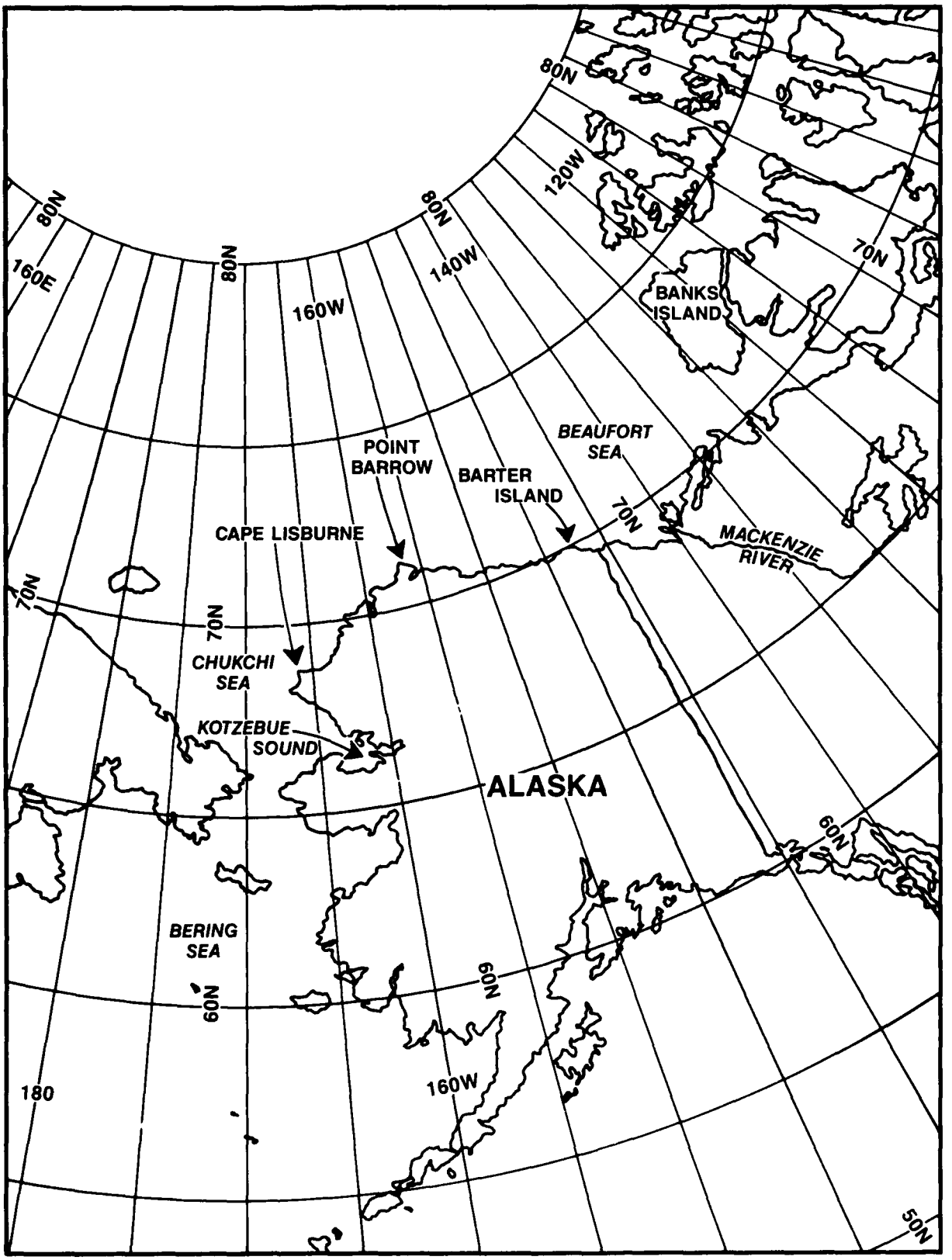

Figure 2-20. Chukchi Sea and Beaufort Sea Region.

2.5.3 Ice Distribution in the Canadian Archipelago

The Canadian Archipelago (Fig. 2-21) is a large area covering thousands of square miles with hundreds of narrow channels throughout the islands. Most of its waterways are completely covered with ice except for very short periods in the late summer or early fall. Many of these channels are never open to transit, even by an ice breaker. The most important factors affecting ice distribution in the archipelago are currents and weather conditions. For this discussion the archipelago is divided into four areas: the Queen Elizabeth Islands, Eureka Transit Route, McClure Strait to Lancaster Sound Route, and the Southern Archipelago.

Queen Elizabeth Islands

The predominant ice type throughout the Queen Elizabeth Islands area is multiyear ice. The exceptions are Wellington Channel, which is mostly winter ice with some polar ice, Jones Sound, and Central and Lower Eureka Sound, which are dominated by winter ice. Multiyear ice fringes all the island coasts, with the exception of the southern coasts of Melville Island, Bathurst Island, Cornwallis Island, and Devon Island where first year fast ice predominates. Freezeup starts in late August with puddles on the ice freezing. By mid-September the leads and cracks freeze.

Breakup and disintegration of the ice starts in March or April even though the maximum ice thickness is not reached until May. By late July much of the ice is rotten, but concentrations remain at eight-eighths. By mid-August the fast ice parts from the shore, and the concentration decreases to six- to seven-eighths in some areas. Navigation by ship is not feasible in the Queen Elizabeth Islands area at any time of the year.

Eureka Transit Route

The Eureka Transit Route is in the eastern portion of the Queen Elizabeth Islands and leads west along the south coast of Ellesmere Island and then north along the west coast of the island. The route goes through Jones Sound, which is dominated by first year floe ice and first year fast ice. The route then enters into Cardigan and Hell Gate Straits, which remain relatively ice free throughout the year because of swift currents. Some fast ice forms along the shorelines of these straits. Next, the route enters Norwegian Bay, which is dominated by multiyear floe ice with multiyear fast ice along the coastline. Finally the transit route enters Eureka Sound, which is dominated by first year and multiyear floe ice.

Freezeup begins in Jones Sound by mid-September, and it is usually frozen solid by the end of October. Cardigan and Hell Gate Straits do not freeze up due to swift currents. Norwegian Bay starts to freeze by late August and is completely consolidated by late September. Freezeup starts early in September in Eureka Sound and is completed by early October.

Because of the westerly winds, breakup in Jones Sound begins in July as ice loosens and moves into Baffin Bay. The minimum amount of ice is present in Jones Sound in late August or early September. Cardigan and Hell Gate Straits remain nearly ice free throughout the year, although heavy floes from Norwegian Bay can block the straits during any season.

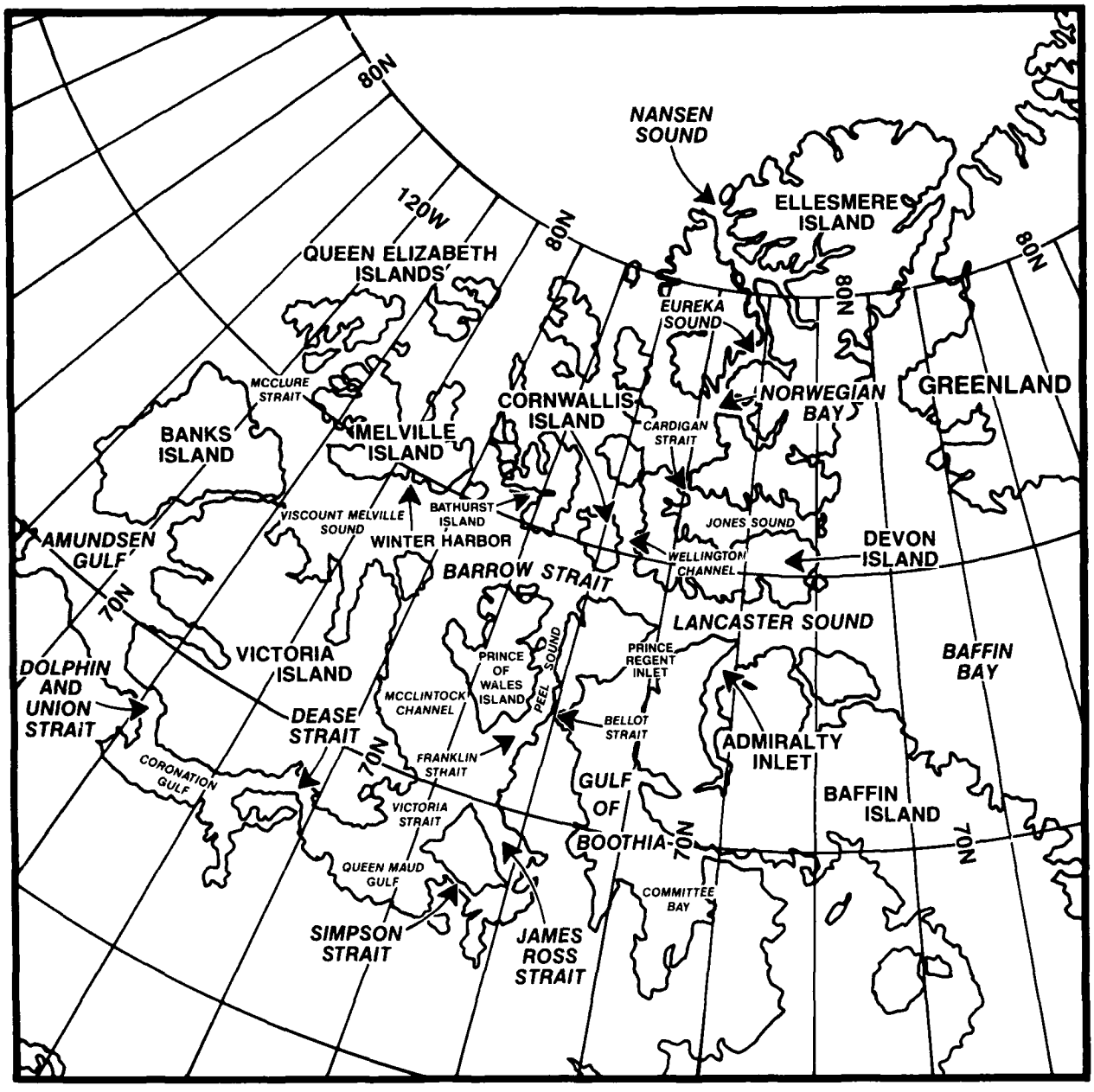

Figure 2-21. Canadian Archipelago.

In favorable years in Norwegian Bay puddling and loosening of the ice begins in July, with navigation possible by mid-August. The ice in Eureka Sound starts to loosen in July, and navigation is possible by mid to late August.

Due to the swift, dangerous currents, coupled with multiyear ice floes, the greatest danger to ships is found in the Cardigan and Hell Gate Straits. The greatest resistance to navigation is the heavy multiyear ice concentrations in the upper two-thirds of Norwegian Bay. During the navigation season ice conditions are as follows: (1) Jones Sound is ice free to two-eighths ice coverage, with belts and patches of greater concentration; (2) Cardigan and Hell Gate Straits generally have less than one-eighth ice coverage, but the straits may

be blocked by multiyear floes for short periods; (3) Lower Norwegian Bay, five- to seven-eighths ice concentration; (4) Upper Norwegian Bay and Lower Eureka Sound, six- to eight-eighths ice coverage often under heavy pressure; and (5) Upper Eureka Sound, one- to two-eighths or less concentration with occasional influx of belts and patches of greater concentration and of multiyear ice floes from Nansen Sound.

McClure Strait to Lancaster Sound

This east-west waterway consists of Lancaster Sound in the east, then Barrow Strait, Viscount Melville Sound, and finally McClure Strait in the west. Ice conditions become progressively worse from east to west. Lancaster Sound and Barrow Strait are dominated by multiyear and first-year ice floes while Viscount Melville Sound and McClure Strait are dominated by heavy concentrations of multiyear ice floes.

Freezeup in Lancaster Sound and Barrow Strait usually begins in October, and they are frozen solid by early November. Viscount Melville Sound usually freezes by mid-September although ice may remain in motion until late November. McClure Strait usually remains clogged with ice all year.

The breakup in Lancaster Sound and Barrow Strait begins in late May; it is normally well advanced by mid-June in the eastern portion of Lancaster Sound and by late June in the remainder of the area. Viscount Melville Sound never completely clears of ice. The ice does loosen, however, and prevailing winds can pack it against the southern shores, leaving its northern shores open but not navigable until sometime in late August or September. McClure Strait usually remains choked with ice throughout the summer.

Navigation is normally possible in the eastern portion of this waterway and almost never possible in the west. The navigation season for Lancaster Sound and Barrow Strait is from mid-July to late September. The area is subject to an influx of ice from the west, and from Wellington Channel, so that even in the best season western Barrow Strait has a concentration of six- to seven-eighths ice. To the east, drifting belts and patches are common particularly along the southern coastal boundary. In Viscount Melville Sound and McClure Strait, navigation is not considered feasible west of Winter Harbor, and, in many years, it is not even possible to get to Winter Harbor.

Southern Archipelago

Nearly all of the waterways in this area are completely frozen for most of the year, but nearly all have at least a short period when they are open to navigation. All of the islands are rimmed with first year fast ice during the ice season. The central water areas remain the most congested with ice during the summer season. The following areas are dominated by first-year ice floes, with large amounts of multiyear ice also present: (1) Admiralty Inlet, (2) Prince Regent Inlet, (3) Gulf of Boothia, (4) Committee Bay, (5) Bellot Strait, (6) McClintock Channel, (7) Peel Sound, (8) Franklin Strait, (9) Victoria Strait, (10) James Ross Strait, and (11) Rae Strait. The following areas are dominated by first-year ice floes with little or no multiyear ice: (1) Simpson Strait, (2) Queen Maud Gulf, (3) Dease Strait, (4) Coronation Gulf, (5) Dolphin and Union Strait, and (6) Amundsen Gulf.

Freezeup starts throughout this area in early to late September, and by late October to mid-November the area is generally frozen solid.

Breakup varies considerably throughout the area. In Prince Regent Inlet ice starts to slacken late in June but rarely clears before mid-August. In Admiralty Inlet a great deal of ice occurs the year round, with large variations each year. Some years the minimum amount of ice occurs during August, and in other years a considerable amount of ice is present the entire season. The Gulf of Boothia clears later and has more ice than Prince Regent Inlet. Committee Bay usually contains six- to eight-eighths ice coverage the entire year. In Bellot Strait swift tidal currents keep some open water in this area all year. Sometimes the strait is open by mid-July but subject to great year-to-year variations. McClintock Channel is covered by six- to eight-eighths of ice the entire year. Shore leads occasionally exist from time to time along the west coast of Prince of Wales Island, while Victoria Strait is covered by four- to eight-eighths of ice throughout the year. Heavy polar floes often enter the strait from McClintock Channel. In Peel Sound cracks and puddling begin in early July, with the ice becoming very loose by mid-August. Breakup in the Franklin and James Ross Straits begins in June, and the ice melts and disappears by late August in good years. The western side of Amundsen Gulf breaks up in late June, and by late July the gulf becomes free of local ice. Dolphin and Union Strait ice starts to loosen in the early part of July, with the minimum amount of ice occurring during the last weeks of August. In Coronation Gulf the ice begins to break up in late June or early July and clears out by late August or early September. Ice in Queen Maud Gulf begins to loosen in late June. In July a wide shore lead develops along the shore of Victoria Island. Late August and early September is usually the most ice-free period. Simpson Strait ice loosens rapidly in July, with patches of open water appearing. The amount of clearance depends on the direction and strength of the winds. In Rae Strait rotting and puddling of the ice begins in late June or early July. Minimum ice conditions occur in late August or early September. Finally, in Dease Strait the ice loosens in June and by early August clears to a few eighths.

Most of the waterways of the Southern Archipelago have at least a short period when they are open to navigation. The periods of navigation are (1) Dease Strait and Coronation Gulf—late July to early August, (2) Dolphin and Union Strait, and Amundsen Gulf—mid-July, (3) Prince Regent Inlet, Gulf of Boothia, Committee Bay, Simpson Strait, and Queen Maud Gulf—mid-August to late September, (4) Admiralty Inlet and Bellot Strait—late August to mid-September, (5) Franklin Strait—late August to early September, and (6) James Ross Strait, Rae Strait, and Peel Sound—late August to early October. Victoria Strait and McClintock Channel are not navigable.

2.5.4 Ice Distribution in the Labrador Sea

Rarely does any remnant pack ice occur in the Labrador Sea (Fig. 2-22) before freezeup. During the freezeup a steady southward progression of the ice extent occurs. In late November fast ice begins to form in the northern coastal indentations. As December progresses, fast ice forms farther and farther south until by the end of December it has reached the southern coastal limit. At the same time that fast ice formation has progressed southward, it has progressed seaward. Depending on the latitude and the distribution of off-shore islands, it may extend 20 to 30 n mi (35–55 km) seaward from the coast proper. Throughout the winter and early spring it continues to grow in thickness. The pack ice or drift ice is brought southward from Baffin Bay in the Labrador Current, and, emanating from Hudson Strait,

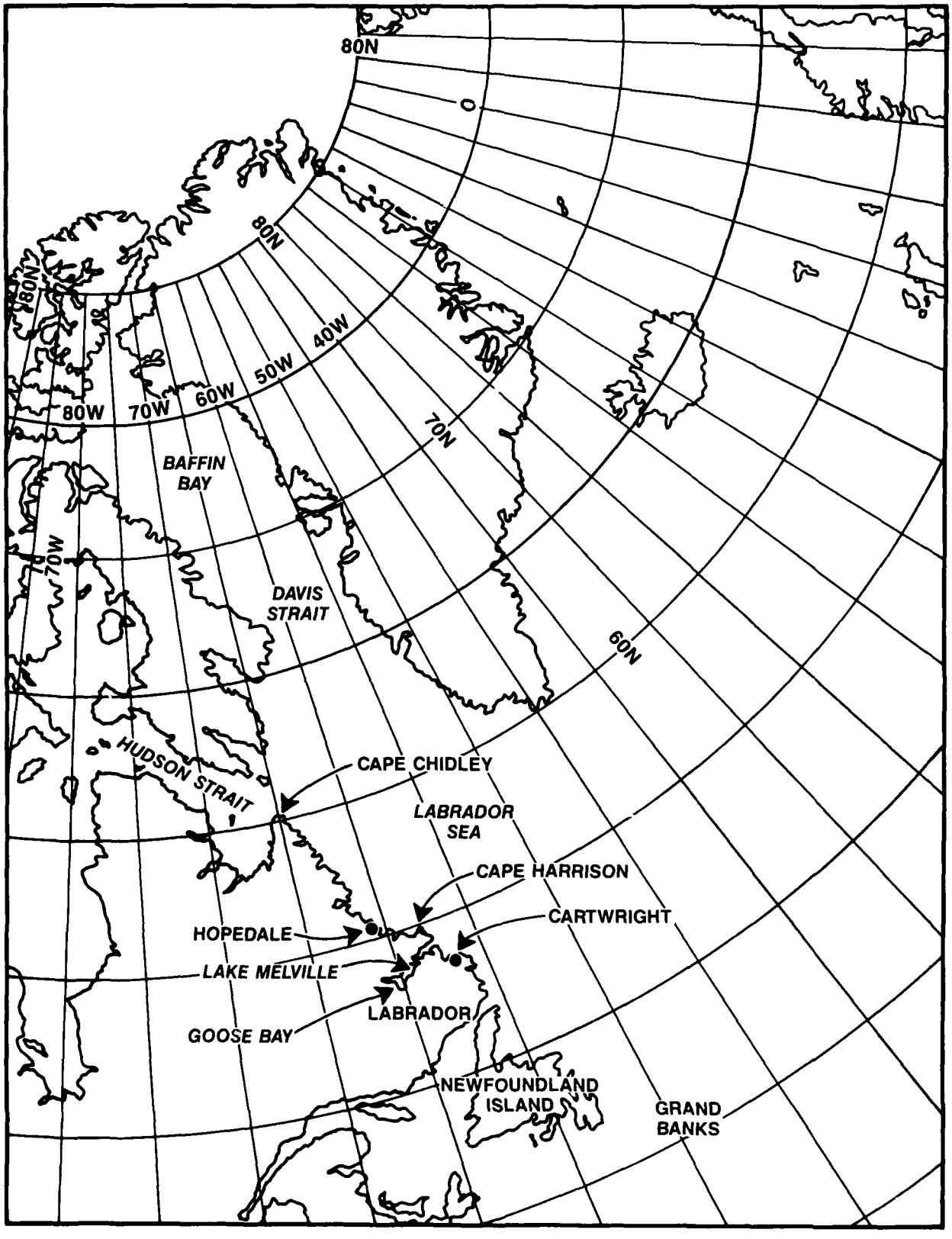

Figure 2-22. Labrador Sea Region.

it first appears off Cape Chidley in early December. By late December drift ice has reached the southern extremity of Labrador. The width of this stream of drift ice, its concentration, and general behavior depend on a number of factors. Among them are the amount of ice available from Baffin Bay and its tributary sounds, the rapidity with which the pack ice is released to the southward directed current, the speed of the Labrador Current, and the prevailing winds. The latter can be particularly effective in creating both favorable and unfavorable conditions for transit. Winds from the north or west tend to spread the ice by decreasing the concentration. Winds from the south or east tend to decrease the areal extent of the ice, hence increase the concentrations. With the advent of spring, the seaward extent of drift ice off the Labrador coast shows a marked increase until it reaches its maximum in May. In May, it extends seaward in the latitude of Cartwright for a distance of 120 to 140 n mi (220–260 km), narrowing rapidly toward the north until it extends only about 50 n mi (90 km) or less in the latitude of Cape Chidley.

Icebergs are normally encountered off the Labrador coast at any time of the year. The distribution of bergs throughout the coast waters of Labrador depends primarily on the number of bergs calved off the glaciers of western Greenland and conditions during the previous winter in Baffin Bay. The largest number of bergs are normally present during early spring.

Disintegration of the fast ice begins in March in the southern areas and extends into more northerly latitudes throughout April. Once disintegration has begun, it progresses quite rapidly, so that by the end of May nearly all coastal areas are free of fast ice. Hopedale and Cape Harrison are two significant areas that retain their fast ice longer. In late April and May the pack ice begins to disintegrate along the Newfoundland coast and along the entire ice edge south of 60 °N. During June great variability occurs in the position of the ice pack. Usually the concentration of the ice along the ice edge is open pack, with heavier concentration and fast ice along the coast. By the end of July the entire area south of 60 °N is normally ice free. In April a small ice area in the outer approaches to Goose Bay decreases to about three-eighths coverage. The fast ice in Lake Melville becomes well puddled in early or mid-May and melts by early June. The pack ice edge is, however, often south of the Goose Bay approaches through much of June, but by the end of June or the first of July, in a normal ice year, the approaches are ice free and ships can transit the area without the aid of an icebreaker.

Accessibility to the Labrador coast for shipping is largely dependent on two ice factors: (1) drift ice from the north and (2) local fast ice formation. The entire coast is normally ice free and navigable from late June or early July to late November and is normally closed to all shipping from late December to early June.

2.5.5 Ice Distribution in Baffin Bay and Davis Strait

In Baffin Bay and Davis Strait (refer to Fig. 2-12) a wide variation in ice conditions occurs with both time and locality. The major factors responsible for these variations are oceanographic features, latitude, and meteorological conditions. September is the month of least ice in this area. At that time, only scattered, rotten remnants of the Baffin ice pack, drifting small floes, polar ice cakes from the north, icebergs, BERGY BITS, and GROWLERS remain.

Baffin Bay

In October the freezing process begins for both the fast ice and pack ice. In October fast ice forms in Melville Bay, in the northern coastal indentations of Baffin Island, and the inner recesses of Cumberland Sound and Frobisher Bay. As the winter progresses, formation of ice is far from uniform, latitude for latitude. Fast ice continues its southward extent but much more rapidly along the Baffin Island coast than along the Greenland coast. By the end of November, fast ice extends the length of Baffin Island, but its southward extent along the Greenland coast is only slightly south of Melville Bay. The extent of both fast and pack ice continues to increase until the maximum is reached in March. At this time the fast ice along the Greenland Coast extends as far south as Disko Bay. Farther south, it is found only in the deep coastal indentations. Fast ice reaches its maximum seaward extent in the Melville Bay area and along the coast of Baffin Island from about Cape Christian northward. In the vicinity of Home Bay it frequently exceeds 30 n mi (55 km), and from there northward, the seaward edge is characterized by a pronounced shear line and heavy ridging. The remainder of the fast ice is relatively smooth except for glacial ice frozen in the fast ice. Off Cape Dyer the fast ice is often completely absent and rarely exceeds 1 n mi ($\approx$2 km) in extent.

Young pack ice first forms along a line from northeastern Baffin Island to the Cape York area, forming first in the west and then in the east. The growth and extent of the pack ice is similar to that of the fast ice as it forms first in the west and north and then grows eastward and southward. In November the drift ice has reached south of Cape Dyer, but in eastern Baffin Bay the southern limit is about 74 °N, leaving the eastern two-thirds ice free. The pack ice reaches its greatest extent in March. The southern limit of the drift ice at this time approximates a line from Sondre Stromfjord southwestward to within 50 mi east of Cape Chidley. The ice in the Baffin pack proper is in continual motion, hence the pack is composed of floes of all sizes and contains many cracks, leads, and areas of rafting and ridging. Its average thickness, excluding topographic features, is about 4 ft (1.2 m). That portion of the pack lying off the central coast of Greenland is weak and unstable even at the time of maximum extent and thickness.

The breakup starts in April though not necessarily in all areas, and follows the reverse pattern of the freezeup. This stage is more complex than the freezeup, however, because disintegration in one area may result in an increased ice concentration in another area. As disintegration begins, flaw leads appear in the Melville area and off the northern half of Baffin Island. The pack proper begins to break up so that the southward drift increases. The pack limit off the Greenland coast recedes northward and fast ice in the southern Greenland indentations, off the central Greenland coast and in the interior of Frobisher Bay, starts to break up and move out. By mid-June the pack south of 73 °N is well puddled, while the width of drift ice past Cape Dyer and the south Baffin coast has decreased. Greenland's coastal area is essentially ice free as far north as Upernavik, and the North About Route is open. The North About Route is a lead that normally extends through Melville Bay along a line connecting Nagssuaq, Holms Island, Thom Island, Bryants Island, Bushnans Island, and Cape York. While this lead is at its best, another lead, called the Middle Passage, is opening. This opening extends along a line connecting the Upernavik area to Cape York. By mid-July this lead is preferred over the North About Route, which normally becomes congested with ice as the fast ice of Melville Bay moves out. The fast

ice along the Baffin coast moves out about two weeks later, but ports are subject to drift ice from Lancaster Sound until mid-August. By late August, only a mass of rotten floes remains along the east coast of Baffin Island.

Icebergs in the Baffin Bay and Labrador Sea are calved from Greenland glaciers, particularly those along the west coast from Disko Island to 80°N. Because an iceberg's draft is generally significantly greater than the volume above water, icebergs are more responsive to ocean currents than to winds. Their distribution, therefore, follows closely the paths of prevailing currents. Icebergs from glaciers north of Disko Island are the main source of bergs encountered in the Grand Banks region. These icebergs drift with the currents that flow northward following the west Greenland coast, then turn westward and southward flowing along the coasts of Baffin Island and Labrador. Of the 20 major glaciers along the west Greenland coast, the two located in Disko Bay are estimated to contribute 28 percent of all bergs appearing in Baffin Bay and the western Labrador Sea. The greatest concentration of bergs occurs in this vicinity, particularly during June and July, when the fast ice breakup liberates hundreds of icebergs. The rugged Baffin Island and Labrador coastline, with its many indentations, trap many bergs that disintegrate in place. Estimates indicate that 1 iceberg in 20 survives the trip from west Greenland to Newfoundland. Those that do survive usually require about 3 years to complete the 1,800 n mi (3,335 km) journey.

An interesting feature of the sea ice distribution in the Baffin Bay area is the North Open water. This wide area has an ice concentration that is generally less than that of the surrounding regions. The North Open water seems to result from the constricting effect of Smith Sound, which shuts off the supply of ice from the north causing an ICE JAM in the vicinity of Cape Sabin. The southern limit of this jam is an arc convex to the north. To the south, ice is continually being removed by winds and currents, producing a zone of lower ice concentration. Here the ice is weak and unstable, and open water exists even in midwinter.

The extreme southwest coast of Greenland is subjected to an influx of hard polar ice known as *storis*. This ice has been brought from the polar regions in the East Greenland Current. The drifting storis first rounds Cape Farewell in December. Its amount and extent, both seaward and northward, increases until the maximum is reached in May. At this time the storis reaches as far north as Godthaab and extends approximately 70 to 100 n mi (130–185 km) seaward in the vicinity of Julianehaab. By September little or no storis is drifting around the southern tip of Greenland.

Frobisher Bay

In early October young ice begins to form along the entire coastal area of Frobisher Bay, and tidal action continually breaks it up. By late October or early November enough ice has been deposited along the shore to seriously hamper loading or lighterage for shipping operations. By mid-November the upper bay is solidly frozen and the southeastern half of the bay is covered with young ice; but the offshore approaches are essentially free of hampering ice conditions. As the fast ice continues to grow and is subjected to wide tidal ranges, large quantities are beached and heavy ridging occurs. Another factor that contributes to the heavy ridging is the extremely low temperatures to which the ice is subjected. The lower bay and approaches become blocked by drifting sea ice in December, with concentrations of seven- to eight-eighths by January. This sea ice is normally heavily ridged. The fast ice continues to thicken, reaching a maximum in April or May.

By late May or early June melt and disintegration begin, with scattered puddles and tidal cracks appearing. By July the fast ice is in the advanced stages of disintegration, but the lower bay and approaches remain blocked by drifting sea ice. By the end of July icebreaker entry is possible, and by mid-August unescorted entry is possible. In September the lower bay and approaches are essentially ice free except for icebergs, bergy bits, and growlers, which are present throughout the year.

Although ice conditions in Frobisher Bay vary greatly from year to year, normally the bay is open to icebreaker entry in late July and to unescorted entry in August. The bay generally closes to unescorted shipping by mid-October and to icebreaker entry by mid-November. Consequently, the best month for shipping is September.

Thule to Alert Route

The route between Thule and Alert (Fig. 2-23) is never ice free and is not considered safe for navigation by anything but an icebreaker. North of Smith Sound the passage is covered by five- to seven-eighths of heavy polar pack ice even in the best month of August. Throughout this area the wind is the major factor in determining the transit route and its dangers. In this north-south waterway, from the breakup in July to the freezeup in September, a changing wind direction will cause the leads to shift from coast to coast. A strong southerly wind will open a lead north of Robeson Channel permitting easy transit around Cape Sheridan to Alert, but a northerly wind will keep this area so congested with ice from the Lincoln Sea that transit of this area may be hazardous. These rapidly changing ice conditions can make the passage impossible to navigate even by an icebreaker. Ice conditions throughout this route are progressively worse from south to north and the navigation season is progressively shorter. Alert, at best, is accessible for only a few weeks, with refreezing starting in late August.

Thule and Its Approaches

Freezeup begins in October with the formation of grease ice that slowly thickens to young ice, becoming fast to the shore. Changing tides and foehn winds (warm katabatic winds) can change the ice concentrations rapidly during this time and may move the ice totally out of the bay. With a shift in wind the ice can also move rapidly back into the bay. In November or December the ice freezes permanently and increases to 3 ft (1 m) thick by the end of December. Tidal cracks form next to the shoreline of islands and the mainland. The ice continues to thicken to about 70 in ($\approx$ 180 cm) in late April. The ice in the bay around Thule is quite smooth with a snow cover of 1 to 3 ft (0.3–0.9 m), which is blown off the adjacent mountains and icecap.

Breakup in the bay begins in May as puddles and cracks start to form. Strong easterly winds can move most or all of the ice out of the bay as early as mid-June. Absence of these winds may result in ice lingering in the bay as late as mid-July. Also, ice blown out of the bay could move back into the bay if a wind shift occurs. From mid-July through September, after the fast ice is blown out of the bay, the area is essentially ice free. During this period, however, an increase in icebergs, bergy bits, and growlers occurs.

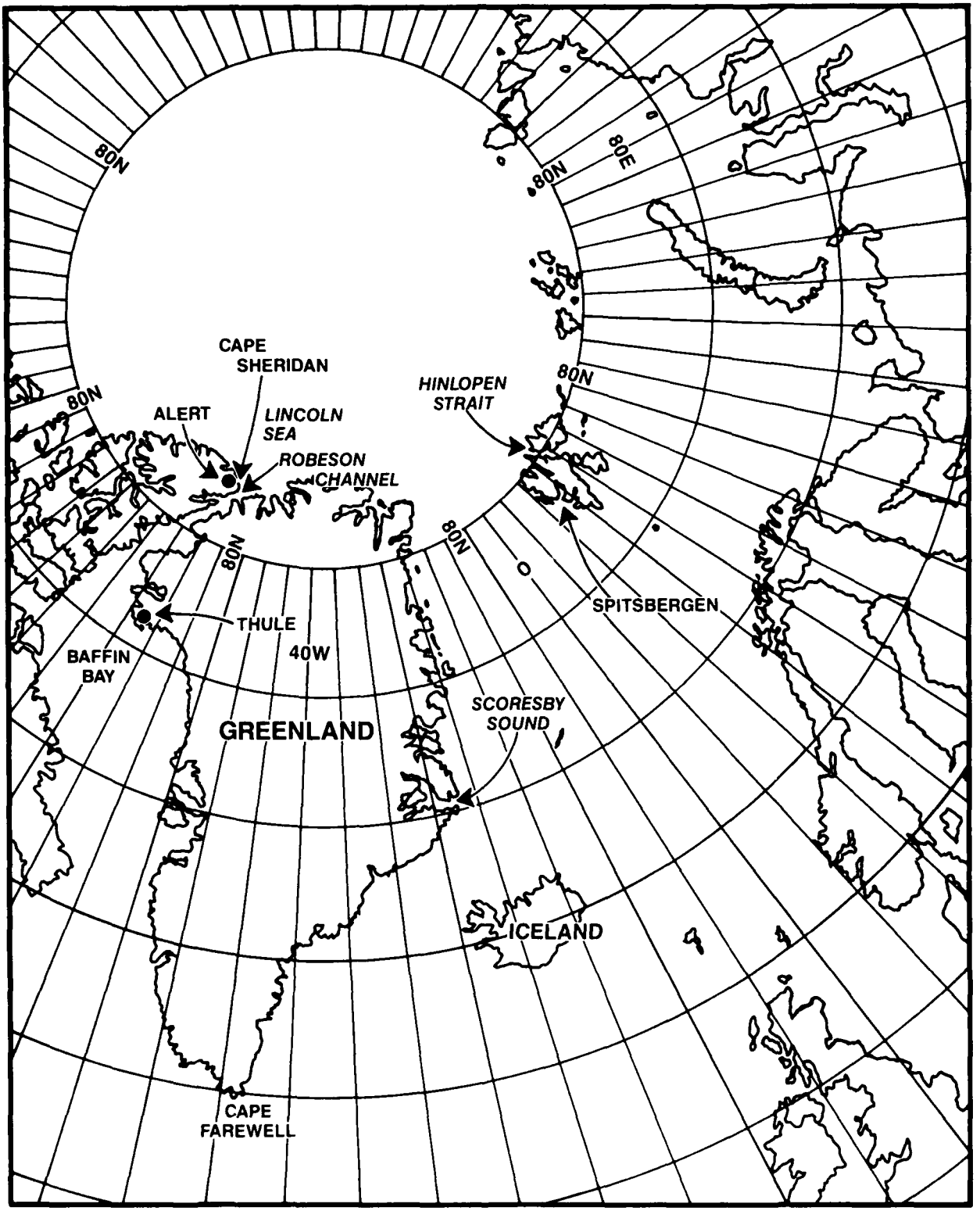

Figure 2-23. Greenland/Iceland Region.

Sondre Stromfjord

Fast ice formation in the fjord is the only problem concerning ship transit into Sondre Stromfjord. Fast ice growth is usually sufficient to halt unescorted shipping by late December, but with icebreaker support transit may be possible throughout the winter. By January or February, fast ice in the upper one-third of the fjord reaches a maximum thickness of about 60 in ($\approx$ 150 cm), while in the central third of the fjord the maximum thickness is about 25 in ($\approx$ 65 cm). This difference may be due to foehn winds in the lower fjord. Tidal ranges of 8 to 11 ft (2.5–3.5 m) help keep the ice weak and elastic throughout the winter.

Breakup occurs from March through May, and the ice becomes heavily puddled and rotten by the end of the period. In late May an icebreaker usually will make one or more runs up the fjord to break up the fast ice. The ice fractured in this manner will either melt or move out in two to three weeks. Icebergs may be encountered off the entrance to Sondre Stromfjord, however, none in the fjord. The fjord is generally ice free from mid-June through November or early December.

2.5.6 Ice Distribution in the East Greenland, Iceland, and Spitsbergen Areas

East Greenland

The east Greenland coastal area is regarded as one of the most inaccessible areas in the world because of the continual flow of multiyear polar ice from the Arctic Ocean via the East Greenland Current. Approximately 95 percent of the total polar ice expelled from the Arctic Ocean each year is carried southward in this strong current. Throughout the year this mass of drifting ice extends 100 to 300 n mi (185–555 km) offshore to the north of Scoresby Sound. South of Scoresby Sound, the maximum offshore extent is reached in the spring, when the ice may extend nearly 200 n mi (370 km) offshore. The minimum extent in this area occurs in August and September, when only belts and patches are present. The drifting multiyear ice is at its maximum extent from December through May, when it drifts around Cape Farewell.

Most of the fast ice along this coast is found in protected coastal fjords, bays, and sounds (sunds). South of Scoresby Sound, this ice is cleared out of these indentations many times throughout the winter due to the foehn wind effect.

Navigation along the east coast of Greenland, even south of Scoresby Sound, has only been attempted by extremely skilled and adventurous seamen. Icebreaker entry into Scoresby Sound should be possible, however, from early August to early or mid-October, but it is considered extremely hazardous. A limited number of unescorted entries are made each year by skilled Danish pilots in ships of special design and construction.

Iceland

Iceland is generally ice free throughout the year except for fast ice extending to the outer harbor entrances on the north coast and for weak unstable ice in bays along the southern coast. Even when the pack ice off the east Greenland coast drifts to its maximum extent,

normally a 50 n mi (90 km) wide area of open water exists between Iceland and the ice pack. On a few occasions, however, the ice has drifted down and touched the north coast of Iceland for a short period of time.

Spitsbergen

Ice conditions along the south and west coasts of Spitsbergen differ drastically from those on the north and east coasts. The north and east coasts have heavy fast ice formations during the winter and are usually subject to closing by polar pack ice throughout the year. The south and west coasts have only a narrow band of fast ice in winter and some areas are ice free all year. Under normal conditions the north coast is navigable by late July or early August, but the east coast does not open until mid to late August. In the area of the Hinlopen Strait usually some ice occurs throughout the year.

2.5.7 Ice Distribution in the Seas of the Soviet Union

In the ice pack off the north coast of the U.S.S.R., a conglomeration of all types of ice occurs. The predominant ice within the coastal seas is winter ice. The North Atlantic Drift is a warm current that enables the island of Iceland to have a fairly temperate climate for its latitude and also causes the Barents Sea (refer to Fig. 2-1) to be the most navigable of the U.S.S.R. polar seas. During the winter months, the entire coastline from the Chukchi Sea to the Kara Sea is frozen fast, and only the western part of the Barents Sea is found to be ice free. Conditions remain as such during the winter months until June, when the great rivers of the U.S.S.R., which empty into the Arctic Ocean (the Ob, Yenisei, Lena, and Kolyma), begin to break up in their southern areas and cause great amounts of fresh meltwater to run over the top of the downstream river ice, and carry great amounts of dirty water to their mouths and out onto the sea ice. This darker discoloring of the ice reduces its albedo and increases its ability to absorb heat; thus it melts more rapidly, so that by mid-July, a narrow shore lead exists along the coastline. The lead is discontinuous, but by August a navigable area extends along the entire coast. This navigable area is open to shipping until October. The freezeup takes place first in the Chukchi and Laptev Seas, as the increasing northerly and northeasterly winds push the Arctic ice pack onto the shore. This occurrence is followed by the closing of the East Siberian Sea and then the Kara Sea in November. In December, the strait between Novaya Zemlya and the mainland is closed by winter ice, and the freezeup is almost complete except for the formation of fast ice in the protected bays of the Barents Sea.

Icebergs calved from glaciers on the islands of Svalbard, Franz Josef Land, Novaya Zemlya, and Severnaya Zemlya are small in number and structure, owing to the shallow glacial ice. Bergs from these islands calve mainly on the north side; they tend to move with the prevailing currents but seldom are encountered near the north coast of the U.S.S.R. In the Barents Sea maximum iceberg occurrence is coincident with the withdrawal of the pack ice northward, with the greatest number found near the ice edge.

Barents Sea

The predominate forms of ice in the Barents Sea (Fig. 2-24) are winter and young ice, with some polar ice found occasionally between Franz Josef Land and Spitsbergen. During the winter and spring the Bear Island Current carries colder polar water and some polar ice into the vicinity of Bear Island.

In average ice years the entire west coast of Novaya Zemlya will be icebound from November through May. In winter the bays and gulfs of the eastern Barents Sea become icebound. The deeper portion of the sea is covered with drift ice consisting of both hummocked and level ice floes. The hummocks are usually 5 to 15 ft (1.5–4.5 m) in height. These hummocky floes normally come from the Polar Basin area. The ice reaches its greatest extent in March and April. Rapid melting takes place from May to August, after which the process decreases and freezing commences. In early June, during very mild ice years, a small portion of the southwest coast may be free of ice. Beginning in mid-July through October the west coast of Novaya Zemlya is normally ice free.

The Norwegian and North Cape Currents keep the Norwegian coast ice free in all months, except for the ice formed within some of the fjords. Ice is no hindrance to navigation within about 400 n mi (740 km) of the west Norwegian coast and 150 n mi (280 km) of the north Norwegian coast. The Norwegian coast and most of the Murmansk coast are kept free of ice by the warm Atlantic water throughout the year.

White Sea

The White Sea is dominated by winter fast ice and winter pack ice. Freezeup starts in October in the deep bays and usually forms a continuous strip of thin ice by December. The whole interior of the sea is filled with drift ice of varying strengths and thicknesses. Depending on wind conditions in the White Sea the ice will either break up and raft, or remain level. Ice reaches its greatest concentration during February and March. Breakup of the fast ice begins in April, and by May the drift ice in the middle of the sea melts rapidly so that by June little drift ice is left in the White Sea. At Archangel the average ice lasts from early to mid-November to early to mid-May. Very little ice drifts from the White Sea into the Barents Sea and any that does melts in a short time in the warmer waters of the Murmansk coast current. Generally, the shipping season in the White Sea is from June to late September.

Kara Sea and Its Approaches

Winter ice is the predominate type in the Kara Sea, with some polar ice along the east coast of Novaya Zemlya. Freezeup starts in late September, and the Kara Sea will be frozen solid by December. The ice comes under considerable pressure, resulting in ridges piled as high as 25 ft (7.5 m). This ice drifts with the currents or becomes stranded on shoals where it can remain for several years. The ice begins to break up in June and continues throughout the summer, with the minimum amount of ice occurring in September.

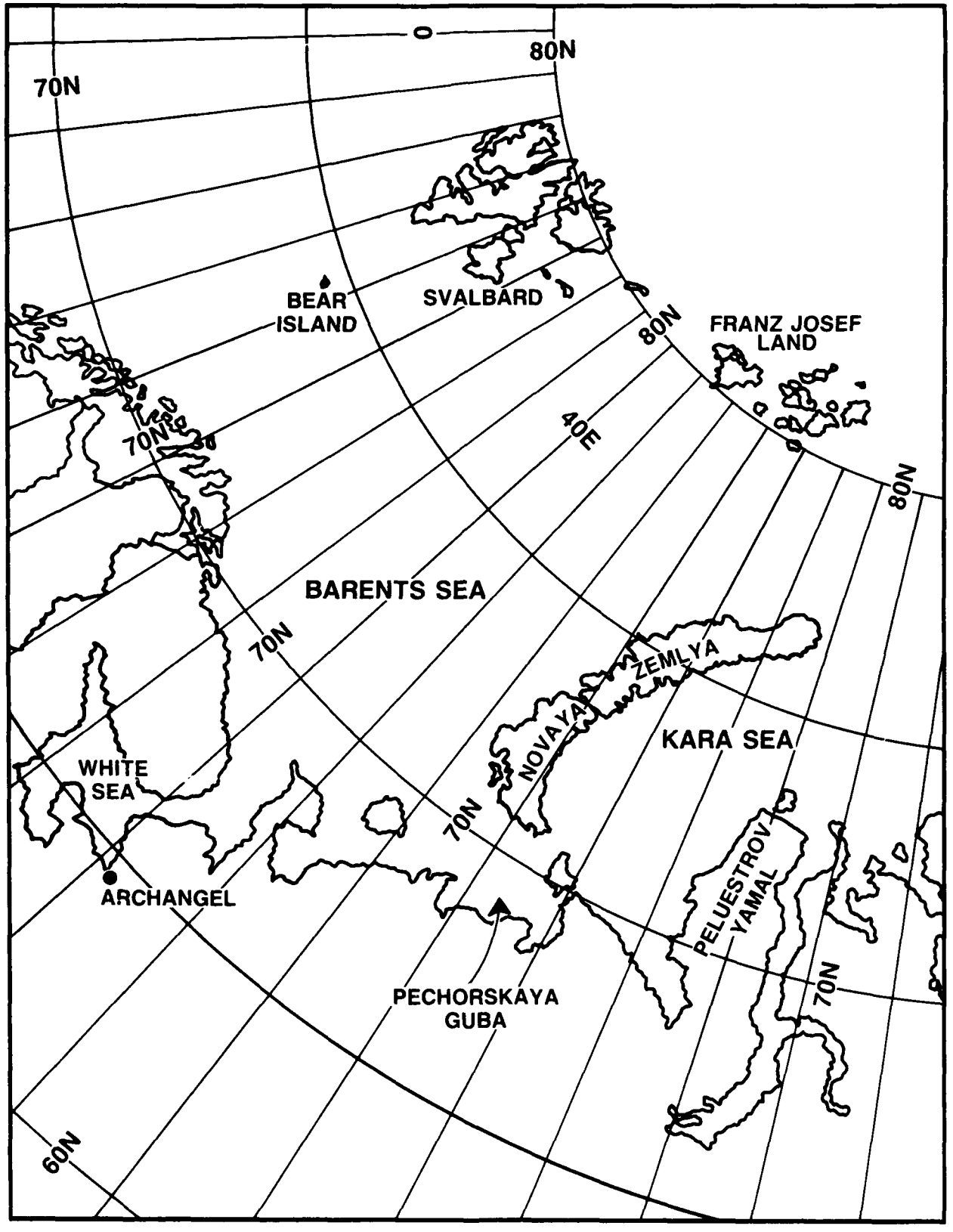

Figure 2-24. Barents Sea and Kara Sea Region.

Generally the area is navagable from July through October, with the best conditions occurring in late September. Navigation is the most difficult in the southwestern section of the Kara Sea, in the bay between Novaya Zemlya and Peluestrov Yamal, in the straits between the Kara Sea and the Barents Sea and Pechorskaya Guba. This difficulty is due primarily to the counterclockwise current regime of the Kara Sea, which concentrates ice in the southwestern section.

Laptev Sea

The Laptev Sea (Fig. 2-25) is predominated by winter ice with varying amounts of polar ice. Ice formation usually begins along the coastal areas of the offshore islands in mid-September due to seasonal cooling. Generally, the Borisa Vilkitskogo Strait, between the Kara Sea and Laptev Sea, contains compact fields of ice by mid-October, and the straits in the eastern part of the sea are completely ice covered in November. From November through June the entire sea normally is dominated by compact ICE FIELDS. Rapid changes in ice conditions take place in early July, with the introduction of the relatively warm river water and rapid decrease in ice concentration occurring alongshore. By early August open water exists along the southern shores of the sea. The straits are subject to temporary closing in all months because of the general southwesterly drift of ice into the area, which is associated with counterclockwise currents in the sea.

The best navigation period is July through late September. Navigation is considered most difficult along the coast of the Taimyr Peninsula and in Borisa Vilkitskogo Strait. Here the most severe ice conditions are found. The coastal ice is carried eastward by currents toward Cape Chelyuskin. Polar pack ice is carried southeastward along the east coast of Severnaya Zemlya to the vicinity of the Taimyr Peninsula. Heavy pack ice accumulates in the center of the Laptev Sea, forcing the shipping lane close in along the coast of the Taimyr Peninsula, but the southern and southeastern parts of the sea are usually ice free. The surface currents here have a great influence on the distribution of ice.

East Siberian Sea

The East Siberian Sea (Fig. 2-25) is dominated by winter ice with some polar ice. The coastal waters usually freeze from west to east. Ice formation usually begins in Dmitriya Laptev Strait, between the Laptev and East Siberian Seas, in September, near Medvezhi Ostrova in October, and near Cape Shelagski at the beginning of November. Normally this area is closed to shipping by October and frozen over by November. Thawing usually begins in May but the breakup of ice does not normally occur until July. The winter ice melts rapidly as the result of summer heating and the discharge of warm water from the numerous Siberian rivers. Between the Indigirka and Kolyma Rivers ice breakup occurs within the first two weeks of July, near Cape Shelagski about the third week of July, and near Cape Schmidt about the last week in July.

The polar pack ice is prevented from spreading southward into the East Siberian Sea by the New Siberian Islands, with the result that the East Siberian Sea coast is nearly ice free during the summer season. Fast ice extends northward from the mainland to the 15 fathom ($\approx$ 27 m) contour and includes the entire area of the New Siberian Islands. North of this fast ice lies continuously moving drift ice, whose movement is predominantly from the southeast toward the west-northwest. When strong southerly winds prevail, wide polynyi

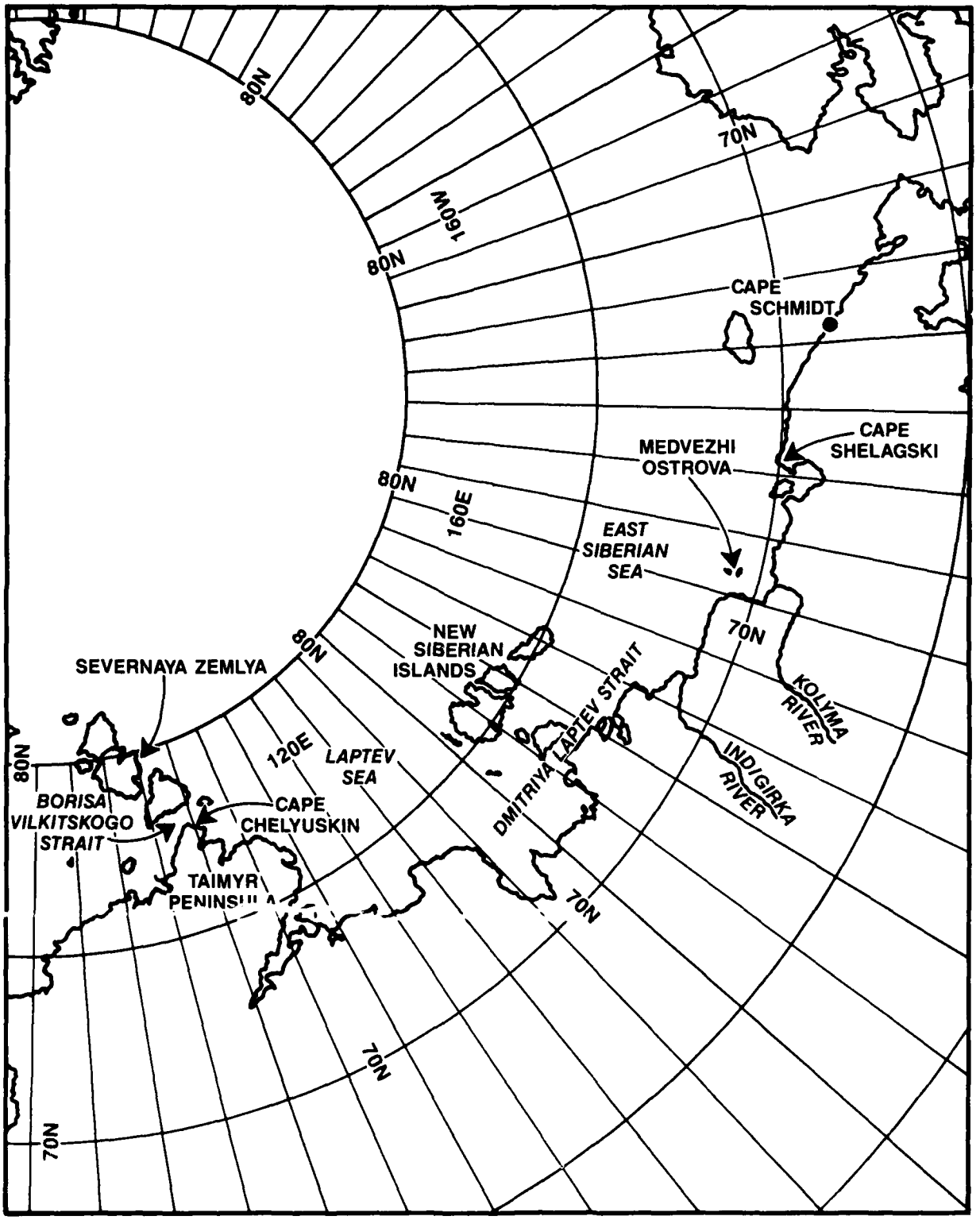

Figure 2-25. Laptev Sea and East Siberian Sea Region.

form on the seaward side of the fast ice. When strong northerly winds prevail, these polynyi become filled with drift ice, which eventually is piled high along the edge of the fast ice. In the deeper, eastern part of the East Siberian Sea, this process is likely to occur closer to the coast, which may result in belts of ice hills that finally come to rest on the bottom. These ice hills are known as stamukhas. The limit of their extent is usually between the 10- to 15-fathom ($\approx$ 18–27 m) depth curves. In the summer, ice-free water is found between the stamukhas and the coast, providing a fine shelter for ships from the drift ice still present in the northern part of the sea. This area also may be used as an anchorage by a ship forced to winter over. The navigation season in the East Siberian Sea is from July to September, with minimum ice conditions occurring in late September.

2.6 Ocean Currents

In addition to winds, ocean currents have a major influence on the motion of the ice. Several sources of oceanic currents exist causing the currents to be quite complex at times. The motion of the water due to tides can also be complex, particularly in shallow and long embayments. (This short section does not attempt a complete treatment of the subject.)

Several centuries of observations have yielded considerable knowledge of the major current systems in the Earth's oceans. Yet, as late as 1961, a major and important current in the equatorial Pacific Ocean was discovered. Although published charts of oceanic currents appear to imply steady and constant currents, this is not really the case. These charts represent averages and generalizations. The accompanying chart (Fig. 2-26) shows the known current systems in the Arctic. Where data are available, the magnitude of these currents is given in knots as well as the direction of the current.

The magnitudes of oceanic currents are not large when compared to wind velocities. Nevertheless, they are much more constant and, therefore, can add a significant component to ice drift, especially over periods of time greater than one day.

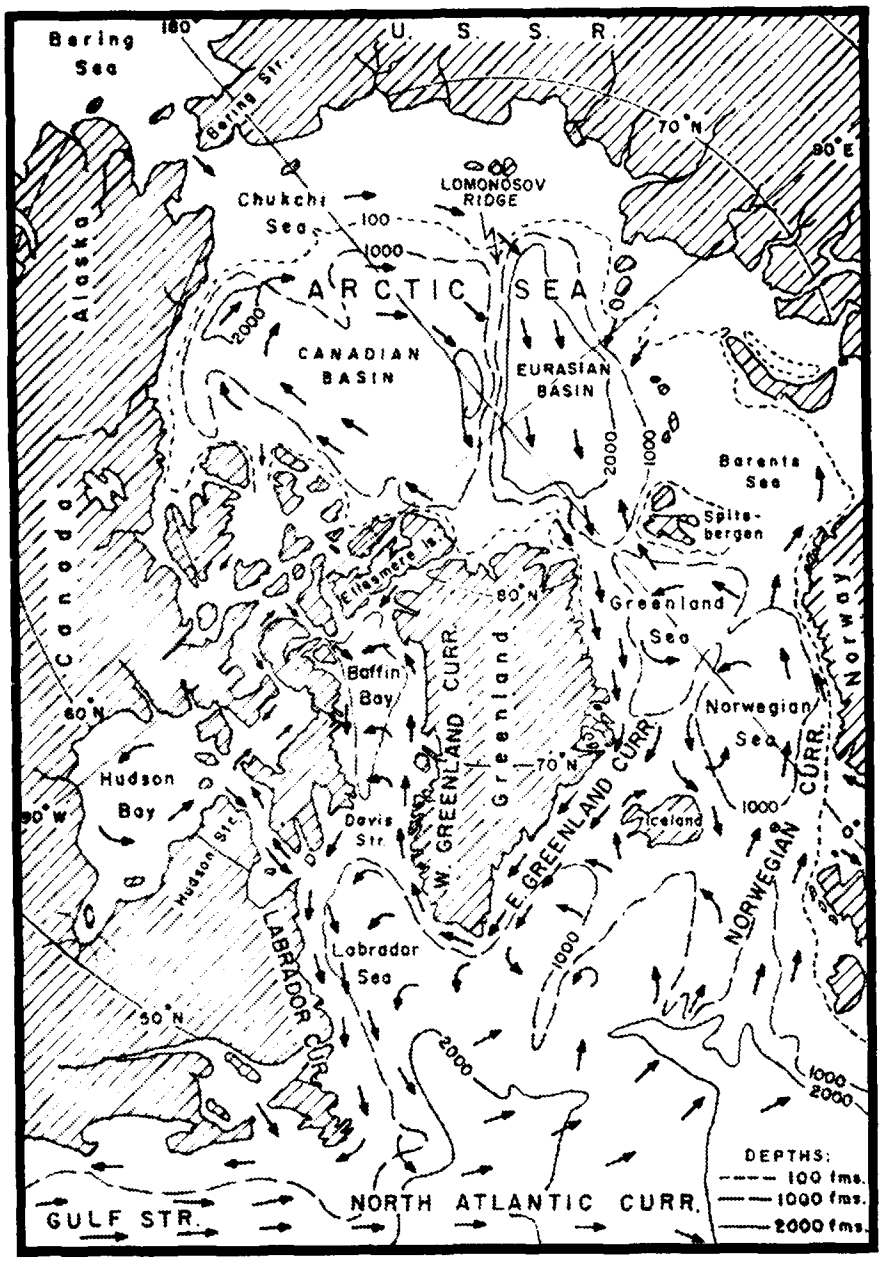

Figure 2-26. Surface Currents of the Arctic.

THIS PAGE INTENTIONALLY LEFT BLANK

3. ARCTIC CLIMATOLOGY

Knowledge of climatic characteristics of a region helps the new forecaster by providing information on the general types of weather systems to expect in day-to-day forecasting situations. Armed with such information, along with good analyses, numerical model forecast aids, and frequent high quality satellite data, the forecaster, through prolonged onsite experience, should be able to develop successful prediction techniques. Use of forecaster handbooks, such as this one, can reduce the onsite time required to become a proficient forecaster.

This chapter will first discuss the major factors that go into determining the climate of the Arctic. Second, individual weather elements will be considered in view of their regional and seasonal variations. Third, local topography and its influence on climatic conditions will be examined. In Chapter Two the physical characteristics of the Arctic regions were described and shown in various locator maps in order to relate them to the profound effect they can have on local atmospheric pressures, temperatures, winds, clouds, and precipitation. Perhaps the most conspicuous causes of these local effects include (1) the Brooks Range and North Slope of Alaska; (2) the vast, elevated ice sheet of Greenland; (3) the land/water complex of the Canadian Archipelago; (4) the fjords of Greenland and Norway; (5) the mountains of eastern U.S.S.R.; and (6) the pack ice and Arctic Ocean itself.

The four characteristics of the Arctic that are primarily responsible for its weather and climate are summarized in the following subsection. These indicators are (1) duration of daylight; (2) the circumpolar vortex; (3) surface snow and ice cover; and (4) strong temperature inversions.

3.1 Major Factors Affecting the Arctic Climate

3.1.1 Duration of Daylight

The regime of daylight and darkness in the polar regions combined with the low Sun angle ensure long periods of heat loss. North of the Arctic Circle in summer, the Sun is always above the horizon, albeit at various elevations. In winter, the Sun is always below the horizon, but there too, the degree of darkness varies throughout the period. Only at the pole itself are there 6 months of Sun below and 6 months above the horizon. Table 3-1 shows the duration of sunlight for various latitudes at the middle of the months. The figures apply to level, unobstructed locations and may differ for stations on hills and in valleys.

TABLE 3-1. TOTAL POSSIBLE DURATION OF SUNLIGHT ON THE 15TH OF EACH MONTH

Month	North Latitude											
	60°		65°		70°		75°		80°		85°	
	hr	min	hr	min	hr	min	hr	min	hr	min	hr	min
January	6	43	5	02	–	–	–	–	–	–	–	–
February	9	12	8	28	7	20	5	10	–	–	–	–
March	11	44	11	40	11	33	11	23	10	50	9	50
April	14	34	15	11	16	09	17	56	24	00	24	00
May	17	08	18	43	22	41	24	00	24	00	24	00
June	18	49	21	53	24	00	24	00	24	00	24	00
July	18	05	20	15	24	00	24	00	24	00	24	00
August	15	41	16	39	18	15	23	19	24	00	24	00
September	12	56	13	07	13	26	13	57	15	10	18	15
October	10	13	9	46	9	06	7	58	5	00	–	–
November	7	34	6	16	3	52	–	–	–	–	–	–
December	5	56	3	42	–	–	–	–	–	–	–	–

An alternate way of looking at the duration of sunlight is shown in Fig. 3-1 below.

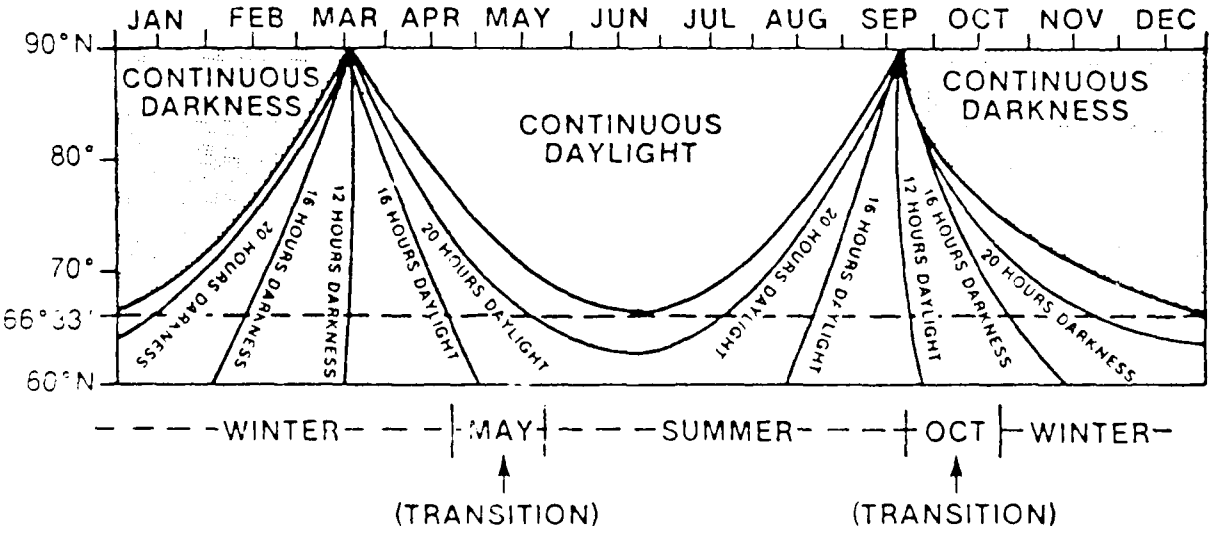

Figure 3-1. Duration of Daylight 60°N to 90°N (Walsh et al., 1986).

The notions of daylight and darkness can be misleading. For example, at the pole, only about 80 days of real night occur. For 20 days after the setting of the Sun at the pole on 24 September, a newspaper can be read by twilight if the skies are clear. Complete darkness does not occur until 12 November. The period of total darkness ends on 30 January, and the twilight grows progressively brighter until the reappearance of the Sun on 19 March.

Note the difference in the definition of civil as opposed to astronomical twilight. The former is said to occur when the Sun is less than 6 degrees below the horizon; the latter when it is less than 18 degrees below.

Another factor is that the Earth is closer to the Sun in the Southern Hemisphere winter than in the Northern Hemisphere winter. As a result, the polar day, defined as the time interval between the last sunrise in spring and the first sunset in fall, is shorter in the south polar regions. At the North Pole only one sunrise and one sunset occur per year, the duration is 189 days for the polar day and 176 days for the polar night; at the South Pole it is 183 and 182, respectively.

Figure 3-2 shows the reason for the polar region heat loss. The poles receive solar heat throughout the year, but the loss by infrared cooling results in a net heat loss poleward of 38 degrees latitude.

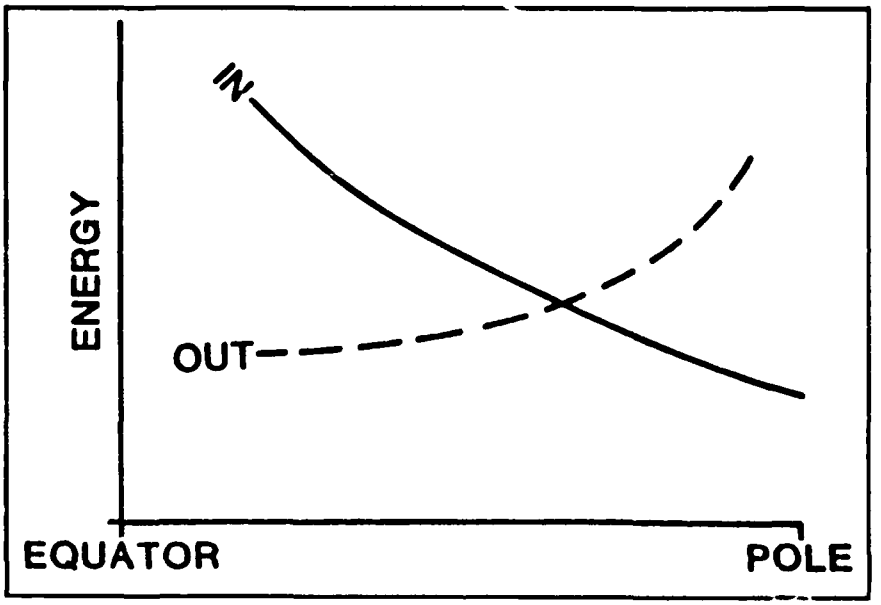

Figure 3-2. Net Radiational Heat Loss at the Poles.

3.1.2 The Circumpolar Vortex

The dominant feature responsible for the Arctic's unique weather is the cold core, circumpolar vortex in the middle and upper atmospheres. The strongest north-south temperature gradients appear in midlatitudes where the mean jet stream occurs. The westerly jet streams have their maximum wind speeds between 30,000 ft (9,144 m) and 40,000 ft (12,192 m). The jets steer surface cyclones and anticyclones and are also responsible for their formation, location, and dissipation. Weather variations at the surface are largely determined by the position and strength of the polar vortex and its associated jet streams.

The areas below the periphery of the vortex typically experience eastward moving frontal cyclones. Areas directly under the vortex are characterized by old, occluded, and stagnant lows with very cold air in them. The location of these cold air pockets aloft determines where the static stability of the underlying troposphere will be minimal and lead to convective type cloudiness.

The circumpolar vortex displays a multiwave pattern that reflects the influence of land forms, oceans, and mountains of the Northern Hemisphere. The Southern Hemisphere with its lack of these topographic features supports a much simpler circulation pattern. In any case, the continent-ocean temperature contrasts of the Northern Hemisphere result in several major troughs in the vortex proper. Five-day mean 700-mb charts for each month are extremely useful in describing the circumpolar vortex throughout the various seasons. Such charts appear in Appendix B, but for purposes of the present discussion, one such chart, representative of mid-January, is given as Fig. 3-3. In winter, three troughs appear: one over the Canadian Archipelago, one passing from Novaya Zemlya southward, and one over Siberia curving past Kamchatka and extending southward into the Sea of Japan. A minor trough extends east-southeast from Kamchatka into the Aleutians. The main ridges lie over the eastern Pacific and the Rocky Mountains, and over the eastern Atlantic and Scandinavia, with a third weaker ridge over the Urals and western Siberia.

The north-south temperature gradient relaxes during the spring and summer causing the circumpolar vortex to contract and weaken until a single center lies over the pole. When this occurs, the jet stream retreats northward, taking with it the principal cyclone tracks. Cyclone frequency diminishes during this period of less baroclinicity as more zonal (westerly) flow replaces the largely meridional (north-south) flow of winter. Then, again in the fall the vortex expands and strengthens, and the flow around it becomes shifted to lower latitudes and is more meridional.

In the more active winter season, the circumpolar vortex is an ever-changing, dynamic center of action. As the wave number increases (more troughs and ridges appear), cyclogenesis is more frequent, and a greater variety of weather is noted. In this chapter the climatology of storm tracks will be discussed. Also, the possibility of blocking (large-scale obstruction of the normal west-to-east progress of migratory cyclones and anticyclones) action can cause a persistence of certain weather systems over a given region.

In summary, Sater (1969) has noted some general features of the circumpolar vortex and the accompanying circulation as follows:

(1) Large scale patterns tend to persist. Regionally these stalled systems can result in extended periods of abnormally cold or mild temperatures, drought, or heavier than usual snowfall, high winds, or other extreme conditions.

(2) The modification of the tracks and frequency of surface cyclones and anticyclones is importantly influenced not only by relief barriers but also by the dynamic barriers formed by persistent well developed upper ridges and high centers. Areas of most frequent blocking are Scandinavia, Alaska, the Ural region and the Davis Strait Greenland sector. Blocking is characteristic of the spring when anticyclonic conditions are most frequent over the continental areas of the high Arctic. During this season the snow and ice cover is still intact, the air is stable, and visibility is good so that flying conditions are generally at their best.

(3) The degree of expansion or contraction of the vortex can have serious effects on Arctic operations by causing abnormal displacement of the upper westerlies.

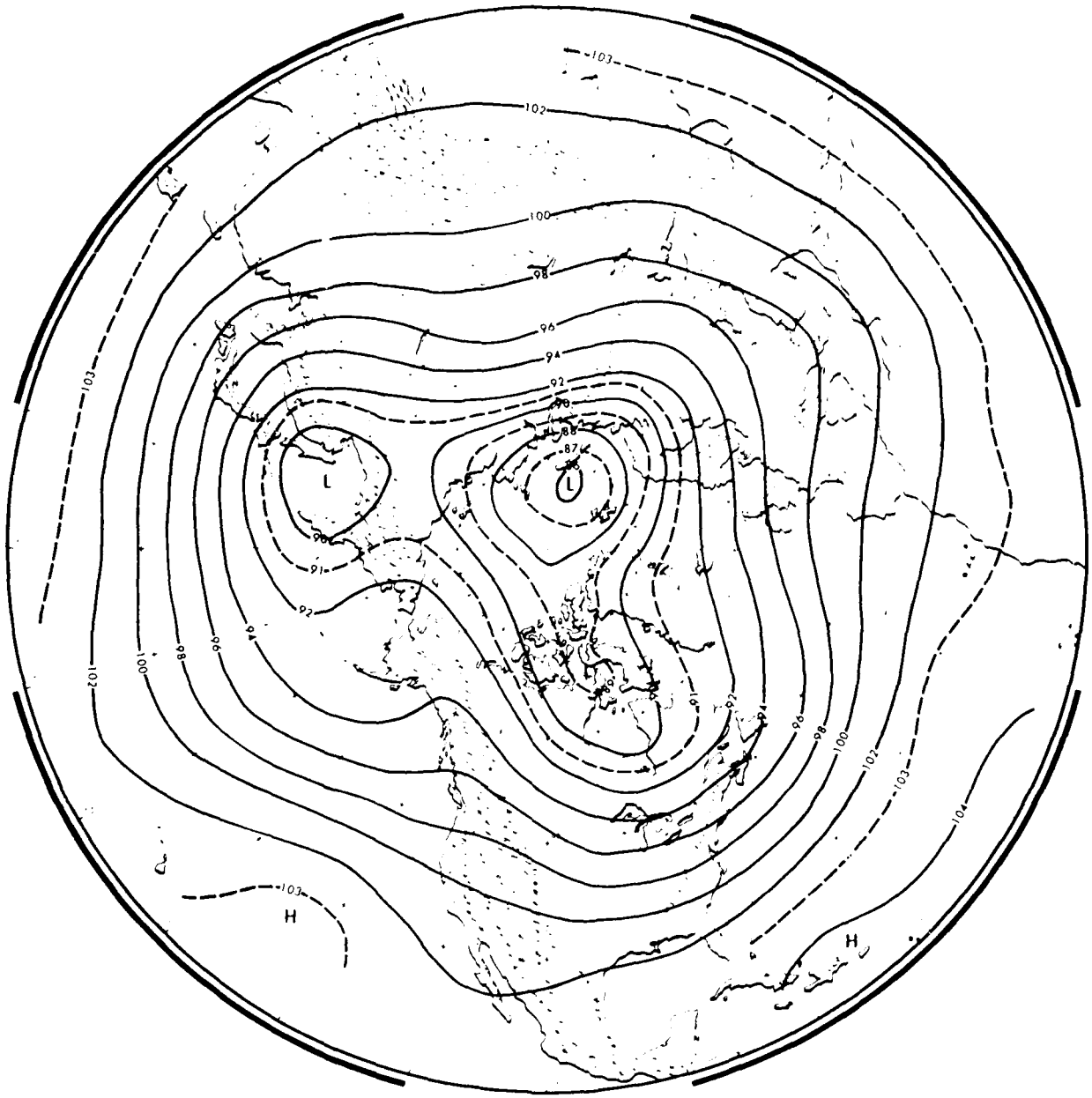

Figure 3-3. Mean 700-mb Chart for Mid-January (Wahl & Lahey, 1969).

3.1.3 Surface Snow and Ice Cover

The amount of snow and/or ice cover in any region of the Arctic determines, to a large degree, the radiation budget for that region. Solar absorption over snow-free land (low albedo) may be as high as 80 percent, and as a result, temperatures in summer may easily rise to 75 °F or 80 °F (24 °C or 27 °C). Over the ice pack the solar absorption is much less, (high albedo) perhaps 20 percent. This characteristic and the lack of enough heat input to change phases help to keep temperatures over the ice pack near 32 °F (0 °C).

At the marginal ice edges temperature and moisture gradients will often be quite large. Thus, in these areas greater than normal precipitation, cloudiness, fog, and even altered cyclone tracks may be expected. These large gradients are also present near open leads and polynyi, which are also significant sources of heat and moisture. In general, open water produces a moderating effect on local temperatures. By contrast, snow-covered land and ice tend to maintain extremely cold temperatures.

Although the actual amount of snowfall may be small due to the lack of water vapor at low temperatures, average depths of the maximum snow cover in March or April ranges from 8 to 20 in (20–50 cm) over the frozen oceans to 16 to 28 in (40–70 cm) over the subarctic.

The most spectacular changes from winter to summer occur over the interior landmasses, but they are primarily in the subarctic. For landmasses north of 60 °N, the spring melt begins first in the region of Scandinavia, which is to be expected because of the warm branches of the Gulf Stream entering the area. The melt spreads into western U.S.S.R., and, at the same time, the west coast of Greenland shows signs of reduced snow cover. By late spring practically all of the Arctic land areas show the effects of warming on the snow cover, and only the icecap of Greenland, Labrador, and north-central Siberia show significant remaining snow cover. By August the snow cover is an absolute minimum in the Arctic region. In the following weeks it will increase to its typical winter distribution.

The net effect of the variations in snow cover is reflected by the fact that the transitional periods between winter and summer are very short in the high Arctic. Spring and fall typically last only a few weeks.

3.1.4 Temperature Inversions

Unique to the Arctic and Antarctic regions are the spectacular temperature inversions that can frequently occur in certain special locations. In extreme cases temperature increases of 20 °C to 30 °C in the lowest 330 ft (100 m) have been recorded by sounding devices. The reason, of course, for these spectacular inversions lies in the nature of the polar regions themselves.

Extreme inversions occur when the lowest levels of the atmosphere experience strong cooling. This cooling is most favored under the following conditions: (1) Nighttime radiational cooling of the surface; (2) light surface winds, which preclude mixing down of warmer air aloft; (3) clear skies, which maximize the radiational cooling; and (4) snow cover surfaces, which also enhance the cooling because snow is a good radiator to space. All of these conditions can be optimized in the polar regions because of the length of the polar night and the presence of all requisite factors for long periods of time. Surface inversions are not as strong over sea ice compared to land stations due to the heat flux through the ice from the warmer ocean.

As will be discussed subsequently, these extremely strong inversions have many implications with regard to Arctic weather. To begin with, the presence of the inversion ensures that the low levels of the atmosphere have a good deal of static stability. This stability, in turn, precludes mixing and contributes to the entrapment of fog, pollutants, and/or low clouds under the inversion. Convection is also suppressed. Inversion induced refractive phenomena of the Arctic have serious impact on radio communications throughout the region. Figure 3-4 presents a typical Barrow, Alaska sounding, showing extreme surface cooling.

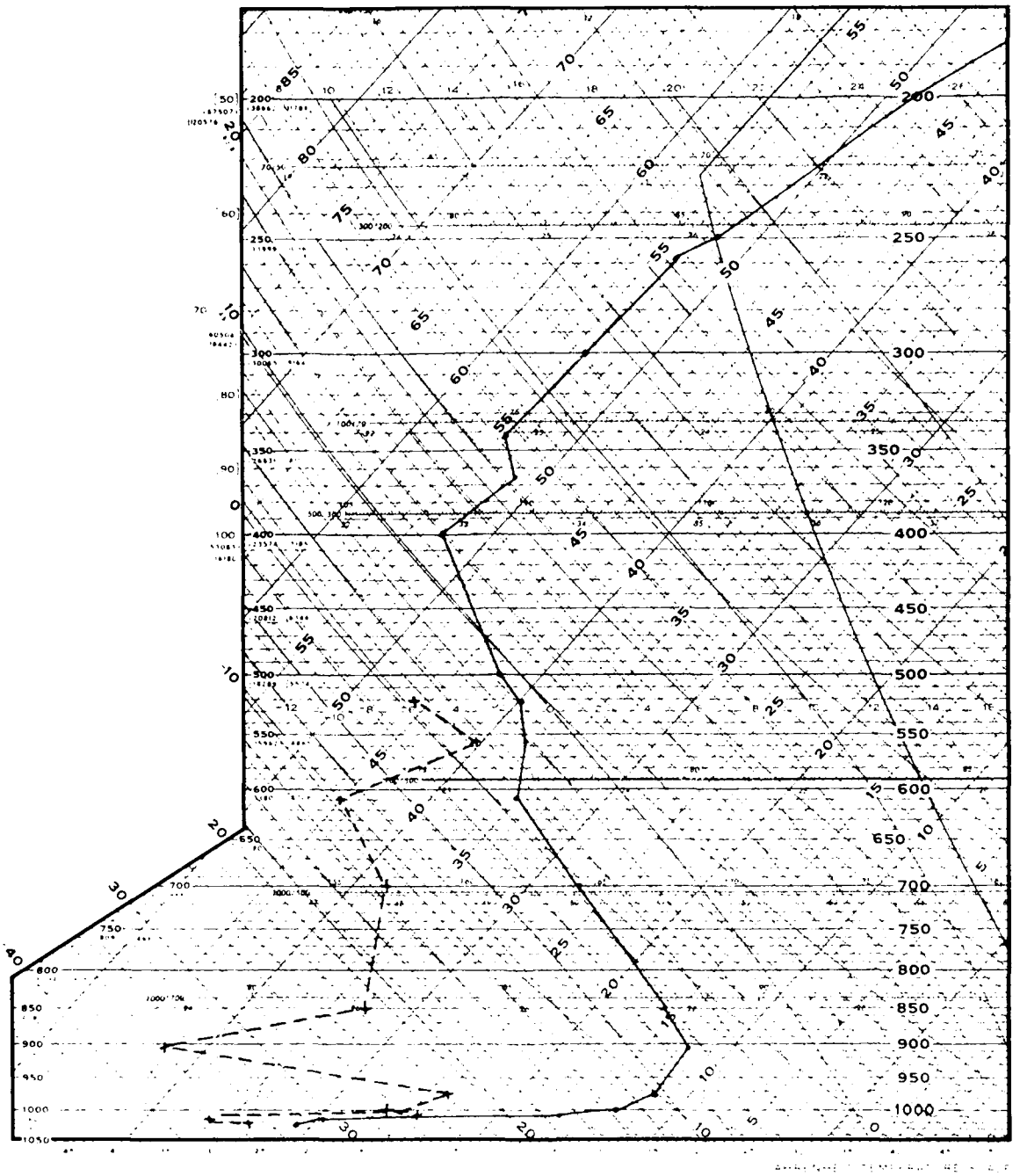

Figure 3-4. Typical Sounding from a Station in the Arctic.

3.2 Individual Atmospheric Elements

3.2.1 Fog

Arctic weather stations experience fog conditions on the order of 100 days per year, mostly in summer. During periods of the year where some daylight is present, fog will usually occur during the early morning and nighttime hours. The regions bordering the

East Siberian and Laptev Seas present an exception. Here fog frequency is greatest around midnight. At noon the fog possibility is least. Low-level mixing in the boundary layer over the Barents and Norwegian Seas makes these areas the least foggy in summer.

Fog can be caused by a number of different mechanisms. Knowledge of these mechanisms aids the forecaster in anticipating the likely occurrence of fog at various locations. The four main fog types are

Advection Fog. Advection fog forms in summer when warm, moist air flows over the melting pack ice and cold, open water. High wind speeds will normally cause the fog to lift, resulting in low stratus. Advection fog is usually patchy and lasts only a relatively short time. June and July are the months of highest probability of advection fog. At present few studies have been made of the climatology of fog occurrence in the Arctic. The areas around southern Greenland and Iceland have received, however, considerable study because of the proximity to shipping lanes. The studies suggest that these areas are subject to considerable advection fog, and the probabilities of occurrence are highest in summer when the temperature contrast between ocean and air is greatest.

Radiation Fog. Radiation fog occurs most frequently with clear, calm conditions over snow and/or ice covers. The surface layer of air is cooled by outgoing radiation during the night, temperatures are reduced to the dewpoint, and condensation occurs. These fogs can occur over the pack ice, but they are most frequently found along river valleys where air movement is minimal and drainage renders the air quite cold. They are most common in the lower Lena and Mackenzie River Valleys. Radiation fogs may also occur in the Yukon Valley and in some of the valleys of northward flowing rivers in Siberia. Radiation fogs are generally thin and shallow and burn off in the daytime. In the lower Mackenzie 20–25 fog days may occur in a month. The radiation fog is also a good indicator of a strong low-level inversion that inhibits vertical mixing. As may be expected, radiation fogs are most common in fall and early winter.

Steam Fog. Steam fog develops when very cold, dry air comes into contact with a relatively warm water surface (leads, polynyi, etc.), causing a rapid transfer of heat and moisture from the water surface to the air. The heating from below produces an unstable lapse rate, and associated small scale convective eddies carry the warm, moist surface air aloft where it mixes with the colder, dryer air above. Condensation occurs in the form of fog, but with further mixing of the dry air the fog will dissolve. Steam fog is sometimes referred to as Arctic sea smoke.

Ice Fog. The fogs mentioned previously are usually water fogs. Ice fog occurs during the winter when large amounts of water are added to extremely cold air ($< -22\,°F$ or $-30\,°C$). The resulting light ice particles (crystals) settle slowly and therefore remain suspended in the air for long periods of time. These ice fogs are common around inhabited areas where a variety of moisture sources can be found. During the Coordinated Eastern Arctic Experiment (CEAREX) in the MIZ, a mild version of ice fog, which had little impact on visibility but which was almost always evident, was referred to as "diamond dust."

3.2.2 Clouds

As in other parts of the world, Arctic clouds are produced by one of several cooling mechanisms: (1) Dynamic lifting in low pressure systems or at convergence lines and fronts; (2) Radiational cooling, which is responsible normally for low clouds and fog; and (3) Orographic lifting, which produces clouds in the vicinity of land and sea features conducive to forced ascent and subsequent cooling of the air to condensation. The following characteristic cloudiness features are found in several different regions of the Arctic.

The Norwegian Sea. Because of the warm waters of the North Atlantic Drift current, wintertime cloudiness in this region is generally of the convective type. Cold outbreaks from the north in winter, when reaching the warm waters off the Norwegian coast, result in a destabilization of the air such that cumulonimbus clouds are possible. Despite this, cumulus cloudiness is less pervasive than stratified clouds of summer and, therefore, winter is less cloudy than summer. Cloud cover in this period reaches only up to 40 percent, whereas in summer it can reach 80 percent. Since less cyclonic activity occurs in summer, the clouds tend to be middle clouds.

East Siberian Type. In winter the central U.S.S.R. can be expected to be dominated by anticyclonic conditions. Because of the moisture supply, however, the clearest areas are east of 100 °E at around 140 °E. The cloud type is generally cirrus about 40 percent of the time. Middle clouds occur only with rare cyclonic activity, and stratocumulus under inversions occurs only infrequently. As in the Norwegian Sea area, cloudiness is greatest over the eastern Siberian area in summer. At this time anticyclonic conditions are less frequent, and open seas are a supply of abundant moisture. This situation tends to produce low and middle convective cloudiness at this time. Spring and fall are not similar in terms of cloudiness because of the rapid freezeup in the fall that ties up the moisture supply. The gradual thaw of spring assures longer lasting or persistent cloudiness.

Polar Ocean Type. Because of the extensive ice cover in winter, cloudiness over the Arctic Ocean is least in winter and greatest in summer here also. In summer a high frequency of stratus and stratocumulus occurs. It may reach 80 percent during this season, as relatively warm air condenses by cooling due to the ice cover of the ocean below. These stratus clouds often exceed 1,500 ft (457 m) in thickness. The water content of these clouds diminishes from the coast to the pole, naturally. The seasonal change in cloudiness is quite rapid during the short transition periods of spring and fall.

Figures 3-5 and 3-6 present cloud cover in percentages for winter and summer, respectively. The major differences are (1) increased cloud cover from winter to summer over the Greenland icecap; (2) a general increase in cloud cover over the East Siberian Sea from winter to summer; and (3) an increase from winter to summer over the Canadian Archipelago.

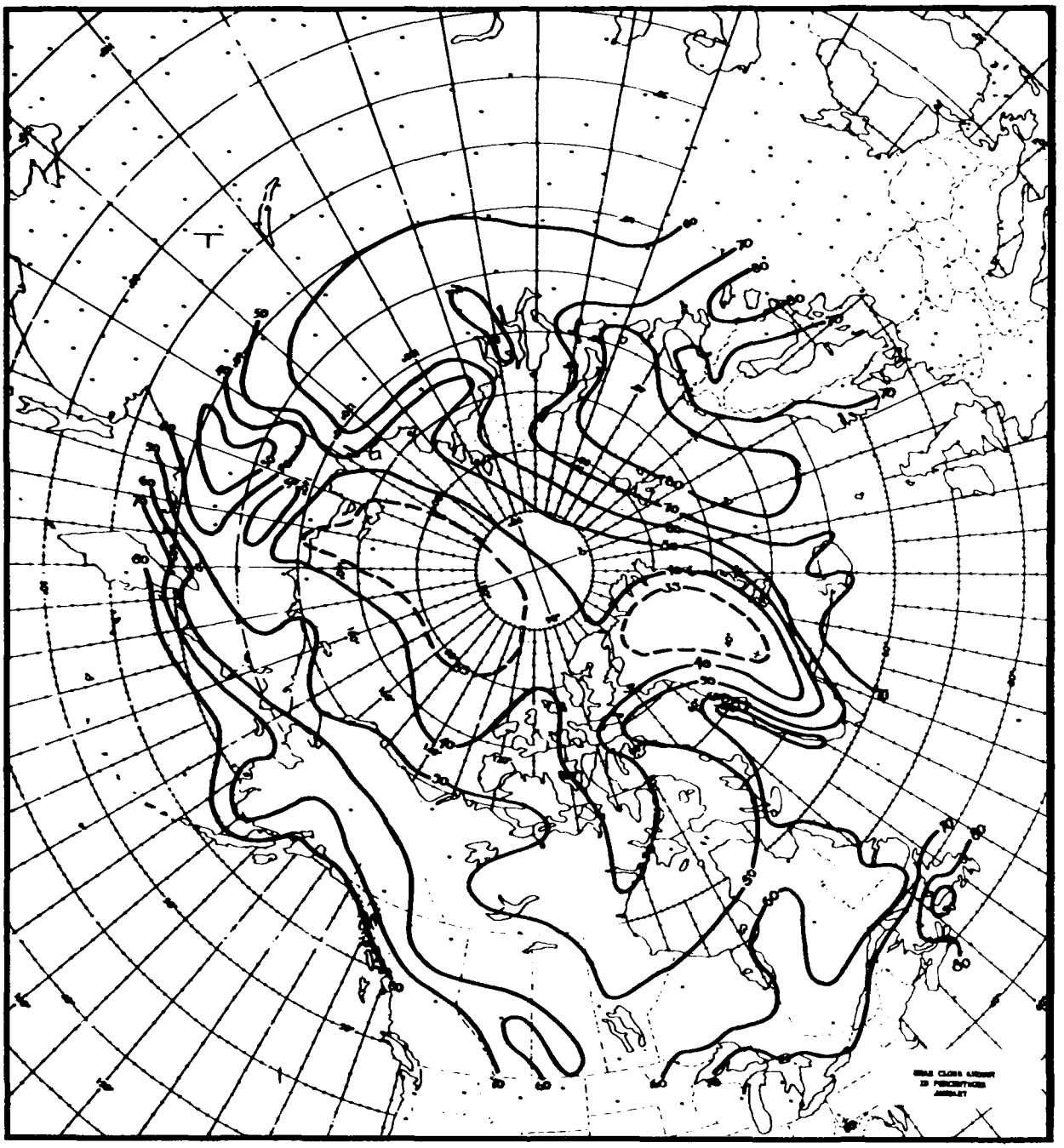

Figure 3-5. Winter Cloud Cover in Percentages (Navy Arctic Manual, 1970).

3.2.3 Precipitation

In winter, Arctic snowfall is light primarily due to the low moisture content of cold air. The annual precipitation over the Arctic Ocean itself is a meager 5 in (13 cm). Along the margins of the Arctic Ocean, where more measurements are taken, the winter accumulation is less than 10 in (26 cm). The coasts of Siberia and the Canadian Arctic

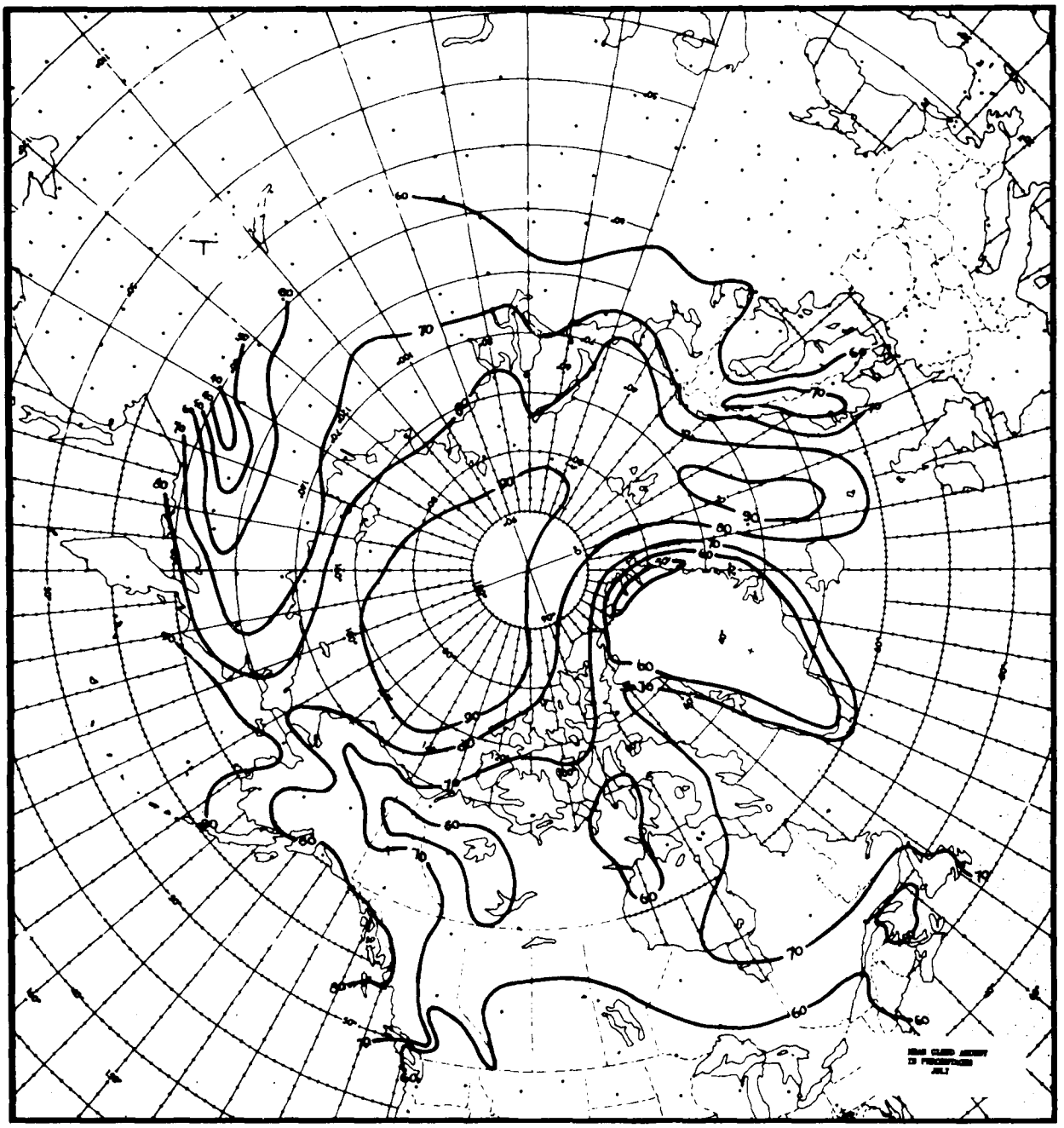

Figure 3-6. Summer Cloud Cover in Percentages (Navy Arctic Manual, 1970).

receive as little as 5.5 in (14 cm) per year, including rain and the water equivalent of snow. This precipitation is mainly snow and falls mostly in the late spring and early autumn and is due primarily to frontal systems. Frequent light snow showers will occur near leads and polynyi, and locally heavy snow showers will occur when severe cold air is aloft.

Although the amount of precipitation along the Arctic coasts is small, the ground remains saturated for long periods in summer. This condition is a result of the lack of drainage in the permafrost (permanently frozen ground). A continuous stratum of permafrost

is found where the annual mean temperature is below ≈23 °F (−5 °C). Further south at inland stations drought conditions can prevail even though the absolute amount of precipitation is greater than in the north. Drought conditions probably prevail because summer temperatures are so high in the south that evaporation exceeds precipitation.

The characteristics of the snow cover, such as thickness and duration, have important climatic effects on the heat and moisture exchange at the surface. Steady snow melt caused by solar radiation usually begins by mid-June. While marked differences occur from year to year, the ice is usually snow free by the middle of July. Over the central Arctic Ocean the snow cover becomes reestablished in late August, with a thickness up to 15 in (38 cm) by late spring.

3.2.4 Wind

Three main factors affect wind speeds in the Arctic. These components are (1) the pressure gradients associated with cyclones and anticyclones; (2) the static stability of the air in the layer near the ground; and (3) features of the local topography.

Since most cold, interior continents contain high pressure systems in winter, stations there will experience lighter winds than will the coastal stations. Examples of stations with strong winter winds are Jan Mayen, Vardo, Barter Island, and Dikson Island. Each of these islands is exposed to steep wintertime pressure gradients. In contrast, it is interesting to compare these stations to Angmagssalik and Anchorage, which are coastal but have small wintertime wind velocities due to sheltering effects, while the unsheltered Arctic coast of Alaska has frequent gales.

Generally, continental interiors have the lightest annual winds due to the moderating effect of high pressure systems. Subsidence in the area of anticyclones produces dry air promoting inversions that inhibit vertical mixing and keep the winds light in winter. Some exceptions do occur, however: Baker Lake, in the Northwest Territories, (NWT) is situated in the flow between the semi-permanent winter high over Yukon/Alaska and lower pressure over the eastern Arctic. Baker Lake's January mean temperature is −27 °F (−33 °C) and a mean wind speed of 13 kt (7 m/s). In winter, many areas bordering on continental interiors experience persistent strong winds due to cold air drainage from the interior that flows through mountain passes and river valleys. In summer, the absence of cyclones and weak pressure gradients keep the winds to a minimum. Examples are Verkhoyansk, Fairbanks, and Watson Lake.

The dearth of extreme wind speeds is due to the high frequency of inversions and the lack of topographic effects. Wind speeds average between 8 to 10 kt (4–5 m/s) and gales (>28 kt [14 m/s]) are infrequent, occurring only a few times a year with 40-kt (21-m/s) winds being an upper limit.

In central Greenland the wind is greatest in winter and least in summer. Here the inversion persists in every season, but since the ice mass is so high the wind speed is determined by the 700-mb contour gradient, which is steepest (strongest) in winter.

Other regional characteristics are present in the Arctic wind systems over land. For example, in eastern Siberia a monsoonal change in wind direction is experienced. During winter southerly winds prevail, being strongest over the coast and light or calm in the interior. At Verkhoyansk winds average less than 4 kt (2 m/s) for the months of September through April. The frequency of storms there is greatest during the months of June, July, and August,

with an average of two or three per month. During these months, the thermal low pressure system shows greatest development over the interior. Along the coast the frequency of storms is least during the summer. Tiksi Bay has an average of one storm per month from April through September. During the colder months, when the anticyclone is well developed over the continent, no gales occur in the interior at Verkhoyansk; but during these same months at Tiksi Bay, gale frequency is greatest. From October through May an average of four storms occur each month.

The wind regime of Alaska, like that of eastern Siberia, is to some extent monsoonal in character. In the warmest months a thermal low develops over the interior of Alaska, whereas, in winter, high pressures are prevalent. As a result, winter winds at Fairbanks are regulated by the Arctic high pressure system to the north and migratory lows from the southwest. Surface winds at Fairbanks itself are light because the town is located in a sheltering valley in which the average winter surface wind speed is 4 kt (2 m/s). In summer the air pressure increases over the Gulf of Alaska, and a local thermal low is established over the interior. The prevailing winds at Fairbanks are southwesterly at about 5 kt (2.5 m/s).

Climatology records show that a north and northwesterly air flow is directed over the Canadian Archipelago throughout most of the year. The flow is strongest during winter.

The Bering Strait and the land areas immediately to the east and west of it are low in elevation and present no obstacle to the free interchange of air between the Arctic Basin and the region of the Bering Sea. During the winter the prevailing wind through this region is northerly, and this flow of cold air replenishes the air moving from the Bering Sea into the Pacific Ocean. During this season the Aleutian Low is well established, and the surface winds and upper winds at Nome, Alaska confirm this. Sixty percent of the surface winds at Nome are from the north to northeast at about 9 kt (5 m/s) and continue from that quadrant up to heights of 6,000 ft (1,828 m).

High surface wind speeds at many Arctic stations are often enhanced by local topographic effects. Many stations show locally preferred wind directions due to topography, and surface wind data from Arctic land stations must not be taken as typical of the wind over larger areas. The following examples indicate the wide variety of conditions under which strong winds occur:

Narsarssuak, Greenland. This station lies at the head of a fjord on the south coast of Greenland. Strong winds occur with low pressure to the south or southwest of the station and high pressure to the north or northeast. The wind blows toward low pressure, descending from the icecap that rises to an elevation of 8,000 ft (2,440 m) a short distance inland from the station. The wind speed is roughly proportional to the pressure gradient along the southeast coast and occasionally exceeds 100 kt (51 m/s). The wind is warm and dry and obviously belongs in the foehn category.

Thule, Greenland. Thule is located in a valley on the west coast of Greenland, with the main body of the icecap lying to the east. To the southeast a tongue of ice about 2,500 ft (762 m) in elevation protrudes outward from the icecap. The strong winds, almost without exception, blow from the southeasterly quadrant and are associated with relatively warm temperatures. These winds are due in part to turbulent mixing, in part to adiabatic descent from the ice arm, and in part to

the advection of air that is of more southerly origin. A strong pressure gradient between Thule and Upernavik, 300 mi (483 km) to the southeast, is a major factor in the occurrence of the "Thule Wind." Strong katabatic winds at Thule are triggered by northward-moving occlusions and/or their parent lows.

Alert, Ellesmere Island. Alert is located at the northeastern tip of Ellesmere Island close to Robeson Channel, which divides this island from Greenland. Two mountain systems with permanent snow and ice fields lie well to the west and southwest of the station. The valley between these systems is oriented northeast-southwest, paralleling Robeson Channel, and is generally below 3,000 ft (914 m) in elevation. The strong, relatively warm winds blow mostly from the southwest at times when the pressure gradient is strong and is oriented in such a way as to force the air to flow in this direction. A foehn effect is suggested, but the humidity is sometimes quite high both at the surface and aloft so that channeling and barrier effects are of importance.

Barter Island. This small, flat island located immediately off the north coast of Alaska is occasionally visited by strong and persistent winds that blow parallel to the coast, either in an easterly or westerly direction. The abnormal wind speeds are caused by a funneling of the air around the semicircular-shaped protrusion of the Brooks Range, located 50 mi (80 km) to the south of the station.

Juneau, Alaska. Juneau is located on the southeast coast of Alaska on a narrow shelf that rises abruptly to an ice plateau of roughly 5,000 ft (1,525 m) elevation. The strong winds that occur there are known as *takus,* since they are popularly associated with the nearby Taku Glacier. These winds are of the bora type, however, being always associated with a large pressure gradient either in conjunction with a deep low offshore or, in the more spectacular instances, with a powerful high over the inland plateau. The cold temperatures associated with the wind are due to the outflow of very cold air from the interior. In cases where the inland temperatures are less extreme, the adiabatic warming may be sufficient to produce a local warming and thus place the Taku in the foehn rather than the bora category.

Big Delta, Alaska. Although strong Arctic winds are characteristically associated with coastal localities, they may occur at inland stations as well, provided that the proper terrain features and meteorological conditions are met. Big Delta (located near the mouth of a long valley, oriented approximately west-northwest to east-southeast with mountains on either side) is an example of an inland site that experiences occasional outbursts of strong and gusty winds. The winds blow most frequently from the east-southeast (along the axis of the valley) and less frequently from south to southeast. They are invariably associated with a large pressure gradient in the direction of the valley and with relatively warm temperatures. The warming is most pronounced with a southerly wind from the mountains, in which case the wind may be classified as a foehn. In the more common case of down-valley flow, the warming is due mostly to the destruction of the surface inversion by turbulent mixing, and the high velocities are attributed to a funneling effect.

3.3 Some Regional Coastal Climatology

Three main factors control climate, in the Arctic as elsewhere. These components are latitude, distribution of land and water, and pressure.

Latitude is important in the Arctic because it causes the marked variation in amount of solar radiation throughout the year. The long hours of sunlight in summer and the absence of sunlight in winter result in a wide range of temperatures, while the oblique angle at which the Sun's rays reach the Earth greatly reduces their effectiveness.

The effect of latitude on weather is modified by *land and water distribution* because landmasses heat and cool rapidly, whereas water heats more slowly and retains its heat longer. It is well known that continental climates are characterized by extreme temperatures and maritime climates by moderate temperatures. In the Arctic, however, the water areas are completely ice covered for more than half the year, and the insulating power of the snow and ice reduces the modifying influence of the water temperatures. A tendency exists, therefore, for the climate of the Arctic Ocean and Canadian Archipelago to be characteristically continental in winter and maritime in summer.

The third factor, *pressure,* is closely linked with the differential heating of land, water, and ice. Thus, in winter the weather of the Canadian Arctic is dominated by a high pressure system over the land and ice of the western Arctic and a trough of low pressure in the area of Davis Strait and Baffin Bay, where open water is commonly present. As a result of this pressure pattern, cold dry air covers the western and central parts much of the time, bringing clear skies and good weather, while in the eastern Arctic cyclonic activity is present with frequent storms moving northward into the Baffin Bay area. Consequently, it is not unusual for Thule, Greenland to have temperatures considerably higher than Edmonton and Saskatoon.

3.3.1 Brooks Range and North Slope of Alaska

The climate of Alaska depends primarily on three factors: (1) latitude; (2) proximity to oceans; and (3) influence of mountains. Since this discussion is confined to the North Slope and Brooks Range, consideration will be given to the impact of each of these factors on Alaska's Far North.

At the latitude of Barrow, which is 71 °N, during a 2-month period in winter (December–January) "day" is only a few hours of twilight (no sunlight). Contrast this with Anchorage at 61 °N where, for the same 2 months, sunlight duration is about 5.5 hours.

The Arctic Ocean to the north has year round sea ice. While the ice may be driven well offshore in the summer months, the water temperatures are usually not much above freezing. In winter, the blanket of sea ice over the water can chill to well below freezing. In this respect, it becomes almost an extension of the continent.

A number of mountain chains in the state act as barriers to the free flow of oceanic air (Fig. 3-7). Southward from the Arctic Ocean is the Brooks Range, the northernmost extremity of the Rockies, with a lateral extent of nearly 500 mi (800 km) and elevations over 9,000 ft (2,750 m). Next is the great Alaskan Interior, a jumble of unglaciated uplands and broad river valleys. South of that lies the majestic Alaska Range, dominated by Mt. McKinley, elevation 20,320 ft (6,194 m). This chain is followed by another complex

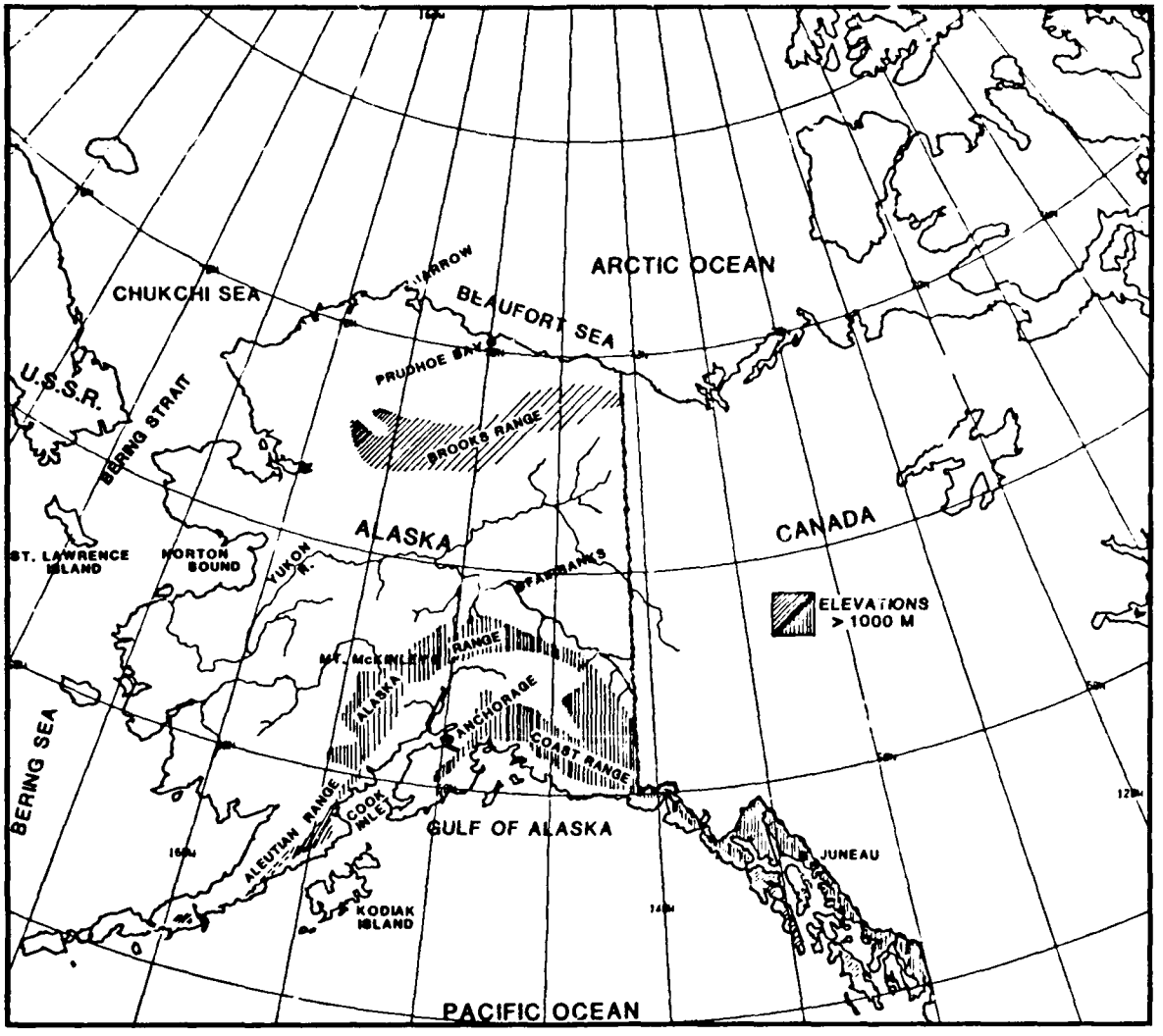

Figure 3-7. Land Features of Alaska.

of lowlands and mountains and finally the Coast Range complex, which rings the north and east sides of the Gulf of Alaska. The overall pattern is one that allows unmodified oceanic air to reach the Alaskan interior only from the west. The climate of the Arctic Slope is strongly affected by air masses from the Arctic Ocean, and that of the Coast Range by the Pacific Ocean. Consequently, the climate of the state is powerfully zoned by the mountains.

Clearly a truly Arctic climate exists on the North Slope of the Brooks Range. Precipitation is quite light, less than 8 in (20 cm) per year. Trees are nearly nonexistent. Mean summer temperatures along the coast are somewhat lower than in the western Aleutians; for example, Barrow, at the northernmost tip of Alaska, has a mean July temperature of 39 °F (4 °C). Cloud overcast is infrequent in spring but almost constant in summer. Midwinter mean temperatures are marginally lower than those of the interior, but the spring warming is far slower. February is usually colder than January. Absolute minimum temperatures are not as extreme as in the interior, but combinations of low temperatures

and high winds are frequent, resulting in extreme wind chill conditions. Along the entire North Slope, permafrost is continuous and extends to considerable depths (over 1,500 ft [457 m]). In the Brooks Range itself, as expected, colder temperatures at higher elevations and more snow and higher winds are likely except in strong inversions.

The following regional features influence the climate of Alaska's Far North:

Mountain Wave Clouds. The mountains of Alaska frequently create spectacular cloud formations. These overcasts range from local wave clouds to much more extensive cloud streets and vortex structures. An example of a wave cloud is shown in Fig. 3-8. Undulating waves occur when moist air is forced to rise over mountain ranges or mountain peaks. If humidity is high and the layer is relatively stable, the air waves become clearly visible by the clouds that form on the mountain crests. Photographs from polar orbiting satellites have captured some of these fascinating shapes and have revealed how surprisingly far they extend downwind.

The types of waves and vortices are determined by the speed of the wind and the size of the obstacle they encounter. They may be accompanied by turbulence and may be hazardous to aircraft.

Sea Breezes. Sea breezes are common mesoscale features in coastal areas around the world. The intensity, duration, and extent of the sea breeze circulation are mainly

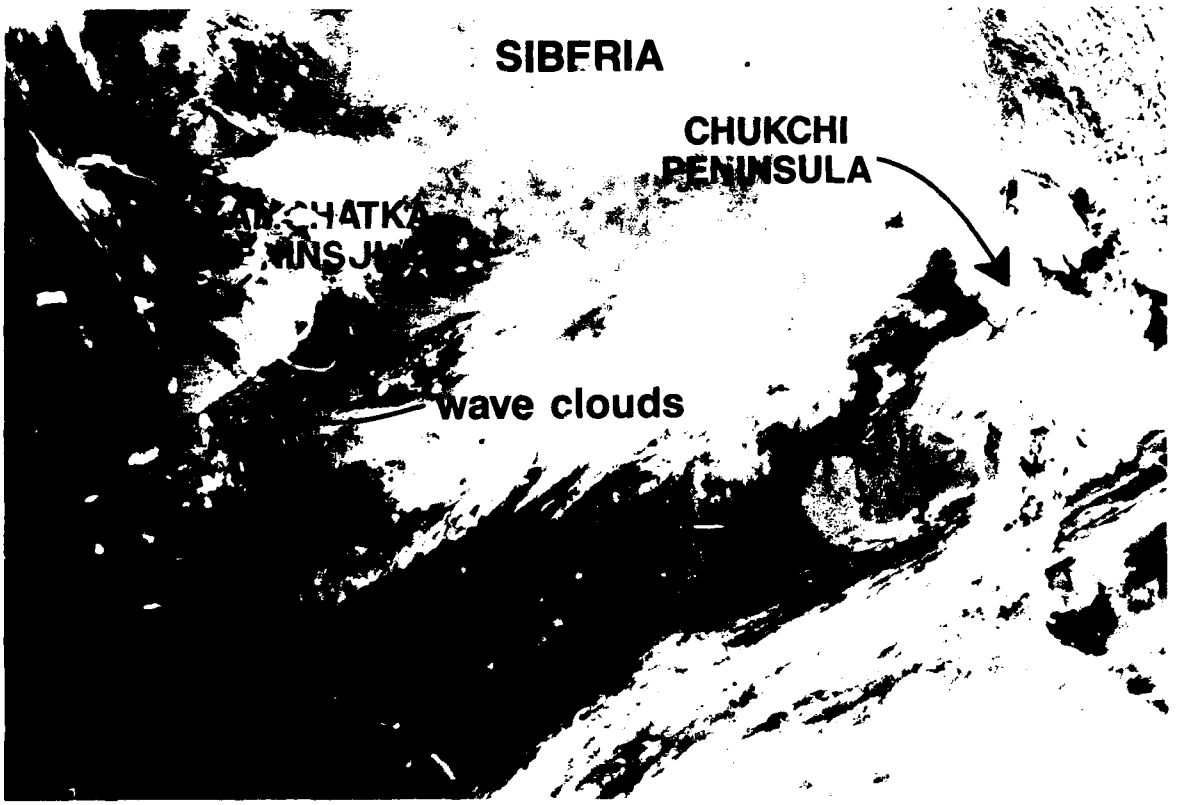

Figure 3-8. Mountain Wave Clouds over Kamchatka Peninsula (11 October 1986).

determined by horizontal gradients of temperature between land and water. The horizontal gradient in surface heating is caused by a difference in the responses of land and water to solar radiation. For equal amounts of incoming radiation, the surface temperature of the water will be less than the land because more energy is used for evaporation, and the rest of the energy reaches greater depths due to water turbulence and water transparency.

Coastal lands warming in the morning cause an increased thickness of isobaric layers over land and a downward sloping upper pressure surface from land to sea. The resultant horizontal pressure gradient force accelerates air from land to sea aloft. This air movement causes an increase in sea-level pressure offshore (mass excess) and a decrease onshore (mass defect). The result is a sea-level pressure gradient force that accelerates air from sea to land. This circulation is normally reversed at night when the land-sea temperature differential reverses, and the land becomes cooler than the ocean. In the Arctic such a circulation is not expected, however, because (1) the great stability of the air here inhibits vertical circulation of any kind, which would preclude a sea breeze, and (2) since the land-sea temperature does not reverse at night in the Arctic, no land breeze would be expected. From data collected in August of 1976, 1977, and 1979 (along the Beaufort Sea Coast of Alaska), Kozo (1982) has shown, however, both circumstantial and direct evidence of the existence of sea breezes as far north as 70°N latitude. Evidently the sea breeze can occur even though the stability is great. The counteracting effect of a low-level temperature difference between land and sea can be as much as two times as great as the contrast in temperatures in low and middle latitudes. The land breeze, however, does not appear because the temperature difference between land and sea does not reverse at night along the Beaufort Sea coast.

The foregoing theory is borne out by the following observations:

(1) The Arctic sea breeze is largely responsible for the increased persistence of surface onshore (northeasterly and easterly) winds as confirmed by historical data for August along the Beaufort coast.

(2) Normal planetary boundary layer turning, usually the result of a three-way balance between the Coriolis force, the large-scale pressure gradient force, and the viscous force should show winds shifted about 20° counterclockwise from their free stream direction to their 10-m direction. Along the Beaufort coast a more extreme turning occurs. The apparent "turning" is more likely to be in excess of 120 degrees from the free-stream level to the surface.

(3) Since the Coriolis parameter for 71°N is 37 percent greater than that for midlatitudes and because the summer sea breeze along the Alaskan Arctic coast is not followed by a land breeze, temporal clockwise rotation (northerly to easterly) of the sea breeze stops at the coast, hence the increase in frequency of easterly flow in August.

The Arctic sea breeze initially faces a strong ground based inversion that implies extreme stability and small eddy thermal diffusivity. This factor limits the vertical extent of the circulation since the depth of the landward flow is often seen to be less than 1,300 ft (400 m). The initial conditions faced by the Arctic sea breeze are similar to those encountered by midlatitude land breezes.

This stability typically occurs under calm synoptic conditions. Whenever actual synoptic offshore winds exist, however, they retard the shoreward movement of the breeze and cause a cold front type system, which has been referred to as a sea breeze of the second kind. Note that early morning offshore flow advects warm air from land out over the water to start the sea breeze offshore rather than near the coast. It has also been noted that when the large-scale wind is from land to sea, the sea breeze develops at sea and advances more slowly landward, reaching the coast much later in the afternoon, acting like a front with a characteristic wind shift.

The database for Arctic sea breeze studies has been enhanced by the discovery and development of the Prudhoe Bay oil fields in the mid-1960s. Since the nearshore ocean current flow along the Alaskan Beaufort Sea coast is primarily wind driven, a direct application to oil spill trajectories in lagoons and embayments exists. This possibility has given rise to still other studies of wind and ocean circulations in this critical area of the Arctic. A discussion of these studies follows, and Fig. 3-9 shows the locations of most of the oil rigs in the Beaufort Sea.

Corner Effect of the Brooks Range. In a study of topographic effects on the wind in Alaska, Dickey (1961) concluded that strong ageostrophic winds occurred at Barter Island due to the "knob" of the Brooks Range. Dickey observed that during periods of high surface winds, Barter Island has a wintertime abundance of west to southwest winds, while Barrow, less than 300 mi (483 km) to the northwest, has an east to northeast bias in its wintertime weather observations.

Schwerdtfeger (1975) took issue with the knob effect and showed rather elegantly that when a stable air mass is moving toward a mountain barrier without being heated from

Figure 3-9. Oil Rig Locations in the Beaufort Sea (Atmospheric Environment Services, 1985).

below, the increased elevation will alter the isothermal surfaces, thus changing the horizontal surface pressure gradient. This pressure change results in a horizontal temperature gradient directed toward the barrier and hence, a thermal wind parallel to the barrier. The flow then becomes deflected toward the east, and its strength increases markedly along the north slope. Schwerdtfeger also found that the remarkable difference between the resultant wind vectors of Barrow and Barter Island is not restricted to the surface layer; it is found up to about 6,500 ft (2,000 m).

Kozo (1980) has verified Schwerdtfeger's findings with observations from the buoys deployed by the Polar Science Center of the University of Washington. His results indicate that the average turning of the wind from above the boundary layer to the surface was 140 degrees during periods of what he calls "the mountain barrier baroclinity." The horizontal extent of this phenomenon ($\approx$75 mi [120 km]) indicates that surface wind measurements in winter months for a coastal zone from east of Barter Island to Prudhoe Bay may be poor indicators of the stress exerted on nearshore ice. The implications for wind and ice movement forecasting is clear.

Strong Valley Winds. Contrary to popular thought, most authorities on Alaska's weather discount the presence of katabatic winds in the mountain valleys. Rather, in Alaska the increases in temperature of the valley surface during wind episodes always occur during the cold season. The surface temperature inversions that occur under clear sky conditions are broken by these winds as the warmer air aloft is brought to the surface by mixing, and the valley surface temperature rises nearly to that of the surrounding mountain top temperatures.

To locate the areas of strong valley winds with accompanying blowing snow and severe turbulence, use can be made of the infrared sensor on the NOAA polar-orbiting satellites. Marvill and Jayaweera (1975) discussed this possibility while reporting on two valley wind episodes in early 1975. The ability of the satellite to view these areas of warming and associated turbulence will alert forecasters to valley wind episodes for which no conventional surface observations or pilot reports are available. When strong valley winds occur during the winter months, the infrared (IR) imagery from the Defense Meteorological Satellite Program (DMSP) satellites shows a dark band (relatively warm surface) as illustrated in Fig. 3-10.

Unlike clouds, this band on the IR imagery appears with a very smooth texture and is coincidental with the valley. Since most valleys have very small slopes, drainage effects are not usually responsible for the high winds. Consequently, synoptic-scale surface pressure gradient seems to be the most important parameter to initiate and maintain strong valley winds. Marvill and Jayaweera observed the presence of a large amplitude, 500-mb ridge to the west of the area of interest at the beginning of both windy periods. This ridge location places the interior valleys under the region of the flow pattern that typically produces subsidence, clear skies, and strong radiational cooling at the surface. The surface high center was in the southern half of the Yukon Territory, creating a surface pressure gradient nearly parallel to the valleys. This situation appeared to be ideal for the production of strong valley winds and for good satellite detection of the area affected by these winds. Once the upper air ridge had moved east of Alaska, satellite viewing was hampered by cloudiness.

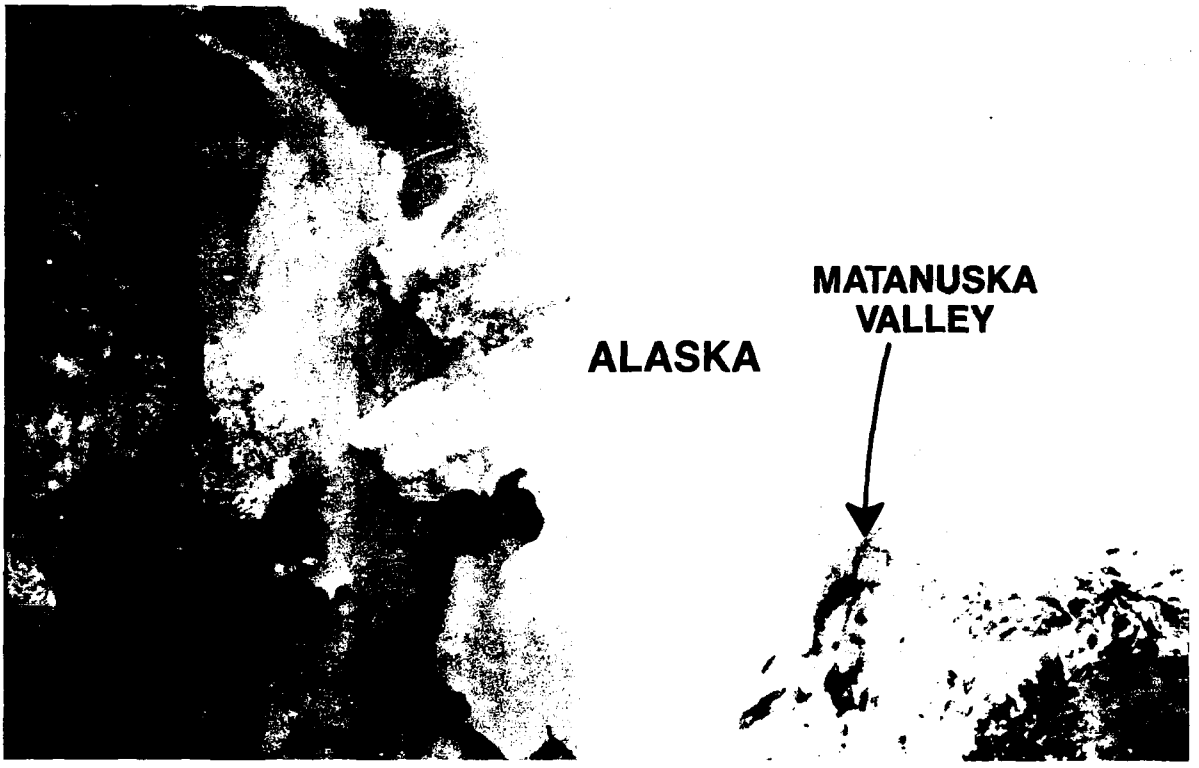

Figure 3-10. IR Imagery Showing Dark Band in Warm Valley.

3.3.2 Canadian Archipelago

In summer a flat pressure gradient is characteristic of the Arctic Ocean and the Canadian Arctic. The maritime influence asserts itself, so that differences between temperatures at 75 °N and the pole are negligible. A frontal zone is generally found along the north coast of the continent, although its position varies from day to day. Disturbances developing along this front are a feature of the weather over the Arctic during this season. The following review of the characteristics of Arctic weather patterns shows that a difference of about 2 months occurs in the length of the summer between the far north and the mainland, and a corresponding difference in the other seasons.

Airmasses. The main properties that distinguish the continental airmass from the maritime airmass in winter are the large temperature inversion at the surface, stability, low temperatures, and dryness. In summer the continental airmass is drier, warmer, and less stable than the maritime airmass.

Pressure Patterns Unique to the Area. The weather of Arctic North America is dominated by the Arctic High, the Icelandic Low with its westward extension, the Baffin Bay Trough, and the Aleutian Low. (Refer to monthly mean sea-level pressure maps, Appendix B).

Arctic High. In the fall pressures build up over eastern Siberia and the Arctic Ocean, and the two systems are often shown on weather maps as a single ridge. This condition persists until spring, when the Siberian High dissipates and the center of the Arctic High moves to a position northwest of the Canadian Archipelago, with a ridge extending south toward Churchill. It reaches peak intensity in April and May. In summer the gradient weakens to such an extent that the Arctic High practically loses its identity and is frequently displaced by migratory lows.

Yukon High. The Yukon High can be described as a ridge extending from the Arctic High over the Mackenzie Valley. It commences to build up in November, reaches its peak in February, and disappears in the spring.

Baffin Bay Trough. The Baffin Bay Trough is the name generally applied to the westward extension of the Icelandic Low. The Baffin Bay area is one of almost continuous cyclonic activity, and migratory lows enter it in all seasons. Many come from the south, others from the Gulf of Alaska across Canada, while some come from the Bering Sea via the Beaufort Sea and the Canadian Archipelago. Occasionally a storm arrives by way of the Arctic Ocean. Most have passed their peak intensity by the time they reach the area.

This trough, like the Icelandic Low itself, is most intense in winter, and it frequently extends westward over the islands from the head of Baffin Bay. In spring the trough begins to fill and during the summer is usually centered off northern Labrador. During this season it frequently loses identity because of the weak pressure gradient. Occasionally the Baffin Bay Trough becomes part of a weak trough, associated with the Arctic Front, that lies in an east-west direction along the north mainland coast.

The extent and permanent nature of the Baffin Bay Trough has a strong influence on the weather of the eastern Canadian Arctic, and the circulation over the archipelago is influenced more by the Icelandic-Baffin Bay Low than by systems originating in the Pacific.

Thule Low. During late summer and fall a "closed" low appears frequently at the northern end of Baffin Bay, which is generally called the Thule Low. Usually little weather is associated with it, and the cloud cover is thin and diffused.

While the preceding paragraphs described the prevalent weather patterns of the Canadian Archipelago, the following paragraphs will address the various wind, cloud, precipitation, and temperature regimes of the Canadian Archipelago.

Winds. In winter the general pressure distribution over the Canadian Archipelago consists of a ridge extending from the Arctic Ocean southeast to the central provinces, and a trough over Baffin Bay and Davis Strait. The prevailing winds near the surface are therefore generally north-northeast over the Canadian sector of the Arctic Ocean; northeasterly over Ellesmere Island, backing to the north and northwest over the central and western part of the archipelago; and generally northwesterly over the mainland. Storms moving into Davis Strait may alter the pattern in the eastern part of the archipelago and similarly in the western part when storms arrive from Alaska. Aloft the pattern is much the same, with northwest winds usually dominating except over northern Ellesmere and the North Pole area, where they may be easterly.

In summer, owing to the weak pressure gradient, winds are variable and subject to frequent changes as migratory lows drift across the region. At this time of year the frequency of winds increase from the east and south. In general terms, the mean circulation aloft is similar to the winter pattern.

Wind speeds over the Canadian Arctic average from a low of about 4 kt (2 m/s) at Arctic Bay, which is sheltered, to a high of 16 kt (8 m/s) at the Resolution Island site (eastern Hudson Strait), which is located on the top of a small rocky island at an elevation of 1,207 ft (368 m) and experiences many storms.

Clouds. Throughout the Canadian Arctic and the Arctic Ocean the maximum cloudiness is in autumn and the minimum in winter. This effect is in direct contrast to more temperate latitudes, where winter is usually the cloudiest season. Cloudiness increases in the spring and reaches a secondary maximum in late May or June. Land areas, away from coastal regions, may have a secondary minimum in July. In August cloud coverage increases in all areas, building to the fall maximum. Over the Arctic Ocean and some coastal areas the spring maximum is delayed and the fall maximum advanced so that they merge into one.

Precipitation. Throughout most of the Canadian Arctic and the polar basin precipitation is light, and some areas of the Archipelago are among the driest in the world. A large proportion of the precipitation falls in summer; in the Arctic 90 percent occurs between May and October. Locator maps in Chapter 2 can be used as references for the following discussion. At Eureka 70 percent of the precipitation falls in summer; in north and east Baffin Island (NWT) 75 percent; in Victoria Island (NWT) and the Beaufort Sea region 65 percent; on the mainland 70 percent; while in southeast Baffin Island and Hudson Strait summer, autumn, and early winter are the seasons of greatest precipitation. South of Hudson Strait, however, considerable precipitation occurs throughout the winter.

The annual precipitation over the Arctic Ocean and the low lying western island of the archipelago averages about 6 in (15 cm). In Axel Heiberg and Ellesmere Islands (off northwest Greenland) the average is less than 5 in (13 cm), and only 1.74 in (4.4 cm) per year at Eureka, which is comparable to the desert areas of the world. Generally speaking precipitation increases southward. For the area between 75 °N and the Arctic Circle, the annual range is about 5 to 10 in (13–25 cm). North Baffin Island has about 6 to 7 in (16–18 cm). On the east coast of Baffin Island, the Clyde River area has about 7 in (18 cm), and the Home Bay region about 9 in (23 cm). In southeastern Baffin Island precipitation is higher, from 10 to about 18 in (25–46 cm), and in Hudson Strait the yearly average is from 12 to 18 in (30–46 cm), the highest in the Canadian Arctic. Cyclonic activity and open water in Davis Strait are largely responsible for this high figure.

The Arctic Ocean and the low-lying western islands of the archipelago receive about 25 in (64 cm) of snow per year. In the high elevations of the interiors of Ellesmere and Axel Heiberg Islands the snowfall is very light, averaging 10 to 15 in (25–38 cm) annually at Eureka, the least in the Canadian Arctic. In coastal areas the average is much higher; about 70 in (178 cm) at Alert and 65 in (165 cm) at Craig Harbor. In the Baffin Bay area the snowfall is about 60 in (152 cm), but at Pond Inlet and Arctic Bay in northern Baffin Island it is only about half as much. In southeastern Baffin Island the snowfall is much

heavier, the inland areas averaging approximately 40 in (102 cm) and the coastal regions 100 in (254 cm), the heaviest snowfall in the archipelago. In the coastal areas of the Beaufort Sea and Amundsen Gulf the total annual snowfall is between 50 and 60 in (127–152 cm).

In the Arctic Ocean and the archipelago north of latitude 75 °N, the greatest average monthly snowfall is usually in September. Between 75 °N and the Arctic Circle the maximum generally occurs in October; in Davis Strait and southern Baffin Island in November and early December. Generally snow falls in small particles, particularly in winter, so that the number of days on which snowfall is reported is out of proportion to the total accumulation.

Temperature. Three distinct types of climatic conditions are found in the Canadian Arctic: continental, maritime, and coastal, each having their own characteristic temperature curve.

The continental climate, which is typical of the mainland west of Hudson Bay and possibly Victoria Island, has a high summer temperature with a distinct maximum, and a very low winter temperature with a pronounced minimum. The annual range of mean temperatures is about 75 to 95 Fahrenheit degrees (42–53 Celsius degrees). The change from summer to winter, and vice versa, is rapid.

The climate of the maritime areas produces flat temperature curves for both summer and winter, and the mean annual range seldom exceeds 35F° (20C°). The most striking example of an Arctic maritime climate is found at Resolution Island. In the Arctic Ocean the climate is maritime in summer, but because of the almost solid ice pack it is more continental in winter; the mean range of about 60F° (34C°) is found around the coasts of many of the Arctic islands, particularly along the south and east coasts of Baffin Island, in the Beaufort Sea region, and around Labrador.

3.3.3 Greenland Icecap

Scorer (1988), in his presidential address delivered to the Royal Meteorological Society, credited Greenland with a major role in affecting the weather of the Northern Hemisphere. He contrasted the roles of the Tibetan Plateau and the Greenland Icecap. The former serves as an atmospheric heat source while the latter is just the opposite, a cold source. The implications of this fact are rather far reaching. Fig. 3-11 presents Greenland's topography measurements.

To begin with, Scorer pointed out a general slope downward to the north and west from a high point near east-central Greenland. On the plateau a permanent katabatic flow occurs toward the west coast, which can extend upward to heights of 1,640 ft (500 m) or more. It follows that the northwest coast of Greenland will be subject to significant katabatic winds. Also, in southeast Greenland at the fjord of Kangerlugssuaq, which has a very steeply sloping hinterland, the adiabatic warming is usually perceptible on IR satellite imagery (Fig. 3-12).

Of course, the even steeper slope (noted in Fig. 3-11) on the east-central coast can lead to significant katabatic flow in the Kangerlugssuaq Fjord (as seen in Fig. 3-12). Because of the strength of the katabatic flow, weather-producing land breezes can be expected to be associated with these katabatic outflows. The land breeze on the west coast is frequently made visible by a line of cloud lying up to 54 n mi (100 km) out to sea. Scorer also pointed

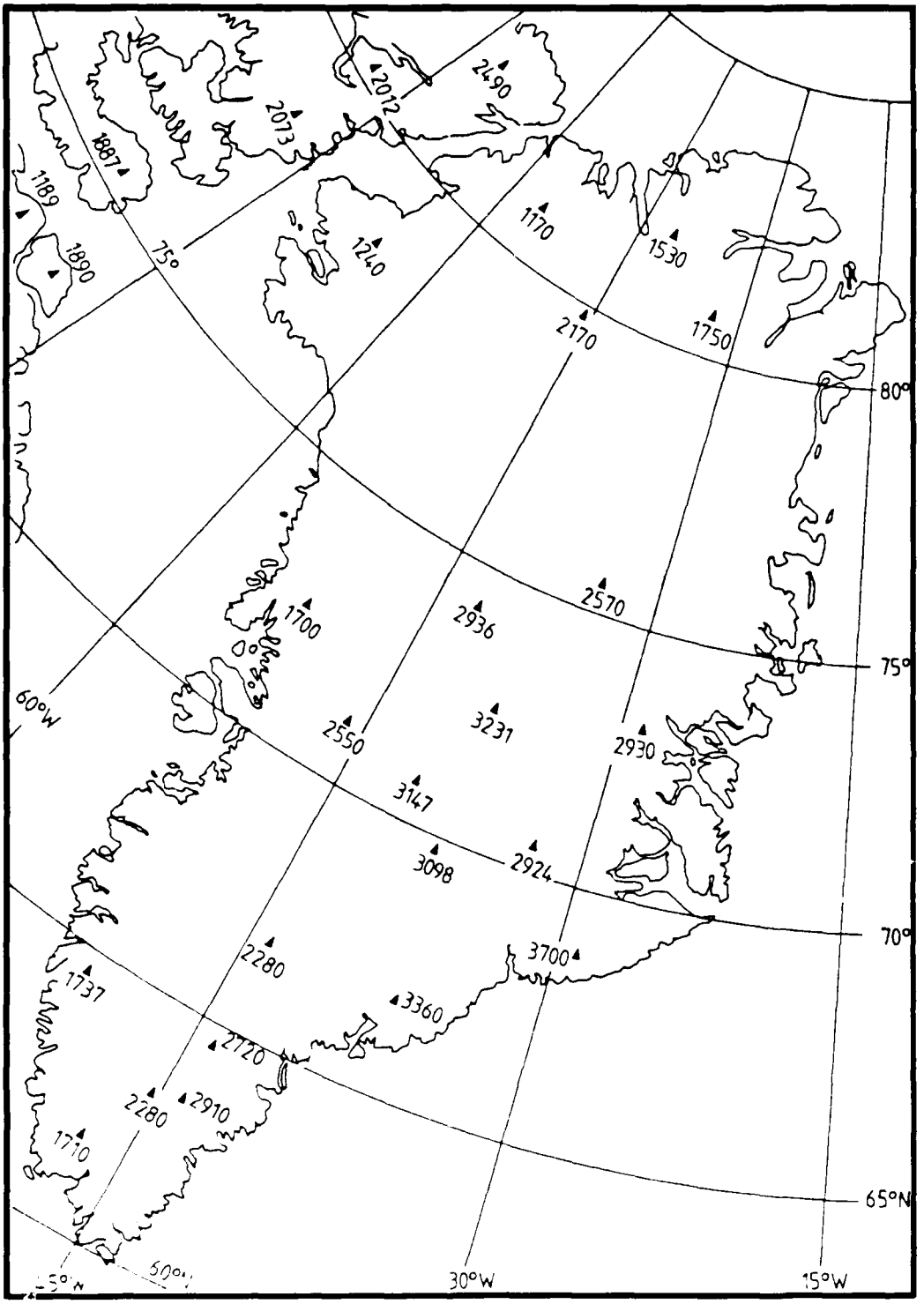

Figure 3-11. Greenland Topography with Measured Altitudes (Scorer, 1988).

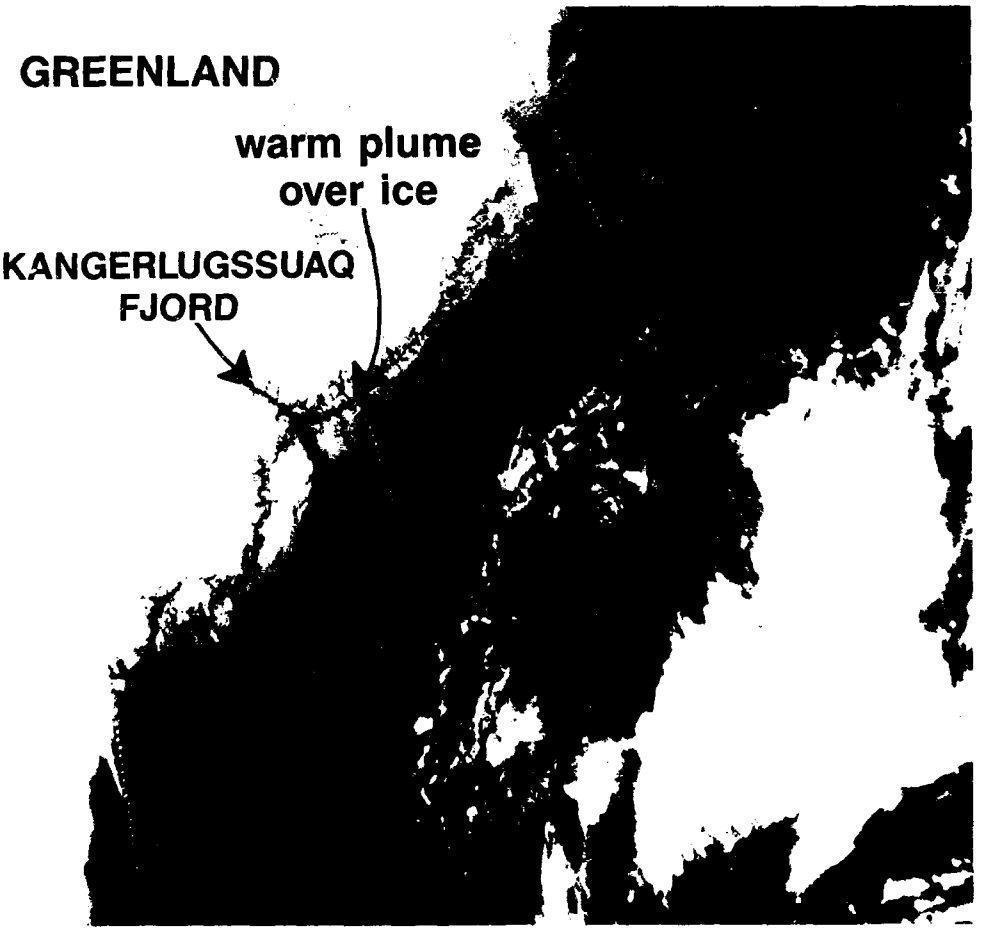

Figure 3-12. The Katabatic Warming of a Greenland Fjord.

out that being a cold source in a cold region it does not fill the upper troposphere with cloud, and the area is, therefore, relatively sunny for the latitude. With an albedo close to 1.0, the land breeze remains a cold source even at midday in June.

The main meteorological feature in the Greenland area is the so-called Icelandic Low. Scorer considered this a misnomer because it is in reality a low formed in the wake of the huge Greenland Icecap, which is a complete obstruction to the advance of air at sea level. For this reason isobars on surface analyses in the Greenland area should not be shown over the plateau. More representative would be the 700-mb height contours.

In any case, as the Icelandic Low moves from Cape Farewell toward Svalbard it causes a prevailing wind from the north or northeast along the lee coast that drives ice as far as Cape Farewell all year round. The Earth's rotation causes the ocean current to turn the cape and occasionally carry ice 50 to 100 n mi (100–200 km) up the west coast. During the fall and winter months many systems moving across the Labrador Sea and the northwest Atlantic split at the southern tip of Greenland, with a portion moving rapidly up the west coast of Greenland and the major portion continuing northeastward. Baffin Bay is often referred to as the graveyard of lows, and many of these lows move through Davis Strait.

Another feature often observed in the Greenland area is the marked anticyclonic curvature of lines of cirrus. This cirrus is seen in the air spreading out at a high level from a cyclone over Greenland, which is not accompanied by parallel surface air flow. Cirrus also originates in the high-level wave that exists above the air descending to the sea from the plateau. Because the surface air shows no convergence into Greenland it indicates that snowfall accompanying the cirrus moving inland is slight or nonexistent.

One new feature discovered by satellite imagery is the formation of rows of small, short-lived cyclones. They occur when the cold air behind a front has spread eastwards so that the front is aligned roughly east-west with the cold air on the south side. The warm air, originally on the south side and coming from the southwest, now lies on the north side of the front. In this manner an "inverted front" is regenerated by the easterly motion of the cold air, and new small cyclones come to life on it. This feature occurs in other Arctic locations such as the Bering Sea (Fig. 3-13).

Storm systems are often "steered" around Greenland and only occasionally penetrate over the plateau and then neither far nor for long. While Svalbard, Iceland, and other landforms near Greenland are some of the cloudiest places on earth, Greenland is relatively sunny, and yet it remains a very significant source of cold.

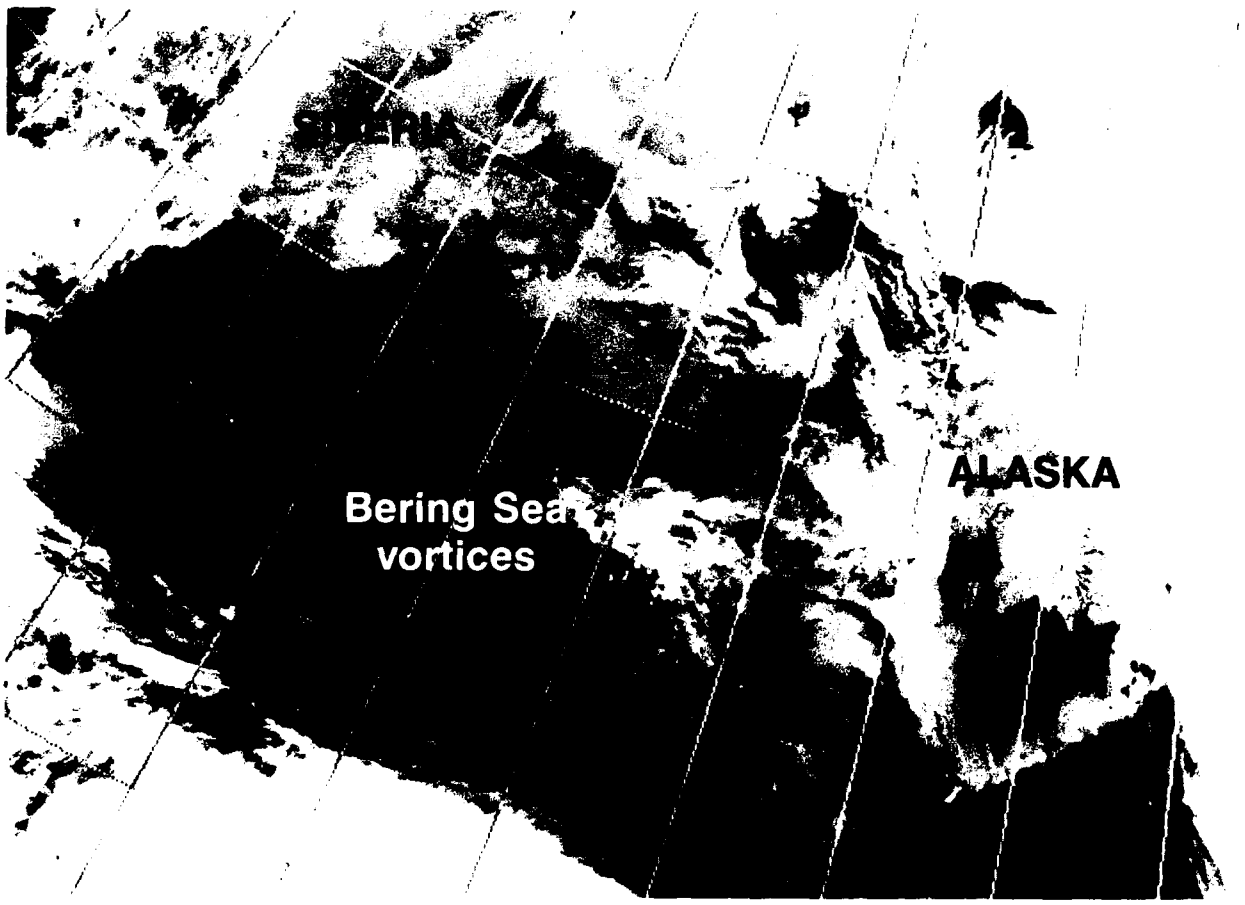

Figure 3-13. Row of Small Lows in the Bering Sea.

During a cruise on an icebreaker in 1979 Wadhams and Squire (1980) observed an ice-water vortex off the Greenland coast in the Fram Strait. The LANDSAT image they acquired appeared on the cover of EOS. Since then, many satellite observations have been made of similar vortices; for example, Figs. 3-14(a) and 3-14(b) are visible and IR images showing ice vortices near the Greenland coast. The eddy-like features are to the west and southwest of Iceland in the Denmark Strait. A comparison of the outline of the ice edges in this region shows that the edges on the IR image do not correspond to the edges in the visible image. In fact, at all points, the cold, bright boundary on the IR image extends seaward (closer to Iceland) than the visible boundary. This observation, which implies that cold, fresh, meltwater exists south of the ice boundary, is apparent in the visible imagery. The boundary of the water is uniquely revealed in the IR data (Fig. 3-14(b).

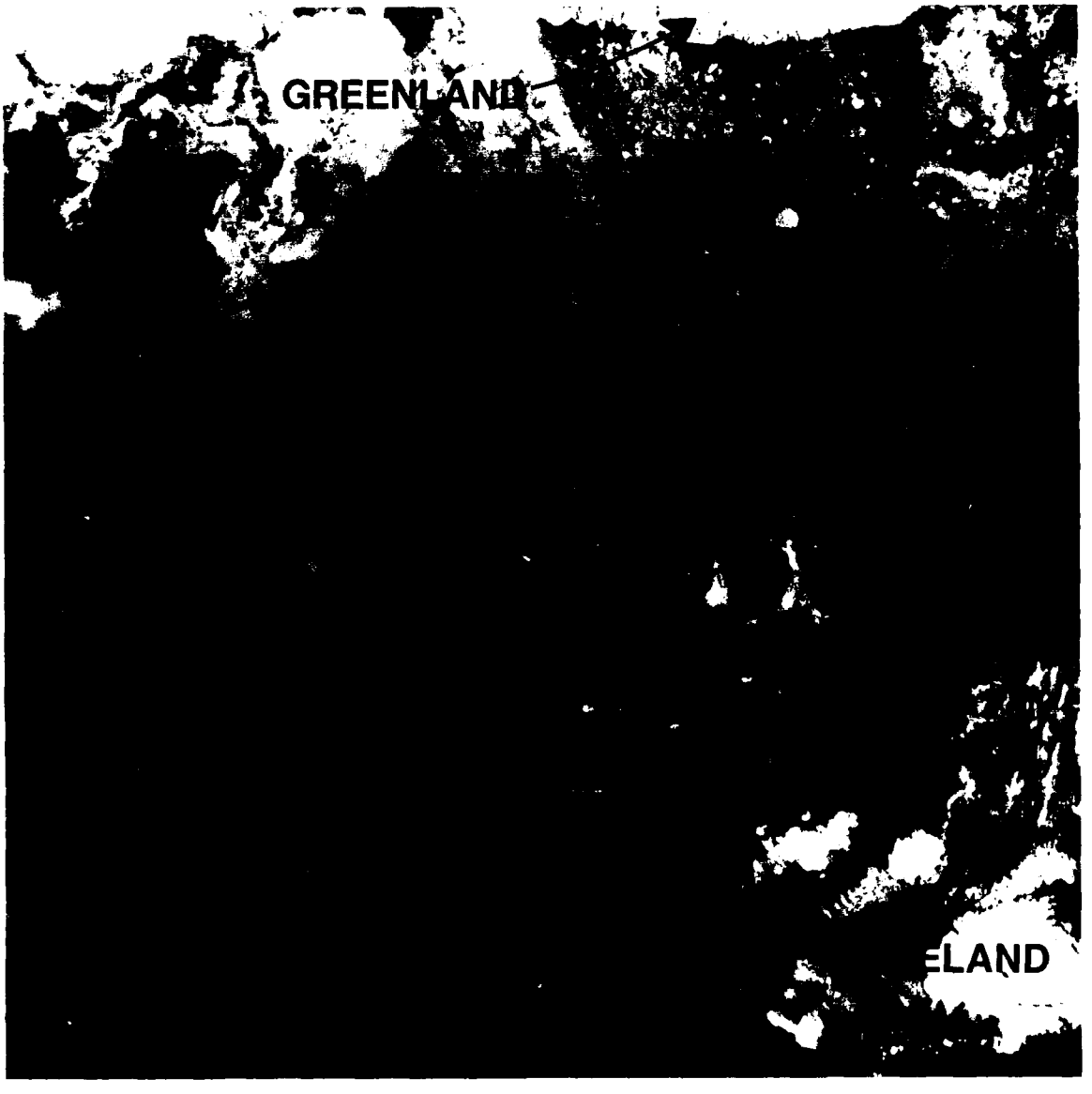

Figure 3-14(a). Ice-Water Vortex in the Denmark Strait (visible).

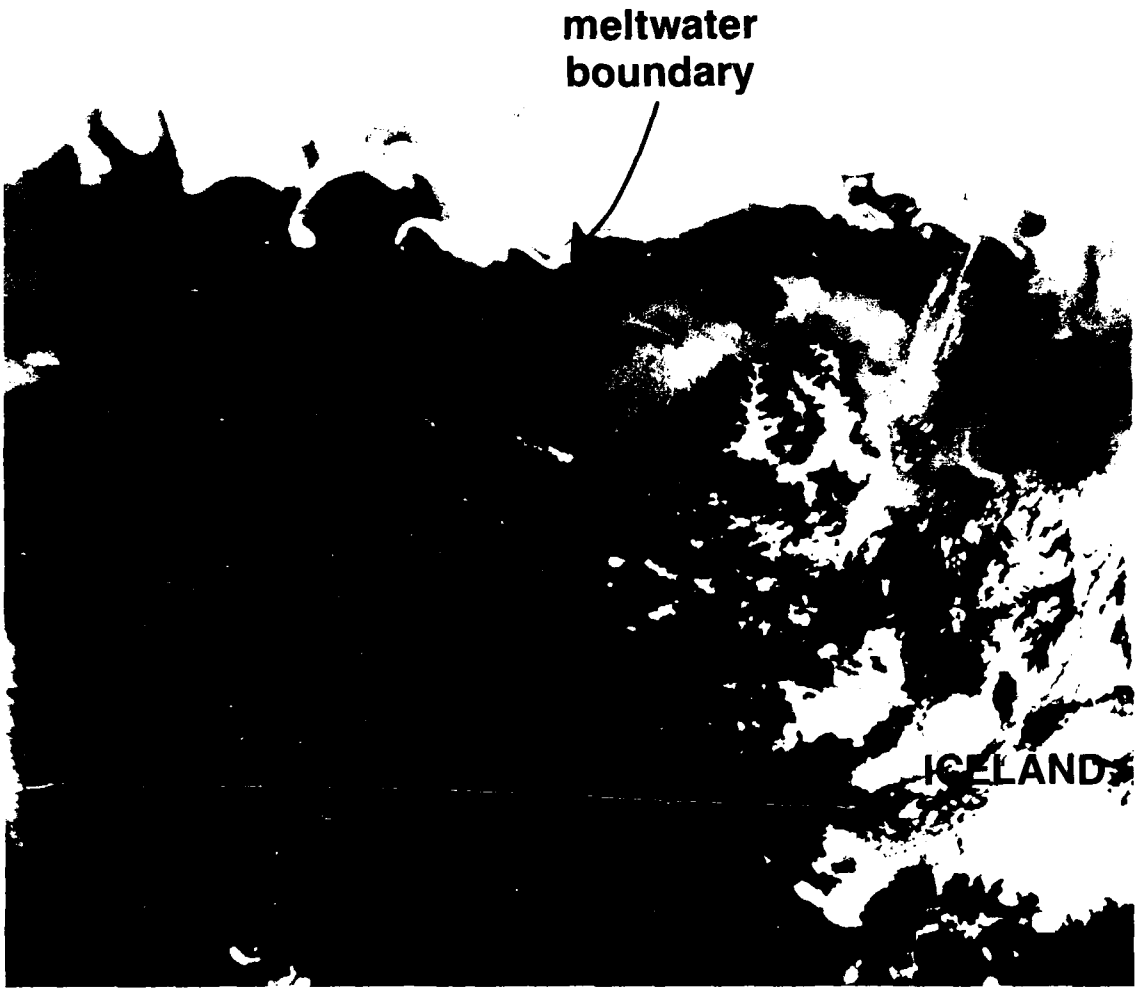

Figure 3-14(b). Ice-Water Vortex in the Denmark Strait (IR).

3.3.4 European U.S.S.R. and Siberia

The weather in this large region (Fig. 3-15) is unified by the movement of cyclonic storms throughout the area, which impart rapid and intense fluctuations in weather that stand in sharp contrast to the more stable conditions to the southeast. In fact, the northern half of the West Siberian Lowland is known to be one of the two areas on Earth (the other being the North American Great Plains) that record the greatest day-to-day variations in weather phenomena, particularly temperature. There are great meridional movements of air masses from Kazakhstan or the southern plain of the European U.S.S.R. As fronts sweep through the area these air masses interchange very rapidly and rival the frequency and magnitude of changes that take place in interior North America, east of the Rocky Mountains.

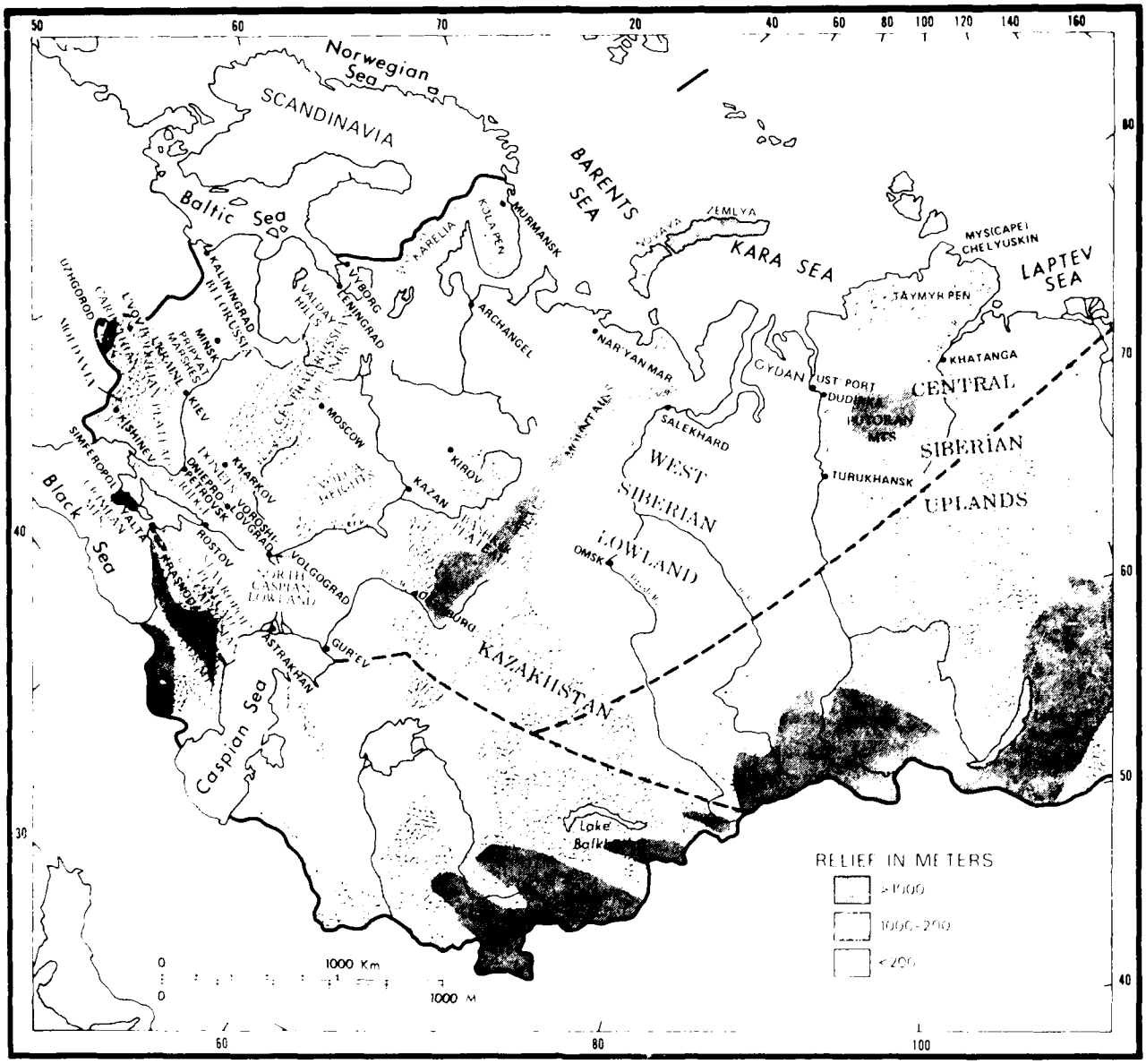

Figure 3-15. European U.S.S.R. and Siberia (Lydolph, 1977).

The entire Arctic coast experiences a monsoonal reversal of winds by season because of the great temperature contrasts between the land and sea. During midsummer, under constant sunlight, surface temperatures in the open water along the coast are held consistently near 32 °F (0 °C) by melting ice floes. The land, with higher thermal conductivity than the water, warms more strongly. Winds blow inland from the sea with average speeds during summer of 12 to 15 kt (6–7 m/s), which is significantly greater than even in the steppe regions to the south. These winds carry the cool humid influence of the sea onto the land and produce much cloudiness and fog. North of the Arctic Circle the region receives about 240 hours of sunshine (total hours the Sun is up minus cloudy hours). As cloudiness decreases somewhat inland, the hours of sunshine increase to about 300 in the southern

part of the tundra, which is the greatest number of sunshine hours during the summer of any part of western Siberia. Fog occurs about 80 days per year along the coast, and more than half of it occurs during the 3 summer months.

Added to the severity of the winter is the dreariness of the skies, which are cloud covered much of the time. During January much of the tundra zone averages at least eight-tenths cloud cover day in and day out. In the estuaries of the Ob and Yenisey more than 210 days per year experience overcast skies.

Precipitation is frequent but light. Some precipitation falls during 160 to 170 days of the year, and the annual total amounts to about 10 in (25 cm) along the coast and 14 in (35 cm) further inland. The precipitation maximum usually comes in late summer when frequent instability showers occur in the cool Arctic air that is being warmed as it moves southward over the land surface. Few thunderstorms occur.

Although the Ural Mountains have not been accorded the status of a separate region, they obviously cause the climate to change locally with elevation and induce enough perturbations in the west-east air flow across the Eurasian plain to produce significant differences in weather on both sides of the range. Although they are relatively low and broken, in many places they rise to 4,900 to 6,550 ft (1,500–2,000 m); such elevations have very significant effects on radiation, temperature, precipitation, and atmospheric circulation.

During the winter the topography of the Urals is significant in stagnating cold air, so that great temperature differences occur between enclosed lowland basins and upper slopes. Strong temperature inversions are the rule. In summer, usually a rather steep lapse rate develops along the mountain slopes, averaging approximately 4.4 °F/1,000ft (8 °C/km). One significant difference between the Urals and the surrounding plains is the amount of cloudiness. At the observation station of Taganay in the south-central Urals at an elevation of 3,616 ft (1,102 m), overcast skies occur more than 60 percent of the time every month of the year. During the average year fog is recorded for 230 days at Taganay. This high fog frequency must relate to stratus clouds that have been formed by orographic uplift and are lying on the ground at this elevation. Snow storms occur an average 97 days per year at Taganay, and the maximum depth of snow cover averages about 35 in (90 cm).

Apparently, a rain shadow effect exists on the eastern side of the Urals; these precipitation amounts may be due more to favorite routes of cyclonic storms than to the mountains themselves. Precipitation on the western side of the mountains is often about 12 in (30 cm) per year less than on the windward eastern side. Eastern Siberia (Fig. 3-16) is characterized by the highest degree of continentality on Earth. The Asiatic High brings consistently cold, clear, calm weather to the region. The area is predominantly mountainous, with the most rugged topography along the southeast. The nature of the topography has great influence on all local climatic elements.

3.4 Storm Tracks and Cyclogenetic Regions

Section 3.1.2 described the nature of the Arctic circumpolar vortex. Owing to the strong southerly and northerly components of the main westerly current around this vortex (caused by superimposition of the long wave pattern onto the polar vortex), cold, dry Arctic air is carried far to the south over central and eastern North America and eastern Asia. Mean

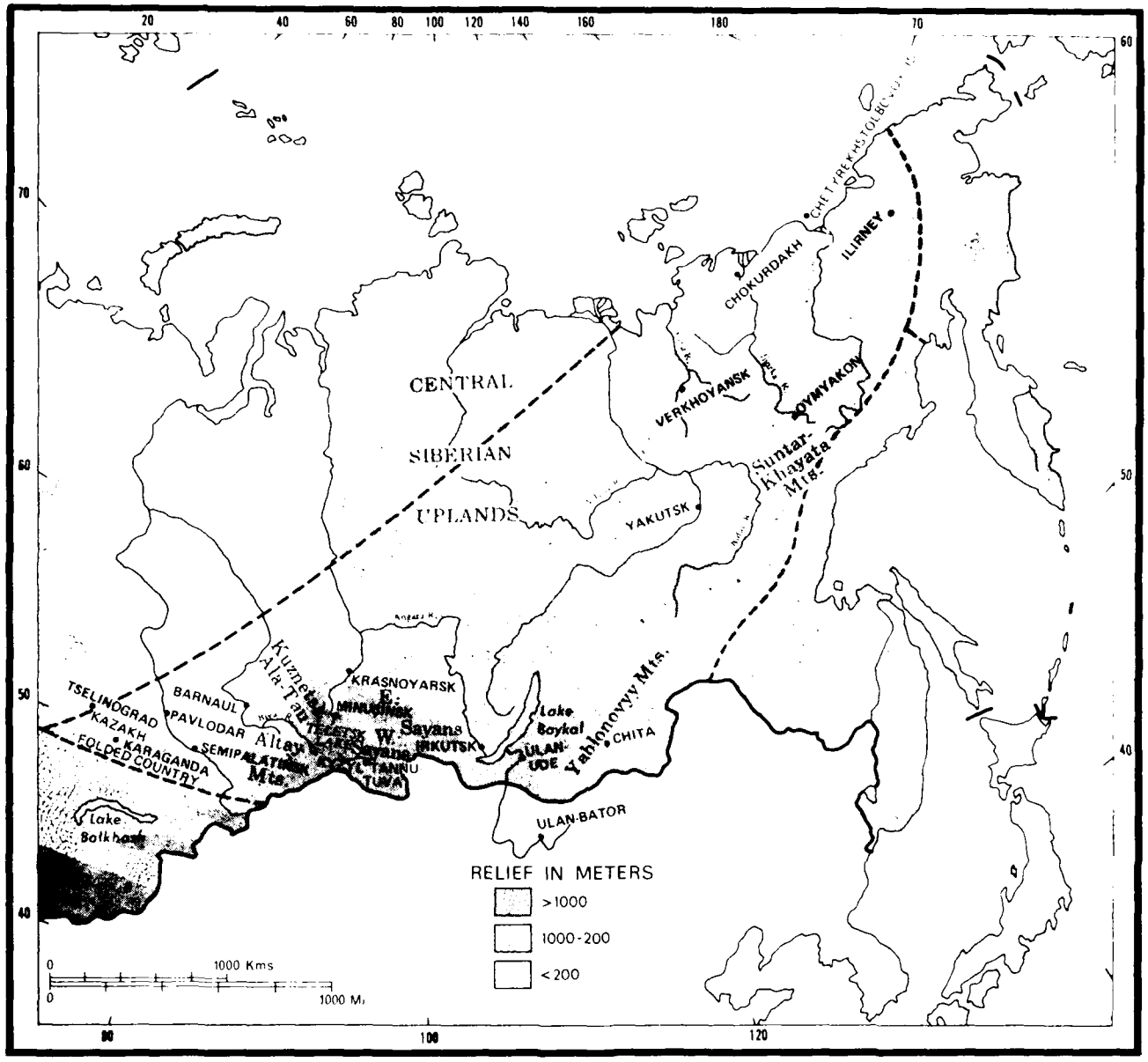

Figure 3-16. Eastern Siberia (Lydolph, 1977).

while, warm, moist air over the oceans of lower latitudes is drawn northward over the western Atlantic and Pacific Oceans toward the Arctic. In the troughs over eastern North America and Asia temperature gradients between continental and oceanic air are strongest, and here are located the major cyclogenetic regions of the hemisphere. The surface cyclonic disturbances, steered in the direction of the upper air flow, move northeast toward polar latitudes and frequently spiral in toward the upper vortex centers. As the disturbances approach high latitudes, they generally lose much of their temperature contrast, and the warm air is undercut and lifted off the ground by the colder air (i.e., the cyclone becomes occluded).

Over the north Pacific Ocean (Bering Sea area) and the Atlantic Ocean (Davis Strait area) many storms stagnate and fill. Occasionally cyclones are regenerated at the ice-water

margin, and storms continue toward the central Arctic Basin. Anticyclogenesis occurs just east of the major ridges, with the Yukon showing a particularly high frequency. Occasionally systems move out to the southeast, but they can remain stationary for many days at a time.

3.4.1 Alberta Low

Cyclogenesis occurs over Alberta where systems from the Pacific produce closed surface lows on the eastern (lee) slope of the Rockies. These cyclones generally move east-southeast to a center of maximum frequency over the Great Lakes region where tracks converge from the southwest and south. Most of these disturbances are then steered northeast to Newfoundland. Here they are joined by cyclones from the east coast of the United States, an area that favors cyclogenesis because of thermal contrasts between the cold continental and warmer maritime air masses. From Newfoundland storms generally migrate either toward Iceland (their high frequency resulting in the semi-permanent Icelandic Low) or along the west or east coasts of Greenland. A few disturbances also enter Davis Strait by way of Hudson Bay or drift erratically from western Canada below the cold upper vortex center, and an area of high cyclonic frequency is located west of Greenland.

In summer the most marked change over North America is the northern displacement of the track of the Alberta Low. The Canadian prairie provinces have one of the highest frequencies of cyclonic activity in the Northern Hemisphere. Most of these storms cross Hudson Bay to the Davis Strait-Baffin Bay area where they stagnate. Over the Atlantic, to the east of Iceland, the primary track is more zonal in July with a drop in the frequency of storms entering the Arctic Basin, and a well-defined storm path extends from the eastern Atlantic into Siberia at about 60 degrees.

3.4.2 Icelandic Lows

Storms breaking away from Iceland usually move northeast to the Norwegian Sea-Barents Sea area, and a primary track continues along latitude 75 °N. These frequent storms play an important role in the climate of the northern Europe and Siberia coastlands. This primary track is joined by tracks from the Baltic, Black, and Caspian Seas. Some storms stagnate near Novaya Zemlya, others regenerate and curve toward the pole, where cyclones outnumber anticyclones by a factor of 2 to 1.

3.4.3 Greenland Lows

Another area of high cyclonic activity appears over Davis Strait and Baffin Bay. In cases where deep lows lie south of Greenland-Iceland, the easterly flow over the Greenland ice sheet will trigger rapid intensification to the west over Baffin Bay. In other cases, surface lows will often regenerate on the east side of Greenland after air passes over the huge ice sheet.

3.4.4 East Asian Lows

Over Asia the westerly jet stream is split into northern and southern branches by the Himalayan Massif. To the north of these mountains no cyclonic development occurs comparable with that over continental North America. Cyclones moving eastward over western Siberia are often old occluded storms and rapidly lose their intensity, although secondary cyclones occasionally form near Lake Baikal and deepen rapidly while moving toward the Pacific coast.

When a strong blocking ridge over the Urals weakens, surface centers move to the southeast causing outbreaks of intensely cold air over China and Mongolia. These outbreaks are associated with strong cyclogenesis off the coast of east Asia. The majority of these east coast storms are steered northeastward toward the semipermanent Aleutian Low to then stagnate or curve north. Occasionally, storms enter the Arctic Ocean over northeastern Siberia or the Bering Strait. From time to time new storms develop on the north side of these mountains after primary storms have stagnated to the south. In general, storms over the Beaufort Sea appear to be largely of the cold low type that is characterized by colder air near its center rather than around its periphery.

4. SATELLITE CASE STUDIES

This chapter presents five selected case studies that include synoptic charts and satellite imagery. Several additional case studies (without satellite imagery) for the Canadian Arctic can be found in Lewis (1987).

4.1 Case I: Cyclone Development in the Chukchi Sea, 30 March Through 4 April 1989

4.1.1 Introduction

Cyclogenesis in the Arctic is usually difficult to predict even with modern numerical techniques. Case I exemplifies how satellite imagery can often show early evidence of cyclone development. Knowledge of these precursor signatures on satellite imagery can be of significant aid to the Arctic forecaster.

In this example, satellite imagery is used to supplement surface and 500-mb charts of the area centered on the Bering Strait (65 °N 170 °W). A time series of changing weather conditions at Barrow, Alaska will document the approach of the storm; the changes in the vertical structure of the atmosphere over Barrow will be shown with the appropriate soundings.

4.1.2 Early Evidence of the Developing Low

A locator map is provided as Fig. 4-1 for the following analysis. The surface chart for 0000 GMT 30 March 1989 (Fig. 4-2) shows a high pressure ridge extending northeast-southwest just south of the Bering Strait. A weak low pressure trough extends southeastward along the northern coast of the Chukchi Peninsula from a low centered near 73 °N 165 °E. Figure 4-3 is the 500-mb chart for the same time as the surface map. It shows a very weak ridge extending along the Chukchi Peninsula coast. Reported winds in that area average 30 kt (15 m/s) at this level and help define the ridge line.

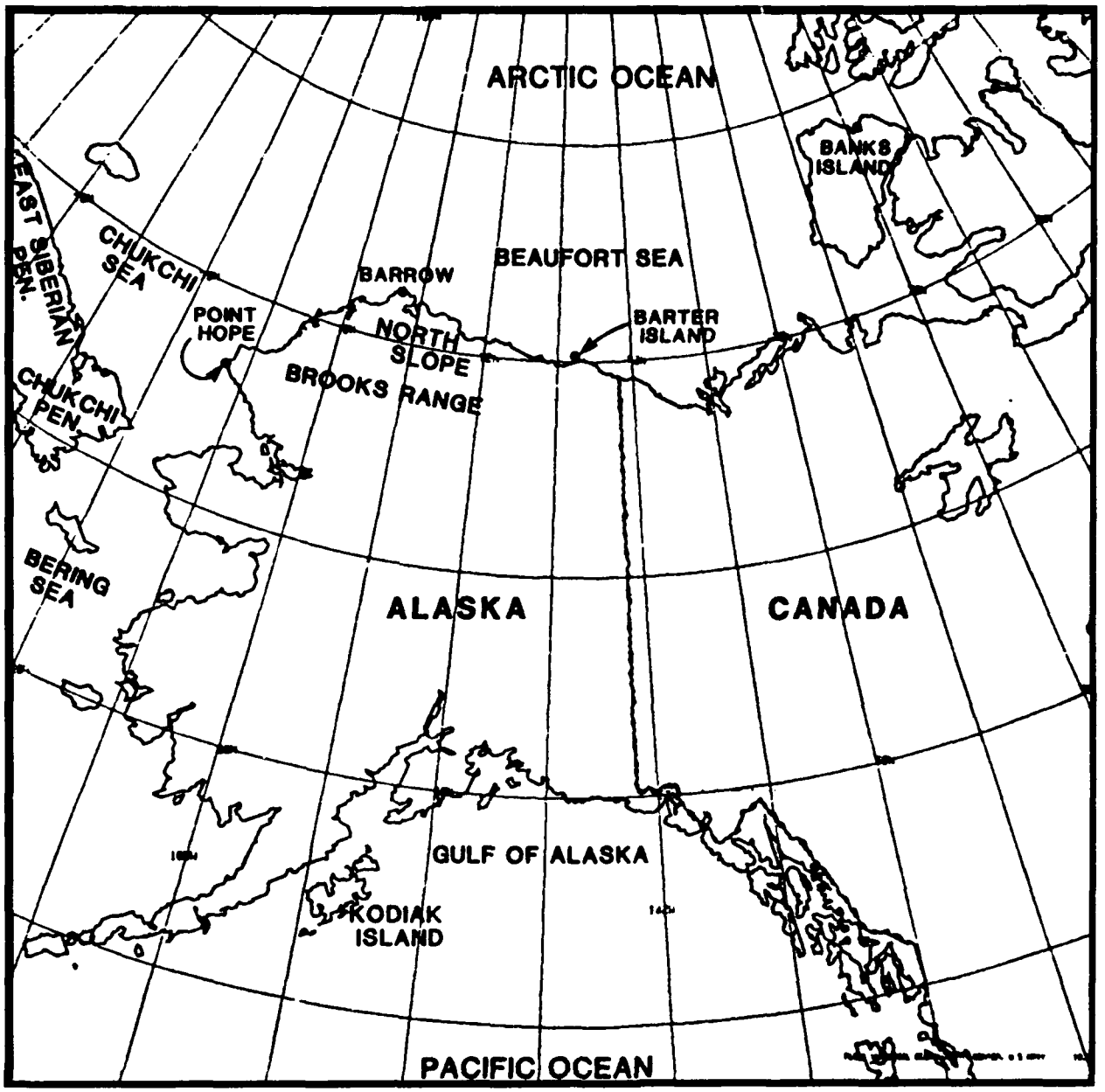

Figure 4-1. Locator Map for Chukchi Sea and Beaufort Sea Area.

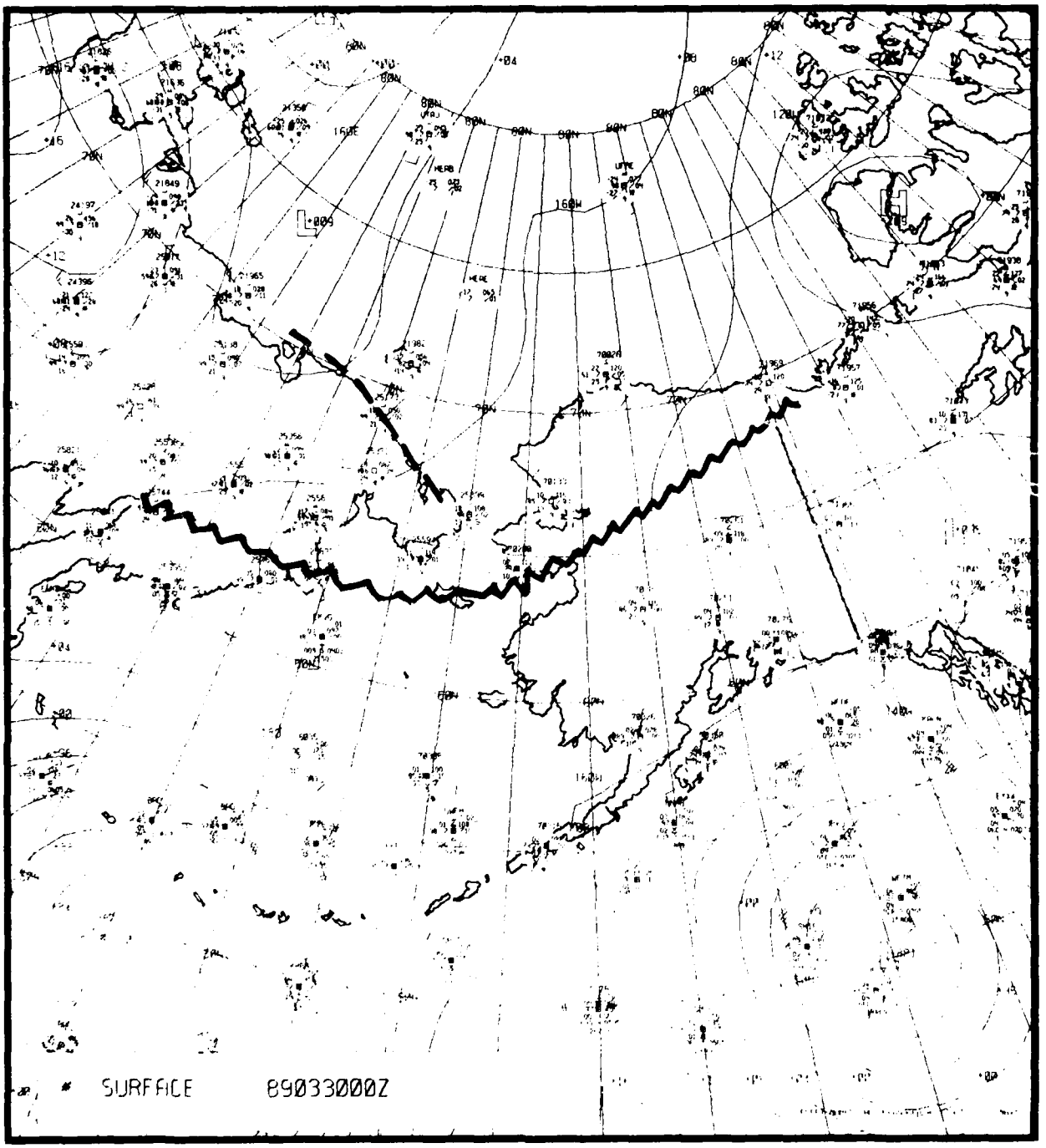

Figure 4-2. FNOC Surface Chart, 0000 GMT 30 March 1989.

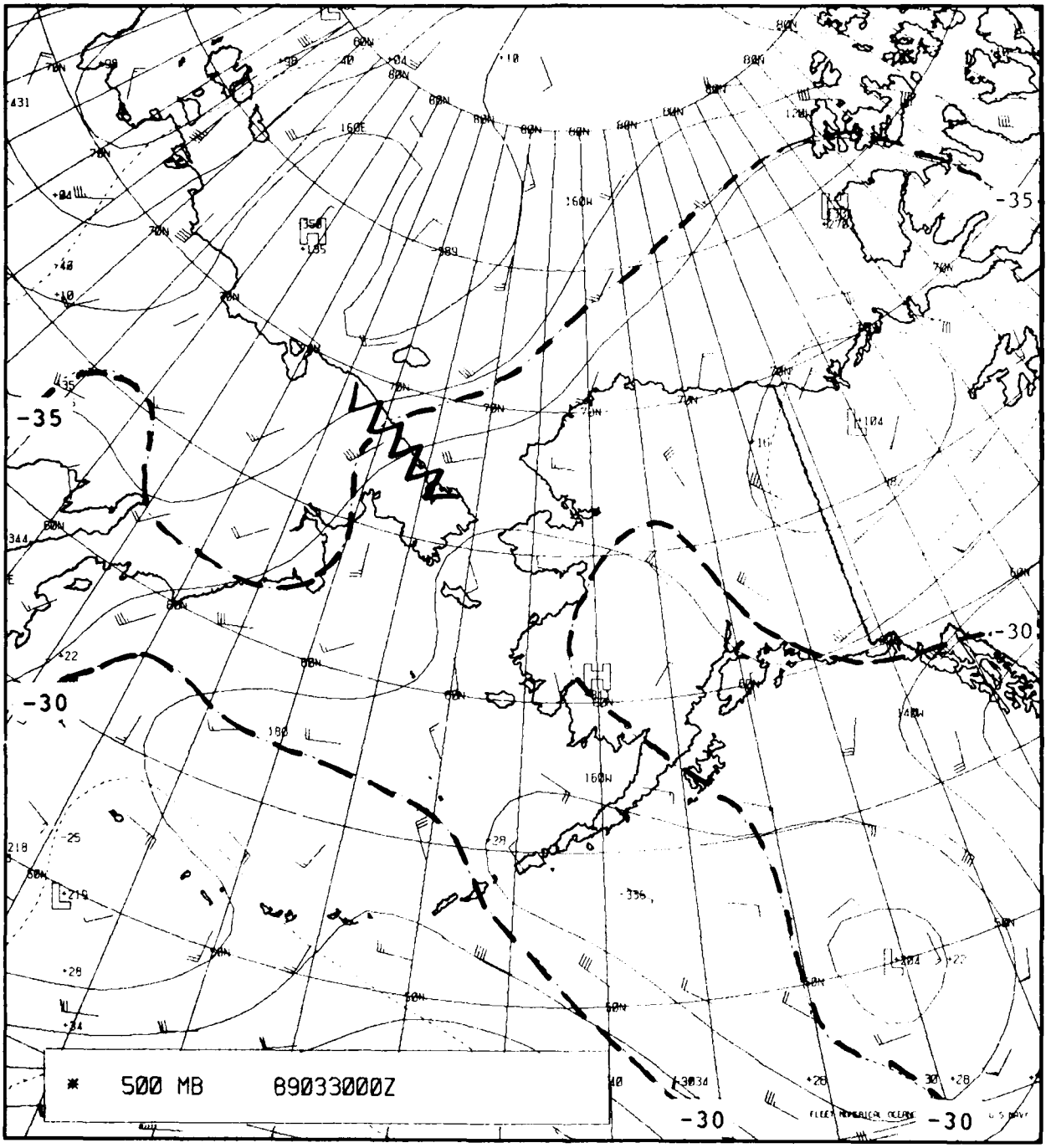

Figure 4-3. FNOC 500-mb Chart, 0000 GMT 30 March 1989.

Of particular interest is a pool of cold air situated over the East Siberian Peninsula and outlined by the −35 °C isotherm. This feature is, perhaps, some evidence of imminent cyclogenesis in the vicinity of the Chukchi Range, as indicated by the cyclonic turning of winds in that region.

The first hard evidence for cyclogenesis appears in the IR satellite imagery for 0806 GMT 30 March 1989, given as Fig. 4-4. Here, in the region of the Chukchi Peninsula, is a swath of cirrus clouds. This characteristic pattern of high cloudiness is an excellent precursor of cyclone development. The forecaster should be alert to these patterns for development can be rapid and intensive.

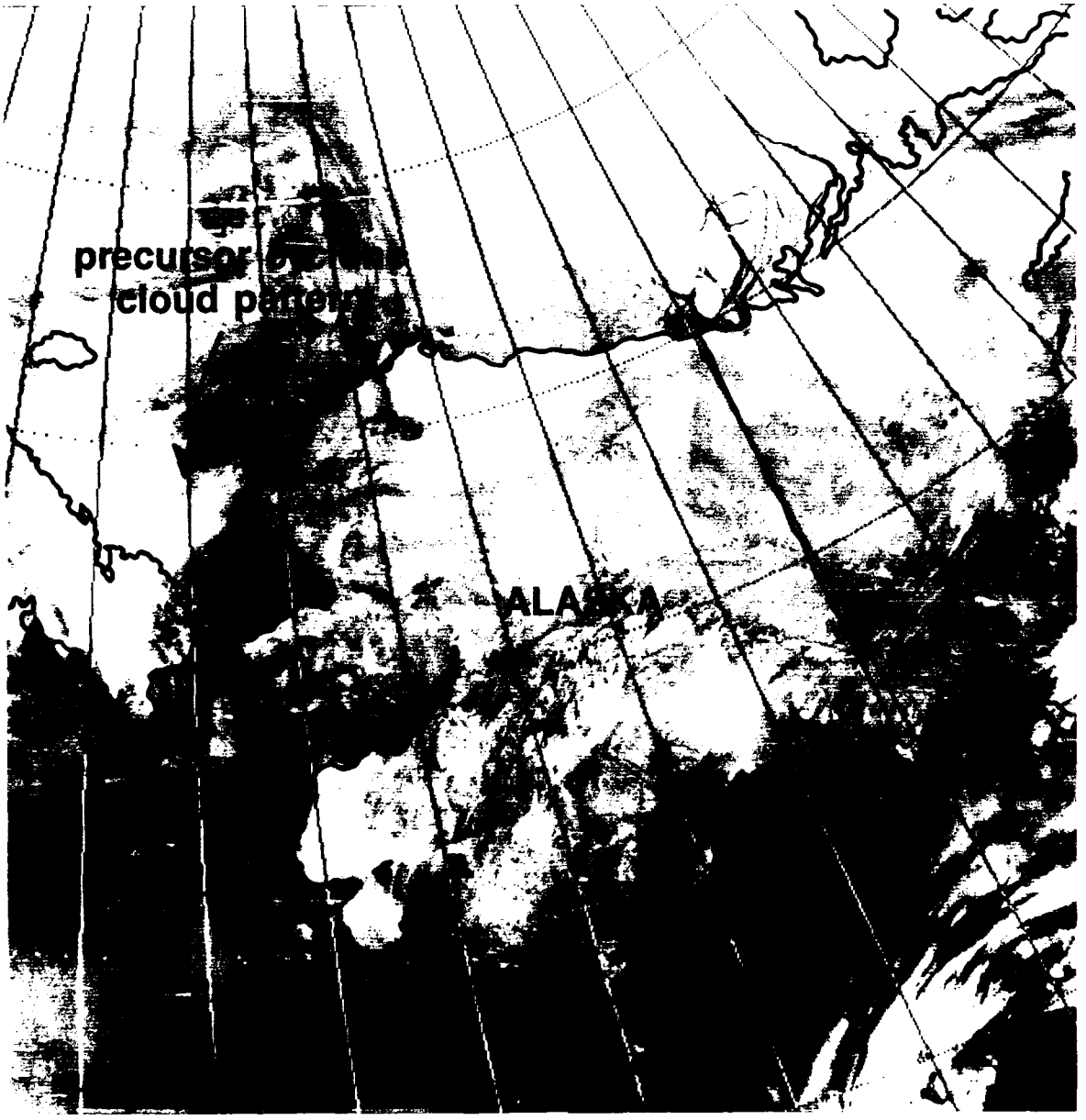

Figure 4-4. IR Satellite Imagery, 0806 GMT 30 March 1989.

4.1.3 The Maturing Storm

After 1200 GMT 30 March 1989, the developing storm is difficult to follow. For example, at 0000 GMT 31 March 1989 no closed low center is evident on the surface chart (Fig. 4-5). There is, however, a rather sharp north-south trough over the Chukchi Sea. The Barrow time series (Fig. 4-6) shows weather at 0000 GMT consistent with low pressure toward the southwest, that is, the winds are southeasterly and the pressure is falling.

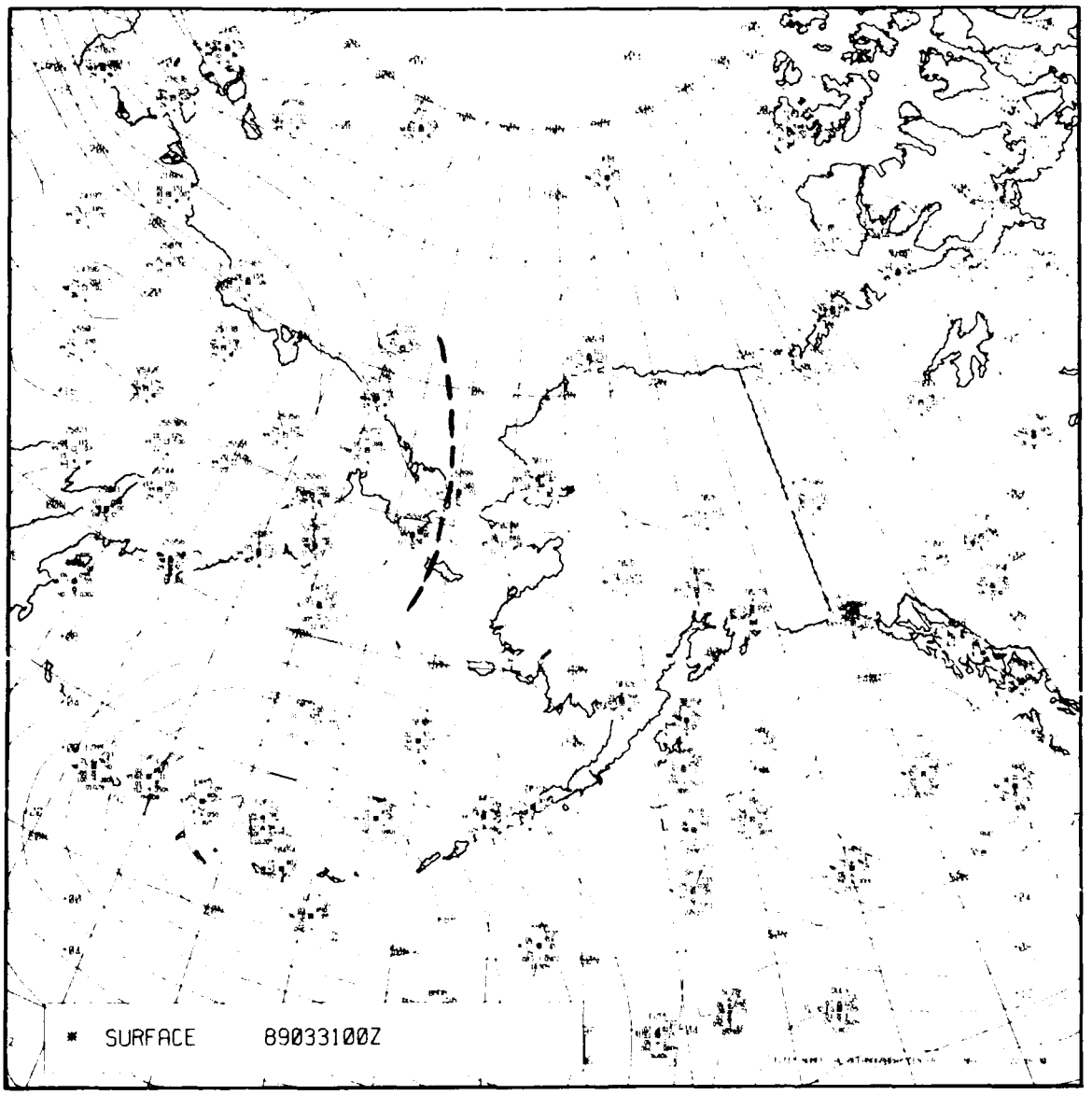

Figure 4-5. FNOC Surface Chart, 0000 GMT 31 March 1989.

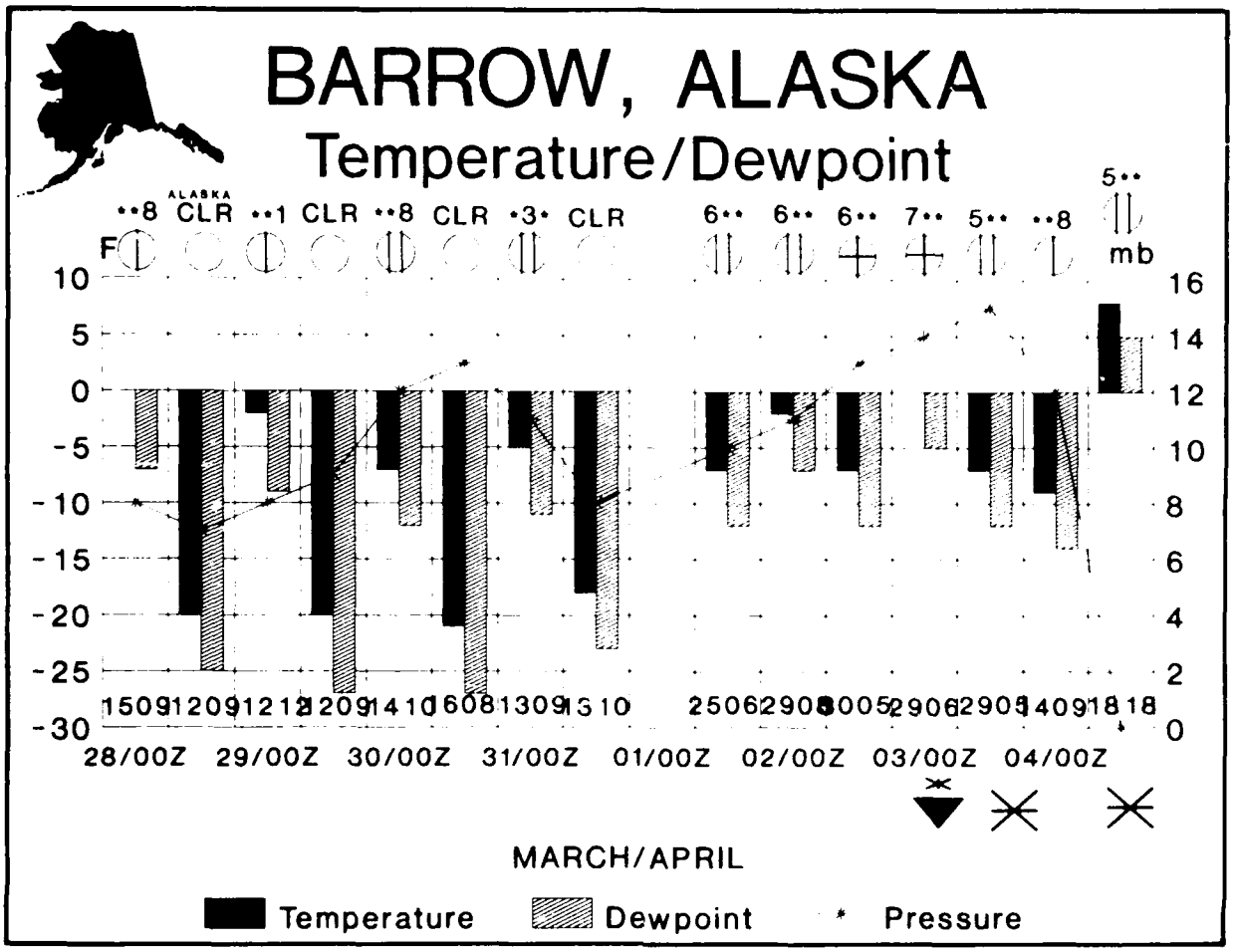

Figure 4-6. Weather Time Series for Barrow, Alaska. (Left ordinate is temperature [°F], right ordinate is pressure [mb], and cloud type [low, mid, high] appears above the sky cover symbol. Wind direction and speed [DDFF in tens of degrees and knots] are shown in the block below temperature/dewpoint data. Present weather symbols are shown below the date/time group information.)

Evidence for the storm is also rather weak on the 500-mb chart for 0000 GMT 31 March 1989 (Fig. 4-7). Note, however, that the ridge previously over the Chukchi Peninsula has weakened considerably. Correspondingly, the winds at that level are somewhat weaker and mostly southwesterly in direction. The isotherm pattern at 500 mb shows the colder air penetrating southeasterly along the coast of western Alaska toward Kodiak Island. The −30 °C isotherm suggests a warm tongue extending into south-central Alaska. This thermal pattern indicates that only weak support exists for any developing surface system and that the cool pocket, warm tongue system is undoubtedly related to the old cutoff low far to the south in the Gulf of Alaska. This thermal pattern had even greater amplitude earlier, as shown in Fig. 4-3.

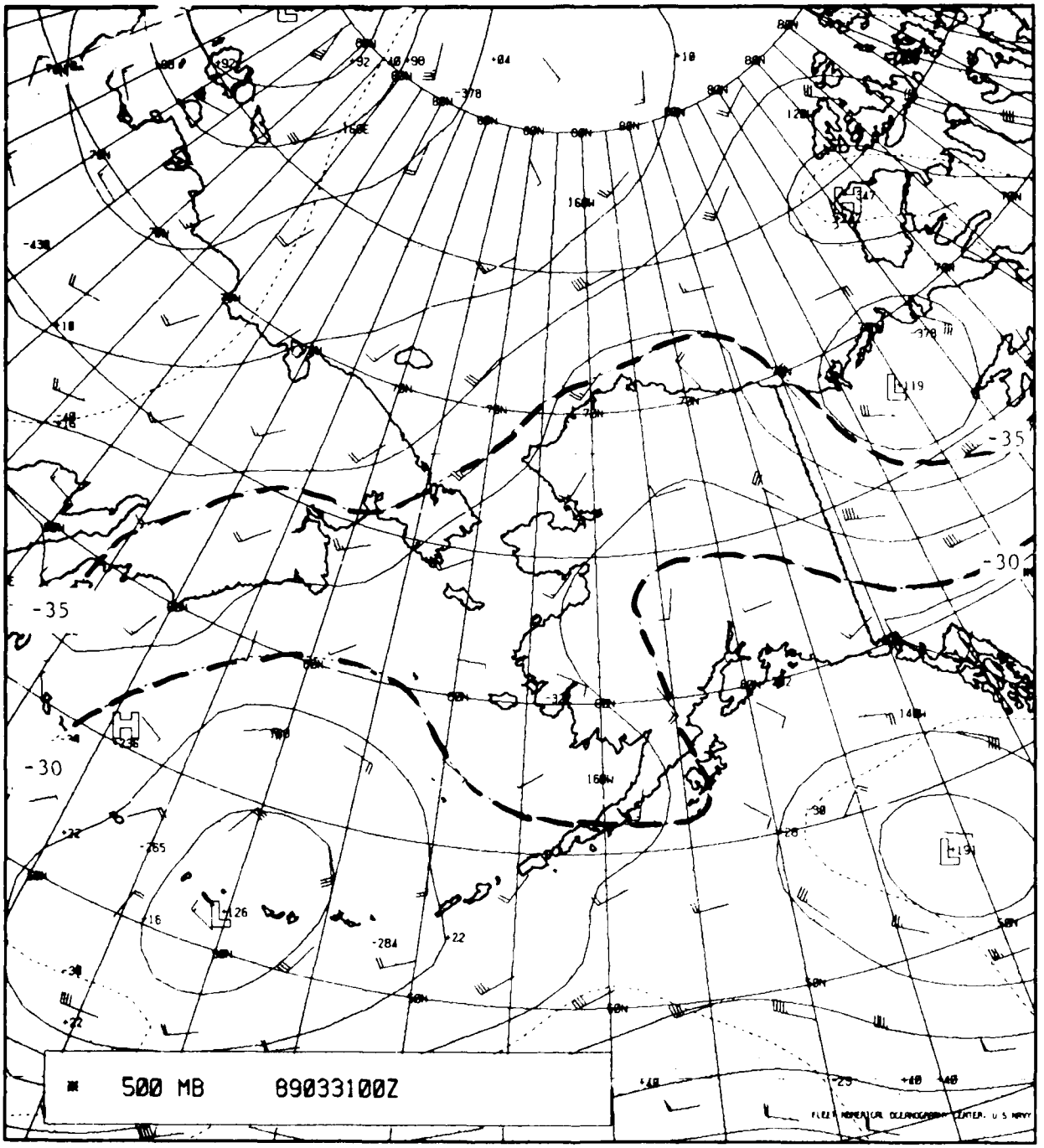

Figure 4-7. FNOC 500-mb Chart, 0000 GMT 31 March 1989.

Examination of the satellite imagery at 0000 GMT 31 March 1989 supports the notion that the surface system at that time is indeed weak. The IR image (Fig. 4-8) at 2341 GMT shows a weak vortex west-southwest of Barrow. This vortex is evidence for a definite circulation over the Chukchi Sea. Figure 4-9 is the visible image corresponding to the IR image. Because of the banded cloud structure north of the Alaskan coast and the frontal-like band over the Chukchi Peninsula, a hint exists that this storm system, although shallow and weak, may cover a rather extensive area.

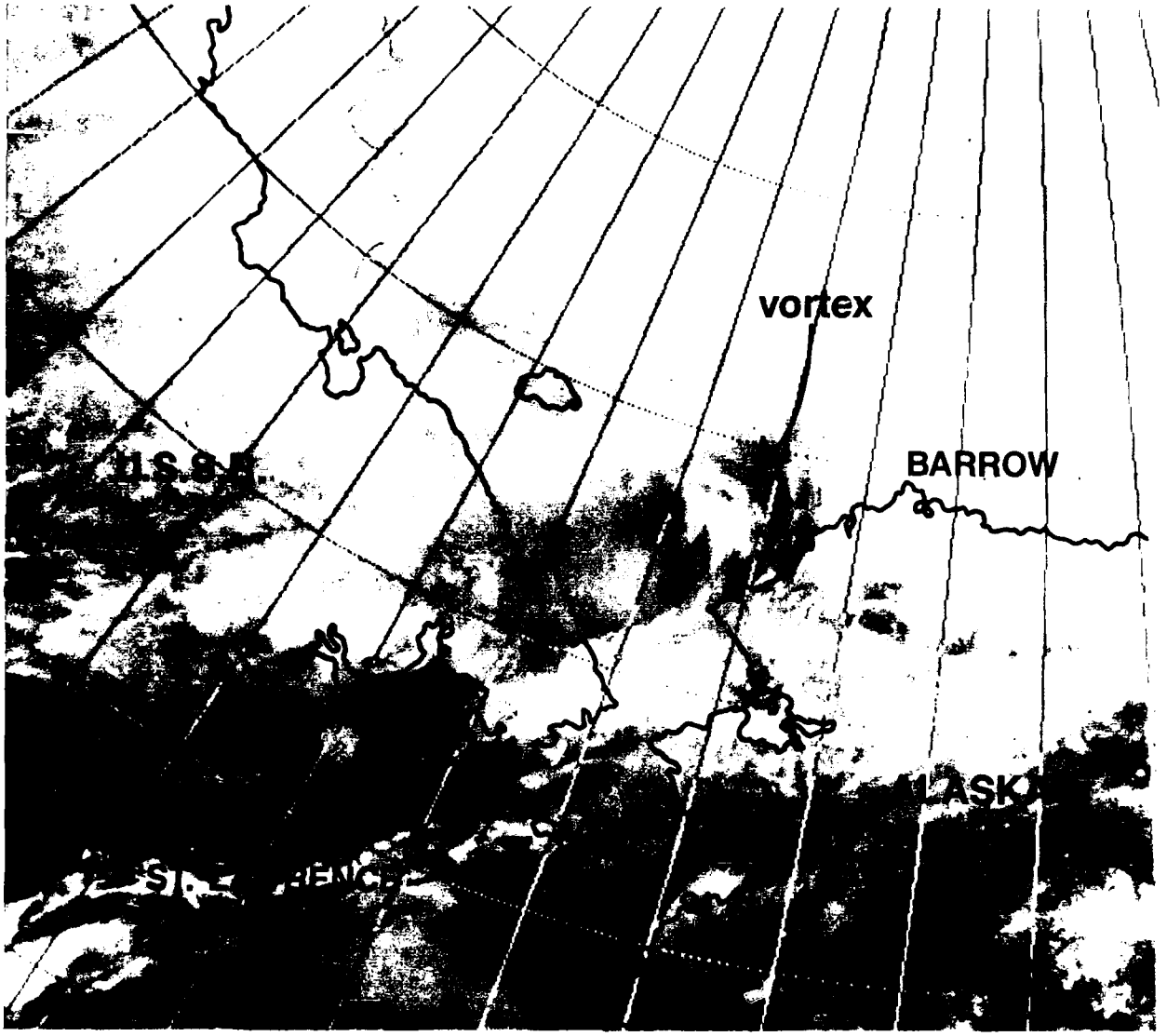

Figure 4-8. IR Satellite Imagery, 2341 GMT 30 March 1989.

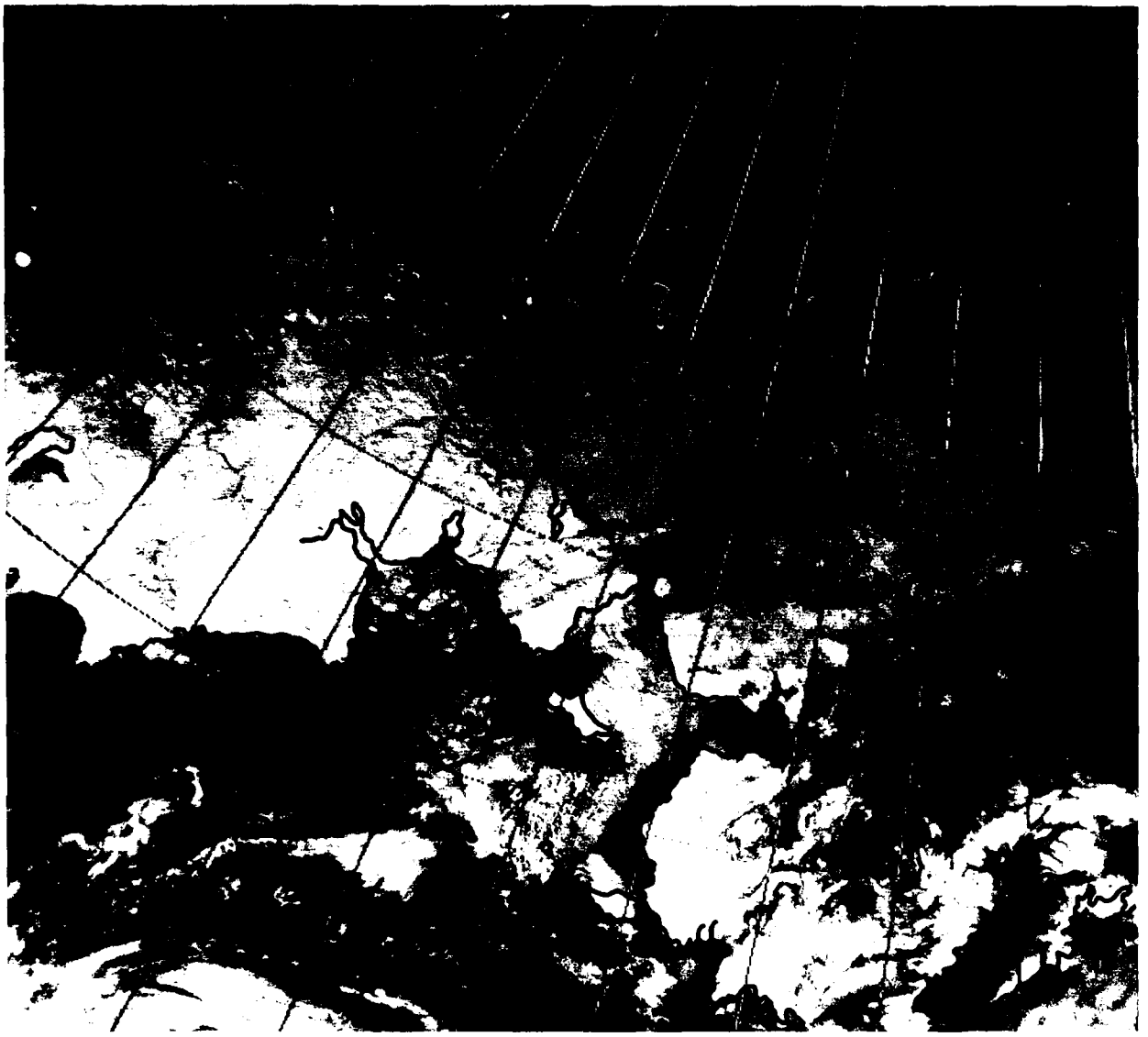

Figure 4-9. Visible Satellite Imagery, 2341 GMT 30 March 1989.

4.1.4 The Mature Storm

Referring again to Fig. 4-6, unfortunately, the data are missing for 0000 GMT 1 April 1989. At this time the storm is probably closest to Barrow, and the minimum pressure is reached. In any case, clearly, Barrow is affected by low pressure, low cloudiness, temperature and dewpoint rises, and a significant wind shift from 130 degrees at 1200 GMT 31 March to 250 degrees at 1200 GMT 1 April. Snow showers are recorded at 0000 GMT 3 April with overcast skies. So, however weak and shallow this system may be, it does significantly affect the weather at Barrow and other stations along the North Slope of Alaska or on the Beaufort Sea.

The visible image from the DMSP satellite for 1855 GMT 2 April 1989 (Fig. 4-10) shows an extensive circulation in the cloud pattern with its center near Prudhoe Bay. The system has the appearance of a mature circulation by this time. Recall that this impressive storm was detected 3 days earlier as a small swath of high cloudiness on IR satellite imagery. This particular feature is often followed by cyclone development in the area. Its uniqueness can be recognized as the cloud pattern expected in a short-wave pattern between the trough line and the downstream ridge line. In this region of the wave, high clouds tend to form in the moist, ascending air (see Fig. 4 11). Thus, high cloudiness is a good precursor of cyclone development.

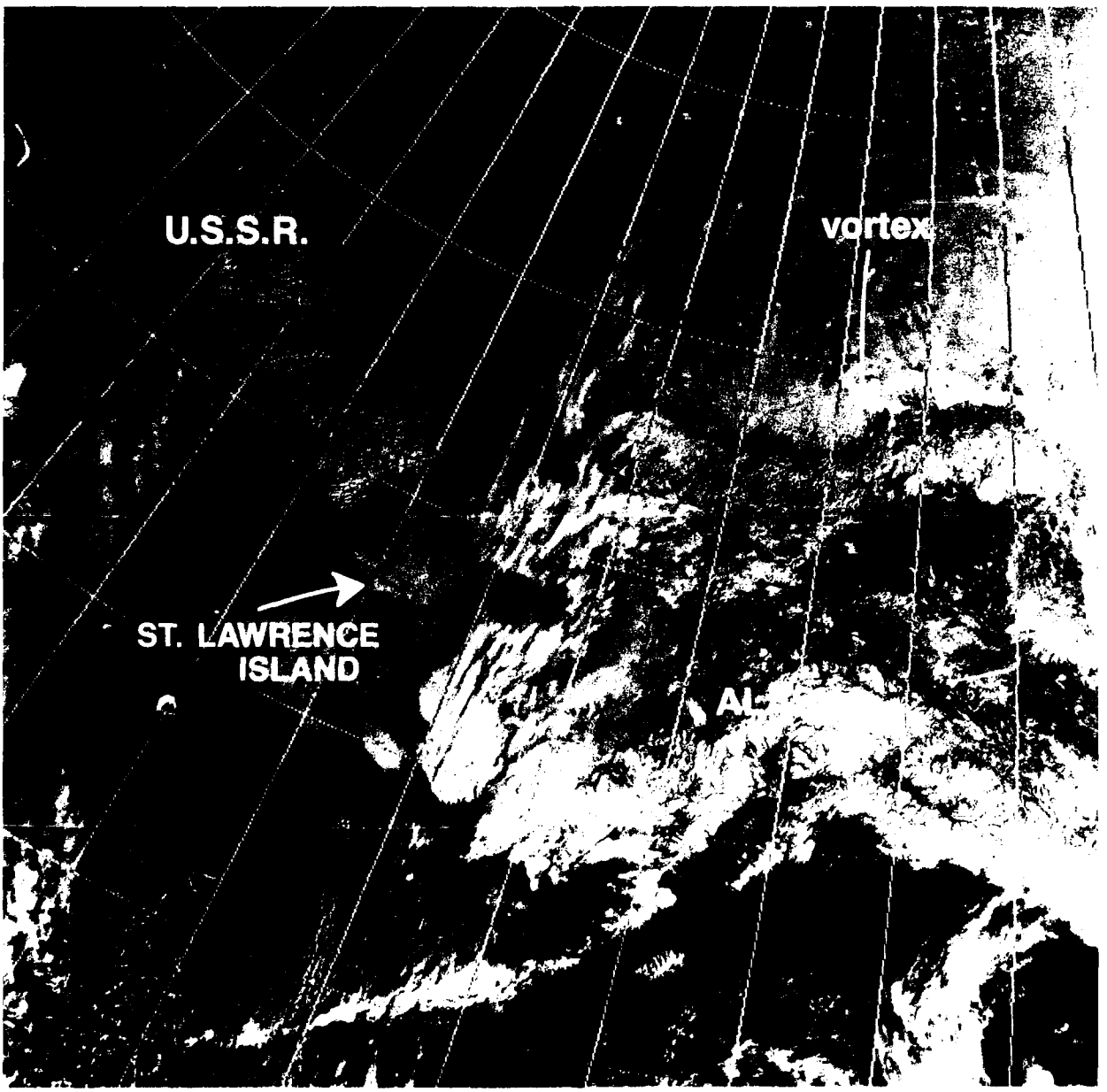

Figure 4-10. Visible Satellite Imagery, 1855 GMT 2 April 1989.

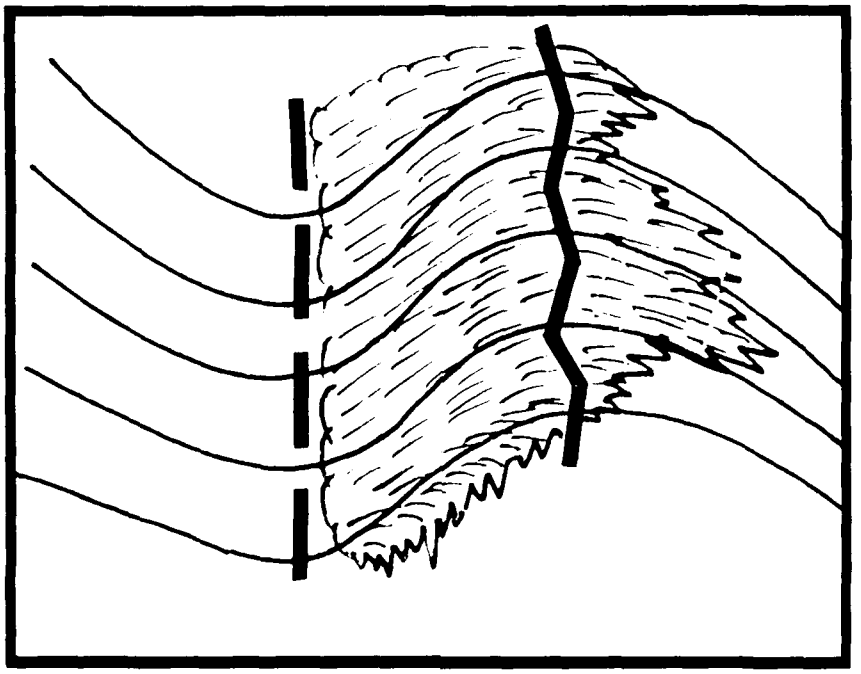

Figure 4-11. Schematic Cloud Pattern for a Short Wave (Weber and Wilderotter, 1981).

4.1.5 Summary

In conclusion, a comparison of interest is that of Barrow radiosonde observation (RAOB) soundings before and after the storm passage. Figure 4-12 is the sounding for 1200 GMT 30 March 1989, and Fig. 4-13 shows the 1200 GMT 2 April 1989 sounding. Comparison of the two soundings and the surface time series (Fig. 4-6) before and after the storm produces the following salient features:

1. Nighttime surface temperature warmed from about −21 °F to −7 °F (−29 °C to −22 °C) as skies changed from clear to cloudy, preventing nighttime loss of heat through long-wave radiation. The change in wind direction from southeast (offshore) to west-southwest (onshore) as the vortex moved past the station was probably an associated factor.
2. By contrast, midlevel temperatures cooled an average of 5 °C throughout most of the atmosphere below 450 mb.
3. Surface winds shifted from southeast to northwest, with little change in speed.
4. Winds aloft were westerly and appeared more southwesterly after storm passage.
5. Levels below 850 mb became saturated as low clouds moved into Barrow.

In some ways the weather changes associated with this frontal passage seem rather subtle compared to the normal diurnal changes in the Arctic. The latter changes can be far more pronounced than most fronts. The changes can be particularly large in Arctic coastal locations subject to land breeze and sea breeze effects. But, the difference is that after the frontal passage, nighttime temperatures tend to remain relatively high for several days due to cloud cover.

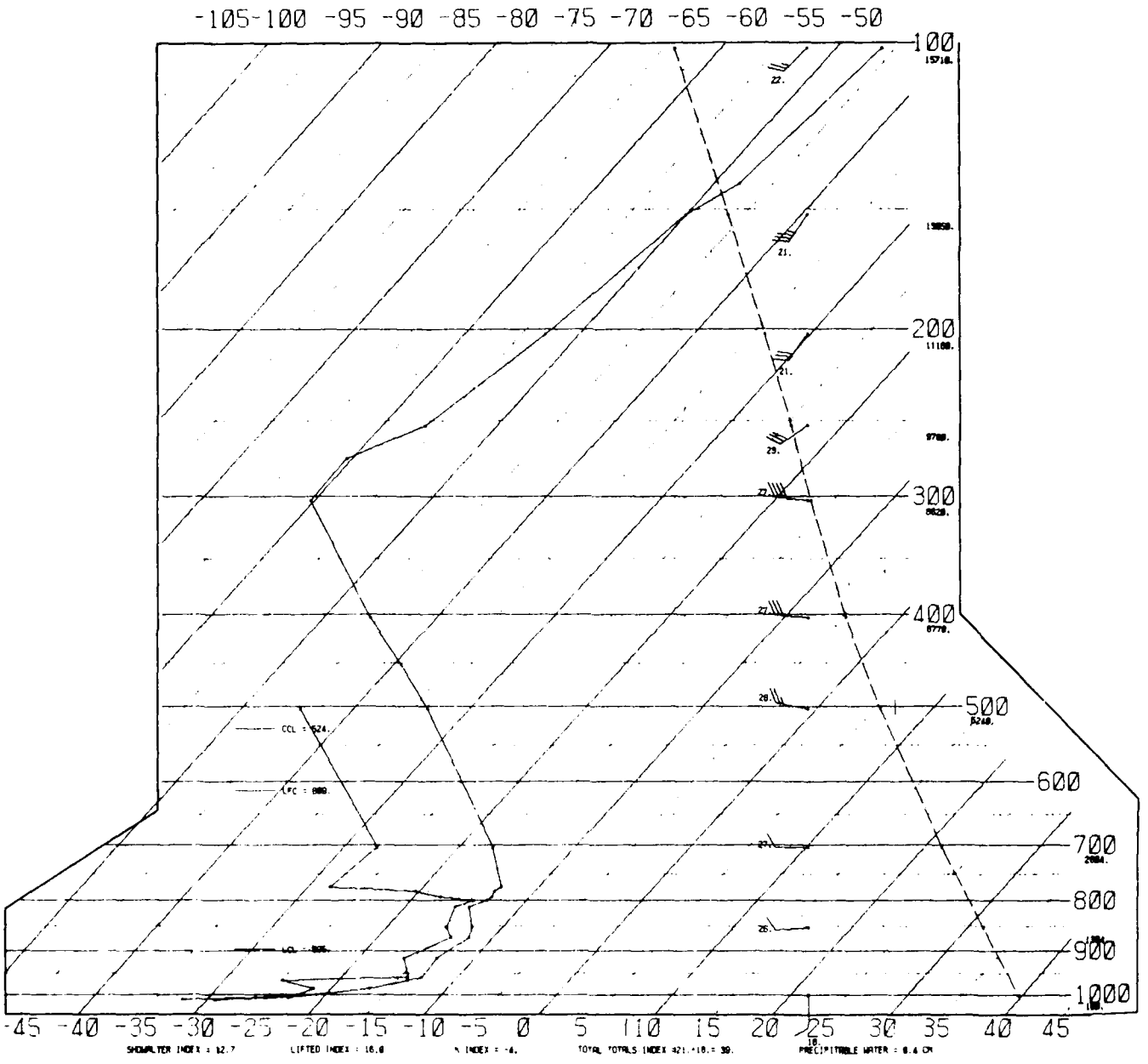

Figure 4-12. Barrow Sounding, 1200 GMT 30 March 1989.

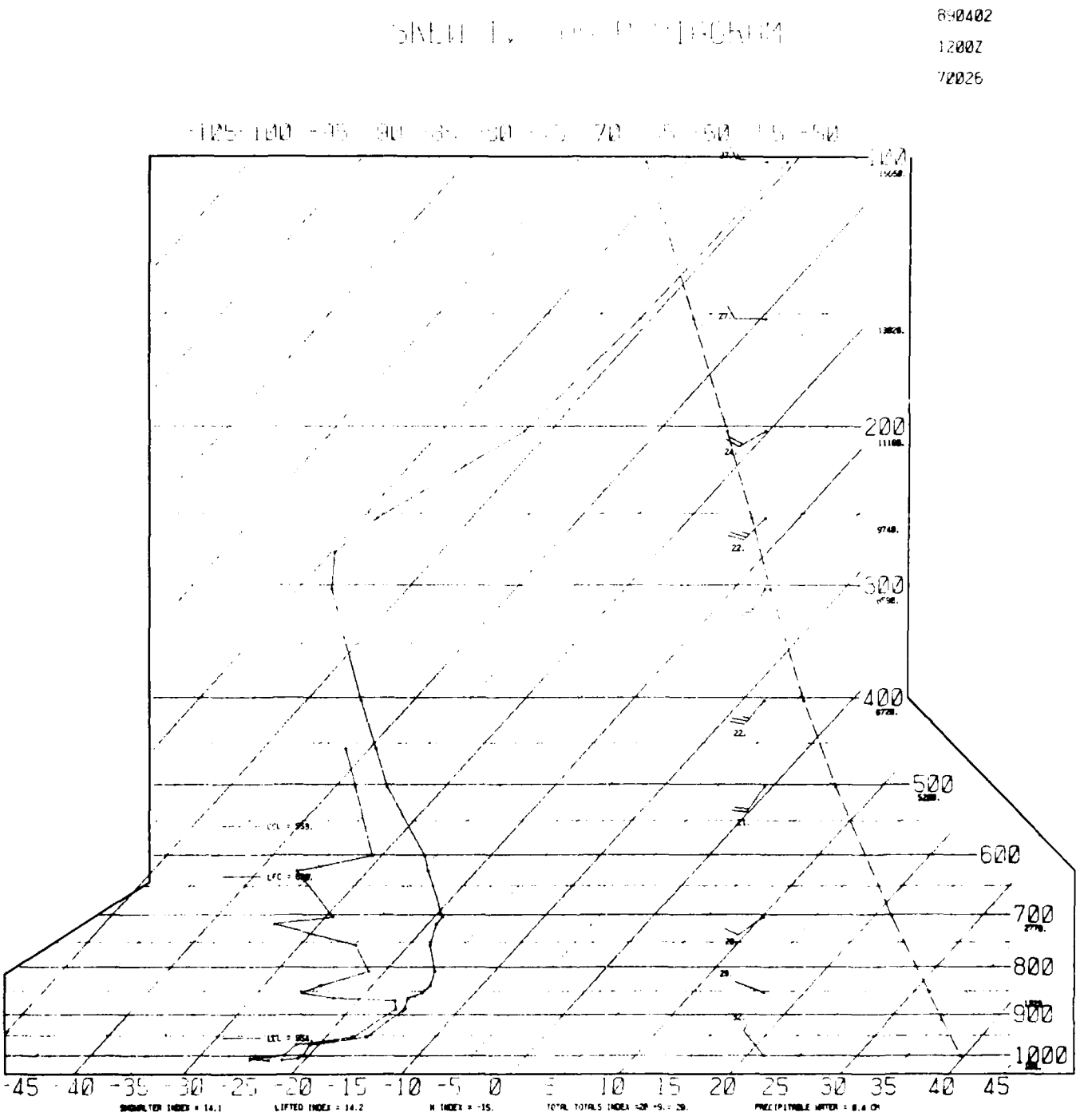

Figure 4-13. Barrow Sounding, 1200 GMT 2 April 1989.

4.2 Case II: Frontal Passage at Barrow, 15 February 1989

4.2.1 Introduction

As noted in the previous case study, diurnal changes of weather elements can often be as great or even greater than those caused by frontal passages. In the present study an impressive example of a frontal passage at Barrow, Alaska is diagnosed. In this particular case the frontal passage aloft behaved as a classical and well-defined cold front. At the surface, however, temperatures cooled as the front approached and warmed after the front passed.

The roles of wind direction, duration of sunlight, and cloud cover will be emphasized in investigating some unique properties of Arctic fronts. Surface and upper air charts are studied and satellite imagery is provided along with time sections of surface and RAOB at Barrow.

4.2.2 Initial Frontal Location and Structure

Figure 4-14 is the surface chart for the Alaska region at 0000 GMT 15 February 1989. In the vicinity of the Chukchi Sea and Alaska (see locator map, Fig. 4-1) an east-west trough appears just southwest of Barrow. Contrast the southeast wind at Barrow with the southerly winds south of that station. The wind shift aids in the location of the trough line. The relatively strong temperature gradient north of the trough is also noteworthy.

Infrared satellite imagery near this time is given in Fig. 4-15 and shows Barrow to be located under the frontal cloud band. The 850-mb chart (Fig. 4-16) shows a weak, warm trough, highlighted by the $-5\,^{\circ}C$ isotherm, just north of Barrow. Otherwise, little evidence supports a thermal gradient or front approaching Barrow at this level. Obviously, however, a previous front passed Barrow earlier and is approaching Banks Island at this time since the thermal gradient is strong in that area.

Looking at the 700-mb chart (Fig. 4-17), a significant thermal gradient southwest of Barrow is noted. This feature suggests that an upper front exists in this area and may be approaching Barrow at 0000 GMT 15 February 1989.

To confirm this approaching front, the 500-mb chart (Fig. 4-18) shows a pronounced thermal gradient in the same area at that time. Since the leading edge of the gradient is in approximately the same position at both levels, a conclusion could be drawn that the front was nearly vertical in the region between 700 and 500 mb. In any case good evidence here supports an upper front approaching Barrow at 0000 GMT 15 February 1989.

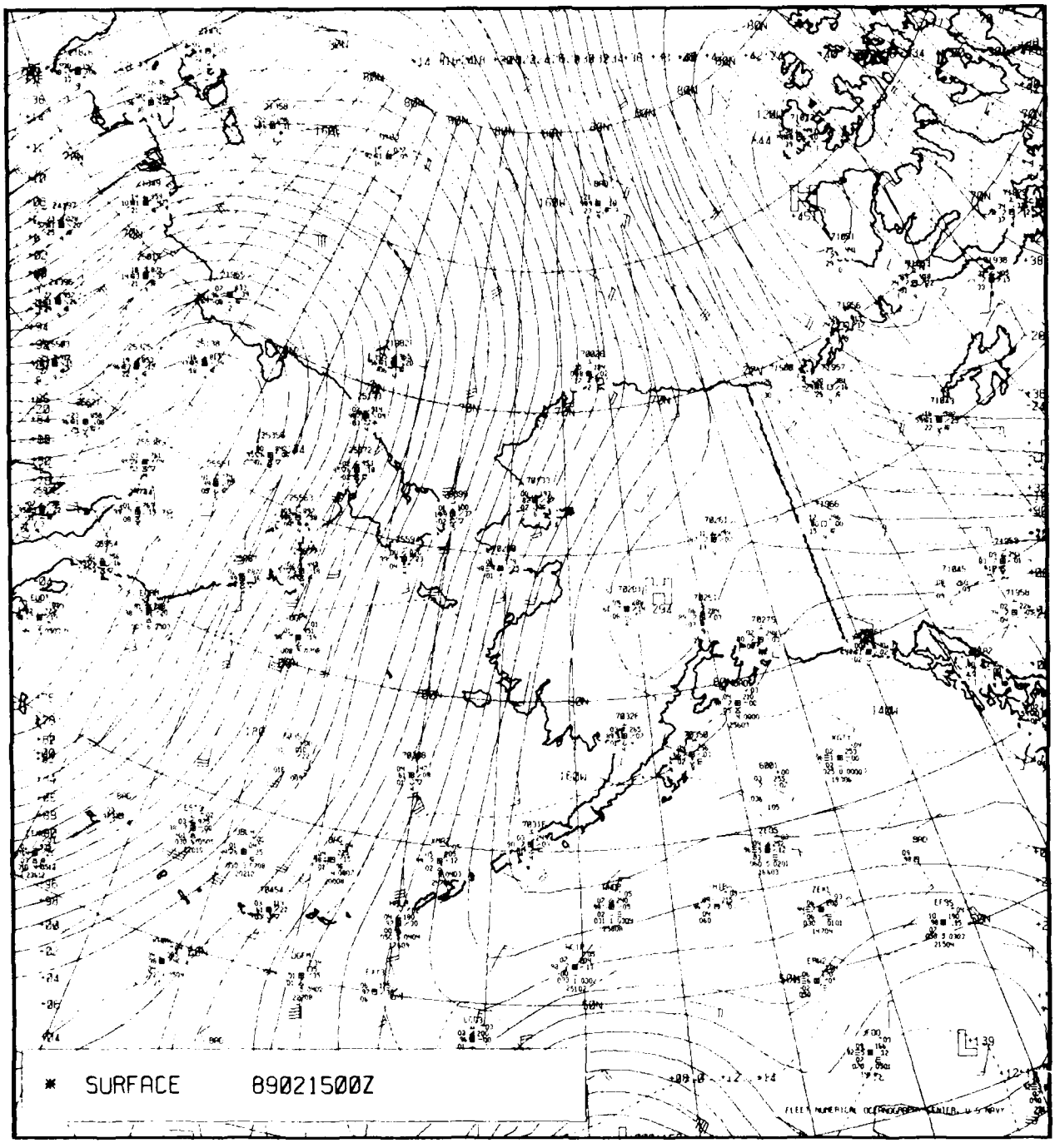

Figure 4-14. FNOC Surface Chart, 0000 GMT 15 February 1989.

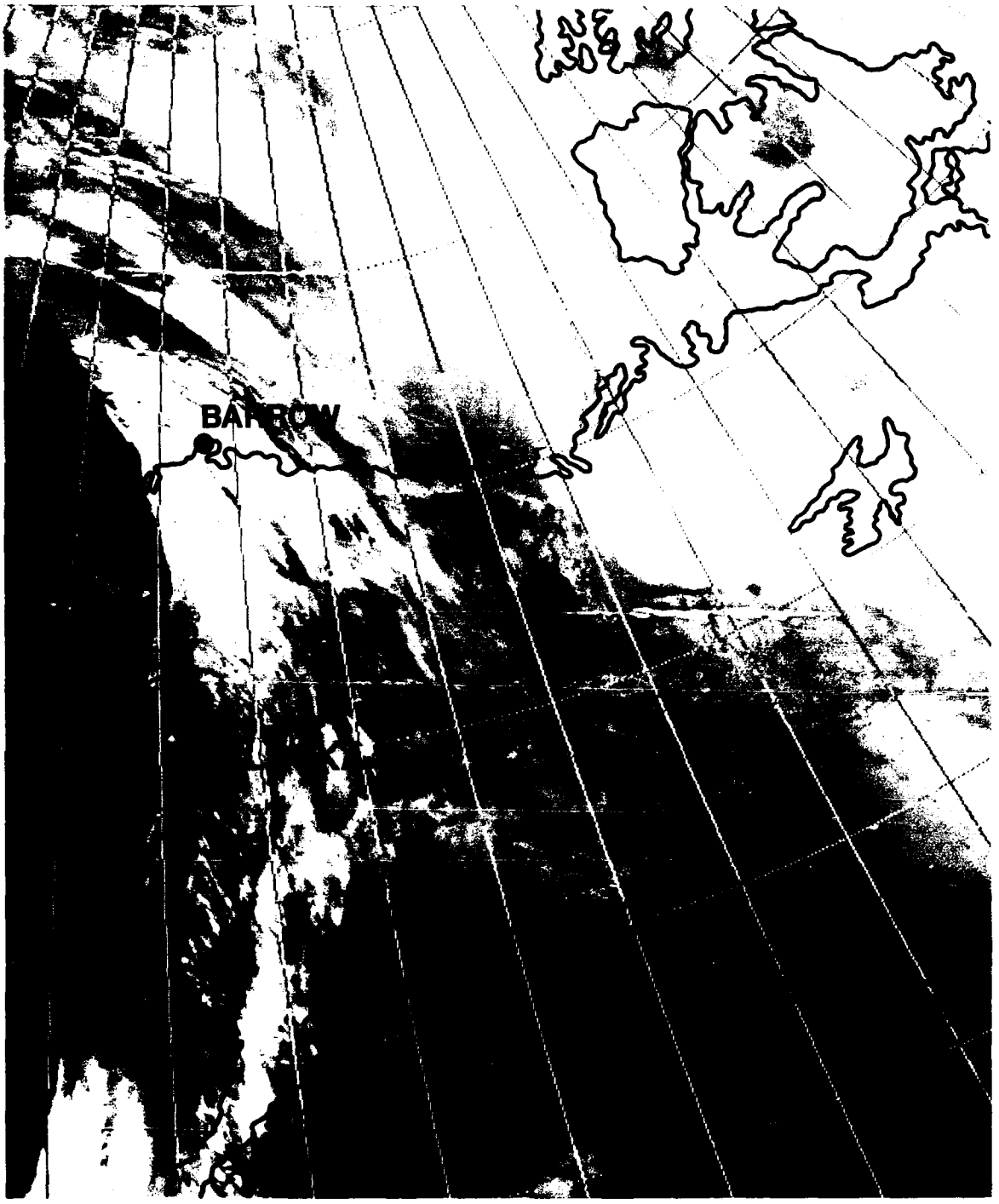

Figure 4-15. IR Satellite Imagery, 0359 GMT 15 February 1989.

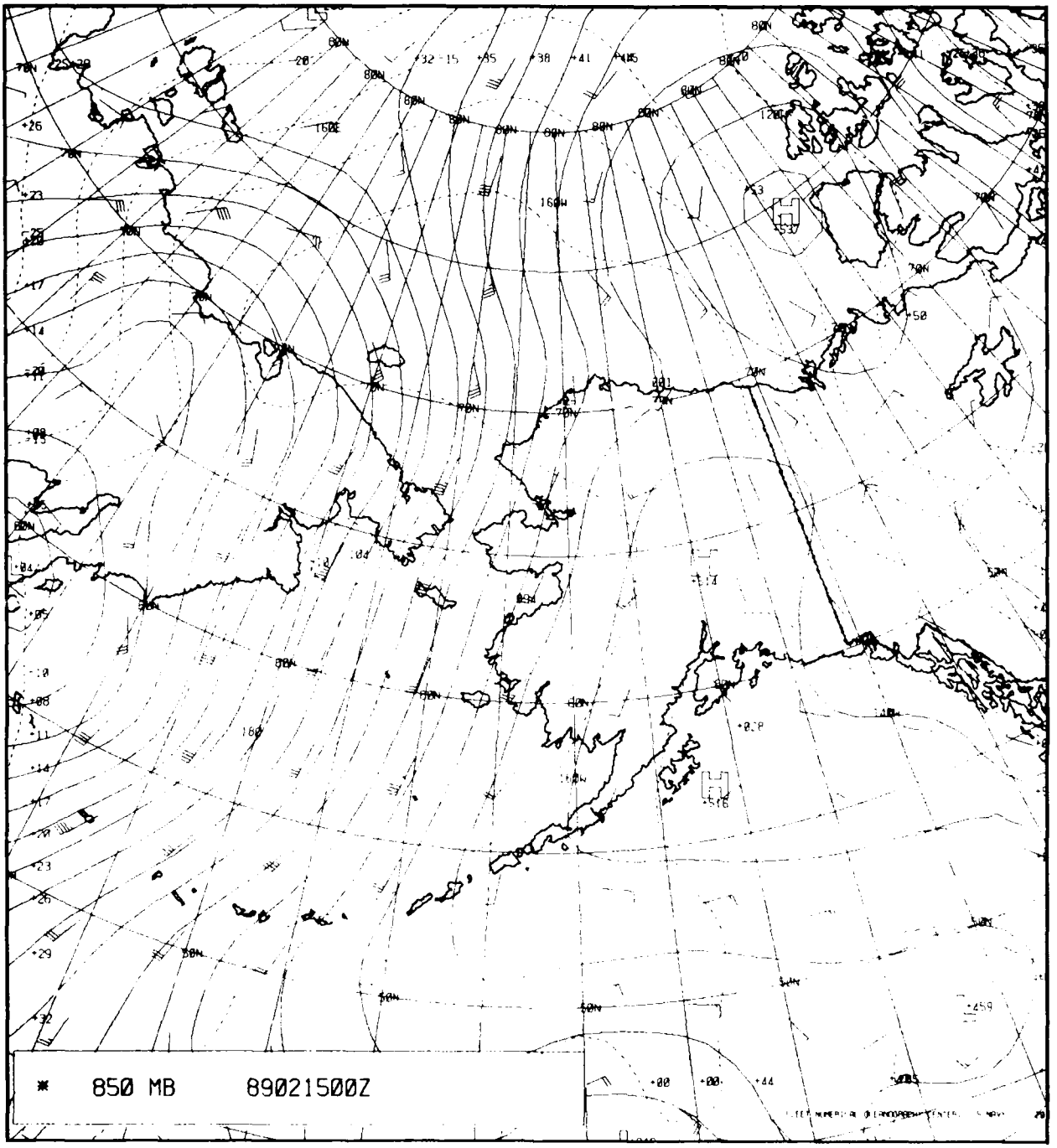

Figure 4-16. FNOC 850-mb Chart, 0000 GMT 15 February 1989.

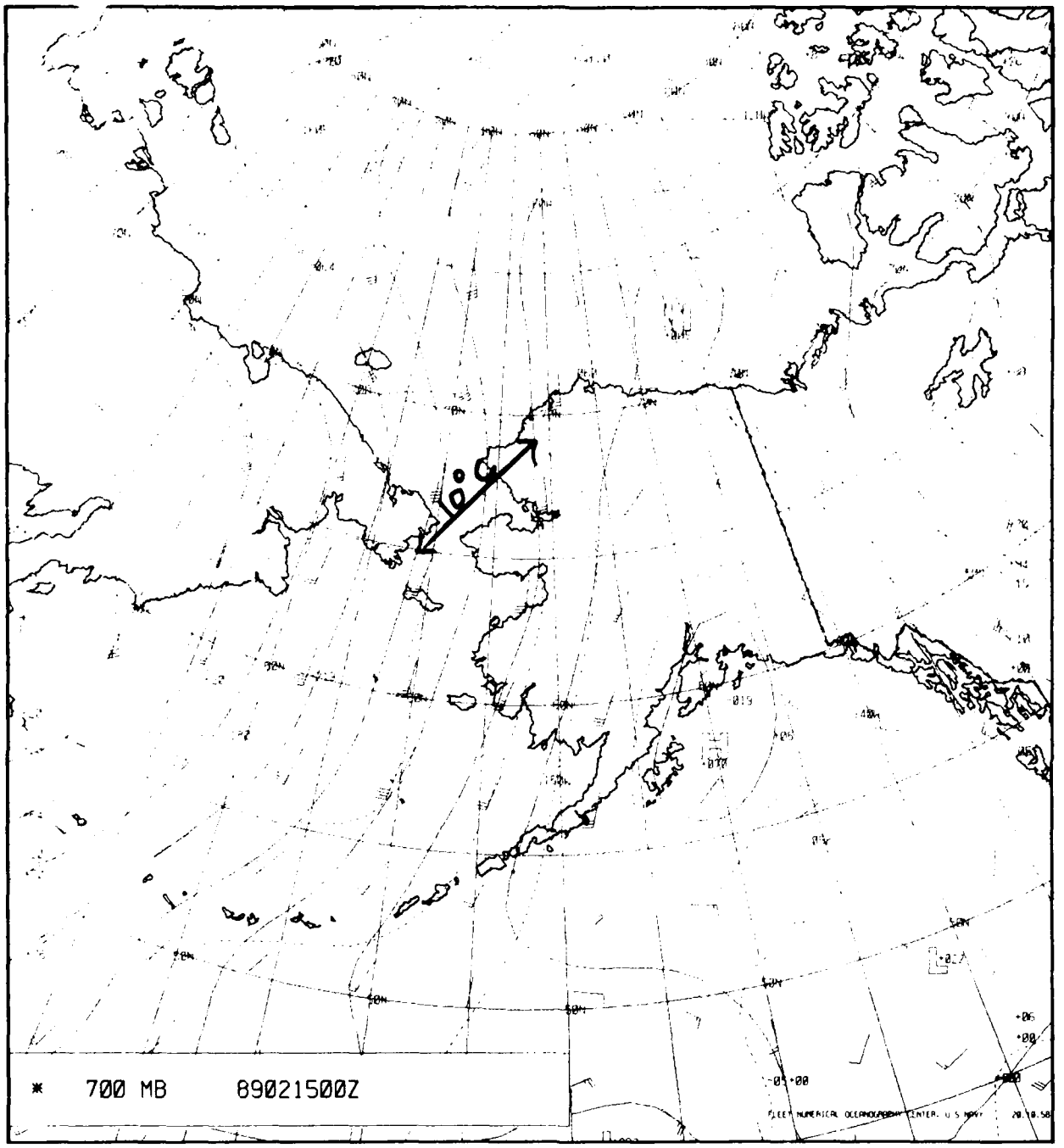

Figure 4-17. FNOC 700-mb Chart, 0000 GMT 15 February 1989.

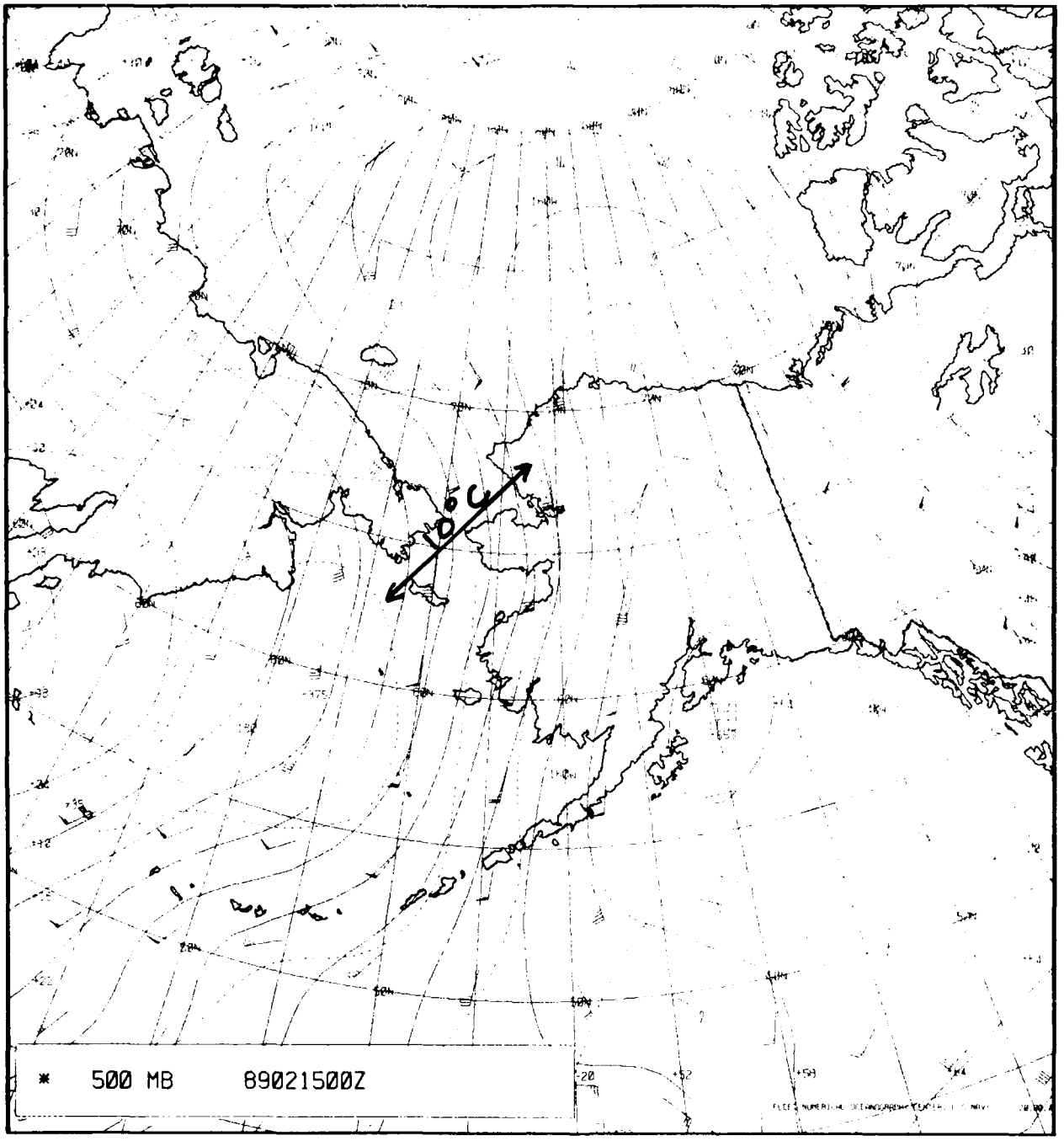

Figure 4-18. FNOC 500-mb Chart, 0000 GMT 15 February 1989.

The sounding for Barrow at 0000 GMT on the 15th, as shown in Fig. 4-19, indicates a strong low-level inversion and southerly winds from the surface to 250 mb. Between 1000 mb and 800 mb, the sounding is nearly isothermal. This evidence is weak for the proximity of a frontal zone. The dewpoint curve suggests some low- and high-level cloudiness, but dry air in the midlevels.

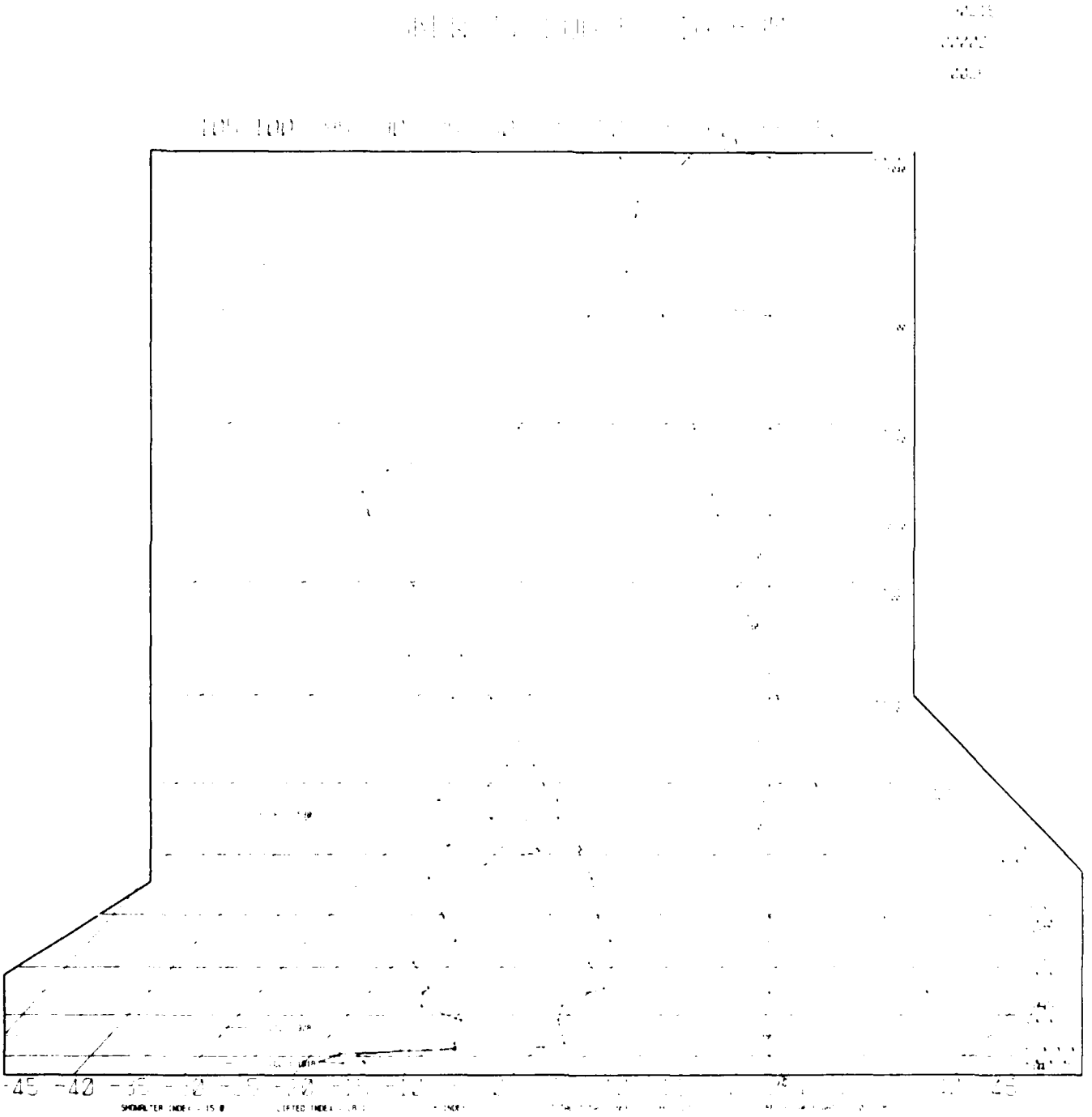

Figure 4-19. Barrow Sounding, 0000 GMT 15 February 1989.

At this point it is useful to examine the time series of surface weather conditions at Barrow. In Fig. 4-20, note that at 0000 GMT on the 15th, the temperature is 5 °F (−15 °C), the wind is from the southeast at 22 kt, and drifting snow is reported with overcast skies and low and high cloudiness.

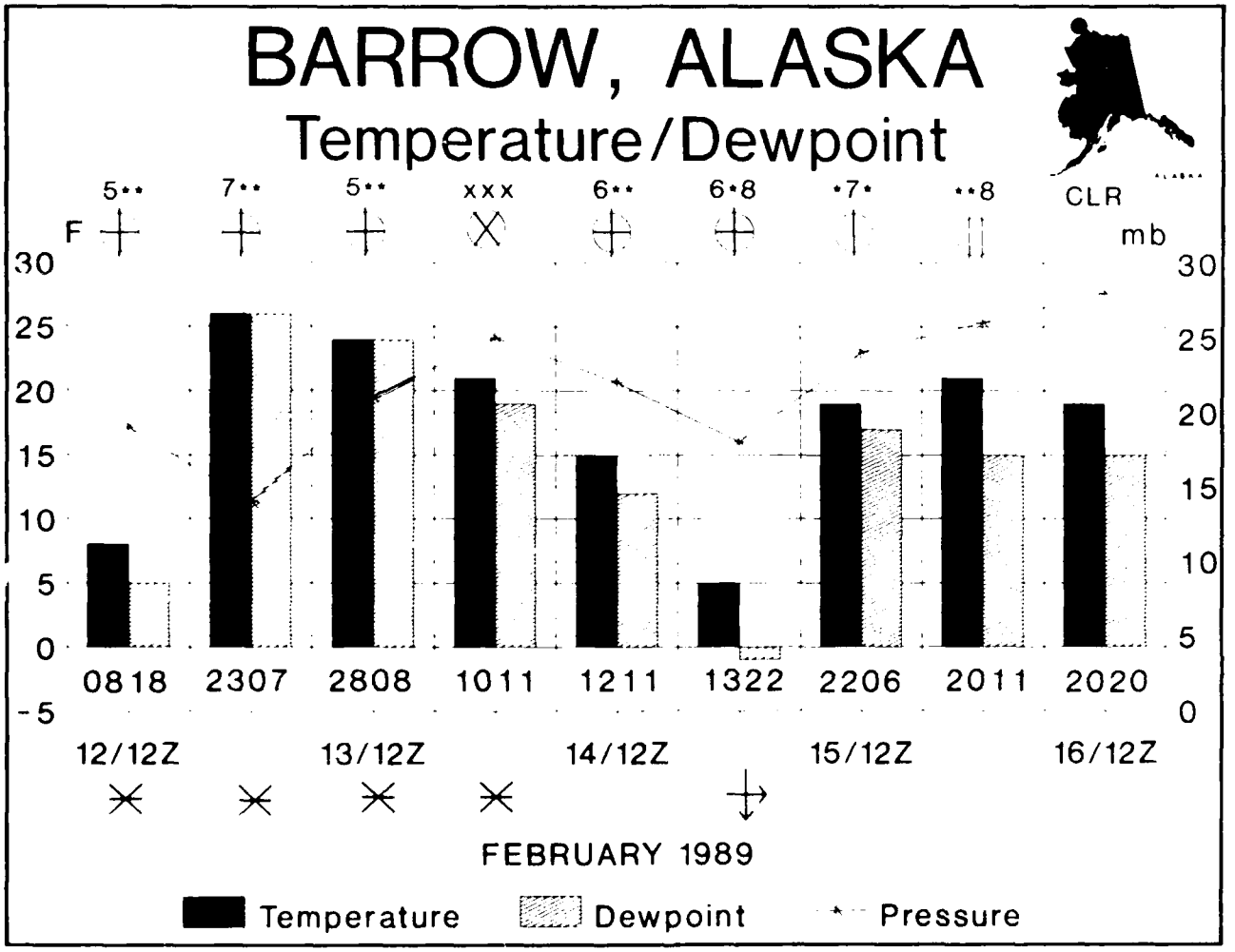

Figure 4-20. Time Series of Surface Weather for Barrow, Alaska. (Left ordinate is temperature [°F], right ordinate is pressure [mb], and cloud type [low, mid, high] appears above the sky cover symbol. Wind direction and speed [DDFF in tens of degrees and knots] are shown in the block below temperature/dewpoint data. Present weather symbols are shown below the date/time group information.)

Prior to 0000 GMT on the 15th, surprisingly, falling pressures were accompanied by falling temperatures. Normally, rising temperatures are expected on the approach of a surface cold front. The low pressure at 13/0000 GMT suggests an earlier frontal passage and will not be described here.

After the lowest pressure and temperature had been reached at Barrow on the 15th, skies began to clear, the wind shifted into the southwest, and temperatures rose dramatically. Again, a normal cold frontal passage would be accompanied with falling temperatures. Clearly, a careful diagnosis of the situation is indicated inasmuch as these anomalous temperature changes associated with this cold front are quite unexpected in midlatitude cyclones.

4.2.3 Vertical Structure of the Front

Figure 4-21 is a vertical time section of the Barrow RAOB for the period 1200 GMT 12 February through 1200 GMT 16 February 1989. Prior to the frontal passage near 0000 GMT on the 15th, the lower atmosphere was characterized by considerable stability as noted by the horizontal and vertically packed isentropes (isopleths of potential temperature) in the time section.

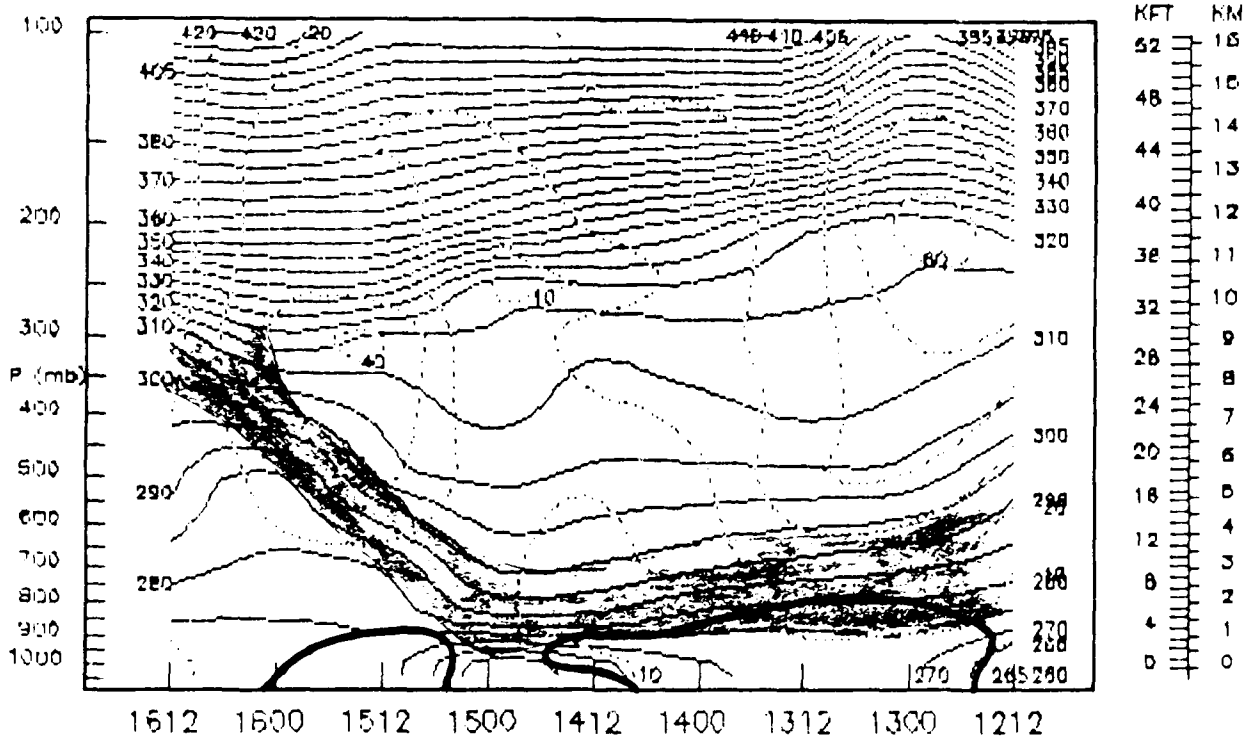

Figure 4-21. Vertical Time Section for Barrow, Alaska, 1200 GMT 12 February through 1200 GMT 16 February 1989. (Solid lines are isopleths of potential temperature [K], dotted lines are isotachs [m/s], the dark solid line represents the mixing ratio equal to 2g/kg, and the frontal zone is shaded.)

The surface cooling, mentioned earlier, was obviously accompanied by some low-level drying as revealed by the gradual lowering of the 2 g/kg line. Low-level winds were relatively light but reached a maximum of 20 kt at the surface at 0000 GMT 15 February 1989 (Fig. 4-20).

After the frontal passage, the most dramatic change occurred in the stability of the lower levels beneath 500 mb (large spacing between potential temperature lines indicates more unstable conditions). This destabilization almost certainly produced a good deal of mixing in the lowest 500 mb, with the result that the soundings before and after the frontal passage look quite different. A comparison of the two soundings at 0000 GMT (Fig. 4-19) and 1200 GMT 15 February 1989 (Fig. 4-22) shows the effects of the mixing. The earlier

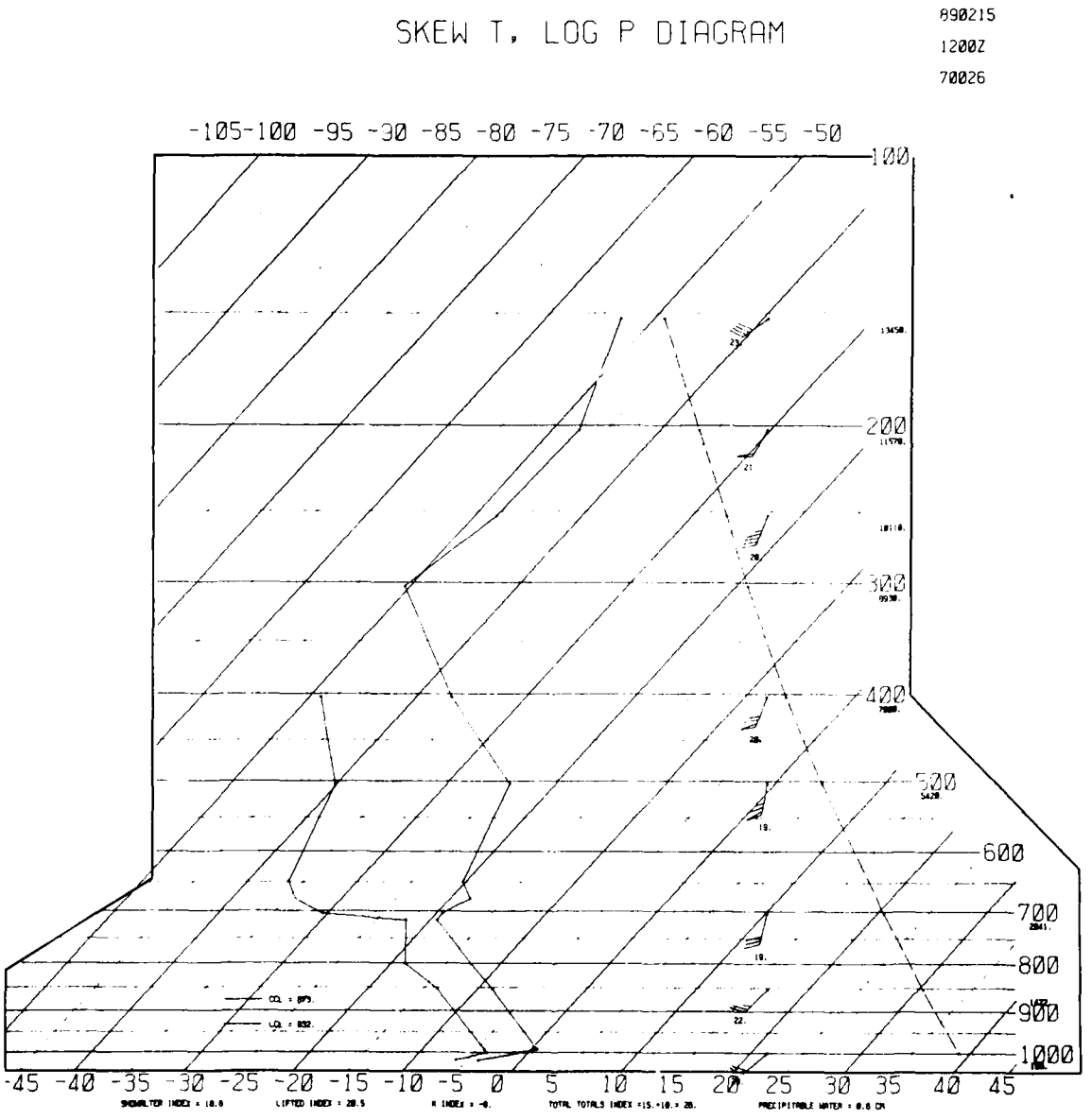

Figure 4-22. Barrow Sounding, 1200 GMT 15 February 1989.

sounding shows a strong, shallow inversion at Barrow, with a surface temperature of 5 °F (−15 °C) and 36 °F (2 °C) at the top of the inversion at 970 mb. The later sounding shows a surface temperature of 19 °F (−7 °C), while above the inversion there is deep cooling. Apparently mixing had brought considerable amounts of warm air down to the surface while appreciable cooling occurred aloft.

The vertical wind shear on the soundings shows slight warm advection at 0000 GMT near the surface (wind is veering with height between 1000 and 850 mb). In contrast, the 1200 GMT sounding suggests moderate cold advection (backing winds) between 850 and 500 mb. Moreover, the surface wind direction at Barrow changed from southeast to southwest (Fig. 4-20) after the frontal passage. The possibility exists that this change in wind direction may have brought in air, warming through compression, from higher elevations to the south and west.

At least three mechanisms may have contributed to the postfrontal warming at the surface in Barrow:

1. Mixing of warm air downward through the inversion.
2. Warm advection near the surface and cold advection aloft.
3. Surface wind shift that produced downslope warming.

Returning to Fig. 4-21, confirmation of the continuity of the front (both temporally and spatially) is possible. At 1200 GMT 15 February 1989 the Barrow sounding (Fig. 4-22) shows this front as a nearly isothermal layer between 700 and 500 mb. The frontal structure shows good agreement between the soundings and the vertical time section. The reader may want to study them carefully. Note also that the tropopause (the bottom of the packed isentropes) descended from about 250 mb at 0000 GMT on the 15th to nearly 300 mb at 1200 GMT on the 15th.

Finally, the clearing of the cloud cover after the frontal passage probably has only a small effect on the local surface temperature changes. The impact is lessened because, in mid-February, Barrow is still under the influence of the polar night and in almost total darkness throughout the day.

4.2.4 Tracking the Front Eastward

The IR imagery (Fig. 4-23) shows that the cloud band associated with the front under discussion has not yet passed over Barrow at 0716 GMT on the 15th. The intensity of the IR imagery suggests very cold clouds (i.e., cirrus) over Barrow. Precipitation was not observed at Barrow and convective type clouds may or may not be embedded in the cirrus at this time. The time series (Fig. 4-20) indicates that some clearing of the cloud cover had begun at Barrow prior to 1200 GMT 15 February 1989. Figure 4-24, the IR satellite imagery for 1411 GMT, confirms the clearing since the frontal cloud band at this time is past Barrow.

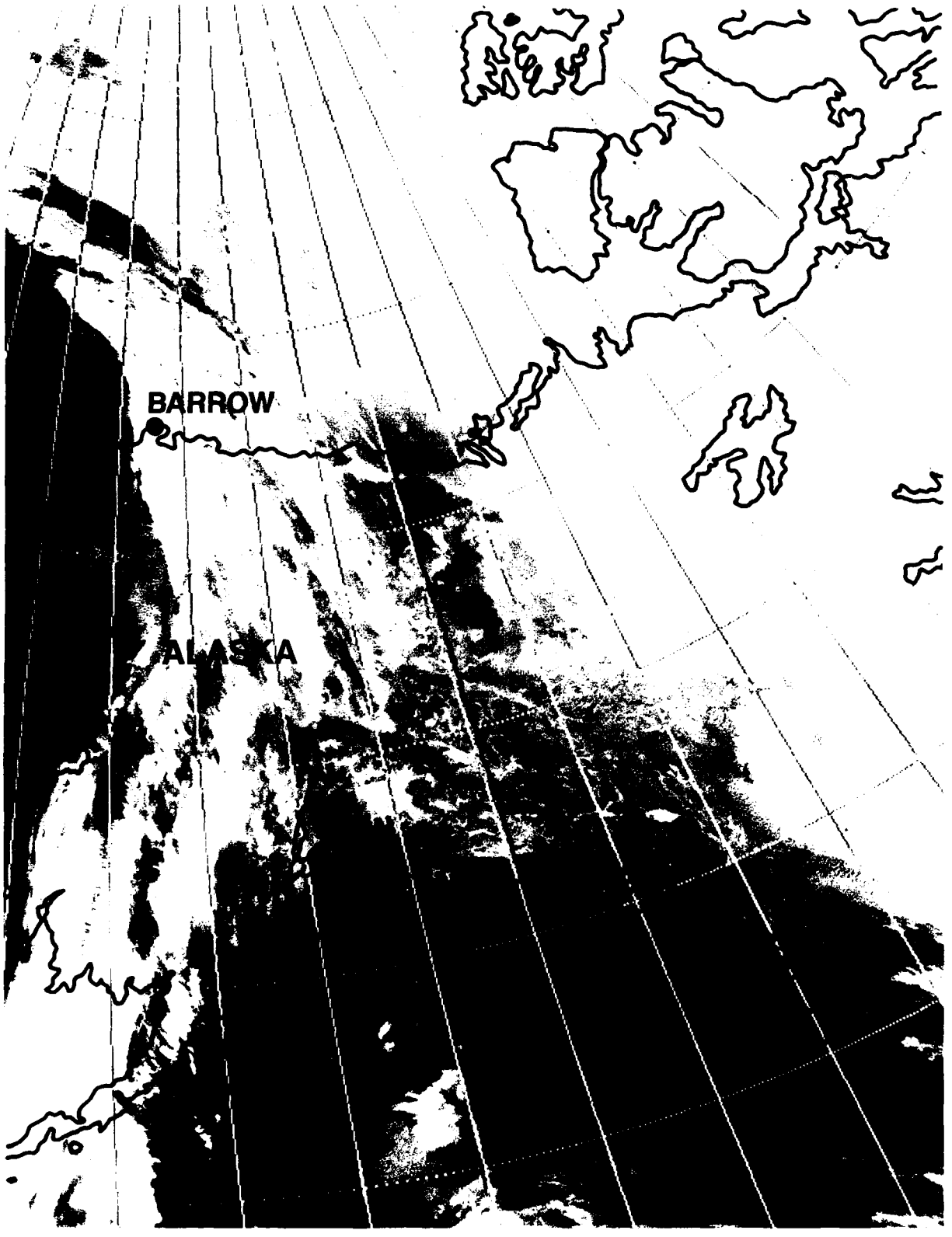

Figure 4-23. IR Satellite Imagery, 0716 GMT 15 February 1989.

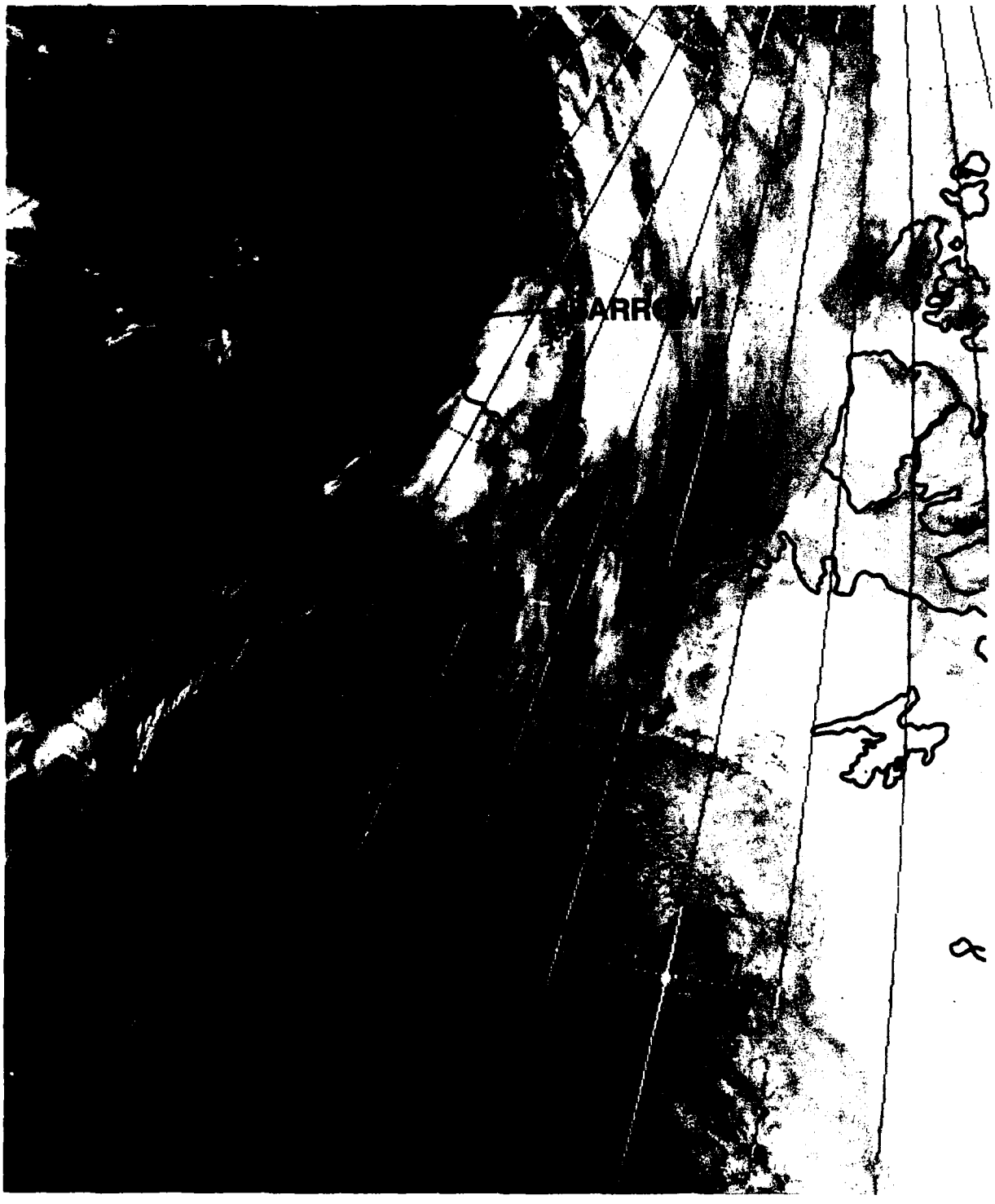

Figure 4-24. IR Satellite Imagery, 1411 GMT 15 February 1989.

Figures 4-25 throuth 4-29 include the surface and upper air charts for 0000 GMT 16 February 1989. They are included for purposes of noting the horizontal thermal structure of the front as it moves eastward toward Banks Island. Since the isentropes of the vertical time section for Barrow (Fig. 4-21) can be translated into isotherms on constant pressure surfaces, the time section can be easily compared with the constant pressure isotherm gradients in the vicinity of the front.

Some highlights of an inspection as suggested are

1. The surface frontal position is well east of Barrow at 0000 GMT 16 February 1989. A very stable, low-level layer remains near the surface at all subsequent times. This stability suggests that the cold air never mixed *all the way down* to the surface and helps explain the lack of cooling associated with this frontal passage at the surface. Some low-level mixing is not precluded, however, through the inversion just above the surface. Note that in the two soundings warming below and cooling above occur near the inversion base.
2. At 850 mb, no evidence supports a thermal gradient in the vicinity of Barrow (Fig. 4-26); this lack of evidence is consistent with the vertical time section (see Fig. 4-21) that shows only horizontal isentropes spread apart in the vertical and suggests relatively unstable conditions.
3. The 700-mb chart, Fig. 4-27, also shows that Barrow is not in the stronger temperature gradient at this level. This evidence is supported in the vertical time section as well. By contrast and to show the three-dimensional consistency between the horizontal charts and the vertical section, in Fig. 4-28, the 700-mb chart for 1200 GMT 15 February 1989 at Barrow is still in the stronger temperature gradient and between the $-15\,^{\circ}C$ and $-20\,^{\circ}C$ isotherms, agreeing with the time section.
4. Again, both the time section and the 500-mb chart (Fig. 4-29) show a well defined upper front over Barrow at 0000 GMT 16 February 1989.

4.2.5 Summary

Weather changes at the surface in the Arctic are often masked by large, low-level stability that allows local effects to predominate over classical frontal behavior. Time of day, wind shifts from land to sea, and cloud cover often dictate surface weather changes. These local effects can lead the unwary forecaster to minimize the effect of frontal passages on weather changes above the surface and/or misinterpret consequences of the frontal passage.

This case study shows that in spite of rather ambiguous weather changes at the surface, fronts aloft can be very strong indeed. The strong upper front depicted in this study suggests that upper fronts are common and strong in the Arctic. The significance of these strong upper fronts is that, although surface weather changes may be rather innocuous, fronts aloft may introduce large gradients of potential vorticity and wind shear. These gradients and shears may be dangerous to aircraft inasmuch as they are often related to clear air turbulence, icing, and other hazards to aircraft.

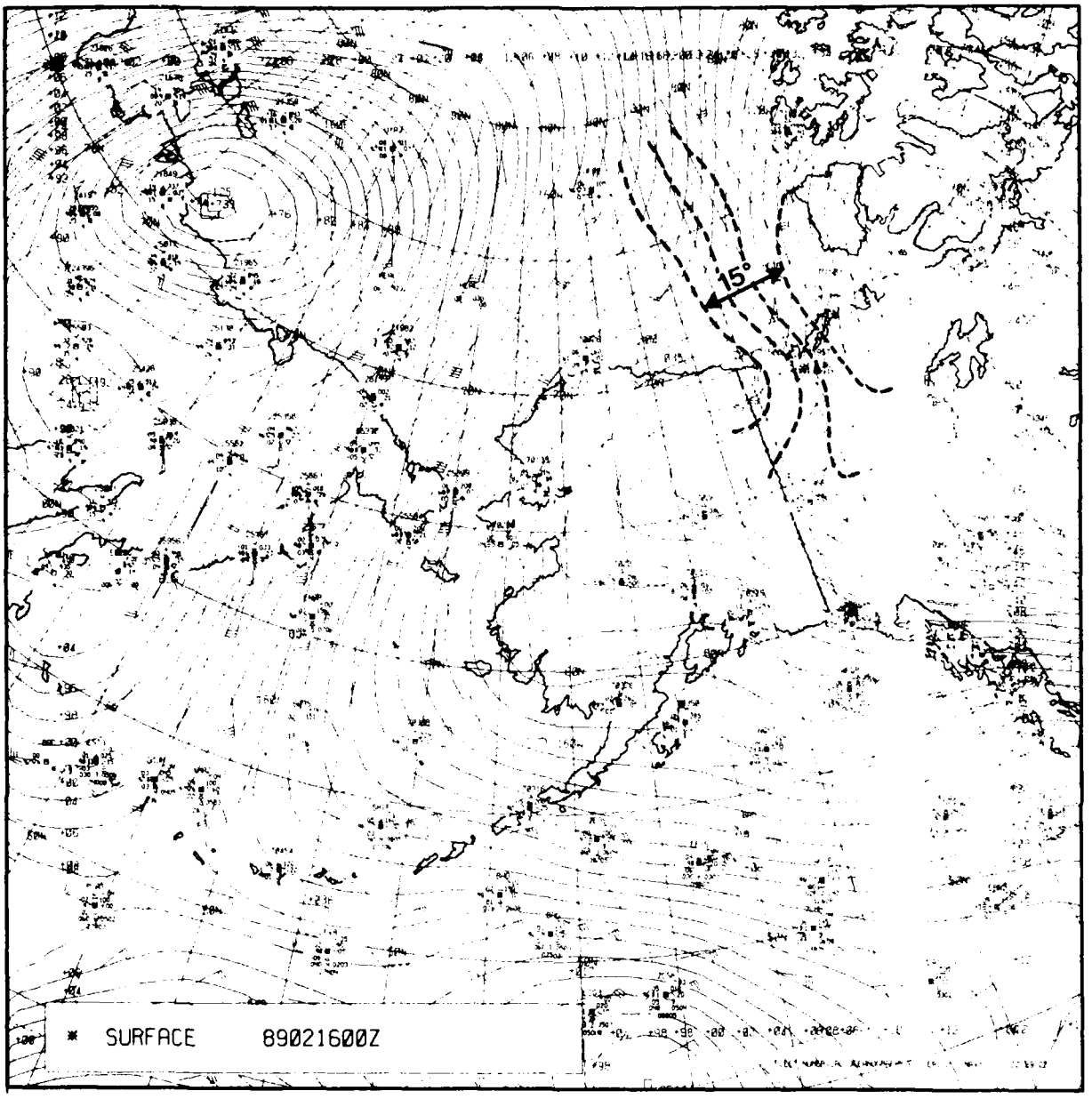

Figure 4-25. FNOC Surface Chart, 0000 GMT 16 February 1989.

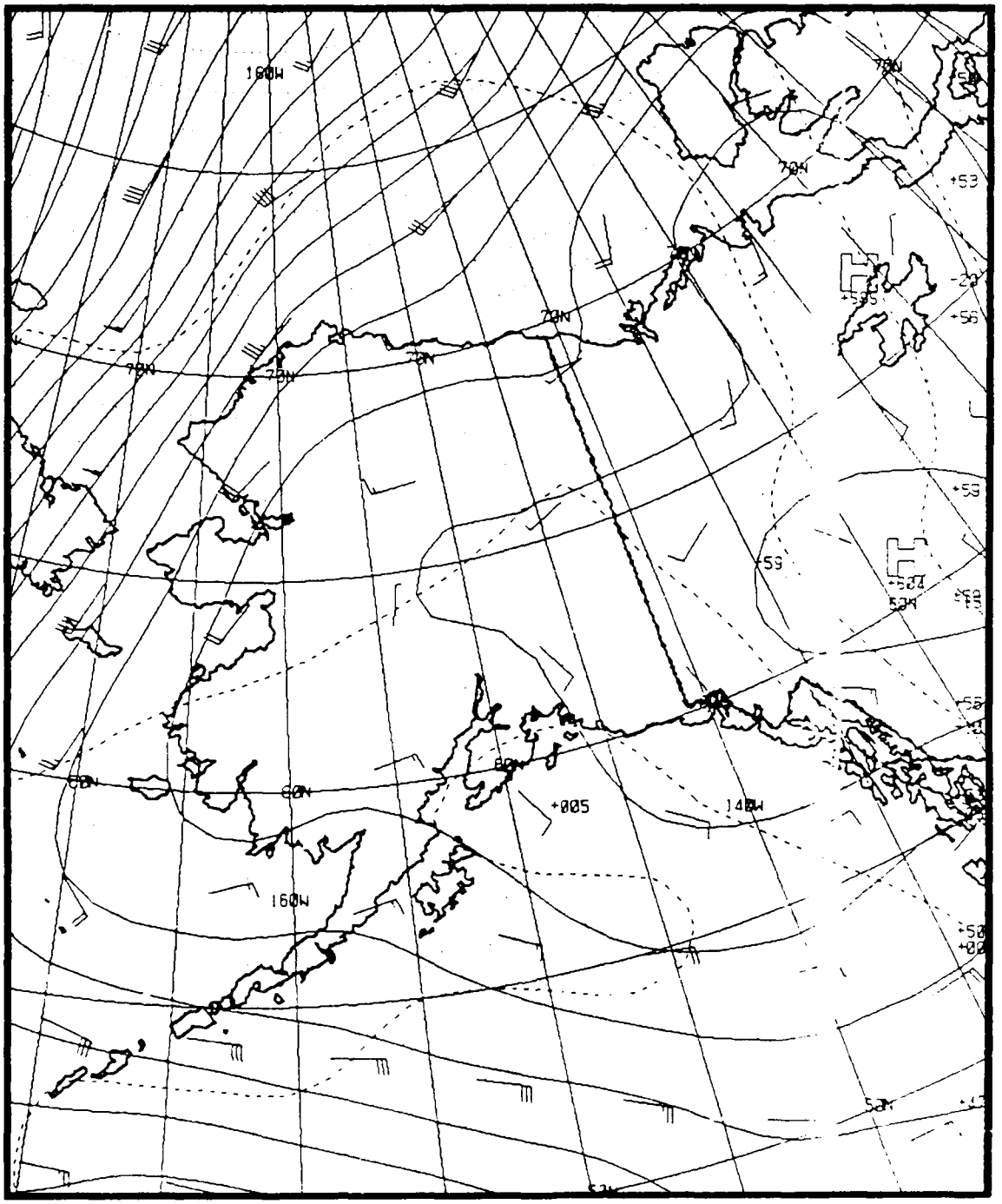

Figure 4-26. FNOC 850-mb Chart, 0000 GMT 16 February 1989.

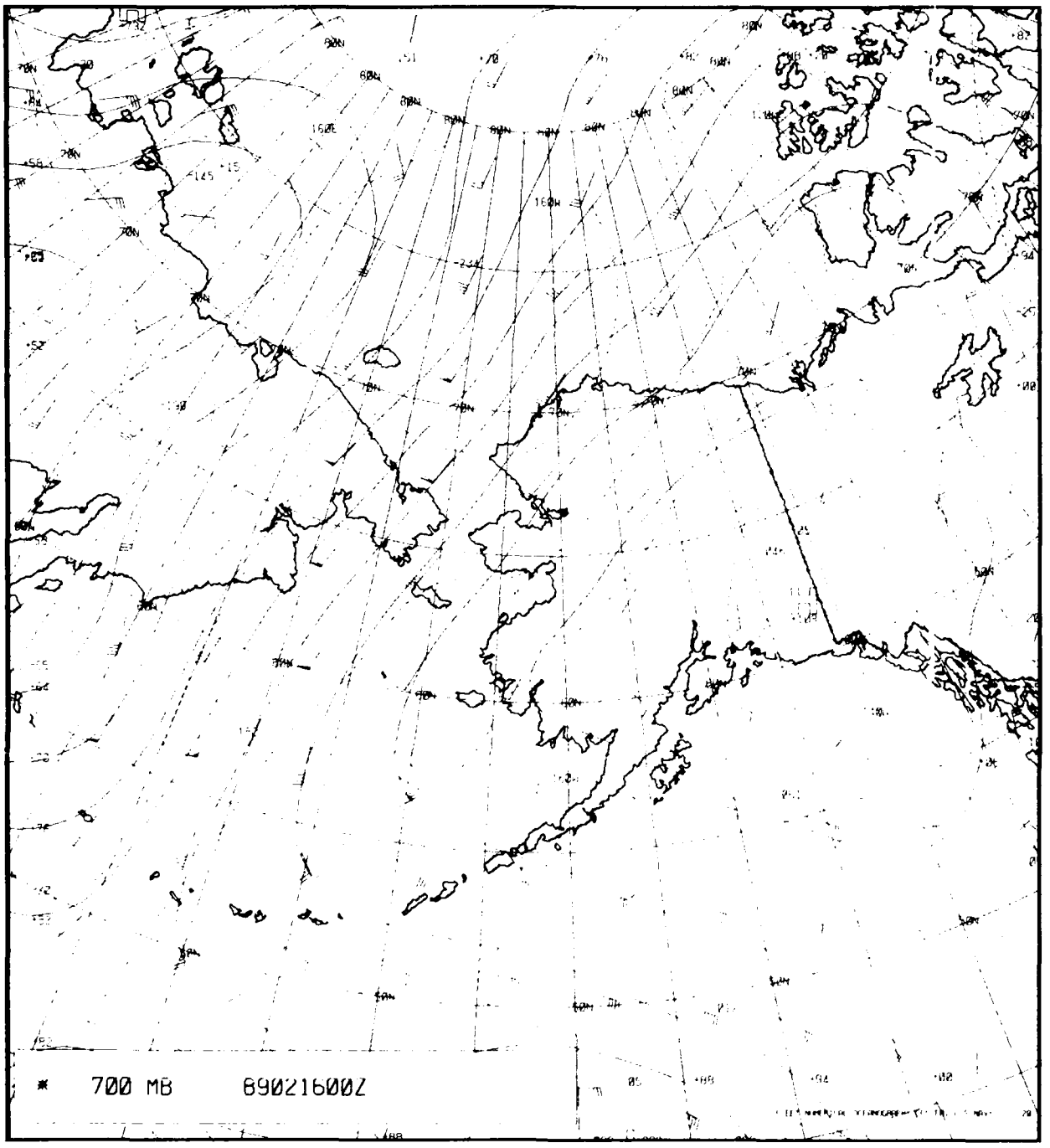

Figure 4-27. FNOC 700-mb Chart, 0000 GMT 16 February 1989.

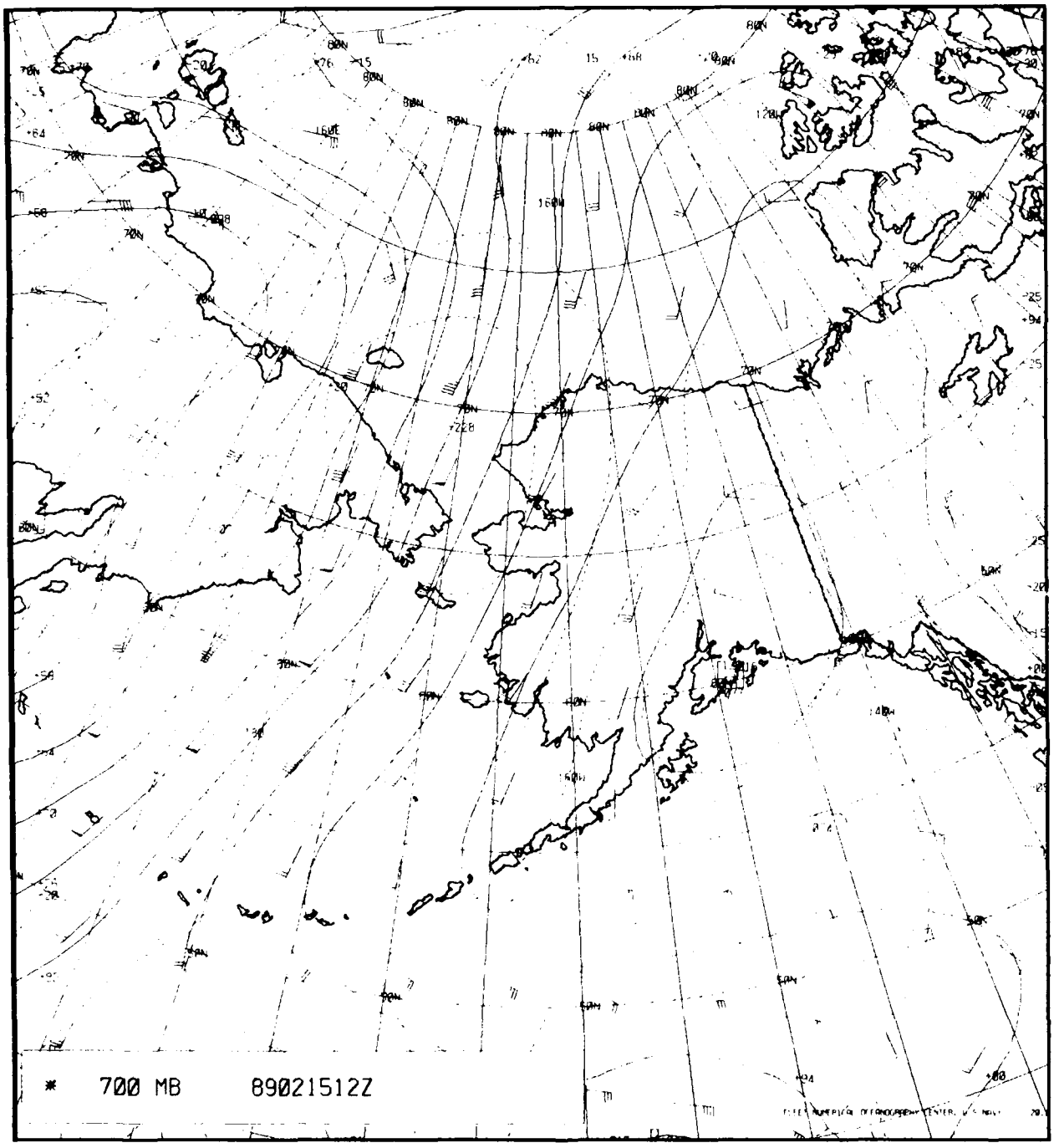

Figure 4-28. FNOC 700-mb Chart, 1200 GMT 15 February 1989.

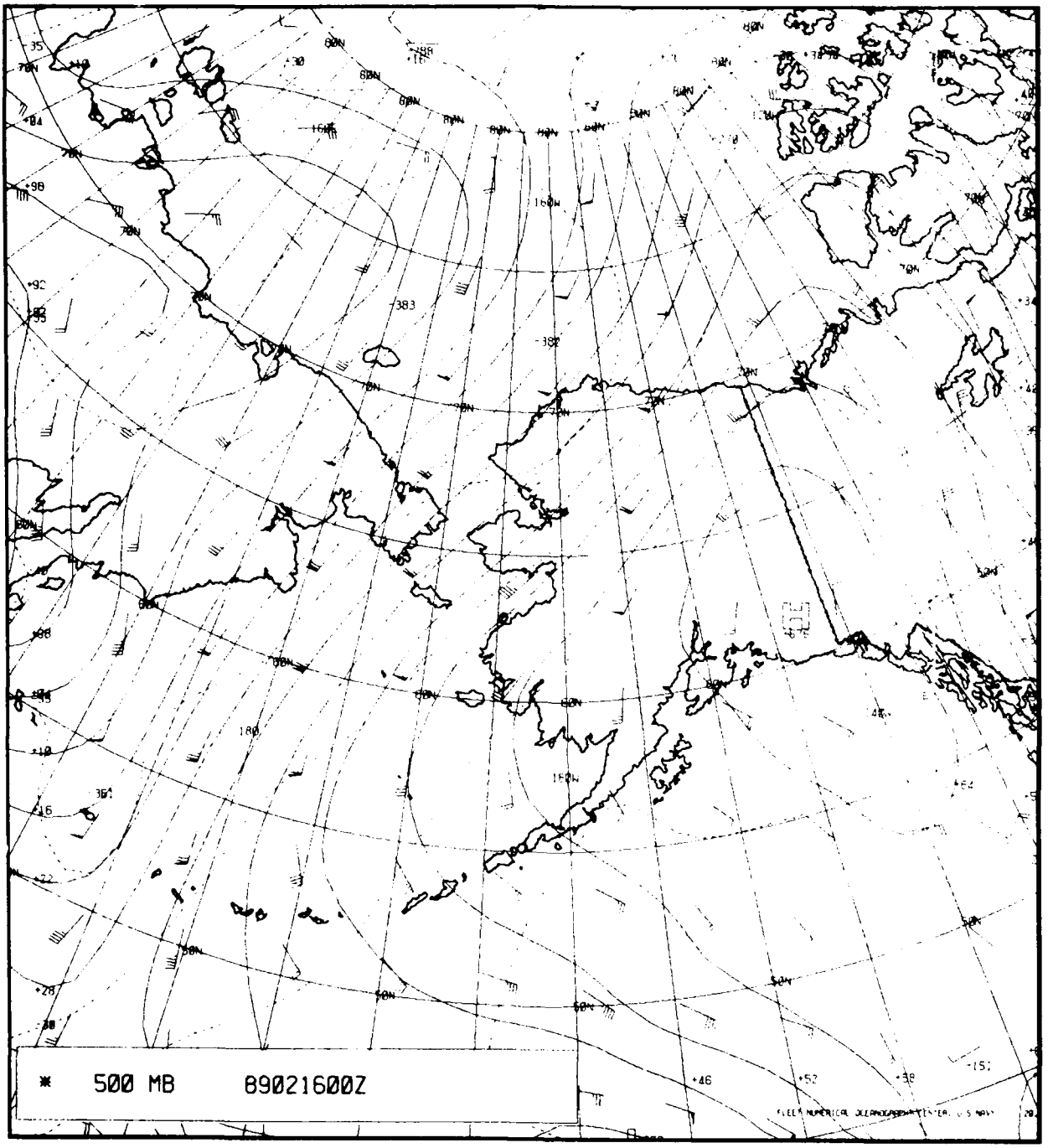

Figure 4-29. FNOC 500-mb Chart, 0000 GMT 16 February 1989.

4.3 Case III: Temperature Swings at Barter Island, 12 Through 16 October 1988

4.3.1 Introduction

Temperature changes at coastal stations in the Arctic can be extreme. Such extremes are commonly observed during periods when wind direction shifts from onshore to offshore. Subtle changes in wind direction can translate to large changes in local temperature. The change is accentuated when low cloudiness or fog under a low-level inversion exists offshore over the ice while continental areas are clear. Under such conditions, especially with limited daylight hours, loss of thermal energy through radiation to space is restricted over the offshore low-cloud regions but is almost continuous over the clear land areas. Warming then occurs with even slight onshore flow trajectories while rapid cooling follows with offshore trajectories (elevation changes not considered).

Arctic fronts are so named to distinguish frontal activity and associated jets over the ice cap from coexisting polar frontal activity of midlatitudes. Arctic fronts are generally less intense than polar fronts, however, marked changes in total cloudiness, in wind direction and speed, and in temperature often accompany their passage.

Figure 4-30 shows, in summarized form, meteorological changes at Barter Island during the period 12 through 16 October 1988. Of special interest for purposes of this study is the sudden drop in temperature on 14 October from about 14 °F (−10 °C) at 0000 GMT to −12 °F (−24 °C) 12 hours later. This decrease was then followed by a rise in temperature to 23 °F (−5 °C) in the following 12 hours. Note that sky conditions cleared as winds backed from west-northwest to south-southwest; this development was followed by increased cloudiness as winds veered back to a westerly direction. The suggested cause for these changes, according to the preceding discussion, is simply a change from onshore to offshore flow and then again to onshore flow. Examination of satellite data and weather charts for the same period is of interest, however, for verification and/or additional factors that might account for such changes.

4.3.2 12 October 1988

Infrared DMSP data received at 0632 GMT (Fig. 4-31) shows a good view of the Alaskan region. Low cloudiness in this IR view radiates at a warm (dark) temperature, reflecting the fact that this cloudiness has formed under the strong, low-level inversion normally existing over the region during the cold months. A swath of low cloudiness extends inland from Barrow to the foothills of the Brooks range. The Beaufort Sea between Barrow and Banks Island appears largely free of clouds, and individual ice floes are well resolved. A plume of clouds generated by air movement over open water near Banks Island extends southwestward, implying northeasterly flow in that region. Barter Island (although difficult to locate in Fig. 4-31) appears to be on the edge of a low cloud bank.

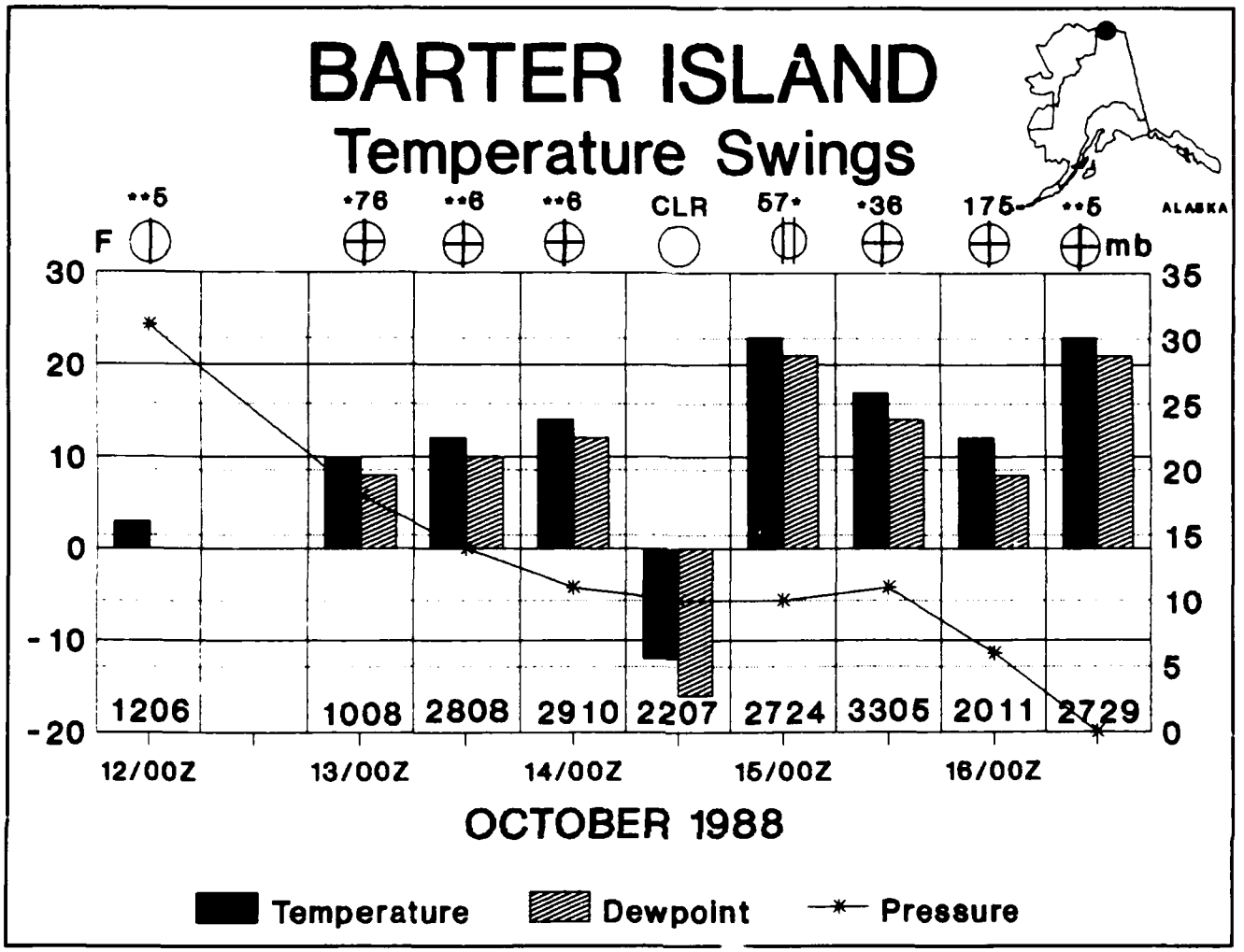

Figure 4-30. Weather Time Series for Barter Island, Alaska. (Left ordinate is temperature [°F], right ordinate is pressure [mb], and cloud type [low, mid, high] appears above the sky cover symbol. Wind direction and speed [DDFF in tens of degrees and knots] are shown in the block below temperature/dewpoint data.)

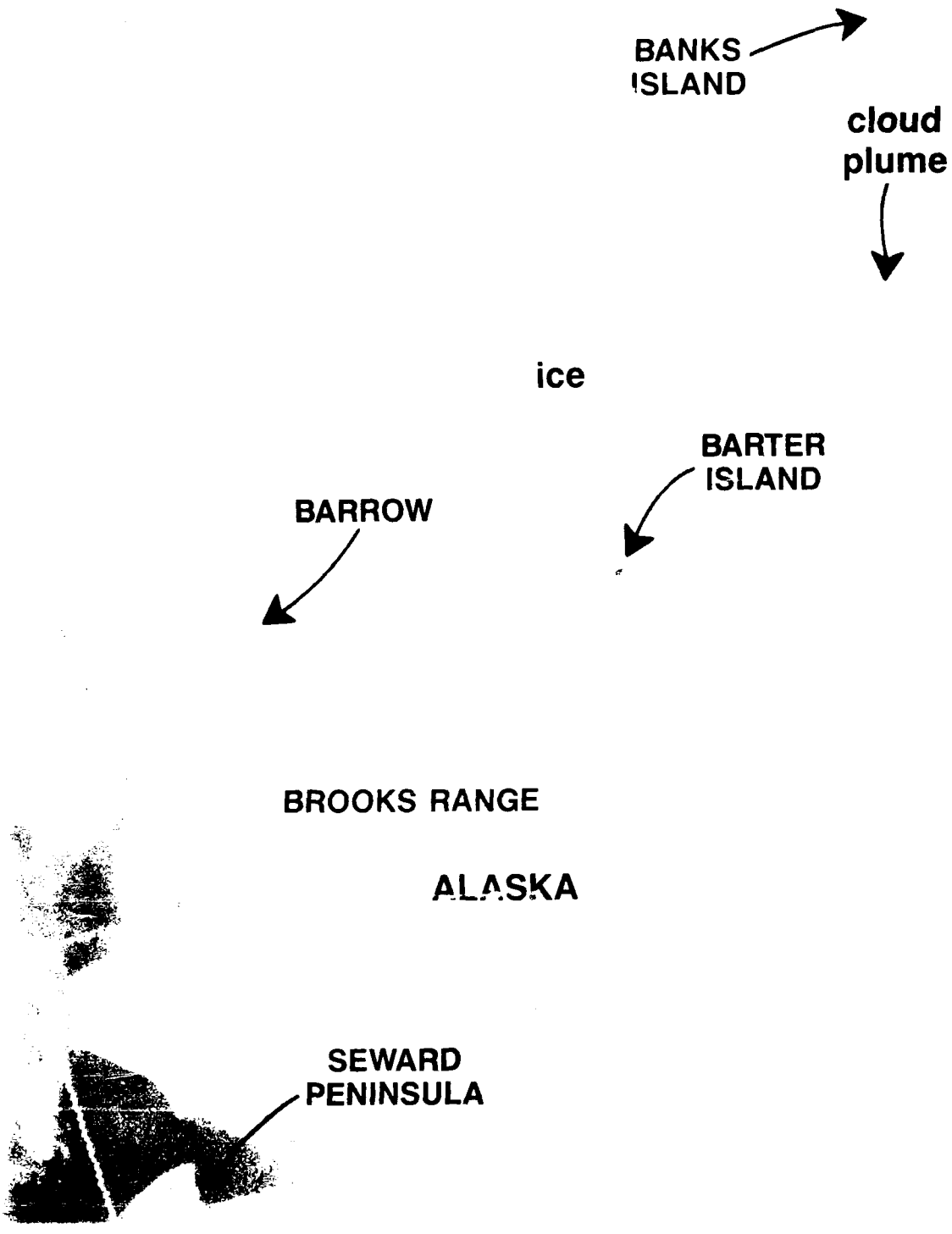

Figure 4-31. IR DMSP Satellite Imagery, 0632 GMT 12 October 1988.

The FNOC surface analysis for 1200 GMT (Fig. 4-32) shows a ridge extending from near the Seward Peninsula east-northeastward toward Banks Island. Winds of 25 kt (13 m/s) from the east-northeast are shown to exist south of Banks Island, agreeing with the plume alignment shown in the DMSP data (Fig. 4-31).

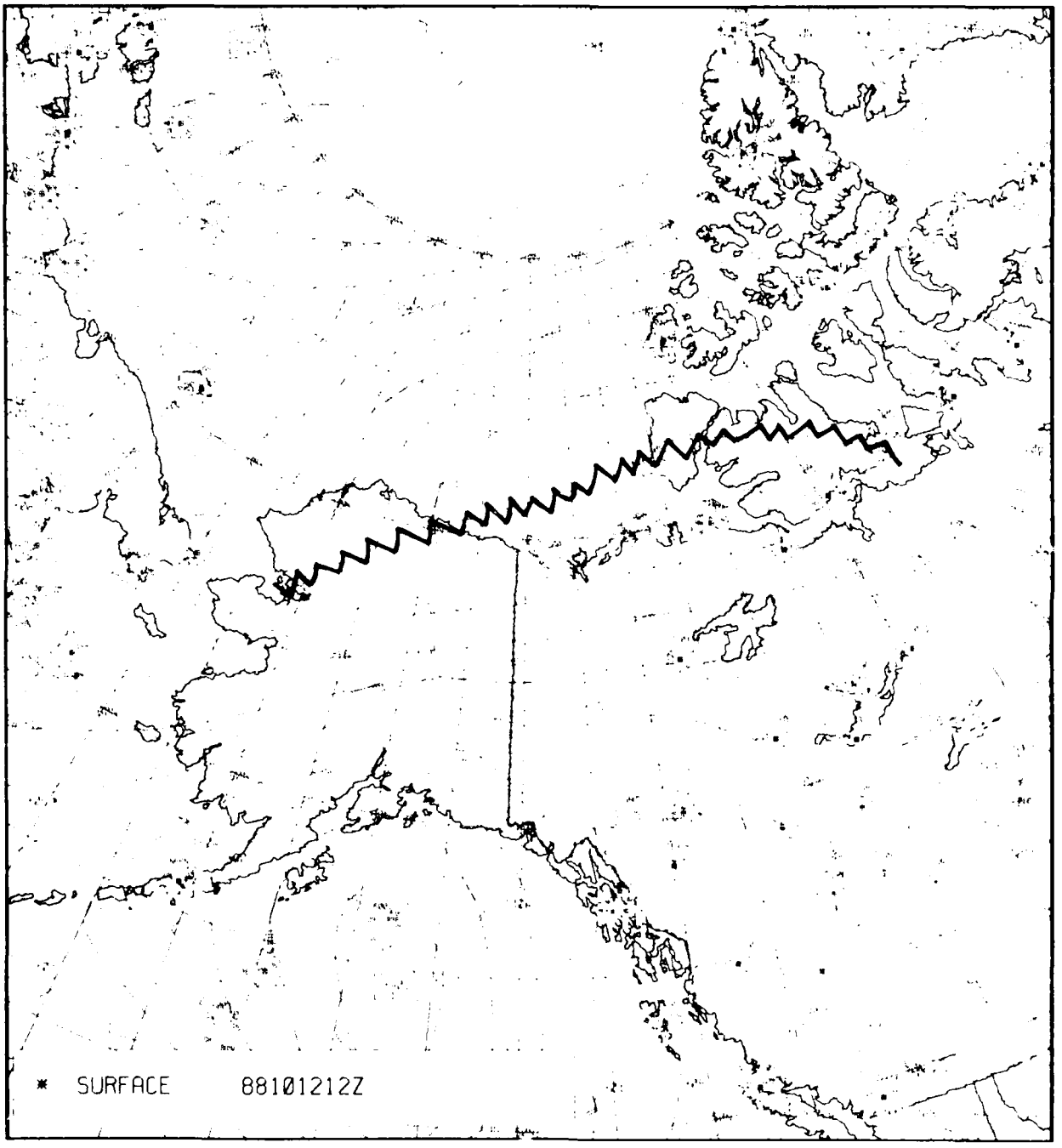

Figure 4-32. FNOC Surface Analysis, 1200 GMT 12 October 1988.

Another IR DMSP image at 1502 GMT (Fig. 4-33) reveals similar features, with Barter Island apparently in the clear. The satellite indications of cloudiness agree quite well with the Barter Island actual reports of three-eighths, two-eighths, and one-eighth of low cloudiness at 0000, 0600, and 1800 GMT, respectively.

Figure 4-33. IR DMSP Satellite Imagery, 1502 GMT 12 October 1988.

The 850-mb analysis at 1200 GMT (Fig. 4-34) shows a high pressure cell over the Beaufort Sea. Convergence associated with the approaching trough may account for the low cloudiness shown in the satellite data for that region.

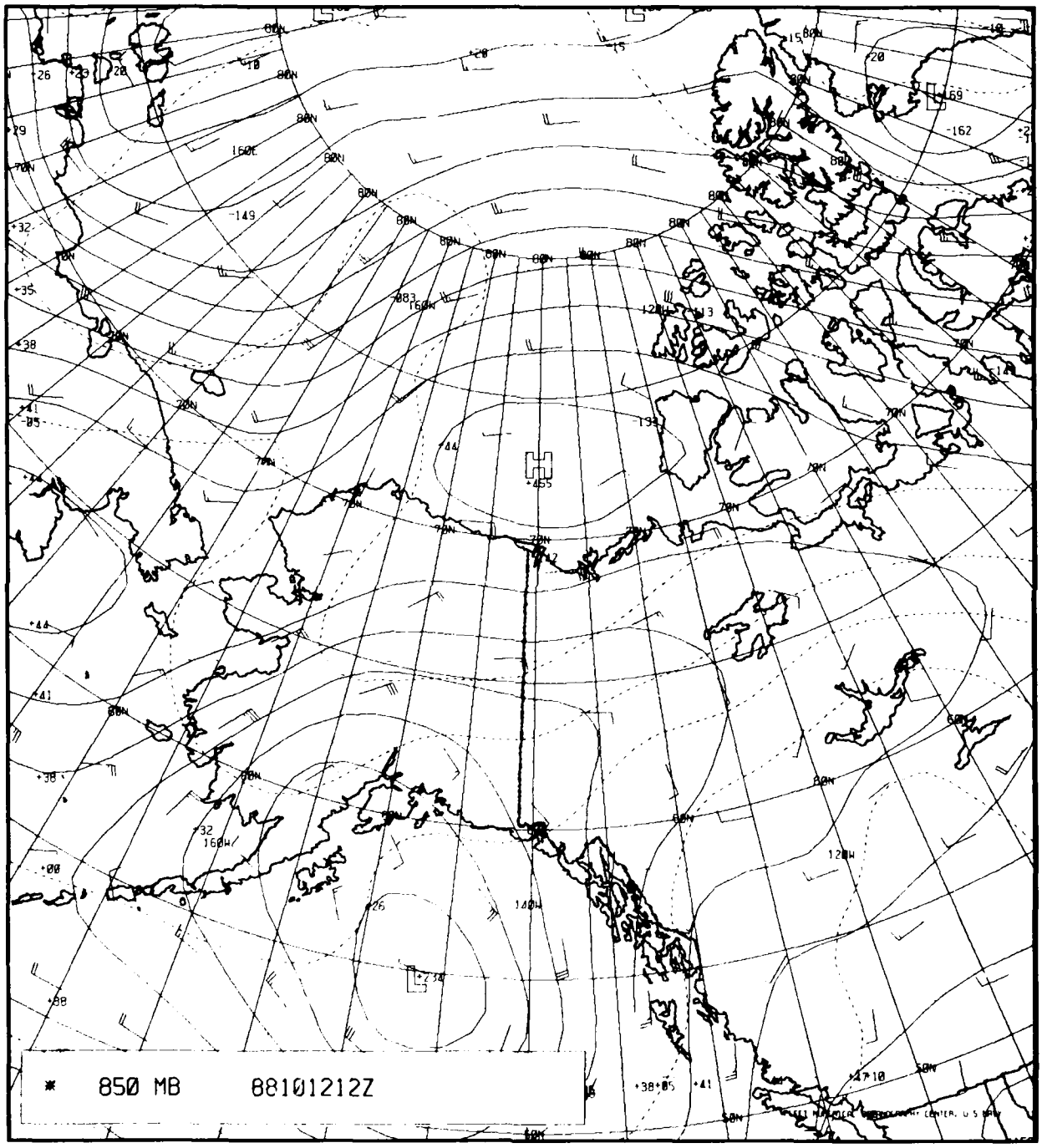

Figure 4-34. The 850-mb Analysis, 1200 GMT 12 October 1988.

4.3.3 13 October 1988

Sky conditions changed to overcast over Barter Island on this date (see Fig. 4-30), as verified by IR DMSP satellite data acquired at 0438 GMT (Fig. 4-35). The low cloudiness that was noted over northwest Alaska has moved eastward and is just beginning to obscure Barter Island. Cirrus cloudiness sweeping northeastward just east of Barter Island appears to be associated with a short-wave disturbance moving from the south into the area.

Figure 4-35. IR DMSP Satellite Imagery, 0438 GMT 13 October 1988.

As expected, the disturbance is not well resolved on the surface analysis for 0000 GMT (Fig. 4-36), which shows a ridge extending from the Seward Peninsula toward Banks Island. Barter Island's wind at this time is still east-southeasterly. The disturbance apparently moved northeastward past Barter Island by 1200 GMT as winds suddenly shifted to westerly (see Fig. 4-30). DMSP infrared data at 1449 GMT (Fig. 4-37) suggests a forming vortex northeast of Barter Island, with the low cloudiness over the island being caught up in the cyclonic circulation.

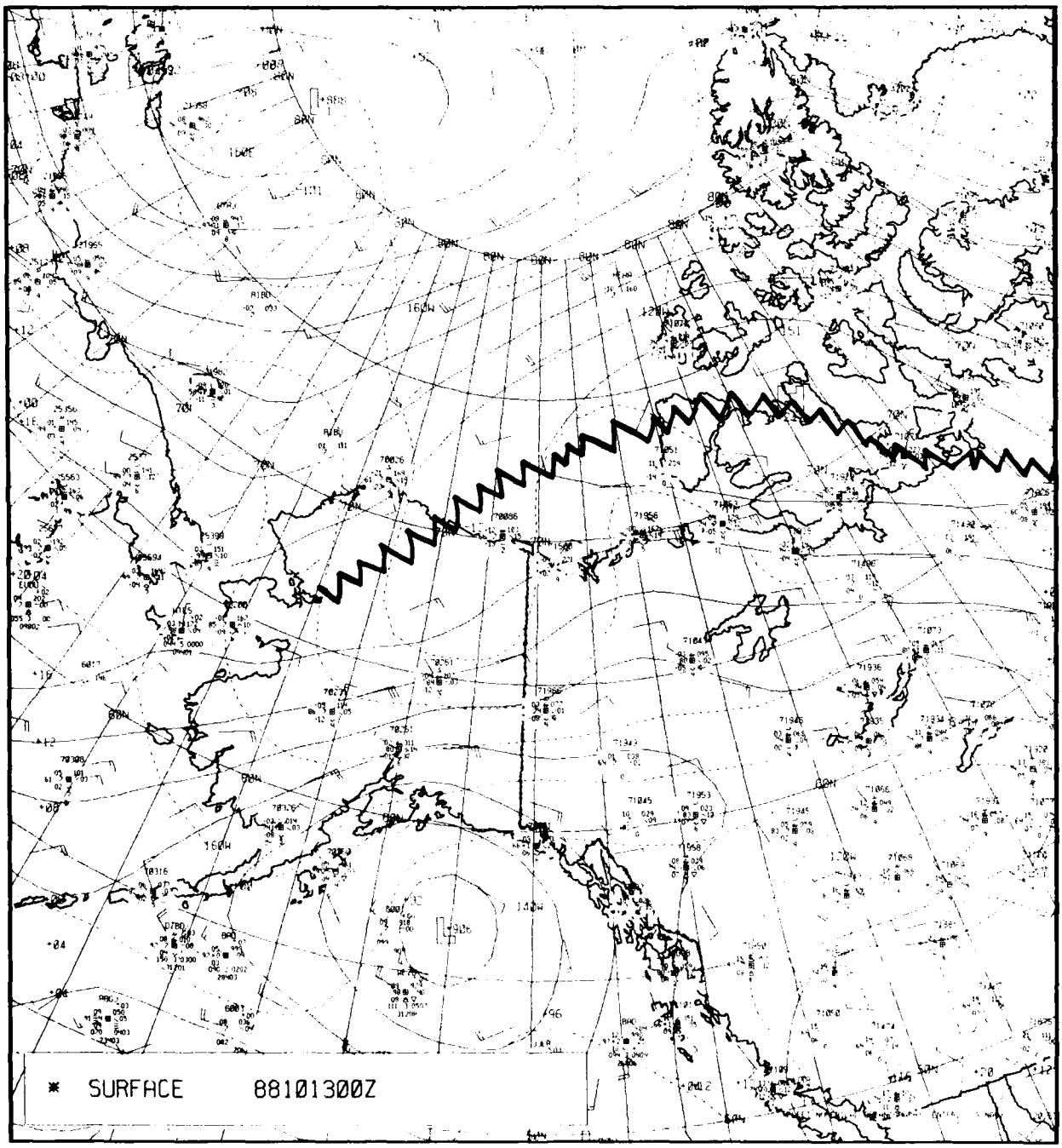

Figure 4-36. FNOC Surface Analysis, 0000 GMT 13 October 1988.

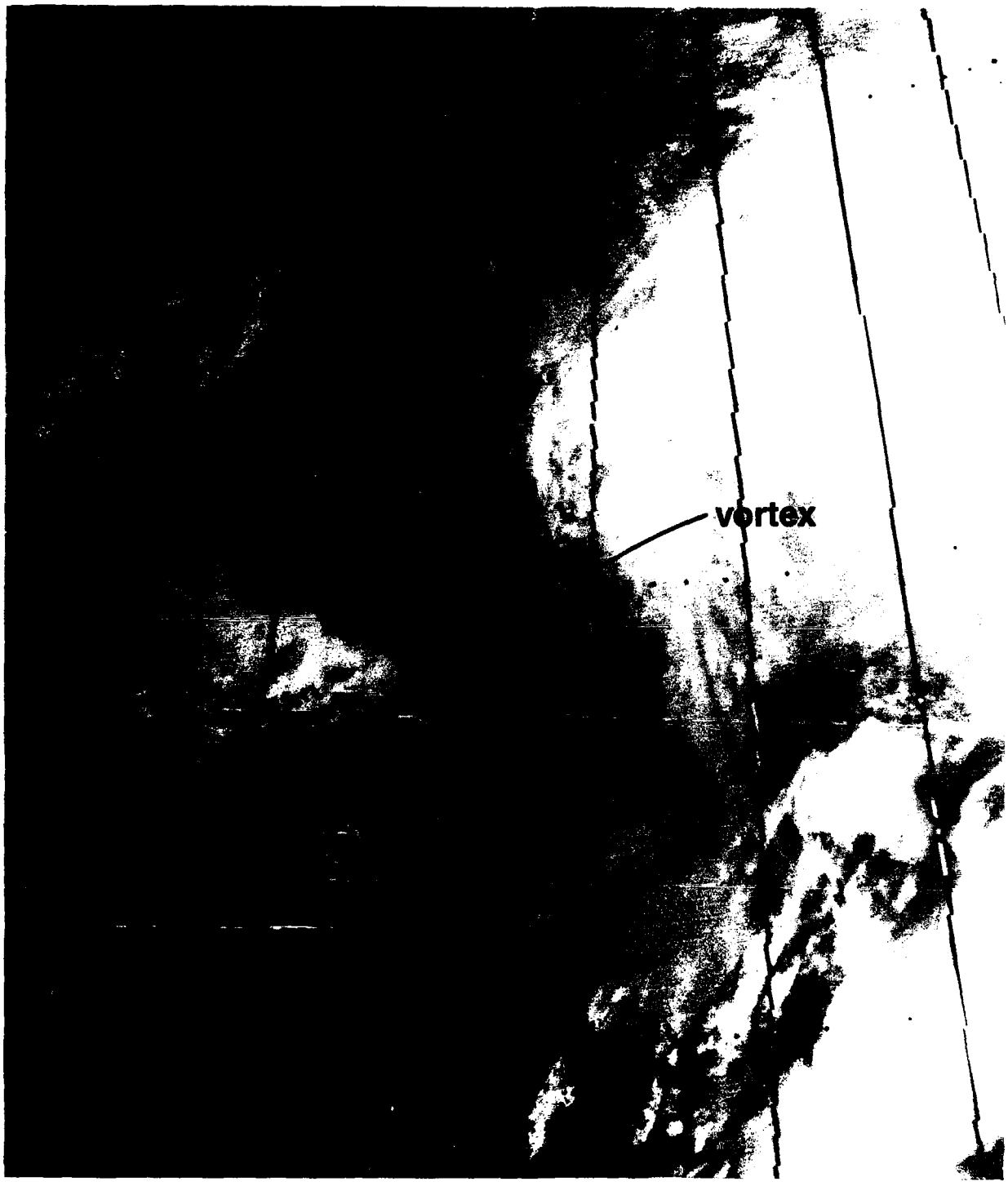

Figure 4-37. IR DMSP Satellite Imagery, 1449 GMT 13 October 1988.

The FNOC surface analysis for 1200 GMT (Fig. 4-38) shows a trough line passing east of Barter Island, with the cyclonic turning of winds in that region suggesting a possible closed circulation.

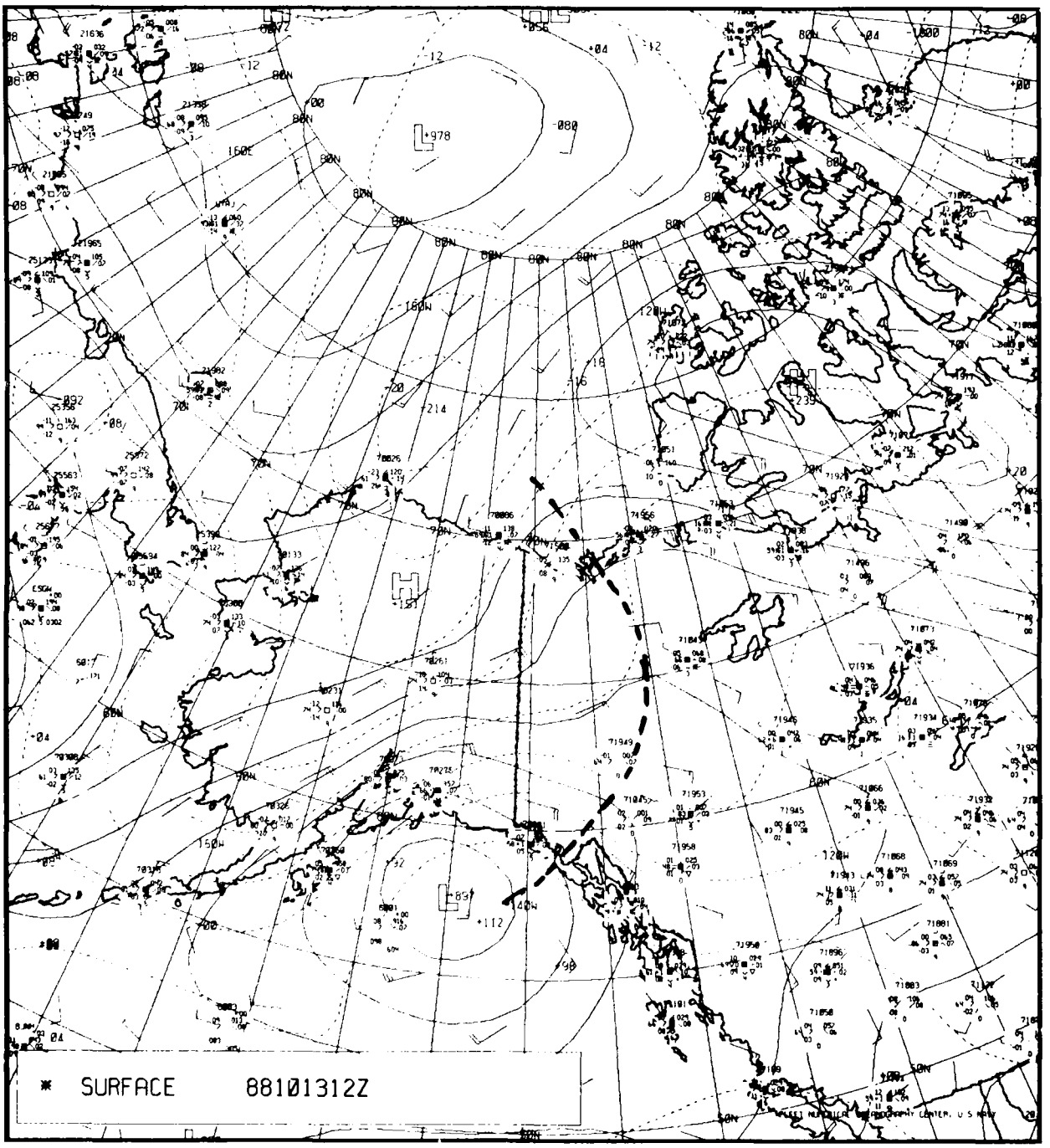

Figure 4-38. FNOC Surface Analysis, 1200 GMT 13 October 1988.

4.3.4 14 October 1988

Infrared DMSP data at 0607 GMT (Fig. 4-39) suggests a vortex forming just southeast of Banks Island. Low (warm) cloudiness seems to be caught up in this circulation, with Barter Island on the southern fringe in overcast conditions. An Arctic front extends northward through the central Beaufort Sea.

Figure 4-39. IR DMSP Satellite Imagery, 0607 GMT 14 October 1988.

The FNOC surface analysis for 0600 GMT (Fig. 4-40) shows a low center just south of Banks Island. Note the excellent definition of the trough, associated with the Arctic front, north of Barrow. Barter Island's wind on this analysis has shifted to west-southwest as it appears to be coming under the influence of a high pressure ridge to the south. Sky conditions are reported as overcast in fog with a visibility of 3 mi.

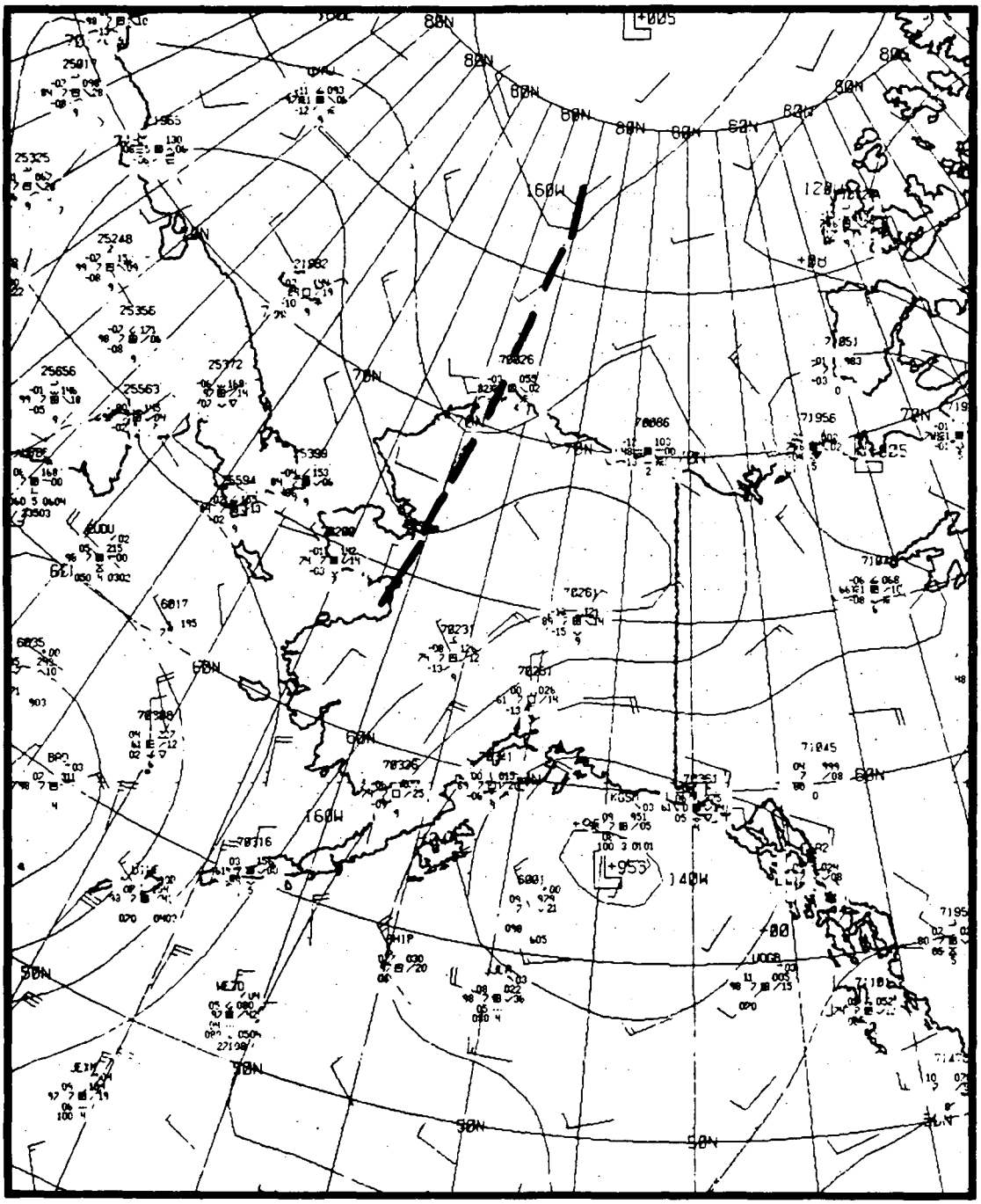

Figure 4-40. FNOC Surface Analysis, 0600 GMT 14 October 1988.

Infrared DMSP data at 1437 GMT (Fig. 4-41) reveal Barter Island apparently in the clear as low overcast cloudiness has moved northeastward, following the vortex center near Banks Island. The Arctic front remains well defined over the central Beaufort Sea, with its southern extremity sweeping low overcast cloudiness into the Barrow region.

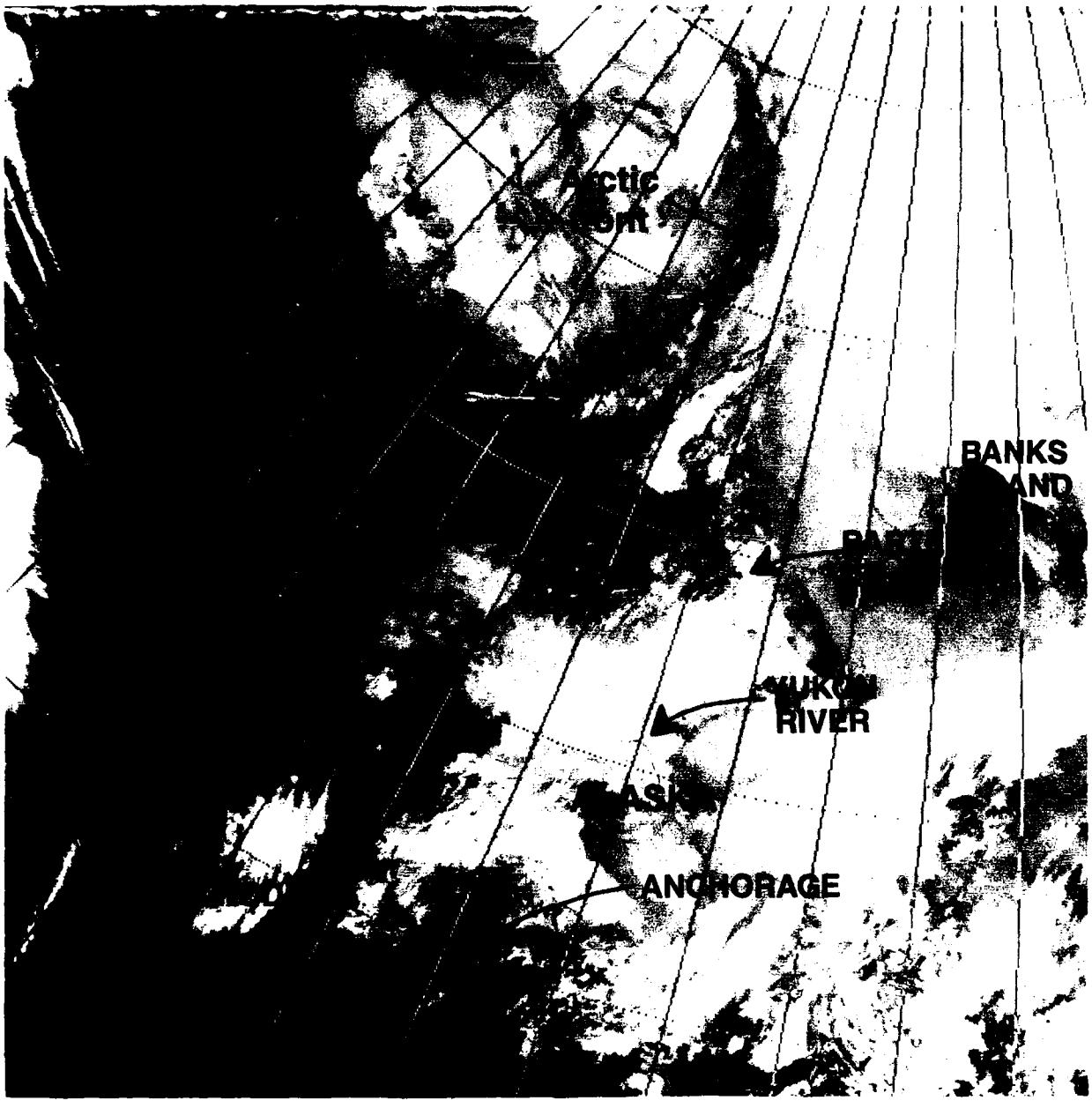

Figure 4-41. IR DMSP Satellite Imagery, 1437 GMT 14 October 1988.

The FNOC surface analysis for 1200 GMT (Fig. 4-42) shows high pressure dominating central Alaska and a low pressure system in the Amundson Gulf southeast of Banks Island. The trough associated with the Arctic front has passed Barrow, which is now reporting a northerly wind with rising pressure tendencies. At this time Barter Island's temperature dropped to −12 °F (−24 °C) in light southwest flow under clear sky conditions. Local time for this analysis was 0200, so that cooling through radiation was an important factor associated with the temperature drop.

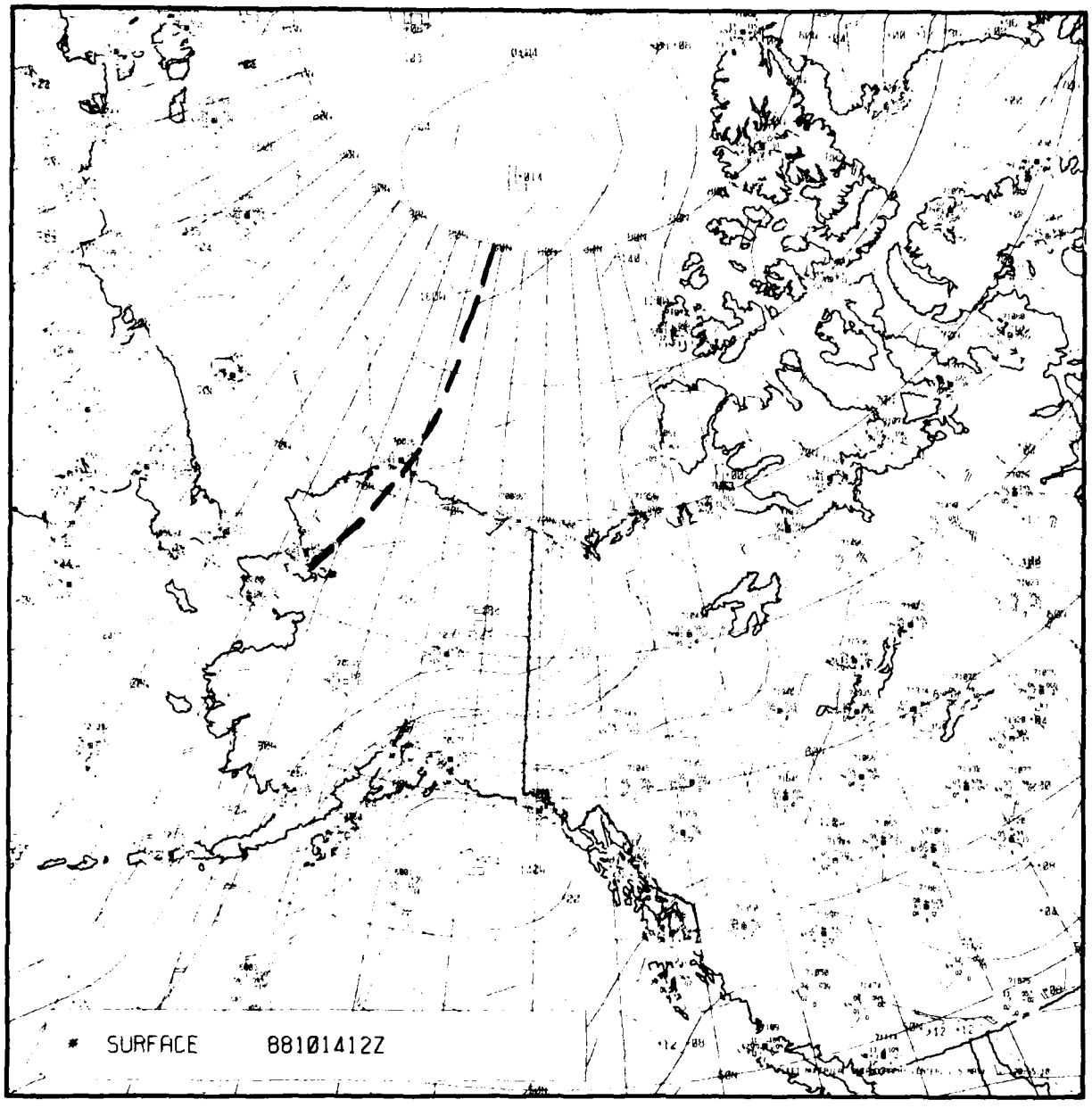

Figure 4-42. FNOC Surface Analysis, 1200 GMT 14 October 1988.

By 1800 GMT (0800 L), as shown in the FNOC surface analysis (Fig. 4-43), the Arctic front had reached Barter Island, bringing overcast skies, a shift in the winds to 280 degrees, and a sudden warming from −12 °F to 19.4 °F (−24 °C to −7 °C). This warming, a peculiarity of so-called cold frontal passage is due to the change in air trajectory. Prior to frontal passage the winds were southwesterly, bringing in air cooled by passage over the cold landmass. After frontal passage, the air trajectory was from over the relatively warmer water modifying the air behind the front because of the heat and moisture flux into the air from open water.

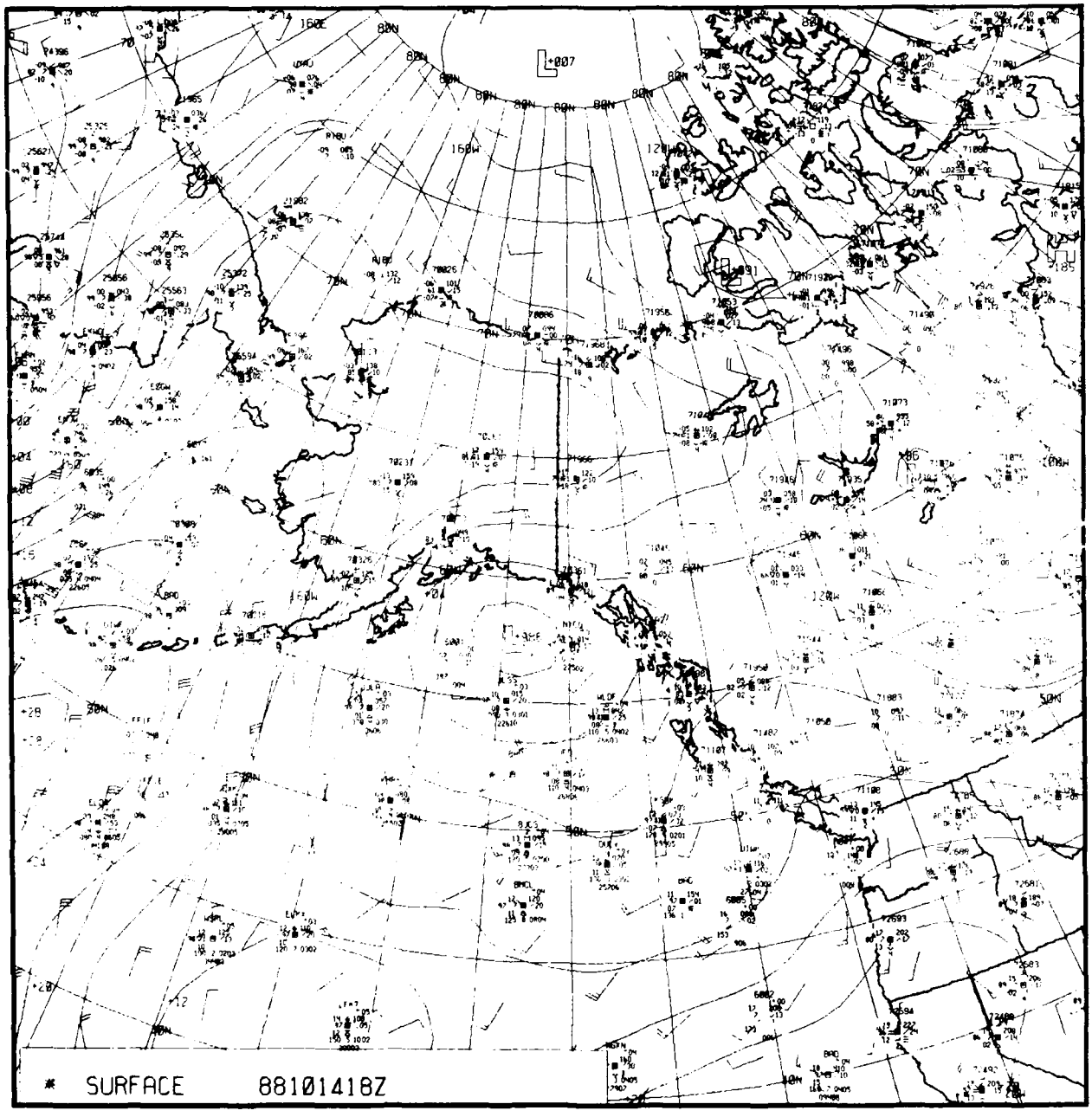

Figure 4-43. FNOC Surface Analysis, 1800 GMT 14 October 1988.

4.3.5 15 October 1988

Infrared DMSP data acquired at 0413 GMT (Fig. 4-44) show Barter Island in apparently low overcast conditions. The Arctic front has weakened and is indistinct in the satellite view. The low to which the front was connected, however, was still apparent to the northwest while the other low, formerly over Banks Island, has moved to a position north of Banks near Prince Patrick Island. New, dynamic developments were to follow as an intense Arctic front formed off the low to the northwest and eventually swept through the North Slope region.

Figure 4-44. IR DMSP Satellite Imagery, 0413 GMT 15 October 1988.

Neither of these systems is shown very well in the FNOC surface analysis for 0000 GMT (Fig. 4-45). The Prince Patrick Island low is shown about 200 mi east of its satellite position and the low to the northwest is not analyzed.

4.3.6 Conclusion

Good quality high resolution satellite data are required for accurate analysis in the Arctic—just as in other regions where observations are more plentiful. The systems observed are often unimpressive; however, the local weather changes they cause capture immediate attention.

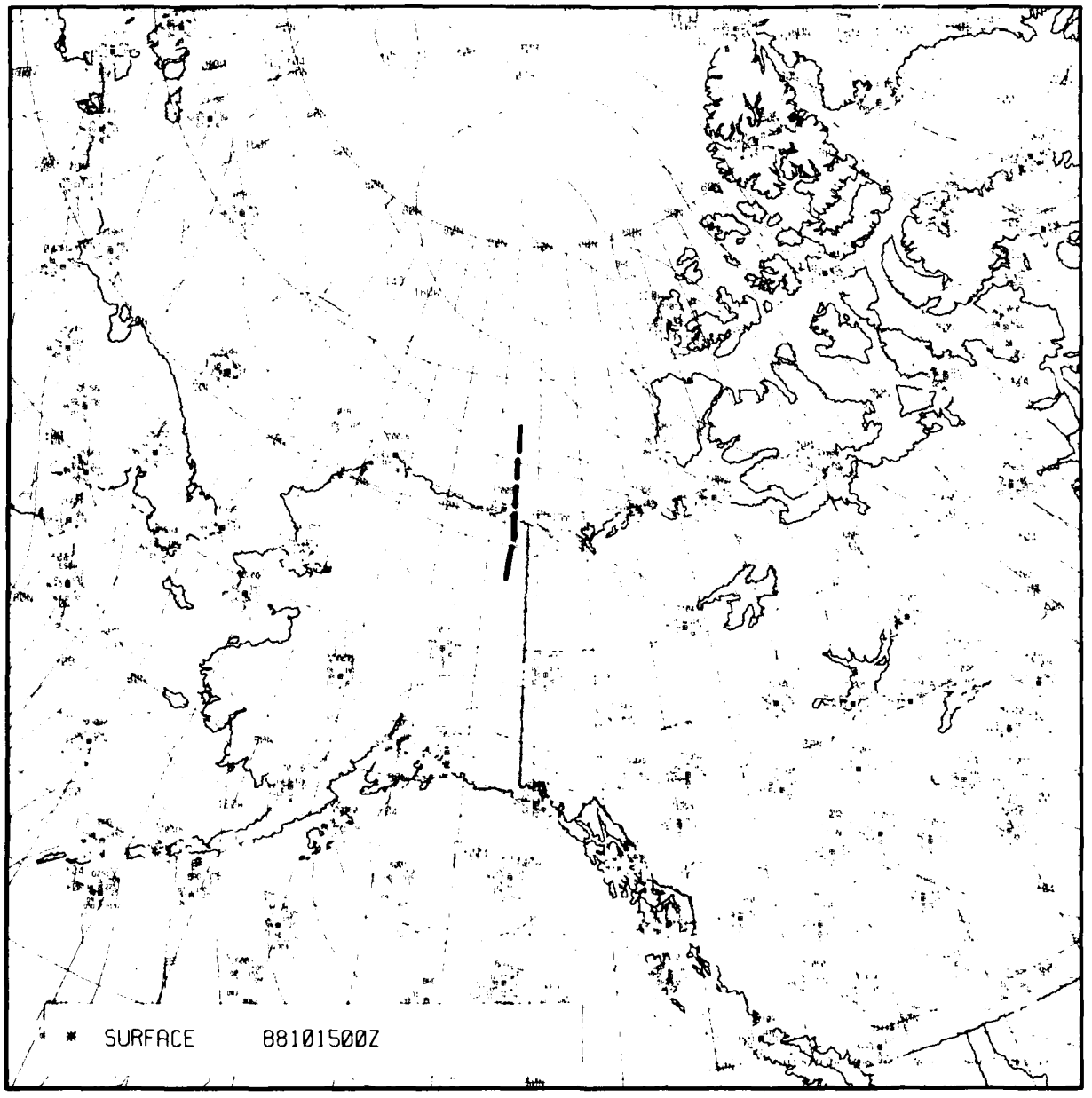

Figure 4-45. FNOC Surface Analysis, 0000 GMT 15 October 1988.

4.4 Case IV: High Winds in Smith Sound, 7 April 1989

4.4.1 Introduction

High winds in the Arctic are certainly not uncommon but they may originate from a large variety of synoptic and local conditions. Among these cases are cold outbreaks being enhanced by downslope flow over the glaciers.

The present case is an example of pre-cold frontal winds being strengthened by a channeling effect as southwesterly flow, ahead of a cold front, funnels into Smith Sound between Ellesmere Island and northern Greenland. Winds in excess of 66 mph and perhaps up to 100 mph were observed at Ice Camp APLIS 89 most of the day on 7 April 1989. The synoptic situation will be described with surface and upper air charts, visible and IR satellite imagery, and time series of the observed weather parameters.

4.4.2 0000 GMT 7 April 1989

Figure 4-46 is a locator map for the area involved in this case study. Ice Camp APLIS 89 at the time of the highest winds was located in Smith Sound approximately 13 miles from the Greenland coast.

Figure 4-47 is the 500-mb chart for 0000 GMT 7 April 1989. The pertinent feature on this chart is the relatively short-wave trough oriented northeast-southwest and extending from northwestern Ellesmere Island to southwestern Victoria Island. At this time, therefore, an upper trough is approaching Smith Sound and the winds in that region are westerly.

At the surface (Fig. 4-48), for the corresponding time, the trough is in a position east of the 500-mb trough that would be expected, considering the slope of cold troughs. More precisely, the surface trough lies between Victoria and Baffin Islands.

The thermal pattern on the surface chart shows the $-16\,^{\circ}C$ isotherm outlining a relatively *warm pocket* of air (normally, cold air would be expected) moving eastward toward Ellesmere Island. Consequently, at this time increasing cloudiness and increasing southwest winds could be expected as the trough approaches Smith Sound; significant warming must also be anticipated.

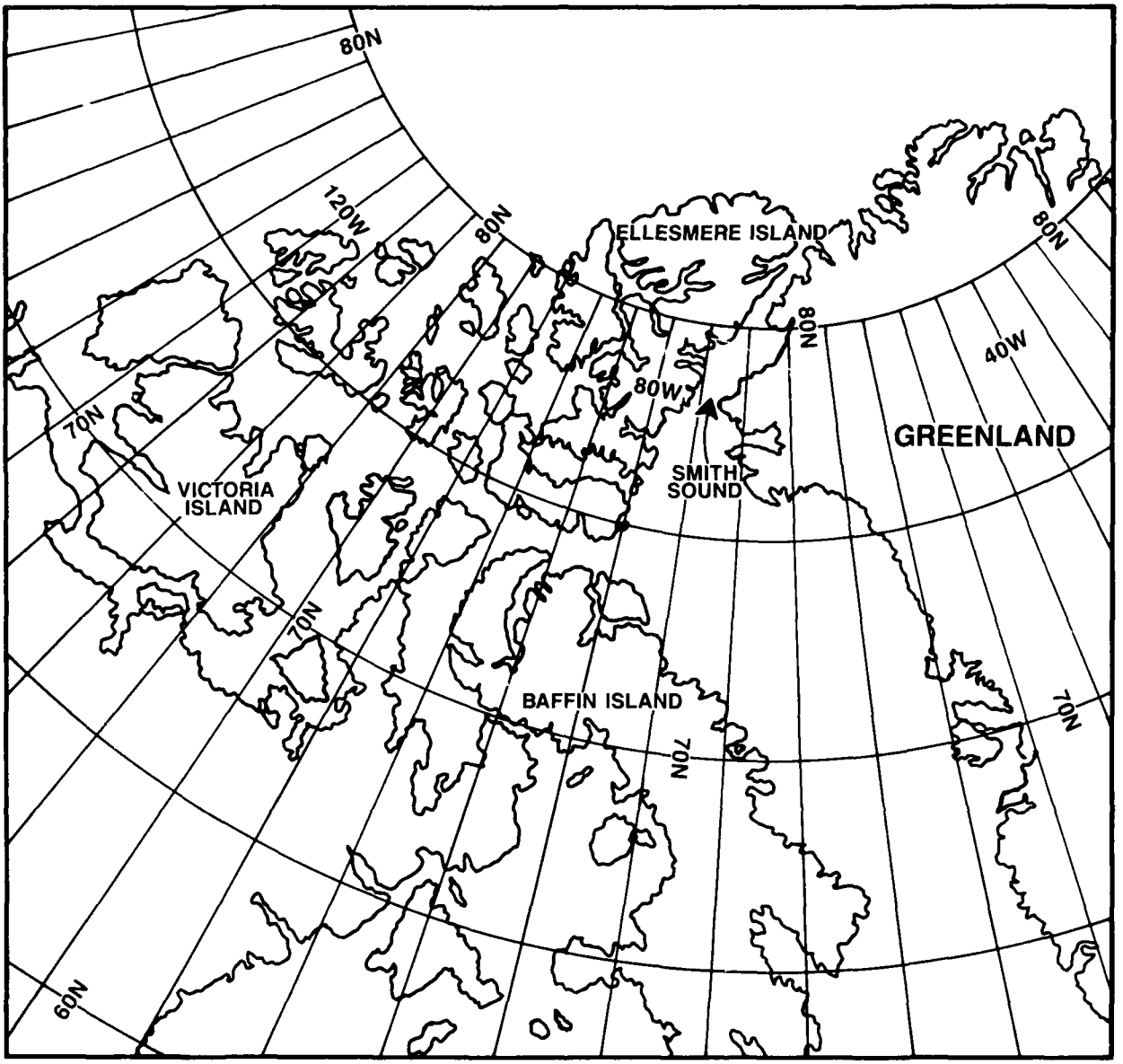

Figure 4-46. Locator Map for the Smith Sound Region.

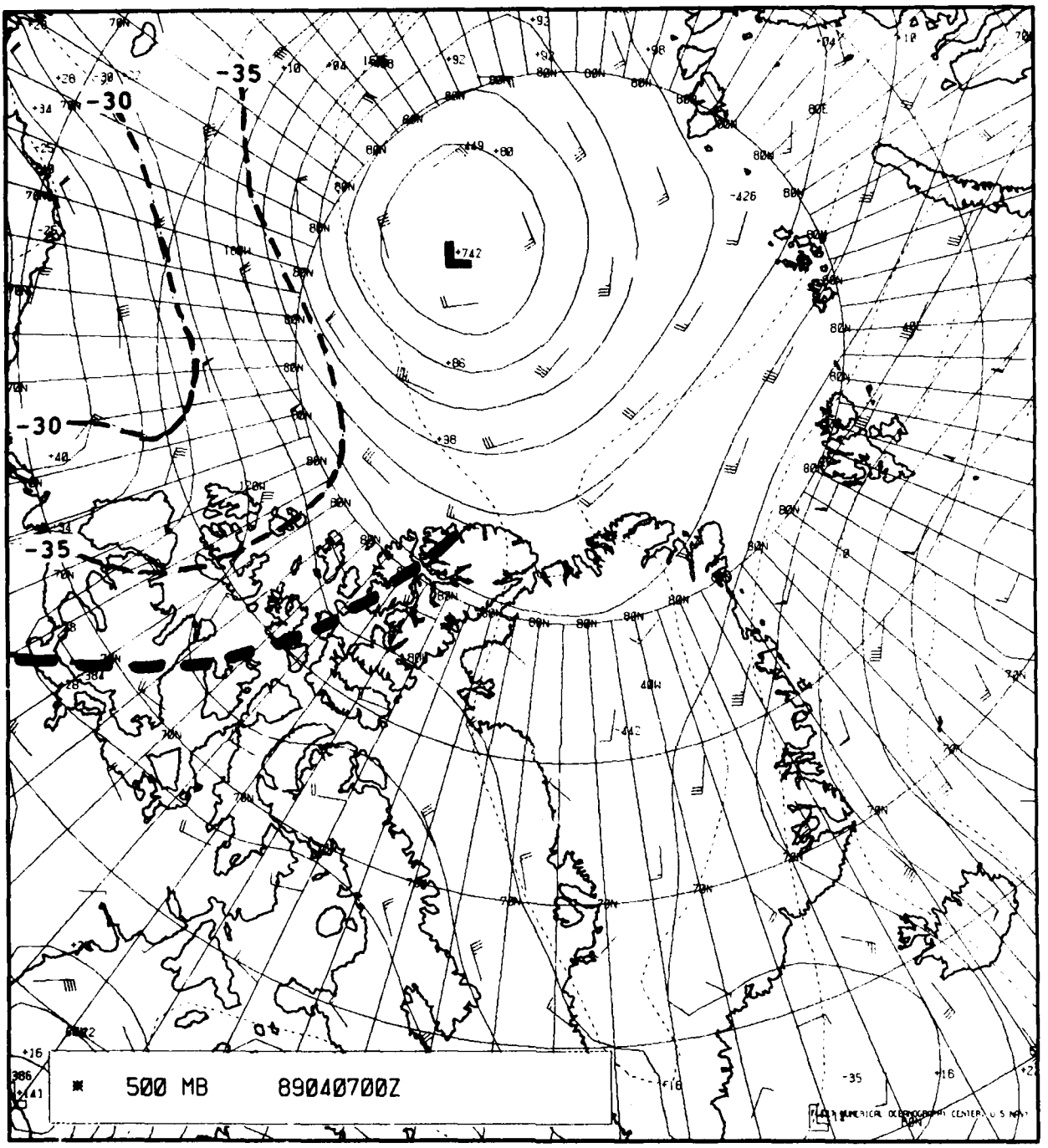

Figure 4-47. FNOC 500-mb Chart, 0000 GMT 7 April 1989.

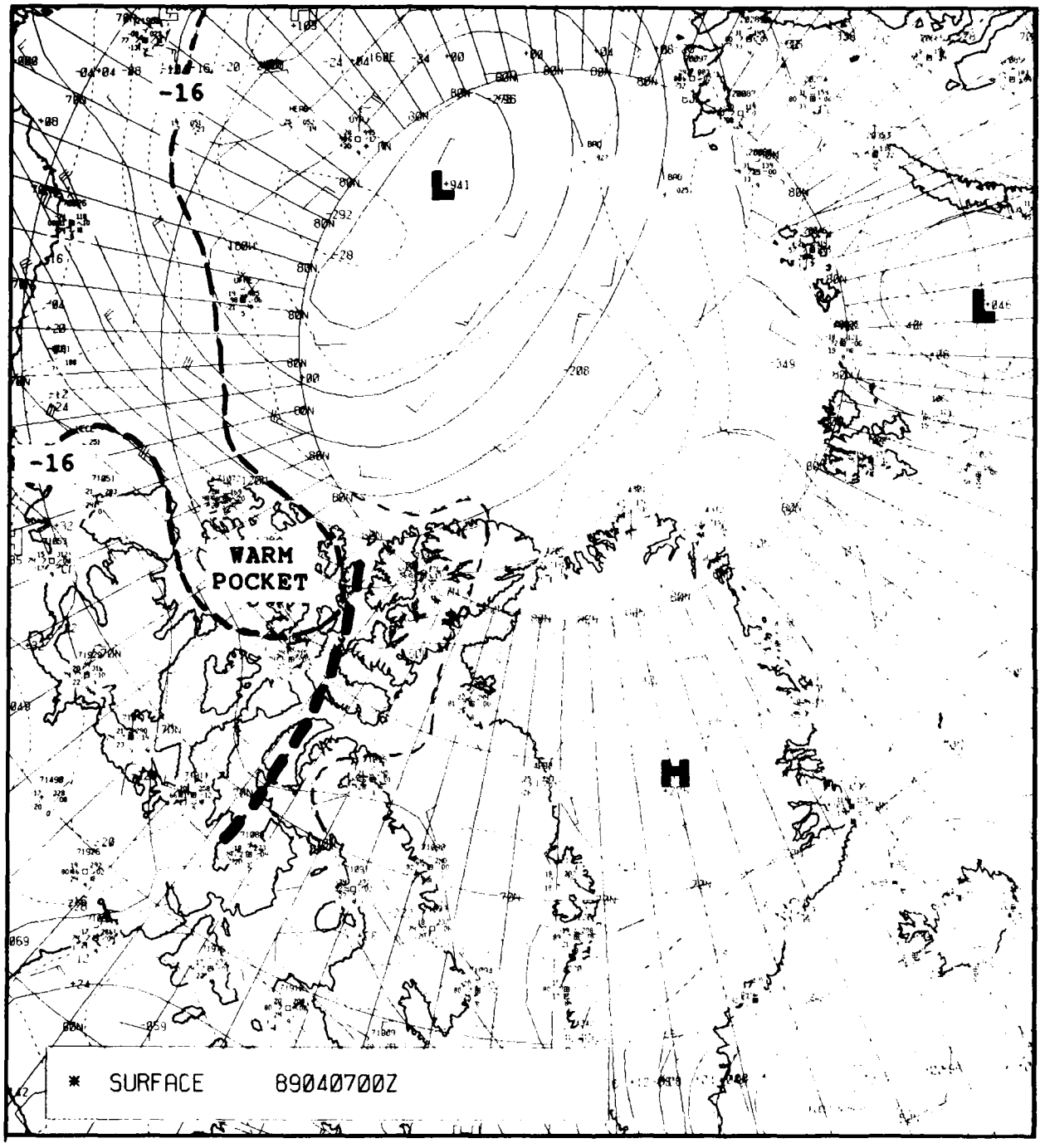

Figure 4-48. FNOC Surface Chart, 0000 GMT 7 April 1989.

4.4.3 1200 GMT 7 April 1989

The well defined surface trough in the vicinity of Ellesmere Island, which appeared on the 0000 GMT chart, weakened somewhat during the subsequent 12 hours, as can be noted on the 1200 GMT surface chart for 7 April 1989 (Fig. 4-49). The flow in the area of interest has become slightly more westerly, and the pressure gradient to the southwest of Ellesmere has intensified. Interestingly, the trough appears to have separated, with the northern portion of the trough moving more rapidly eastward than did the southern portion. The northern portion of the trough is over the west coast of Greenland at this time while the southern portion loses its identity. In the meantime, the warm tongue, outlined by the −16 °C isotherm, has advanced eastward also, bringing warmer air closer to Smith Sound.

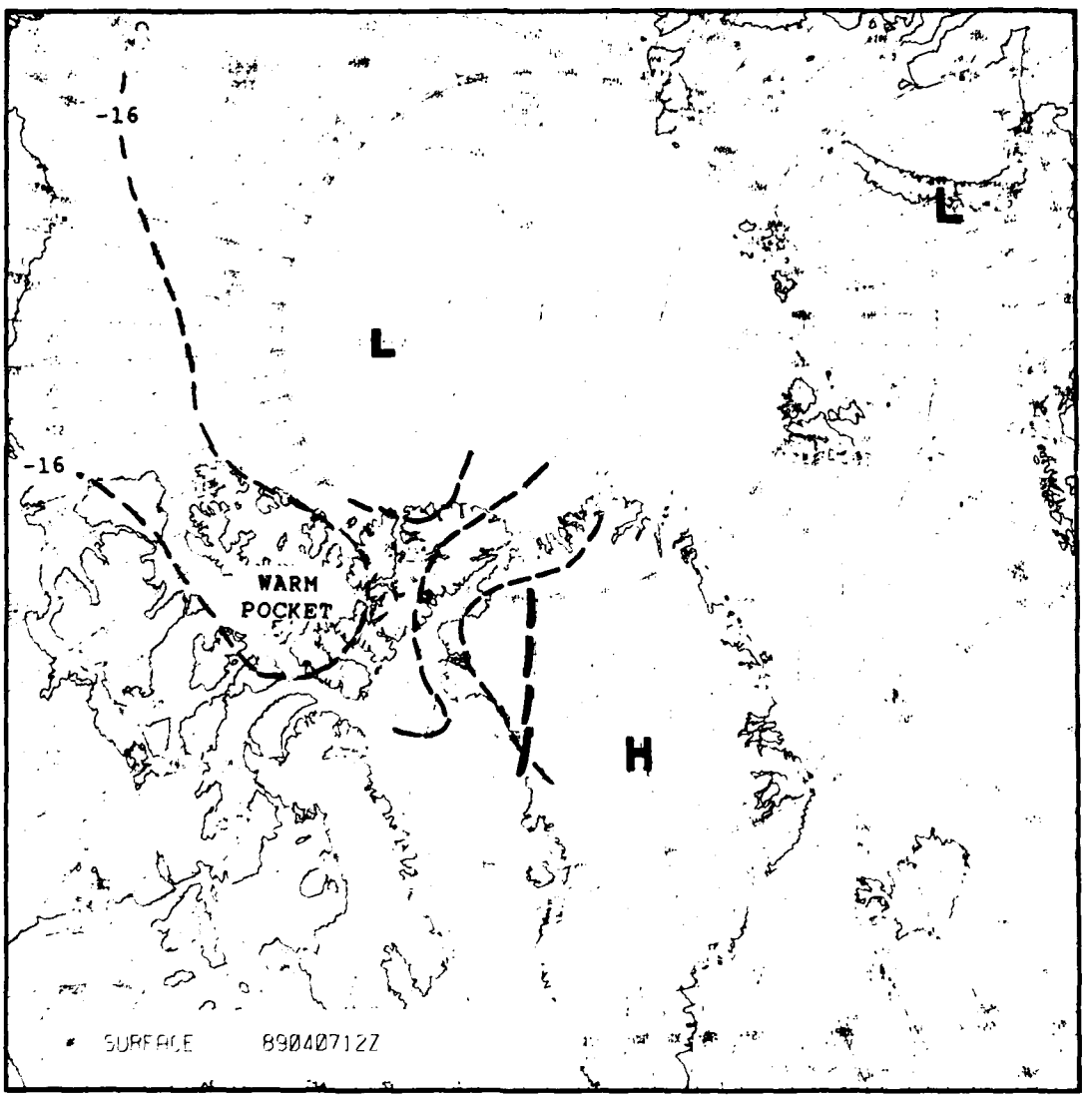

Figure 4-49. FNOC Surface Chart, 1200 GMT 7 April 1989.

At 500 mb (Fig. 4-50), the separation of the northern and southern portions of the trough is even more obvious. The northern portion of the trough at 1200 GMT approached central Greenland while the southern portion lingered over northern Baffin Island. This separation of the trough may have implications that are not obvious at this time.

Note that a comparison of the surface and 500-mb charts shows warm advection common to both in the area of interest around Ellesmere Island. The surface warm advection appears, however, to be much stronger near the surface than at 500 mb, which implies that some destabilization of the air is occurring. Also note that warm advection decreasing with height can be just as effective in the destabilization process as low level warm advection topped by upper level cold advection.

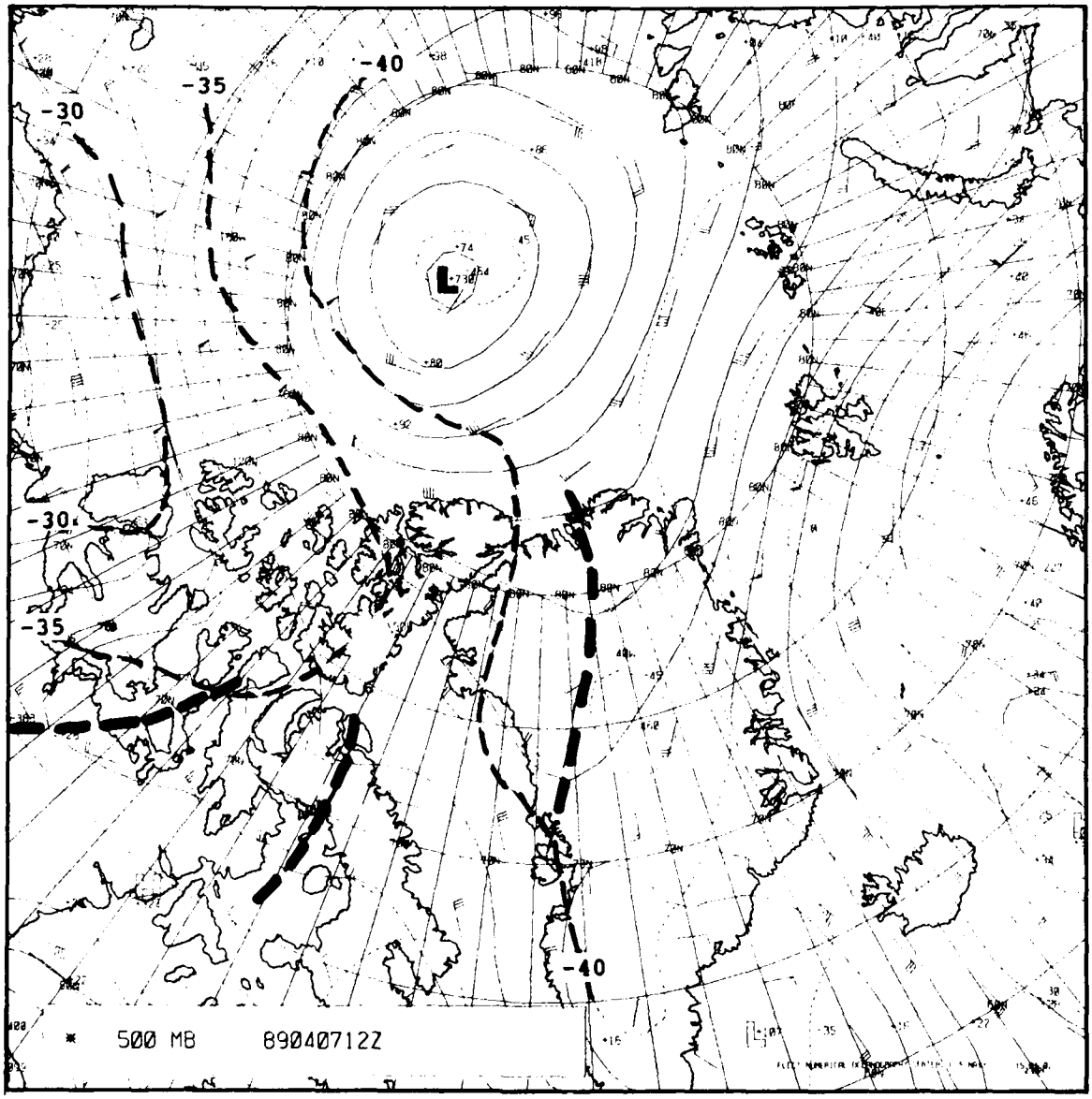

Figure 4-50. FNOC 500-mb Chart, 1200 GMT 7 April 1989.

Satellite imagery for this time is presented in Figs. 4-51 and 4-52. Figure 4-51, the visible DMSP imagery, shows a wide frontal band stretching northeast-southwest just north of Ellesmere Island and Greenland. Significantly, a developing wave appears on the frontal band and indicates cyclogenesis just north of the area in which strong winds developed on 7 April. The structure and intensity of the wave is better defined in the IR DMSP satellite imagery (Fig. 4-52). Clearly, Smith Sound is southeast of this deepening wave and would lie in the developing warm sector of the system.

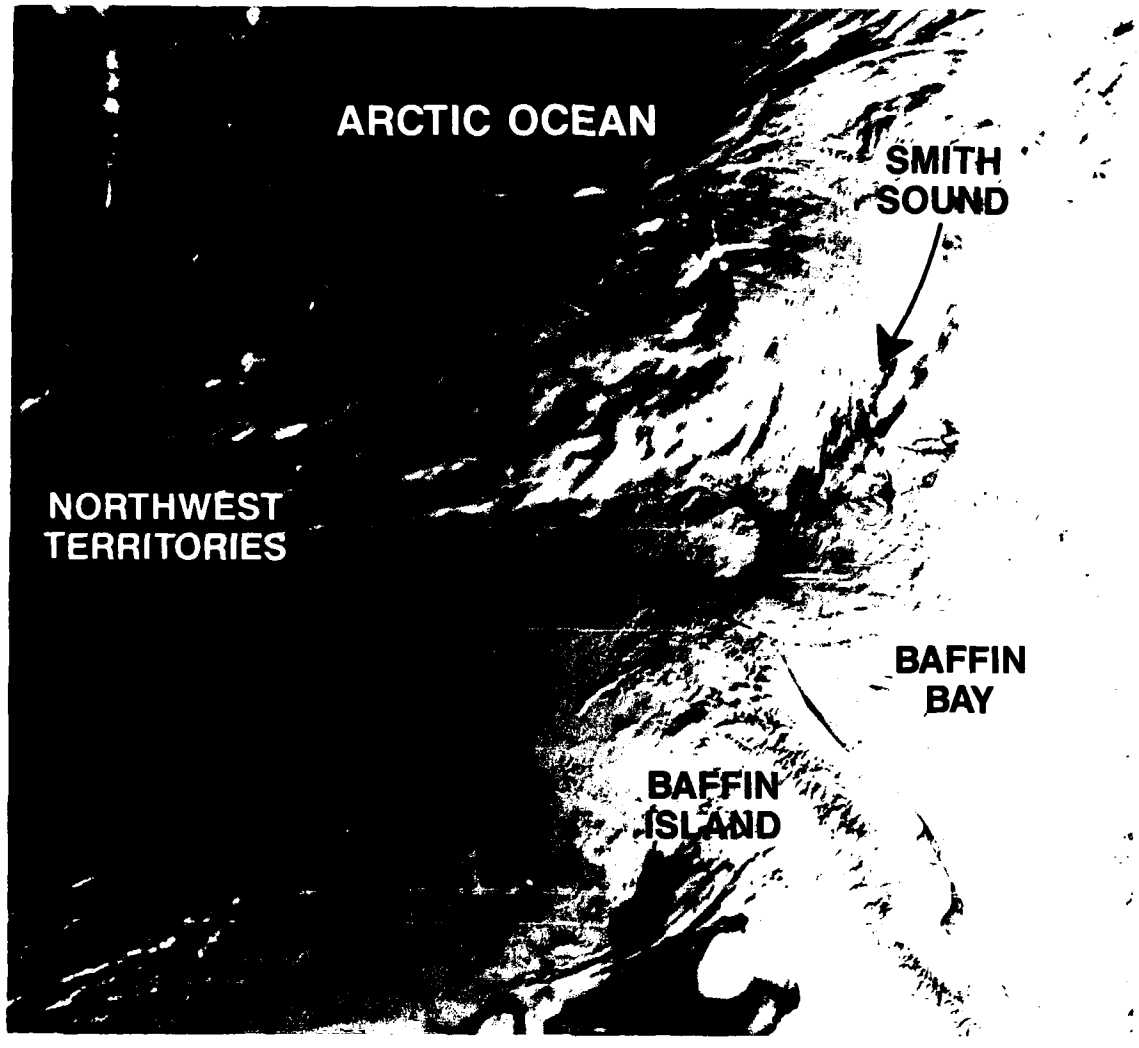

Figure 4-51. Visible DMSP Satellite Imagery, 1400 GMT 7 April 1989.

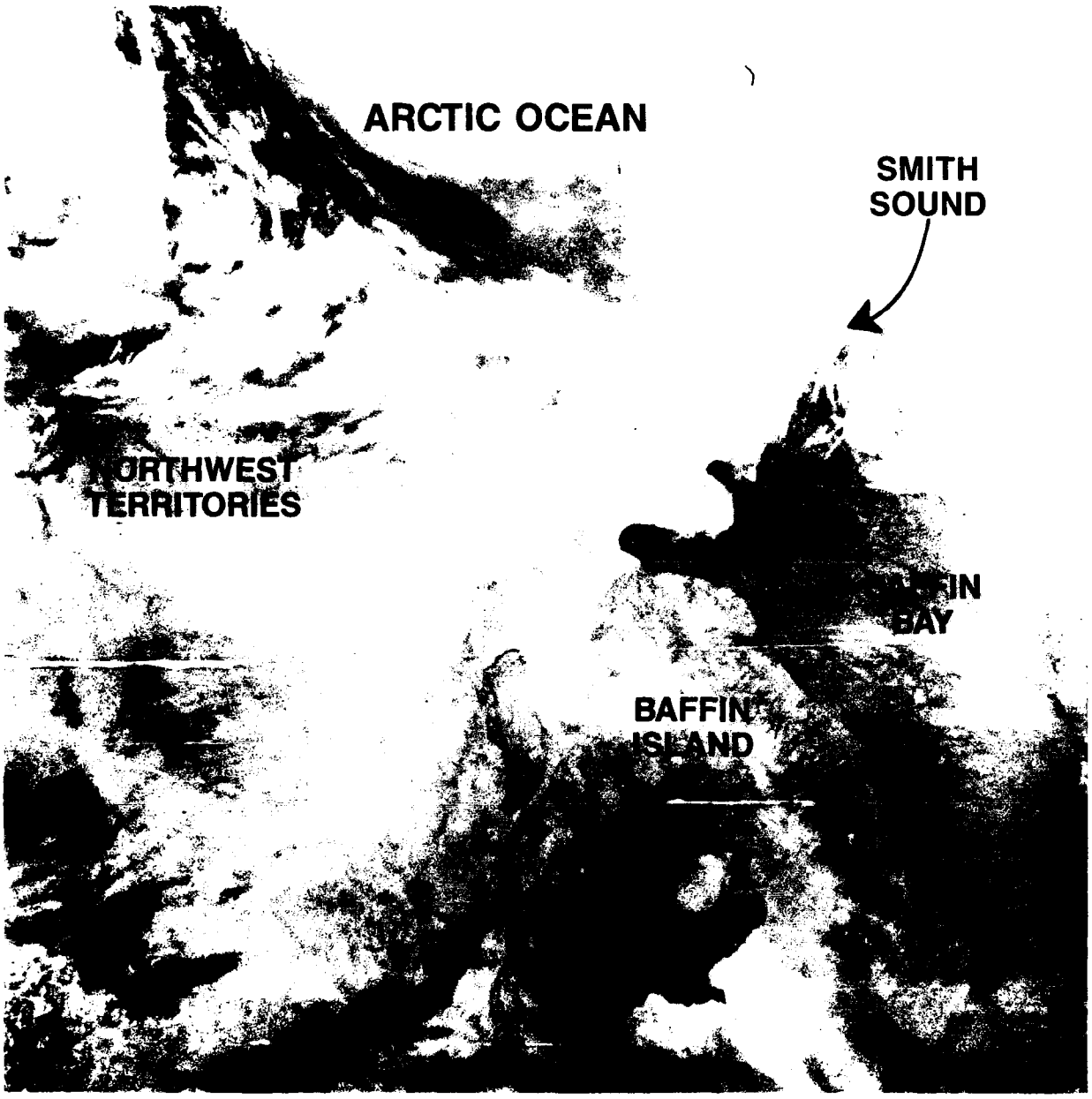

Figure 4-52. IR DMSP Satellite Imagery, 1400 GMT 7 April 1989.

Figure 4-53 is a time series of various weather parameters as observed at Ice Camp APLIS 89. Clearly, as shown in this figure, considerable warming occurred at the surface during the morning hours of 7 April. This trend is consistent with the earlier observation of warm advection on the surface chart (Fig. 4-49).

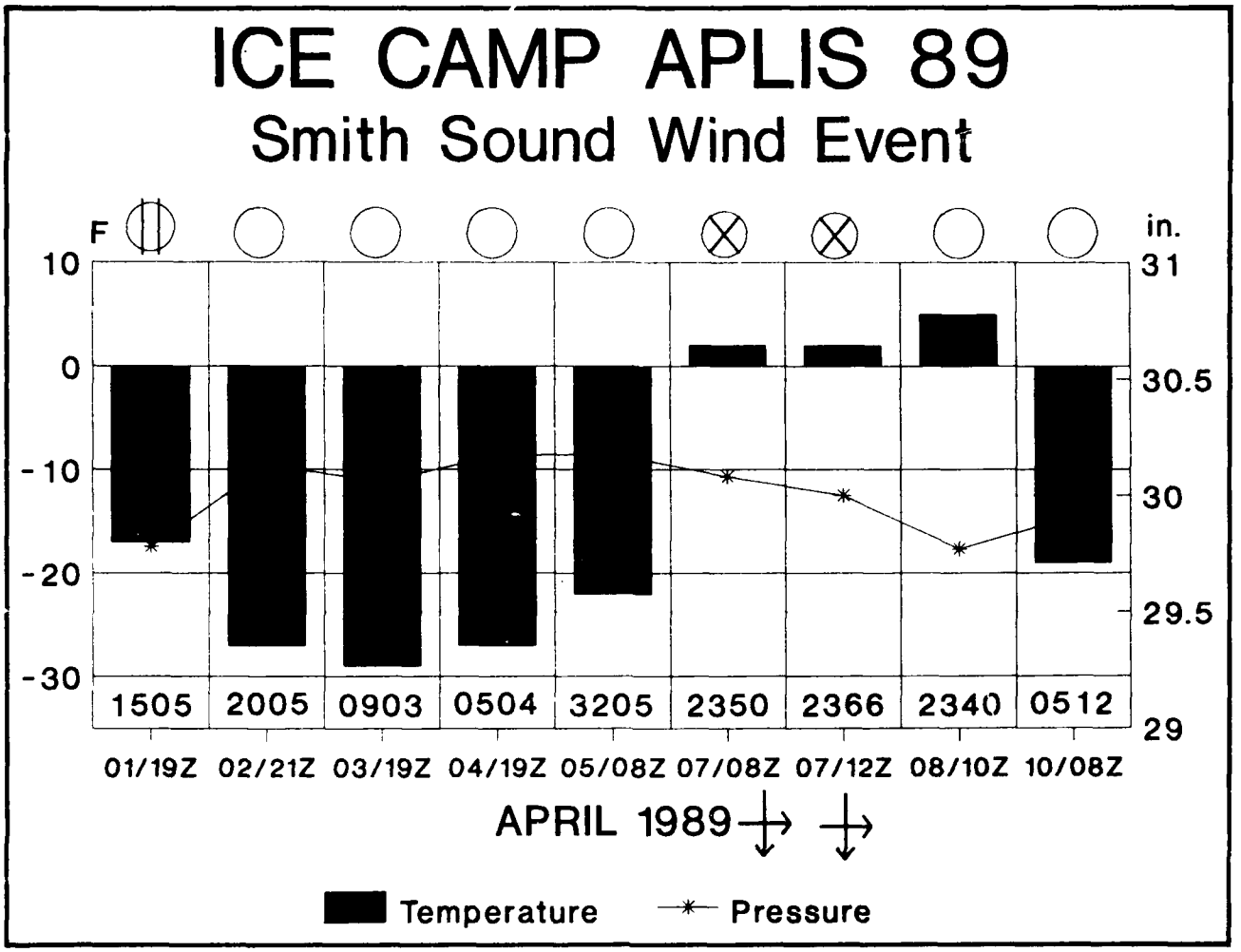

Figure 4-53. Time Series of Surface Weather for Ice Camp APLIS 89. NOTE: Observation times are irregular. (Left ordinate is temperature [°F] and right ordinate is pressure [mb]. Wind direction and speed [DDFF in tens of degrees and miles per hour] are shown in the block below the temperature/dew-point data. Present weather symbols are shown below the date/time group information.)

Accompanying the warming was the onset of overcast skies and a considerable increase in wind speed and the onset of blowing snow. The fact that winds increased from very light winds on 5 April (5 mph) and 6 April (15 mph—not shown) to 50 and then 66 plus mph by 1200 GMT indicates that dangerous wind conditions approaching hurricane force reached Smith Sound during this period and persisted throughout most of the day at the ice camp. Records from the ice camp show that the winds did not abate until the next day (8 April) when skies cleared and the surface pressure reached its minimum value of 29.67 in of mercury.

Navy Captain Dorman of the Arctic Submarine Laboratory at San Diego was at the ice camp during this high wind event and attests to the fact that the situation was life-threatening, the camp being only 2 mi ($\approx$ 3 km) from open water. Captain Dorman maintains that the wind speed may have reached as high as 100 mph; however, since the anemometer blew away, this estimate cannot be confirmed.

This case study shows how an otherwise innocuous synoptic situation can be enhanced by local effects. Perhaps southwesterly flow in advance of an approaching trough routinely produces extremely heavy weather in the Smith Sound area due to a channeling effect. In any event, these strong winds were not forecasted. Thus it behooves the Arctic forecaster to anticipate similar future events.

4.4.4 Conclusions

1. In regions of the Arctic, an approaching trough can produce extreme wind events if the flow is channeled from a larger to a smaller body of water when the wind is upchannel.
2. In spite of deep warm advection, significant vertical mixing can occur as long as weak, warm advection aloft overlies strong, low level, warm advection. This mechanism is just as effective for destabilization in cases where low level, warm advection is accompanied by strong, cold advection aloft.
3. The strongest winds associated with a cold frontal passage may be dangerously stronger ahead of the front rather than behind if local channeling effects are present.

4.5 Case V: Cloud Plumes in the Arctic

4.5.1 Introduction

The existence of cloud plumes, emanating from selected islands and/or adjoining polynyi in the Arctic, has attracted attention since Kienle et al. (1983) suggested a possible volcanic origin for plume development near Bennett Island (Ostrov Bennetta) in the East Siberian Sea. Matson (1986), reported on another plume, this one emanating from the vicinity of Novaya Zemlya, an island that separates the Kara Sea from the Barents Sea. Matson also suggested a geomorphic or anthropomorphic origin for this case plume (see Chapter 5, Section 5.2). Parmenter-Holt (1987) argued rather convincingly that the latter plume was not geomorphic or anthropogenic but rather a naturally occurring, orographically-induced event, which signaled cloud formation as a result of lee mountain wave activity.

Research at NEPRF substantiated Parmenter-Holt's conclusion as valid for both of the preceding examples and distinguishes differences between orographic plumes and lower level polynya-produced plumes, also often noted during the cold months over the Arctic region. NEPRF further suggested that the orographic plumes are often excellent indicators of Arctic frontal location and associated jet stream activity.

4.5.2 18 February 1983

Figure 4-54, IR NOAA-6 imagery for 18 February 1983, shows the Bennett Island plume that attracted so much early attention. The plume is colder than the surrounding environment, radiating at a temperature of about −45 °C. Zhokhova is the small island outlined in the figure to the east-southeast of Bennett. The 0000 GMT sounding for Zhokhova on 18 February is shown in Fig. 4-55. The sounding indicates that the plume top was located below the tropopause near the 400-mb level. From Fig. 4-54 the source of the plume appears to be over the polynya, apparent as a warm region on the east side of Bennett Island. (Note the polynya effect also apparent on the east side of Zhokhova.) The suggestion that the plume has its source over the polynya, however, is ruled out for two reasons: (1) the low-level inversion shown on the Zhokhova sounding would have been a strong influence tending to prevent the cloud from extending to altitudes above the lowest levels, and (2) data from NOAA-7 at 0047 GMT (Fig. 4-56) reveal that the northernmost plume extends inland, over the island, at that time. A second plume appears slightly southeast of the first plume. Unfortunately the outline of Bennett Island is rather crudely drawn on the original image, used in the 1983 article (Fig. 4-54). A more exact outline of the island, showing topographical features, is shown in Fig. 4-57. This outline was superimposed over the NOAA-7 image and is shown in Fig. 4-58. It reveals that the first plume had developed downstream but in the lee of a 1,398 ft (426 m) mountain; the second southernmost plume also developed in the lee of higher terrain (exact height not specified) near the southeastern tip of the island. Consequently, more than likely both plumes are effects of vertically propagating mountain waves of the type commonly seen in the lee of mountainous terrain over other islands in the Arctic and other regions of the world (see Chapter 5, Subsection 5.5.1). The turbulent appearance of the particular plume of this example is different from the more stratified and striated appearance of many plumes more commonly seen (Subsection 4-5.3). The difference may be attributed to the fact that this particular plume was generated as the result of airflow over an isolated mountain peak, rather than the more commonly seen flow over the crest of a lengthy ridge oriented perpendicular to the prevailing flow.

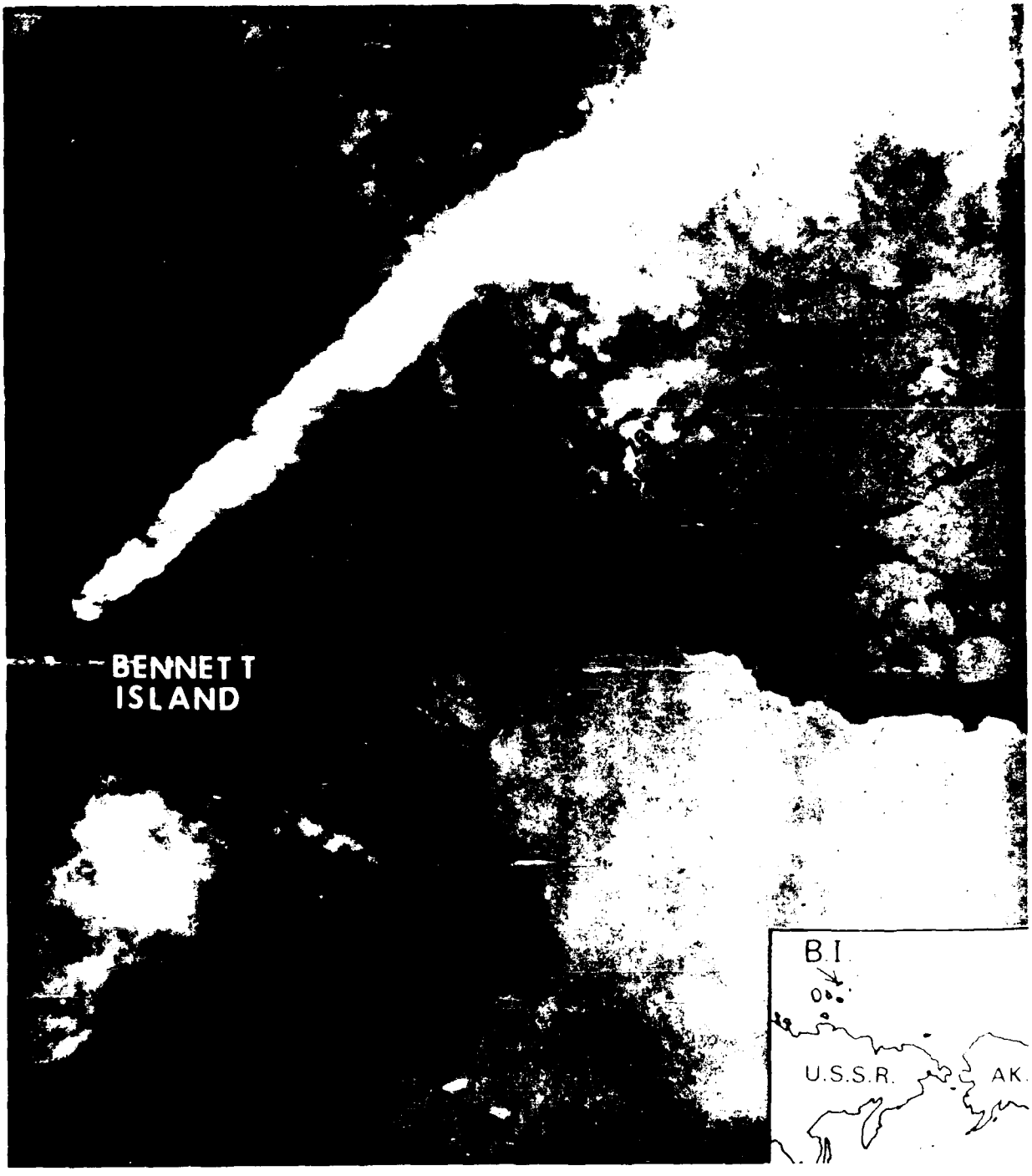

Figure 4-54. IR NOAA-6 Imagery, 0615 GMT 18 February 1983.

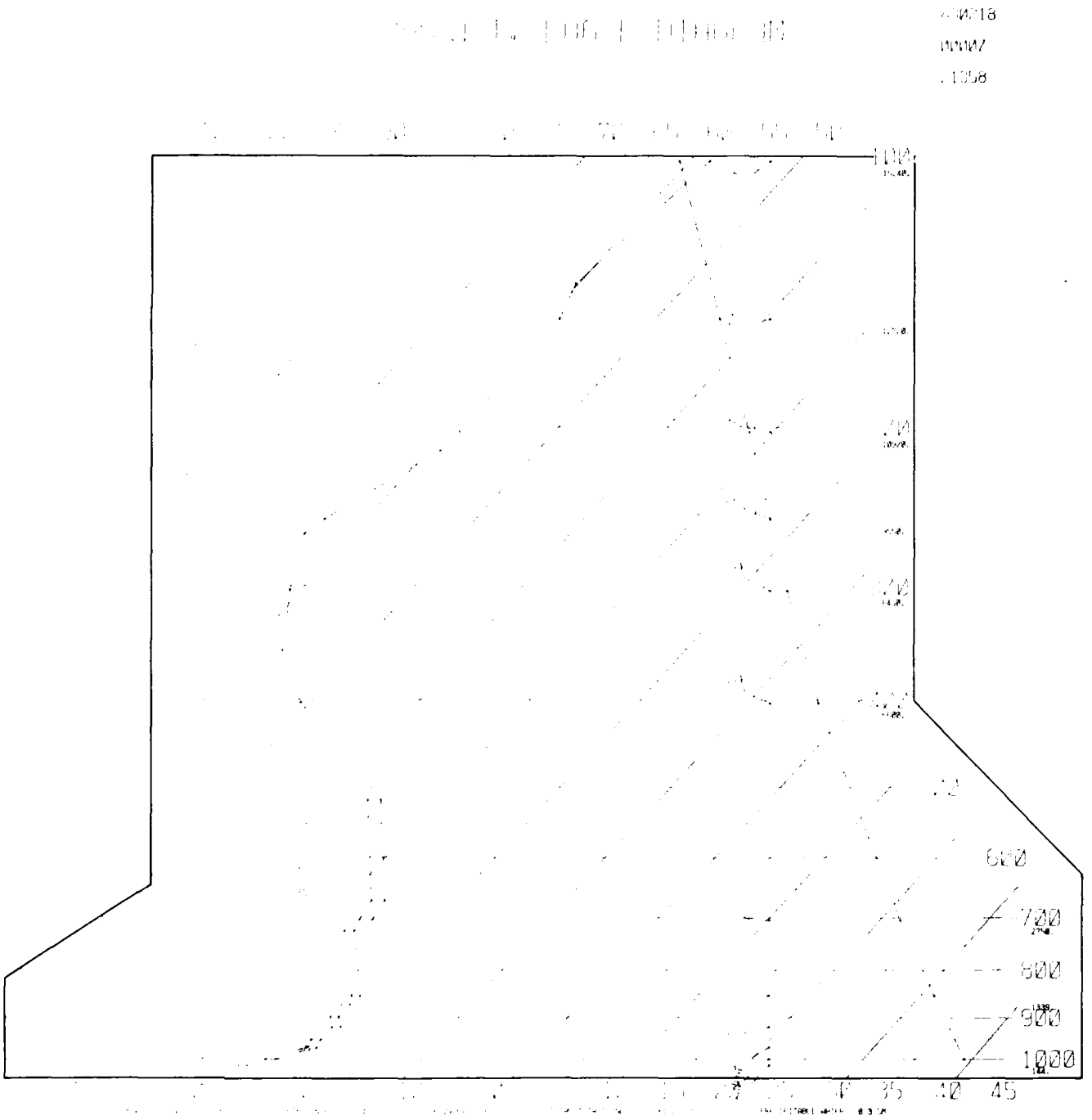

Figure 4-55. Radiosonde Data for Zhokhova Island (Station 21358), 0000 GMT 18 February 1983.

Figure 4-56. IR NOAA-7 Imagery, 0047 GMT 18 February 1983.

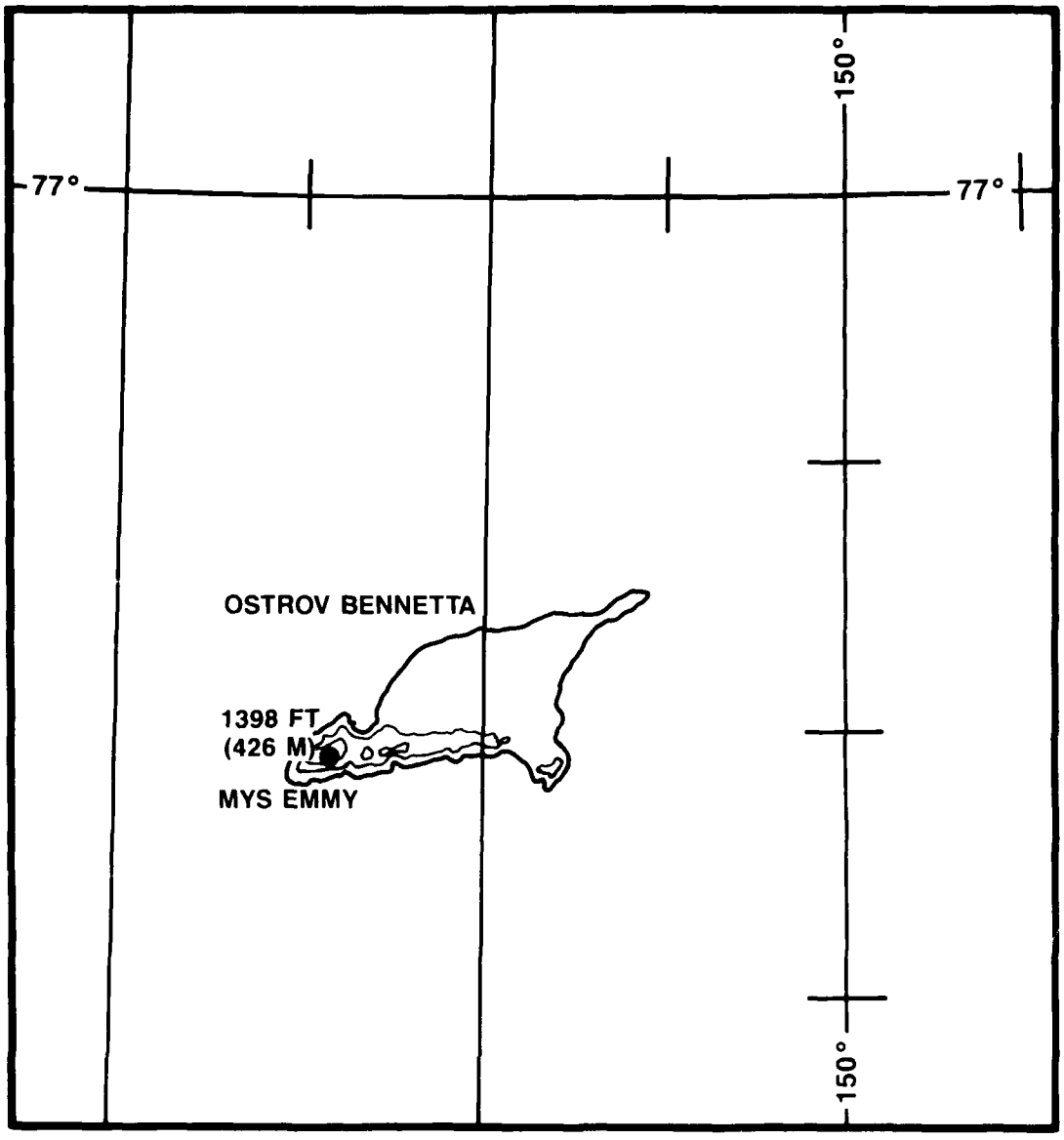

Figure 4-57. Map of Bennett Island.

Figure 4-58. IR NOAA-7 Imagery with Outline of Bennett Island Superimposed, 0047 GMT 18 February 1983.

An important consideration to bear in mind is that the apparent plume source region can appear to shift with time, probably depending upon a sudden relaxation, or conversely, intensification, in the strength of the wind flowing over the obstacle. A good example is shown by plume cloud development in the lee of the island of Kvitoya, just east of Svalbard, on 28 March 1987. The image for this example (Fig. 4-59) shows the region as observed by NOAA-10 in IR channel 4 data at 1114 GMT. Apparently the plume's source is the

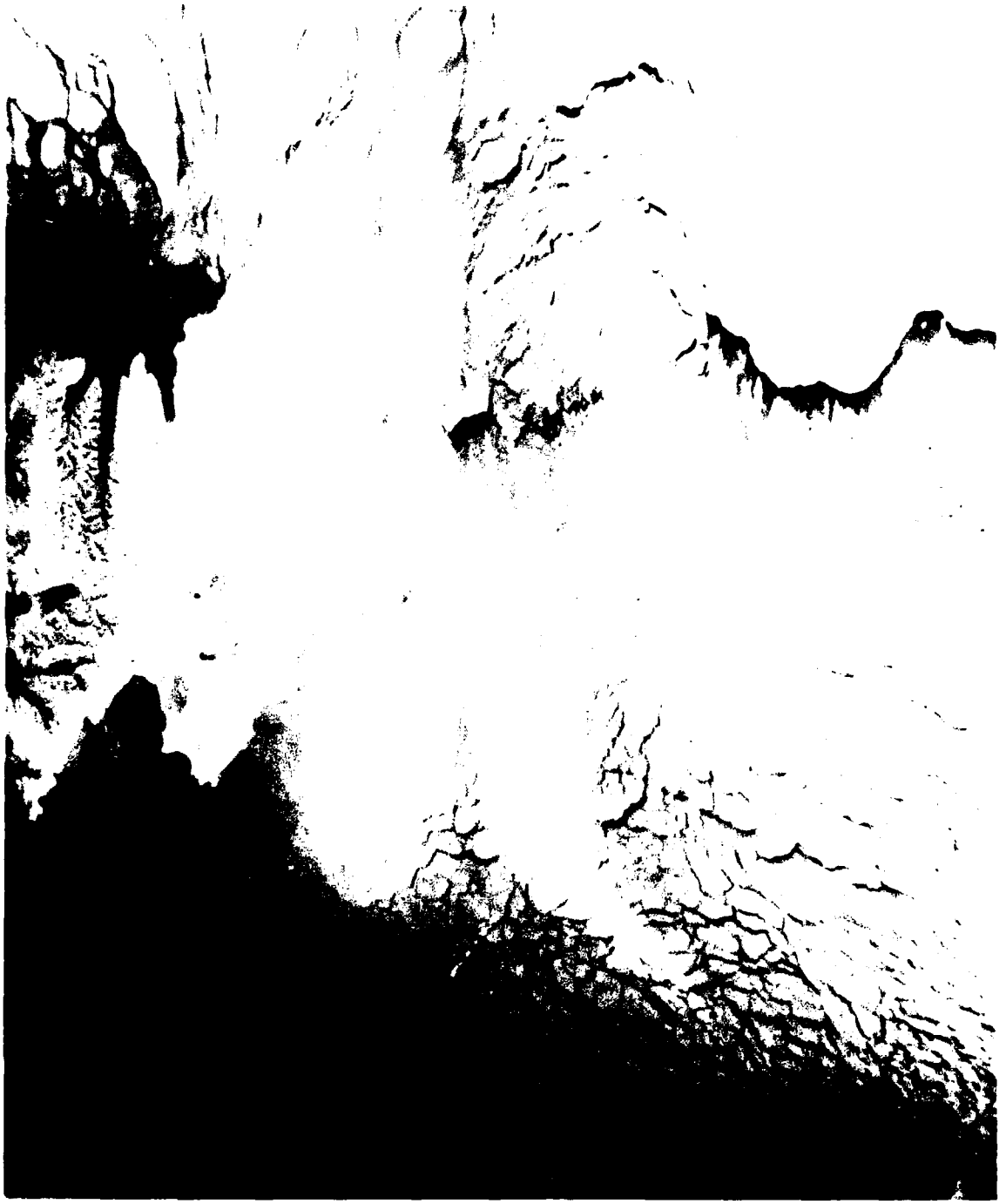

Figure 4-59. IR NOAA-10 (Channel 4) Imagery, 1114 GMT 28 March 1987.

polynya on the south lee of the island. A later NOAA-10 channel 4 view at 1515 GMT (Fig. 4-60) shows, however, the main plume formation very near or even very slightly over the southern shore of the island. A second thinner plume also emanates from the shoreline near the southeastern tip of the island. Figure 4-61 is a map of the island showing that a ridge line exists between two peaks aligned east-west on the island. The width of the ridge line correlates well with the width of the larger plume. The contours indicate an additional separate peak near the southeastern end of the island, which aligns quite well with the thinner cloud plume extending from the shore of the island. Conclusive proof of formation, as a result of island topography, is provided much earlier in the day by IR DMSP (2 n mi resolution) imagery (Fig. 4-62). These data, acquired on 28 March 1987 at 0254 GMT, show plume formation clearly over the island on the lee slope of the ridge line and the smaller southeastern peak. Note that cloud-top temperatures are colder at the plume source, immediately adjacent to the highest terrain—an indication of greater wave amplitude and highest cloud-top altitude in that region.

Figure 4-60. IR NOAA-10 (Channel 4) Imagery, 1515 GMT 28 March 1987.

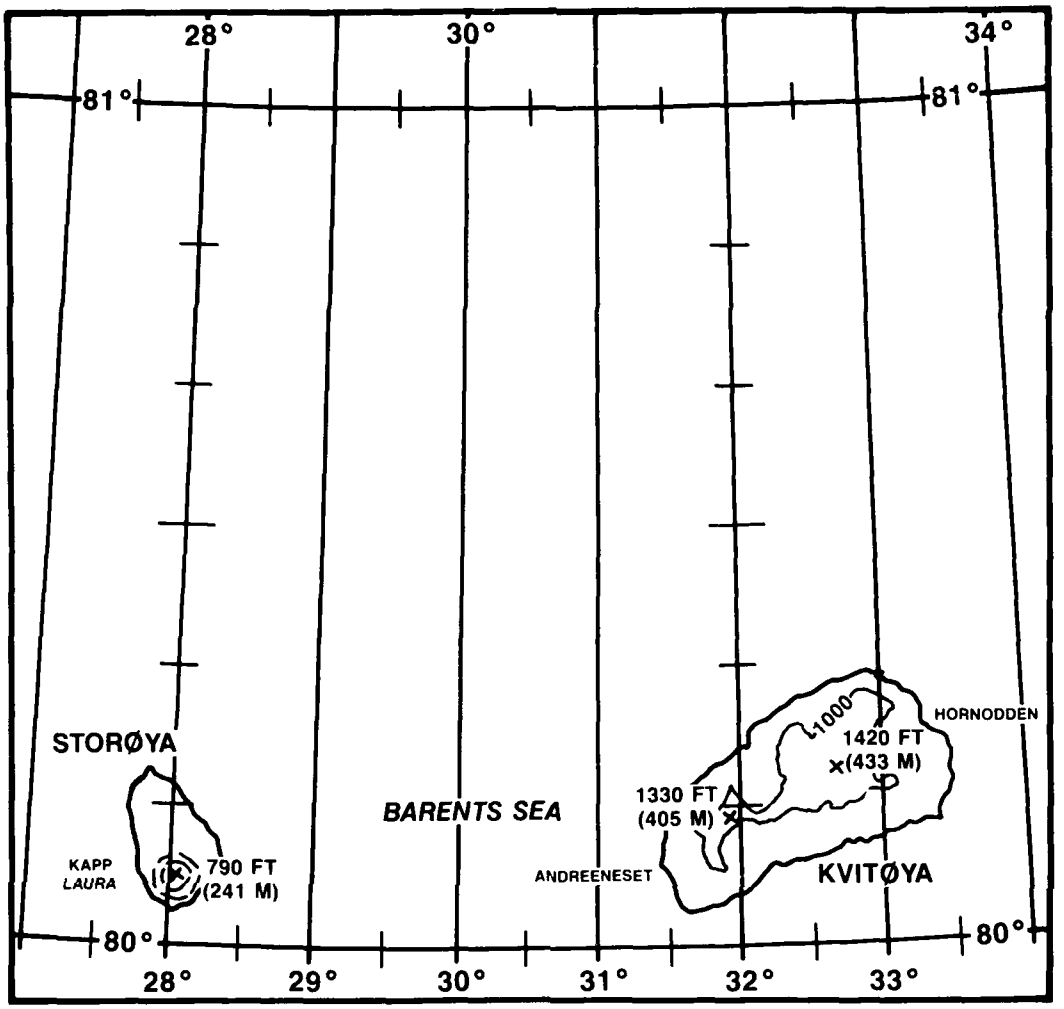

Figure 4-61. Map of Kvitoya Island.

4.5.3 Polynya Plume Examples

In the NOAA-10 satellite image of Fig. 4-60 some obvious small plumes emanating from lead features in the southeastern portion of the figure can be seen. Probable polynya plumes also extend from apparent open water areas south of Franz Josef Land in the upper right of the image. As indicated and illustrated in Chapter 5, Section 5.2, polynya-produced plumes in cold Arctic regions generally appear warmer than the surrounding, ice-covered sea surface over which they lie, due to formation under a pronounced low-level inversion. The plumes in Fig. 4-60 appear colder than the surrounding region. This illustration suggests that the air was more unstable than normal at lower levels and that the plumes were forming under an inversion base whose temperature was colder than the surface temperature.

Figure 4-62. IR DMSP (Thermal Smooth) Imagery, 0254 GMT 28 March 1987.

A sounding for Heysa (Fig. 4-63), located at 80.6°N 58.0°E on Franz Josef Land, north of the polynya region, confirms this potential. Air from the north flowing from the ice over the open water of the polynya would be rapidly moistened and warmed by several degrees, depending on length and duration of the path over the water. Resulting plume formation would be capped near the base of the inversion, which is shown to be colder than the surface temperature.

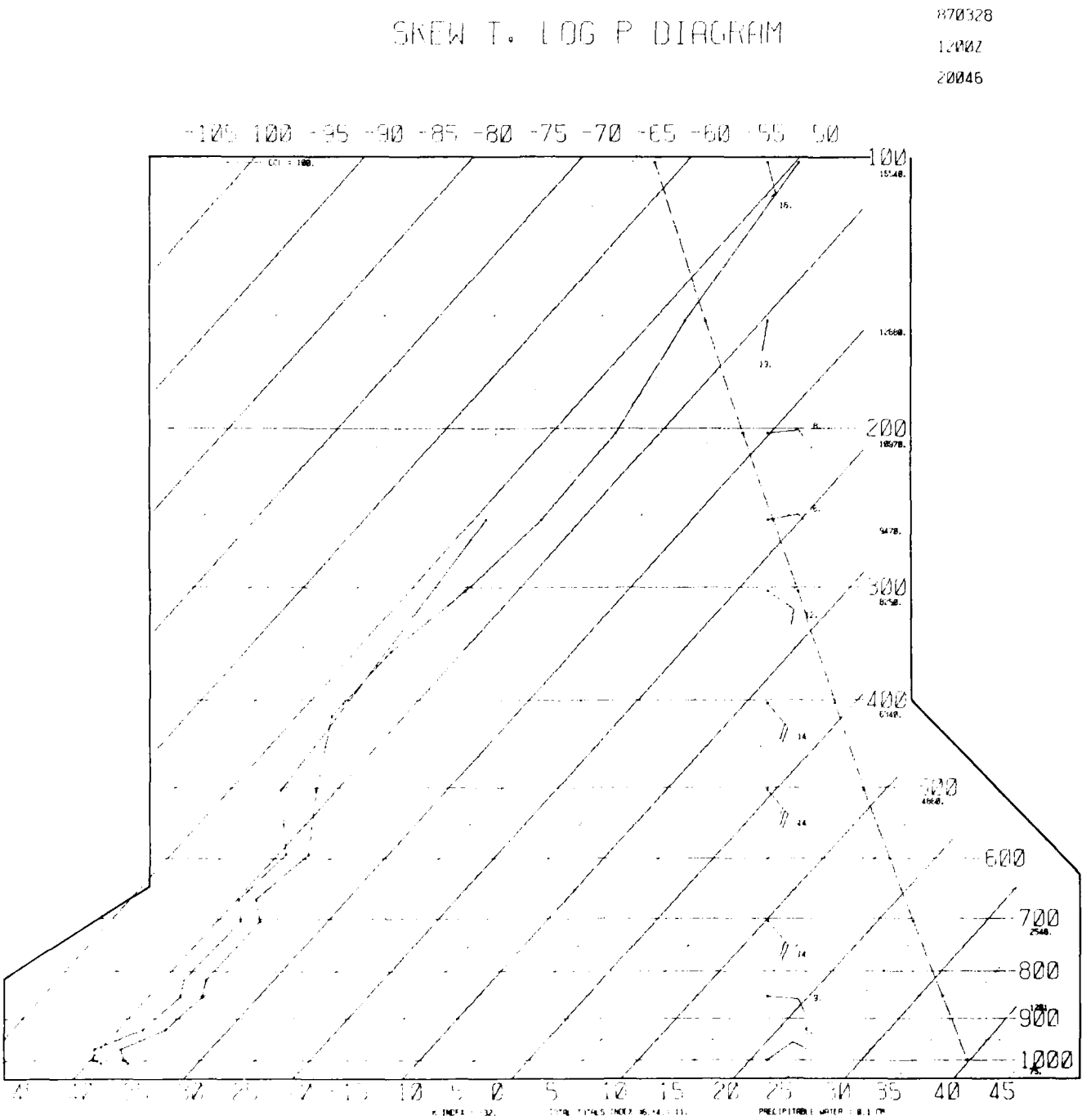

Figure 4-63. Radiosonde Data for Heysa (Station 20046), 1200 GMT 28 March 1987.

4.5.4 Association of Arctic Plumes and Arctic or Polar Frontal and Jet Stream Location

An examination of Arctic plume formation over the Svalbard-Barents Sea region (Fett, 1990(a)) showed that the plumes could often be used as indicators of Arctic frontal position and coexisting jet stream location. Plume generation requires strong winds aloft, and sufficient moisture, characteristic of frontal zones. Since Arctic fronts are often ill defined over the relatively flat ice surface, the sudden generation of a plume over mountainous island terrain may be an early unambiguous signal of Arctic frontal position.

Figure 4-64 exemplifies the concept for a polar front, slightly south of Arctic latitudes, over the Aleutian Islands area. The image is from IR DMSP thermal smooth (TS) data received at Elmendorf Air Force Base on 11 May 1990. Arctic plume generation is apparent over Unimak Island in obvious close association with a polar front position and accompanying low pressure center or cloud vortex. Note that plume formation at this time is restricted to Unimak Island, where the front is located, and not over equally mountainous terrain to the east-northeast or west-southwest. This fact makes the use of island plumes valuable in meteorological analysis. An additional excellent example of lee wave formation in association with an Arctic front is shown in Chapter 5, Fig. 5-16.

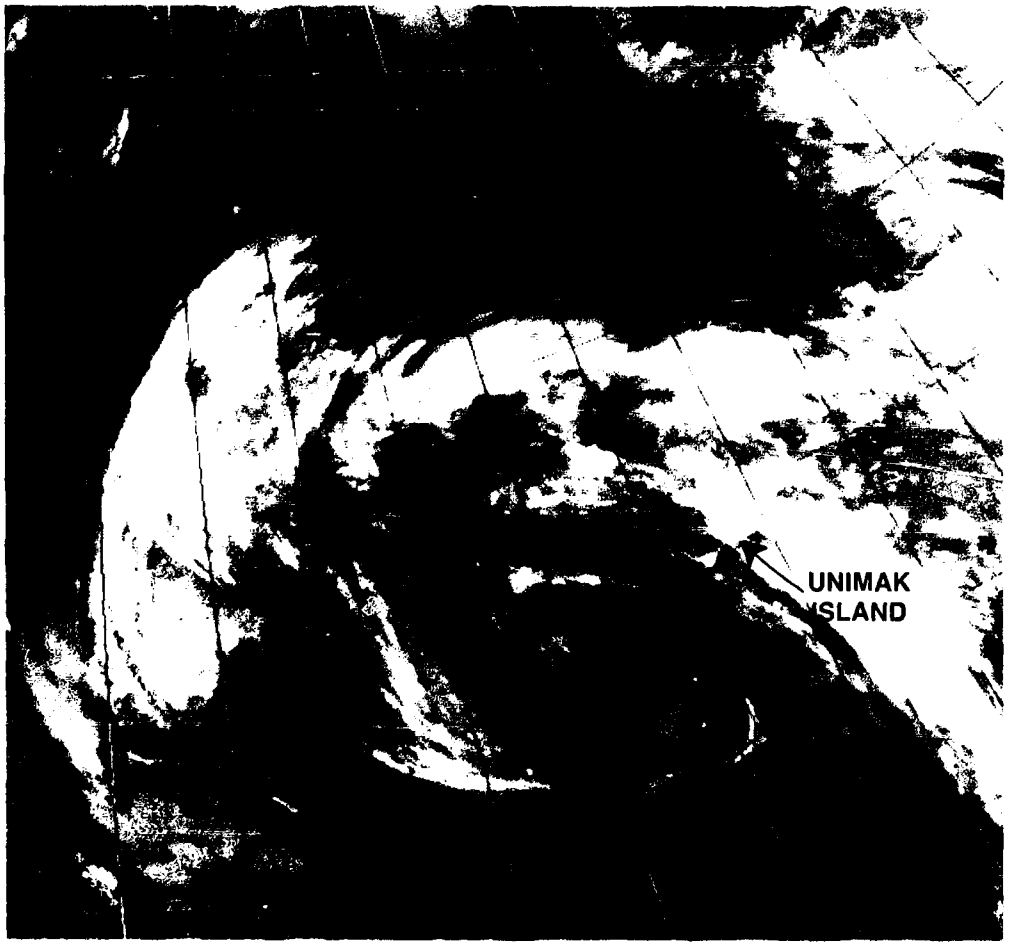

Figure 4-64. IR DMSP (Thermal Smooth) Imagery, 0613 GMT 11 May 1990.

5. SPECIAL WEATHER FEATURES OF THE ARCTIC

5.1 Pollution Versus Arctic Haze

A popular notion exists that the vast, underpopulated, and pristine regions of the Arctic must have crisp, clean air. But such is not the case. In fact, the Arctic atmosphere is beclouded by at least two distinct types of turbidity. On the one hand, population centers like Anchorage and Fairbanks in Alaska produce in situ pollution, and on the other hand, industrial pollutants from midlatitudes have been traced all the way to the Arctic Ocean.

The principal implications regarding the climate of the Arctic due to Arctic haze and pollution involve a significant change in the heat balance of the Arctic and the acidification of Arctic waters. This section concentrates on pollution problems in Alaska for which adequate information is available. Populated areas of the Arctic are shown in Fig. 5-1.

In situ pollution will be discussed first. As elsewhere in the world, locally produced air pollution results when three factors are present: a source of polluting material, light winds, and strong temperature inversions. Anchorage and Fairbanks have all three. In fact, previous sections described how very common and persistent light winds and strong inversions are in the Arctic, especially in winter months. Elevated inversions occur when a layer of warm air glides up over a cold air layer, such as in frontal inversions. Inversions will form right at the ground, however, if radiational cooling of the Earth's surface is the main cooling mechanism. In the Arctic the latter type inversion can occur during the day as well as at night due to the radiative properties of snow and ice cover and because long periods occur in winter when no sunlight is present.

Under the low temperature conditions of winter in Fairbanks, according to Benson and Rizzo (1980), the most visible type of air pollution is ice fog. Ice fog occurs at $-30\,^{\circ}F$ ($-35\,^{\circ}C$) or below when all water vapor emitted into the atmosphere (from car exhausts, houses, industrial plants, and open water surfaces) condenses onto hygroscopic nuclei and forms droplets. These droplets then freeze almost at once to form tiny ice crystals. Because of this origin, ice fog can be considered as a type of air pollution, in which the major pollutant is ice.

In addition to water, however, other air pollutants, including lead, sulfur dioxide, nitrogen oxides, carbon monoxide, and hydrocarbons are present and often in high concentrations. Pollutant concentrations in the Fairbanks area in winter are, in fact, found to be as high as those in cities such as New York, Detroit, and Los Angeles.

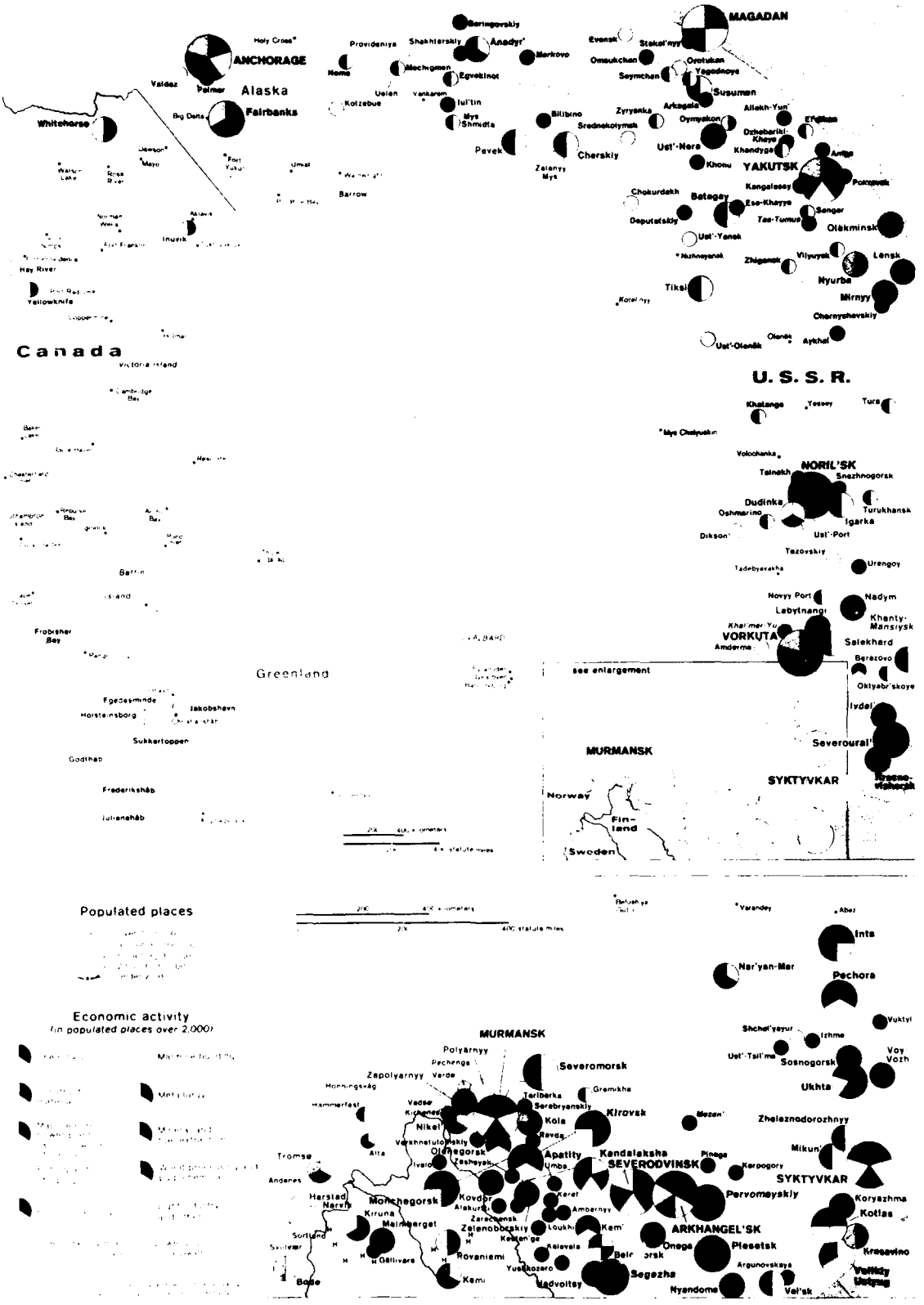

Figure 5-1. Population Centers of the Arctic (Jones and Bartlett, 1981).

Air pollution has even surfaced on the Arctic coast of Alaska, with the petroleum development at Prudhoe Bay. One of the most striking examples is the exhaust plumes from oil rigs extending for 20 mi (30 km) or more across the Arctic tundra and adjacent Arctic Ocean, which can be seen in satellite imagery (Fig. 5-2). The plumes originate from the exhaust of heating units aboard the rigs.

The difference between Arctic in situ pollution and Arctic haze was outlined by Shaw (1980). Evidence of widespread haze over the northern regions in late winter and early spring was presented. Aircraft observations showed that the haze concentration increases from the ground up, reaching a maximum at an altitude of several thousand meters, then decreasing again above that. This pattern indicates that the haze is not produced by a nearby surface source as is the in situ pollution.

In 1976 a series of chemical sampling experiments were carried out by Rahn and Borys (Shaw, 1980) from the University of Rhode Island. These experiments were aimed at determining the composition of Arctic haze. The findings were rather surprising inasmuch as they indicated that the haze is rich in elements associated with industrial pollution, such as vanadium and manganese. Researchers now suspect that the source of the haze may be in Europe, the U.S.S.R., and sometimes the northeast United States. On rare occasions the haze is composed of "crustal" materials that appear to have come from the Gobi and other great Asian deserts. A schematic representation of the principal pathways of industrial pollutants and desert dust being injected into the Arctic is given in the Shaw diagram, presented as Fig. 5-3.

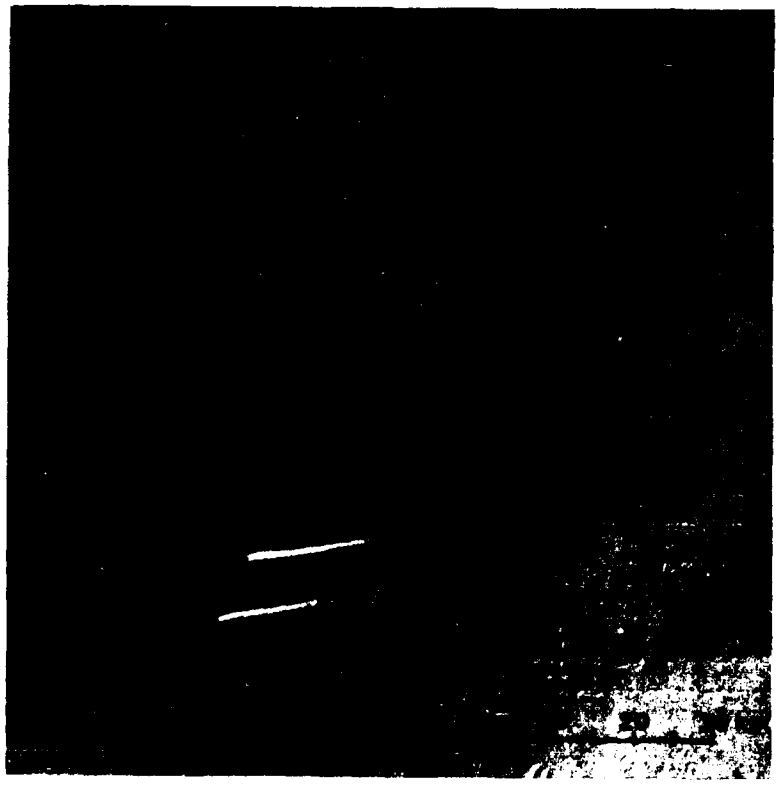

Figure 5-2. Oil Rig Exhaust Plumes, Prudhoe Bay, Alaska (LANDSAT Image, 12 February 1977) (Benson and Rizzo, 1980).

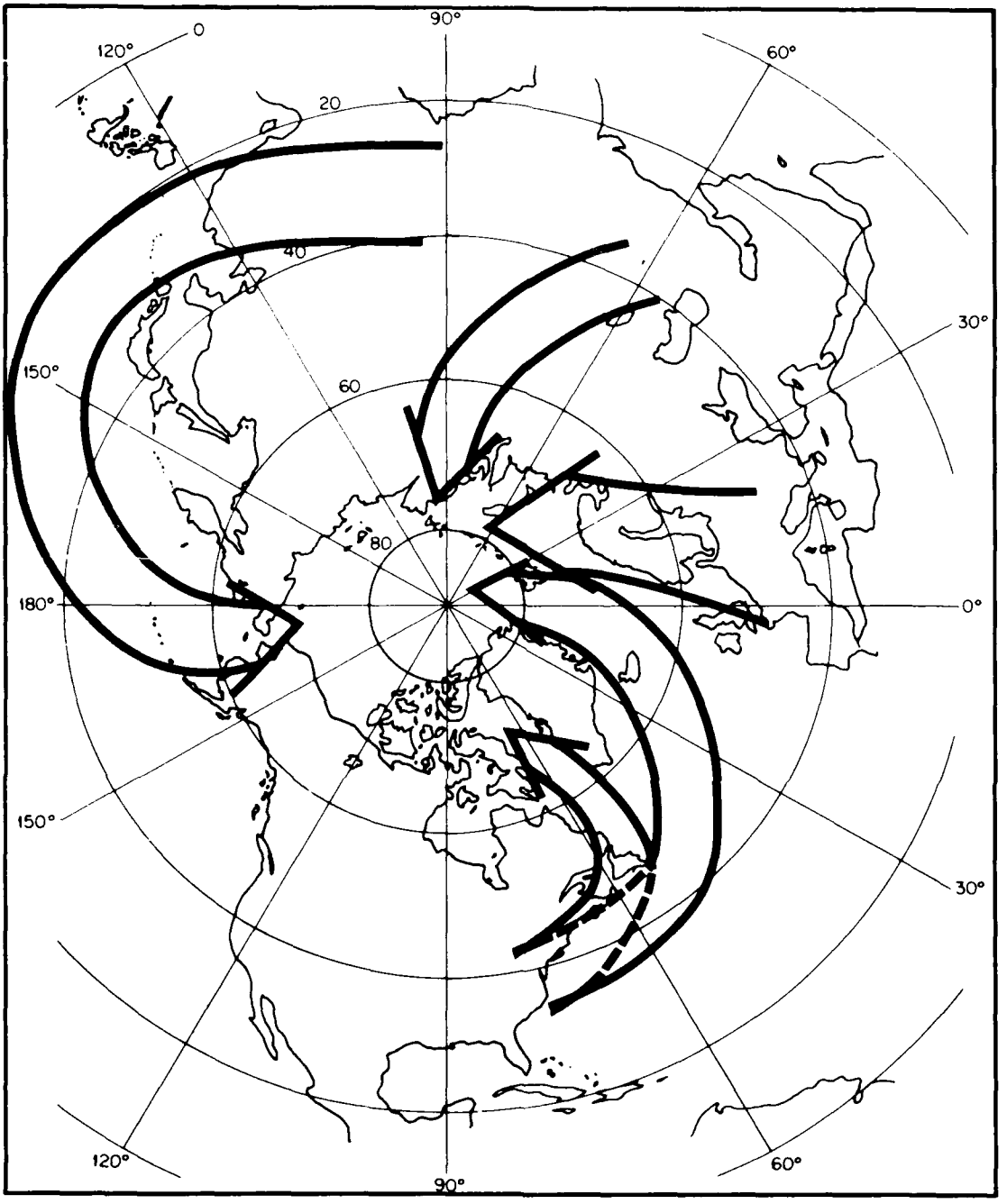

Figure 5-3. Source Regions of Arctic Haze (Shaw, 1980).

In addition to the presence of vanadium and manganese, a strong indicator of pollution is the gray coloration on filters taken from air sampling devices. The color comes from the presence of sooty, unburned carbon, an element that most likely originates from manmade combustion processes. Also, an abundance of sulfates is found in the haze particles over Barrow, Alaska. Presumably, these sulfates come from conversion of sulfur dioxide gas, the major source of which is midlatitude pollution.

Arctic haze investigators were initially surprised that the Arctic haze made its appearance in winter whereas summer haze is more characteristic of the midlatitudes. The winter-summer contrast is apparently Arctic-wide. Samples from the air at Thule, Greenland, at Spitsbergen, and near Fairbanks in interior Alaska all show pronounced winter maxima. In general, Arctic air can be termed clean in summer but dirty in winter. Four possible reasons account for the fact that the Arctic haze is most pronounced in winter: (1) increased winter emission of pollutants, (2) more rapid and efficient poleward transport, (3) greater prevalence of strong inversions (greater stability/less mixing) in winter, and (4) longer atmospheric residence times of the haze particles in winter due to the lack of precipitation to scavenge the pollution particles from the air.

5.2 Arctic Plumes

Matson (1986) reported that in a routine search for satellite ice imagery of the Soviet Arctic, large cold plumes were discovered emanating from Novaya Zemlya Island, U.S.S.R. (74 °N 57 °E). Since then numerous other instances of such plumes have been found. Figure 5-4 is a dramatic example of such plumes. The plume is 95 n mi (175 km) long and originates from the northern part of the island.

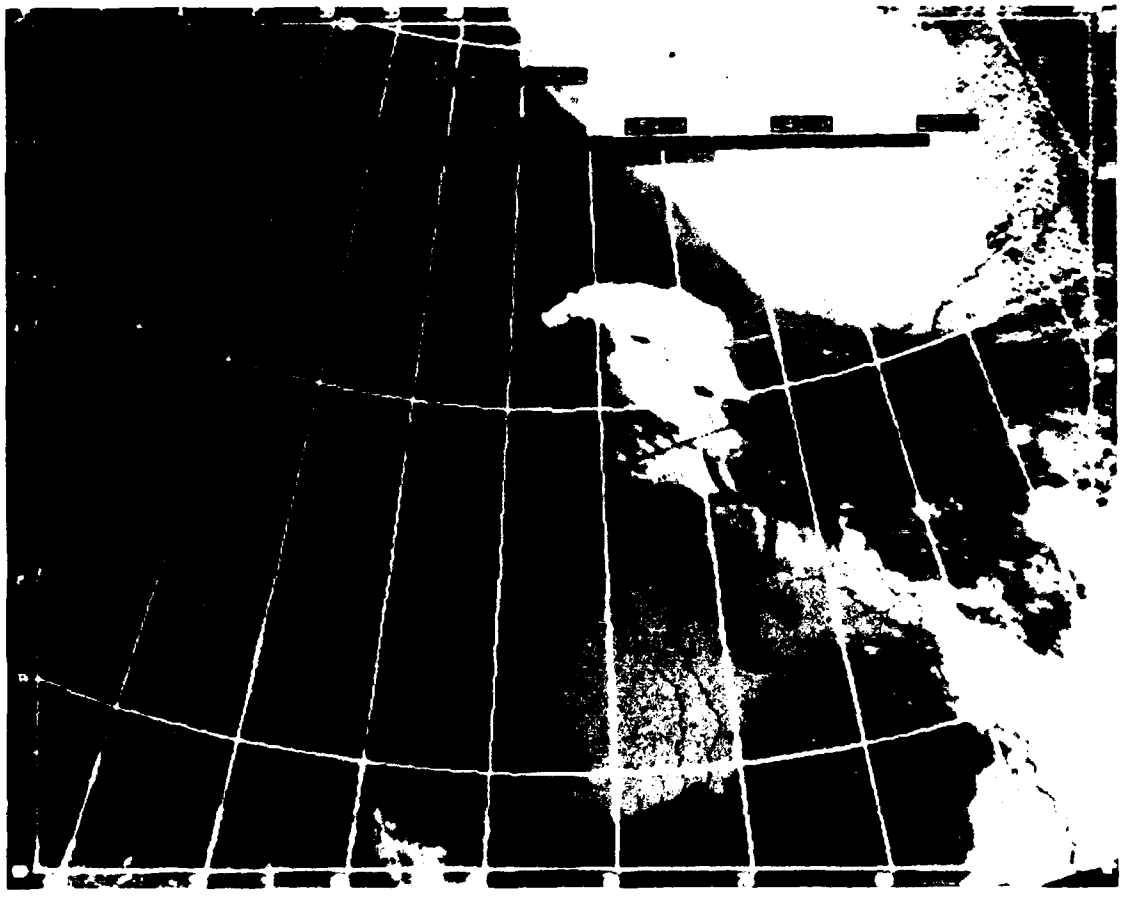

Figure 5-4. IR Image of Novaya Zemlya Plume, 12 March 1982 (Matson, 1986).

Subsequent plumes ranged in length from 95 to 200 n mi (175–375 km). Gray scale temperatures suggest the plume-top temperatures are around −76 °F (−60 °C). Maximum plume altitudes appear to be in the 23,000- to 33,000-ft (7–10 km) range.

Of course, the interesting question about these plumes is: What is their origin? In his article Matson speculated on the following: (1) the origin is volcanic, (2) methane gas released from coal beds decomposing beneath the sea floor is responsible, and (3) the island is used for military testing, and the plumes result from huge energy sources.

In no instance, however, was the author able to define the originating mechanism conclusively. No known volcanoes exist in the area, and it is difficult to find a mechanism that could lift the methane gas to altitudes as high as the observed plumes. Finally, the energy required to account for these plumes far exceeds any likely ordnance on Novaya Zemlya. (The Soviets have not replied to any of the author's contact efforts.)

A year later, Parmenter-Holt (1987) challenged Matson's hypotheses and suggested that the cold plumes were naturally occurring, orographically induced events. She pointed out that Novaya Zemlya Island is a northeast-to-southwest-oriented island. The topography of the northern portion of the island, where the plumes were observed, is characterized by a continuous glacial ridge located at the center of the landmass. This glacier rises quickly from sea level to more than 2,500 ft (760 m) as shown in Fig. 5-5. In addition, the northern portion of the island arcs to the northeast, generally perpendicular to the movements of prevailing winds and weather systems.

Depending on wind strength, static stability, and moisture availability, air flow over an orographic barrier, such as Novaya Zemlya, establishes lee waves. Figure 5-6 illustrates the atmospheric motions and resulting cloud distribution of the long orographic gravity wave, or arch cloud.

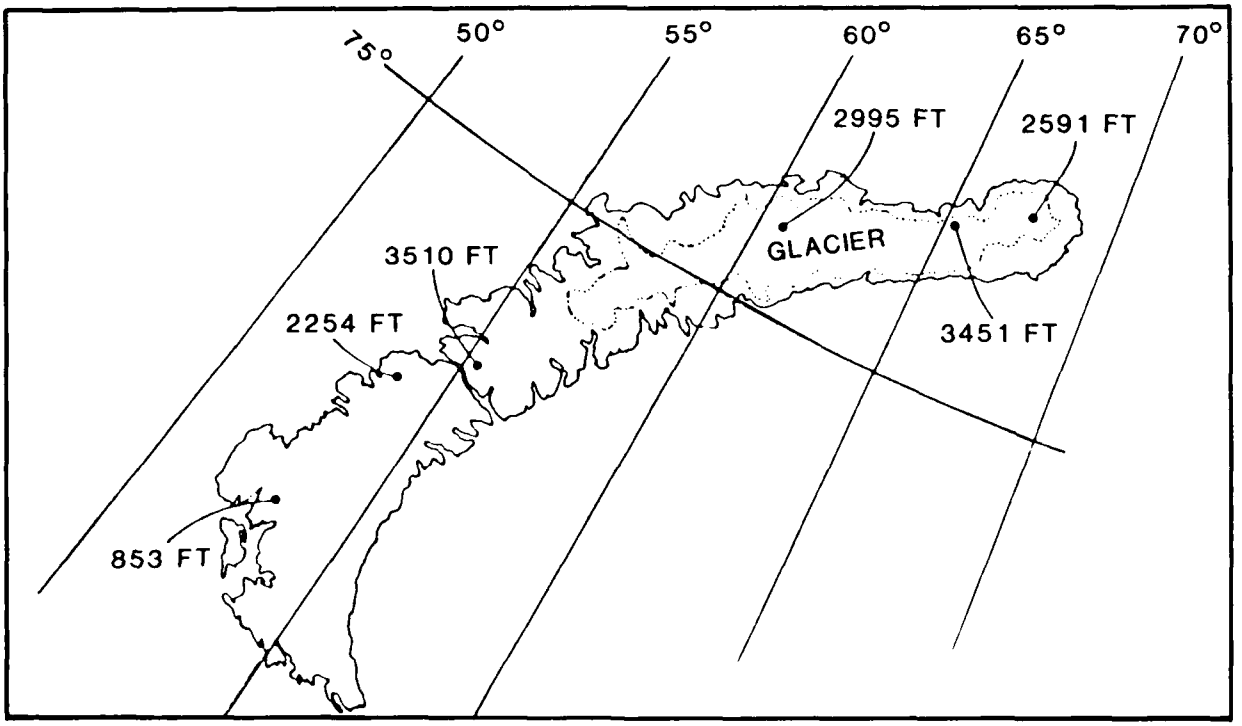

Figure 5-5. Major Features of Novaya Zemlya Island (Parmenter-Holt, 1987).

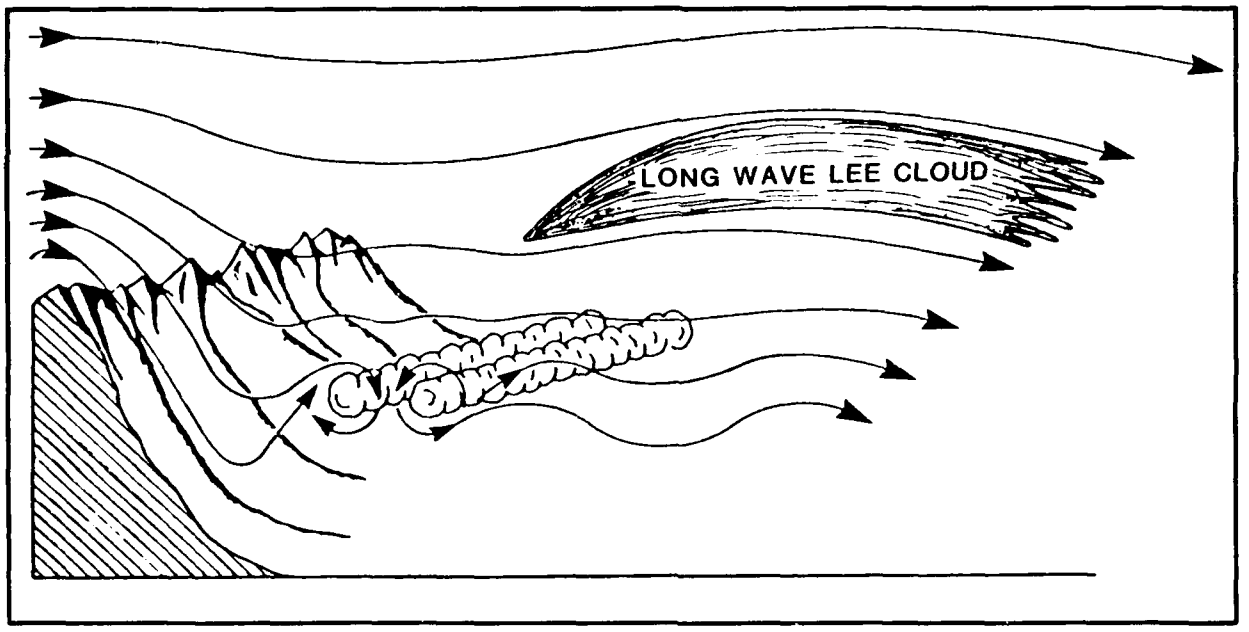

Figure 5-6. Air Flow and Mountain Formation (Parmenter-Holt, 1987).

According to Parmenter-Holt, when viewed from above, a point source plume and an orographic cloud may appear similar. This resemblance may be due to the right combination of terrain, stability, winds, and moisture. Regarding moisture, the northeast end of Novaya Zemlya often appears ice free because prevailing winds blow the ice away from the coast. The suggestion is that Novaya Zemlya may be a source of both polynya-produced plumes and orographic plumes. Note that orographic plumes are often accompanied by strong upper level turbulence and mountain waves that can be extremely hazardous to aircraft operations.

Recent satellite imagery shows evidence of plume generation in many areas of the Arctic. Examples include plumes from Wrangel Island, Spitsbergen, Franz Josef Land, Ellesmere Island, Jan Mayen, and even Bear Island. Polynya-produced plumes are generally revealed in IR satellite data as warm plumes radiating at temperatures reflecting the low-level inversion below which they form. Stronger inversions act as a lid, preventing further vertical development. Under weaker inversions, or more unstable conditions, polynya-produced plumes may break through the inversion or extend to higher altitudes, so that in IR satellite data, the plumes appear as colder, rather than warmer, than the surrounding environment. In such instances polynya-produced plumes can be readily confused with plumes generated as a result of orographic effects. The polynya plumes are generated as cold, dry, low-level air from over the ice advects over the relatively warm open water of the polynya. Interestingly, plumes generally form when relatively high speed, sinking air is in the vicinity. This characteristic suggests that plumes are also related to the presence of the jet stream; however, more work must be done on this subject before conclusive relationships can be made. Figure 5-7 is an example of a polynya plume.

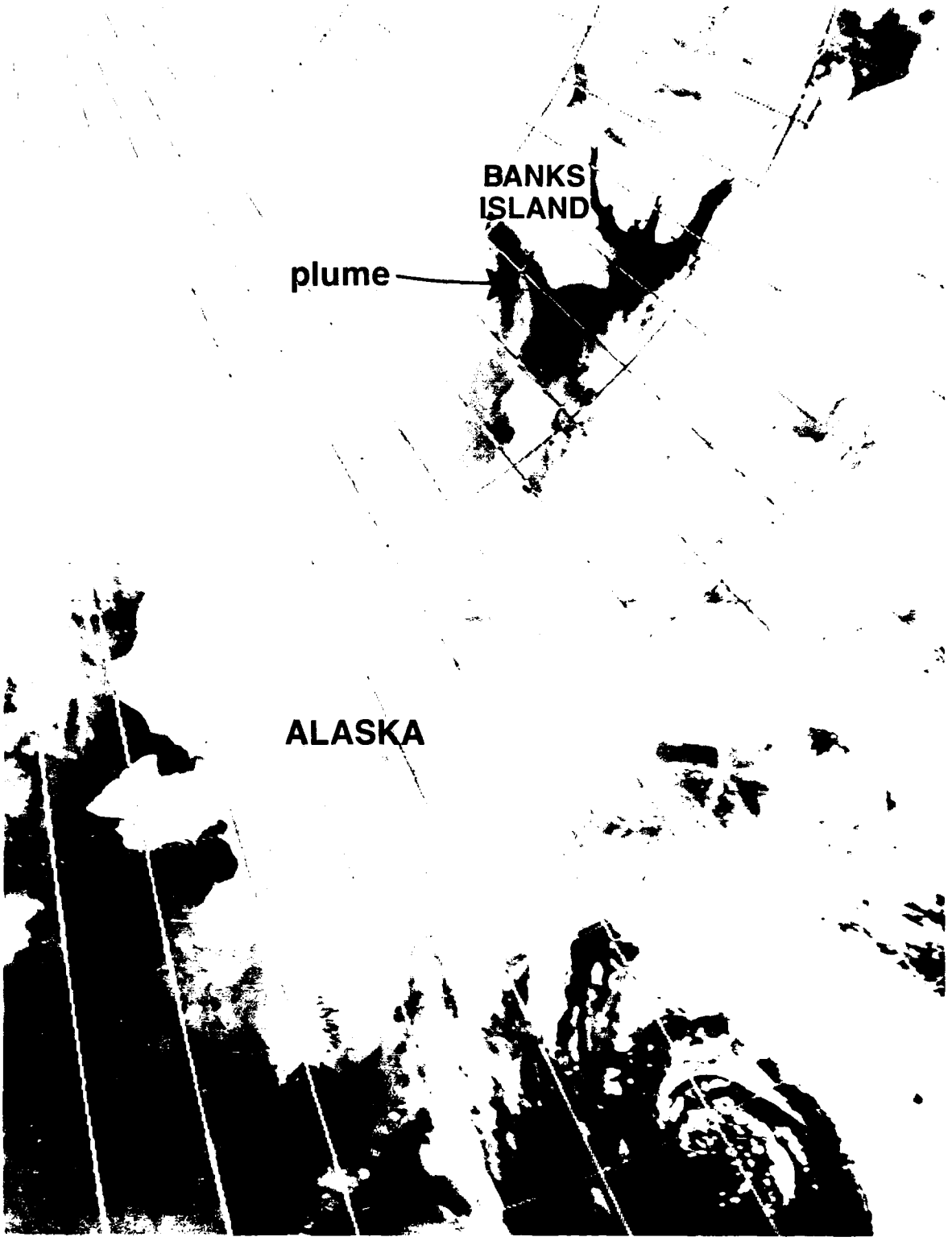

Figure 5-7. A Polynya Plume.

5.3 Small Island Wakes

Even the casual observer of satellite imagery will sooner or later come upon distinctive cloud signatures formed in the wake of small islands, especially in the northeast Atlantic Ocean. Jan Mayen (east of Greenland/north of Iceland) produces a variety of wake clouds that can shed some light on synoptic conditions in the area.

Scorer (1986) chose to present dozens of images of wakes in the lee of Jan Mayen (Chapter 2, Subsection 2.3.10) and discussed the probable synoptic and subsynoptic features associated with them. Jan Mayen is the closest landmass to Greenland and Iceland, a distance of 270 n mi (500 km) and 325 n mi (600 km), respectively. The Norwegian Sea is southeast of Jan Mayen, and it remains unfrozen during the winter. By contrast, the Greenland Sea, to the west, is frozen most of the time during winter and frozen within 110 to 160 n mi (200–300 km) of the coastline of Greenland during the summer.

Aside from the orographic plume patterns previously described, two additional flow patterns are set up by the island: the ship wave pattern and the vortex street. According to Scorer (1986), the ship wave pattern occurs when the air passes over the top of the higher peak and the flow below is not restricted, by a stable layer, from flowing over the top everywhere on the island. The vortex streets are produced when a low level, stable layer prevents the flow below from passing over the island so that the flow can only pass around the ends of the island (see *Navy Tactical Applications Guide* [NTAG] Vol. 1, Sec. 2C). Often the lower peak and ridge line may produce wave clouds while the higher peak produces a vortex street. The wake patterns and vortex streets provide evidence of the direction of low-level flow and of the existence of a low-level inversion in the area. Figure 5-8 shows both a ship wave pattern and a vortex street in the wake of Jan Mayen. Figure 5-9 shows another example of a vortex street in the wake (south) of the Aleutians.

Another isolated island in the Arctic is Bear Island. Lying 130 n mi (240 km) south of the southern tip of Spitsbergen, Bear Island, on occasion, displays ship wave patterns in its lee wake. Due to the relatively flat topography, Bear Island signatures are rather rare.

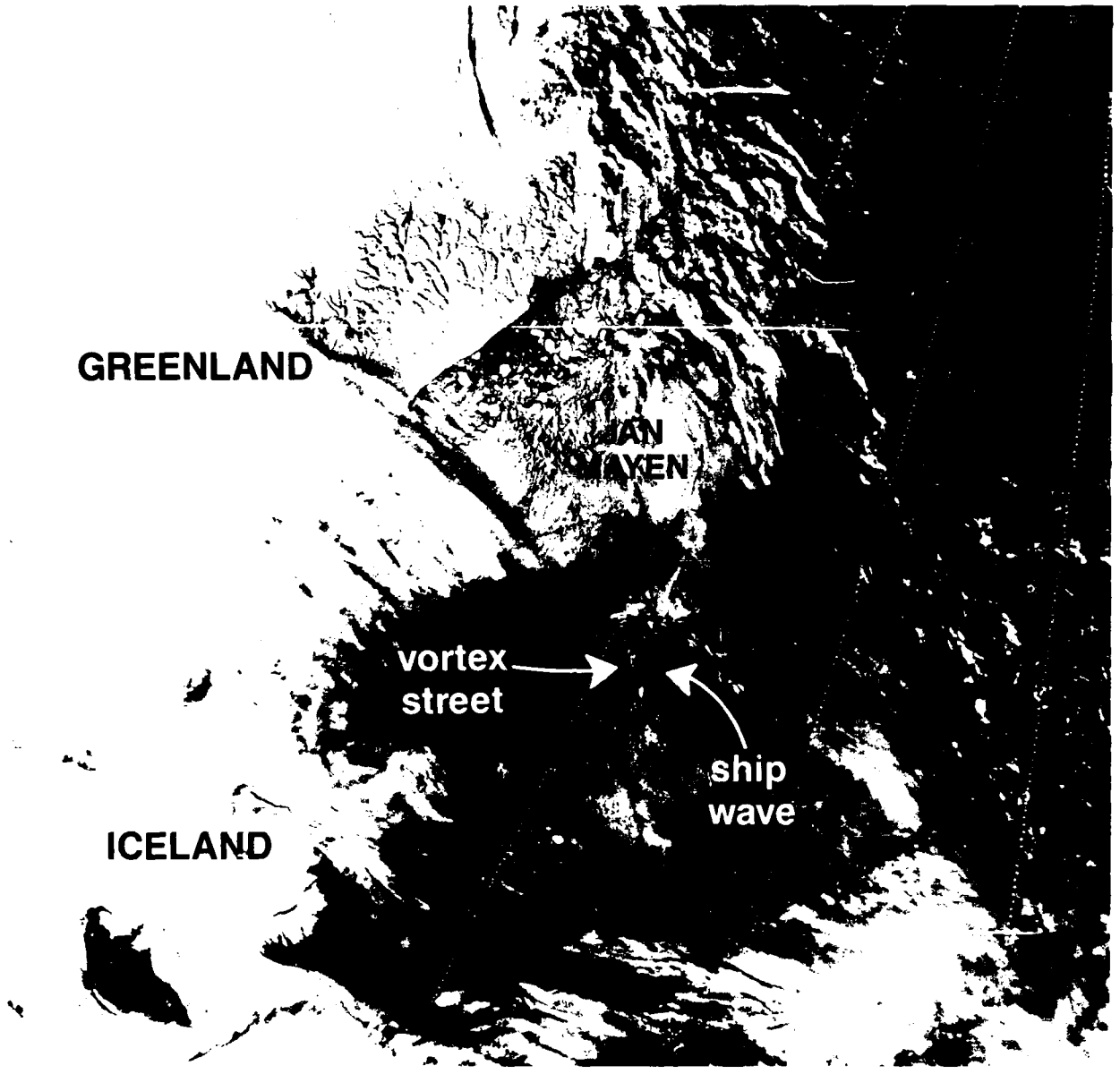

Figure 5-8. Ship Wave and Vortex Street Pattern.

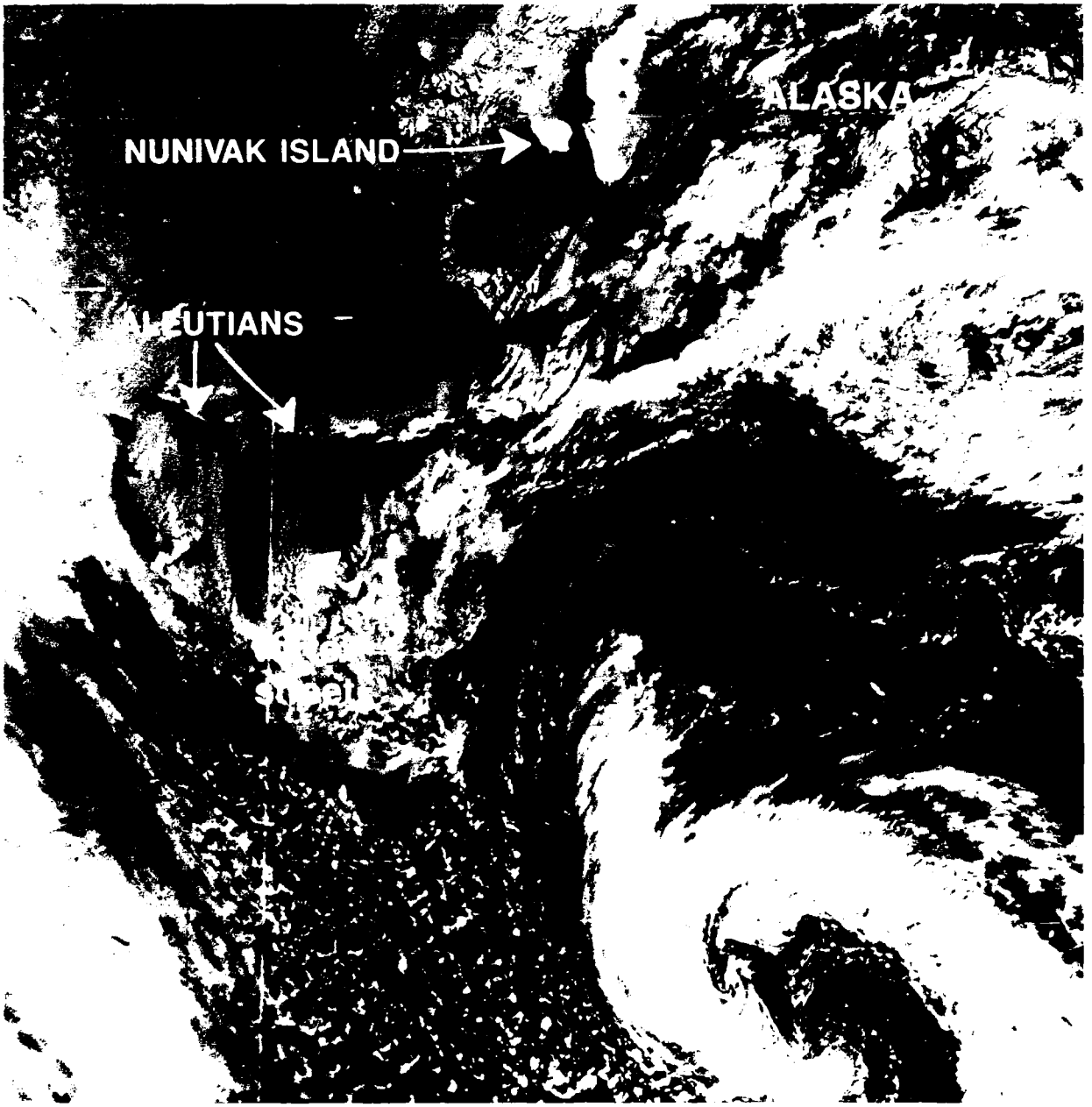

Figure 5-9. Vortex Street.

5.4 Contrails and Ship Trails

In Europe and in the North Atlantic Ocean, contrails can be seen in satellite imagery most frequently in the latitude belt between 45 °N and 60 °N. Arguably, three requirements exist for the formation of contrails: (1) the air must be ice saturated, (2) it must be water unsaturated, and (3) it must be colder than −40 °F (−40 °C).

Contrails are often easy to see in the infrared, but are difficult to see in the visible satellite imagery except over darker ocean and land areas. They are often perceptible due to their shadows on layer clouds below, and both the trail and its shadow are visible when the area below has an intermediate shade. In Channel 3 (3.53–3.93 μm) imagery, the trail and its shadow often appear with equal intensity as darker than the scene below. Occasionally the trails are especially white, an indication that they are composed either of smaller than normal water drops or of unusually small ice particles, as might be the case if the air were only just saturated for ice. Also the possibility exists that with small ice crystals (about 5 millimicrons), sufficient forward scattering may occur in this wavelength for the crystals to appear white when viewed toward the Sun. Figure 5-10 shows contrails over the Beaufort Sea in IR DMSP imagery.

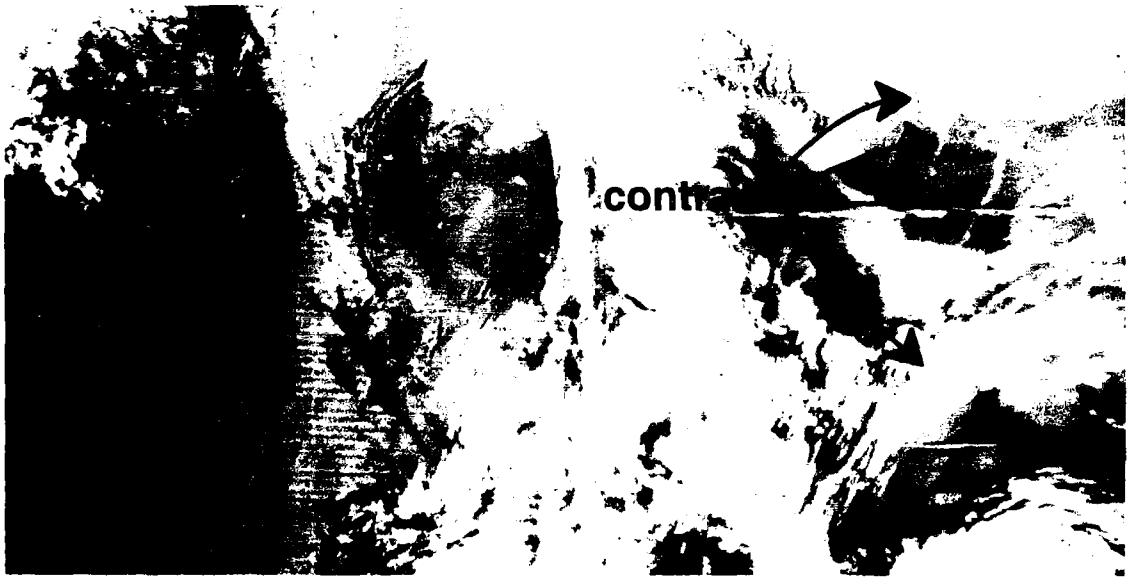

Figure 5-10. Satellite Imagery Showing Aircraft Contrails.

Figure 5-11 is included here to facilitate the forecasting of contrails. To use the graph to evaluate potential contrail formation on a Skew T, Log P Diagram, the trace of the temperature curve on the diagram is related to the "yes," "possible," or "no" sectors of the graph. That portion of the temperature curve in the "yes" sector indicates that contrails will form; in the "no" sector, contrails will not form; and in the "possible" sector, formation will be determined by the relative humidity at the selected temperature versus pressure level. A manual (*Air Weather Service*, 1960) is available for detailed guidance on contrail forecasting for jet aircraft.

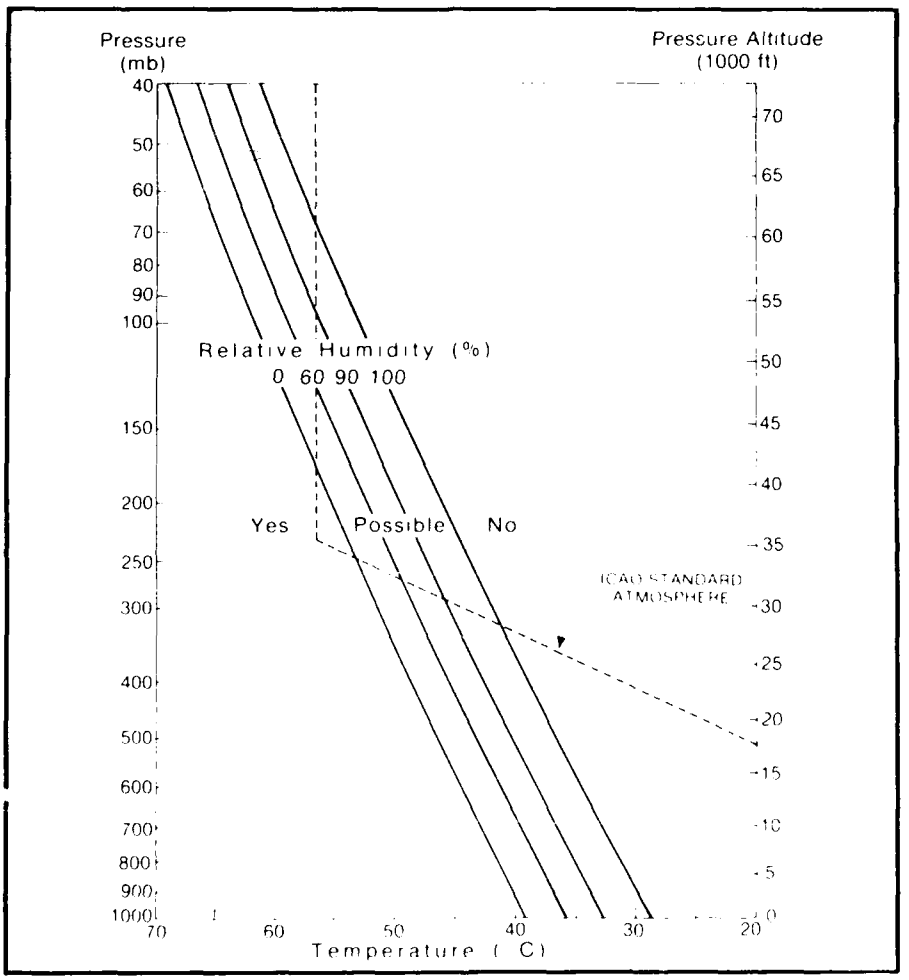

Figure 5-11. Graph of Relative Humidity Required for Jet Aircraft Contrail Formation as a Function of Pressure and Temperature (Fett, 1983).

Ship trails, conversely, form at lower levels and seem to be quite rare at high latitudes. That such trails can be seen on satellite imagery is not surprising when considering that these trails form in stable air and extend, relatively undisturbed, over hundreds of miles. Figure 5-12 shows a local view of a ship's trail.

Ship trails are seen in thin stratus over the sea where the cloud has a cellular structure induced by the loss of heat by radiation from the cloud top. The water vapor and condensation nuclei emitted from the ship rise into the cloud, but no further, inducing a helical circulation with rising motion in the center of the plume and sinking motion along the edges (see NTAG, Vol. 2, Sec. 1C). The broken nature of the cloud reduces the radiative heat loss so that the overturning of the mixed layer down to the sea surface is very slow. The trail of air with more moisture remains visible for many hours. Even so the trail undergoes a widening that can be seen clearly. The point of formation of the trail is at the narrow tip, and the widening is a measure of the horizontal spreading by the internal motion in the layer.

Ship trails are rare, probably because the ship makes a difference to the cloud only when the cloudy air is very clean and deficient in numbers of condensation nuclei. Figure 5-13 shows ship trails in the eastern Pacific.

Figure 5-12. Pollution from a Cruise Ship (Benson and Rizzo, 1980).

Figure 5-13. Ship Trails in the Eastern Pacific.

5.5 Wind Fields of the Arctic

5.5.1 Mountain Waves

When the wind blows over a relatively narrow mountain ridge (< 60 mi or < 100 km), air parcels are displaced in the vertical, and, if the atmosphere is stably stratified, they descend and may oscillate about their equilibrium positions. The gravity waves that result, called mountain waves or lee waves, have been observed in mountainous regions all over the world.

The presence of mountain waves is frequently revealed by distinctive orographic clouds that form in the wave crests. Various types of mountain waves produce the different types of wave clouds. An identification of a particular type of wave cloud can be used to make some qualitative deductions about the vertical variation in wind speed and stability over the mountains.

Large amplitude mountain waves can produce several weather phenomena that significantly affect human activity and, therefore, require the attention of the weather forecaster. The strong downslope winds observed along the lee slopes of mountain barriers are usually associated with large-amplitude waves. Dangerous regions of clear air turbulence and sustained, strong downdrafts are also produced by these waves.

Wave induced orographic clouds are often evident in satellite photographs. When interpreting these photographs, however, operational meteorologists tend to assume that all cloud producing mountain waves propagate horizontally. In fact, vertically propagating waves commonly generate clouds as well, and usually the two types of clouds can be distinguished. Horizontally propagating waves are trapped, due to an inversion, and indicate stable conditions in the area of the clouds. Vertical propagating waves are not trapped by an inversion and are allowed to propagate upward in unstable air. Once the type of wave has been identified, certain general conclusions can be drawn about the atmospheric conditions in the vicinity of the waves. The two types are clouds from trapped waves and clouds from vertically propagating waves.

Figure 5-14 is an IR NOAA-9 view of the northern Norway coastal region on 9 March 1988. Trapped wave clouds are evident stretching for several degrees from south-southwest to north-northeast along the rugged coastal terrain. Just inland from the trapped wave clouds occur a series of vertically propagating wave clouds in the region of Tromsø, Norway. An observer at the Earth's surface would view the trapped waves as rows of middle and high clouds.

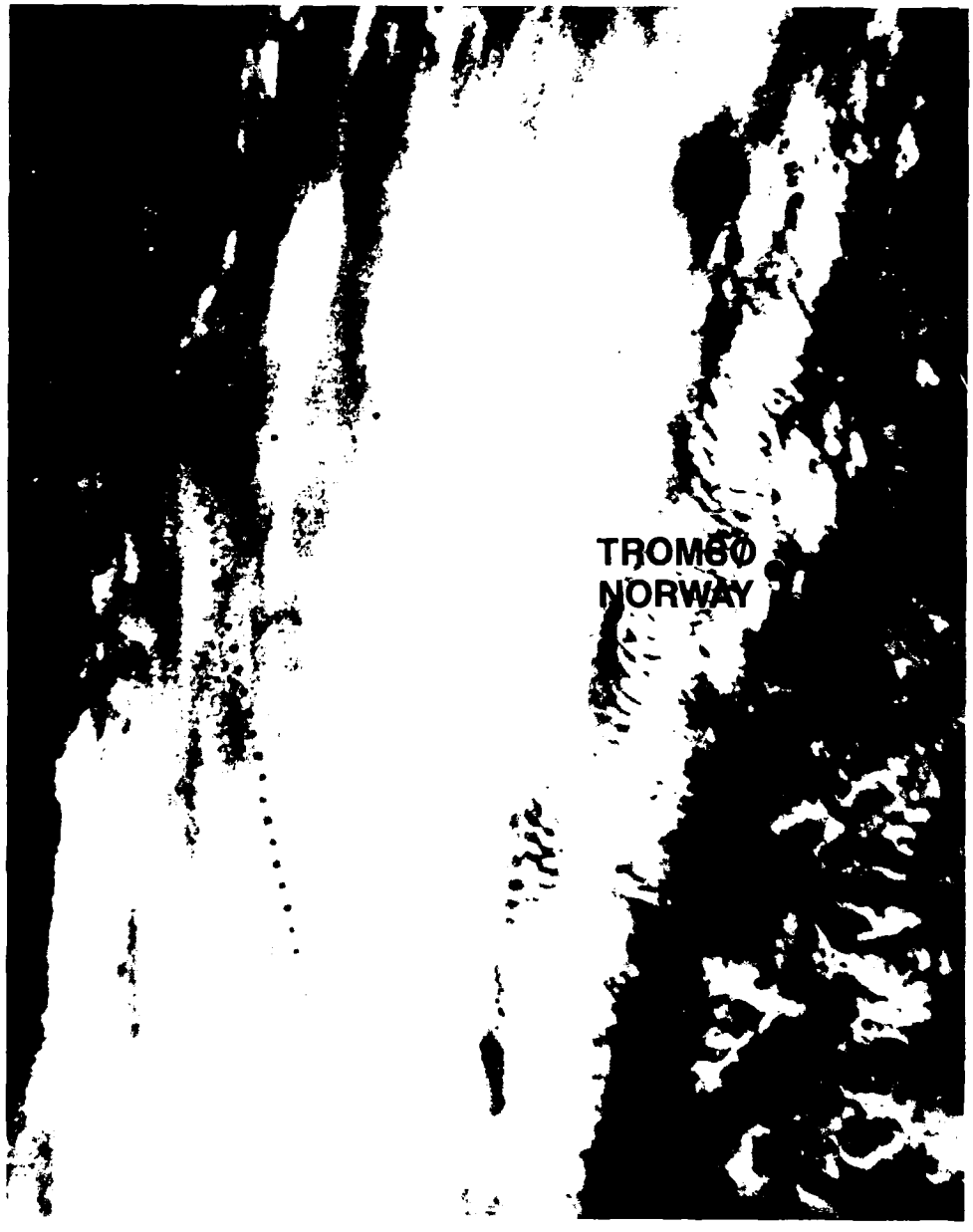

Figure 5-14. Satellite Imagery of Two Kinds of Lee Waves.

The vertically-propagating wave clouds are layered and stacked vertically. Figure 5-15 is a photograph of the wave cloud just west of Tromsø, taken from a hotel window looking westward within minutes of the satellite view.

The two types of lee waves obviously have very different characteristics. These features are summarized in the following paragraphs.

Figure 5-15. Observer's View of Vertically Propagating Lee Waves.

Trapped waves can be recognized by (1) multiple wave crests occurring downstream from the initial disturbance and (2) a characteristic wavelength that varies between 6 and 13 mi (10–25 km). Given that the waves are trapped, general conclusions can be drawn about the state of the atmosphere in their vicinity. In order for mountain waves of any type to exist, a sufficiently strong wind must be directed across the mountain at the ridge-top level. The minimum wind speed required for waves will vary with the size and shape of the mountain but seems to lie in the range from 15 to 30 kt (7–15 m/s). Also, usually a large vertical wind shear will occur, or an increase of wind speed with height, and the presence of one or more stable layers in the lower troposphere. Moist layers that contain the wave clouds are also apparent in these cases.

Vertically propagating waves have only one wave crest visible, and the horizontal wavelength (though hard to determine) exceeds the width of the wave cloud, which is roughly 60 mi (100 km). As mentioned earlier, the wavelength for trapped waves is much shorter. Given that the waves are vertically propagating, a significant flow across the mountains should be expected, but in this case the vertical wind shear may be less pronounced, and the low level stable layers are weaker than in the trapped wave case.

Note that topographical differences may exist. For example, a wide mountain range will tend to force long waves that can propagate vertically even with small, vertical wind shear and weak, stable layers. Conversely, trapped waves indicate stronger vertical shear and stronger stable layers. Figure 5-16 provides a unique opportunity to examine an extremely interesting case of a vertically propagating lee wave.

Figure 5-16. Vertical Propagating Lee Wave (Brooks Range).

At first glance, the clouds on the south side of the Brooks Range appear perhaps to be associated with southerly flow being orographically lifted and subsequently saturated on the windward slope. If this were the case, a narrow region of clearing would also be expected on the lee (north) side of the range. But this case is not simple orographic lifting.

The first clue that the above analysis is faulty appears as a long stretch of jet stream cirrus extending from the North Slope northward toward the pole. Additionally, a vortex is suggested to the northeast just off the North Slope of Alaska. The FNOC surface analysis near the time of the DMSP data on 30 October 1985 at 0000 GMT (Fig. 5-17) provides additional information.

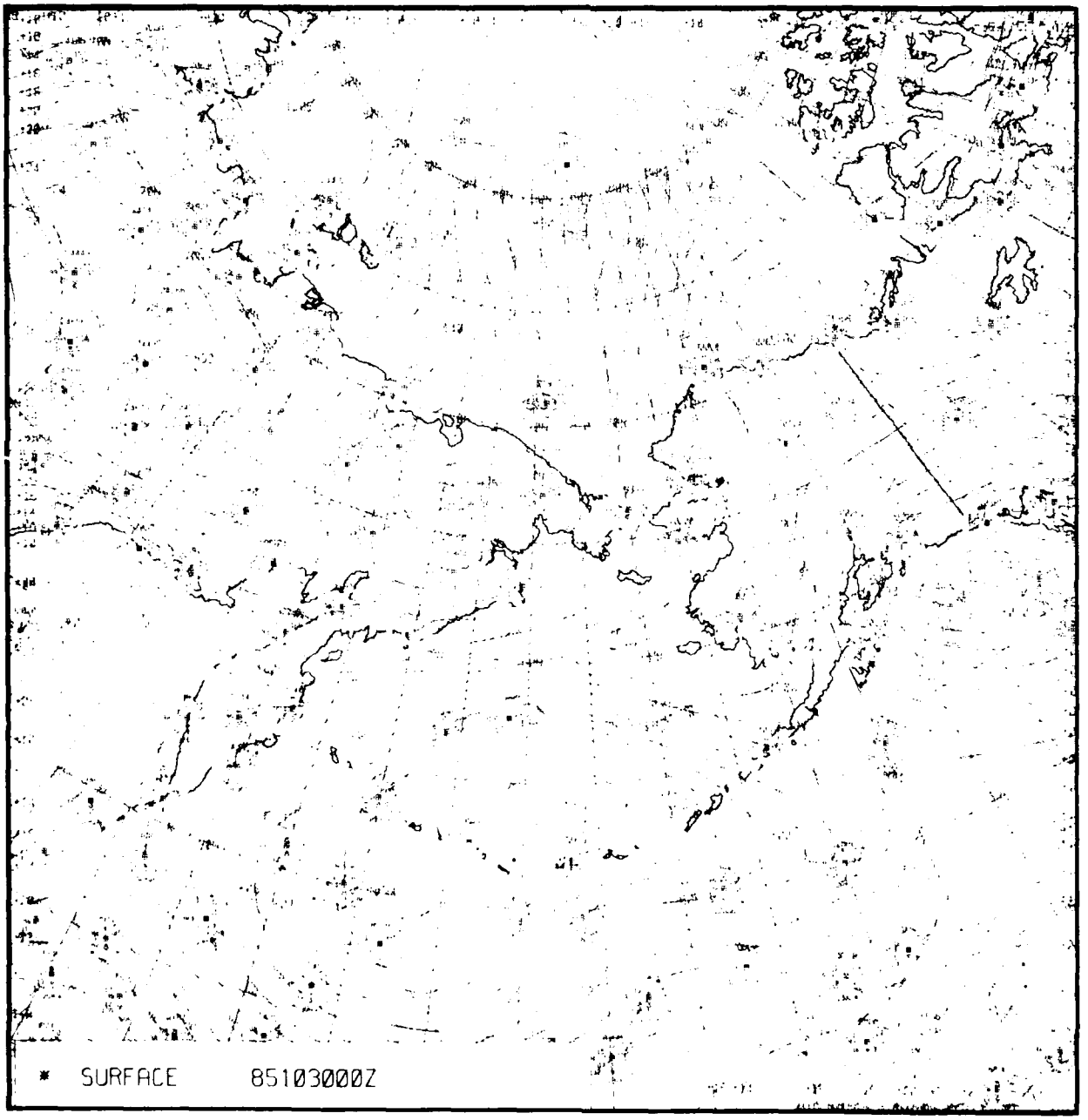

Figure 5-17. Surface Chart, 0000 GMT 30 October 1985.

The analysis shows a low centered just west of the McKenzie River delta, therefore, the flow over the North Slope of Alaska and the Brooks Range is northerly—not southerly. So instead of orographic lifting being the mechanism for the clouds on the south side of the Brooks Range, the northerly flow suggests a classical case of a vertically propagating lee wave characterized by a clear area on the windward side of the ridge and lee side cloudiness. To better understand the formation of vertically propagating lee waves and the attendant cloudy/clear regions relative to the ridge, the results of a lee wave numerical diagnostic model (Durran, 1986), presented in Figs. 5-18(a) and 5-18(b), should be examined. The example shown as Fig. 5-18(a) displays a steep windward slope and a gentle lee slope. In this configuration pronounced subsidence occurs at midlevels over the ridge but rather gentle upward motion to the lee.

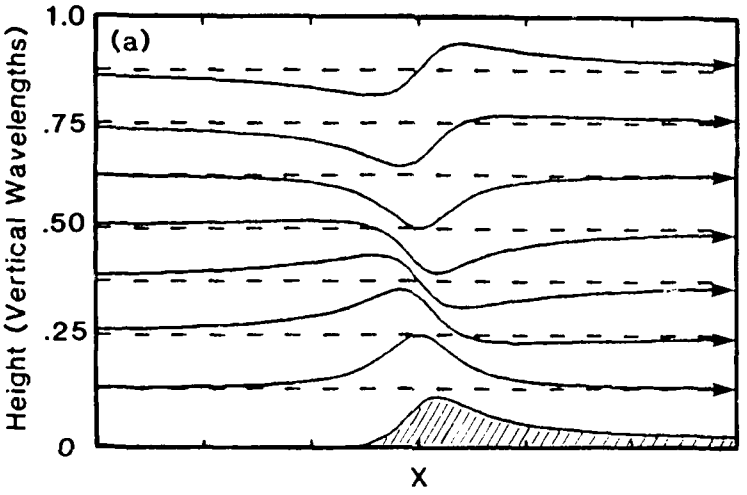

Figure 5-18(a). Streamlines in the Steady Airflow over an Isolated Asymmetric Ridge with a Steep Windward Slope.

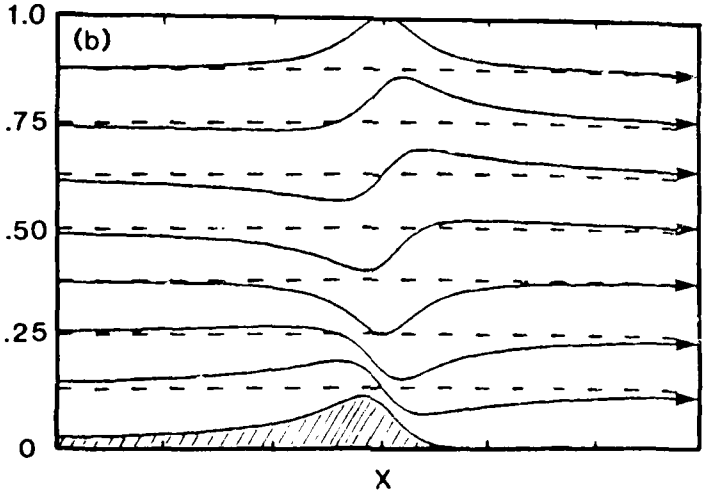

Figure 5-18(b). Streamlines in the Steady Airflow over an Isolated Asymmetric Ridge with a Steep Leeward Slope.

The Brooks Range, however, has a reverse configuration, with a more gentle slope on the north side and a very severe slope to the south. Figure 5-18b illustrates the Brooks Range configuration and relates very well to the satellite data (Fig. 5-16) that suggest strong subsidence down the lee slope, followed by vigorous upward vertical motion to the lee. This pattern of circulation is required to produce the pronounced vertically propagating wave cloud found south of the Brooks Ridge.

Fortunately, a radiosonde observation is available from Barrow, Alaska on the north coast, which is the windward side in this case. Figure 5-19 may be typical of the vertical structure on the windward side of a mountain producing a vertically propagating lee wave. Its main features are (1) a deep, moist layer from just above the ground to 450 mb, (2) a strong, low-level inversion between 900 and 950 mb, and (3) strong, vertical wind shear from the surface (20 kt) to 400 mb (75 kt).

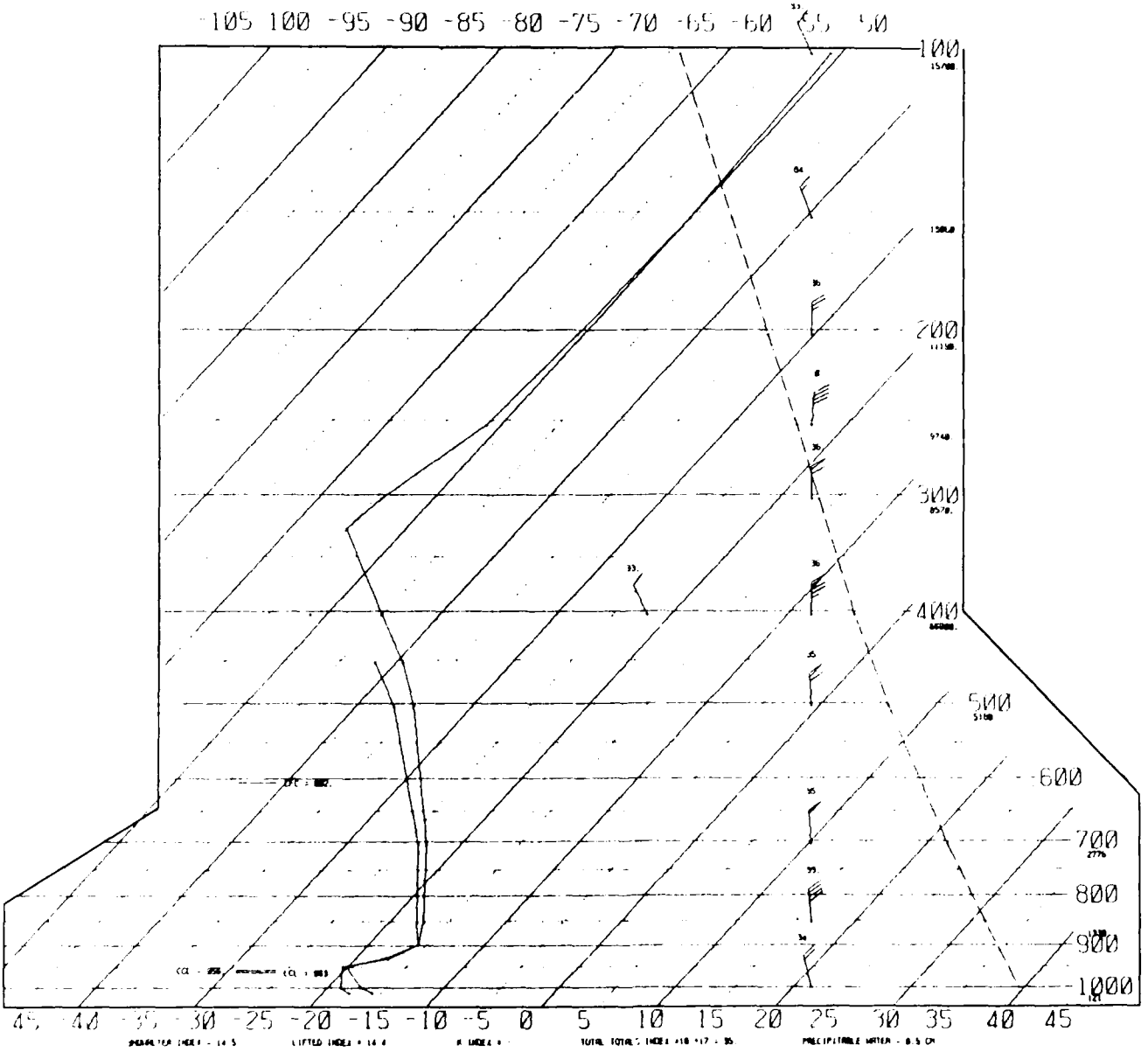

Figure 5-19. Sounding for Barrow, Alaska, 0000 GMT 30 October 1985.

The following guidelines should be helpful in forecasting the conditions in which strong lee waves will develop:

1. The mountain barrier in question has a steep lee slope. Asymmetric mountains with steep leeward and gentle windward slopes are the most effective generators of large amplitude mountain waves.
2. The wind is directed across the mountain (roughly within 30 degrees of being perpendicular to the ridge line) throughout a deep layer of the troposphere. The wind speed at the level of the crest should exceed a terrain-dependent value of 15 to 30 kt (7–15 m/s) and should increase with height.
3. The upstream temperature profile exhibits an inversion or a layer of strong stability near mountain-top height, with weaker stability at higher levels. Weak, low-level stability also favors development of waves in the lee of the mountain.
4. If strong waves of any type are forecast, clear air turbulence and downslope winds are likely to develop as well.

5.5.2 Drainage or Slope Winds

Drainage and slope winds are usually diurnal in nature and arise from the daily cycle of local solar heating in the daytime and long wave radiational cooling at night. Consider the left-hand side of Fig. 5-20, which represents the daytime situation.

During the day the south slopes of hills receive abundant short wave solar heating. By contrast, a point at the same elevation above the valley will be relatively cool during the day because of the lack of an effective absorbing medium. This thermal gradient in the horizontal requires, by the thickness equation, that pressure surfaces in the warm air be separated further than the pressure surfaces in the cooler air. This condition will give rise to the configuration of isobars as shown in the figure on the left. Thus, on the level surface (A to A′) a pressure gradient is set up that will accelerate air parcels at this level

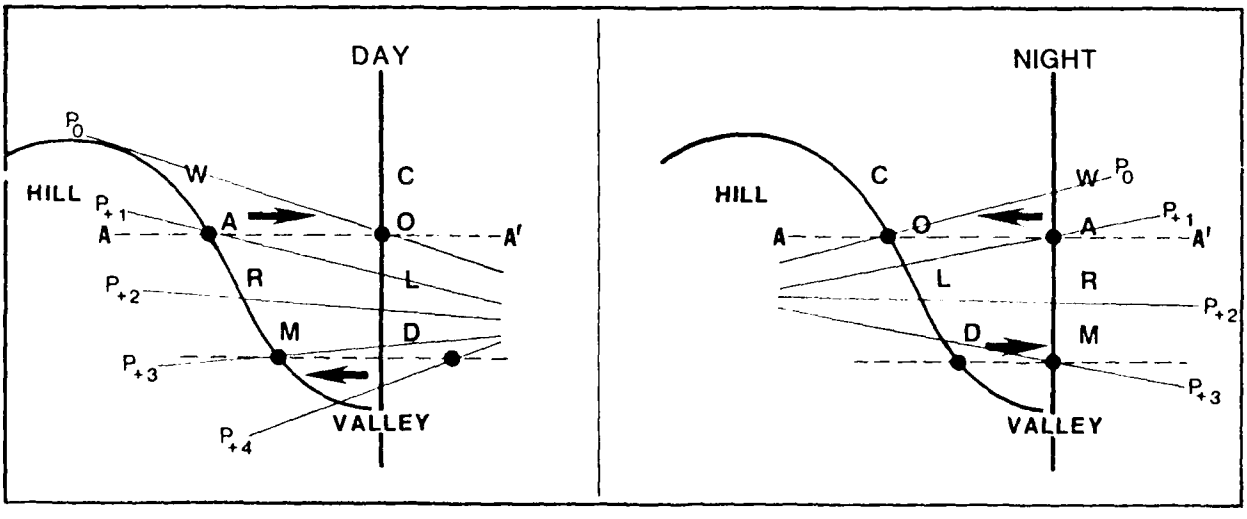

Figure 5-20. Slope Wind Schematic.

from a point over the hill to a point over the valley. Continuity then requires that the converging air over the valley will sink and spread out near the surface in such a way as to set a direct thermal circulation in the hill-valley system. A direct thermal circulation is one in which cold air sinks and warm air rises. An indirect circulation prevails when warm air sinks and cold air rises. This latter situation normally arises from some dynamic forcing of the wind and temperature fields, such as in the vicinity of jet cores. During the day the flow will be up the hill and subsidence will occur in the valley. These conditions could, in the presence of sufficient moisture, induce cloud formation at the top of the ridge and clearing in the valley. Note that the pressure surfaces at low elevations in the figure dictate gradient flow from the valley to the ridge slope.

In the evening the slopes of the hill will cool rapidly as long wave radiational cooling takes place over the previously heated ground. At corresponding elevations over the valley, the infrared cooling is much less because the air there is a poor radiator compared to the land on the side of the hill.

As a result of the reversal of the horizontal temperature gradient, the pressure surface at night must conform to the pattern shown on the right side of Fig. 5-20. This pattern reverses the direction of the thermal circulation such that, at night, air sinks down into the valley. The circulation is still a direct thermal circulation, but it is reversed from night to day because of the heating/cooling reversal.

At the base of Parry Peninsula in Canada's Northwest Territories, west of the village of Paulatak, a drop of about 600 ft (182 m) occurs over a distance of 10 mi (21 km) (Fig. 5-21). The interior drainage, as indicated by the rivers, is toward the north-northwest. To the east and west higher terrain, up to 1,500 ft (457 m), occurs so that a broad pass is centered roughly at the base of Parry Peninsula. Darnley Bay and Franklin Bay on either side of the peninsula remain ice free well into December. For this reason, a strong temperature gradient often occurs through the pass and down the slope. Infrequently, southerly flow develops, and the winds down the slope may reach velocities of hurricane force (64 kt plus). Due to lulls that occur, these winds are locally referred to as "pumping winds."

Slope winds also occur in the eastern foothills area of Alberta. The Rockies lie northwest-southeast. With a flow of stable air from the north or north-northeast, the winds tend to be very strong along and just windward of the foothills. From old reports of damage to buildings, speeds over 100 kt (50 m/s) must have occurred occasionally. Another good example is Resolute, which is on the south side of Cornwallis Island. Although winds over 50 kt (26 m/s) are usually from the north-northeast to east-northeast, winds of 35 kt (18 m/s) are frequent when the flow is from the southeast or south-southeast, with an onshore or upslope component.

5.5.3 Glacier Winds

Although glacier winds are related to slope winds, the presence of an ice surface changes the physics by adding another factor: the ice surface cannot be warmer than 32 °F (0 °C). Also, glaciers begin at high elevations and have slopes that are usually flat at the source but increase downward. A shallow downdraft along the icy surface of the glacier continues all day, therefore, regardless of insolation. Its thermal cause is the continuously present

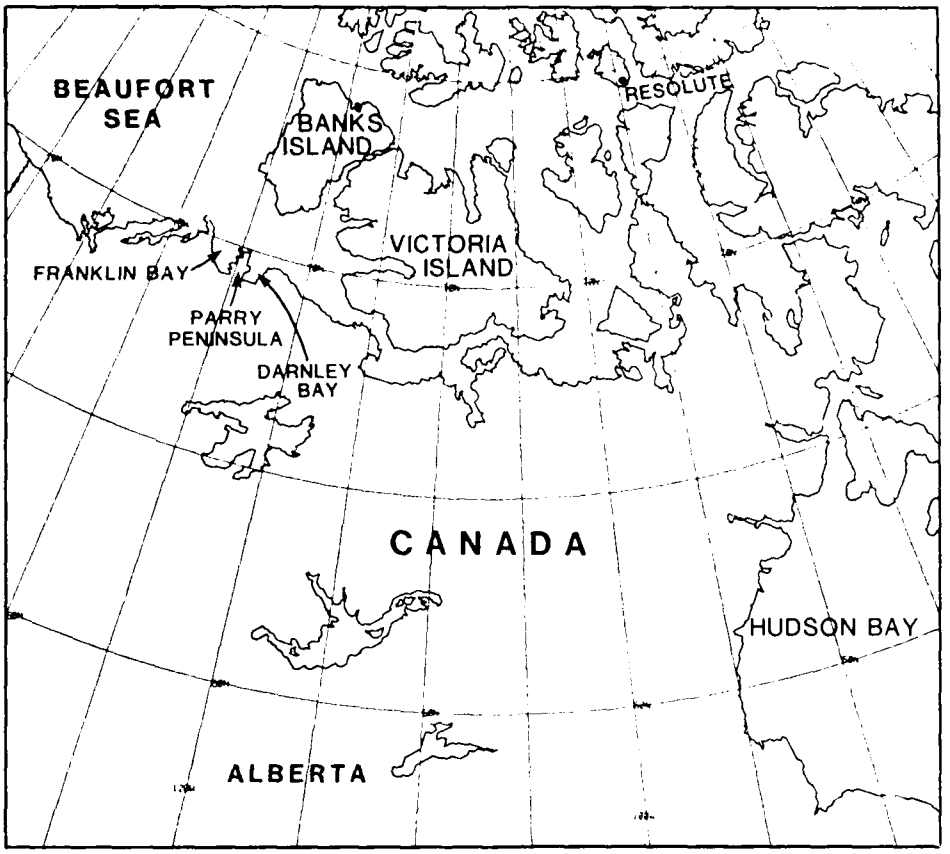

Figure 5-21. Locator Map for Parry Peninsula.

temperature difference between the glacier surface and the free air at the same altitude (analogous to the Arctic sea breeze regime). For this reason, the glacier wind has no diurnal period as does the slope wind. Since the wind is a function of this temperature difference, it reaches a maximum intensity and greatest vertical extent (165 to 1,310 ft [50–400 m]) in the early afternoon.

The glacier wind always appears, even on cloudy days. In daytime the wind fades out soon after leaving the glacier because its kinetic energy is dispersed by ground friction. The glacier wind often collides with the upvalley wind and, being colder, slides under it. At night, after leaving the glacier, it blends into the mountain wind, which has the same downslope direction. A characteristic of the glacier wind is its strongly turbulent flow, which, in a more moderate form, is also a feature of the nocturnal slope wind.

The term "katabatic" (downslope winds such as foehn and bora) and "anabatic" (upslope) are often used in the literature. A katabatic wind is, however, more than simple thermally induced nighttime downslope flow. Unless the slope is very long and steep, the katabatic wind component is not usually impressive with regard to speed. Combinations of favorable stability, thermal gradient, and geostrophic wind can, nevertheless, produce extremely strong winds in the downslope direction. Due to the concomitant adiabatic warming caused by the sinking of the air, occasionally instances can be seen of katabatic and glacial winds on IR satellite imagery (see Chapter 3, Fig. 3-12 for example).

5.6 Fog Near Marginal Ice Zones

The Marginal Ice Zones (MIZ) of the Arctic are defined by Kozo and Diachok (1973) as "the active part of the ice canopy between the ice edge and the point where consolidated multiyear ice predominates." They are regions of strong horizontal temperature and moisture gradients and, therefore, areas where fog formation often occurs.

Fog is reported, under World Meteorological Organization (WMO) guidelines, when the horizontal visibility is reduced to 1 km or less (except for present weather code 10, which is used for visibilities over 1 km). Ships and aircraft operating near the edge of the MIZ are subject to icing and severely reduced visibility under conditions of off-ice flow. Since fog often consists of supercooled water drops, impact with superstructures can cause instantaneous formation of rime ice.

Guest (1989) experienced a variety of fog and icing conditions during his work aboard ships recording observations during the MIZEX in 1984, 1987, and 1988. He noted, in particular, various causes of fog near the MIZ. First, radiation fog tends to form during long wave radiational cooling in the absence of clouds. Second, advection fog forms when warm, moist air flows from the sea to the ice surface and is cooled by the air over the ice.

Guest described another fog type known as stratus-lowering fog. This type occurs when a stratus deck lowers to the surface, normally happening when the top of the stratus cools to such an extent that it is colder than the underlying air, a thermally unstable situation. This instability then results in mixing, which extends the cooling to the surface, and produces fog, and usually occurs also during sea-to-ice winds. Another mechanism producing fog in the vicinity of the MIZ is precipitation into a lower, dryer layer that then becomes saturated to the point where "rain fog" or scud (stratus fractus) forms.

Finally, fog can be expected to form over leads and polynyi in winter when a sort of steam fog forms as cold, dry air moves over the warmer, moisture source in the lead or polynya. Figure 5-22 is a NOAA satellite image of low stratus or fog along an ice edge. The stratus, or fog, appears darker in the infrared than the surface snow cover because the top of the stratus, or fog layer, is near the top of an inversion with temperatures higher than the surface.

Fog formation is frequent in areas of the Arctic away from the MIZ. Fog is frequently observed around the *periphery* of high pressure centers and in the ridges emanating from the centers, especially in regions of "wet" ice or other moist areas. Fog is not often found in the *center* of Arctic highs because subsidence there is strong enough to overcome fog formation.

Another place to look for Arctic fog is along coasts, wherever an onshore component of the wind occurs. This is a form of upslope fog.

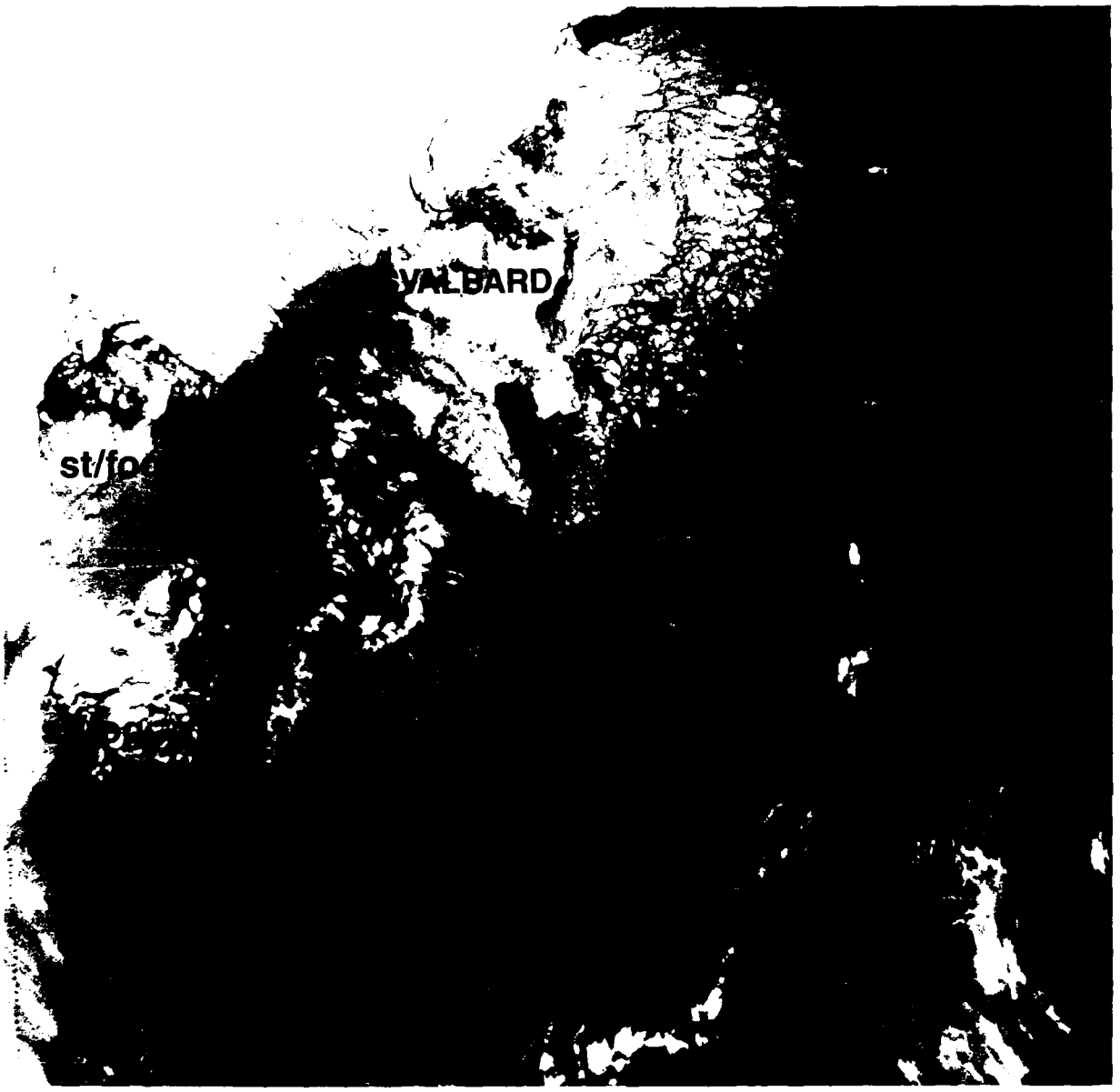

Figure 5-22. IR Satellite Imagery of Fog near the MIZ.

River valleys represent drainage areas for cold air, and the water, if not frozen, serves as a moisture source for dense radiation fog, just as in any valley where moisture is available. Figure 5-23 shows an excellent example of extensive fog or low stratus emanating from a low drainage valley ringed by mountainous terrain in northern Siberia. The Kolyma River flows on the east side of this valley that contains hundreds, if not thousands, of small lakes, rivers, and ponds.

Figure 5-24 is an example of a pollution plume extending westward from Prudhoe Bay on 23 July 1986. Cause of the plume is unknown. Because of low-level stability, however, the plume persists under a low-level inversion causing overcast skies and presumably poor visibility over a large area of the North Slope west of Prudhoe.

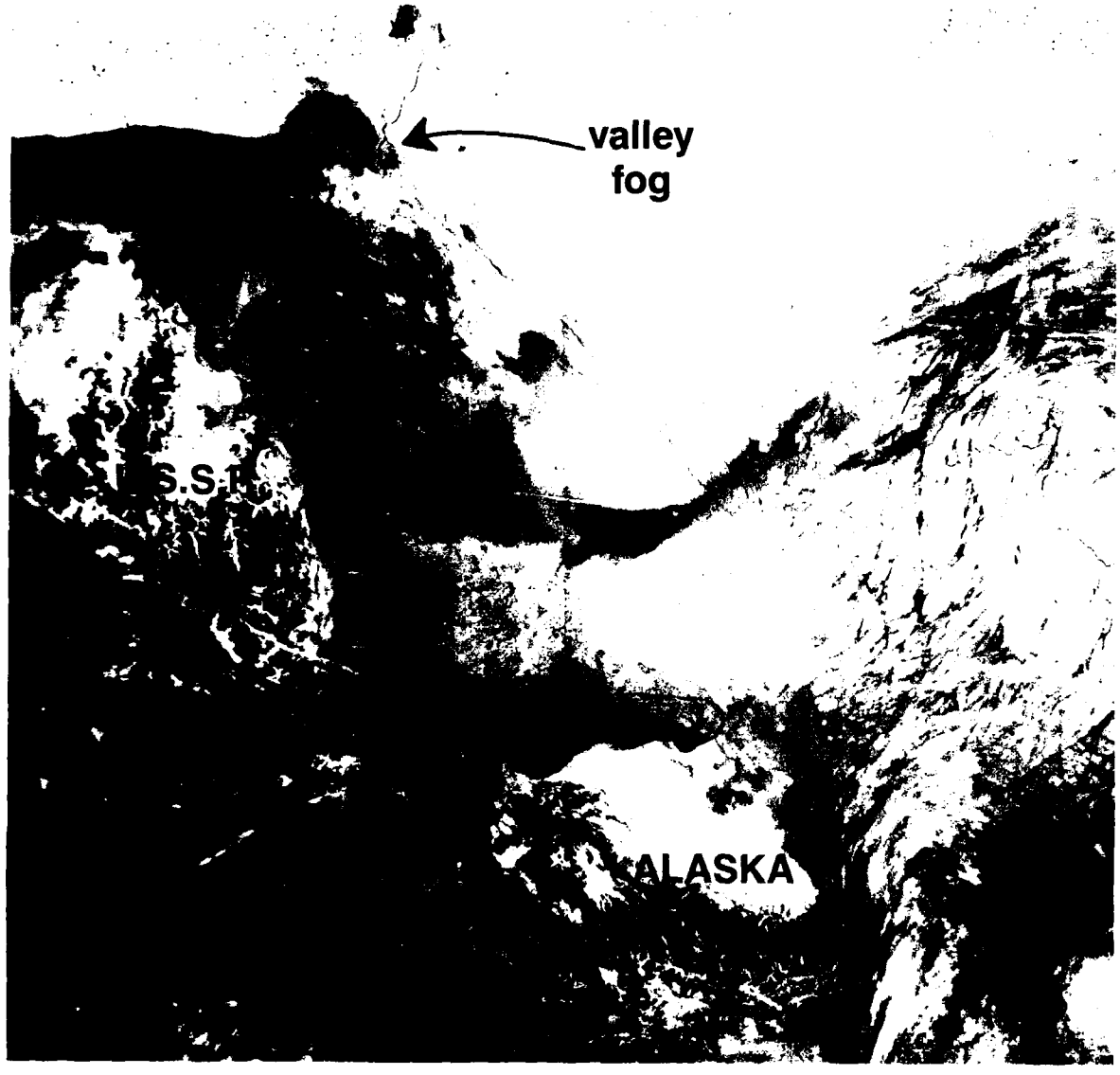

Figure 5-23. IR Imagery Showing Fog in the Kolyma River Valley.

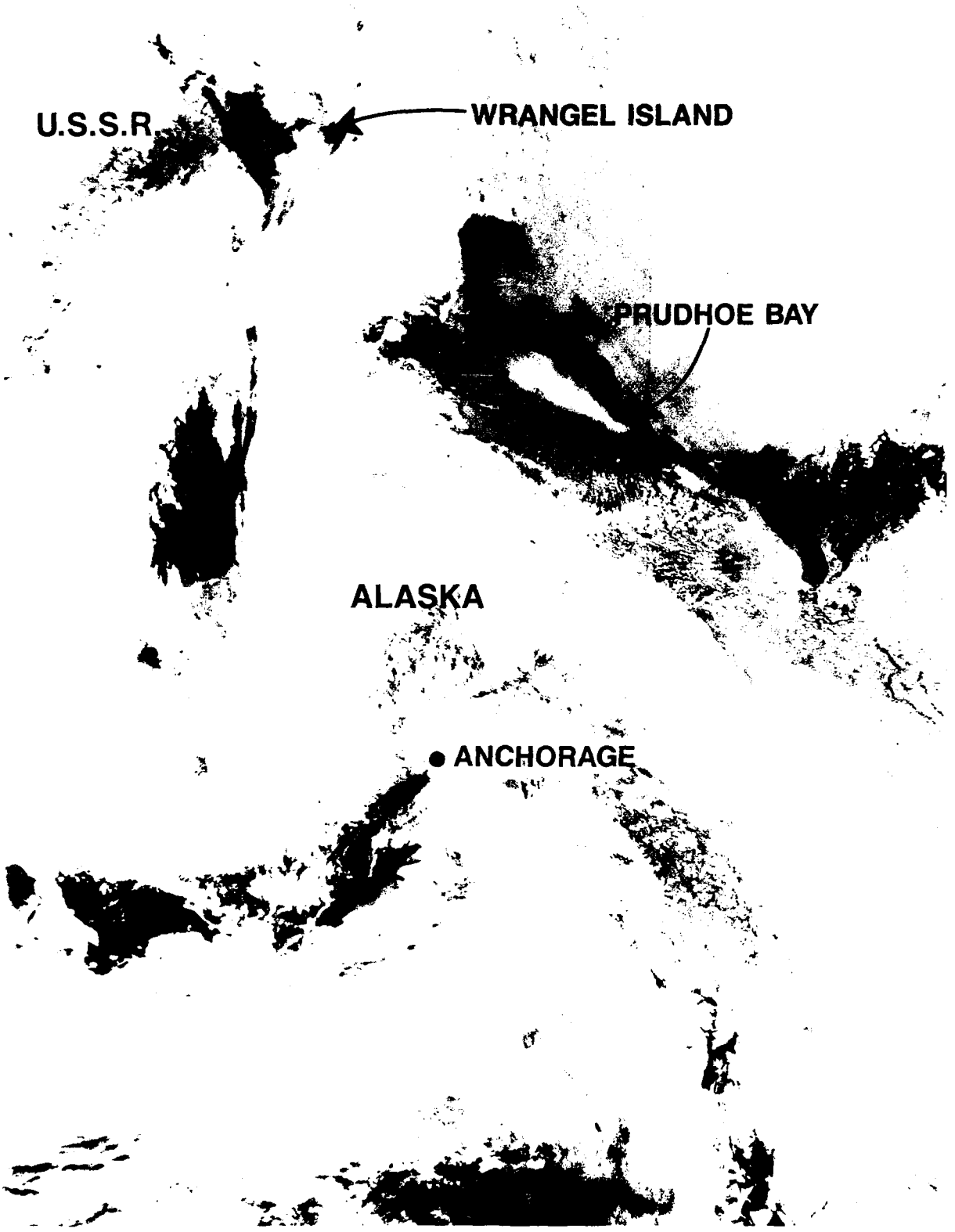

Figure 5-24. Pollution Plume Extending from Prudhoe Bay, Alaska.

A typical example of fog and/or low stratus banked up against the North Slope coast is shown in Fig. 5-25, an IR DMSP view of the region on 17 June 1985. All of the North Slope coastal stations were reporting overcast skies in low stratus or fog at the time of these data. Barter Island's visibility was reduced to 2 mi in the fog. Some of the overcast had spread inland in the region just east of Barrow.

In addition, cases are known where fog will occur in the vicinity of low pressure systems positioned partially over the ice and partially over open water. Normally a strong surface-based inversion exists over the ice. On the west side of the low, as the air moves from the ice in northerly flow over the water, the heat and moisture fluxes from the water will initially erode the inversion only slightly. Steam fog results, and it spreads out under the inversion that gradually rises to the south. After about 60 to 120 n mi (100–200 km) the fog will dissipate and cloud streets develop, reflecting the effect of cold air flowing over warm water. This fog is often noted when drift ice is present, as opposed to consolidated pack ice. Steam fog also occurs over polynyi and leads when air moves from over the ice to over the moisture source.

5.7 Boundary Layer Fronts

Satellite imagery revealed an especially significant boundary layer frontal type in the Fram Strait during MIZEX in 1984 and 1987. The front is formed as relatively strong flow, normally from the east or northeast, comes off the ice pack and over the open water. Winds turn strongly anticyclonically as they approach the front. An enhanced cloud band appears, which represents the leading edge of the boundary layer front. A streamline analysis of the wind field associated with a boundary layer front takes on the appearance of an inverted trough—much like an easterly wave. Another example of a boundary layer front in the Bering Sea appears in Fig. 5-26. Often a band of convective cumulus development occurs in the vicinity of the boundary layer front. In any case it has a distinctive signature in satellite imagery, as can be noted in Fig. 5-26.

Shapiro et al. (1987) contributed an exhaustive study of one of the 1984 cases through the use of extensive observations made by aircraft flying in the vicinity of Spitsbergen. Schultz (1987) described a boundary layer front that occurred during the 1987 MIZEX period. In both cases, the boundary layer front was associated with the outbreak of cold Arctic air advected southward by north winds east of Svalbard. A major difference between the findings of Shapiro and Schultz was the location of the higher inversion layer. In the Shapiro case study, the boundary layer inversion was higher over the west side of the front. In the Schultz study, the boundary layer front was observed to propagate across the Fram Strait from east to west, while in Shapiro's study it was a stationary ice-edge front. Also among the differences was the lack of a low-level wind maximum in the Schultz case. The Shapiro study, by contrast, shows a low-level jet at 870 mb with speeds up to 60 kt (30 m/s).

Figure 5-25. North Slope Fog.

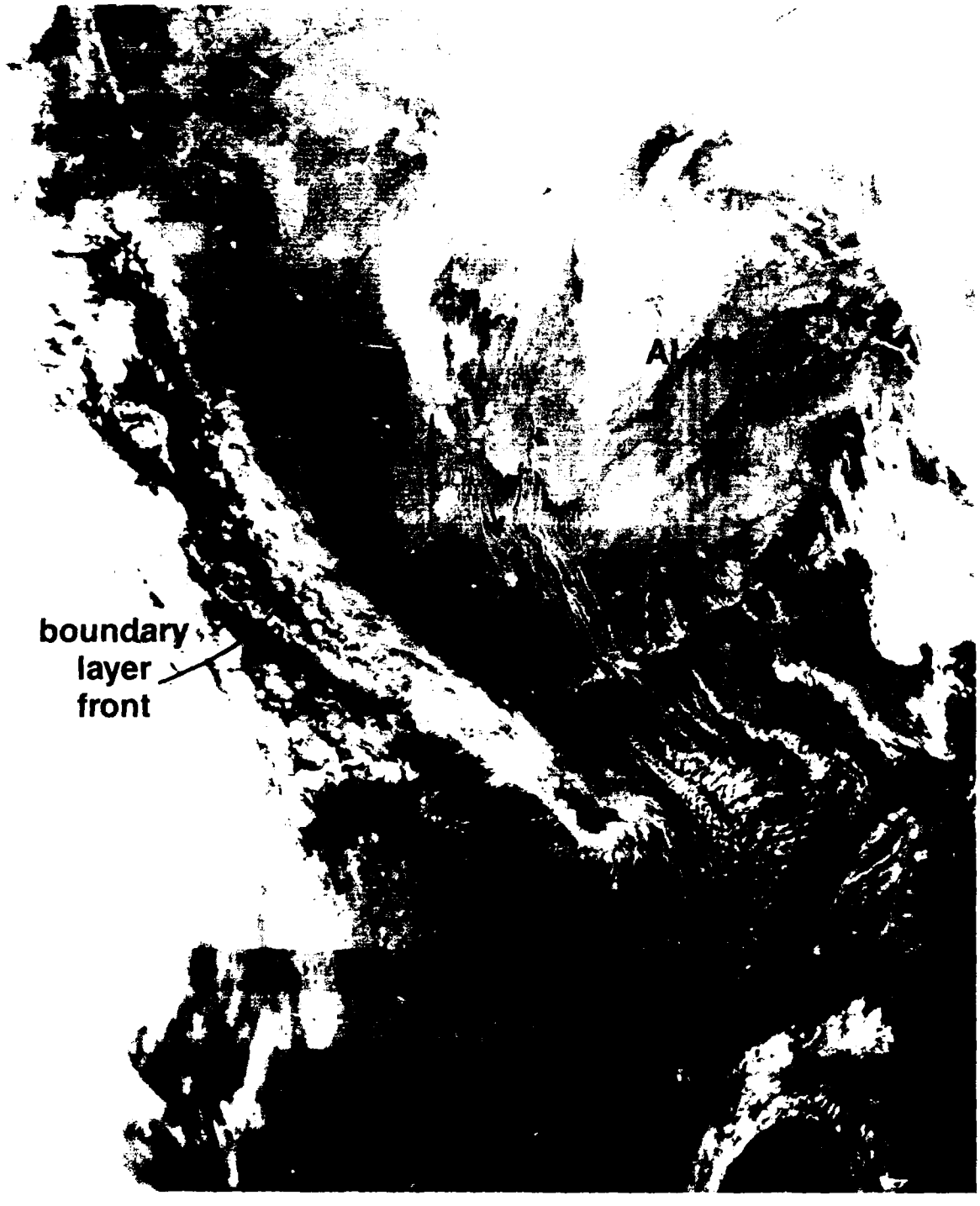

Figure 5-26. IR Imagery of a Boundary Layer Front.

Fett (1990(b)) observed that wind speeds were higher in the southeasterly flow east of the front and lighter in the northerly flow west of the April 1987 front. This wind pattern maximizes the cyclonic vorticity at the frontal boundary, which is favorable for vortex development. Fett also links development of the infamous polar lows of the Arctic with the boundary layer fronts. Chapter 6 is devoted entirely to descriptions of the structure and evolution of polar lows in the Arctic.

5.8 Turbulence

Turbulence has been the subject of many publications, and any attempt to present such a wealth of knowledge in this section is unrealistic. For indepth information on turbulence some good references are Ellrod, 1985; Ellrod, 1989; and Lee et al., 1979. A brief summary on turbulence follows.

Satellite imagery gives some signs of telltale cloud patterns in areas where turbulence should be expected.

1. Turbulence of some degree can be expected near any convective activity. Severe turbulence can occur in the enhanced cumulus pattern near vorticity centers or in the dry tongue.
2. Turbulence occurs near jet streams (Fig. 5-27). Around the polar jet, turbulence can be expected in the upper two-thirds of the cirrus shield. Clear air turbulence near jet streams is encountered in three areas where wind shear is strongest: just north of the jet axis, near the tropopause and level of maximum winds, and elsewhere in regions close to the tropopause or level of maximum winds. Typically, clear air turbulence will occur where the vertical wind shear is in excess of 8 kt per 1000 ft (4 m/s per 300 m). The term "clear air turbulence" may be misleading. Although the majority (75 percent) of wind shear turbulence occurs in clear air, it will also occur in cloudy areas that contain shear.
3. Mountain wave turbulence is indicated by lee-side rotor or lenticular clouds where mountain wave activity is indicated (see Fig. 5-16).

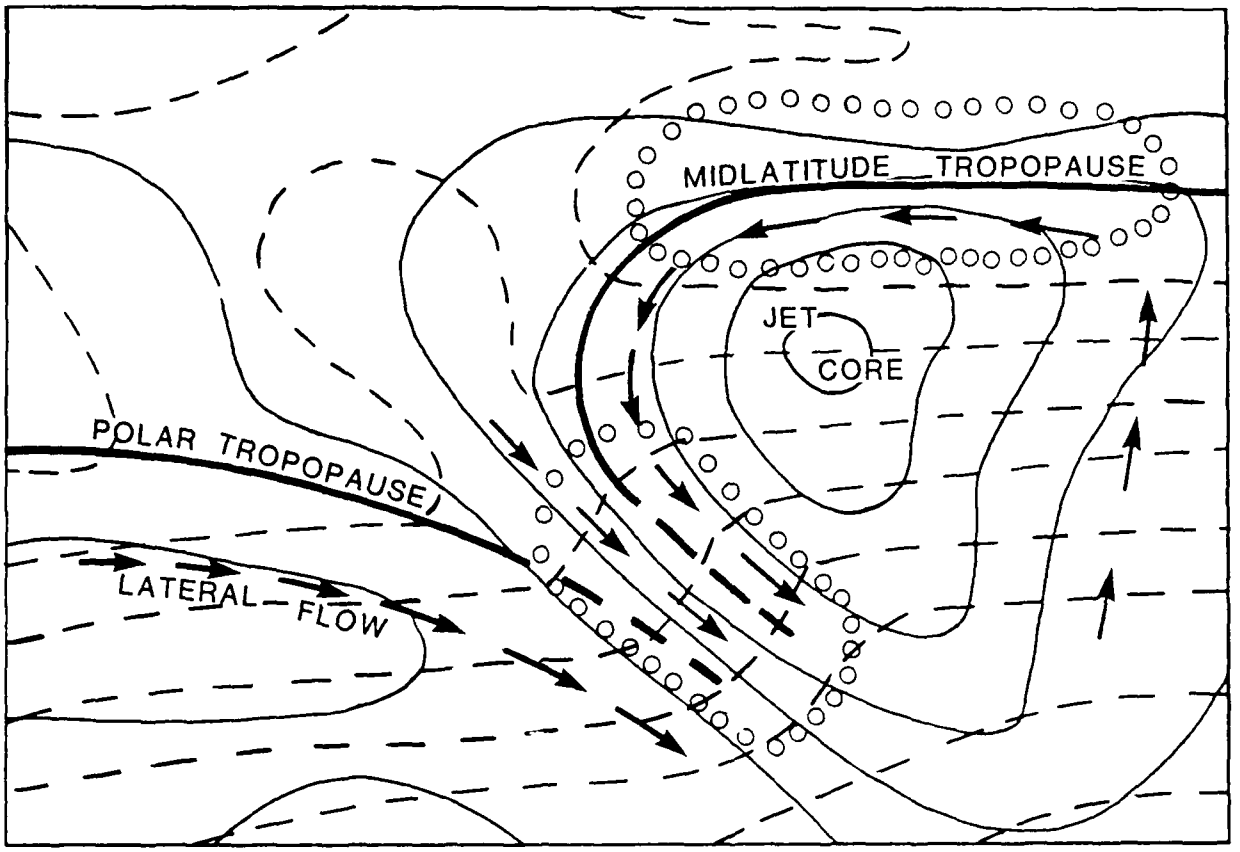

Figure 5-27. Location of clear air turbulence in typical jet stream (Lee et al., 1979). Solid lines are isotachs, dashed lines are isotherms, and open circles indicate regions of possible clear air turbulence.

6. POLAR LOWS

6.1 Characteristics of Polar Lows

Polar lows are intense lows that occur generally north of and/or west of the Arctic front, on the cold air side of the 500 mb polar jet and quite often in areas of pronounced low level cyclonic shear. They vary in size, from 100 n mi (160 km) to 700 n mi (≈ 1,000 km) in diameter. Surface wind speeds can reach hurricane force (60 kt plus). Polar lows are typified by an atmosphere exhibiting conditionally unstable conditions through the lower troposphere and midtroposphere. Vertical shear in the vicinity of polar lows is generally weak. The geostrophic wind accompanying polar vortices displays this characteristic and tends to back with height. Polar lows differ from midlatitude lows not only in size but often in the mechanism for development, the speed of development and often dissipation, and in their internal structure. The last attribute is still a subject of some speculation. For example, on the one hand Carleton (1985) concluded that ". . .a cold core and little vertical tilt distinguish the polar low in the mean." On the other hand, Shapiro et al. (1987) in their analysis "of the first research aircraft observations of the three-dimensional structure of a polar low" found that ". . .the polar low possessed a warm inner core, whose layer-averaged thickness temperature exceeded the exterior environmental temperature at 108 n mi (200 km) from the low center by about 9 °F (5 °C)." Temperature analyses at 1,000 ft (300 m), 850 mb, and the 580- to 1013-mb thickness, all indicated a warm core structure.

Rasmussen (1985) also noted that the polar low circulation is strongest near the surface and weakens upward, implying a warm core structure at lower levels. This type of structure agrees very well with the observation that polar lows develop quite frequently in reversed shear atmospheric conditions. In reversed shear conditions the thermal wind in the lower troposphere opposes the surface flow. Reversed shear can be established in a number of ways. Quite commonly it occurs when a cold pool of air moves to the south of a surface low.

In that type of configuration westerly low-level flow around the vortex is opposed by an easterly thermal wind component. The Norwegians (Midtbo et al., 1986) noted that "Investigations on the growth of baroclinic waves are generally dealing with occasions when the thermal wind and the progression of the disturbance are in the same direction. In case of a reversed-shear flow the baroclinic instability takes place in a different way. The wind at the steering level is northerly and directed nearly opposite to the thermal wind." They also noted that the surface wind speeds are generally stronger than expected when compared with ordinary unreversed situations.

Figure 6-1 shows an example of a reversed-shear configuration on 1 November 1985. The figure shows an analysis of the 1000-mb height contours (solid lines), indicating a low over the Norwegian Sea. The 1000- to 850-mb thickness analysis (dashed lines) reveals that the thermal wind west of the low center is southerly (parallel to the thickness lines, with cold air to the left). The thermal wind, then, opposes northerly low-level flow about the low center.

When surface observations are available in the region of polar low development, an analysis of the 3-hourly pressure change reveals falling isallobaric patterns ahead of the low and strong rises to the rear. Figure 6-2 shows such a pattern in the area where a polar low developed near 70°N 0° at 1200 GMT on 1 November 1985. Six hours later (Fig. 6-3), the pattern is even more pronounced as the pattern and storm are displaced southward. Note, as is typical in a polar low development, that the polar low is on the periphery or west of the analyzed low center.

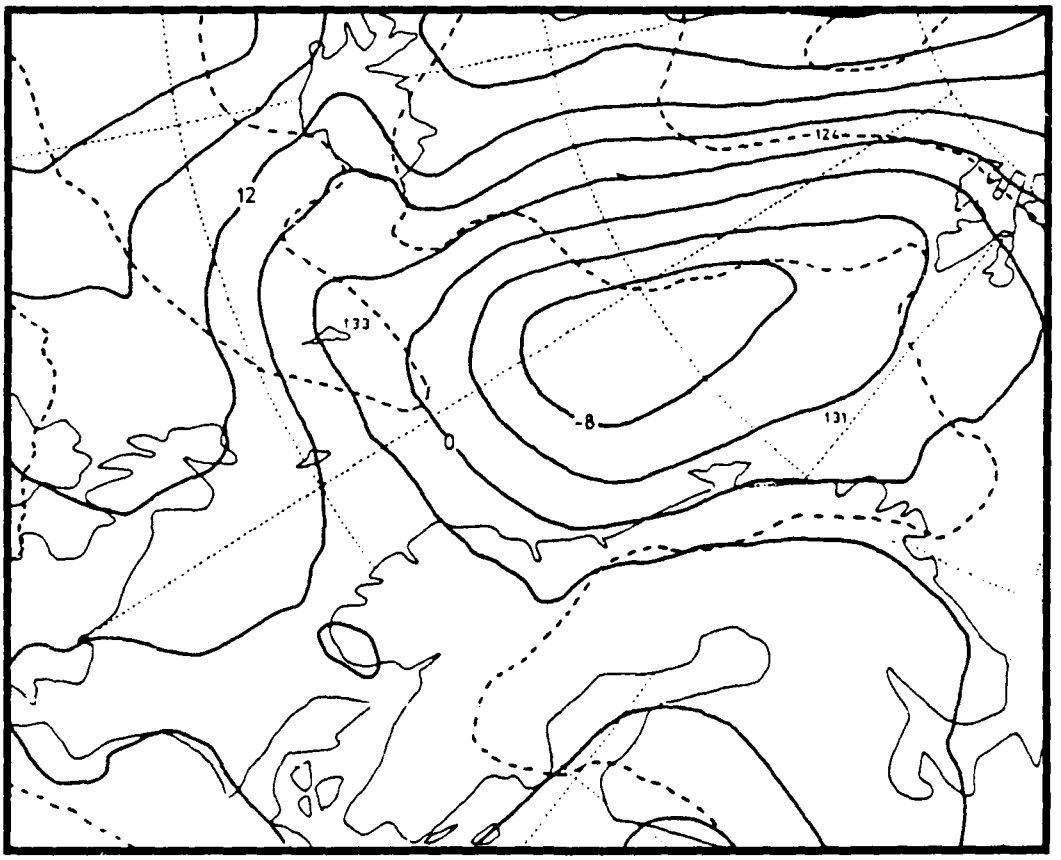

Figure 6-1. FNOC 1000-mb Analysis, 0000 GMT 1 November 1985. Solid lines are height contours (4 decameters) and dashed lines are 1000- to 850-mb thickness (4 decameters).

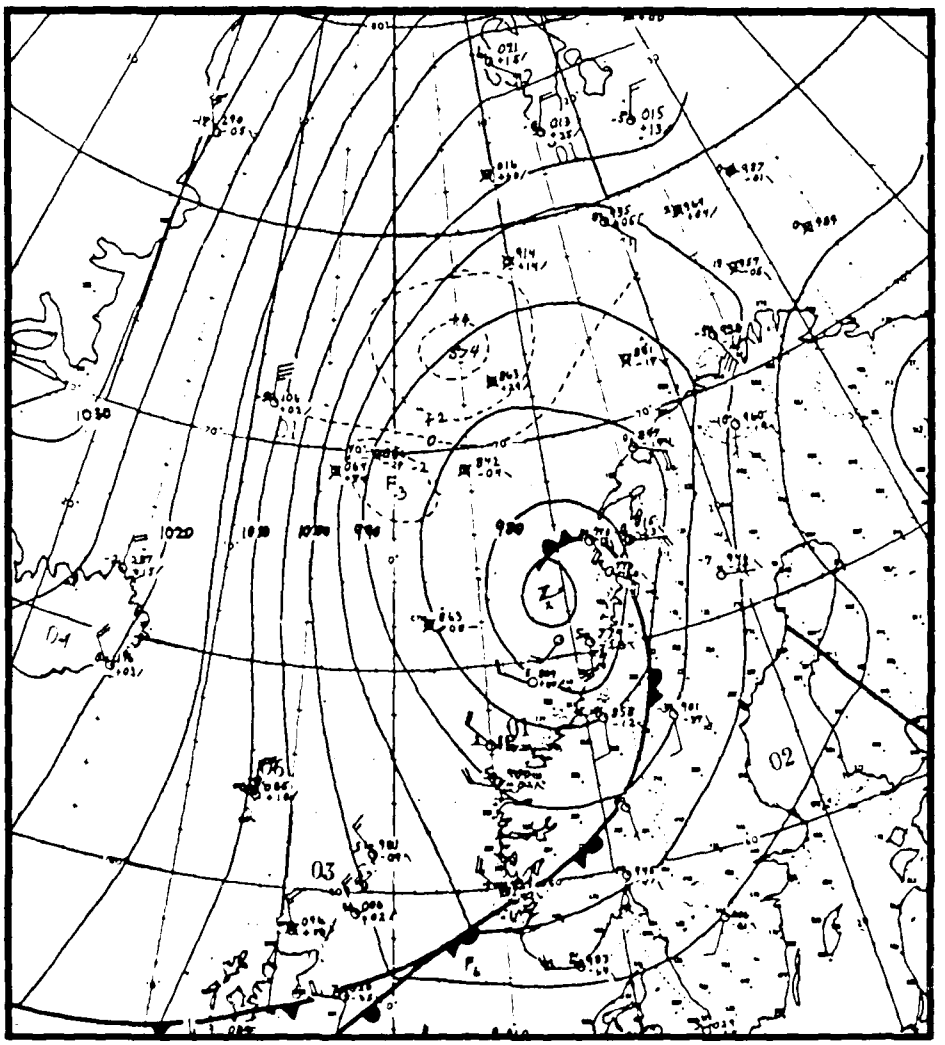

Figure 6-2. FNOC Surface Pressure Analysis, 1200 GMT 1 November 1985.

In the Norwegian report (Mitbo et al., 1986), criteria for selecting likely areas of polar low development were given. These are

1. Cold air advection must be present at the sea surface.
2. The thickness of the layer 850 to 500 mb must be below 13,000 ft (3,960 m). This limit should vary with the sea surface temperature: When the sea surface temperature is low, the limit should be lowered.
3. The curvature of the contour lines in the 500- to 700-mb levels must be cyclonic or zero.

Polar lows probably develop in different regions through either baroclinic instability or conditional instability of the second kind (CISK), and at times by a combination of these and other processes. In the "other" category is a third potential, described by Shapiro et al. (1987), in which essentially unmodified cold Arctic air moving southward over the ice, turned cyclonically, over the water, wrapping itself "about a warm(er) inner air mass, thereby isolating it from its warm air source. . . ."

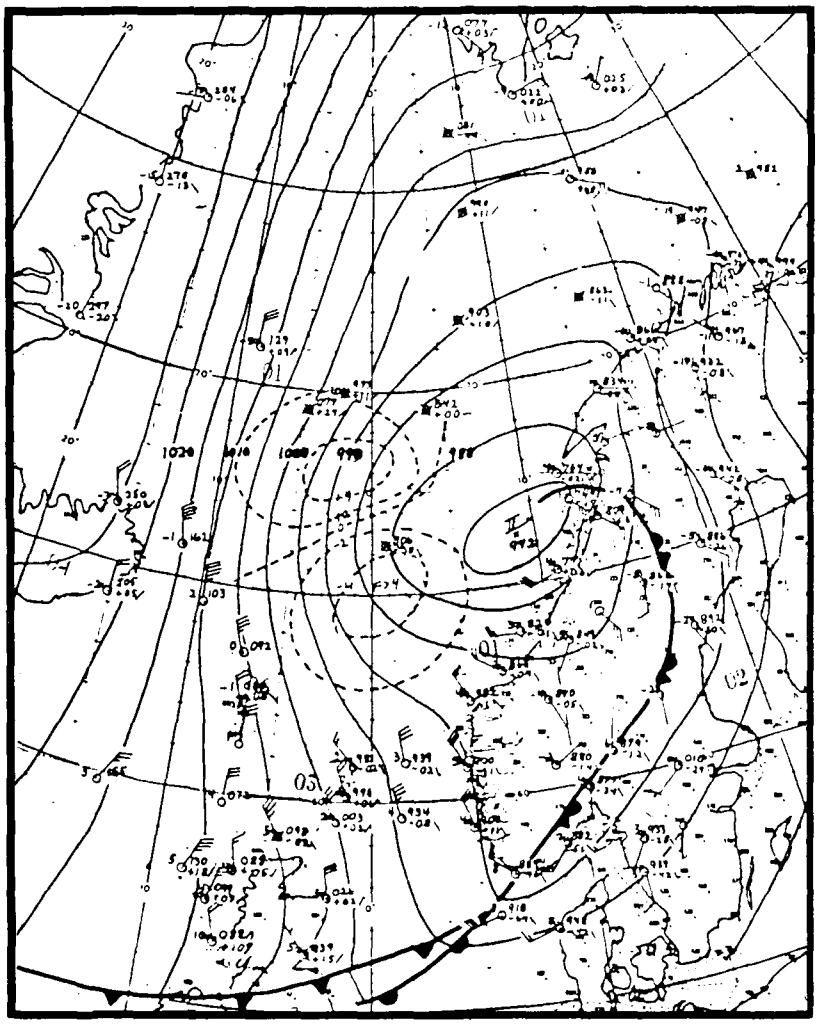

Figure 6-3. FNOC Surface Pressure Analysis, 1800 GMT 1 November 1985.

This process was first described by Bergeron (1928) who termed the process "a seclusion." The importance of the Shapiro study is that the classic definition of a polar low, being one that necessarily develops in a homogeneous cold polar air stream behind the Arctic front, is shown to be incorrect, at least in some instances.

Another important mode of development, believed to be of primary importance in the Bear Island region, was advection of an upper level low across the ice edge in the region of pronounced sea surface temperature gradient (Rasmussen, 1985). The Naval Environmental Prediction Research Facility (NEPRF) hypothesized that the upper cold core low caused the formation of the polar low of the same horizontal scale through the initiation of convection, which transformed the initial cold core system to a low level warm core system by release of latent heat and further development through the CISK mechanism.

Polar lows are difficult phenomena to forecast and seldom are forecast at all by numerical methods. Their life cycle can be completed in as little as 6 to 12 hours, or as long as 2 to 3 days; wind speeds can gust to 115 kt ($\approx$ 60 m/s), and seas can build to 50 ft (15 m) or higher. Structural icing is common and very hazardous for ships because of below freezing ambient air temperature in high winds and resulting spray. Sudden unexpected encounters with polar lows have cost the Norwegians an average loss of three ships a year over a timespan of many years because of these effects. Satellite images every few hours are an essential requirement in detecting polar lows and monitoring their evolution.

6.2 Polar Low Studies

In view of the importance of satellite imagery in studying polar lows, in this section a classic example of polar low development is shown for the area near Iceland. Additional examples over Greenland and the Norwegian Sea support the general concept. Finally, a schematic model is developed to indicate the precursor surface and 500-mb flow conditions associated with polar low development, especially applied to the Greenland Sea region.

6.2.1 Polar Low Evolution Near Iceland, 13 December 1986

Very seldom are conventional observations adequate to define the polar low in its initial development. A series of IR NOAA images on 13 December (Figs. 6-4(a) through 6-4(f)) reveal the complete evolution of a polar low within a period of approximately 14 hours in the area near Iceland. Evolution during this time starts from its inception as a short-wave trough (Fig. 6-4(a)), through cloud cluster development (Figs. 6-4(b) through 6-4(d)) to the beginning of a cloud vortex (Fig. 6-4(e)), and final encirclement of a spiral band to define a nearly cloud-free eye (Fig. 6-4(f)).

Synoptic charts (not shown) reveal that the polar low develops within a massive low pressure system covering the entire North Atlantic between Greenland and Norway, with a center near Iceland. The polar low does not develop near the center of low pressure but rather as an offset feature moving in the cyclonic flow around the periphery of this center. As the main low pressure center moves westward from near Iceland toward the coast of Greenland, the polar low is steered northward from its position in Fig. 6-4(b) toward the west coast of Iceland (Fig. 6-4(c)), and then further northward through the Denmark Strait (Figs. 6-4(d) through 6-4(f)). Because the low is an embedded feature in a larger scale circulation that has a strong pressure gradient extending outward for hundreds of miles, assessment of the intensity of the feature in itself is difficult. Similar appearing vortices passing Keflavik have produced sustained winds of over 50 kt (personal communication, CDR R.T. Pearson, Navy Oceanography Facility, Keflavik, Iceland, 1987).

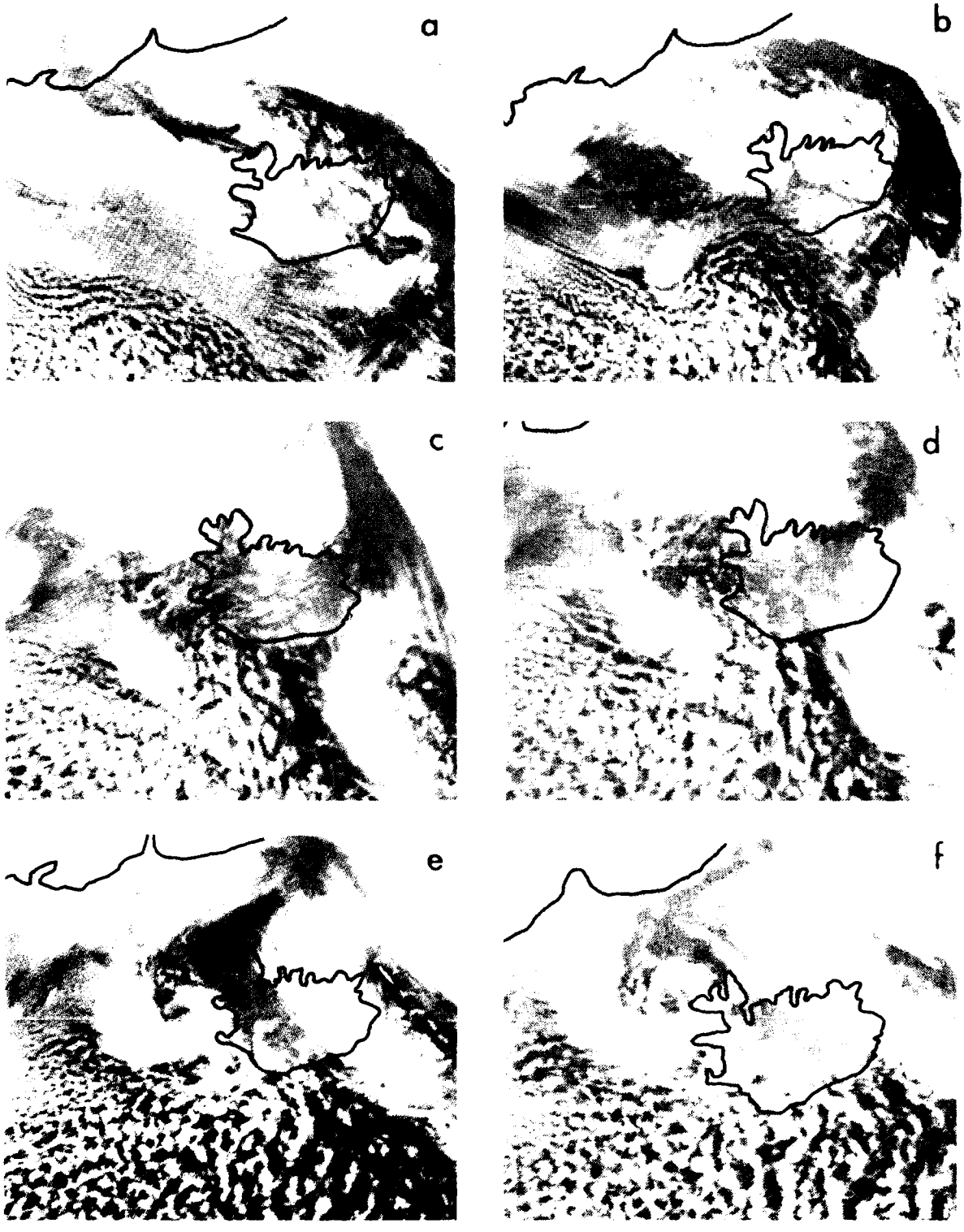

Figure 6-4. IR NOAA 9 and 10 Imagery for 13 December 1986: (a) 0603 GMT, (b) 1051 GMT, (c) 1420 GMT, (d) 1601 GMT, (e) 1904 GMT, (f) 2045 GMT.

Importantly, the small polar low develops within a general low pressure region adjacent to an unusually enhanced field of open-celled cumulonimbus. The 500-mb data (not shown) reveals a cold trough aloft superimposed over the enhanced convection. The trough is preceded by a warm ridge so that upper level winds turn anticyclonically downstream from the trough. This pattern appears favorable for polar low development. From a satellite perspective, the enhanced convection is the clue that an upper cold trough is in the area. This information, combined with other favorable factors, serves as advance notice of potential polar low production.

6.2.2 Polar Low Evolution, 26–27 February 1984

On 26 February the FNOC surface analysis for 0000 GMT (Fig. 6-5) reveals a synoptic-scale low west-northwest of Iceland. An IR DMSP mosaic over the region at about 0200 GMT (Fig. 6-6) fails to reveal a distinct vortex associated with this low pressure region. Readily apparent in the DMSP data, however, is the large field of enhanced, open-celled convection in the region of cyclonic flow southwest of Iceland. Aloft at 500 mb (Fig. 6-7), a cold trough extends over the field of enhanced convection.

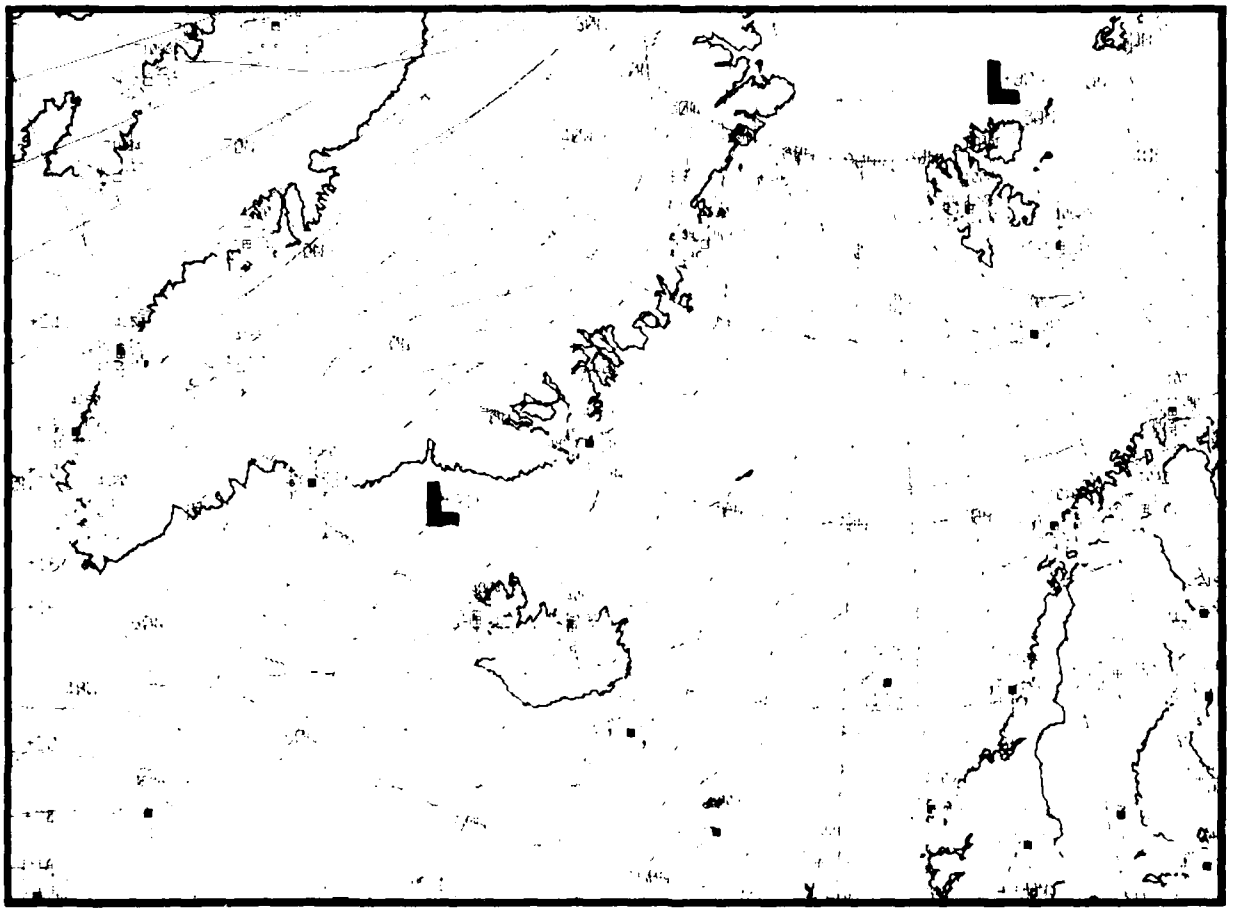

Figure 6-5. FNOC Surface Analysis, 0000 GMT 26 February 1984.

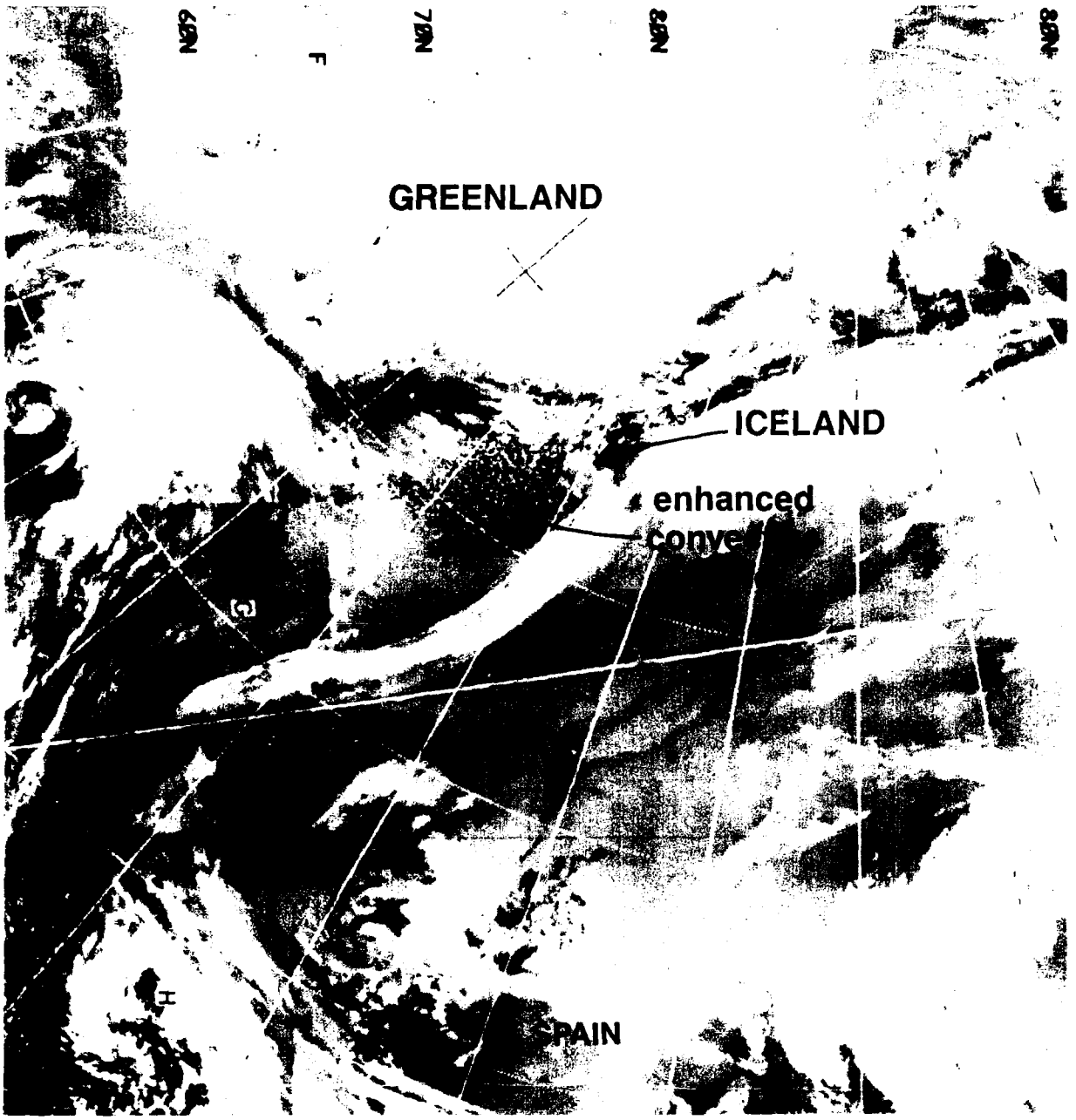

Figure 6-6. DMSP Imagery, 0200 GMT 26 February 1984.

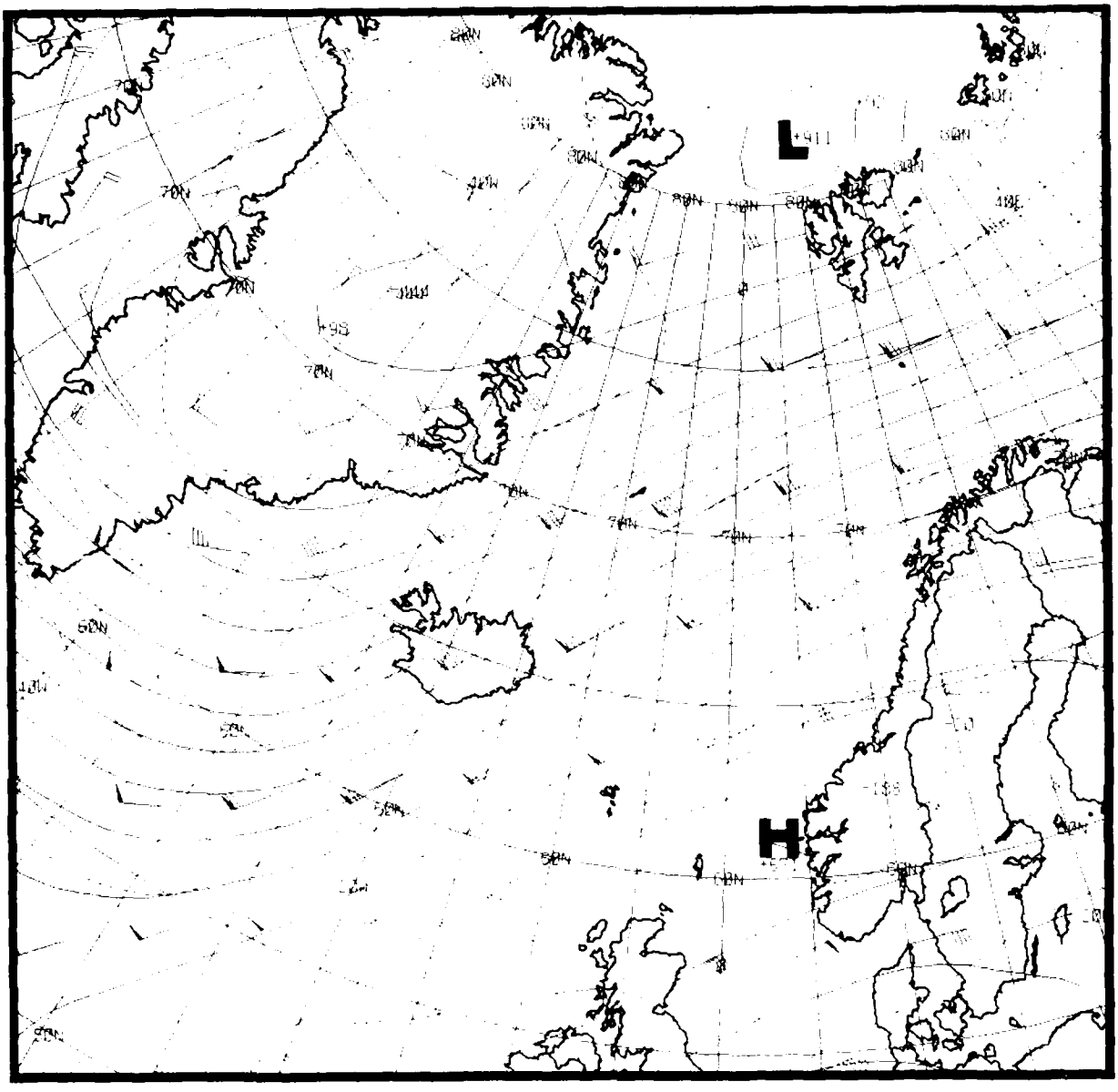

Figure 6-7. FNOC 500-mb Analysis, 0000 GMT 26 February 1984.

By 2330 GMT DMSP data (Fig. 6-8) shows an east-west oriented band of heavy convection north of Iceland, with cyclonically curved bands in the cellular cloud field leading up to the band passing over Iceland. The surface analysis for 27 February at 0000 GMT (not shown) reveals an elongated trough leading through the banded cloudiness toward Bear Island. The 500-mb analysis for the 27th at 0000 GMT (Fig. 6-9) shows the cold trough aloft with flow turning anticyclonically over the banded structure.

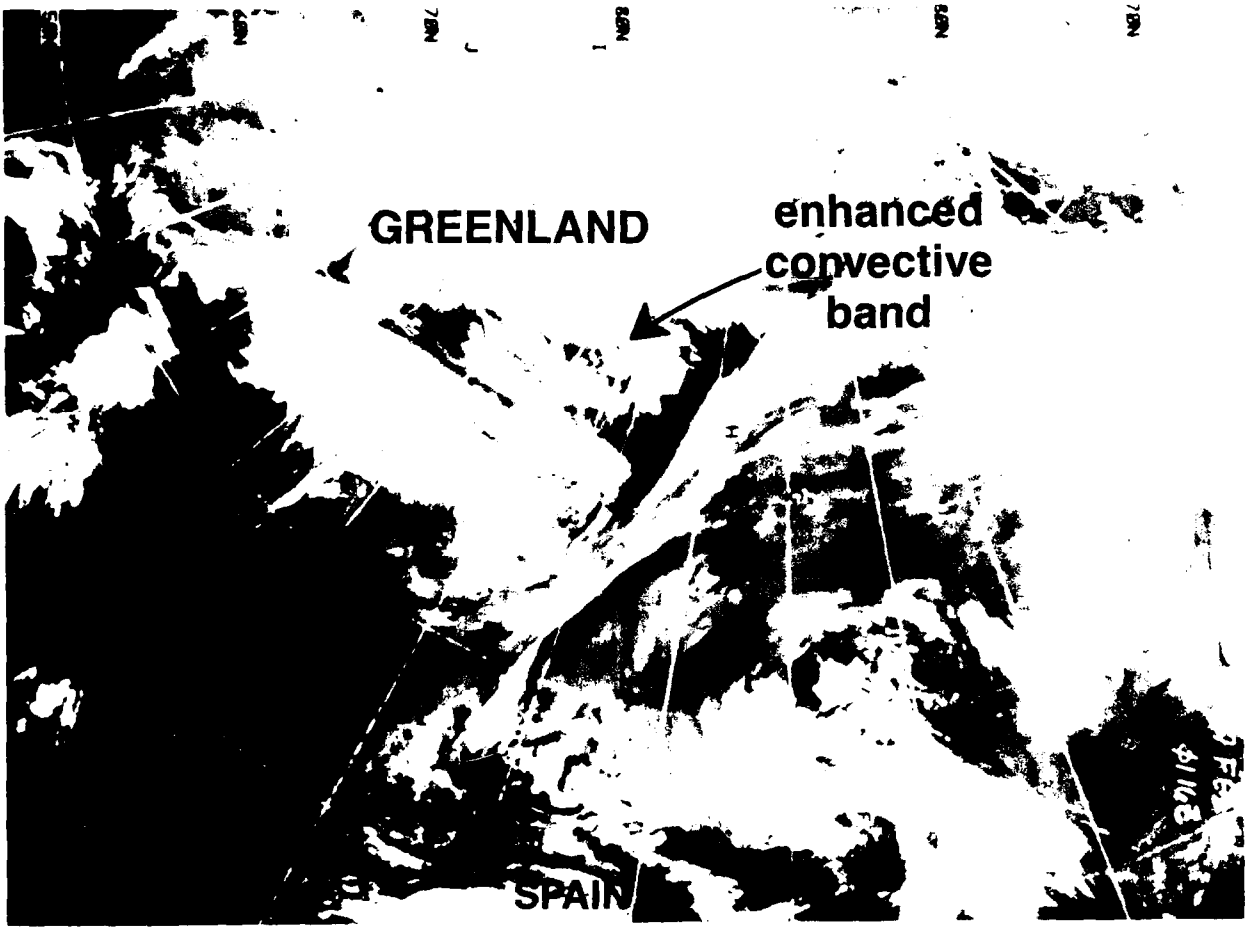

Figure 6-8. DMSP Imagery, 2330 GMT 26 February 1984.

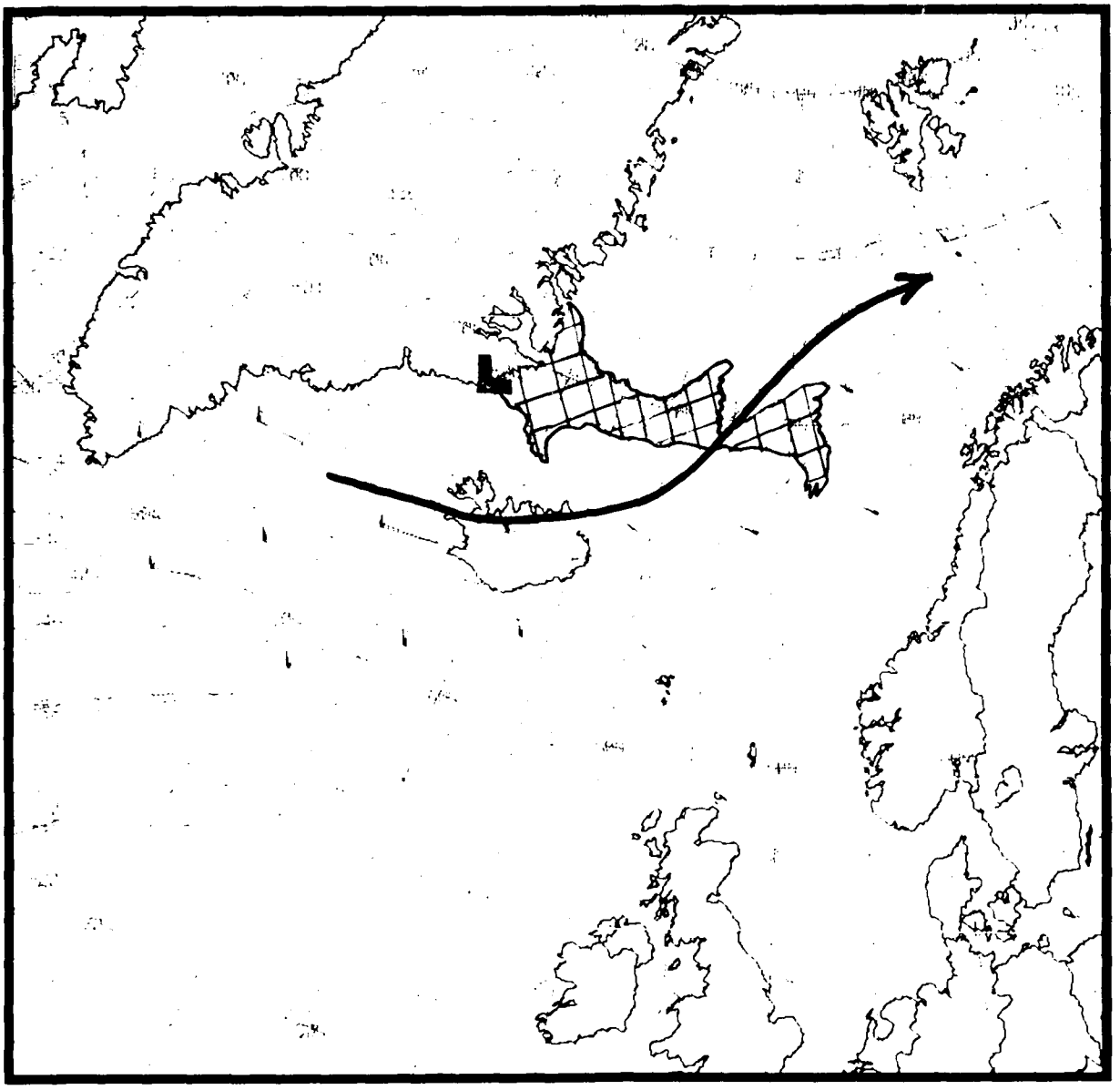

Figure 6-9. FNOC 500-mb Analysis, 0000 GMT 27 February 1984.

Further development of the banded structure revealed by DMSP data near 0700 GMT on the 27th (Fig. 6-10) shows an apparent grouping of at least three distinct cloud clusters. These structures coalesce into a significant polar low, as revealed in NOAA-7 data at 1340 GMT on the same day (Fig. 6-11). This storm was penetrated by a P-3 research aircraft near the time the NOAA data was acquired. Surface winds up to 65 kt (33 m/s) were measured as the storm reached peak intensity (Shapiro, 1986). Again, an important observation is the presence of heavy convection in the storm's southern quadrants associated with a cold trough aloft.

Figure 6-10. IR DMSP Imagery, 0700 GMT 27 February 1984

Figure 6-11. NOAA-7 Imagery, 1340 GMT 27 February 1984.

Figure 6-12 shows the FNOC 500-mb analysis for 1200 GMT on this date with the outline of storm cloudiness superimposed. These data verify the location of the cold trough that traveled with the moving disturbance. The surface analysis, Fig. 6-13, fails (as is common in these circumstances) to locate the center of the major development that had reached hurricane force by this time.

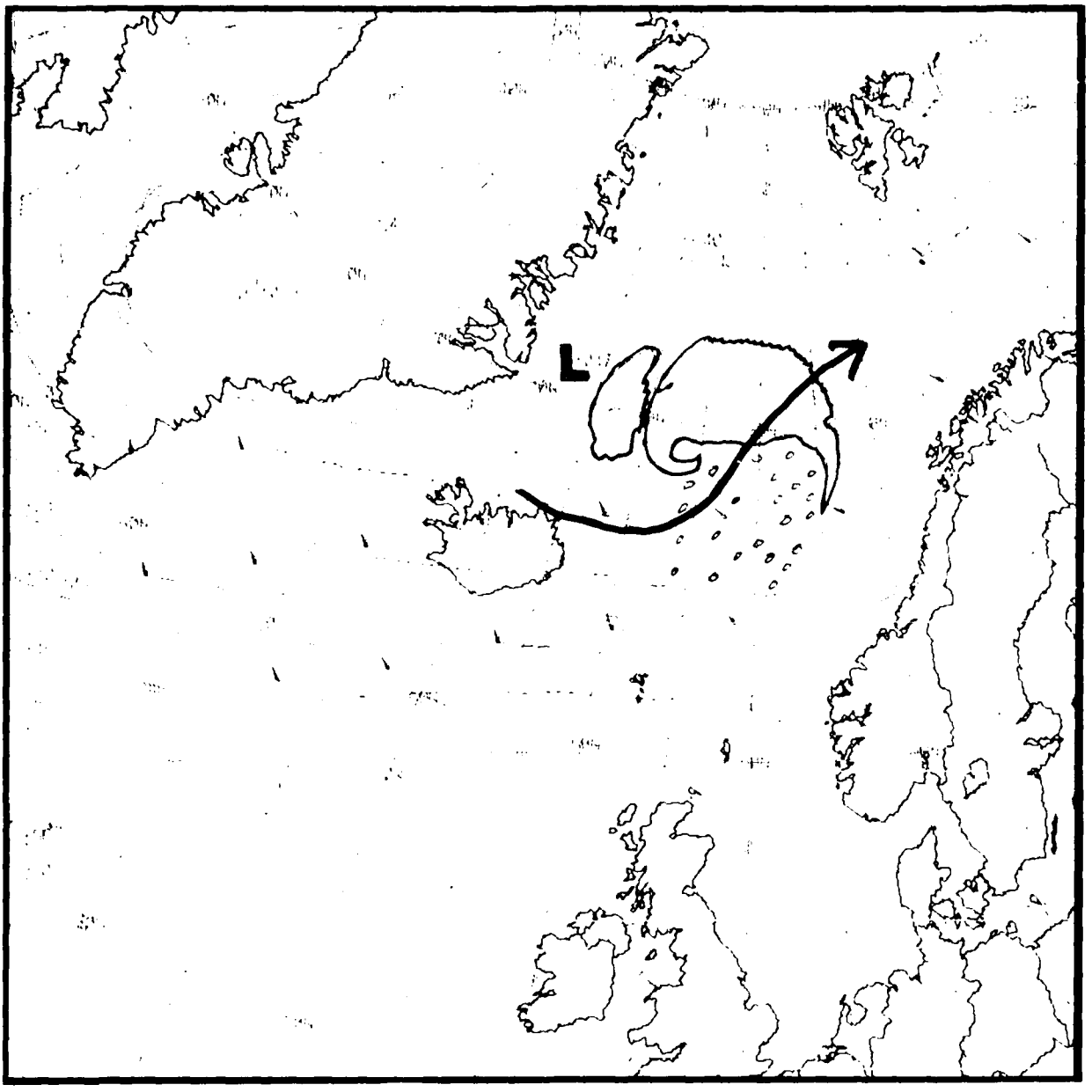

Figure 6-12. FNOC 500-mb Analysis, 1200 GMT 27 February 1984.

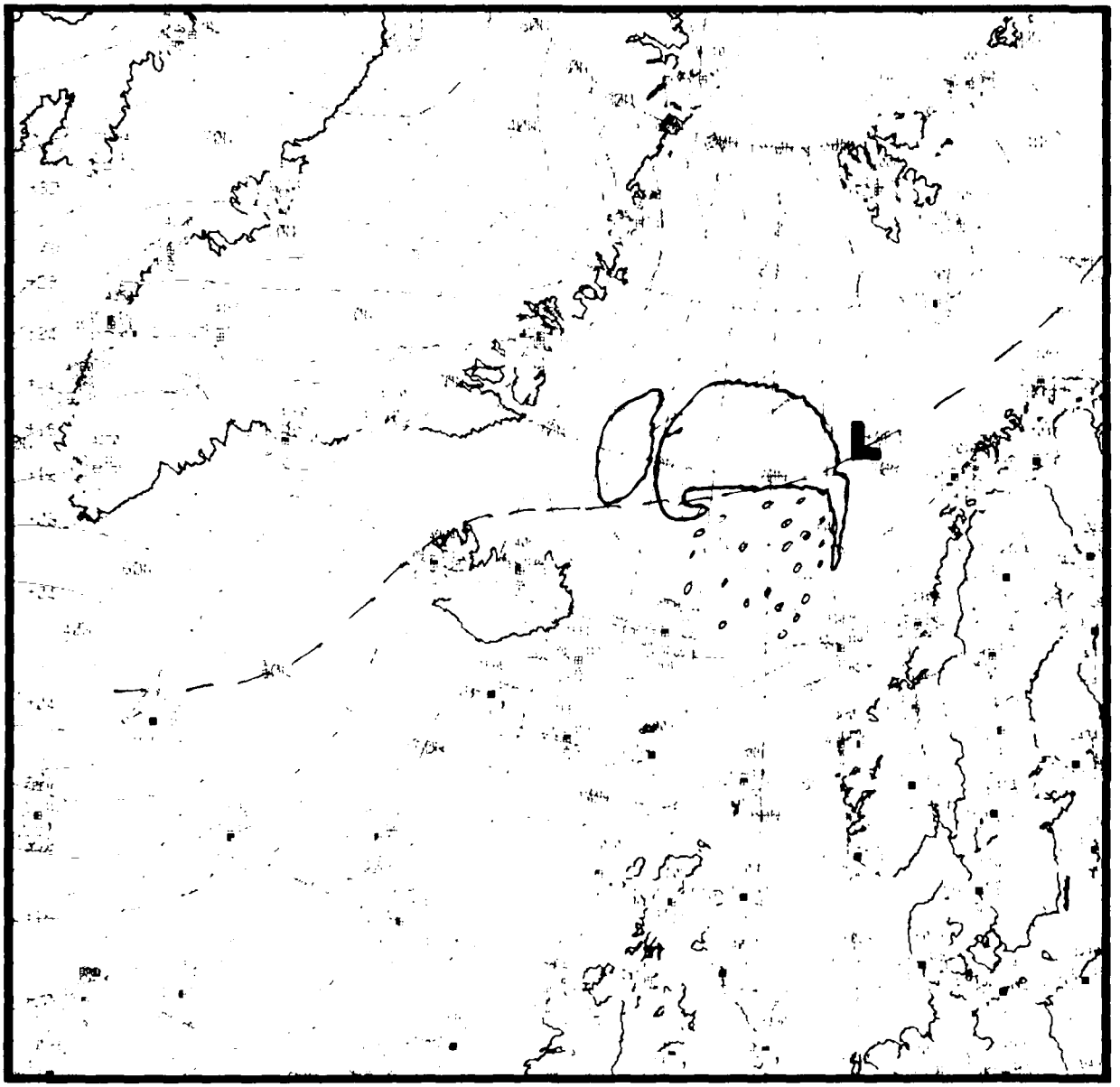

Figure 6-13. FNOC Surface Analysis, 1200 GMT 27 February 1984.

6.2.3 Polar Low Evolution, 13–14 February 1984

Figures 6-14 and 6-15 on 13 and 14 February 1984, respectively, illustrate how effectively enhanced cumulonimbus convection in open-celled areas can be used to track general areas where polar low development is anticipated. This convection occurred in the northernmost cloud cluster of Fig. 6-15, as documented in another P-3 aircraft flight into the storm area on 14 February (Shapiro, 1986). In this example, as in the others, a cold trough aloft triggers deep convection in the general region of surface low pressure. The cloud band north of the convection is associated with an asymptote of convergence in surface streamline flow (not shown). At 500 mb (not shown) the flow tends to turn anticyclonically over the overcast cloud band; therefore, a pattern of low-level convergence and upper level divergence develops very similar to the warm core structure of tropical cyclones that polar lows often resemble.

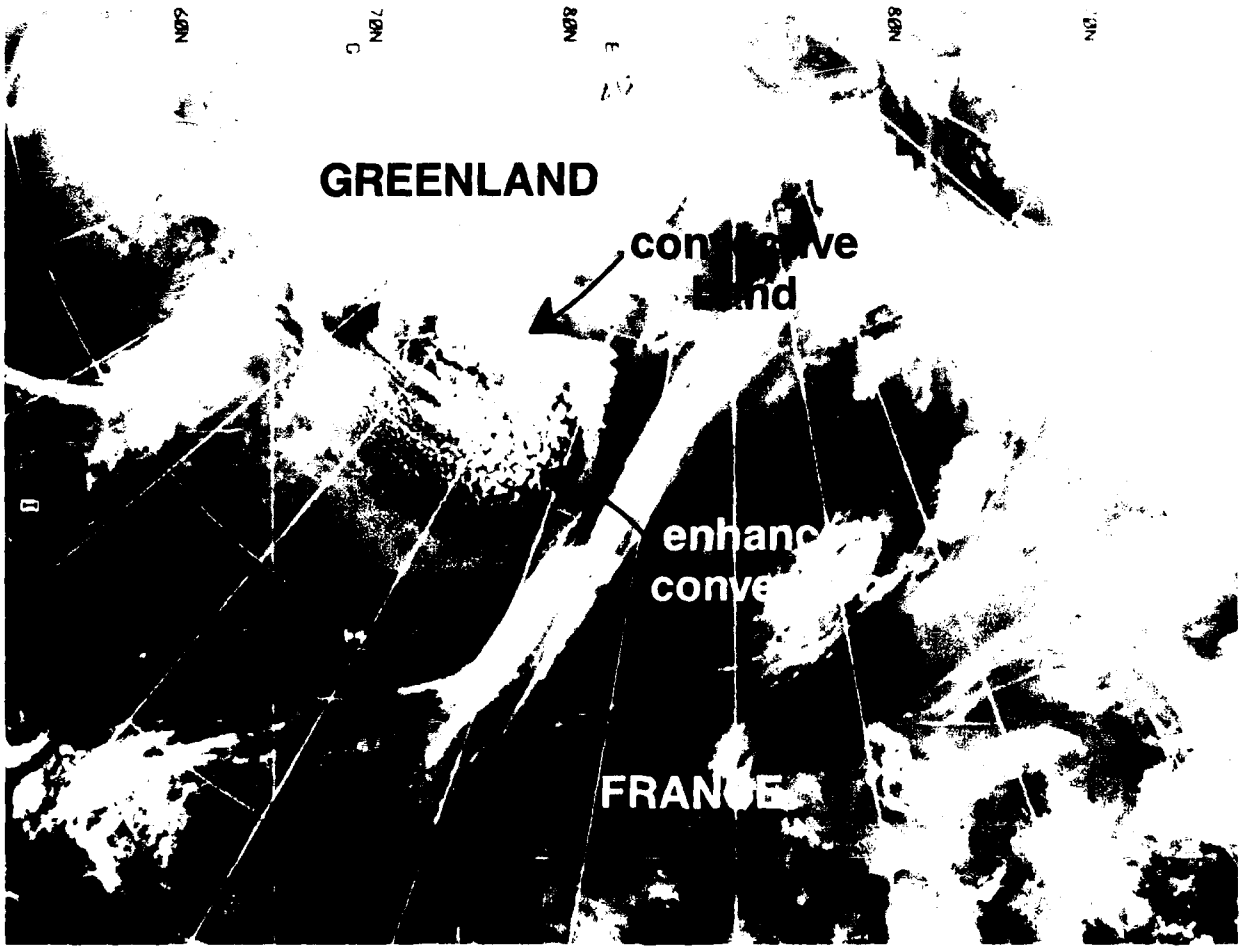

Figure 6-14. DMSP Imagery near Iceland, 0040 GMT 13 February 1984.

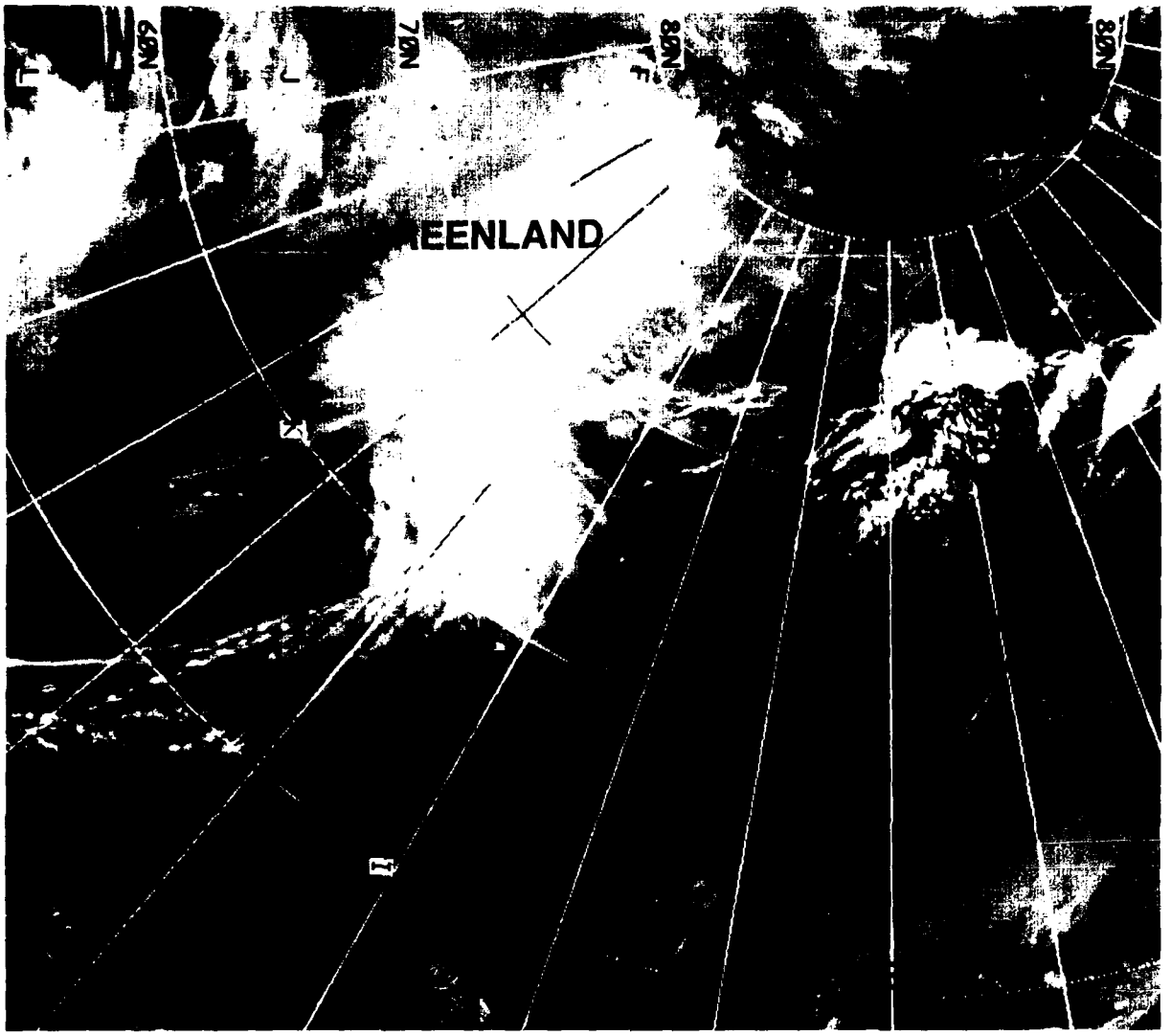

Figure 6-15. DMSP Imagery near Norway, 0234 GMT 14 February 1984.

6.2.4 Polar Low Development Near Bear Island, 12-14 December 1984

The Bear Island region is another area favored for polar low development. The climatologically favored easterly flow past Spitsbergen produces inverted troughs (similar to easterly waves) that move across the Fram Strait between Spitsbergen and Greenland. Vortices develop along and especially at or near the base of the trough axis. Figure 6-16 shows an example collected during MIZEX of 1987. Here fresh southeasterly winds flow off ice from the area just south of Spitsbergen and converge along a distinct, nearly north-

south-oriented cloud band. Winds are much weaker west of the cloud band and turn cyclonically in that region in the manner of an inverted trough. A cloud vortex is apparent at the southern end of the cloud band, and a second, even better developed vortex appears just southeast of the first. Open-celled cloud fields are in the region, but no evidence exists of deep convection that would signal the presence of an upper level cold low or trough. These vortices fail, therefore, to develop further and soon dissipate.

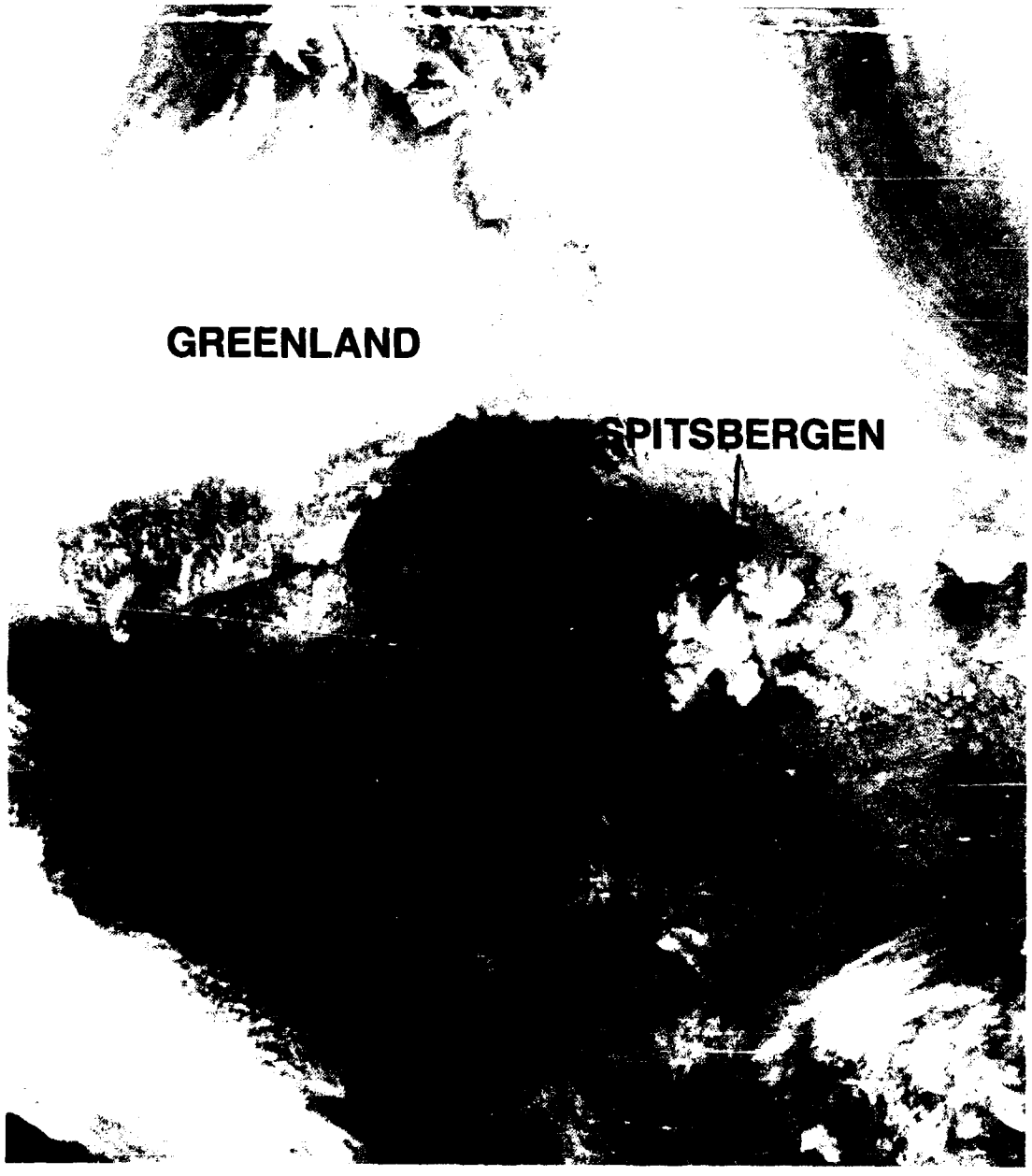

Figure 6-16. DMSP Imagery, 0337 GMT 26 March 1987.

Figure 6-17 shows a similar-appearing vortex at the end of the inverted trough just to the west of Bear Island, indicated by an X (Spitsbergen is marked with an S), on the image. In this example deep convection with abundant cumulonimbus development is evident south of the vortex.

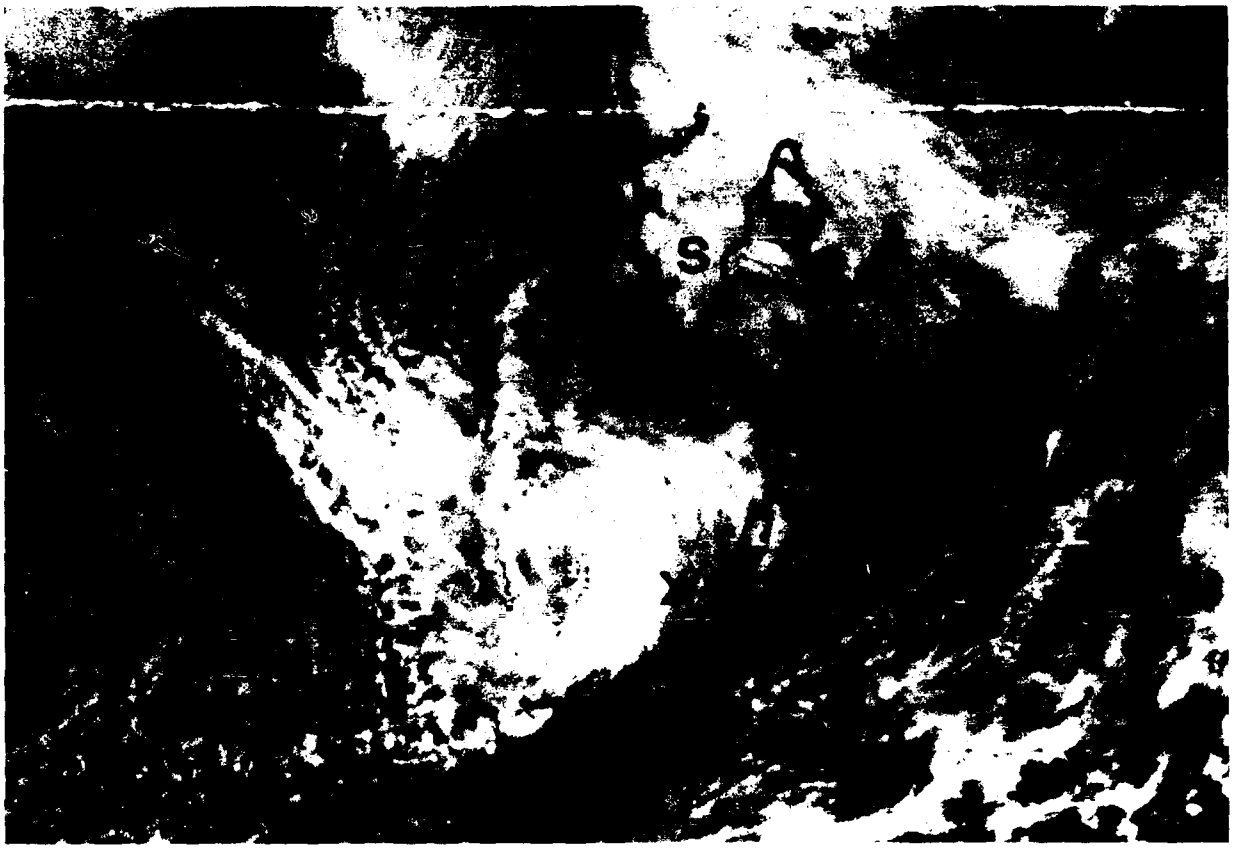

Figure 6-17. IR NOAA 7 Imagery, 1257 GMT 12 December 1982 (Courtesy of University of Dundee).

The 500-mb data (not shown) indicate a deep cold trough over the region with temperatures below −40 °F (−40 °C). Within about 12 hours the storm deepens to an intense-appearing vortex with a clear eye and within 24 hours changes from cold core to warm core structure (Rasmussen, 1985). A NOAA-7 image of the storm at 1245 GMT on 13 December is shown in Fig. 6-18. Characteristic very heavy cumulonimbus activity is evident in all of the southern directions from the storm center.

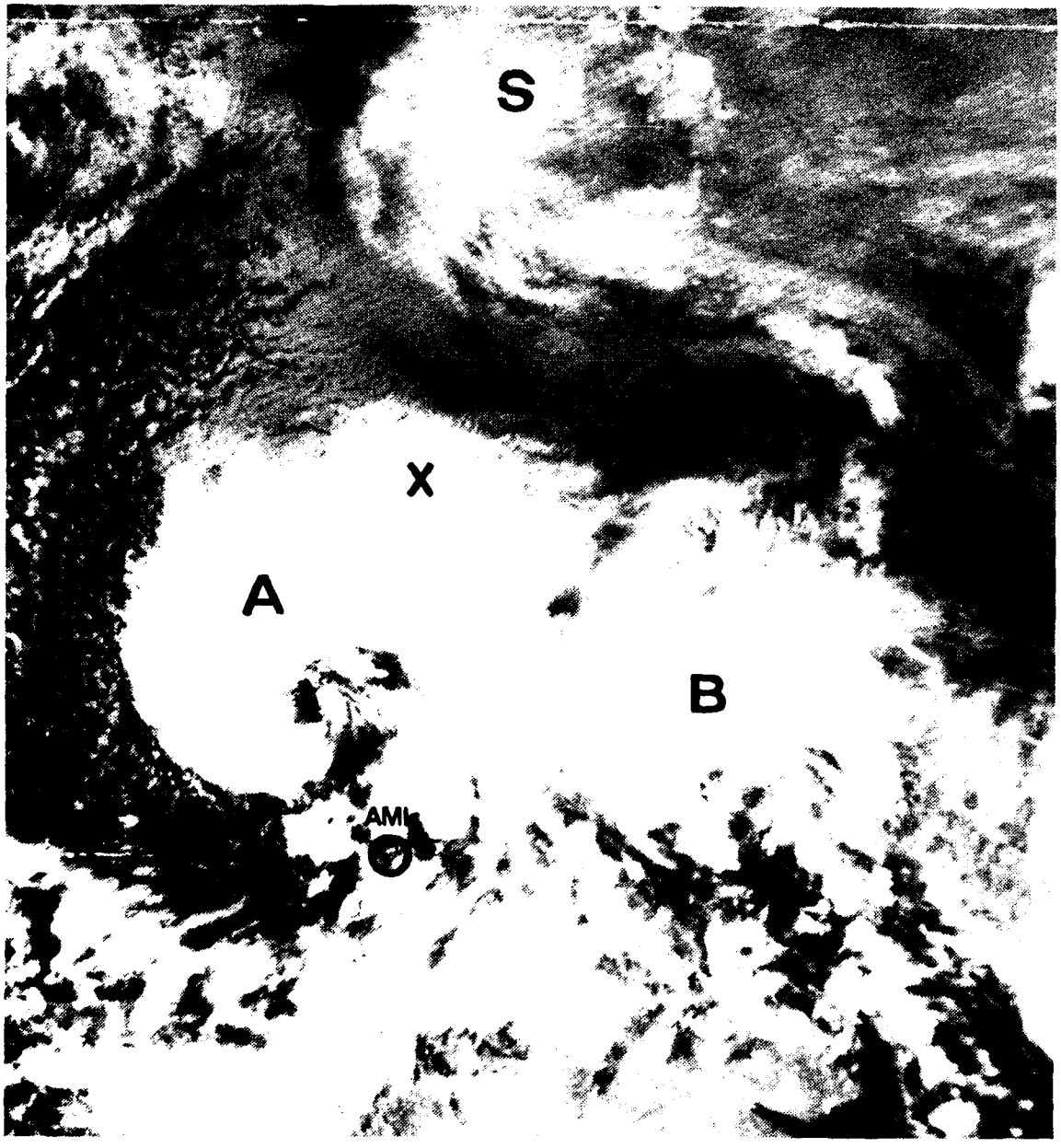

Figure 6-18. IR NOAA 7 Imagery, 1245 GMT 13 December 1982 (Courtesy of University of Dundee).

The 500-mb analysis at this time is shown in Fig. 6-19. The southeast wind direction at Bear Island suggests outflow characteristic of a warm core system. Winds immediately above 500 mb turn to the southwest, indicating even more strongly the outflow characteristic.

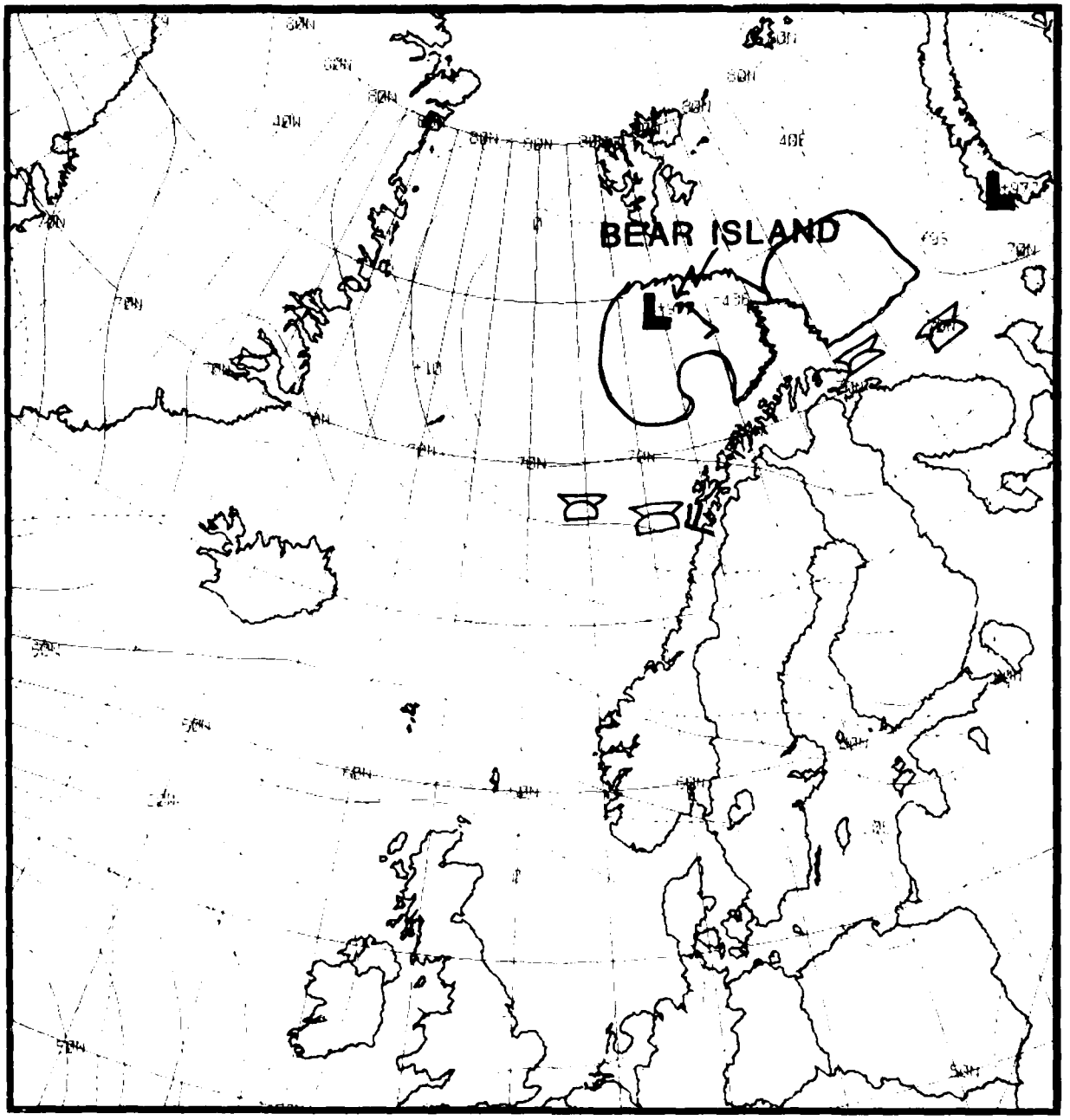

Figure 6-19. FNOC 500-mb Analysis, 1200 GMT 13 December 1982.

6.3 Precursor Surface and 500-mb Flow Patterns

6.3.1 Precursor Surface Conditions

The examples in the preceding section document the importance of an upper cold low or trough relative to polar low development. They also suggest general flow patterns in relation to satellite observed cloud development that are favorable for polar low evolution. Figure 6-20 shows the frequently observed surface pressure pattern associated with polar low development in the region near Iceland. The overcast cloud band may contain one or more vorticity centers from which the major low will develop. The band generally appears offset from the main low pressure center in a region of weak vertical shear. A streamline analysis of the area would reveal an asymptote of convergence in the area occupied by the band. Businger (1985) noted the typical ridging over northwestern Greenland that preceded polar low development. The effect of the ridging, in conjunction with the general trough over Greenland and the Norwegian Sea, results in a northerly flow component of very cold air along the east coast of Greenland, over the MIZ. When this cold air is eventually advected over the warm Gulf Stream Current, which flows past Iceland, an enormous exchange of heat and moisture can contribute to storm intensification.

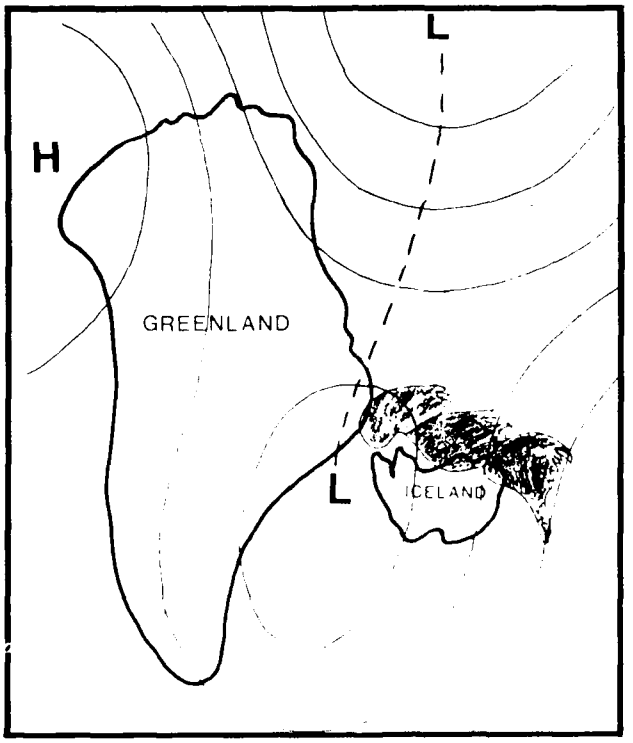

Figure 6-20. Schematic of Surface Conditions Favorable for Polar Lows.

6.3.2 Precursor 500-mb Flow Patterns

Figure 6-21 shows the typical 500-mb flow pattern frequently noted in polar low development. The cold upper level trough triggers deep open-celled convection. Release of latent heat in the convective cloud band may assist in building the warm ridge sometimes observed over this feature. In this configuration the thermal wind component, V_T acts to accelerate the wind flow over the convective cloud band, thereby enhancing upper level divergence (Fig. 6-21). The upper level trough and developing polar low move together with time in mutual interaction.

In conclusion, intense polar low developments can be distinguished from weaker nondeveloping vortices, noted in Arctic regions, by the presence of deep open-celled convection adjacent to banded overcast cloudiness. The deep open-celled convection indicates cyclonic low-level flow with a cold low or cold trough aloft. Good quality, high resolution satellite data are required at frequent intervals to monitor the progress of such developments.

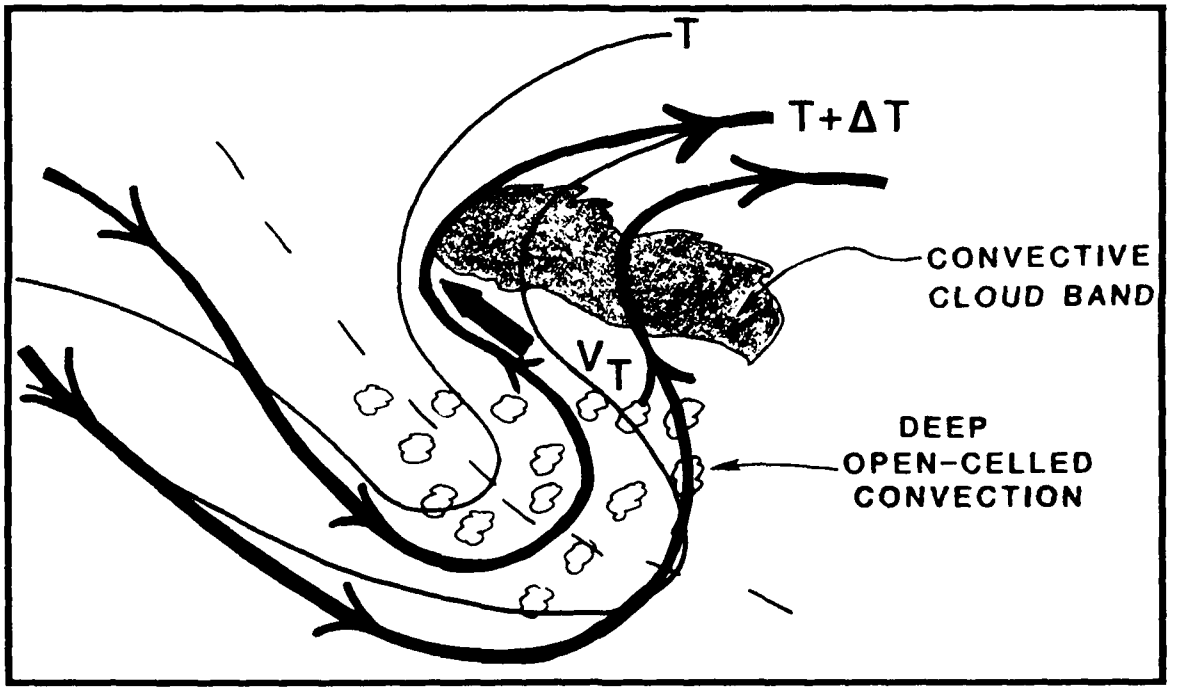

Figure 6-21. Schematic of 500-mb Conditions Favorable for Polar Lows.

THIS PAGE INTENTIONALLY LEFT BLANK

7. OPTICAL PHENOMENA OF THE ARCTIC

One of the unique aspects of an assignment in the Arctic is the ample opportunity to view a host of optical phenomena that occur there. Many of these phenomena arise from the suspension of ice crystals in the polar atmosphere; however, the presence of strong surface inversions is also responsible for refraction of light rays. The combination of these two features of the Arctic atmosphere make for a variety of optical effects.

7.1 Refraction

Sunlight is composed of a mixture of colors ranging from violet to red, not to mention the invisible ultraviolet and IR radiation on the edges of the solar spectrum. A prism, as shown in Fig. 7-1, causes the rays of different colors to be deflected and separated as a result of *refraction*. Refraction comes about because the speed of light depends on the property of the medium through which the light passes. Consider the passage of light from one medium, water, into another medium, air (Fig. 7-2). The wave speed is greater in air than in water, and as a result, when a wave front emerges from the water, it is reoriented because the part of the wave in the air moves faster than the part in water. The bending of light rays is easily demonstrated by observing a pencil partly immersed in water, as in Fig. 7-3. When viewed from the side, the pencil appears shorter than it actually is because the light rays coming from all parts of the pencil under water are deflected at the surface of the water.

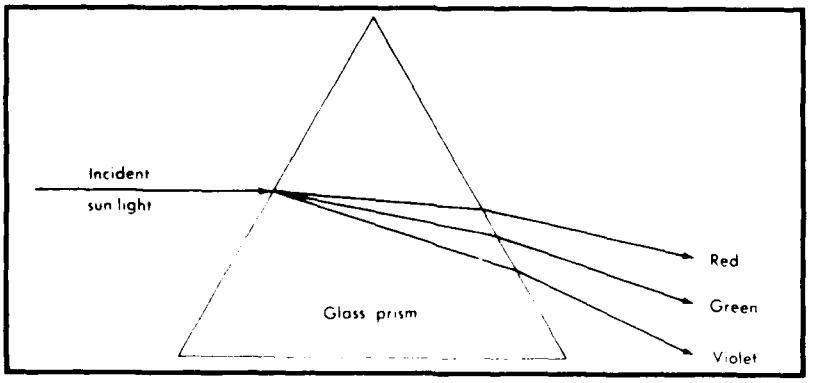

Figure 7-1. Sunlight Passing Through a Prism (Battan, 1984).

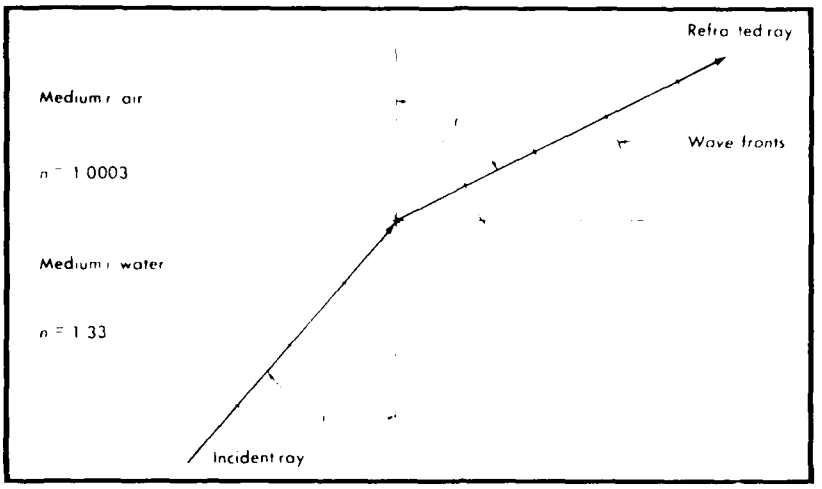

Figure 7-2. An Example of Refraction (Battan, 1984).

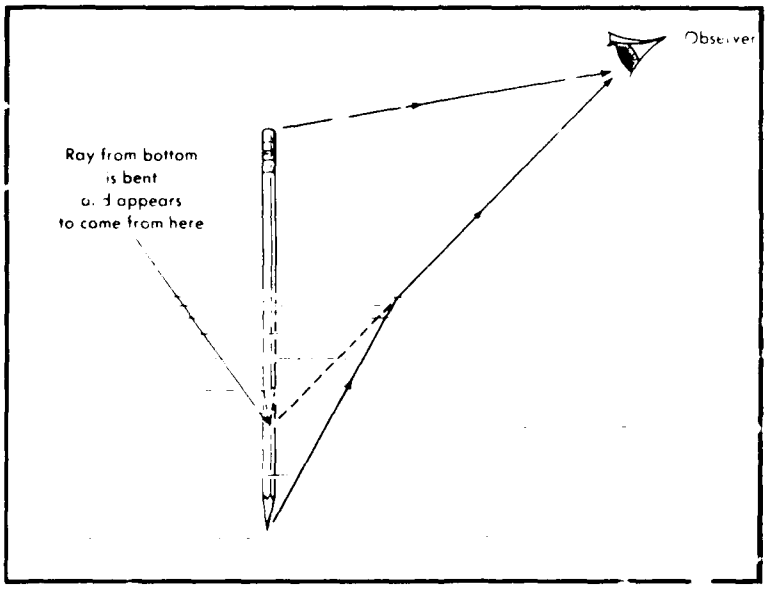

Figure 7-3. Rays Bending from One Medium to Another (Battan, 1984).

The velocity of light in any medium is given by the speed of light in a vacuum (3×10^8 m/s) divided by a quantity called the *index of refraction*. Table 7-1 shows the indices of various substances and the corresponding speeds of light through them. For example, light passes through water at a velocity of 2.26×10^8 m/s, a value substantially less than the speed of light in air. The degree of refraction as a light ray moves from one medium to the next depends on the difference in indices of refraction of the two media.

The change of direction of a light ray is given by *Snell's law of refraction.* The law states that the greater the ratio of the indices of refraction, the greater the bending of the ray as it moves from one medium to the next.

TABLE 7-1. INDICES OF REFRACTION (N) OF VARIOUS SUBSTANCES FOR VISIBLE LIGHT* (BATTAN, 1984)

Medium	n	Speed of light** ($\times 10^8$ m/s)
Vacuum	1.0000	3.000
Air (lower atmosphere)	1.003	2.999
Ice	1.31	2.29
Water	1.33	2.26
Olive Oil	1.47	2.04
Flint Glass	1.61	1.86
Diamond	2.42	1.24

* The values in this table apply specifically to a wavelength of 0.589 μm (yellow), but they are approximately correct for all visible radiation.

** Speed $v = c/n$, where $c = 3.000 \times 10^8$ m/s.

The value of the refractive index depends not only on the properties of the medium but also on the wavelength of the electromagnetic radiation. Over the visible part of the spectrum, the range of the refractive index is small. Nevertheless, the small differences are important because they lead to the dispersion of white light into various color components as the light passes through a glass prism, raindrop, or an ice crystal. Since the refractive indices at the violet end of the spectrum are larger than those at the red end, the violets and blues are refracted more than the yellows and reds, in accordance with Snell's law.

7.2 Rainbows

When the Sun illuminates sheets of water droplets, colorful arcs appear around the antisolar point, i.e., the point 180 degrees away from the Sun along a great circle. These arcs are called *rainbows*, although they may be caused by dew droplets on the ground, or by sprays from waterfalls, fountains, or garden hoses.

The *primary rainbow* has a red outer border whose angular radius is roughly 42 degrees. The *secondary rainbow* is generally a broader and less bright band with red on the inner border and a radius about 50 degrees. The area between these two rainbows appears darker than the rest of the sky. The *supernumerary bows* that appear inside the primary and outside the secondary rainbows are an integral part of these rainbows; they show fewer and less distinct colors and are frequently so faint as to be visible only to an experienced observer. Figure 7-4 shows schematically the geometric optics of primary and secondary rainbows. Considering the primary rainbow, a sunray entering a water droplet is refracted, once reflected, and again refracted on leaving the droplet. Since the various color components of sunlight are differently refracted, the component rays diverge. Thus, only one ray emerging from a droplet may reach a given observer. Moreover, each eye of the observer receives light from a different droplet for each color from every point of the rainbow.

The secondary rainbow is produced in a similar manner, but the light ray is twice internally reflected before being refracted out of the drop. For this reason, the color sequence is reversed, and because of the greater divergence of the emerging color components, the secondary rainbow is broader. It is also only about one-twelfth as bright as the primary bow because of the light lost in the multiple optical processes involved.

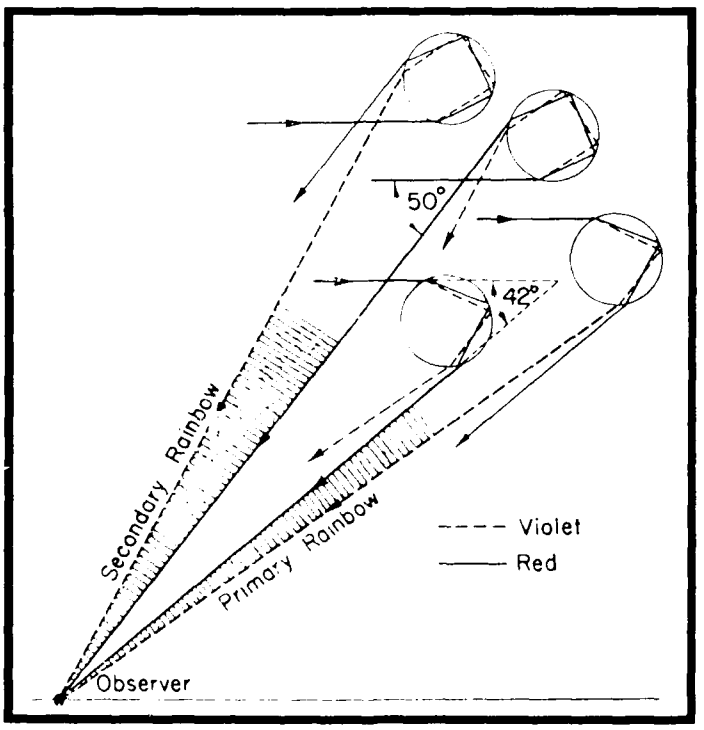

Figure 7-4. Schematic Diagram of Geometric Optics of Rainbows (Neuberger, 1966).

Figure 7-5 shows that a rainbow always appears in the opposite side of the sky from the Sun. By standing in front of the Sun while viewing a distant shower, the observer will be able to see a rainbow. Because of the geometry involved, when rainbows are observed from the ground, they appear as semicircles. Thus, flying over a region of raindrops when the Sun is high in the sky, the observer will have the experience of looking down and seeing a rainbow in the form of a complete circle or ring.

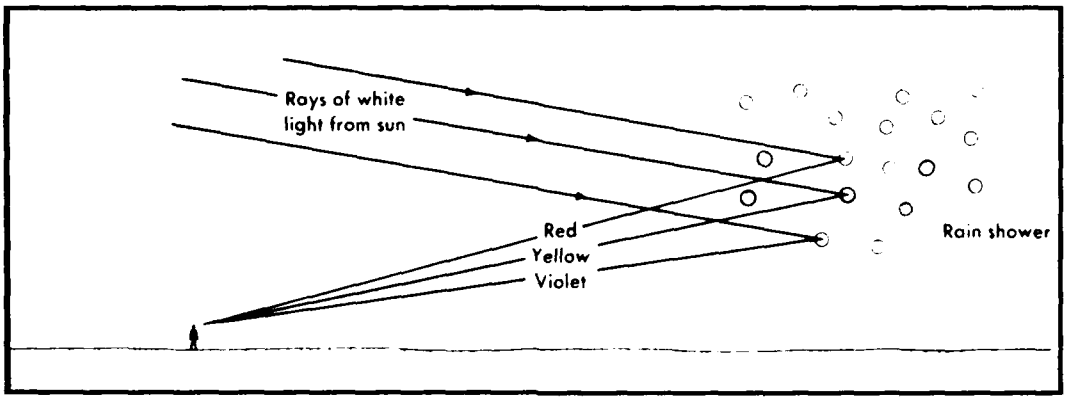

Figure 7-5. The Primary Rainbow (Battan, 1984).

7.3 Halos

Ice crystal clouds can produce a large variety of luminous arcs and circles that are called *halos*. The most common one is a bright ring surrounding the Sun or the Moon and having a colored or whitish appearance. The halo occurs because of the refraction of light as it passes through ice crystals in the shape of hexagonal prisms (Fig. 7-6). When a thin, uniform cirrostratus deck containing such crystals covers the sky, the halo may be in the form of a complete circle having an angular radius of 22 degrees (the angle between lines from the eye to the Sun and to a point on the halo).

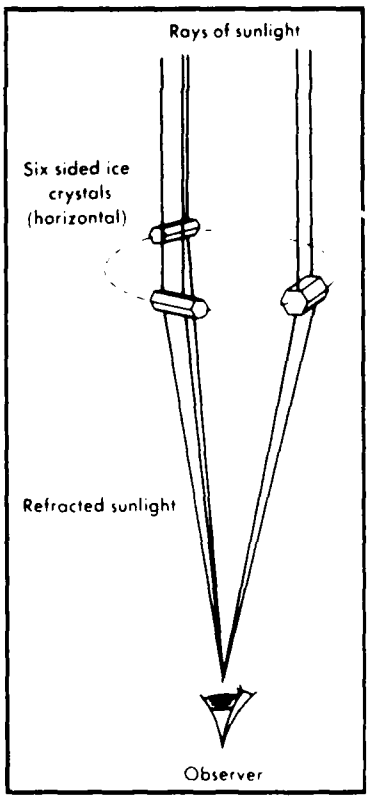

Figure 7-6. Formation of a 22-Degree Halo (Battan, 1984).

More often a cloud of ice crystals covers only part of the sky, and as a result, only a segment of a halo is seen. A hexagonal ice prism in the process of refraction separates white light into its component colors. Since blue waves are bent more than red ones, the inside of the halo is red, the outside blue. Most often the colors are subtle, and thus halos appear mostly white.

Figure 7-7 shows the ray path through a hexagonal platelet or column by which the halo of 22 degrees is produced. In order for a complete ring around the Sun to be visible, the ice crystals must be randomly oriented. This condition also holds true for the halo of 46 degrees that is produced by a refracting angle of 90 degrees; that is, a ray enters the side of a hexagonal prism and leaves the base of the crystal as shown in Fig. 7-8, or the ray enters the base and leaves the side. The 46-degree halo is rarely seen as a complete circle, but exhibits more distinct colors than does the halo of 22 degrees.

Of the great variety of halo forms, only the most common halos are shown in Fig. 7-9, in which the Sun is represented by a small circle in the center. The various features are depicted for the Sun's elevation of about 25 degrees. Thus, the lower portions of this diagram are below the horizon for an observer on the ground.

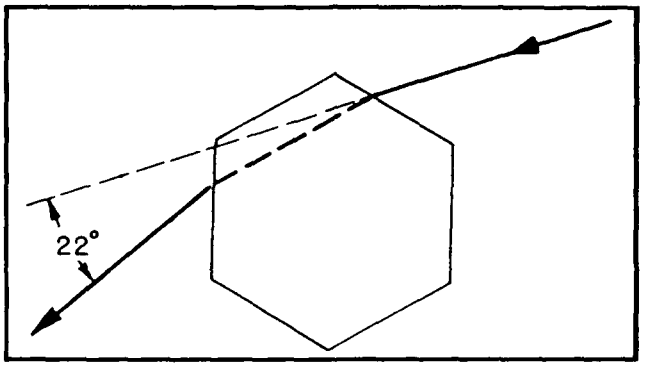

Figure 7-7. Ray Path Through a Hexagonal Crystal (Neuberger, 1966).

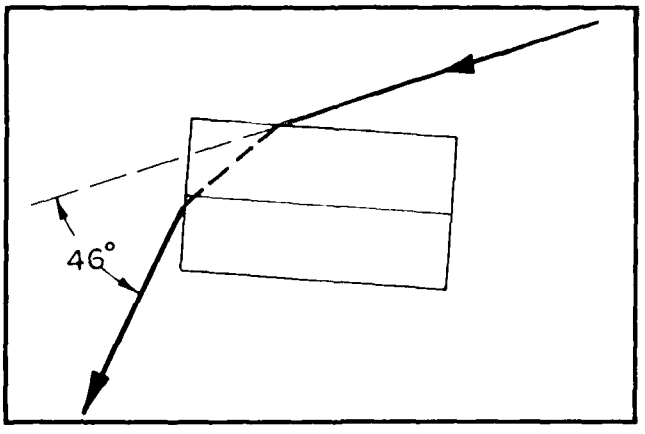

Figure 7-8. Ray Path for a 46-Degree Halo (Neuberger, 1966).

Occasionally a species of halo can be seen consisting of a faint, white circle passing through the Sun and running parallel to the horizon. This unusual effect is called a *parhelic circle.* It is caused by simple reflection from the faces of ice crystals (in the form of hexagonal prisms) having their long axes in a nearly horizontal plane as though they were tiny mirrors.

When ice crystals in the form of hexagonal prisms fall with long axes vertical, refraction causes the formation of luminous spots on both sides of the Sun at an angular distance of 22 degrees. Either of these spots is a *parhelion,* but the more popular name is *sun dog.* Figure 7-10 shows a 22-degree halo with sun dogs embedded to the left and right of the horizon.

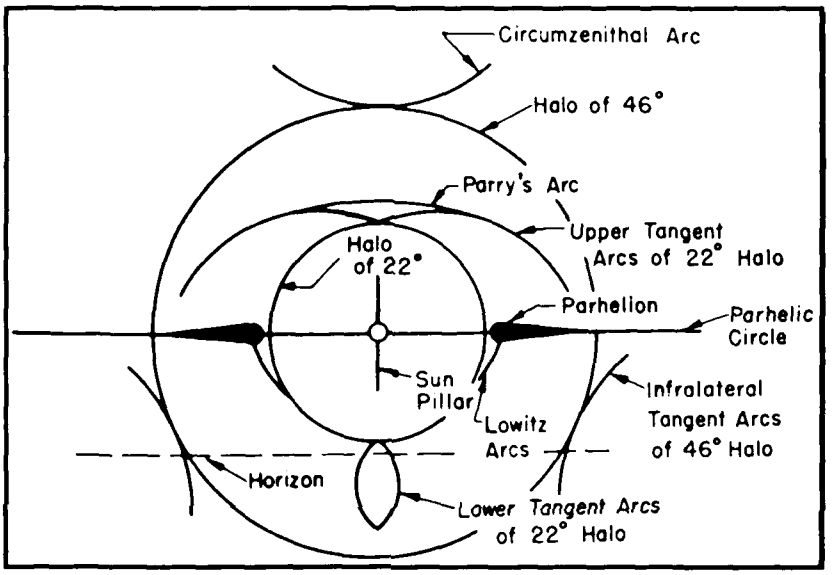

Figure 7-9. Common Observable Halo Phenomena (Neuberger, 1966).

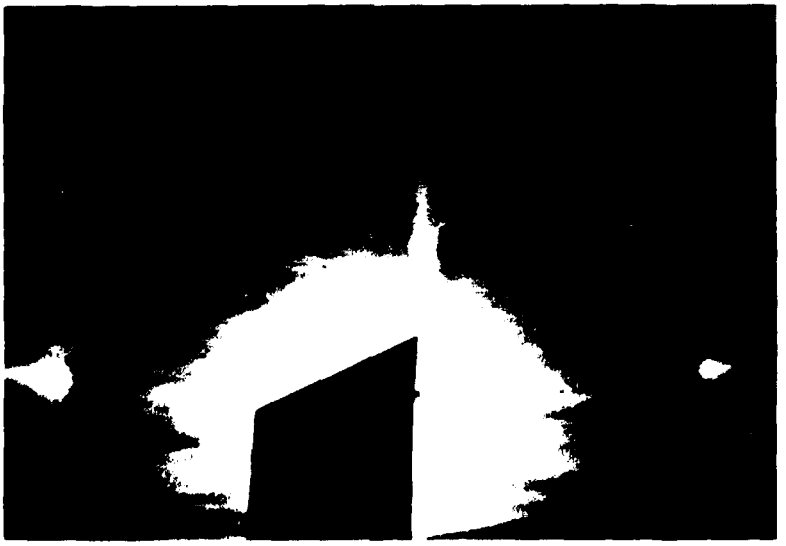

Figure 7-10. Halo with Sun Dogs and Sun Pillar (Battan, 1984).

Occasionally shafts of light extend vertically either directly above or below the Sun. Commonly known as *sun pillars,* they are most frequently seen near sunrise or sunset (Fig. 7-10).

7.4 Coronas and Related Phenomena

Sometimes the Sun or Moon is partially obscured by a thin cloud and is surrounded by a ring of light called a *corona,* a word meaning "crown." At times, a corona may be in the form of a luminous disk having the Sun or Moon at its center. Coronas subtend angles of only a few degrees and therefore are much smaller than the common 22-degree halo. When a corona exhibits coloration, it is blue on the inside and red on the outside, opposite to the order of colors in a halo. Coronas are produced by clouds of water droplets as a result of an effect called *diffraction.* In diffraction, a light wave spreads behind an obstacle into the region that might normally be expected to be in shadow. Light waves coming from the Sun or the Moon toward an observer are slightly deflected around cloud droplets. When the waves interfere with one another on the observer's side of the droplets, concentrations of light occur in circles around the Sun or the Moon. Thus, whenever a corona is visible, the conclusion can be drawn that the cloud partly obscuring the Sun or Moon is made up of water droplets. In general, the smaller the cloud droplets, the larger the radius of the corona. Figure 7-11 shows a corona.

Occasionally, thin clouds high in the sky exhibit patches of color of the purest blue, green, and red. They may appear either when the Sun is low or high. Such clouds, called *iridescent clouds,* usually are observed to be within 30 degrees of the Sun and also are thought to be caused by diffraction. Recall that the Sun's rays are deflected around patches of uniform water droplets, and the light waves interfere with one another in such a fashion as to separate the various color components.

Figure 7-11. An Example of a Solar Corona (Battan, 1984).

The coronal phenomena around the light source have their counterparts around the point opposite the light source, such as around the antisolar or antilunar points. For example, an observer in the mountains seeing his slightly enlarged shadow on a fog bank or cloud beneath (the *brockenspecter*), often sees the shadow of his head encircled by brightly colored rings, the *anticorona or glory.* The anticorona can often be observed from a plane when looking on the shadow cast by the plane on the clouds below it.

7.5 Mirages

Four different types of mirages occur: the inferior image, which projects an image below the source; the superior image, which projects the image above the source; the towering image, which makes something appear taller than it really is; and the stooping image, which makes an object appear shorter.

7.5.1 The Inferior Mirage

An excellent example of the *inferior* mirage is the shimmering lake that appears on freeways or at the base of mountains. In hot, dry regions, air layers near the surface of the Earth are hotter, and therefore less dense, than those above it. When light strikes this superheated, low-density layer of air, it is refracted, or bent, so that it creates an optical illusion. For example, light from the sky may strike the hot air just above the pavement of a highway and be shot into a driver's line of vision. This situation is pictured in Fig. 7-12. The driver appears to see a pool of blue water in the road ahead but is actually seeing a mirrored image of the blue sky.

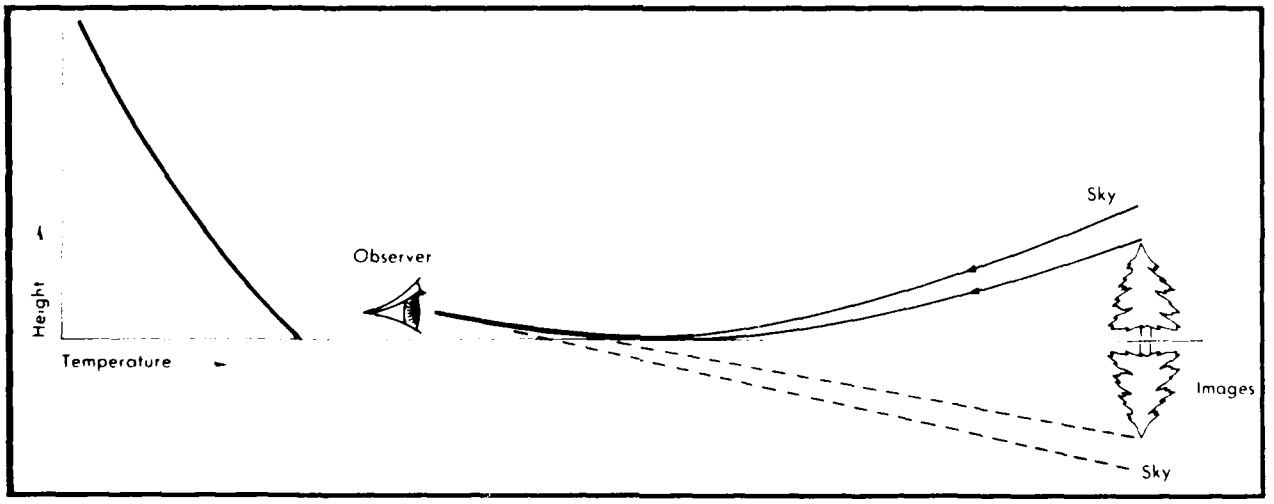

Figure 7-12. The Inferior Image (Battan, 1984).

If the light illuminates clouds or mountains before it is refracted, the driver also see mountains or clouds within the blue sky. Often, depending on the angle at which the light is bent, the images are inverted, making them look very much like reflections in a pool of water.

7.5.2 The Superior Mirage

The *superior* image works the opposite way from the inferior image. If an observer is standing in cool air with warm air above, light may be refracted back from space into the line of vision. Since some light will also travel directly from the source, the observer will see the actual object in the horizon and its inverted image floating in the sky. Figure 7-13 is a representation of the superior mirage effect.

One of the authors once saw in Antarctica a spectacular case of "looming." The location was at a coastal station where the early morning hours were characterized by a very strong surface inversion, on the order of 20 °F–30 °F (−7 °C to −10 °C) in the lower 500 ft. On this particular morning a look seaward revealed what appeared to be hundreds of icebergs rather than the usual ten or twenty. Looming had allowed the observers to see far beyond the horizon to icebergs not normally seen. No doubt many erroneous estimates of distances by early explorers can be ascribed to this phenomenon.

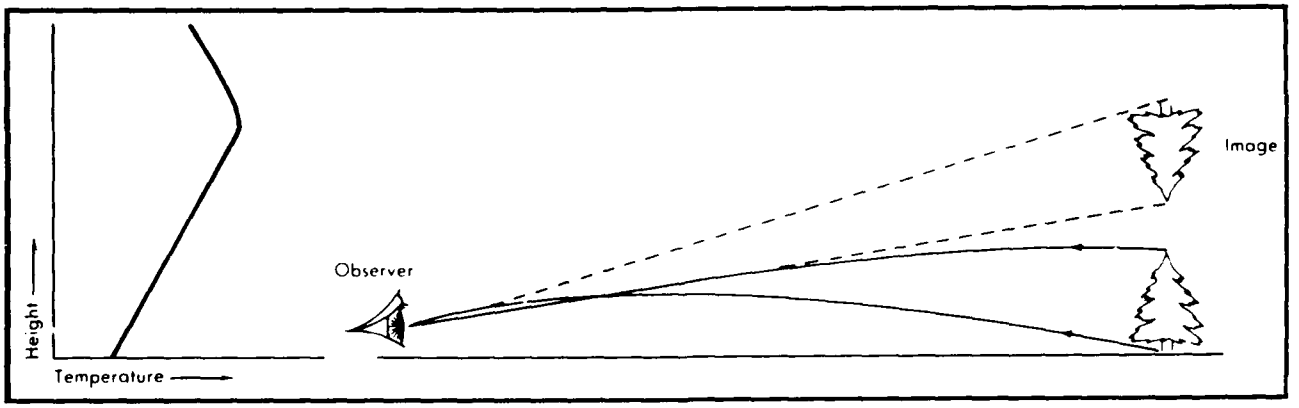

Figure 7-13. The Superior Image (Battan, 1984).

7.5.3 The Towering Image

Depending on the curvature of light rays, towering and stooping mirages also may occur. For example, the sails and mast of a ship may look elongated if seen from a distance. This *towering* mirage is caused by light moving through cool air and hitting warm air as it comes off the upper part (the sail) of the ship. The warm air bends the light back toward the observer. Since the light appears to the viewer to come from a higher source, the sail appears elongated. See Fig. 7-14 for an example of towering.

7.5.4 The Stooping Image

The *stooping* mirage, (Fig. 7-15) is an image that is contracted vertically. It works in basically the same manner as the towering image, but in this case the observer is standing in warm air, instead of cool air, thus forcing the light to level off into the observer's eyes and apparently reducing the vertical size of the object viewed.

Since stooping and inferior mirages occur in conditions where warm air is below cool air, these mirages happen most often on hot, dry land, where air nearest the Earth is usually the warmest in the atmosphere. Conversely, towering and superior mirages appear most often at sea, where air nearest the water is generally cooler than that above.

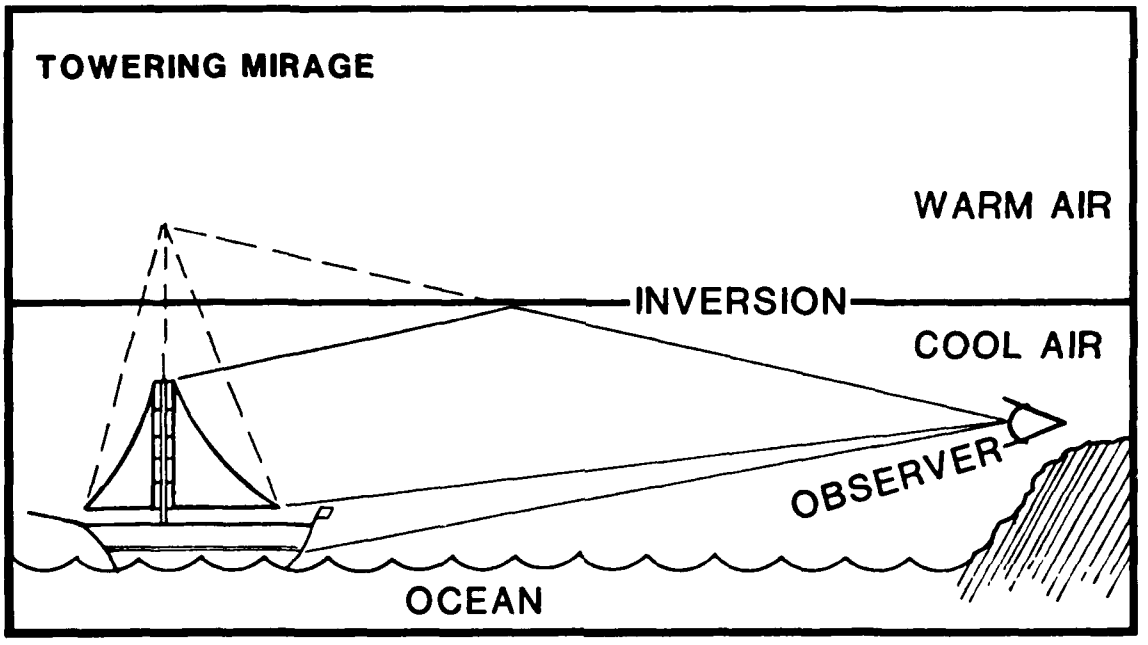

Figure 7-14. The Towering Image.

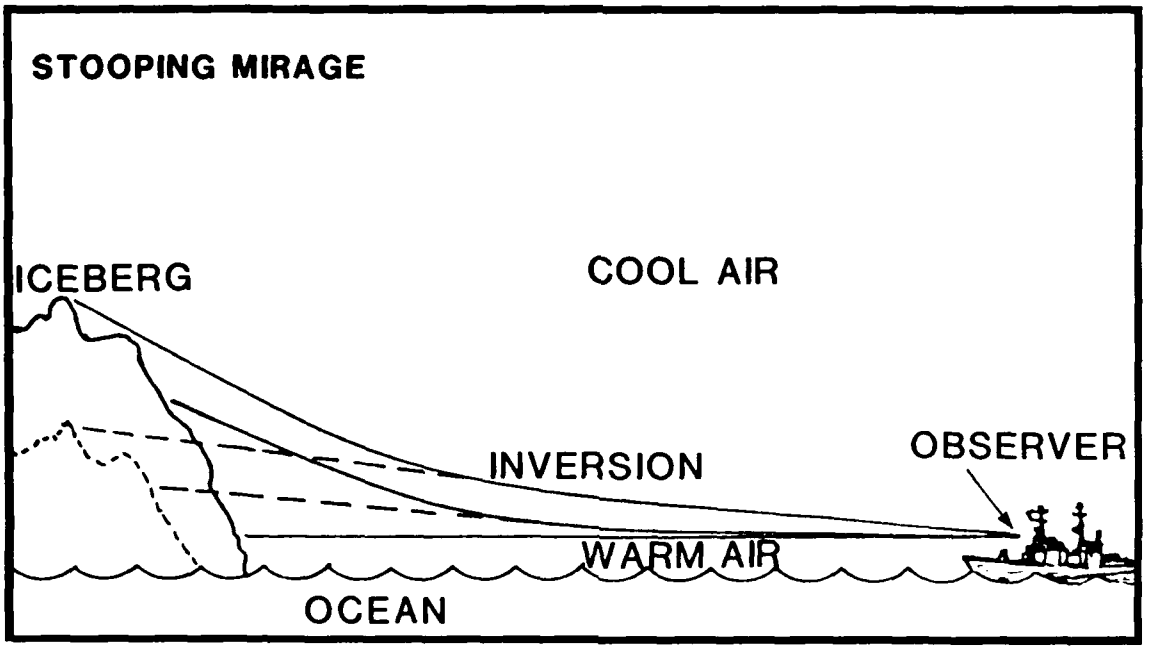

Figure 7-15. The Stooping Mirage.

7.6 Fata Morgana

Fata Morgana is the name given to a complex mirage in which distant objects become greatly elongated in the vertical direction and take on a bizarre aspect. A shoreline may be drawn out into tall cliffs and columns, and houses near the shore may assume the appearance of wondrous castles.

The phenomenon occurs under much the same meteorological conditions as the superior mirage and indeed often contains many of its features, though in more distorted form. The unusual stretching takes place in the layer where the normal upward lapse of temperature ceases and the elevated inversion begins. At the cold point in the sounding the density is at a relative maximum, and the degree of bending of the light rays changes sharply. The result is a vertical magnification of objects in the layer.

The fata morgana may be regarded as an intermediate stage between towering and the superior image, or a mixture of the two conditions. This mixture is evident in Fig. 7-16, where both the stretching and the tendency for formation of inverted images can be observed. Note that Fig. 7-16 is an etching produced from a drawing made in 1820. The subtleties shown in photographs of fata morgana do not reproduce well. Although the etching is overstated, it does provide the reader with the basic concept of fata morgana.

Figure 7-16. An Example of Fata Morgana.

7.7 Iceblink and Water Sky

In summer a white or yellowish-white glare may be seen on the underside of clouds, as a result of the reflection of sunlight from snow or ice fields. When these reflections are intense, they are referred to as *iceblink*. Conversely, under the same circumstances dark patches or streaks may appear on the cloudbase above areas of open water. This condition is known as *water sky*. When other means of reconnaissance are not available, these phenomena are of assistance in navigating through the ice of the polar seas, since they give at least a rough idea of ice conditions at a distance.

THIS PAGE INTENTIONALLY LEFT BLANK

8. REFRACTIVITY IN THE ARCTIC ATMOSPHERE

All electromagnetic radiation (EM) propagation through the atmosphere is affected by the atmosphere. EM energy can be reflected, refracted, scattered, and absorbed by different atmospheric constituents. The extent of these atmospheric effects depends upon both the frequency and power of the EM source and on the state of the atmosphere through which the EM energy must propagate. This chapter summarizes the effects of the environment on E-O, IR, laser, microwave, and radio-wave sensor and communication systems.

In general, environmental effects on communication systems are divided into three categories: attenuation, or loss of energy, of the radiation beam because of beam interaction with absorbing or scattering constituents in the beam path; refraction, or bending of the beam, due to atmospheric density variations along the beam path; and scintillation, or distortion of the beam, due to small scale atmospheric turbulence (Cook and Payne, 1987). Since particulate and density variations are usually greatest in the lower troposphere, it is essential to understand the nature of the atmospheric boundary layer (ABL) in studying electromagnetic propagation. To this end, a discussion of the properties and variations of the ABL will follow the sections on attenuation, refraction, and scintillation.

8.1 Attenuation

Attenuation is the most important environmental effect on nonlaser visible and IR systems. Small airborne particles (aerosols) and air molecules can remove energy from the radiation beam by scattering the energy out of the beam path and/or absorbing the energy and producing heat. The scattering relationship between aerosols and energy is governed by particle size and energy wavelength. Examples of scattering are the attenuations of visible light by clouds, fog, rain, haze, smoke, and snow.

Atmospheric scattering processes are difficult to quantify and forecast accurately because of the lack of appropriate measurements of particle size distributions and chemical properties. Predictions of attenuation due to scattering for visible wavelengths are operationally derived from atmospheric visibilities, which are related to meteorological conditions as shown in Table 8-1.

TABLE 8-1. INTERNATIONAL VISIBILITY CODE, VISIBILITY AND PERCENT ATTENUATION DUE TO SCATTERING FOR A 1 KM PATH

Code No.	Weather Condition	Visibility		1 km Path Attenuation (%)
		Metric	English	
0	Dense Fog	<50 m	<50 yd	100
1	Thick Fog	50 m - 200 m	50 yd - 219 yd	>99.99999 - 99.99999
2	Moderate Fog	200 m - 500 m	219 yd - 547 yd	99.99999 - 99.9
3	Light Fog	500 m - 1000 m	547 yd - 1095 yd	99.9 - 98
4	Thin Fog	1 km - 2 km	1095 yd - 1.1 nmi	98 - 86
5	Haze	2 km - 4 km	1.1 nmi - 2.2 nmi	86 - 61
6	Light Haze	4 km - 10 km	2.2 nmi - 5.4 nmi	61 - 32
7	Clear	10 km - 20 km	5.4 nmi - 11 nmi	32 - 18
8	Very Clear	20 km - 50 km	11 nmi - 27 nmi	18 - <8
9	Exceptionally Clear	>50 km	>27 nmi	<8
—	Pure Air	277 km	149 nmi	<1

Note: Scattering for moderate to heavy snowfall can be approximated by the figures for light fog.

As the table shows, attenuation at visible wavelengths is practically 100 percent for clouds, fog, and snow. Attenuation at IR wavelengths shows a similar increase from pure air to dense fog, except that clear air is slightly more opaque to IR radiation than to visible, and fog and haze generally are slightly more translucent in the IR.

In addition to scattering by aerosols, IR energy is strongly absorbed by atmospheric water vapor. Water vapor is such an efficient absorber of IR energy that the multiple absorption lines overlap to the point of creating a virtual continuum—an extremely broad band IR absorption feature. Since water vapor is so abundant in the atmosphere, IR systems are confined normally to operating within two minimum absorption windows in the spectrum: 3 to 5 μm and 8 to 12 μm.

The attenuation in the 3- to 5-μm region is generally affected less by water vapor absorption than the 8- to 12-μm region; however, aerosol scattering and absorption by CO_2 molecules is more significant at 3 to 5 μm. In low latitudes with high water vapor density conditions, the 3- to 5-μm band is sometimes thought to provide superior transmission because of the heavy absorption of 8- to 12-μm radiation. Haze affects the 3- to 5-μm band more than the 8- to 12-μm band, however, and long haze-free paths through humid atmospheres are rare. The preference in hazy conditions is, therefore, the 8- to 12-μm band. At high latitudes, the low values of water vapor density again make the 8- to 12-μm band the preferred choice. Since objects at ambient temperature radiate with their energy peaked in the 8- to 12-μm band, this window region is a logical choice for target imaging and detection. Hotter targets, such as exhaust plumes, radiate at shorter wavelengths, and when the paths are at high altitudes where the water vapor densities are very low, the 3- to 5-μm band is preferred.

The attenuation of E-O and IR radiation by atmospheric gases and precipitation as a function of wavelength is depicted in Fig. 8-1. (Attenuation due to dry aerosols, such as pollutants and salt from sea spray, is not shown.) The visible region of the spectrum is transparent in clear air, becomes translucent in the presence of precipitation, and is virtually opaque in dense fog. The same is true for the IR window regions. The far IR and submillimeter wave regions of the spectrum are dominated by water vapor absorption.

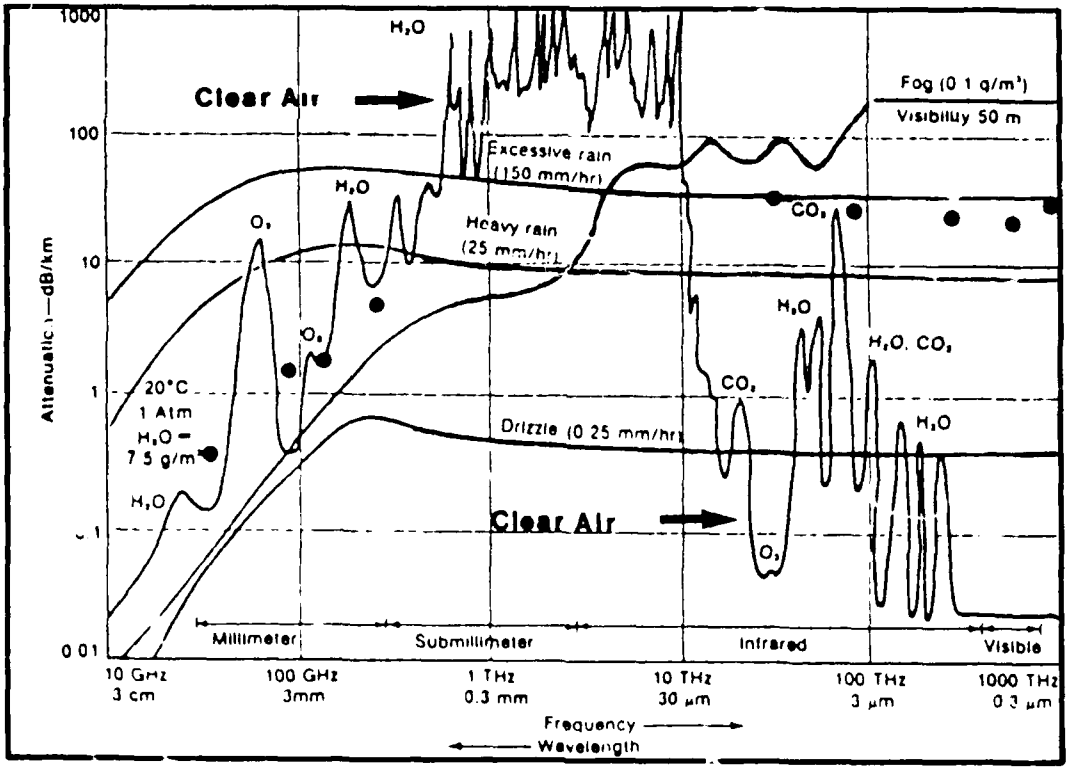

Figure 8-1. Atmospheric Attenuation at Sea Level.

Laser beams are also subject to attenuation as previously described. The proper wave band must be chosen to minimize attenuation because other environmental factors also seriously affect beam quality, spot size, and power on target.

Electromagnetic radiation (radar and communications) passing through the atmosphere is depleted by both absorption and scattering, which are caused by gaseous constituents of the atmosphere and by particles carried by the atmosphere. Molecular absorption and scattering have the greatest effect on super high frequency (SHF, 3-30 GHz) and extremely high frequency (EHF, 30-300 GHz) radiation (Fig. 8-2). This absorption involves well-defined frequencies and thus occurs in narrow bands (or lines), primarily attributable to oxygen and water vapor. Since water vapor concentration varies significantly through the atmosphere, absorption by water vapor also varies significantly.

At microwave frequencies (300 MHz-100GHz), scattering and absorption by particles in the atmosphere are dominated by liquid water drops. These droplets scatter wavelengths roughly the same size as the droplets and thus scatter frequencies above about 300 MHz (ultrahigh frequency [UHF] and higher). Other important scattering particulates include smoke, dust, and insects, which primarily affect UHF, although smoke particles also absorb SHF and EHF.

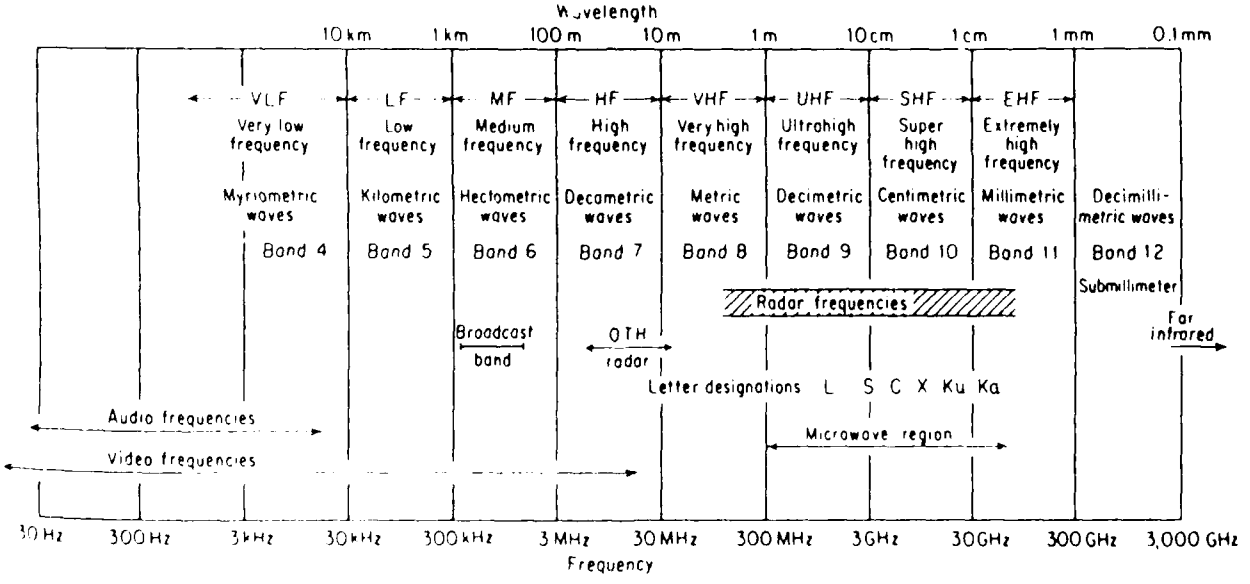

Figure 8-2. The Electromagnetic Spectrum.

8.2 Refraction

Refraction is the bending of light rays due to refractive index (density) changes in the atmosphere. For visible and IR propagation, refraction can cause image distortion, image inversion, and path length changes important for laser ranging. Refractive conditions are characterized by comparison to the refraction expected from a standard atmosphere. Differences from standard conditions are due to temperature and water vapor density fluctuations. Large gradients of these parameters near the ocean surface can seriously affect surface horizontal propagation paths. Propagation over slant paths are usually not seriously affected by refraction.

The index of refraction of a medium, n, is defined by Eq. (8.1) where c is the velocity of an EM wave in free space and v is the velocity of the same EM wave in another medium.

$$n = c/v \tag{8.1}$$

For the atmosphere, the refractive index is defined to be the ratio of the velocity of propagation of an EM wave in a free space to that in the air. Since the velocity of an EM wave in free space is always faster than that in any medium, the index of refraction is always greater than one. In the standard atmosphere, a typical near-sea-level value for n is approximatcly 1.0003 (Bean and Dutton, 1966). For convenience, the refractivity N is defined by Eq. (8.2) such that normal atmospheric values of N units range from 250 to 400.

$$N = (n\text{-}1) * 10^6 \tag{8.2}$$

As stated by Battan (1973), "In dry air the index of refraction has the same value over almost the entire range of the electromagnetic spectrum: it is the same for light and radio waves. However, when water vapor is added to the air, the value of N for the mixture becomes frequency dependent. It is well known that the water vapor molecule is polar in nature and that the dipole moment of the molecule has a different response to different frequencies of radio waves. With the extremely high frequencies of visible light, the water molecules are electronically polarized. With the lower frequencies of radar waves, the water molecules not only acquire electronic polarization, but also reorient themselves rapidly enough to follow the electric-field changes. As a result, the index of refraction of water vapor is greater for radio than for optical frequencies."

Temperature, water vapor, and pressure are the major variables of the atmosphere that determine its refractivity. Bean and Dutton (1966) expressed refractivity in terms of temperature T in Kelvin, with pressure P, and water vapor pressure e, in millibars as follows in Eq. (8.3):

$$N = 77.6\ P/T - 5.6\ e/T + 3.75 * 10^5\ e/T^2 \tag{8.3}$$

In an atmosphere of constant N units, no bending of an EM wave could occur regardless of the value of N. Refraction is dependent upon the gradients of N.

Since gradients of pressure, temperature, and humidity occur throughout the atmosphere, it follows that gradients of N must also exist. Battan (1973) showed that when the gradient of N (i.e., dN/dZ) is equal to -157 km^{-1}, a propagating EM wave will bend with a curvature exactly equal to that of the Earth. Bending would cause a horizontally propagating EM wave to remain constantly parallel to the Earth's surface, always at the same height. Any value of dN/dZ less than -157 km^{-1} would cause an EM wave to bend with greater curvature than the Earth's surface; therefore, -157 km^{-1} is the threshold for "trapping" of an EM wave.

Trapping, or ducting, occurs when the microwave energy is trapped in layers and propagates to greater ranges than normal because of the lack of vertical spreading of the rays. Ducting regions can be elevated or surface based. Radar propagation and coverage are affected by the refractive nature of the atmosphere. Nonstandard refractive conditions lead to anomalous propagation and can cause microwaves to be refracted less than normal (subrefraction), refracted more than normal (superrefraction), or trapped in wave-guide modes (ducted) as in Fig. 8-3.

Over the oceans, a persistent surface ducting mechanism is the rapid, near-surface decrease in moisture due to evaporation, which creates evaporation ducts. The relation for the vertical gradient of refractivity as a function of T, P, and specific humidity (q) is given by Eq. (8.4).

$$dN/dZ = 0.3\ dP/dZ + 7.2\ dq/dZ - 1.3\ dT/dZ \tag{8.4}$$

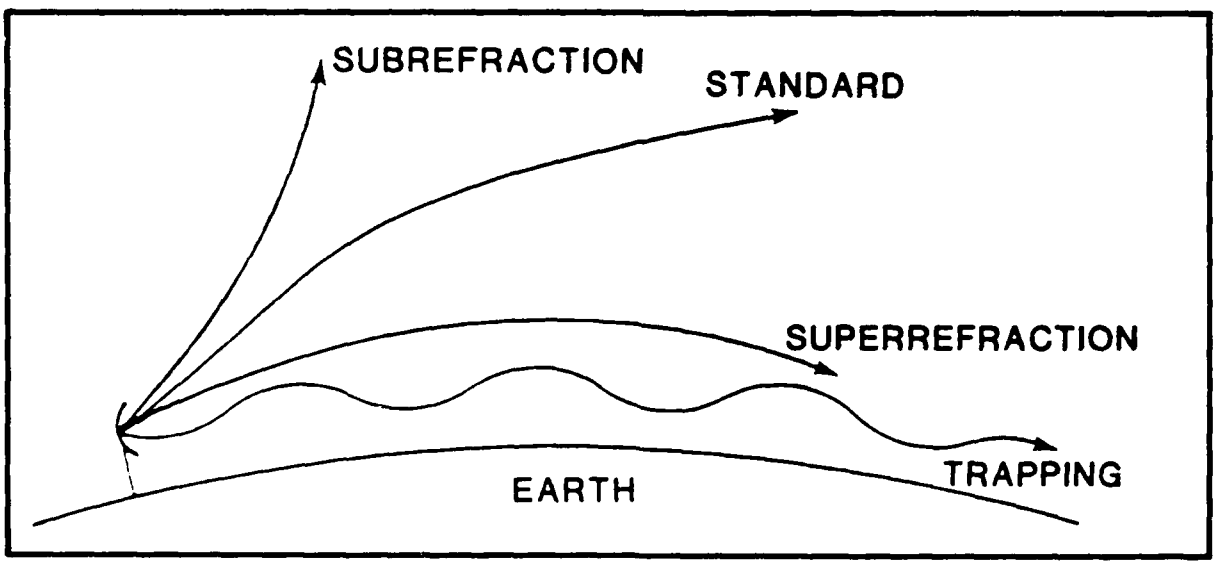

Figure 8-3. Four Basic Categories of Refraction.

It is sometimes convenient to think of the Earth's surface as flat and to represent the EM wave refraction in this frame of reference. This conversion can be done simply by subtracting the Earth's curvature from the EM wave and from the Earth. A modified refractivity M has been developed to take into account the Earth's curvature and to allow for easy identification of ducting. Eq. (8.5) shows the relationship of M to N (Battan, 1973).

$$M = N + 157Z, \; Z \text{ in km} \tag{8.5}$$

8.3 The Integrated Refractive Effects Prediction System

The Integrated Refractive Effects Prediction System is a shipboard environmental data processing and display system that is used to predict the effects of refraction on EM signals for naval surveillance, communications, electronic warfare, and weapons guidance systems. Environmental data usually obtained from radiosondes are processed on a desk-top computer, the Hewlett-Packard 9845, to derive a comprehensive assessment of refractive effects in the lower atmosphere. Knowledge of the refractive environment can be used to maximize tactical advantage. The most recent IREPS, version 2.2, is an integral part of the Tactical Environmental Support System (TESS), now being introduced into the fleet.

IREPS uses M gradients to classify refractive conditions. Table 8-2 shows IREPS classifications of refractive conditions and the relationship of N units to M units.

TABLE 8-2. IREPS CLASSIFICATION OF REFRACTION CONDITIONS

IREPS Classification	dN/dZ km^{-1}	dM/dZ km^{-1}	Range
Subrefraction	>0	>157	Reduced
Normal	0 to -79	79 to 157	Normal
Superrefraction	-79 to -157	0 to 79	Increased
Trapping	<-157	<0	Greatly Increased

The performance of the IREPS model is directly related to the quality and timeliness of atmospheric information entered into the program. Accurate and timely data must be used if the resulting displays are to indicate the true refractive structure of the atmosphere. Knowledge of the immediate environment and its dynamic evolution are necessary for a proper interpretation of IREPS results.

By comparing the IREPS version 2.2, computed atmospheric refractivity conditions for a high resolution and degraded resolution sounding, Dotson (1987) showed the importance of high resolution data. The high resolution data were better able to define the smaller scale refractive structure of the atmosphere and, therefore, allowed IREPS to realistically portray the ambient ducting conditions. By observing the variability in ducting conditions for 120 soundings taken at irregular time intervals over a 47-day period, Dotson found that refractive conditions are in constant dynamic evolution on diurnal as well as synoptic time scales. This discovery implies that timely data must be used to achieve accurate refractivity condition predictions. Contrary to previous arguments that in over 85 percent of the time the horizontal homogeneity was not a factor in refractive considerations, Dotson found that horizontal inhomogeneity does indeed cause significant variability in radar lobe coverage at least 50 percent of the time when near areas of weak sea surface temperature gradients.

Ducting is of primary concern to Navy operations and is caused by trapping layers. A trapping layer is defined as the area where M decreases with height ($dM/dZ < 0$). In this region the ray is bent downward relative to the Earth's surface. A duct is defined as the region in which the energy is confined. A surface-based duct occurs when an EM wave is refracted downward at a curvature greater than the Earth's curvature and is then subsequently reflected up from the Earth's surface. It is the continuous refraction down and the reflection up that forms the duct and makes ducting a concern to the Navy by allowing detection by surface radars far beyond the normal horizon. The type of duct depends on the height, strength, and extent of the trapping layer.

The top of the duct is defined as the height where M reaches a minimum value. It also corresponds with the top of the trapping layer. In practice, thickness of the duct may be found by dropping a vertical line from the top of the duct down toward the surface until it intersects the M profile. Duct strength is defined as the maximum range of M values within the limits of the duct. The optimum coupling height (OCH) is the height where the dM/dZ profile changes from a positive to a negative value.

Three types of ducts commonly exist: (1) the surface-based duct, (2) the elevated duct, and (3) the evaporative duct. Profile (a) of Fig. 8-4 depicts an *elevated* duct that is the type often found when an inversion layer is present. Large temperature and humidity gradients are usually present within the inversion. The boundary layer is cool and moist relative to the overlying air, and over the ocean it is often referred to as the MARINE layer. These jumps in the vertical structure of the temperature and humidity are associated with warming and drying due to subsidence above the inversion and turbulent mixing in the boundary layer. In the Arctic this type of ducting, which causes strong subsidence, is most likely when the Greenland High is well established.

Profile (b) of Fig. 8-4 is an example of a *surface-based* duct. These ducts are formed by relatively warm, dry air being advected over a cool body of water, or by strong subsidence modifying the elevated duct.

Figure 8-4(c) shows an *evaporative* duct. The evaporative duct can be created by two different mechanisms. First, an evaporative duct may be created by the very rapid decrease of moisture immediately above the ocean surface. The air adjacent to the ocean is saturated with water vapor, and the relative humidity is 100 percent. This high relative humidity decreases rapidly in the first few meters to an ambient value that depends on varying

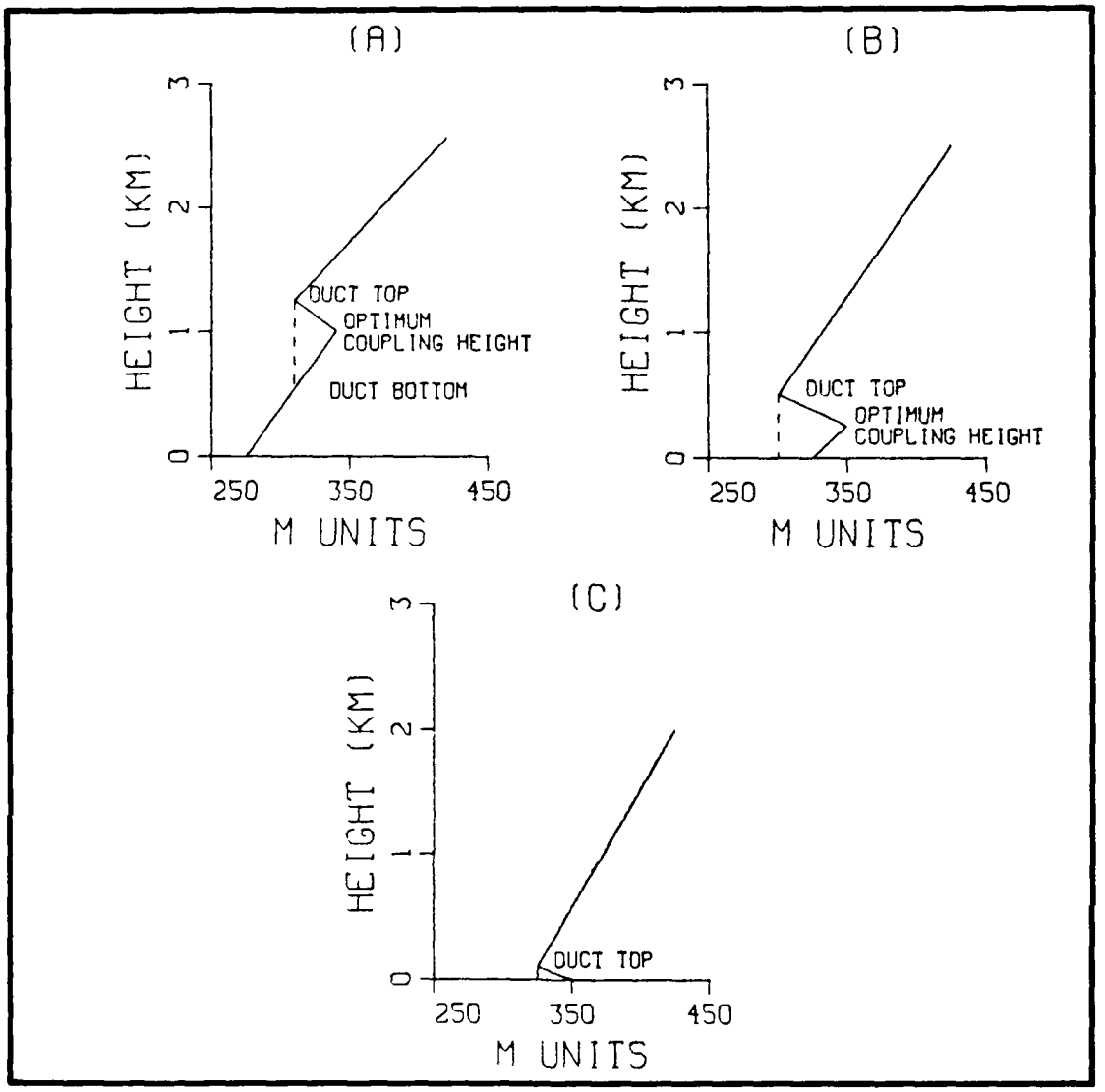

Figure 8-4. Ducting Occurrences for Typical M Profiles.

meteorological conditions. This initial rapid decrease in humidity will cause *M* to decrease with height to a minimum and then *M* will increase with height. The second way in which an evaporative duct can be formed is independent of the decrease in humidity. This evaporative duct is caused by strong cooling at the surface. The cooling can cause a sufficient positive temperature gradient between the air near the surface and the air just above to create a duct. Radiation fog is often associated with this condition because the overlying air is cooled sufficiently by radiational transfer for the relative humidity to increase to the point of condensation. Evaporative ducts almost always occur over the oceans, but it is the strength and upper boundary that are critical in determining the importance of this duct to tactical operations. The evaporative duct, although present, is generally shallow in the Arctic.

Two other important refractive effects are subrefraction and superrefraction. *Subrefraction* is defined as N increasing with height as shown in Table 8-2. In this situation the rays actually bend away from the Earth's surface. The radar range in this situation is reduced. *Superrefraction* is defined in Table 8-2 as N gradients having values between -79 to -157 per km. The EM wave is bent toward the Earth's surface, but not strongly enough to form a trapping layer. With superrefraction the radar range is increased somewhat. The refractive conditions vary from one location to another. In Section 8.6, the assumption made by IREPS that horizontal homogeneity is valid 85 percent of the time is shown NOT to be valid in the Arctic.

8.4 Description of Some IREPS Output Products

Figure 8-5 is a representation of one type of IREPS product. The environmental data list is used primarily for checking the numerical values of the input data. The IREPS-computed output values of dewpoint depression, *dN/dZ* values, *M* units, and a single word description of the refractive conditions give an overall assessment of the atmospheric refractive conditions from each input level to the next.

IREPS REV 2.2

**** ENVIRONMENTAL DATA LIST ****

LOCATION: 31 56N 118 36W
DATE/TIME: 17 JUN 0045Z

WIND SPEED 12.0 KNOTS

EVAPORATION DUCT PARAMETERS:
SEA TEMPERATURE 18.2 DEGREES C
AIR TEMPERATURE 15.1 DEGREES C
RELATIVE HUMIDITY 89 PERCENT
EVAPORATION DUCT HEIGHT 28.0 FEET

SURFACE PRESSURE = 1008.0 mB
RADIOSONDE LAUNCH HEIGHT = 60.0 FEET

LEVEL	PRESS (mB)	TEMP (C)	RH (%)	DEW PT DEP(C)	FEET	N UNITS	N/KFT	M UNITS	CONDITION
1	1,008.0	15.1	89.0	1.8	60.0	340.0	-28.2	342.9	SUPER
2	1,000.0	14.2	87.0	2.1	281.6	333.8	15.6	347.2	SUB
3	993.0	13.9	95.0	0.8	476.6	336.8	-10.9	359.6	NORMAL
4	982.0	13.3	97.0	0.5	785.3	333.4	-176.4	371.0	TRAP
5	972.0	20.4	25.0	20.8	1,071.8	282.9	27.2	334.2	SUB
6	962.0	21.5	34.0	16.6	1,364.9	290.9	-28.9	356.2	SUPER
7	949.0	21.5	27.0	19.9	1,751.3	279.7	-9.4	363.5	NORMAL
8	862.0	20.6	25.0	20.8	4,477.3	254.0	-9.5	468.2	NORMAL
9	850.0	19.7	25.0	20.7	4,873.5	250.2	-7.6	483.4	NORMAL
10	807.0	20.0	25.0	20.7	6,339.1	239.0	-6.0	542.3	NORMAL
11	726.0	14.5	34.0	15.8	9,299.4	221.2	-8.9	666.1	NORMAL
12	700.0	11.8	34.0	15.5	10,305.6	212.2	------	705.3	------

SURFACE REFRACTIVITY: 341 --SET SPS-48 TO 344

Figure 8-5. IREPS Environmental Data List.

The propagation conditions summary, reproduced in Fig. 8-6, is a system independent visual display and plain-language narrative assessment of expected refractive conditions. Vertical profiles of refractivity *N*, as well as modified refractivity *M*, are accompanied by a diagram showing the presence and vertical extent of any existing ducts. Evaporation duct height and surface wind speed information is given along with brief statements concerning anticipated performance of surface to surface, surface to air and air to air EM systems.

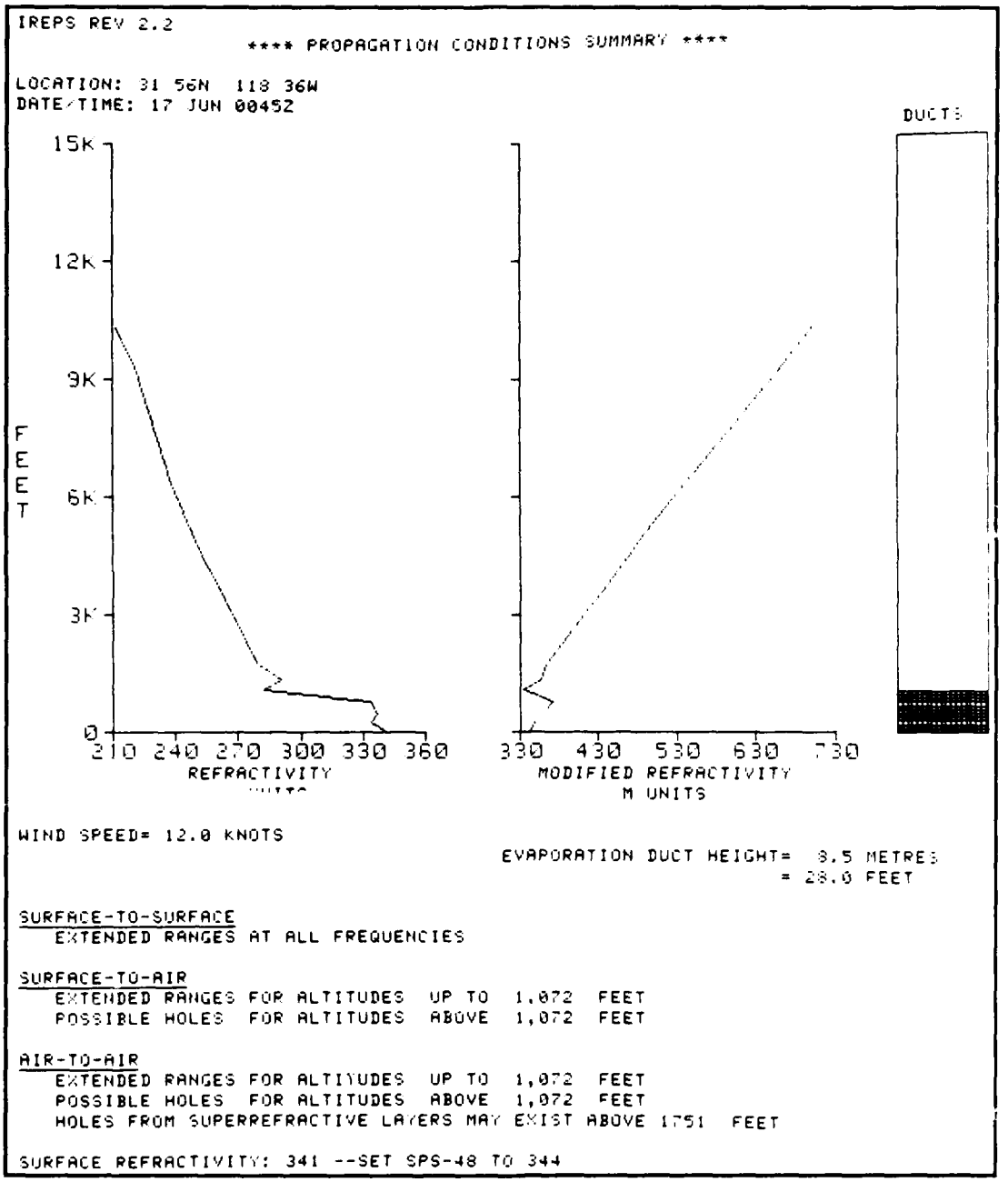

Figure 8-6. IREPS Propagation Conditions Summary.

Propagating radar waves experience constructive and destructive interference as direct path rays coincide with rays reflected from the sea surface. The resultant amplitude of the radar wave is a function of the phase differences among the intersecting waves. As a result, radar lobes (constructive interference) are created with shadow zones (destructive interference) appearing in between. Knowledge of where these lobes and shadow zones occur can become an immediate tactical advantage in both offensive and defensive operations. IREPS version 2.2 produces radar coverage diagrams that display the positions of the lobes and the shadow zones for any specified radar system and target at any desired probability of detection (POD).

Since these lobes and shadow zones are created by reflections from the sea surface, their extent is determined by the roughness of the sea surface. Surface roughness is dependent on the sea state and wind speed, with higher wind speeds and rougher seas leading to relatively reduced coverage; low wind speeds and calm seas lead to relatively increased coverage. Wind speed changes are important indicators of changing radar conditions *not dependent* on refractivity.

Figure 8-7 is an example of the IREPS radar coverage display product that also can be very useful in determining an EM system's maximum range capability. It depicts a specified EM system's area of coverage on a curved Earth, range-versus-height plot. Varying PODs are indicated by variations in the shading of the lobes. A numeric listing of some of the parameters used to generate the display, along with the location and time/date information of the profile, are included at the top and bottom of this product.

8.5 Atmospheric Boundary Layer

Propagating EM waves, unless in a completely homogeneous medium, will experience some degree of bending due to changes in the index of refraction. The Earth's atmosphere is normally a very inhomogeneous fluid. Certain regions, such as the ABL, characteristically have large mean gradients in temperature and/or humidity. Rapid vertical changes in both temperature and humidity create layers that significantly refract propagating EM signals. This phenomenon is readily apparent, for example, in the evaporation duct at the base of the Marine Atmospheric Boundary Layer (MABL) and in the elevated trapping layer associated with the inversion layer at the top of the ABL.

The ABL is defined by Stewart (1979) as the portion of the lower atmosphere that has turbulent flow and is in direct contact with the Earth's surface. The ABL extends from the surface to a height of a few meters in conditions of strongly stable stratification and to thousands of meters in highly convective conditions. On the average, the ABL extends through the lowest 3,300 ft ($\approx$ 1 km) of the atmosphere and contains 10 percent of the mass of the atmosphere. The boundary layer is very important to the dynamics and thermodynamics of the atmosphere because it is in this layer that all momentum, water vapor, and thermal energy exchanges between the atmosphere and the Earth's surface takes place.

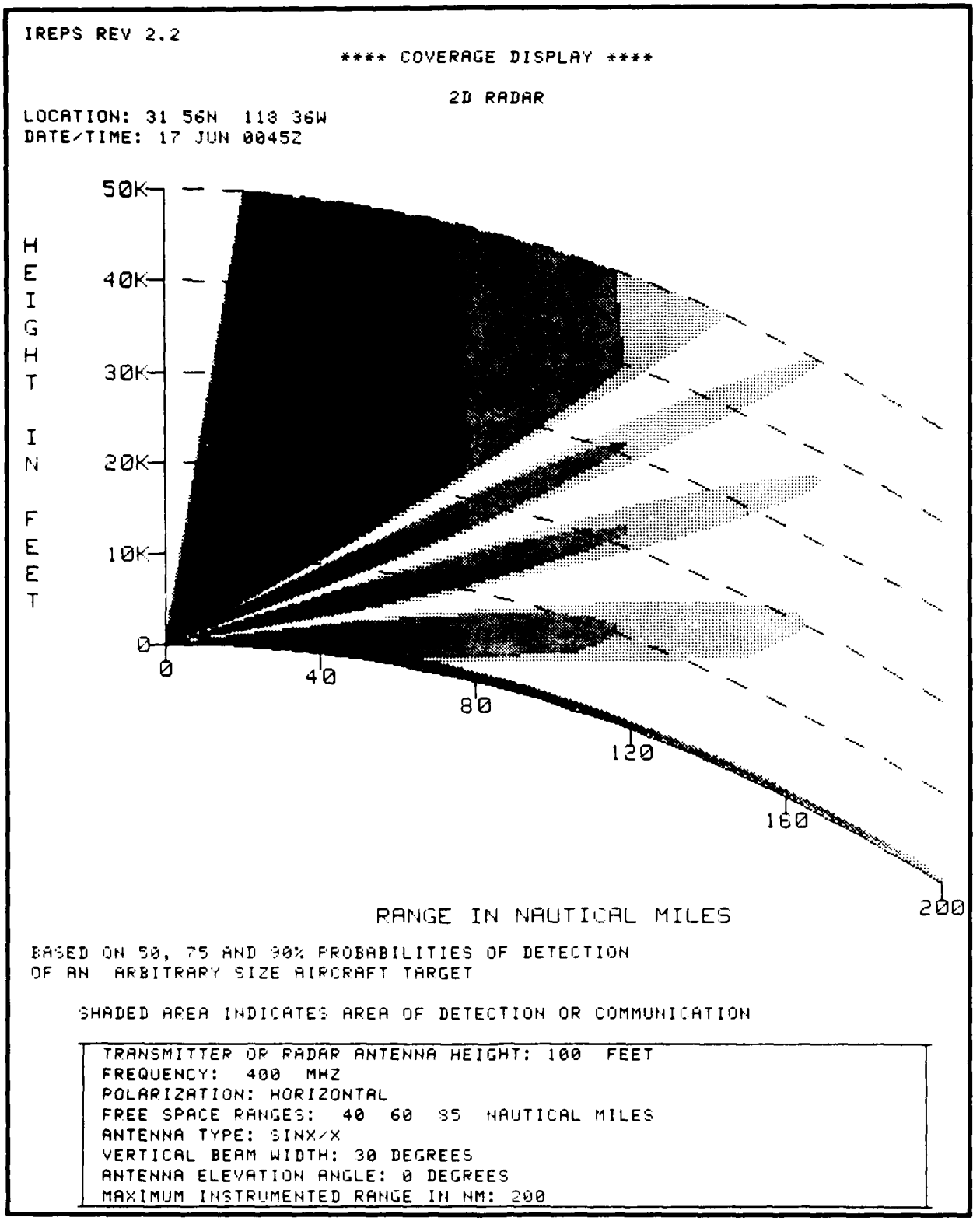

Figure 8-7. IREPS Radar Coverage Diagram.

Physical continuity between the atmosphere and the Earth dictates that wind velocity be zero at the immediate surface over land and equal to the surface drift current over water. Above the surface, velocity increases with height in an approximately logarithmic fashion to the top of the layer. Thus, strong vertical wind shear is common in this layer. It, along with convection, produces turbulence that facilitates the transport of moisture and momentum within the layer. The relatively homogeneous mixed layer directly above the turbulent surface layer constitutes the majority of the unstable ABL. Turbulence tends to continuously erode local gradients and, thus, conditions are well mixed up to the inversion layer. The final 165 to 325 ft ($\approx$ 50–100 m) of the convective ABL is usually an inversion layer where the kinetic energy available for mixing is damped by strong stable vertical temperature gradients. The gradients have a "capping" effect on the convection below and effectively suppress exchange of physical properties with the free atmosphere above.

If the ABL is cooled from below it will be stable. Turbulence is suppressed by the resulting density structure, and generally little mixing will occur except in the surface layer. All exchanges between the atmosphere and the Earth's surface are thus greatly reduced.

In the marine atmospheric boundary layer the oceans and the atmosphere exchange energy directly in the form of turbulent heat, moisture, and momentum fluxes. Gases and solids are also in continuous exchange between each fluid. Wave activity can toss small water droplets directly into the lower atmosphere where they become suspended and eventually evaporate. Normally, evaporation from the sea surface creates a shallow layer of rapidly decreasing relative humidity, from 100 percent at the sea surface to a lower value (80–90 percent) directly above the sea surface. This low level feature produces an extended radar propagation phenomenon known as the evaporation duct because of its formation mechanism. The evaporation duct extends only tens of meters above the ocean's surface, but it is of great importance to the mariner because it occurs in varying degrees throughout all oceanic areas and results in over-the-horizon radar propagation.

The ABL over land shows much more variation than the MABL. Seasonal and diurnal changes are both more pronounced. Larger variations in the vertical temperature structure occur over land than over the ocean, but usually less vertical humidity variation occurs. Radiative heating and cooling can cause large diurnal fluctuations in the height of the ABL from near surface values at night to over 6,500 ft ($\approx$ 2000 m) during the day.

8.6 Arctic Refractive Conditions

Willis (1987) examined the spatial and temporal variability of the refractive structure of the lower atmosphere in the vicinity of the Fram Strait MIZ. The data used in this study were collected by four ships during MIZEX of 1984. The ships operated in the pack ice, at the MIZ, and in the water adjacent to the ice edge.

The results of a spatial study showed that the refractive structure leading to elevated ducting was different over the pack ice and the MIZ from over the open water adjacent to the ice edge. The ducts were generally lower, weaker, and thinner over the pack ice, with the averages of height, strength, and thickness dramatically increasing over the water.

away from the ice edge. Scatter diagrams showed that the duct height, strength, and thickness exhibited a linearly increasing relationship with respect to distance from the ice. The average height, strength, and thickness values increased slightly from the pack ice to the MIZ and then dramatically increased from the MIZ to 115 n mi (≈ 210 km) from the ice edge. This linearly increasing relationship from the pack ice to the open water was strongest with the height data. These differences in the refractive structure over this relatively narrow region are tactically important. An EM wave transmitted from a source located over the ice would be affected differently from an EM wave transmitted from a source over the water. Multiple ducts were seen only at the ice edge and may have reflected the multiple inversions that were seen on sodar traces.

Willis (1987) also made a temporal study by selecting six regimes to assess the effect of the difference in synoptic flow on the refractive structure. In four of six regimes a cyclone passed over the area. When the low passed directly over all four of the ships no ducts were recorded. The greatest number of ducts was associated with the two regimes in which high pressure dominated the period. This situation was the only one in which persistence of the ducts was seen. On two separate occasions two ships reported ducts that persisted for 24 hours. At both of these times, however, only two of the four ships reported ducts; so once again considerable spatial inhomogeneity existed. The longest case on record in which a duct persisted was 36 hours.

Shaw et al. (1989) has presented some results of refractive studies carried out during MIZEX of 1984 and 1987. Several conclusions were drawn from that work derived from numerous summer/winter radiosonde records.

1. Substantial difficulty may occur in obtaining accurate refractivity profiles from rawinsondes in the Arctic if the sensors pass through subfreezing stratus clouds. Many launches from MIZEX of 1984 produced profiles that may indicate erroneous saturation due to frost formation on the humidity sensor.
2. Irrespective of the frost formation problem, trapping layers in the MIZ of the Arctic are in general quite weak and occur within 30 n mi (≈ 56 km) of the ice edge. Furthermore, they occur typically 1,000 to 2,600 ft (300–800 m) above the surface, making them unlikely to affect surface-based microwave devices. There is, however, a decidedly upward slope from ice (shallow boundary layer) to water (deeper boundary layer) of the trapping layer, and this feature may indeed affect surface systems that are well into the ice. Trapping layers are also sporadic in extent. During the 1984 experiment the four ships making measurements never observed a trapping layer at the same time. The majority of the time (61 percent) only one ship observed a trapping layer, and during the remaining time two ships observed a trapping layer concurrently.
3. Horizontal homogeneity is observed less than 13 percent of the time in the Arctic at levels above 65,000 ft (≈ 20 km).

From the Willis and Shaw studies, clearly, anomalous refraction will be of less consequence in the MIZ than in warmer regions of the globe. Equally clear, however, when anomalous refraction is important it will be due largely to horizontal variability of the refractivity field.

THIS PAGE INTENTIONALLY LEFT BLANK

9. NUMERICAL MODELS

The forecaster using numerical model-generated weather products can benefit by acquiring some knowledge of the models and computer systems that produce the charts and data sent to the field. Each numerical model is part of a system that not only creates a forecast but also performs data assimilation, data analysis, and quality control. Many factors combine to determine the quality and usefulness of a model forecast.

A primary consideration to keep in mind is the inherent limitations of numerical models in terms of resolvable spatial and time scales. For example, a model with 50 n mi (90 km) spacing between gridpoints should not be expected to forecast coastal sea breeze circulations explicitly on a scale of 5 to 10 n mi (9–18 km). Similarly, a typical polar low has a spatial scale that is near the lower limit of the current Naval Operational Global Atmospheric Predication System model's (NOGAPS T79) ability to resolve on the model grid accurately (Fig. 9-1). In such cases, the large-scale model forecast can be used to infer the presence or likelihood that a given small-scale feature does exist.

A good rule of thumb is that because of computational errors in wave propagation and advection, numerical models cannot be expected to *resolve features explicitly* that are less than four to six grid points in extent (Ross, 1986). Small-scale features can be introduced into a model through a "bogusing" procedure. Bogusing is commonly done for tropical cyclone forecasts. Of course, features of sufficiently large scale may still be misforecast because observational data are not available or deficiencies exist in the numerical model.

Numerical weather prediction relies on mathematical representation of atmospheric processes such as advection, cumulus convection, and radiative transfer. Properties of the surface, including topography, ground wetness, and surface roughness must also be numerically represented. Processes such as cumulus convection, which are too small to be resolved on the scale of the model grid spacing, are parameterized in terms of the model prognostic variables, including temperature, winds, and moisture. The methods used to parameterize physical processes can vary widely between numerical models and lead to significant differences in model forecast quality and model biases.

The following discussion of Navy operational forecasting models is intended only to provide an introduction and overview of basic model characteristics.

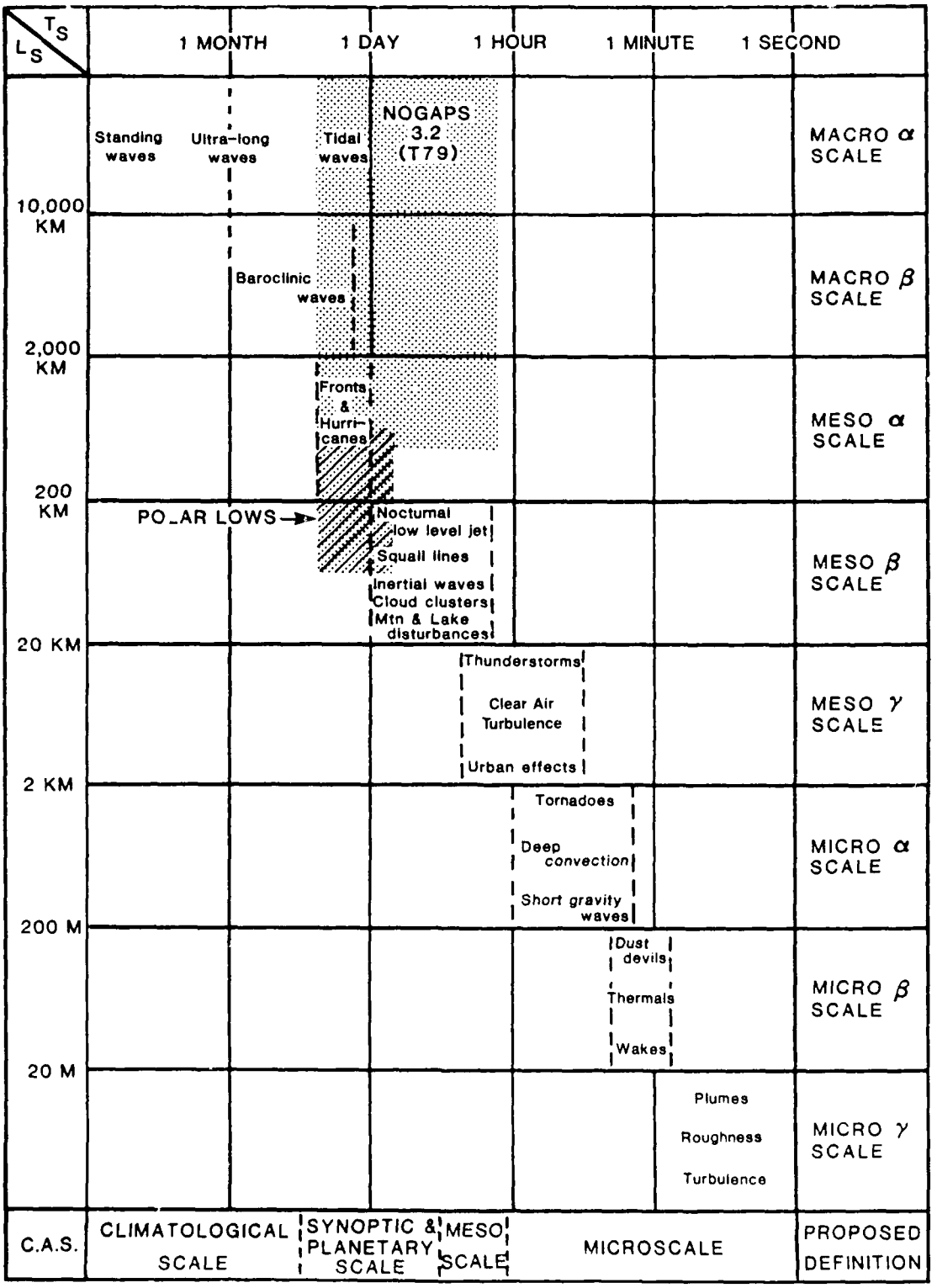

Figure 9-1. Scale Definitions and Various Processes with Characteristic Time and Horizontal Scales.

9.1 Description of Fleet Numerical Models

The Fleet Numerical Oceanography Center in Monterey runs two large scale numerical models on an operational basis. These simulations are the global model NOGAPS and the regional model NORAPS (Navy Operational Regional Atmospheric Prediction System). NORAPS can be run over the polar regions, but current plans call for NOGAPS to provide primary forecast coverage of the Arctic. The operational version of NOGAPS is upgraded frequently; the description included here is accurate as of late 1989.

Until 1981 FNOC ran a hemispheric gridpoint primitive equation (PE) model with a horizontal resolution of 205 n mi ($\approx$ 380 km). NOGAPS 2.0 was the first FNOC global model and had a resolution of 2.4 degrees east-west and 3.0 degrees north-south. NOGAPS 3.0, installed operationally in January 1988, was the first spectral model. This version was a T47 spectral model with equivalent horizontal resolution of 2.5 degrees, equivalent to about 150 n mi (275 km) in the longitudinal direction (and east-west at the Equator).

NOGAPS 3.2 became operational in September 1989 and included a significant increase in horizontal resolution—from T47 to T79 (1.5 degrees, 90 n mi or 165 km). NOGAPS 3.2 has 18 vertical levels, and it contains a complete set of physical parameterizations, including long- and short-wave radiation and cumulus convection (Rosmond, 1989). NOGAPS 3.2 forecasts are made out to 120 hours, with quality considered equal or superior to the National Meteorological Center's global model.

NOGAPS 3.2 is run on the FNOC Cyber 205, taking approximately 15 minutes per forecast day (excluding the input/output time). Planned increases in computer power may allow for an increase in resolution equivalent to 50 n mi (90 km), the current grid spacing now used in NORAPS.

The following section will provide a general description of how NOGAPS performed in Arctic regions. The forecaster should be aware of model biases as well as the inherent limitations of scale in the model.

9.2 Verification of Numerical Model Forecasts

Computer forecast models are in a perpetual state of update, revision, and change. For this reason, continuous monitoring of the accuracy of the model is necessary in hopes of spotting error tendencies. While surveillance is usually performed at the center producing the forecast model, the user should still verify the model forecasts against the analyses for the area of responsibility. An evaluation of a particular model is not included in this handbook, since it would soon be outdated. Rather, a few simple guidelines are given to assist the forecaster in evaluating models.

Insufficient data are a problem that forecasters must face every day. Sometimes a forecast can depend on one crucial observation from one observing station. Computer models are also highly dependent on observational data. Even in data poor areas, such as the tropic and polar regions, analyses must still be produced. Inevitably, schemes must be developed to handle these regions.

The most common method of performing an analysis of the existing atmospheric variables (e.g., temperature, moisture, pressure) employs a first guess field. This field is commonly the 6- or 12-hour model forecast from the previous model run. Observational data are interpolated to grid points and compared with the first guess value at each point. If a number of observations influence a grid point, the first guess field is essentially ignored. In data poor areas, however, the possibility remains that no observational data exist within a reasonable distance of a grid point. In such cases, the first guess field now becomes the analysis at that particular grid point. If only a limited number of observations are found, the data are blended with the first guess field to arrive at an analysis.

Clearly, the first guess field can play a large role in the analysis of the current meteorological variables. Thus, a good first guess field is critical. Without observational data, the analysis field in certain areas is nearly a reproduction of the model's earlier forecast. The result is a catch-22 situation: a poor forecast leads to a poor analysis that leads to a poor forecast. The Arctic forecaster needs to be aware of this possibility. Even though a computer analysis has a low pressure center at a given location and intensity, it may only be a poor forecast from 12 hours earlier.

The sources of data also need to be considered by a forecaster using a computer model. The surface and upper air observational network is fairly well established and widely known. Satellites, however, can provide large amounts of data that are usable by computer-generated analyses. This information is usually supplied in two forms: cloud track winds and vertical thickness soundings.

Cloud track wind data are largely confined to the midlatitudes. They are a man-machine mixture form of data where the human determines the wind direction based on cloud motion and the computer decides on the height of the cloud based on its temperature. Vertical soundings are completely automated (i.e., no human intervention is required) and can provide large amounts of data anywhere over the globe. These data are in the form of temperature/thickness soundings for a single column, similar to that of a radiosonde. The accuracy and vertical density of the data, however, are much less than that of a radiosonde. Still, the value of these data in the Arctic region cannot be disputed.

Another consideration is the time of the model forecast (i.e., 0000 GMT or 1200 GMT). Surface ships often only report during daylight hours. In the Pacific Ocean, for example, more data are available for the 0000 GMT run than for the 1200 GMT run, as seen by comparing Figs. 9-2(a) and 9-2(b). Obviously these data would have a great effect on the surface analysis in this region. Time of day is less of a problem for upper air data such as RAOBS, AIREPS, and satellite soundings.

9.2.1 Model Errors

Computer forecast models are far from perfect. While in some instances the guidance they give is very valuable, at other times they can give erroneous forecasts leading to major busts. Even in the latter situations, the information provided by the model can be useful if the error characteristics of a forecast model are known.

Random observation of a model performance can often lead to incorrect assumptions about a model's behavior. For example, a low that is underforecast 7 mb by a model on a given day does not mean that all lows in all situations are underforecast by the model.

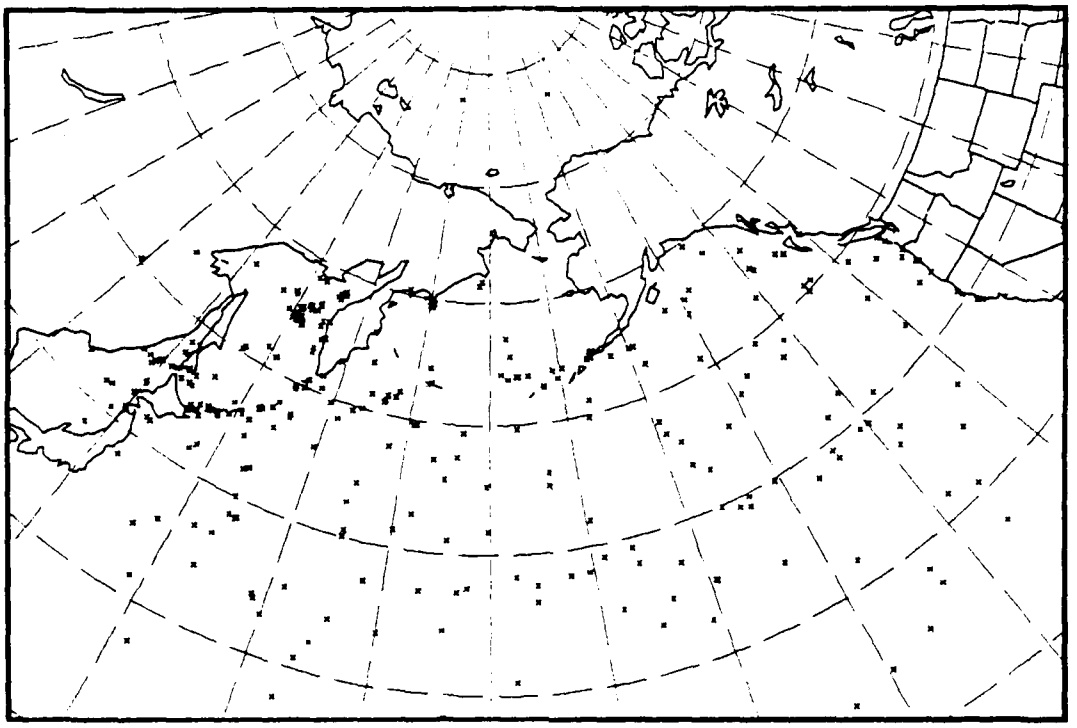

Figure 9-2(a). Location of Surface Ship Observations in the North Pacific, 0000 GMT 18 January 1989.

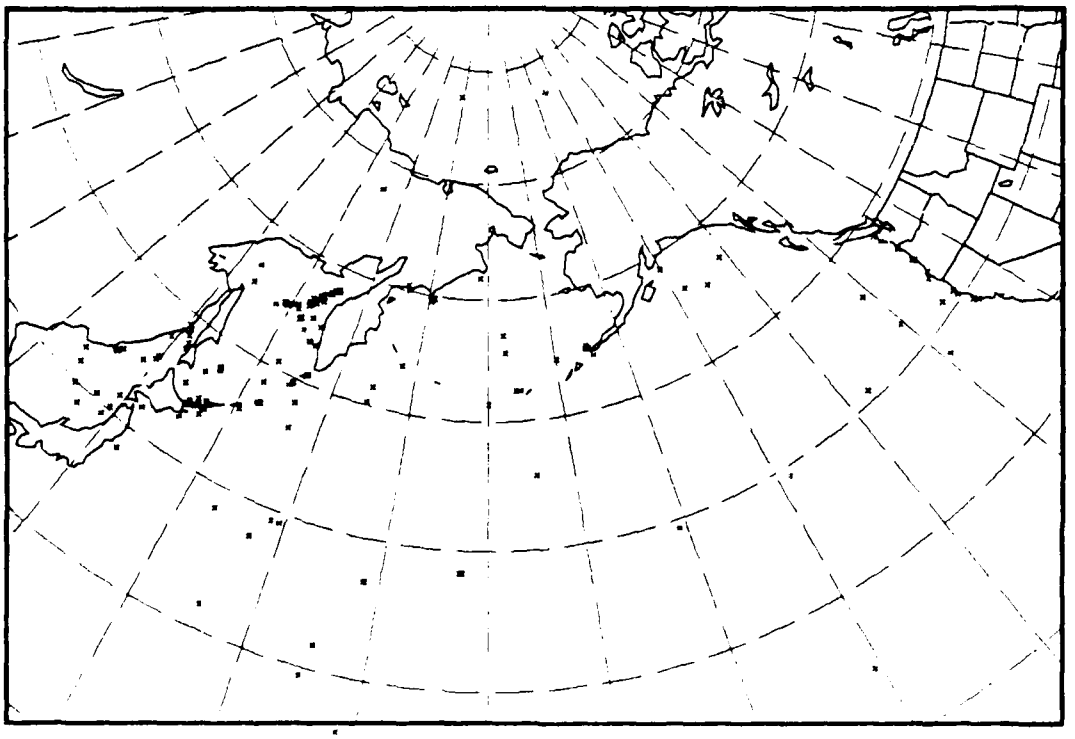

Figure 9-2(b). Location of Surface Ship Observations in the North Pacific, 1200 GMT 18 January 1989.

Rather, the model's performance must be evaluated daily over a period of time to gain an understanding of the error characteristics.

Model errors fall into two classes: model tendencies and systematic errors. The former refers to similar treatment of a situation without regard to season or location. An example would be that the model deepens lows too slowly. Systematic errors refer to an error occurring in the same location and/or at the same time more than once. Knowledge of both kinds of errors can be very useful to a forecaster.

9.2.2 Model Tendencies

Figure 9-3(a) is a NOGAPS 36-hour surface pressure forecast valid 0000 GMT 27 September 1988. The verifying surface analysis is shown in Fig. 9-3(b). The model underforecasts the central pressure of the mid-North Pacific low by 18 mb. Truly, to

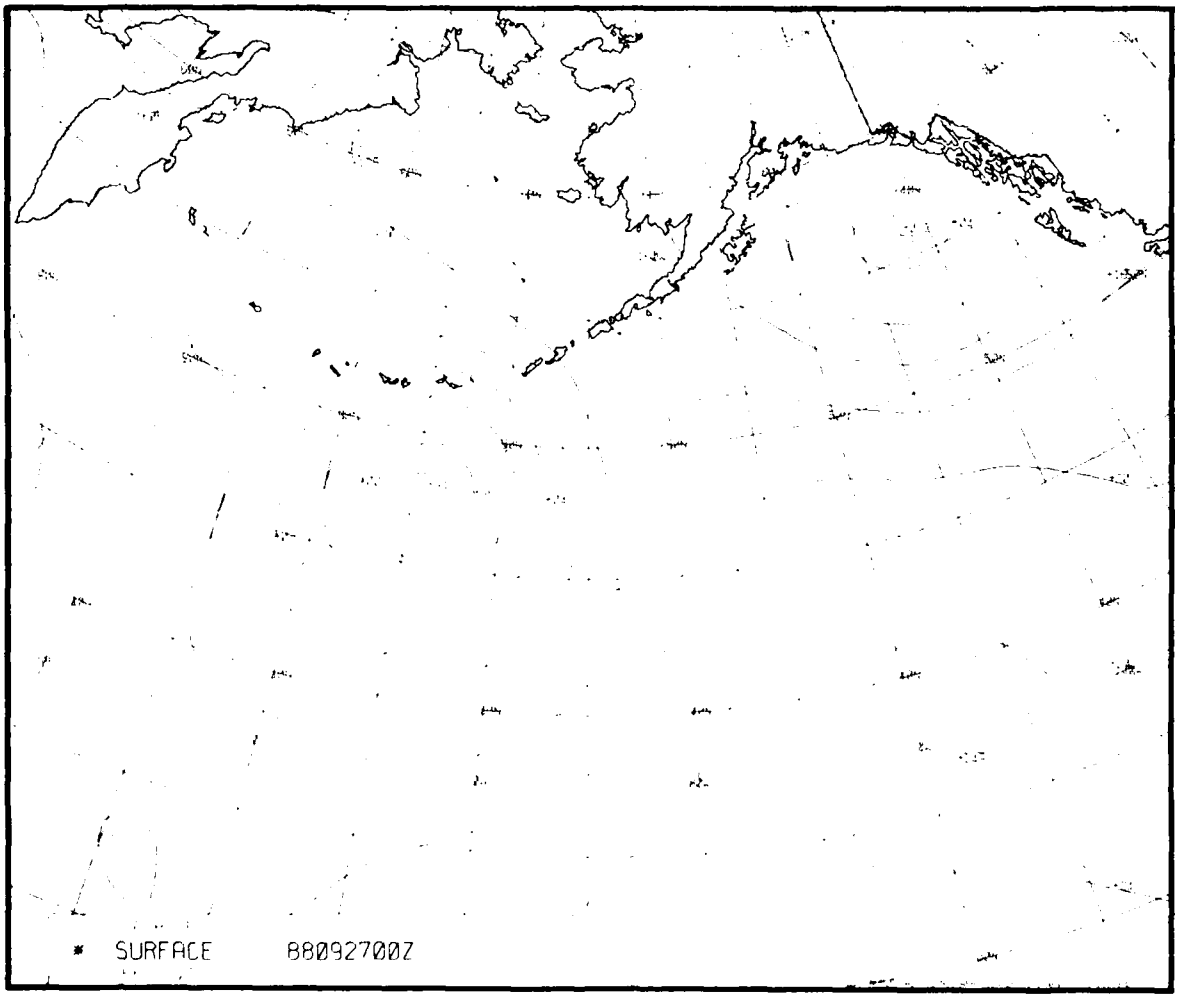

Figure 9-3(a). The 36 hour Surface Pressure Forecast, 0000 GMT 27 September 1988.

determine the model's performance, the forecaster should determine if the low in question is deepening, filling, or unchanged. In this case, the low had deepened 15 mb in the previous 12 hours. The model forecasts 5 mb of deepening. Thus the initial judgment is that the model is slow in deepening the low.

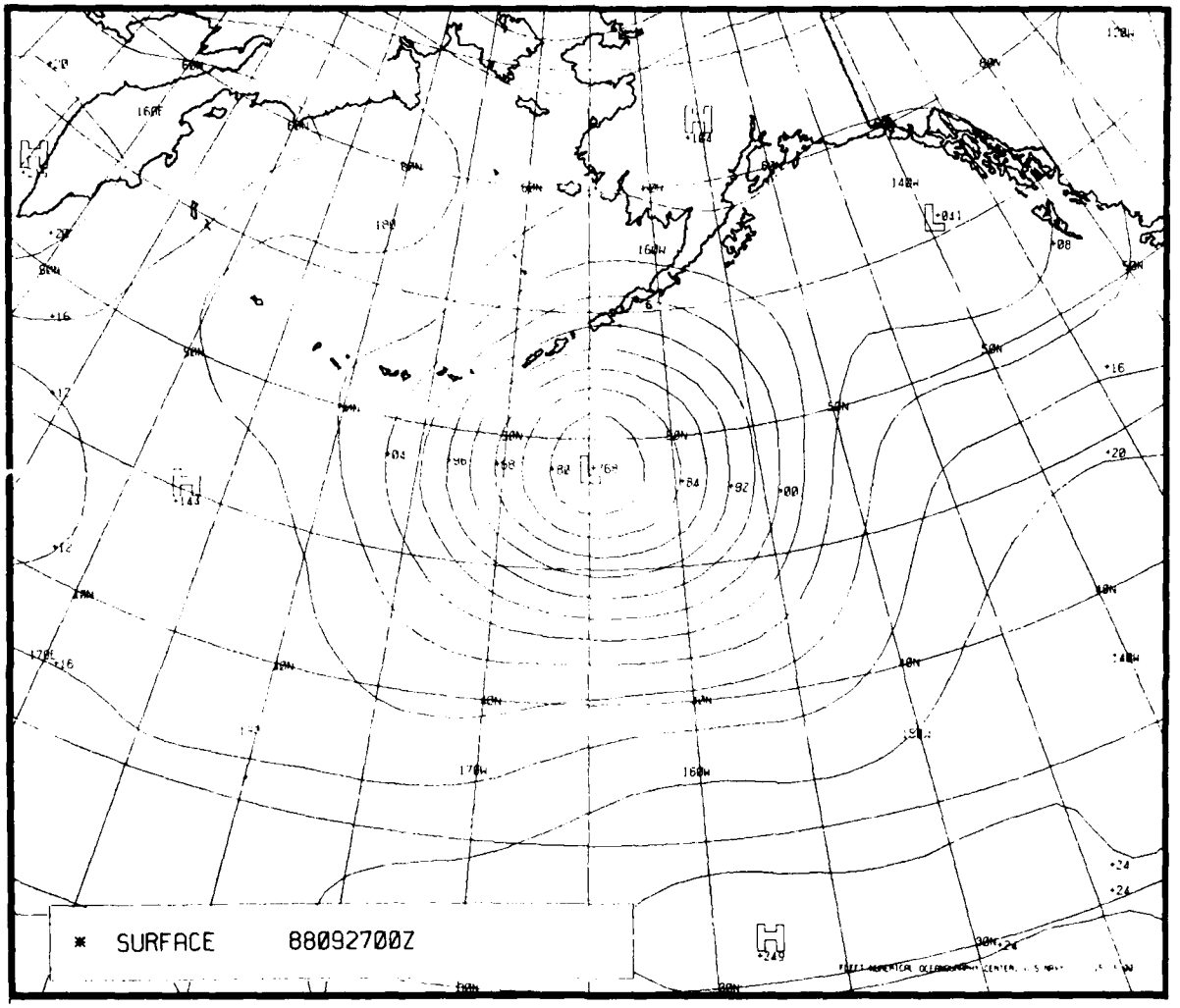

Figure 9-3(b). The Surface Pressure Analysis, 0000 GMT 27 September 1988.

To obtain a complete picture, the life cycle of the low should be charted as found in Fig. 9-4(a). Several notes should be made:

1. The model fails to predict cyclogenesis;
2. While the model correctly forecast that the low would deepen, it is too slow on the rate of deepening;
3. The model continues to deepen the low even after it began to fill;
4. The rate of filling predicted by the model is poor; and
5. The greatest error is during deepening.

From this analysis, clearly, the model has some serious problems forecasting this low. Figure 9-4(b) shows a similar tracing for another low. Note that while some features are the same as those found in Fig. 9-4(a), some differences occur.

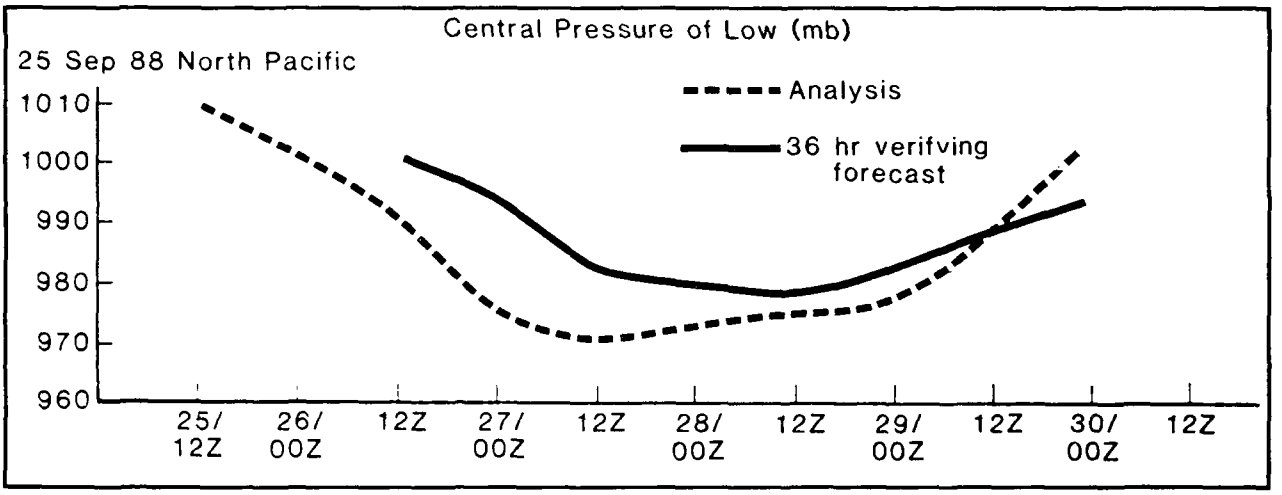

Figure 9-4(a). Forecast and Verifying Central Pressure of the 25–30 September 1988 Cyclone (see Figs. 9-3(a) and 9-3(b)).

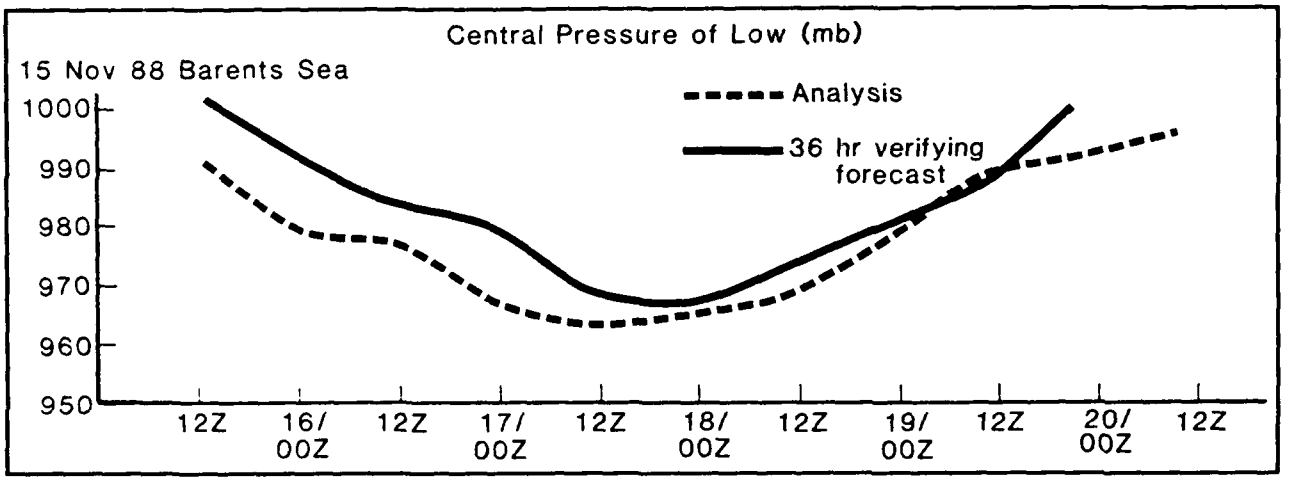

Figure 9-4(b). Forecast and Verifying Central Pressure of the 15–20 November 1988 Cyclone.

The value of such a verification is obvious. It is far too easy to jump to a conclusion to explain why the model busted a forecast. A systematic approach such as the one described yields much more correct and useful information, which can assist the user when making forecasts in the future.

Another example of model tendencies is shown in the four panels of Fig. 9-5. A comparison of the 36-hour forecast for 0000 GMT 25 December 1988 (Fig. 9-5(a)) and the verifying analysis (Fig. 9-5(b)) shows that the model has done a good job forecasting the overall long wave trough-ridge pattern in the North Pacific. But the important short waves are smoothed too much and are difficult to spot on the forecast chart. This error is common in models and stems from the resolution of the model. Gridpoint spacing is often 1 to 3 degrees of latitude/longitude. Small disturbances are often poorly resolved by the gridpoints of the model and lead to poor forecasts.

Figures 9-5(c) and 9-5(d) are the corresponding surface pressure forecast and verifying analysis. Although the model made a good forecast of the large-scale low, the surface troughs near 180 °E and 160 °E (Fig. 9-5(d)) are poorly forecast. Thus, the lack of model resolution affects both surface and upper air forecasts. The forecaster should be aware of such model tendencies since they can have a large effect on the resulting forecast of various parameters such as winds, seas, and ice movement.

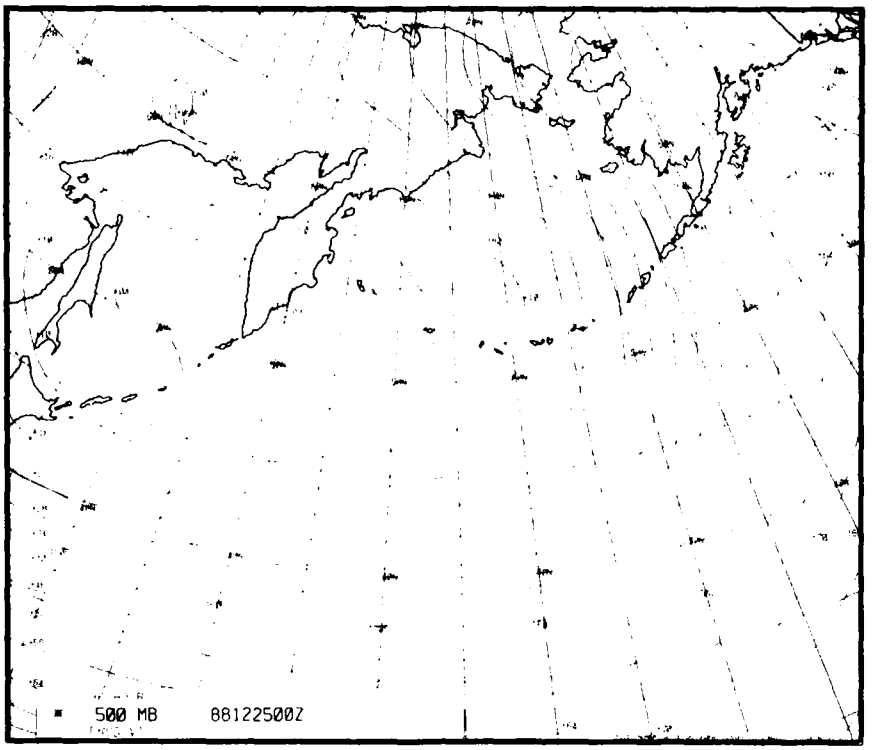

Figure 9-5(a). The 500-mb Height 36-Hour Forecast, 0000 GMT 25 December 1988.

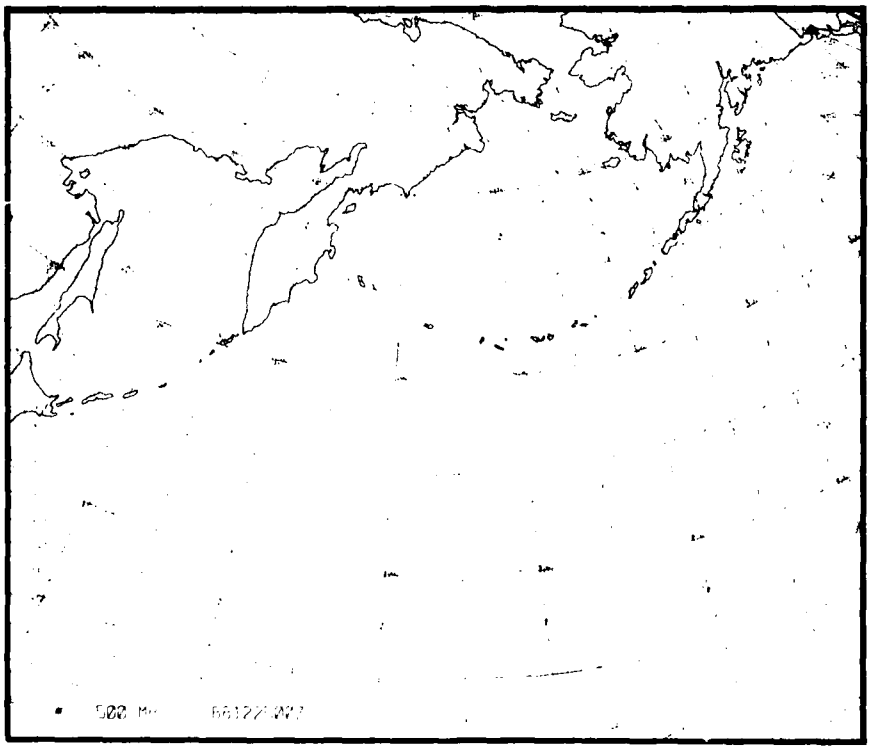

Figure 9-5(b). The 500-mb Height Analysis, 0000 GMT 25 December 1988.

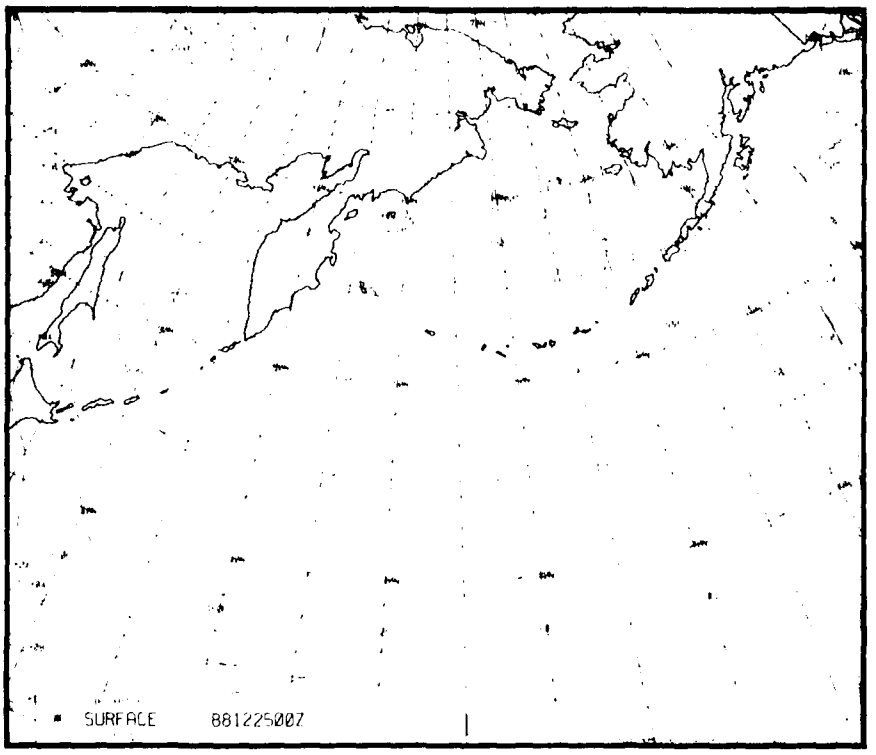

Figure 9-5(c). The 36 Hour Surface Pressure Forecast, 0000 GMT 25 December 1988.

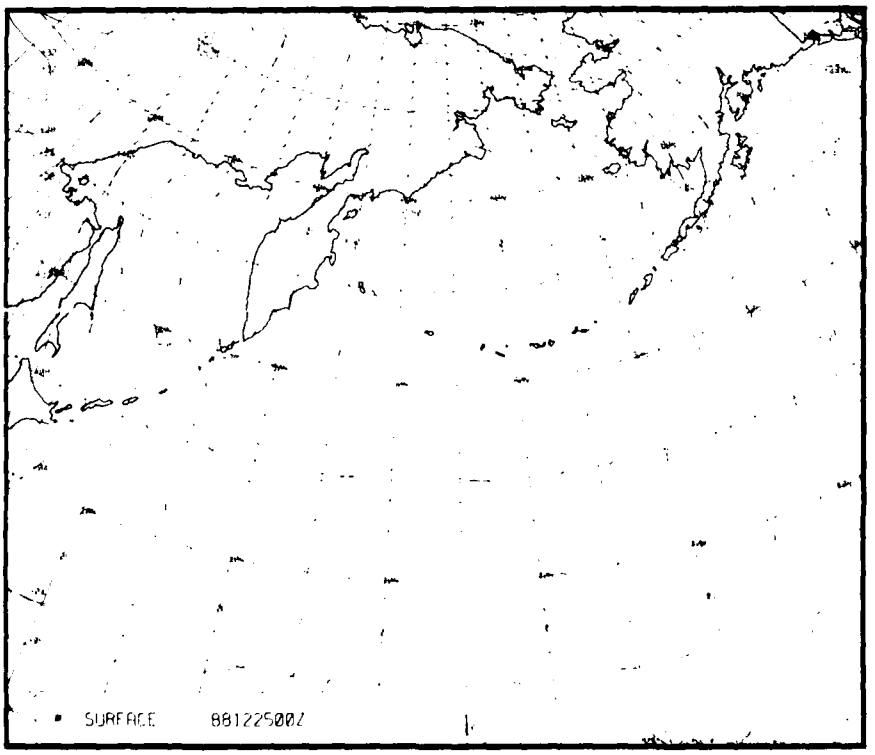

Figure 9-5(d). The Surface Pressure Analysis, 0000 GMT 25 December 1988.

9.2.3 Systematic Errors

The five panels of Fig. 9-6 show a NOGAPS 36-hour surface pressure forecast and verifying analysis. The poor forecast in the Greenland-Norway area is a common problem encountered by models. The low on the Greenland icecap is "locked-in." Figure 9-6(c) is the surface pressure analysis from 36 hours earlier (i.e., the initial field for the forecast in Fig. 9-6(a)). Note the presence of a surface low over Greenland. When a low (or high) exists over high terrain on the analysis, the feature often remains over the high terrain during the entire forecast. This result stems from problems that models have reducing pressure to sea level. The error is systematic, since it occurs in the same location time after time.

Although the model leaves a fictitious low over Greenland, it correctly forecasts the true low to move northeastward to Spitsbergen and is only 2 mb in error on the central pressure. Figures 9-6(d) and 9-6(e) indicate that the model makes a good forecast of the corresponding short-wave trough. This example emphasizes the fact that the forecaster should check model output for vertical consistency. A suspicious surface low may not have any upper level justification for its existence and should thus be considered with caution.

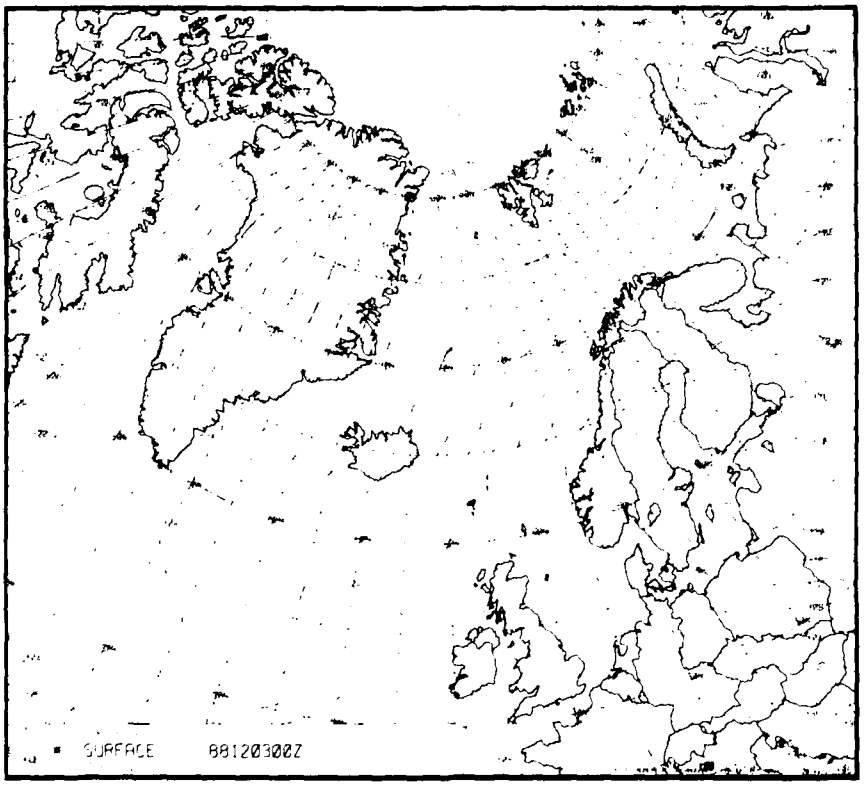

Figure 9-6(a). The 36 Hour Surface Pressure Forecast, 0000 GMT 3 December 1988.

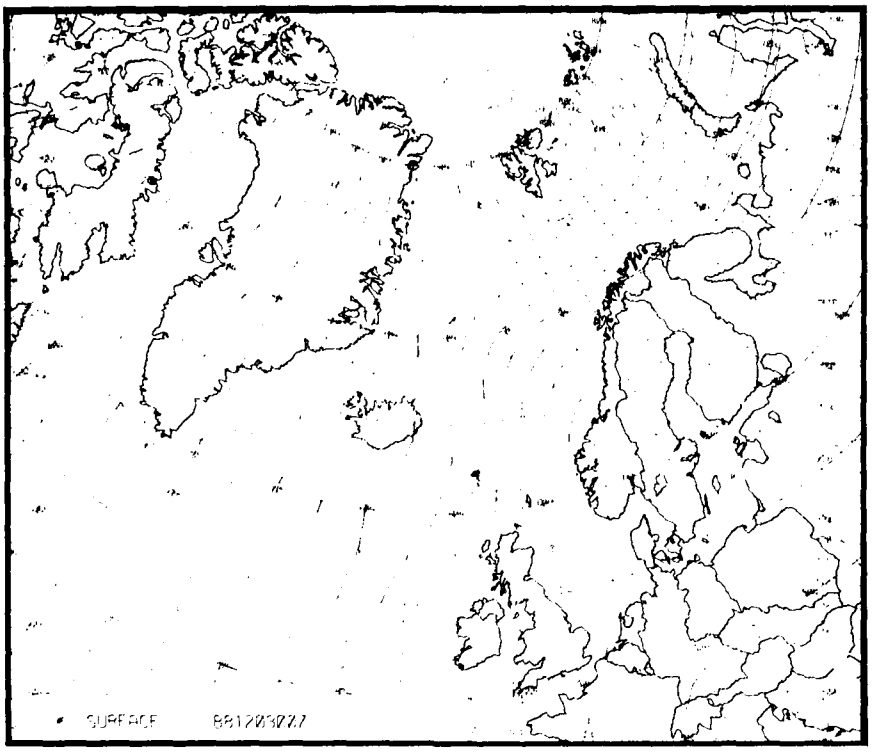

Figure 9-6(b). The Surface Pressure Analysis, 0000 GMT 3 December 1988.

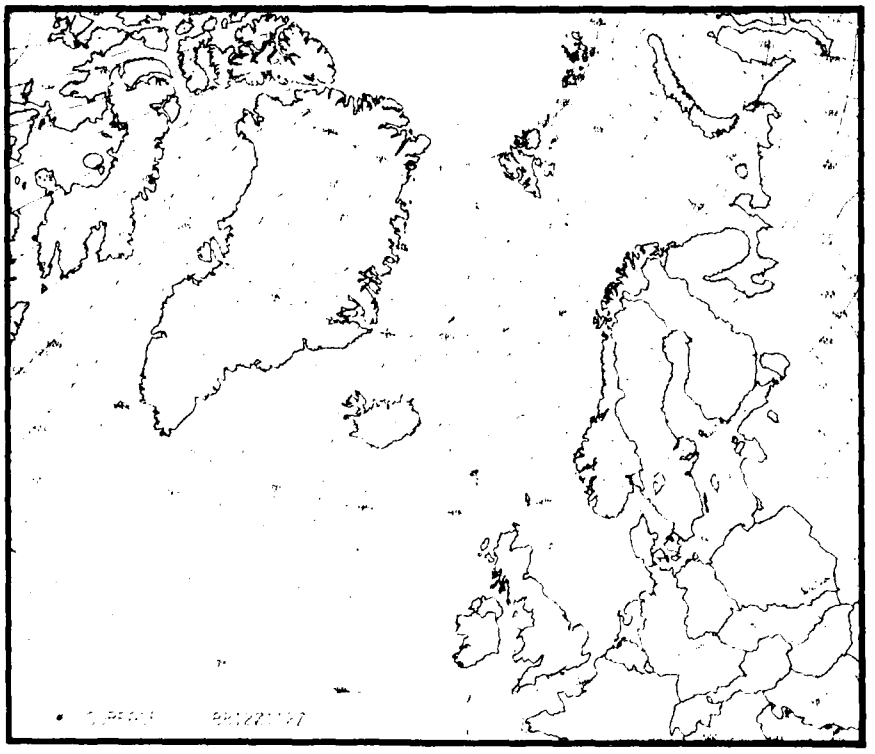

Figure 9-6(c). The Surface Pressure Analysis, 1200 GMT 1 December 1988.

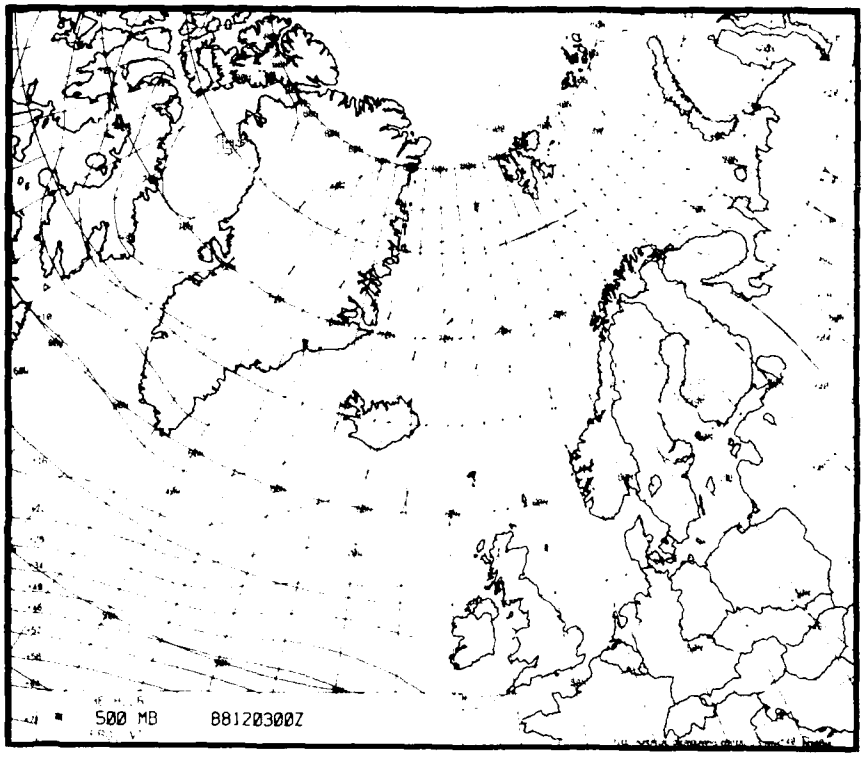

Figure 9-6(d). The 500-mb Height 36-Hour Forecast, 0000 GMT 3 December 1988.

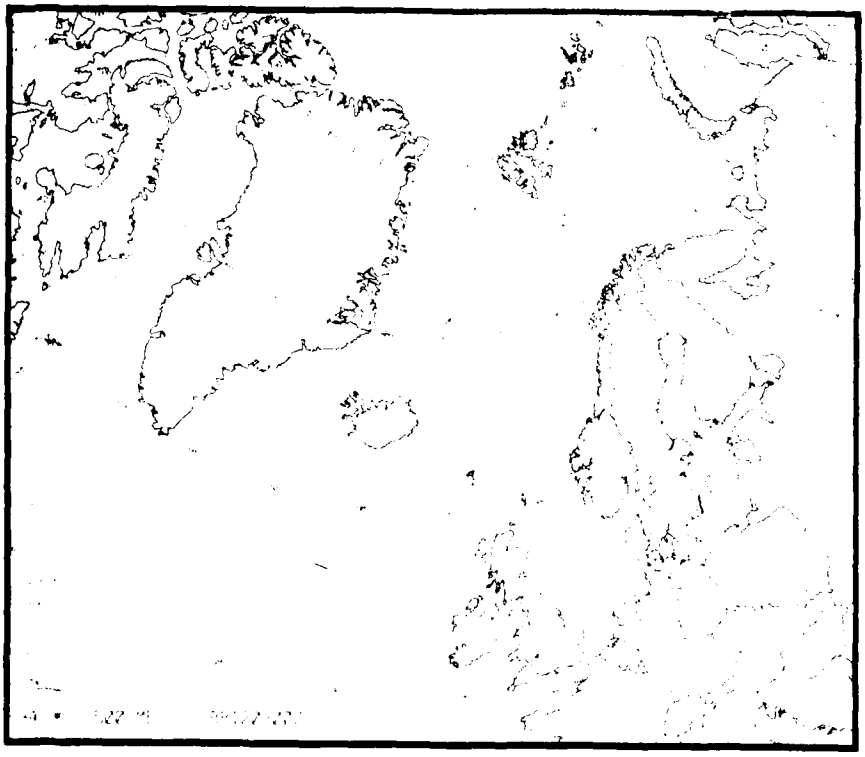

Figure 9-6(e). The 500-mb Height Analysis, 0000 GMT 3 December 1988.

9.3 Summary

Numerical models provide a great deal of information that can assist a forecaster. Unfortunately, the model forecasts are not always correct. It is easy to become too trusting of the computer forecasts, that is, accepting the forecasts as correct without questioning their validity. Eventually, the model has a major bust that leads to an embarrassing situation for the forecaster. A total lack of trust in models usually results.

For this reason, model forecasts should be constantly scrutinized for their accuracy. A working knowledge of systematic errors and model tendencies, such as the examples given in this chapter, will help prevent a forecaster from using erroneous computer guidance that could lead to large forecast errors.

THIS PAGE INTENTIONALLY LEFT BLANK

10. ICING

Inability to forecast vessel icing is one of the most important marine meteorological problems in high latitude waters because rapid accretion on decks and superstructures creates an extreme hazard for vessels due to lack of stability. In the case of smaller ships, the added weight of the ice reduces freeboard and therefore reduces the range of stability of the vessel. Ice formed high on masts, rigging, and superstructure produces a large heeling lever, and the vessel may become topheavy and capsize.

In the case of larger vessels, including warships, accumulation of ice on deck, superstructure, and on deck equipment impairs the ships overall efficiency and maneuverability. In addition, the accumulation of ice on aerials may render the radio and radar systems inoperative.

The regions historically known for producing significant icing conditions are located in the North Atlantic and North Pacific Oceans, as outlined in Fig. 10-1. Icing, however, can occur in other cold weather areas.

10.1 Physical Processes of Icing

The rate of icing depends on (1) precipitation type, (2) wind speed, (3) air temperature, (4) sea surface temperature, and (5) characteristics of the vessel (including size, shape, speed, and heading). Much of the information in this section is taken from Kotsch (1983).

10.1.1 Precipitation Types

Types of precipitation in the Arctic that affect ship icing include freezing rain, Arctic frost smoke, and freezing spray. Snow is not considered a threat due to the inherent lack of adhesion.

Freezing rain will cover a ship or small craft with fresh-water glaze (clear) ice, but the accumulated weights of ice are unlikely to be sufficient to endanger the vessel directly. Because rates of ice accretion depend on the rainfall rates, and the Arctic rainfall rate is not large, the potential hazard is normally not a major one.

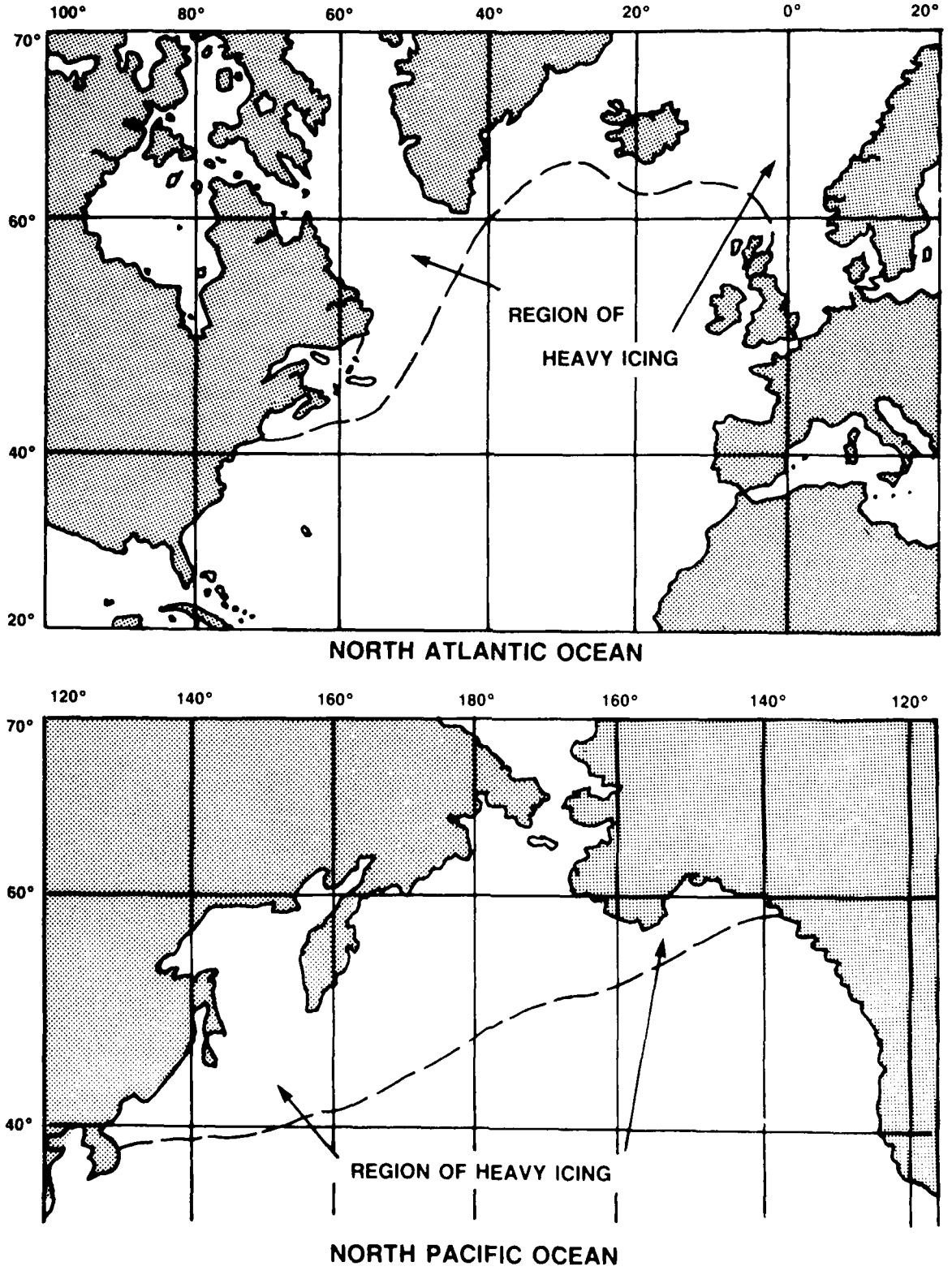

Figure 10-1. Regions of Heavy Icing (U.S. Navy, 1988).

Arctic sea smoke occurs when the air temperature is at least 16 °F (9 °C) colder than the sea. If the air temperature is below 32 °F (0 °C), then the Arctic sea smoke is called Arctic frost smoke. This frost smoke is often confined to a layer only a few feet thick, and trawlermen in northern waters refer to it as "white frost" when the top of the layer is below the observer's eye level. It is referred to as "black frost" when it extends above the observer.

The small water droplets in frost smoke are supercooled. On contact with exposed surfaces on a vessel, part of the droplet freezes immediately while the remainder stays liquid for a short time before it too freezes. The result of the instantaneous freezing of the supercooled droplets is an accretion of opaque, white rime ice with imprisoned air. This rime ice is easier to remove than the clear ice, or glaze (which forms in other circumstances), because rime ice is porous. In one case, a ship (near Bear Island) caught in air temperatures colder than 14 °F (−10 °C), with dense frost smoke, accumulated 4 in (≈ 10 cm) of rime ice on deck in 12 hours. Twelve inches (≈ 30 cm) collected on the ship's side at rail level during the same time. This ice accumulation is equivalent to nearly 2½ tons per hour. Accumulation on isolated structures, such as cranes, can be more than twice as heavy as that on flat surfaces.

Freezing spray is the most dangerous form of icing. It occurs when the air temperature is below the freezing temperature of the sea water, about 28 °F (−2 °C). The spray freezes on the exposed surfaces of the vessel to produce clear ice or glaze. At lower air temperatures, the ice may be opaque, which may be due to the spray being supercooled so that it partially freezes on impact and entraps air. At extremely low temperatures such as 1 °F (−17 °C) and below, as might be encountered in anchorages or close inshore, wind-induced spray may be frozen before it strikes the vessel, so that it does not adhere to the vessel but may form drifts on deck.

With air temperatures below 28 °F (−2 °C), freezing spray is observed in winds of 18 kt (9 m/s) or higher. The lower the air temperature and the stronger the wind, the more rapid is the accumulation of ice. A low sea temperature also increases the rate of accumulation of ice.

Once a spray cloud is produced, the vertical distribution of the cloud is significant as it determines the size of the droplets. In turn, droplet size determines the rate of cooling of the droplet on its trajectory toward the ship. Once the spray reaches vessel surfaces, continued cooling of the ocean water from its sea temperature to the freezing point is determined by the heat flux away from the surface, a function of local wind speed and air temperature.

The freezing process itself is complicated because of the influence of ocean salinity, which affects the freezing temperature. The salinity contributes to forming low density "spongy" ice with air and brine pockets.

10.1.2 Wind

Sea spray generation depends on the wave height and period of waves. Waves, in turn, depend on the duration of the wind and fetch. Generally, the higher the wind speed for the critical temperature ranges (discussed in the following subsections), the greater the ice accumulation.

One factor that can reduce the effect of high wind speeds on icing is the concentration of the ice pack. Obviously, if the ice pack concentration exceeds about 50 percent, wave formation is sharply reduced and freezing spray is minimized.

10.1.3 Air Temperature

The critical range for icing is from 0 °F to 32 °F (−18 °C to 0 °C). At temperatures below 0 °F (−18 °C), the spray striking the structure will usually be in the form of nonadhering small, dry ice crystals. A handy rule of thumb was proposed in a Japanese study: During offshore flow of Arctic air, ship icing is likely when the 850-mb temperature is −4 °F (−18 °C) or colder (Taiyo Fishing Company, Limited, 1972).

10.1.4 Sea Temperature

The critical range of sea surface temperatures are 28 °F to 48 °F (−2.2 °C to 8.9 °C). Seawater of normal salinities is generally frozen below 28 °F. The upper value of 48 °F is not an impediment to freezing since sea spray can be cooled rapidly when air temperatures are below 28 °F.

10.1.5 Vessel Design

To the spray blown from the wave caps is added the spray generated by the vessel herself, so that the total rate of ice accretion will also depend on the design and loading of the vessel, on her heading and speed relative to the waves, and also on the relative wind that determines which part of the vessel is most exposed.

As the dominant wavelength approaches the vessel length, vertical motion is generated between the vessel and the sea, and wave-generated spray is produced. The amount of spray generated by a vessel depends on the ocean wave field, the vessel length, its seakeeping ability, stability, freeboard, hull shape, and vessel heading and speed relative to the wave field.

Finally, note that an accumulation of ice will, in itself, increase the rate of accumulation. The ice already formed increases the effective cross section of rigging, mast, rails, and antennae, exposed to the spray.

10.2 Estimating Rates of Icing

Considering the variety and number of variables to be studied in forecasting icing conditions, no simple or precise rules can be formulated. Over the past two decades, however, research and observations by scientists and mariners have led to some fairly reliable indicators that can be plotted graphically. The results of the most recent studies are summarized in the nomograms of Fig. 10-2.

The nomograms of Fig. 10-2 are based on studies of small ships and are provided as baseline data. As the size of the ship increases, a proportional decrease in the amount of accretion can be expected. These nomograms show potential icing on the ship's superstructure for four water temperature ranges and a ship heading into or abeam of the wind. Ships running downwind will not likely incur accretion rates as high.

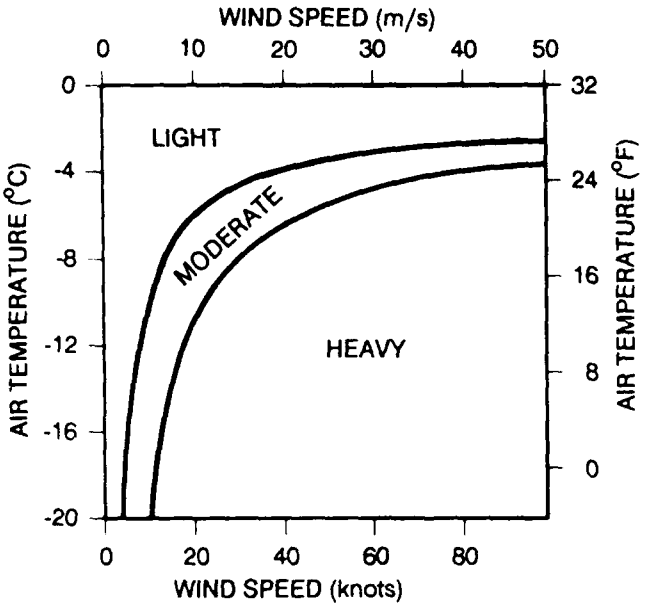

Icing conditions for vessels heading into or abeam of the wind for water temperatures of +1°C (34°F)

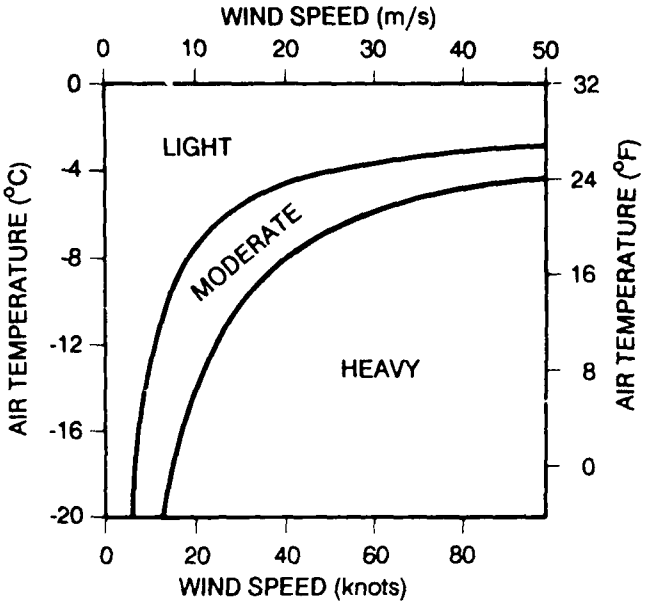

Icing conditions for vessels heading into or abeam of the wind for water temperatures of +3°C (37°F)

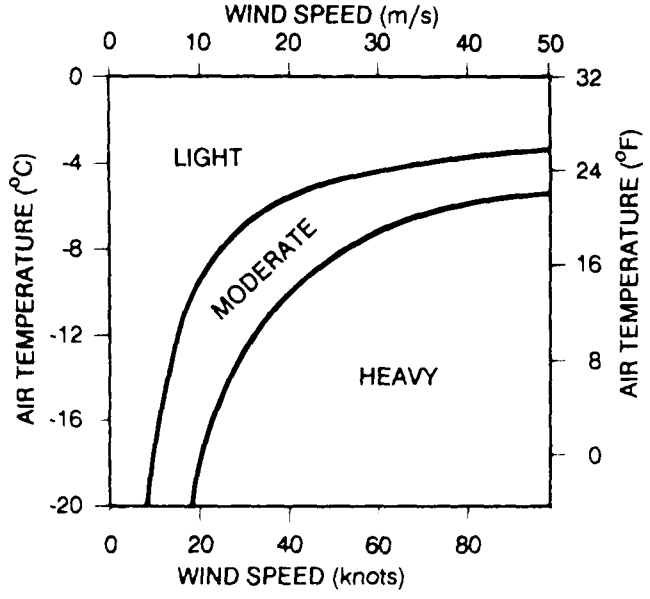

Icing conditions for vessels heading into or abeam of the wind for water temperatures of +5°C (41°F)

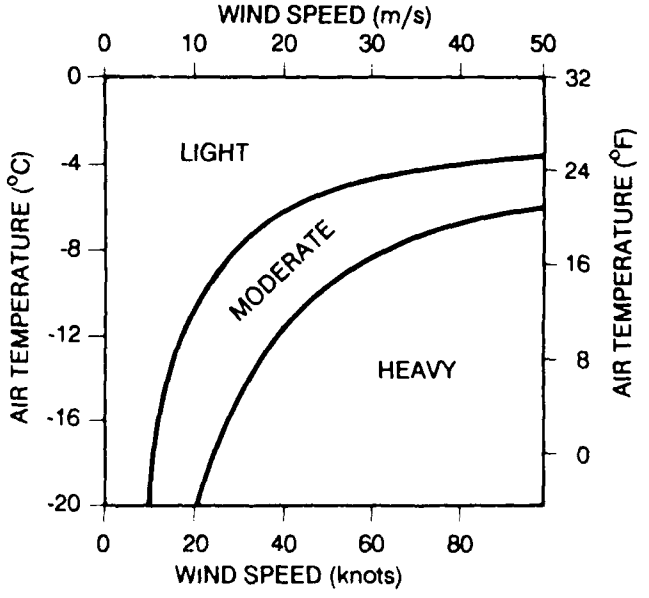

Icing conditions for vessels heading into or abeam of the wind for water temperatures of +7°C (45°F)

Light Icing - Less than 0.7 cm/hr (0.3 in/hr)
Moderate Icing - 0.7 cm/hr (0.3 in/hr) to 2.0 cm/hr (0.8 in/hr)
Heavy Icing - Greater than 2.0 cm/hr (0.8 in/hr)

Figure 10-2. Icing Nomograms (Overland et al., 1986).

These nomograms offer the best prediction method for icing available to the fleet. Laboratory experiments conducted at the Naval Applied Science Laboratory provide some further indication as to the potential weight increase that a ship may experience. A wind speed of 10 kt (5 m/s) and an air temperature of 0 °F (−18 °C) will yield an accretion rate of 8 lb per sq ft (≈ 37 kg per sq m). An Oliver Hazard Perry class frigate has over 7,000 sq ft (650 sq m) of exposed area on the forward one-third of the ship. Therefore, ice accretion could amount to 25 long tons per hour of extra weight. Figure 10-3 is presented to show ice accretion versus wind velocity for six air temperatures. An important note, however, is that icing rates vary with the geometry of structure and orientation, whether horizontal or vertical.

Sea surface temperature has a direct influence on the rate of ice accretion. In addition, warmer sea temperatures frequently mean warmer air temperatures. Since the air temperature also has a strong influence on the rate of ice accretion, the benefit of warmer water may be twofold.

Vessels that seek shelter in the lee of land may still experience low air temperatures, but some reduction of wind speeds and spray blown from the wave caps should be observed. Ship-generated spray in the calmer water will be greatly reduced. Furthermore, attempts to remove the ice will not be thwarted by the vessel's motion and seas sweeping the deck, as would be the case in the open sea.

In very high latitudes, however, ships should not seek shelter in the lee of the ice edge. The ice provides negligible shelter from the wind, and here the coldest air and sea temperatures are found and provide the most severe conditions for icing. If the wind backs

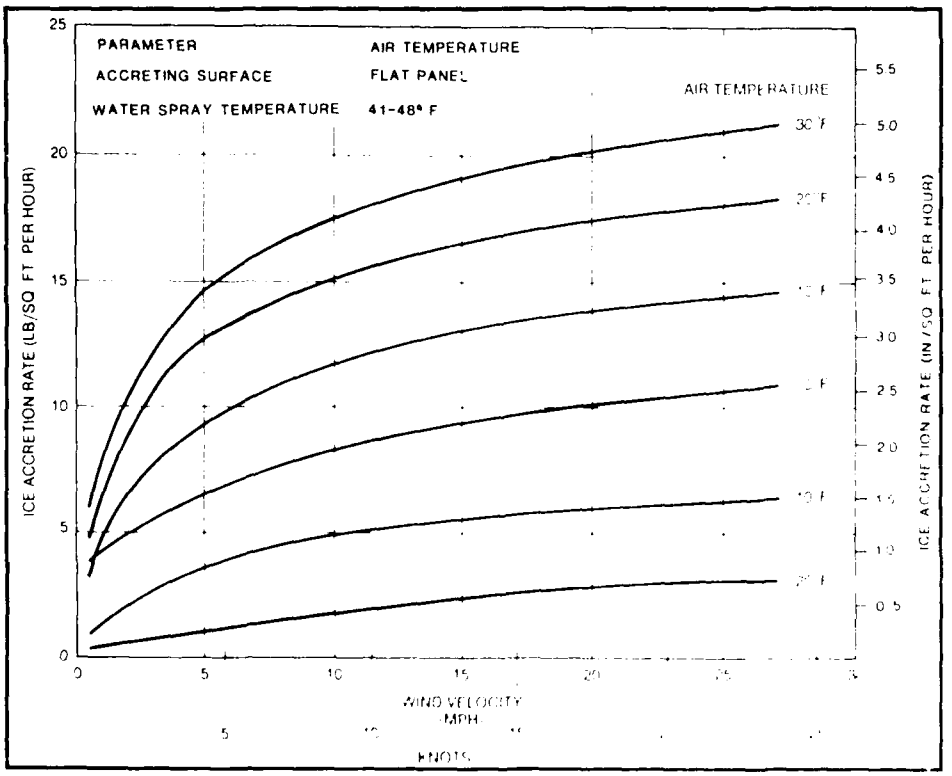

Figure 10-3. Ice Accretion Versus Wind Velocity (U.S. Navy, 1988).

or veers parallel to the ice edge, the air temperature remains very low and heavy seas are soon generated. When ice accumulation reaches 3.9 in (10 cm), dangerous conditions prevail. If this accumulation occurs within 4.5 hours, the condition is one of *extreme icing*. *Heavy icing* would produce this thickness in eight hours, and *light icing* would produce this thickness in one day.

10.3 An Example of Extreme Icing

During the week of 22 to 29 January 1989, the crabbing ship Vestfjord was making its way across the Gulf of Alaska from Cape Spencer, Alaska to the ice edge near Dutch Harbor in the Aleutians (see the locator map Fig. 10-4). As the ship passed south of Kodiak on 28 January the strong westerly winds it had encountered on the previous day intensified significantly and impeded its forward progress. The ship's superstructure began icing up from the supercooled sea spray as the vessel encountered strong cold advection and 50 kt winds.

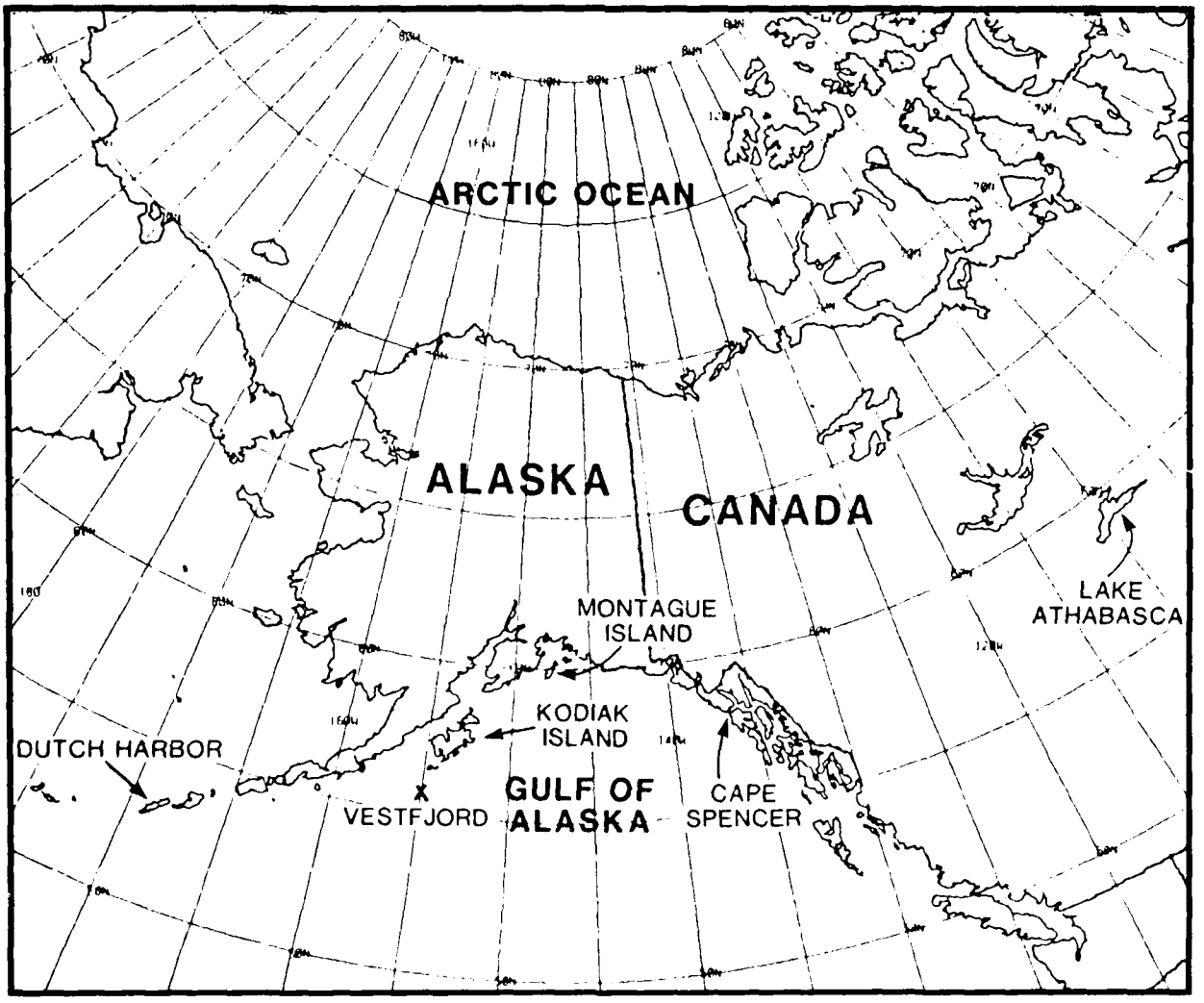

Figure 10-4. Locator Map.

The severity of the situation increased on the 29th, as can be gleaned from the 0600 GMT surface weather map for that date (Fig. 10-5). This surface chart shows a sharp, elongated low-pressure trough oriented nearly east-west and extending from the vicinity of Lake Athabasca, Canada to the central Aleutians. The trough terminated just east of an intense high pressure area centered over the western tip of the Aleutians. Between these two systems was an intense pressure gradient that resulted in northwest winds in excess of 50 kt (26 m/s) with 27 ft (8 m) seas. The air temperature, meanwhile, was about 7 °F (−14 °C) and the sea surface temperature near 39 °F (4 °C).

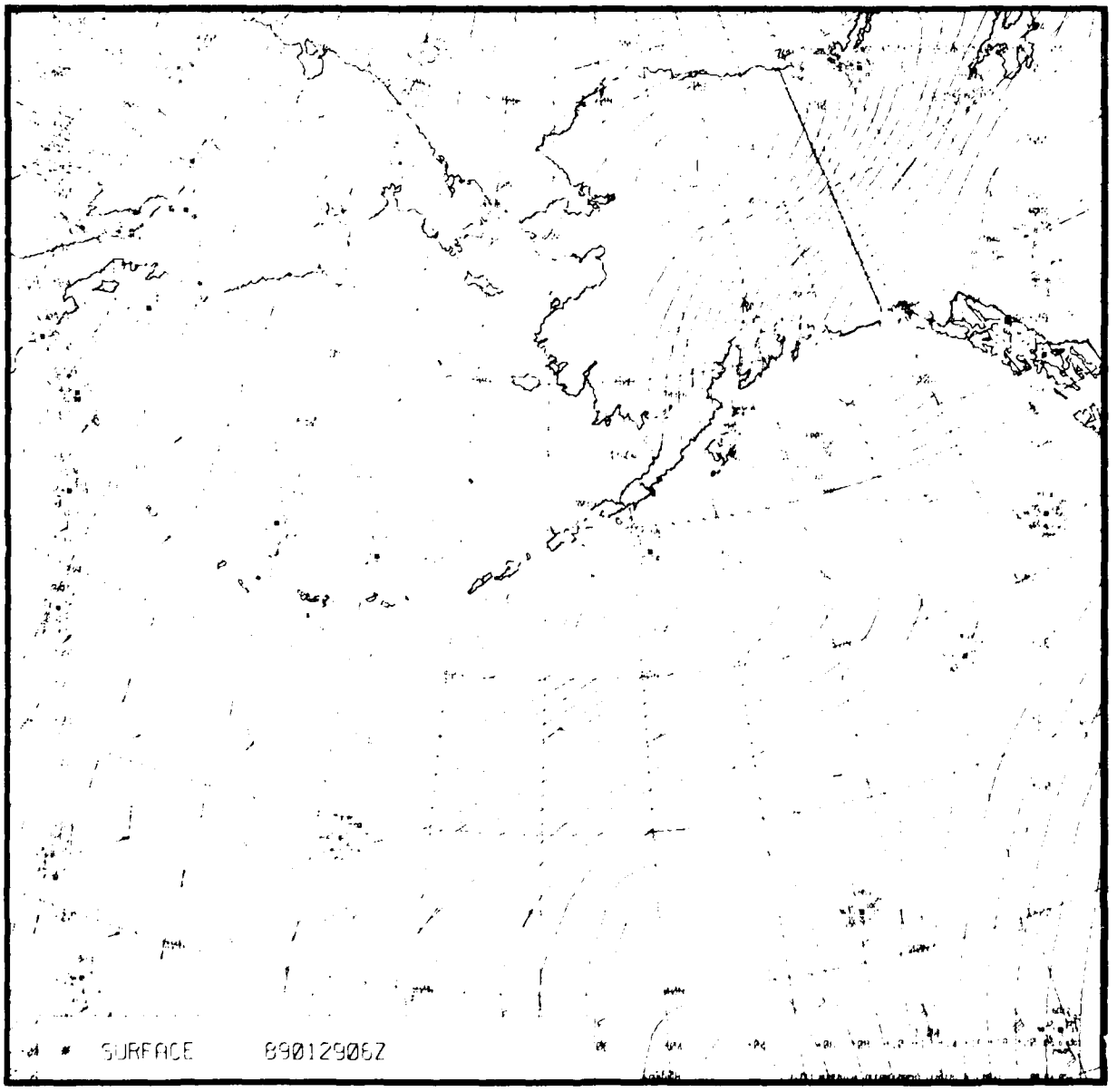

Figure 10-5. The Surface Chart, 0600 GMT 29 January 1989.

The intensity of the cold air advection occurring at the time of heaviest icing is best depicted on the 850-mb chart for 0000 GMT 29 January 1989, as seen in Fig. 10-6. The strongest cold advection on this chart occurs southwest of the low centered near Montague Island on the south-central coast of Alaska. This region is precisely where the ship overturned and sank with all six hands at 1010 GMT on the 29th (last position of Vestfjord shown as an "X" in Fig. 10-4).

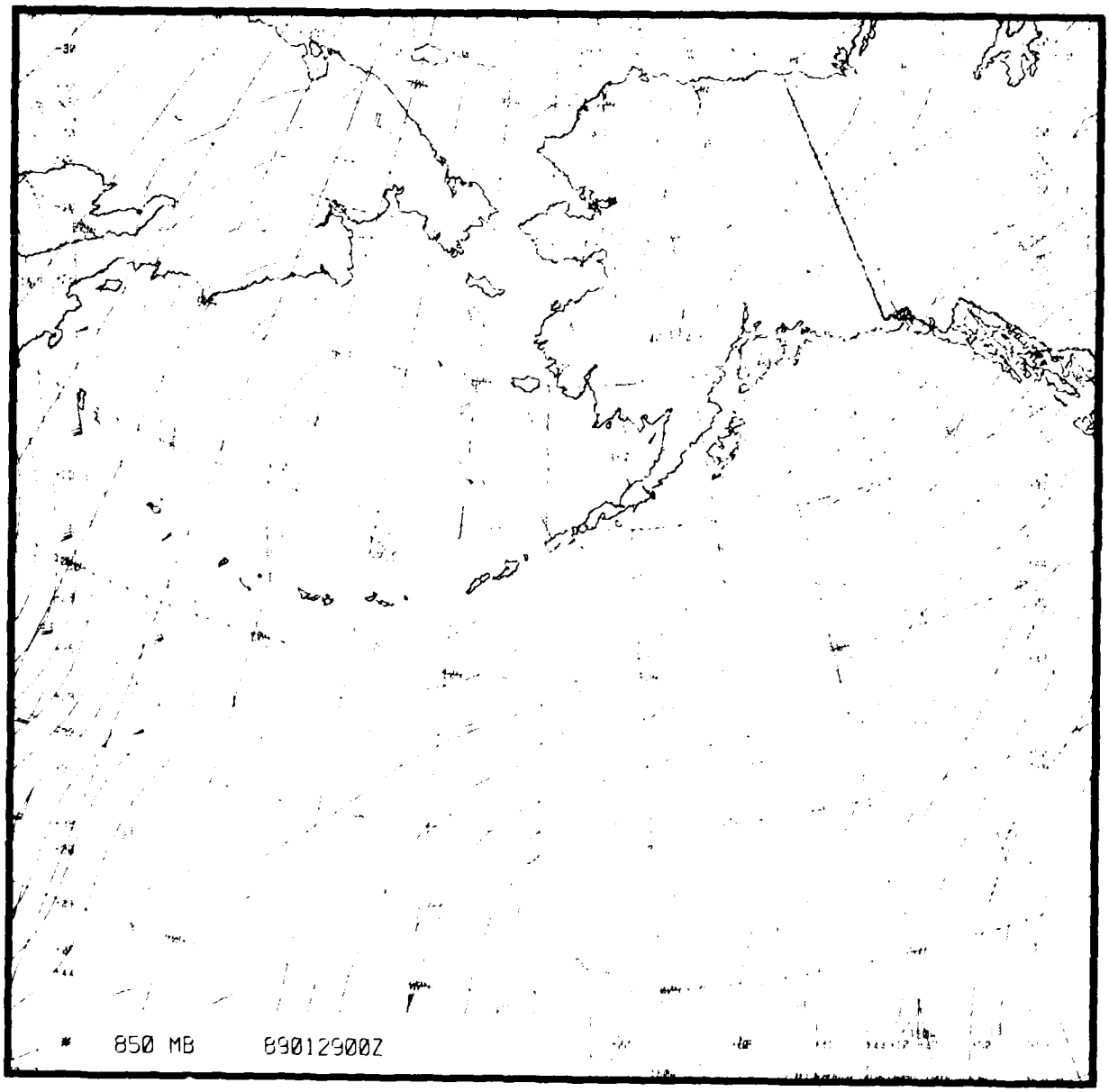

Figure 10-6. The 850-mb Chart, 0000 GMT 29 January 1989.

Figure 10-7 is a satellite imagery from the DMSP satellite for 0552 GMT on the 29th of January 1989. An X marks the approximate location of the ship at that time. The effect of the cold surge on the cloud lines is apparent in the imagery, showing not only strong northwest flow but likely precipitation as well.

Figure 10-7. IR Satellite Imagery, 0552 GMT 29 January 1989.

As Fett (1989) noted in his study of this case, icing can be heavy even with water temperatures as high as 45 °F (7 °C) if the air temperature is cold enough and wind speeds are high enough. He also noted that icing conditions are especially favored in the region in advance of an approaching 500-mb trough. Figure 10-8 is the 500-mb chart for 0000 GMT 29 January 1989 and shows the trough line just east of and parallel to the Aleutians about 10 hours before the ship went under.

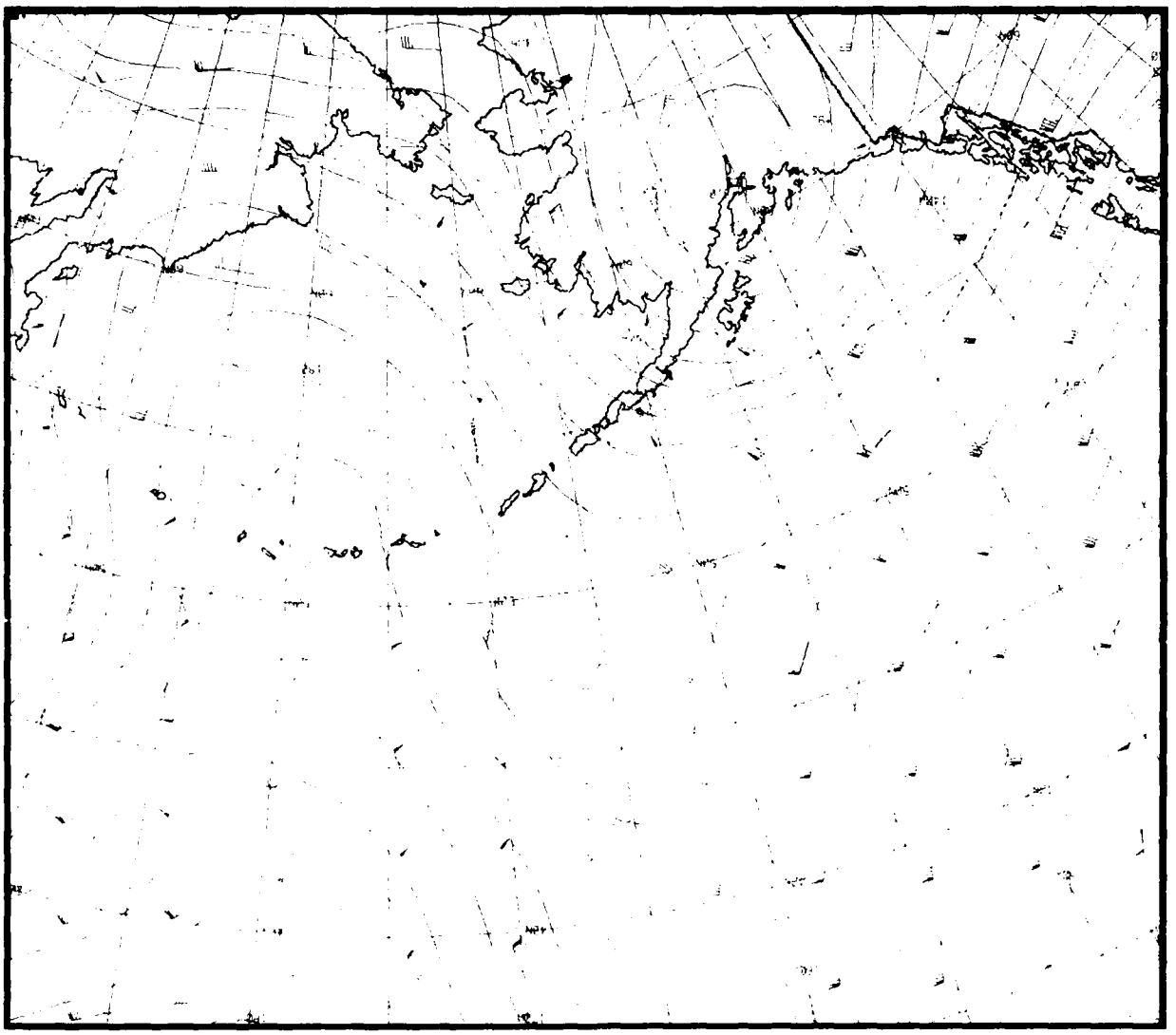

Figure 10-8. The 500-mb Chart, 0000 GMT 29 January 1989.

10.4 Aircraft Icing

Aircraft icing is one of the major weather hazards to aviation. Ice on the airframe decreases lift and increases weight, drag, and stalling speed. In addition, the accumulation of ice on exterior movable surfaces affects the control of the aircraft. Finally, airframe icing greatly increases fuel consumption and decreases range.

The subject of aircraft icing is complex. The following discussion outlines the basic elements of aircraft icing but makes no attempt to encompass all available knowledge on the subject.

10.4.1 The Formation of Ice on Aircraft

Two basic conditions must be met for ice to form on an airframe in significant amounts. First, the aircraft surface temperature must be colder than 32 ° (0 °C). Second, supercooled water droplets, i.e., liquid water droplets at subfreezing temperatures, must be present. Water droplets in the free air, unlike bulk water, do not freeze at 32 °F (0 °C). Instead, their freezing temperature varies from an upper limit near −23 °F (−31 °C) to a lower limit near −40 °F (−40 °C). The smaller and purer the droplets, the lower is their freezing point. When a supercooled droplet strikes an object, such as the surface of an aircraft, the impact destroys the internal stability of the droplet and raises its freezing temperature. Therefore, the possibility of icing must be anticipated in any flight through supercooled clouds or liquid precipitation at temperatures below freezing. In addition, frost sometimes forms on an aircraft in clear humid air if both aircraft and air are at subfreezing temperatures.

10.4.2 Icing Factors

Temperature of the cloud droplets and aircraft surface temperature are only two of the physical factors involved in aircraft icing. Also to be considered are (1) liquid water content, (2) droplet size, (3) collection efficiency, and (4) aerodynamic heating.

Under icing conditions, the *liquid water content* of the cloud is probably the most important parameter in determining the ice accumulation rate. In general, the lower and warmer the base of the cloud, the higher is its water content. Within the cloud, the average liquid water content increases with altitude to a maximum value and then decreases. The maximum concentration usually occurs at a lower level in stratiform than in cumuliform clouds, and the average liquid water content of a stratiform cloud is usually less than that of a cumuliform cloud.

The *size distribution* and median size of the droplets in a cloud are related to the type, depth, and age of the cloud, the strength of the updrafts, the humidity of the air mass, and to other factors. Since both the liquid water content and droplet size are generally greater in cumuliform clouds than other cloud types, at first glance cumuliform clouds would appear to be particularly conducive to icing. The effect exerted by other variables (such as the speed, shape, and size of the aircraft components), however, may be sufficiently great for meteorological conditions leading to trace icing for one type of aircraft to result in light or moderate icing for another.

The icing rate depends to a large extent upon the *collection efficiency* of the aircraft component involved. Collection efficiency, or the fraction of the liquid water collected by the aircraft, varies directly with droplet size and aircraft speed, and inversely with the size or geometry of the collecting surface. The size of an aircraft component is described in terms of the radius of curvature of its leading edge. Those components that have large radii of curvature (canopies, thick wings, etc.) collect but a small percentage of the cloud droplets, especially of the smallest droplets. Components having small radii of curvature (antenna masts, thin wings, etc.) deform the airflow less, permitting a higher proportion of droplets of all sizes to be caught. Once ice begins to form, the shape of the collecting surface is modified, with the radius of curvature nearly always becoming smaller and the collection efficiency increasing. In general, fighter-type aircraft, because of their greater speed and thinner wings, have higher collection efficiencies than do cargo aircraft.

Aerodynamic heating is the temperature rise resulting from adiabatic compression and friction as the aircraft penetrates the air. (The saturation-adiabatic laws, including the effects of fusion and evaporation, apply to flight through clouds.) The amount of heating varies primarily with the speed of the aircraft and the altitude (air density) ranging from about one centigrade degree for very slow aircraft at low altitudes to more than 50 degrees for supersonic jets at low altitudes. Thus, although an aircraft flying through any supercooled liquid water cloud must anticipate icing (as stated in the previous subsection), in actuality, the amount of supercooling must exceed the amount of aerodynamic heating (U.S. Navy, 1985).

10.4.3 Atmospheric Distribution of Icing

The atmospheric distribution of potential aircraft icing zones is mainly a function of temperature and cloud structure. These factors, in turn, vary with altitude, synoptic situation, orography, location, and season.

Altitude and Temperature

In general, the frequency of icing decreases rapidly with decreasing temperature, becoming rather rare at temperatures below −22 °F (−30 °C). The normal vertical temperature distribution in the atmosphere is such that icing is usually restricted to the lower 30,000 feet (9,140 m) of the troposphere.

The type of icing, also, is highly dependent on temperature. Clear ice usually occurs at temperatures just below freezing, whereas rime ice predominates at lower temperatures. The relative frequency of icing by types is as follows: clear, 10 percent; clear-rime mixture, 17 percent; rime, 72 percent; and frost (in flight), 1 percent.

Clouds

Icing in middle and low level stratiform clouds is confined, on the average, to a layer between 3,000 and 4,000 ft (≈ 900–1,200 m) thick. The intensity of the icing generally ranges from a trace to light, with maximum values occurring in the upper portions of the cloud. Both rime and mixed icing are observed in stratiform clouds. The main hazard lies in the great horizontal extent of some of these cloud decks. High level stratiform clouds are composed mostly of ice crystals and produce little icing.

The zone of probable icing in cumuliform clouds is smaller horizontally but greater vertically than in stratiform clouds. Furthermore, icing is more variable in cumuliform clouds because many of the factors conducive to icing depend to a large degree on the stage of development of the particular cloud. Icing intensities may range from generally a trace in small, supercooled cumulus to often light or moderate in cumulonimbus. Although icing occurs at all levels above the freezing level in a building cumulus, it is most intense in the upper regions in a mature cumulonimbus, and to a shallow layer near the freezing level in a dissipating thunderstorm. Icing in cumuliform clouds is usually clear or mixed.

Frontal Systems

Warm frontal icing may occur both above and below the frontal surface. Moderate or severe clear icing usually occurs where freezing rain or freezing drizzle falls through the cold air beneath the front. This condition is most often found when the temperature above the frontal inversion is warmer than 32 °F (0 °C) and the temperature below is colder than freezing. Icing above the warm frontal surface, in regions where the cloud temperatures are colder than freezing, is usually confined to a layer less than 3,000 ft (914 m) thick. For active, warm, fast-moving fronts, moderate icing, usually clear or mixed, can be found 100 to 200 mi (≈ 160–320 km) ahead of the front.

Whereas warm frontal icing is generally widespread, icing associated with cold fronts is usually spotty. Its horizontal extent is less and the areas of moderate icing are localized. Clear icing is more prevalent than rime icing in the unstable clouds usually associated with cold fronts. Moderate clear icing is usually limited to supercooled cumuliform clouds within 100 miles (160 km) to the rear of the cold front surface position and is usually most intense immediately above the frontal zone. Light icing is often encountered in the extensive layers of supercooled stratocumulus clouds that frequently exist behind cold fronts.

Orographic Influences

High or steep terrain, particularly mountains, causes icing to be more intense than is usual under identical conditions over flat terrain. Icing is greater over the ridges than over the valleys and greater on the windward side than on the lee side. Moderate icing, usually clear, is experienced in convective clouds over mountainous terrain. Windward, mountainous coasts in winter are especially subject to extensive aircraft icing zones.

Geographic Distribution

A wide variation of aircraft icing potential exists between geographic areas because of area-to-area variations in temperature and available moisture. For example, icing during the winter season is very frequent over the warm water areas off the east coast of continents, to the lee of large inland water bodies, and over those western portions of continents where winds transport ample moisture inland from the oceans.

Because of the comparatively small amount of moisture in winter Arctic air and the small liquid water content of clouds, icing is seldom regarded as a serious problem in the Arctic in winter. Not surprising, therefore, icing was reported by weather reconnaissance aircraft only 2 percent of the time over the Arctic Ocean at 10,000 ft (≈ 3,050 m). On the other hand, at the same altitude over the northern portion of the North Atlantic Ocean, icing was reported 19 percent of the time. Weather reconnaissance data at 700 and 500 mb over the oceans suggest that the greatest winter icing frequency was found over the northern and western parts of the North Pacific and North Atlantic, and the least over the Arctic Ocean. These data do not imply that icing is never a hazard in the Arctic. In those instances when moisture-laden air from the North Atlantic and the North Pacific invades the Arctic, conditions conducive to copious icing are established.

Normally, winter is the season of maximum icing. The exception is over the Arctic Ocean, where maximum icing occurs in summer because the temperatures and moisture amounts are much too low in winter.

THIS PAGE INTENTIONALLY LEFT BLANK

References

Air Weather Service, 1960: Forecasting of aircraft condensation trails. *Air Weather Service Manual AWSM 105-100 (Navy NAVAIR 50-1p-6)*, USAF Air Weather Service, Scott AFB, Il.

Atmospheric Environment Services, 1985: *Beaufort Weather Office Report.* AES Western Region, Forecast Operations, Edmonton.

Battan, L. J., 1973: *Radar Observation of the Atmosphere.* University of Chicago Press, Chicago.

Battan, L. J., 1984: *Fundamentals of Meteorology.* Second edition, Prentice-Hall, Inc., Englewood, NJ.

Bean, B. R., and E. J. Dutton, 1966: *Radio Meteorology.* NBS Monograph 92, U.S. Dept. of Commerce, National Bureau of Standards, Washington, D.C.

Benson, C. S., and K. R. Rizzo, 1980: Air pollution in Alaska. *Weatherwise 33* (5) 210-215.

Bergeron, T., 1928: Uber die dreidimensional verknufende wetteranalyze. *I. Geofy. Publ.*, (6).

Businger, S., 1985: The synoptic climatology of polar outbreaks. *Tellus 37A*, 419-432.

Carleton, A. M., 1985: Satellite climatological aspects of the polar low and instant occlusion. *Tellus 37A*, 433-450.

Cook, J., and S. Payne, 1987: *Summary of environmental effects on sensors and communications systems.* NEPRF Technical Report TR87-02, Naval Environmental Prediction Research Facility, Monterey, CA.

Dickey, W. D., 1961: A study of a topographic effect on wind in the Arctic. *J. of Meteorol., 18*, 790-803.

Dotson, M. E., 1987: "An evaluation of the impact of variable temporal and spatial data resolution upon IREPS." Master's thesis, Naval Postgraduate School, Monterey, CA.

Durran, D. R., 1986: Mountain waves. *Mesoscale Meteorology and Forecasting*, P. S. Ray (ed.), Am. Meteorol. Soc., Boston, MA.

Ellrod, G. P., 1985: *Detection of high level turbulence using satellite imagery and upper air data.* Technical Memorandum NESDIS 10, National Oceanic and Atmospheric Administration, Washington D.C.

Ellrod, G. P., 1989: *A decision tree approach to clear air turbulence analysis using satellite and upper air data.* Technical Memorandum NESDIS 23, National Oceanic and Atmospheric Administration, Washington, D.C.

Fett, R. W., 1983: Case 5, Contrails, *Navy Tactical Applications Guide (NTAG)*, Volume 5, Part 1. NEPRF TR 83-03, Naval Environmental Prediction Research Facility, Monterey, CA, 1C-47.

Fett, R. W., 1989: Case 2, Ship's Icing. *Navy Tactical Applications Guide (NTAG)*. Volume 8, Part 2. NEPRF Technical Report, Naval Environmental Prediction Research Facility, Monterey, CA.

Fett, R. W., 1990(a): Satellite detection of Arctic weather fronts in the Barents Sea and their role in ice movement prediction. *Weather and Forecasting*, in press.

Fett, R. W., 1990(b): Case 4, Polar Lows, Volume 8, Part 1, *Polar low development at the base of inverted troughs in the Fram Strait.* NEPRF TR89-07, Naval Environmental Prediction Research Facility, Monterey, CA (to be published).

Hogan, T. F., T. E. Rosmond, R. Gelaro, 1990: *NOGAPS forecast model: A technical description.* NOARL Report 13, Naval Oceanic and Atmospheric Research Laboratory, Monterey, CA.

Jones and Bartlett (pub.), 1981: *Atlas of the Polar Regions.* Portola Valley, CA.

Kienle, J., J. G. Roederer, and G. E. Shaw, 1983: Volcanic event in Soviet Union?, *EOS Trans. AGU 20*, 377.

Kotsch, W. J., 1983: Ice accretion—Hazard of significance to seafarers, *Weather for the Mariner*, Chapter 10 Naval Institute Press, Annapolis, MD.

Kozo, T. L., and O. I. Diachok, 1973: Spatial variability of topside and bottomside ice roughness and its relevance to underside acoustic radiation loss. *Arctic Ice Dynamics Joint Experiment (AIDJEX) 19*, Univ. of Washington, Seattle, 114.

Kozo, T. L., 1980: Mountain barrier baroclinity effects on surface winds along the Alaskan Arctic coast. *Geophys. Res. Lett. 7* (5), 377-380.

Kozo, T. L., 1982: An observational study of sea breezes along the Alaskan Beaufort Sea Coast: Part I. *J. Appl. Meteorol. 21* (7), 891-921.

Lee, D. R., R. Stull, and W. Irvine, 1979: *Clear air turbulence forecasting techniques.* AFGWC Technical Note 79/001, Air Force Global Weather Central, Offutt AFB, NE.

Lewis, P. J., 1987: *Severe storms over the Canadian Western High Arctic.* Canadian Climate Centre Report 87-2, Atmospheric Environment Service, Downsview, Ontario.

Lopez, B., 1986: *Arctic Dreams.* Charles Scribner's Sons, New York, 209-211, 252.

Lydolph, P. E., 1977: *Climates of the Soviet Union in World Survey of Climatology*, Volume 7. Elsevier Scientific Publishing, New York.

Matson, M., 1986: Large plume events in the Soviet Arctic. *EOS Trans AGU 67*, 1372–1373.

Marvill, S. and K. Jayaweera, 1975: Investigations of strong valley winds in Alaska using satellite infrared imagery. *Mon. Wea. Rev.* (103) 1129–1136.

Midtbo, K. H., M. Naustvik, V. Hoem, and J. C. Smits, 1986: *Polar low forecasting, Part I: Methods and evaluation*, Polar Low Project. Technical Report 19, Norwegian Meteorological Institute, Oslo.

Navy Arctic Manual ATP-17(A), 1970: U.S. Government Printing Office, Washington, D.C.

Neuberger, H., 1966: *Introduction to Physical Meteorology.* The Pennsylvania State University Press, University Park, PA.

Orvig, S. (ed.), 1970: Climates of the polar regions. *World Survey of Climatology,* Volume 14. Elsevier Publishing, New York.

Overland, J. E., C. H. Pease, and R. W. Preisendorfer, 1986: Prediction of vessel icing. *J. Clim. Appl. Meteorol. 25,* (12) 1793–1806.

Parmenter-Holt, F. C., 1987: The large plumes of Novaya Zemlya. *EOS Trans. AGU,* 1129, 1142.

Rasmussen, E., 1985: A case study of polar low development over the Barents Sea. *Tellus 37A,* 407–418.

Ross, B., 1986: An overview of numerical weather prediction. *Mesoscale Meteorology and Forecasting,* Am. Meteorol. Soc., Boston, MA, 720–751.

Sater, J. E., 1969: *The Arctic Basin.* The Arctic Institute of North America, Washington, D.C.

Sater, J. E., A. G. Ronhovde, and L. C. Van Allen, 1971: *Arctic Environment and Resources.* The Arctic Institute of North America, Washington, D.C.

Schultz. R. R., 1987: "Meteorological features during the Marginal Ice Zone Experiment from 20 March to 10 April 1987." M. S. thesis, Naval Postgraduate School, Monterey, CA.

Schwerdtfeger, W., 1975: Mountain barrier effect on the flow of stable air north of the Brooks Range. *Proc. Climate of the Arctic,* Alaska Science Conference, Aug. 15–17, 1973, Univ. of Alaska, Fairbanks, 204–208.

Scorer, R. S., 1986: *Cloud Investigation by Satellite.* Ellis Horwood, Ltd., Chichester.

Scorer, R. S., 1988: Sunny Greenland. *Quart. J. Roy. Meteorol. Soc. 114* (479), 3–29.

Shapiro, M. A., 1986: *The Arctic Cyclone Expedition, 1984: Research aircraft observations of fronts and polar lows over the Norwegian and Barents Sea, Part I,* Polar Low Project. Technical Report 20, National Oceanic and Atmospheric Administration/Environmental Research Laboratories, Boulder, CO.

Shapiro, M. A., L. S. Fedor, and T. Hampel, 1987: Research aircraft measurements of a polar low over the Norwegian Sea. *Tellus 39A,* 272–306.

Shaw, W. J., K. L. Davidson, Z. Willis, and D. Groters, 1989: Horizontal variability of mean refractive structure in the Arctic. *Proc. Conference on Microwave Propagation in the Marine Boundary Layer,* NEPRF Technical Report TR89-02, Naval Environmental Prediction Research Facility, Monterey, CA.

Shaw, G. E., 1980: Arctic Haze. *Weatherwise 33* (5), 219–221.

Stewart, R. W., 1979: *The Atmospheric Boundary Layer.* World Meteorological Organization, Geneva.

Stringer, W. J., D. G. Barnett, and R. H. Godin, 1984: *Handbook for Sea Ice Analysis and Forecasting.* NEPRF CR 84-03, Naval Environmental Prediction Research Facility, Monterey, CA.

Taiyo Fishing Company, Ltd., 1972: *Study on Preventative Measures Against Icing Induced Marine Accidents of Fishing Vessels,* Japan.

U.S. Navy, 1985: *Aerographers' Mate 1 and C.* NAVEDTDA 10362-B1, U.S. Government Printing Office, Washington, D.C.

U.S. Navy, 1988: *Cold Weather Handbook for Surface Ships.* OPNAV P-03C-01-89, Chief of Naval Operations, Washington, D.C.

Wadhams, P. and V. A. Squire, 1980: Field experiment on wave-ice interaction in the Bering Sea and Greenland waters. *Polar Record 20* (125), 147–158.

Wahl, E. W., and J. F. Lahey, 1969: *A 700-mb Atlas for the Northern Hemisphere.* Univ. of Wisconsin Press, Madison, WI.

Weber, E. M., and S. Wilderotter, 1981: *Satellite interpretation.* Technical Note 3WW/TN-81/001, Third Weather Wing, Offutt AFB, NE.

Welsh, J. P., R. D. Ketchum, A. W. Lohanick, L. D. Farmer, D. T. Eppler, R. E. Burge, and C. J. Radl, 1986: *A compendium of Arctic environmental information.* Report 138, Naval Ocean Research and Development Activity, Stennis Space Center, MS.

Willis, Z. S., 1987: "The spatial and temporal variability of the Arctic atmospheric boundary layer and its effect on electromagnetic (EM) propagation." Master's thesis, Naval Postgraduate School, Monterey, CA.

Appendix A

Glossary of Ice Terms

The following text and photos are adapted from Sea Ice Nomenclature, WMO No. 259, TP 145.

AGED RIDGE: Ridge that has undergone considerable weathering. These ridges are best described as undulations.

ANCHOR ICE: Submerged ice attached or anchored to the bottom, irrespective of the nature of its formation.

BARE ICE: Ice without snow cover.

BELT: A large feature of pack ice arrangement that is longer than it is wide, from 0.5 mi to 65 mi (1–100 km) in width.

BERGY BIT: A large piece of floating glacier ice, generally showing less than 16 ft ($\approx$ 5 m) above sea level but more than 3 ft ($\approx$ 1 m) and normally about 120 to 360 sq yds ($\approx$ 100–300 sq m) in area.

BESET: Situation of a vessel surrounded by ice and unable to move.

BIGHT: An extensive crescent-shaped indentation in the ice edge, formed by either wind of current.

BRASH ICE: Accumulations of floating ice made up of fragments not more than 6.5 ft ($\approx$ 2 m) across, the wreckage of other forms of ice.

BUMMOCK: From the point of view of the submariner, a downward projection from the underside of the ice canopy; the counterpart of a hummock.

CALVING: The breaking away of a mass of ice from an ice wall, ice front, or iceberg.

CLOSE PACK ICE: Pack ice in which the concentration is seven-tenths to eight-tenths, composed of floes mostly in contact.

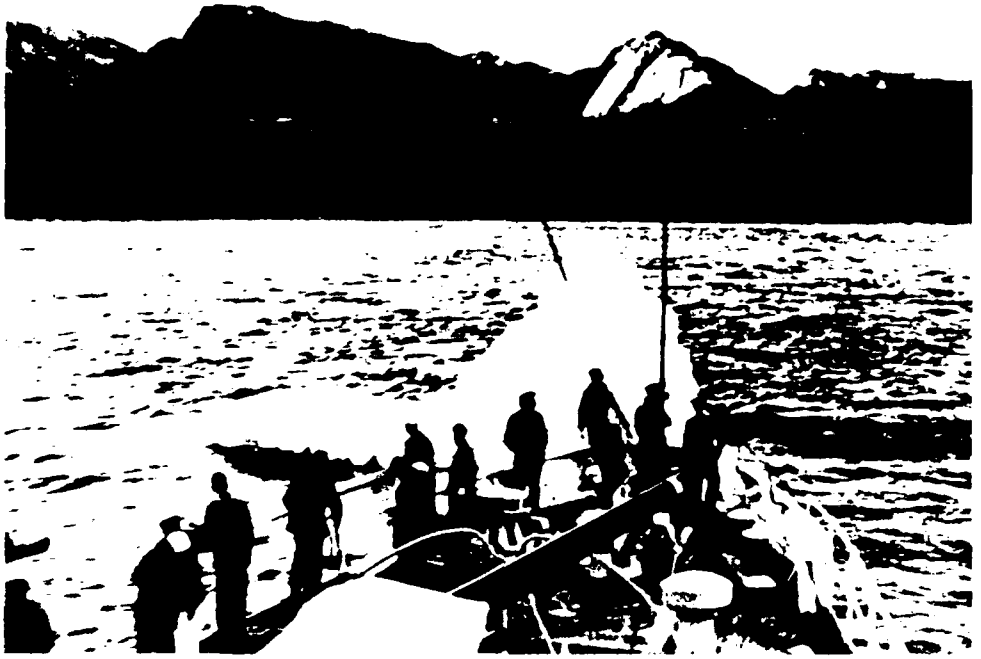

Figure A-1. Example of a Bergy Bit.

COMPACTED ICE EDGE: Close, clear-cut ice edge compacted by wind or current; usually on the windward side of an area of pack ice.

COMPACTING: Pieces of floating ice are considered to be compacting when they are subjected to a converging motion, which increases ice concentration and/or produces stresses that may result in ice deformation.

COMPACT PACK ICE: Pack ice in which the concentration is ten-tenths, and no water is visible.

CONCENTRATION: The ratio in tenths of the sea surface actually covered by ice to the total area of sea surface, both ice covered and ice free, at a specific location or over a defined area.

CONCENTRATION BOUNDARY: A line approximating the transition between two areas of pack ice with distinctly different concentrations.

CONSOLIDATED PACK ICE: Pack ice in which the concentration is ten-tenths and the floes are frozen together.

CONSOLIDATED RIDGE: A ridge in which the base has frozen together.

CRACK: Any fracture that has not parted.

DARK NILAS: Nilas that is under 2 in (5 cm) in thickness and is very dark in color.

DEFORMED ICE: A general term for ice that has been squeezed together and, in places, forced upwards (and downwards). Subdivisions are rafted ice, ridged ice, and hummocked ice.

DIFFICULT AREA: A general qualitative expression to indicate, in a relative manner, that the severity of ice conditions prevailing in an area is such that navigation in it is difficult.

DIFFUSE ICE EDGE: Poorly defined ice edge limiting an area of dispersed ice; usually on the leeward side of an area of pack ice.

DIVERGING: Ice fields or floes in an area are subjected to diverging or dispersive motion, thus reducing ice concentration and/or relieving stresses in the ice.

DRIED ICE: Sea ice from the surface of which meltwater has disappeared after the formation of cracks and thaw holes. During the period of drying, the surface whitens.

EASY AREA: (Opposite of DIFFICULT AREA listed above) Navigation is not difficult.

FAST ICE: Sea ice that forms and remains fast along the coast, where it is attached to the shore, to an ice wall, to an ice front, between shoals or grounded icebergs. Vertical fluctuations may be observed during changes of sea level. Fast ice may be formed on site from sea water or by freezing of pack ice of any age to the shore, and it may extend a few yards (meters) or several hundred miles (kilometers) from the coast. Fast ice may be more than one year old and may then be prefixed with appropriate age category (old, second-year, or multiyear). If it is thicker than about 7 ft (2 m) above sea level, it is called an ice shelf.

FAST-ICE BOUNDARY: The ice boundary at any given time between fast ice and pack ice.

FAST-ICE EDGE: The demarcation at any given time between fast ice and open water.

FINGER-RAFTED ICE: Type of rafted ice in which floes thrust "fingers" alternately over and under the other.

FIRN: Old snow that has recrystallized into a dense material. Unlike ordinary snow, the particles are to some extent joined; but, unlike ice, the air spaces in it still connect with each other.

FIRST-YEAR ICE: Sea ice of not more that one winter's growth, developing from young ice; thickness 1 to 7 ft (30 cm–2 m). May be subdivided into thin first-year ice (white ice), medium first-year ice, and thick first-year ice

FLAW: A narrow separation zone between pack ice and fast ice, where the pieces of ice are in a chaotic state; it forms when pack ice shears under the effect of a strong wind or current along the fast ice boundary.

FLAW LEAD: A passageway between pack ice and fast ice that is navigable by surface vessels.

FLAW POLYNYA: A polynya between pack ice and fast ice.

FLOATING ICE: Any form of ice found floating in water. The principal kinds of floating ice are lake ice, river ice, and sea ice, which form by the freezing of water at the surface, and glacier ice (ice of land origin) formed on land or in an ice shelf. The concept includes ice that is stranded or grounded.

FLOE: Any relatively flat, isolated piece of sea ice 65 ft (≈ 20 m) or more across. Floes are subdivided according to horizontal extent as follows:

GIANT: over 5.5 n mi (10 km)
VAST: 1–5.5 n mi (2–10 km)
BIG: 550–2200 yd (500–2000 m)
MEDIUM: 110–550 yd (100–500 m)
SMALL: 22–110 yd (20–100 m)

FLOEBERG: A massive piece of sea ice composed of a hummock or a group of hummocks, frozen together and separated from any ice surroundings. It may float up to 17 ft (5 m) above sea level.

FLOODED ICE: Sea ice that has been flooded by meltwater or river water and is heavily loaded by water and wet snow.

FRACTURE: Any break or rupture through very close pack ice, compact pack ice, consolidated pack ice, fast ice, or a single floe resulting from deformation processes. Fractures may contain brash ice and/or may be covered with nilas and/or round ice. Length may vary from a few yards (meters) to many miles (kilometers).

FRACTURE ZONE: An area that has a great number of fractures.

FRACTURING: Pressure process whereby ice is permanently deformed, and rupture occurs. Most commonly used to describe breaking across very close pack ice, compact pack ice, and consolidated pack ice.

FRAZIL ICE: Fine spicules, or plates of ice, suspended in water.

FRIENDLY ICE: From the point of view of the submariner, an ice canopy containing many large skylights or other features that permit a submarine to surface. There must be more than ten such features per 30 n mi (56 km) along the submarine's track.

GLACIER: A mass of snow and ice continuously moving from higher to lower ground or, if afloat, continuously spreading. The principal forms of glacier are inland ice sheets, ice shelves, ice streams, icecaps, ice piedmonts, cirque (half-bowl) glaciers, and various types of mountain (valley) glaciers.

GLACIER BERG: An irregularly shaped iceberg.

GLACIER ICE: Ice in, or originating from, a glacier, whether on land or floating on the sea as icebergs, bergy bits, or growlers.

GLACIER TONGUE: Projecting seaward extension of a glacier, usually afloat.

GRAY ICE: Young ice 4 to 6 in (10–15 cm) thick. Less elastic than nilas and breaks on swell. Usually rafts under pressure.

GRAY-WHITE ICE: Young ice 6 to 12 in (15–30 cm) thick. Under pressure more likely to ridge than to raft.

GREASE ICE: A later stage of freezing than frazil ice. It occurs when the crystals have coagulated to form a soupy layer on the surface. Grease ice reflects little light, giving the sea a matte appearance.

Figure A-2. Example of Gray Ice.

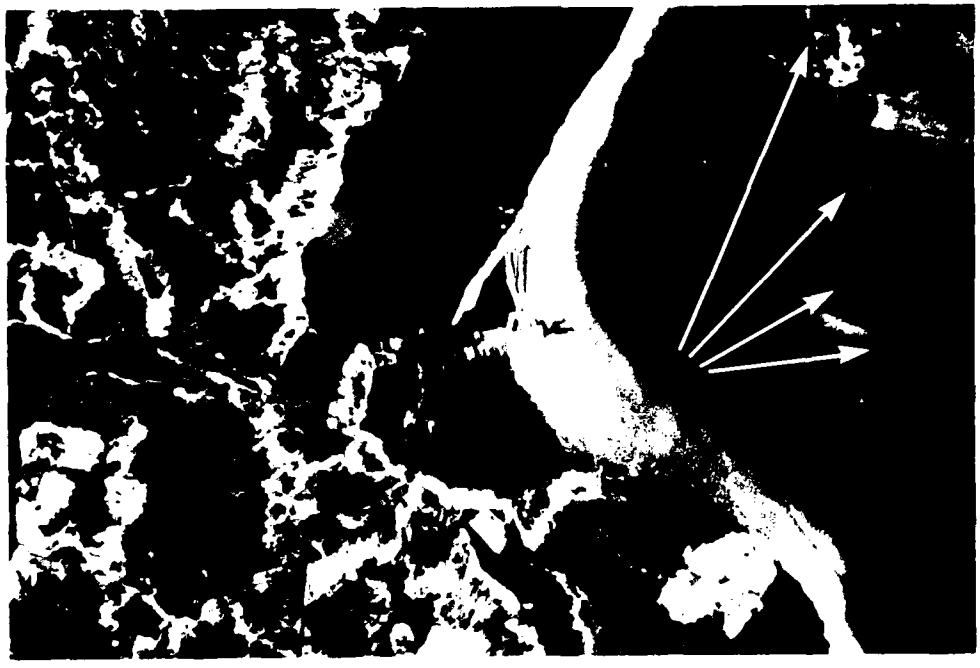

Figure A-3. Example of Grease Ice on Far Right, Nilas to the Left.

GROUNDED HUMMOCK: Hummocked grounded ice formation. Single grounded hummocks occur as well as lines (or chains) of grounded hummocks.

GROUNDED ICE: Floating ice that is aground in shoal water.

GROWLER: Smaller piece of ice than a bergy bit, often transparent but appearing green or almost black in color. Usually extends less than 3 ft (1 m) above the sea surface and normally occupies an area of about 24 sq yd (20 sq m).

HOSTILE ICE: From the point of view of the submariner, an ice canopy containing no large skylights or other features that permit a submariner to surface.

HUMMOCK: A hillock of broken ice that has been forced upwards by pressure. May be fresh or weathered. The submerged volume of broken ice under the hummock, forced downwards by pressure, is termed a bummock.

HUMMOCKED ICE: Sea ice piled haphazardly one piece over another to form an uneven surface. When weathered, it has the appearance of smooth hillocks.

HUMMOCKING: The pressure process by which sea ice is forced into hummocks. When the floes rotate in the process it is termed screwing.

ICEBERG: A massive piece of ice of greatly varying shape, more than 16 ft (5 m) above sea level, which has broken away from a glacier, and which may be afloat or aground. Icebergs may be described as tabular, dome-shaped, sloping, pinnacled, weathered, or glacier bergs.

Figure A-4. Example of a Growler.

ICEBERG TONGUE: A major accumulation of icebergs projecting from the coast, held in place by grounding and joined together by fast ice.

ICE BLINK: A whitish glare on low clouds above an accumulation of distant ice.

ICE BOUND: A harbor, inlet, etc., is said to be ice bound when navigation by ships is prevented on account of ice, except possibly with the assistance of an icebreaker.

ICE BOUNDARY: The demarcation at any given time between fast ice and pack ice or between areas of pack ice of different concentrations.

ICE BRECCIA: Ice of different stages of development frozen together.

ICE CAKE: Any relatively flat piece of sea ice less than 22 yd (20 m) across.

ICE CANOPY: Pack ice from the point of view of the submariner.

ICE COVER: The ratio of an area of ice of any concentration to the total area of sea surface within some large geographic locale; this locale may be global, hemispheric, or prescribed by a specific oceanographic entity such as Baffin Bay or the Barents Sea.

ICE EDGE: The demarcation at any given time between the open sea and sea ice of any kind, whether fast or drifting. It may be termed compacted or diffuse.

ICE FIELD: Area of pack ice consisting of floes of any size that are greater than 5.5 n mi (10 km) across.

ICEFOOT: A narrow fringe of ice attached to the coast, unmoved by tides and remaining after the fast ice has moved away.

ICE FREE: No sea ice present. Some ice of land origin may occur.

ICE FRONT: The vertical cliff forming the seaward face of an ice shelf or other floating glacier varying in height from 6 to 165 ft (2–50 m) or more above sea level.

ICE ISLAND: A large piece of floating ice about 16 ft (5 m) above sea level, which has broken away from an Arctic ice shelf, having a thickness of 100 to 165 ft (30–50 m) and an area of from a few thousand square yards (meters) to 200 sq mi (500 sq km) or more, and usually characterized by a regularly undulating surface that gives it a ribbed appearance from the air.

ICE JAM: An accumulation of broken river ice or sea ice caught in a narrow channel.

ICE KEEL: From the point of view of the submariner, a downward-projecting ridge on the underside of the ice canopy—the counterpart of a ridge. Ice keels may extend as much as 165 ft (50 m) below sea level.

ICE LIMIT: Climatological term referring to the extreme minimum or extreme maximum extent of the ice edge in any given month or period based on observations over a number of years. Term should be preceded by minimum or maximum.

ICE MASSIF: A concentration of sea ice covering hundreds of square miles (kilometers) that is found in the same region every summer.

ICE OF LAND ORIGIN: Ice formed on land or in an ice shelf, found floating in water. The concept includes ice that is stranded or grounded.

ICE PATCH: An area of pack ice less than 6 n mi (10 km) across.

ICE PORT: An embayment in an ice front, often of a temporary nature, where ships can moor alongside and unload directly onto the ice shelf.

ICE RIND: A brittle shiny crust of ice formed on a quiet surface by direct freezing or from grease ice, usually in water of low salinity. Thickness to about 1 in (5 cm). Easily broken by wind or swell, commonly breaking in rectangular pieces.

ICE SHELF: A floating ice sheet of considerable thickness showing 6 to 165 ft (2–50 m) or more above sea level, attached to the coast. Usually of great horizontal extent and with a level or gently undulating surface. Nourished by annual snow accumulation and also by the seaward extension of land glaciers. Limited areas may be aground. The seaward edge is termed an ice front.

ICE STREAM: Part of an island ice sheet in which the ice flows more rapidly and not necessarily in the same direction as the surrounding ice. The margins are sometimes clearly marked by a change in direction of the surface slope but may be indistinct.

ICE UNDER PRESSURE: Ice in which deformation processes are actively occurring and hence a potential impediment or danger to shipping.

ICE WALL: An ice cliff forming the seaward margin of a glacier that is not afloat. An ice wall is aground, the rock basement being at or below sea level.

LAKE ICE: Ice formed on a lake, regardless of observed location.

LARGE FRACTURE: More than 1,640 ft (500 m) wide.

LARGE ICE FIELD: An ice field over 12 n mi (20 km) across.

LEAD: Any fracture or passageway through sea ice that is navigable by surface vessels.

LEVEL ICE: Sea ice that is unaffected by deformation.

LIGHT NILAS: Nilas that is more than 2 in (5 cm) in thickness and rather lighter in color than dark nilas.

MEAN ICE EDGE: Average position of the ice edge in any given month or period based on observations over a number of years. Other terms that may be used are mean maximum ice edge and mean minimum ice edge.

MEDIUM FIRST-YEAR ICE: First-year ice 25 to 50 in (70–120 cm) thick.

MEDIUM FRACTURE: 650 to 1,650 ft (200–500 m) wide.

MEDIUM ICE FIELD: An ice field 8 to 10 mi (15–20 km) across.

MULTIYEAR ICE: Old ice up to 10 ft (3 m) or more thick that has survived at least two summers' melt. Hummocks even smoother than in second-year ice, and the ice is almost salt free. The color, where snow free, is usually blue. The melt pattern consists of large interconnecting irregular puddles and a well developed drainage system.

NEW ICE: A general term for recently formed ice that includes frazil ice, grease ice, slush, and shuga. Theses types of ice are composed of ice crystals that are only weakly frozen together (if at all) and have a definite form only while they are afloat.

NEW RIDGE: Ridge newly formed with sharp peaks and slope of sides usually 40 degrees. Fragments are visible from the air at low altitude.

NILAS: A thin, elastic crust of ice bending easily on waves and swell. Nilas has a matte surface and is up to 4 in ($\approx$ 10 cm) thick. Under pressure it thrusts into a pattern of interlocking fingers (see FINGER-RAFTED ICE). May be subdivided into dark nilas and light nilas.

NIP: Ice is said to nip when it forcibly presses against a ship. A vessel so caught, though undamaged, is said to have been nipped.

OLD ICE: Sea ice that has survived at least one summer's melt. Most topographic features on old ice are smoother than those on first-year ice. May be subdivided into second-year ice and multiyear ice.

OPEN PACK ICE: Pack ice in which the ice concentration is four-tenths to six-tenths, with many leads and polynyas, and the floes are generally not in contact with one another.

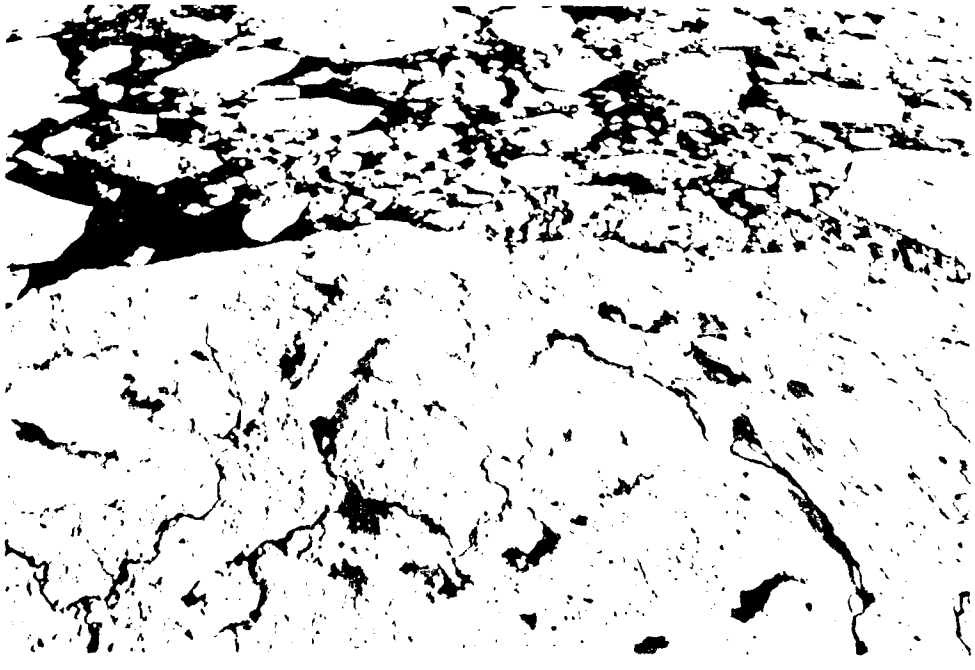

Figure A-5. Example of Multiyear Ice.

OPEN WATER: A large area of freely navigable water in which sea ice is present in concentrations less than one-tenth. When no sea ice is present, the area should be termed ice free, even though icebergs occur.

PACK ICE: Term used in a wide sense to include any area of sea ice, other than fast ice, no matter what form it takes or how it is disposed.

PANCAKE ICE: Predominantly circular pieces of ice from 1 to 10 ft (30 cm–3 m) in diameter and up t. bout 4 in (≈ 10 cm) in thickness, with raised rims due to the pieces striking against one another. It may be formed on a slight swell from grease ice, shuga, or slush, or as a result of the breaking of ice rind, nilas, or, under severe conditions of swell or waves, of gray ice. Sometimes pancake ice forms at some depth, at an interface between water bodies of different physical characteristics, from where it floats to the su. face; it may cover wide areas of water rapidly.

POLYNYA: Any nonlinear-shaped opening in the water but enclosed by ice. Sometimes the polynya is limited on one side by the coast and is called a shore polynya, or by fast ice and is called a flaw polynya. Some polynyi recur annually in the same position.

PUDDLE: An accumulation on ice of meltwater, mainly due to melting snow, but in the more advanced stages, also to the melting of ice. Initial stage consists of patches of melted snow.

RAFTED ICE: Type of deformed ice formed by one piece of ice overriding another.

RAFTING: Pressure processes whereby one piece of ice overrides another. Most common in new and young ice.

RAM: An underwater ice projection from an ice wall, ice front, iceberg, or floe. Its formation is usually due to a more intensive melting and erosion of the unsubmerged part.

RECURRING POLYNYA: A polynya that recurs in the same position every year.

RIDGE: A line or wall of broken ice forced up by pressure; it may be fresh or weathered. The submerged volume of broken ice under a ridge, forced downwards by pressure, is termed an ice keel.

RIDGED ICE: Ice piled haphazardly one piece over another in the form of ridges or walls. Usually found in first-year ice.

RIDGED-ICE ZONE: An area in which much ridged ice with similar characteristics has formed.

RIDGING: The pressure process by which sea ice is forced into ridges.

RIVER ICE: Ice formed on a river, regardless of observed location.

ROTTEN ICE: Sea ice that has become honeycombed and is in an advanced state of disintegration.

SASTRUGI: Sharp, irregular ridges formed on a snow surface by wind erosion and deposition. On drift ice the ridges are parallel to the direction of the prevailing wind at the time they were formed.

SEA ICE: Any form of ice found at sea that has originated from the freezing of sea water.

SECOND-YEAR ICE: Old ice that has survived only one summer's melt. Because it is thicker and less dense than first-year ice, it stands higher out of the water. In contrast to multiyear ice, summer melting produces a regular pattern of numerous small puddles. Bare patches and puddles are usually greenish-blue.

SHEARING: An area of pack ice is subject to shear when the ice motion varies significantly in the direction normal to the motion, subjecting the ice to rotational forces. These forces may result in phenomena similar to a flaw.

SHORE LEAD: A lead between pack ice and the shore or between pack ice and an ice front.

SHORE POLYNYA: A polynya between pack ice and the coast, or between pack ice and an ice front.

SHUGA: An accumulation of spongy white ice lumps, a few inches (centimeters) across; they are formed from grease ice or slush and sometimes from ice rising to the surface.

SKYLIGHT: From the point of view of the submariner, thin places in the ice canopy, usually less than 3 ft (1 m) thick and appearing from below as relatively light, translucent patches in dark surroundings. The undersurface of a skylight is normally flat. Skylights are called large if big enough for a submarine to attempt to surface through them, or small if not.

SLUSH: Snow that is saturated and mixed with water on land or ice surfaces, or as a viscous floating mass in water after a heavy snowfall.

SMALL ICE CAKE: An ice cake less than 7 ft (2 m) across.

SMALL ICE FIELD: An ice field 5 to 10 n mi (10–15 km) across.

SNOW-COVERED ICE: Ice covered with snow.

SNOWDRIFT: An accumulation of windblown snow deposited in the lee of obstructions or heaped by wind eddies. A crescent-shaped snowdrift, with ends pointing downwind, is known as a snow barchan.

STANDING FLOE: A separate floe standing vertically or inclined and enclosed by rather smooth ice.

STRANDED ICE: Ice that has been floating and has been deposited on the shore by retreating high water.

STRIP: Long narrow area of pack ice, about 0.5 n mi (1 km) or less in width, usually composed of small fragments detached from the main mass of ice, and run together under the influence of wind, swell, or current.

TABULAR BERG: A flat-topped iceberg. Most tabular bergs form by calving from an ice shelf and show horizontal banding.

THAW HOLES: Vertical holes in sea ice formed when surface puddles melt through to the underlying water.

THICK FIRST-YEAR ICE: First-year ice over 4 ft (120 cm) thick.

THIN FIRST-YEAR ICE (WHITE ICE): First-year ice 1 to 2 ft (30–70 cm) thick.

TIDE CRACK: Crack at the line of junction between an immovable ice foot or ice wall and fast ice, the latter subject to rise and fall of the tide.

TONGUE: A projection of the ice edge up to several miles (kilometers) in length, caused by wind or current.

VERY CLOSE PACK ICE: Pack ice in which the concentration is nine-tenths to less than ten-tenths.

VERY OPEN PACK ICE: Pack ice in which the concentration is one-tenth to three-tenths and water preponderates over the ice.

VERY WEATHERED RIDGE: Ridge with tops very rounded, slope of sides usually 20 to 30 degrees.

WATER SKY: Dark streaks on the underside of low clouds, indicating the presence of water features in the vicinity of sea ice.

WEATHERED RIDGE: Ridge with peaks slightly rounded and slope of sides usually 30 to 40 degrees. Individual fragments are not discernible.

WEATHERING: Processes of ablation and accumulation that gradually eliminate irregularities in an ice surface.

WHITE ICE: Same as thin first-year ice.

Figure A-6. Example of Thin First-Year Ice (White Ice).

YOUNG COASTAL ICE: The initial stage of fast ice formation consisting of nilas or young ice, its width varying from a few yards (meters) up to 110 to 220 yd (100–200 m) from the shoreline.

YOUNG ICE: Ice in the transition stage between nilas and first-year ice, 4 to 12 in (10–30 cm) in thickness. May be subdivided into gray ice and gray-white ice.

THIS PAGE INTENTIONALLY LEFT BLANK

Appendix B

Mean Monthly Sea Level Pressure, Air Temperature, and 700-mb Height

Note that although anticyclonic flow dominates the Arctic area, cyclonic activity can occur during any month. Appendix B contains monthly charts of mean sea level pressure (mb), mean surface air temperature (°C), and mean heights of the 700-mb pressure surface. The sea level pressure charts (Figs. B-1 through B-13) were derived from drifting buoy data collected from 1979 to 1985 while the air temperature data (Figs. B-14 through B-25) were compiled from several sources, some with data records as long as 60 years. These charts were developed by the Applied Physics Laboratory, University of Washington. The pressure surface charts (Figs. B-26 through B-37), taken from Wahl and Lahey (1969), show data for the 5 days closest to the middle of each month. The original publication included 5-day charts for the entire year.

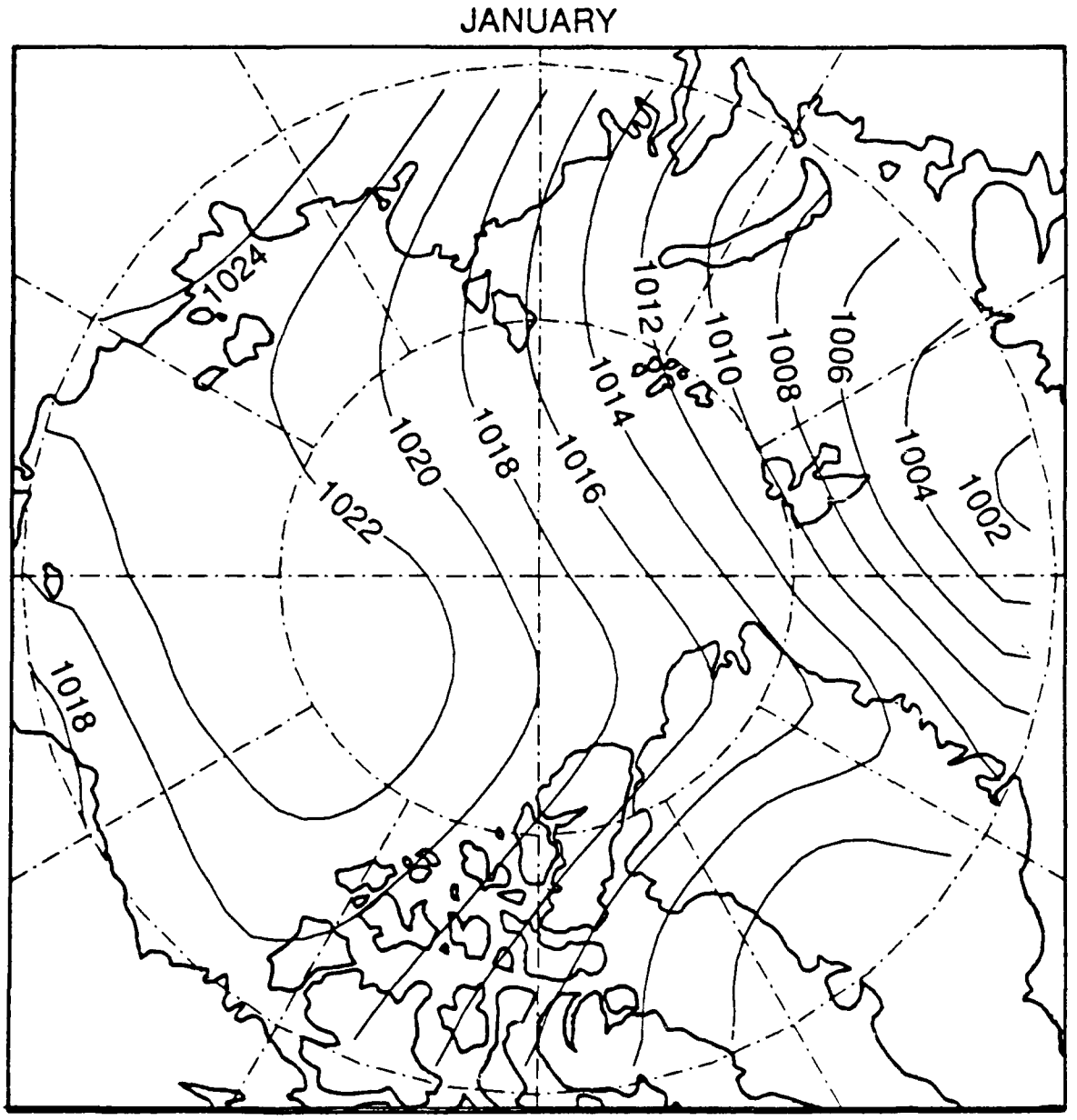

Figure B-1. Mean Sea Level Pressure (mb) for January.

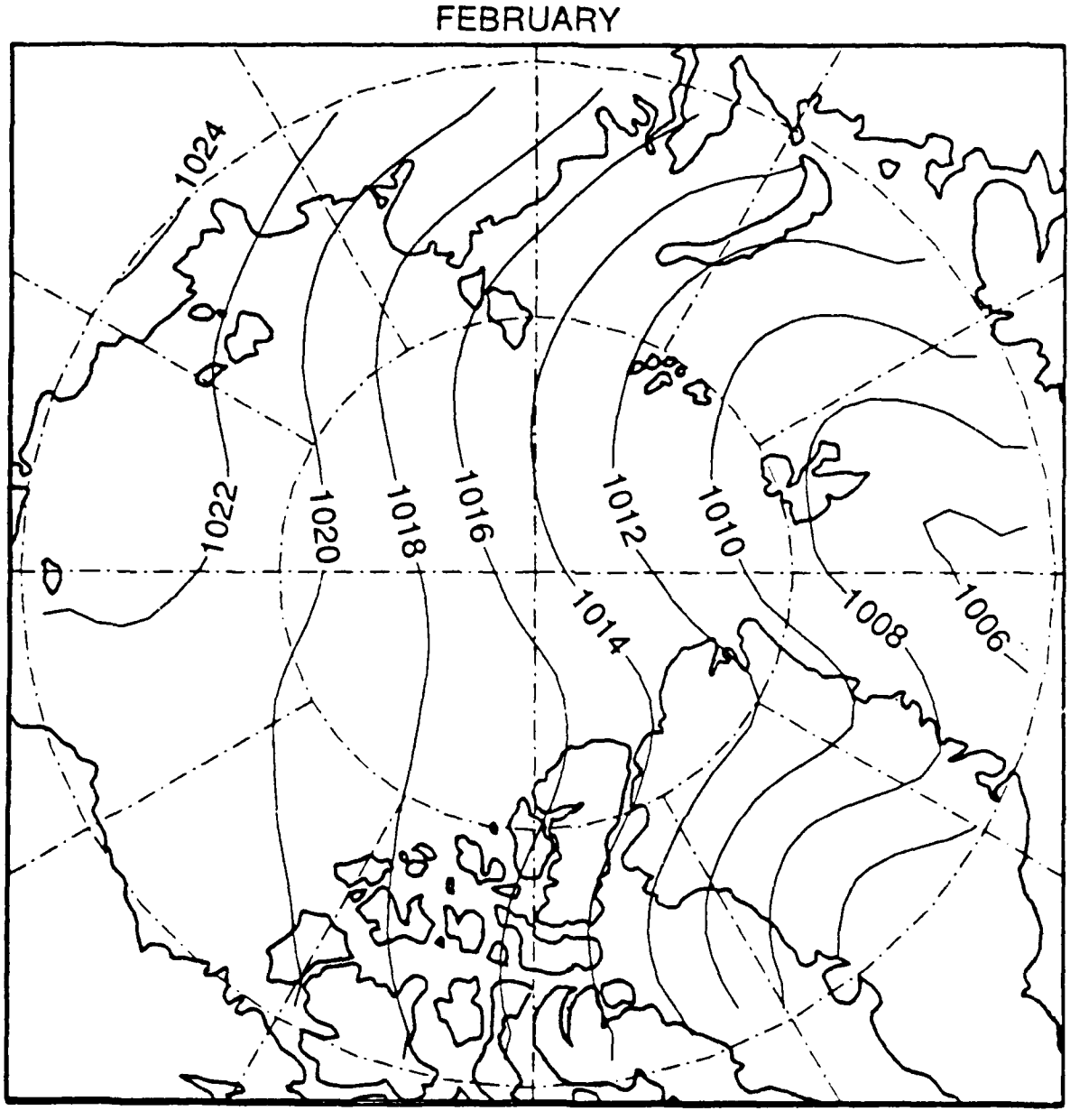

Figure B-2. Mean Sea Level Pressure (mb) for February.

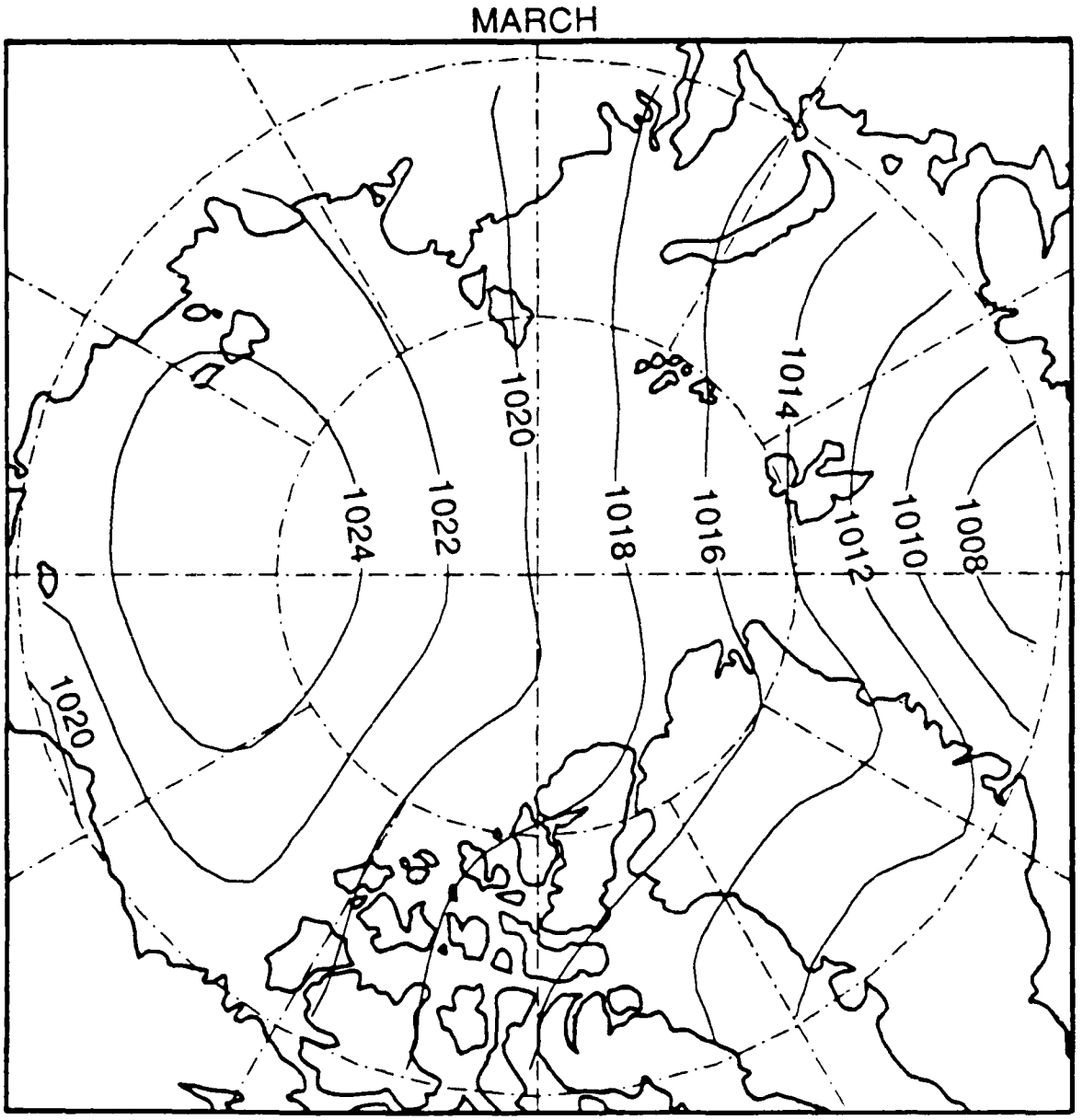

Figure B-3. Mean Sea Level Pressure (mb) for March.

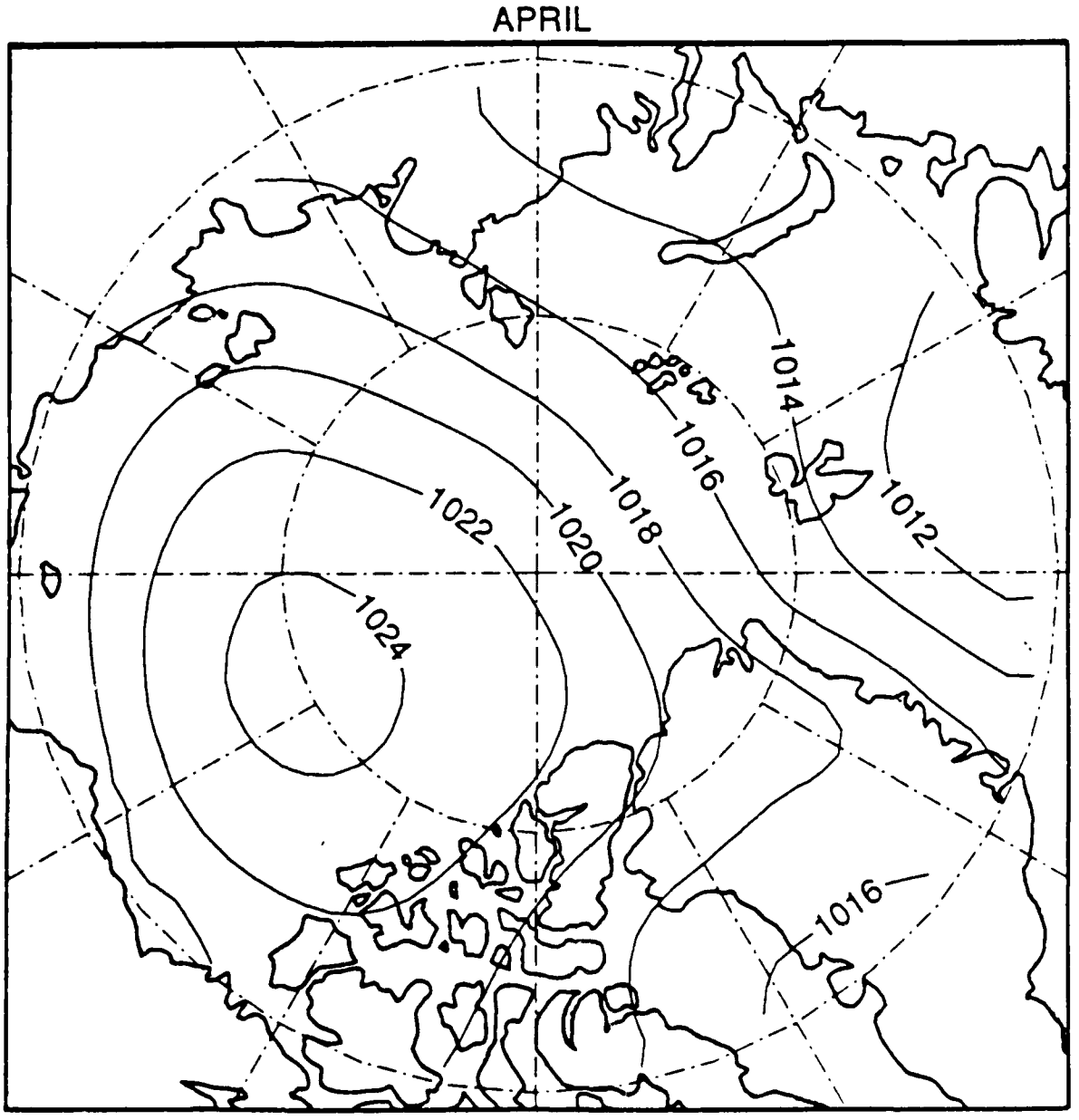

Figure B-4. Mean Sea Level Pressure (mb) for April.

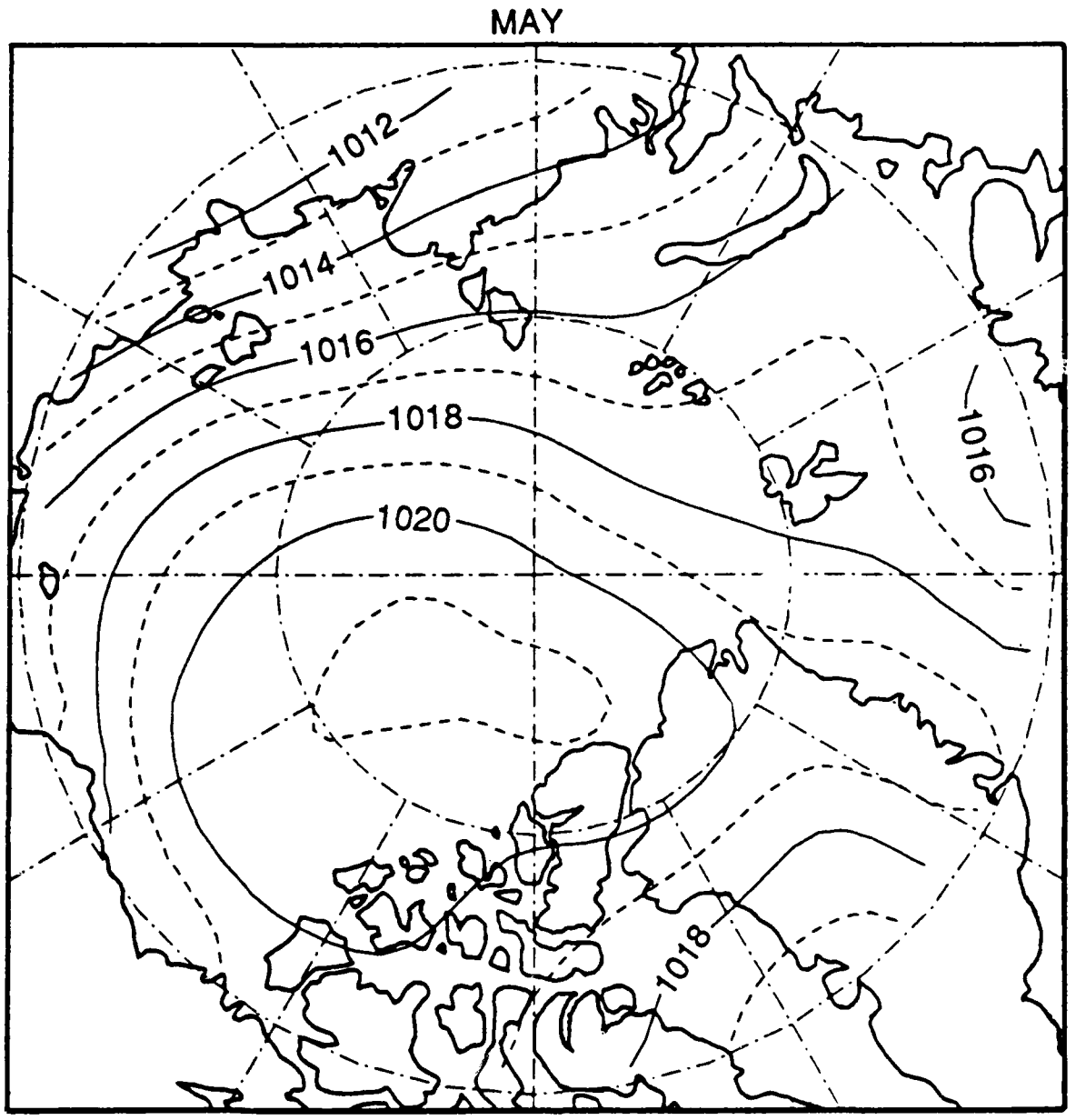

Figure B-5. Mean Sea Level Pressure (mb) for May.

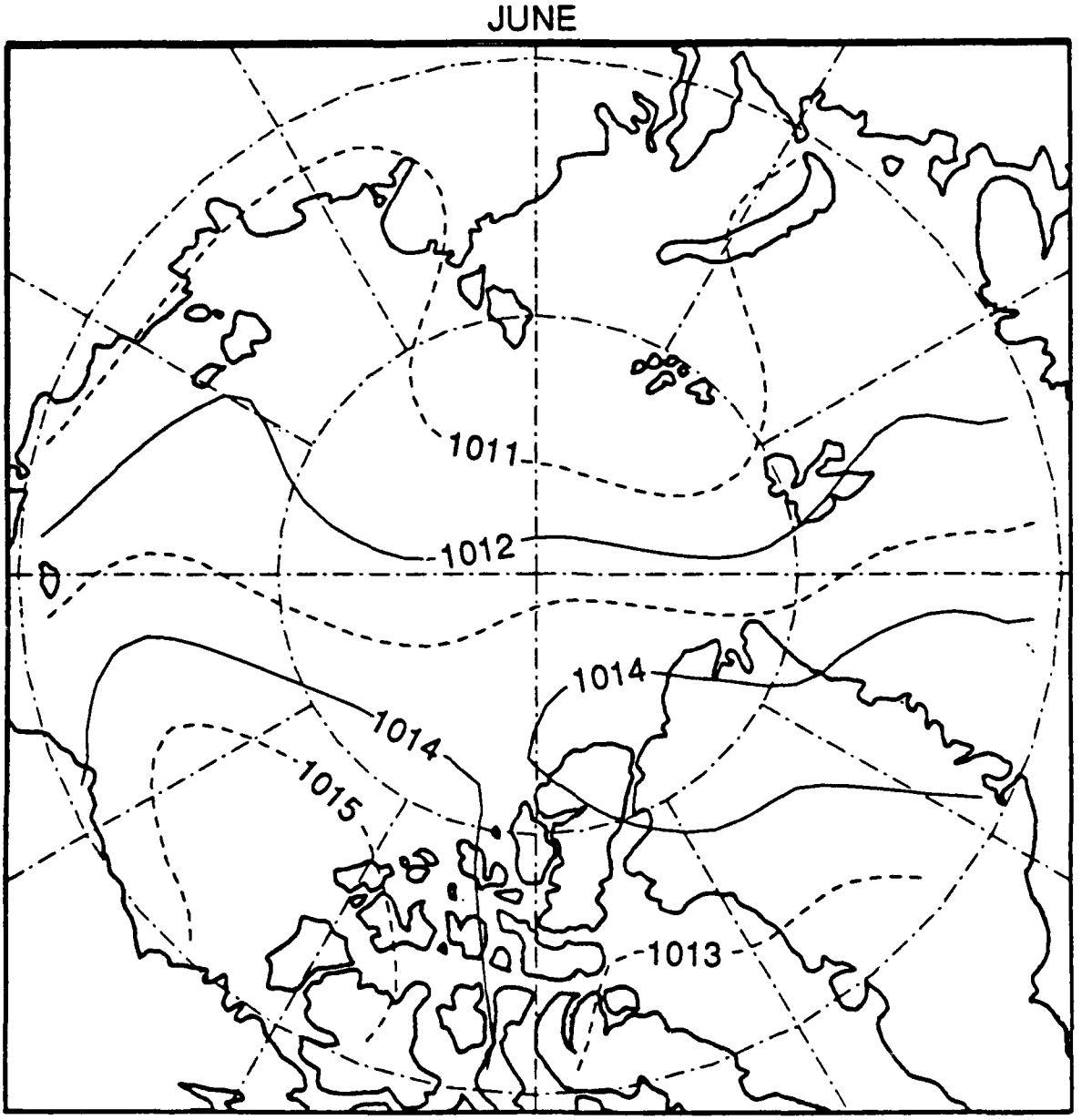

Figure B-6. Mean Sea Level Pressure (mb) for June.

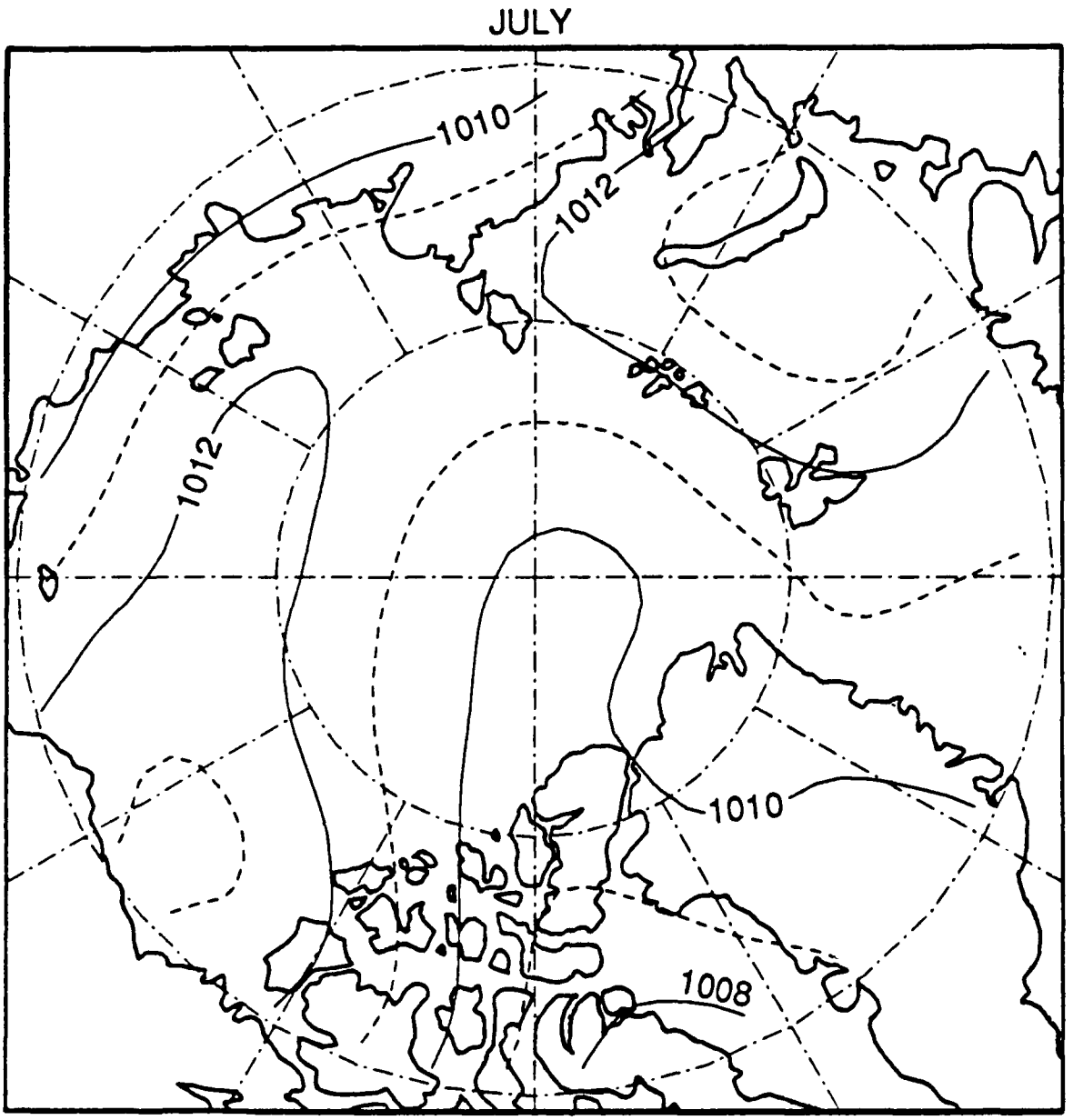

Figure B-7. Mean Sea Level Pressure (mb) for July.

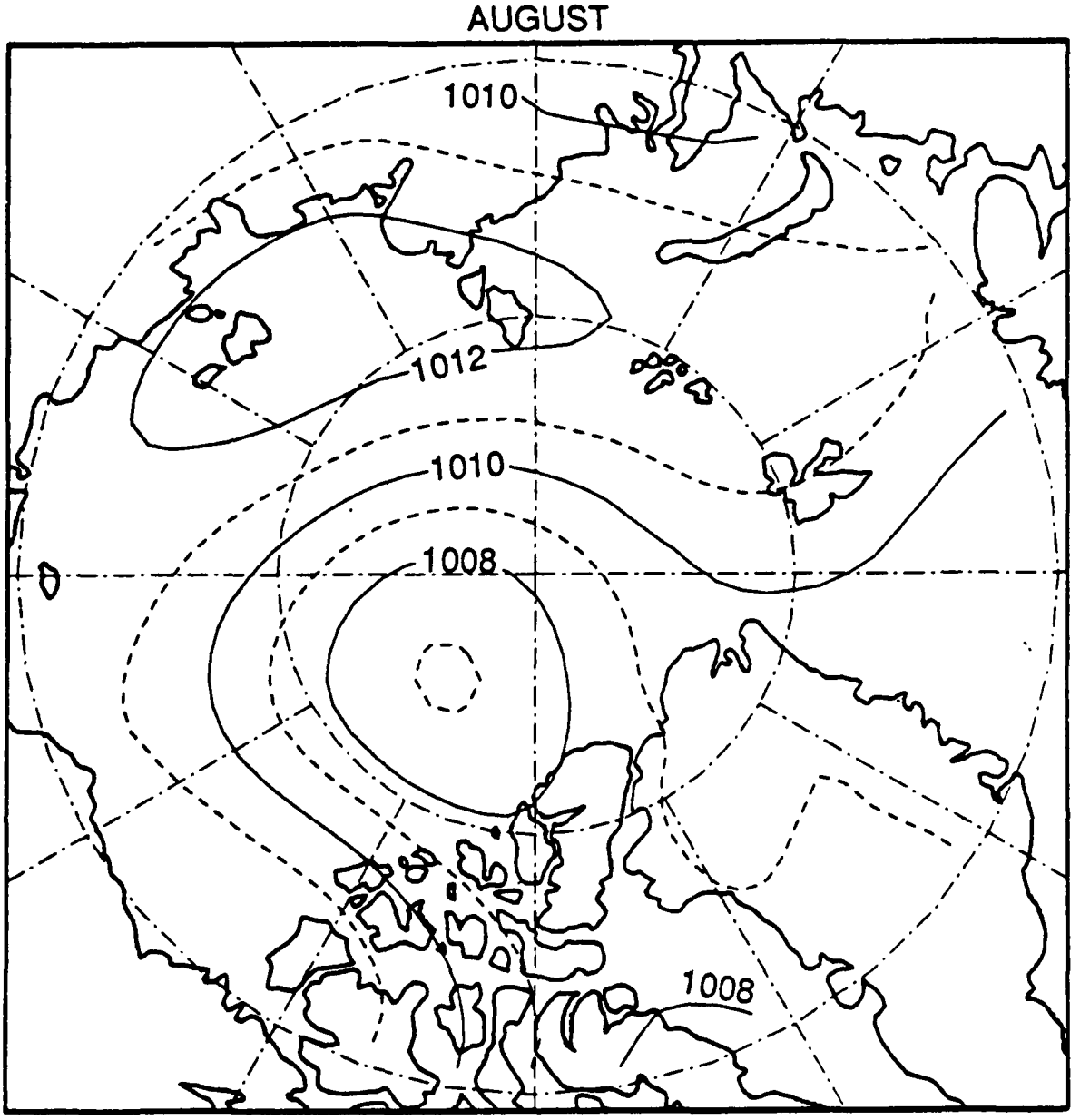

Figure B-8. Mean Sea Level Pressure (mb) for August.

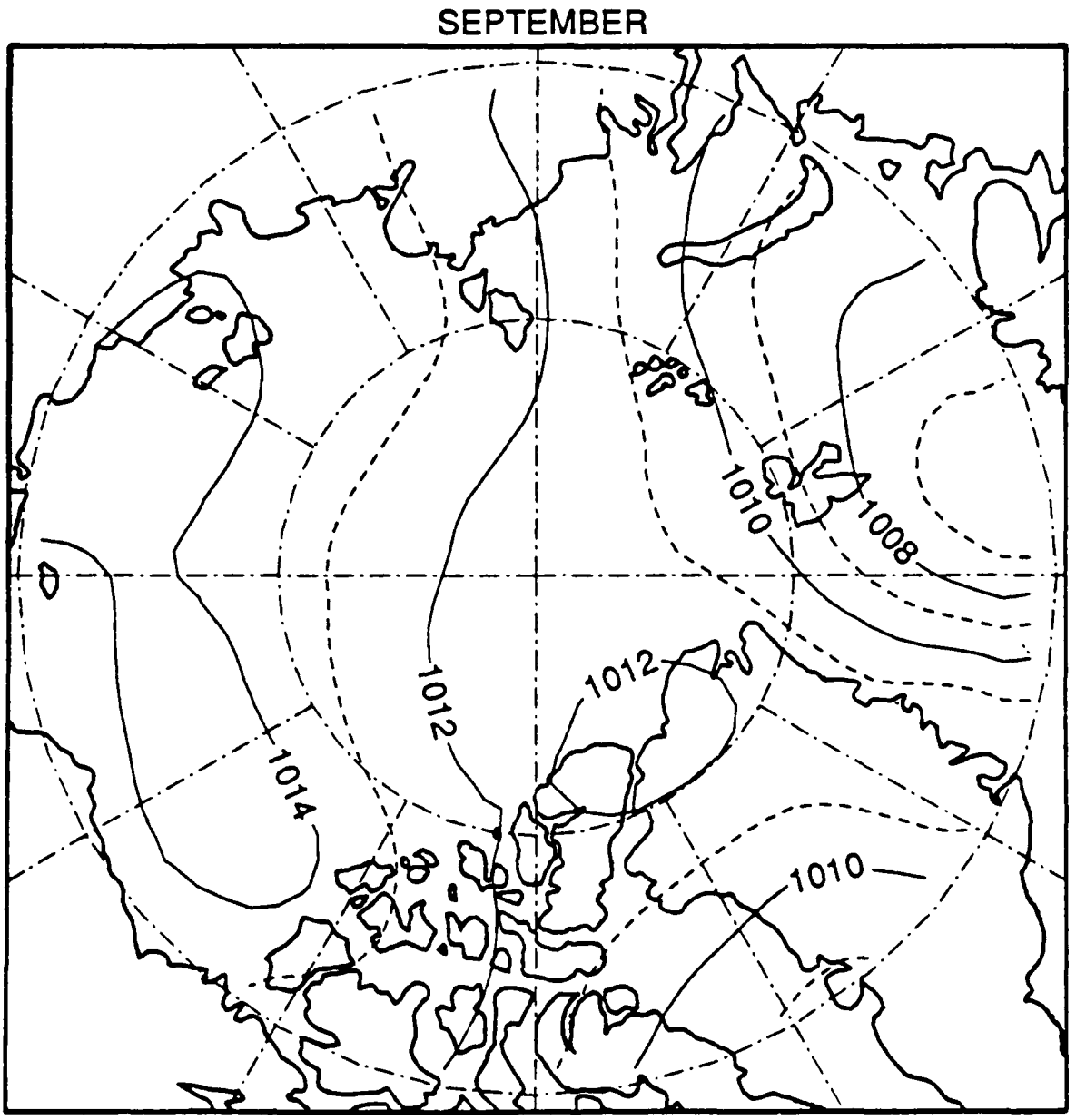

Figure B-9. Mean Sea Level Pressure (mb) for September.

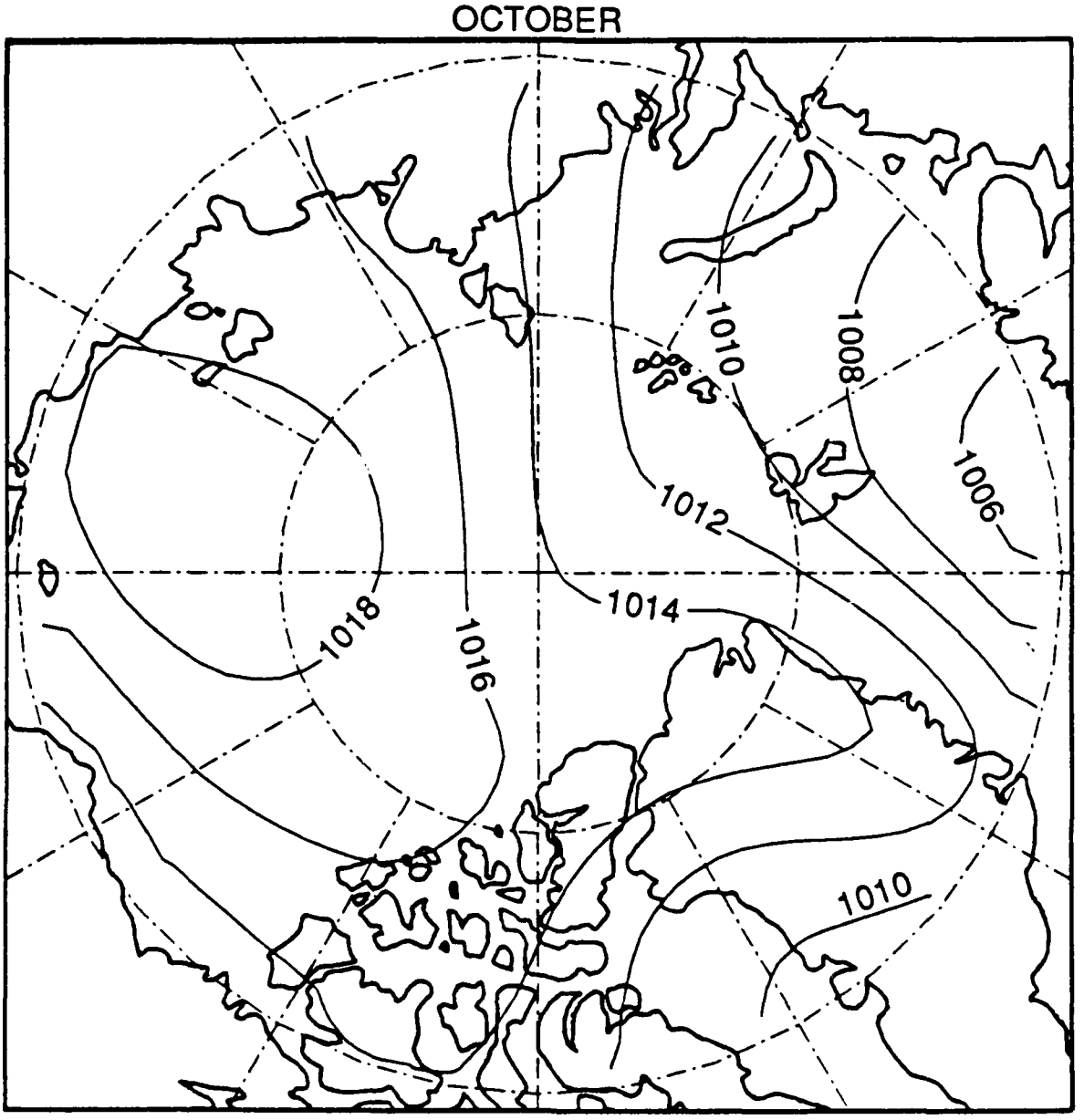

Figure B-10. Mean Sea Level Pressure (mb) for October.

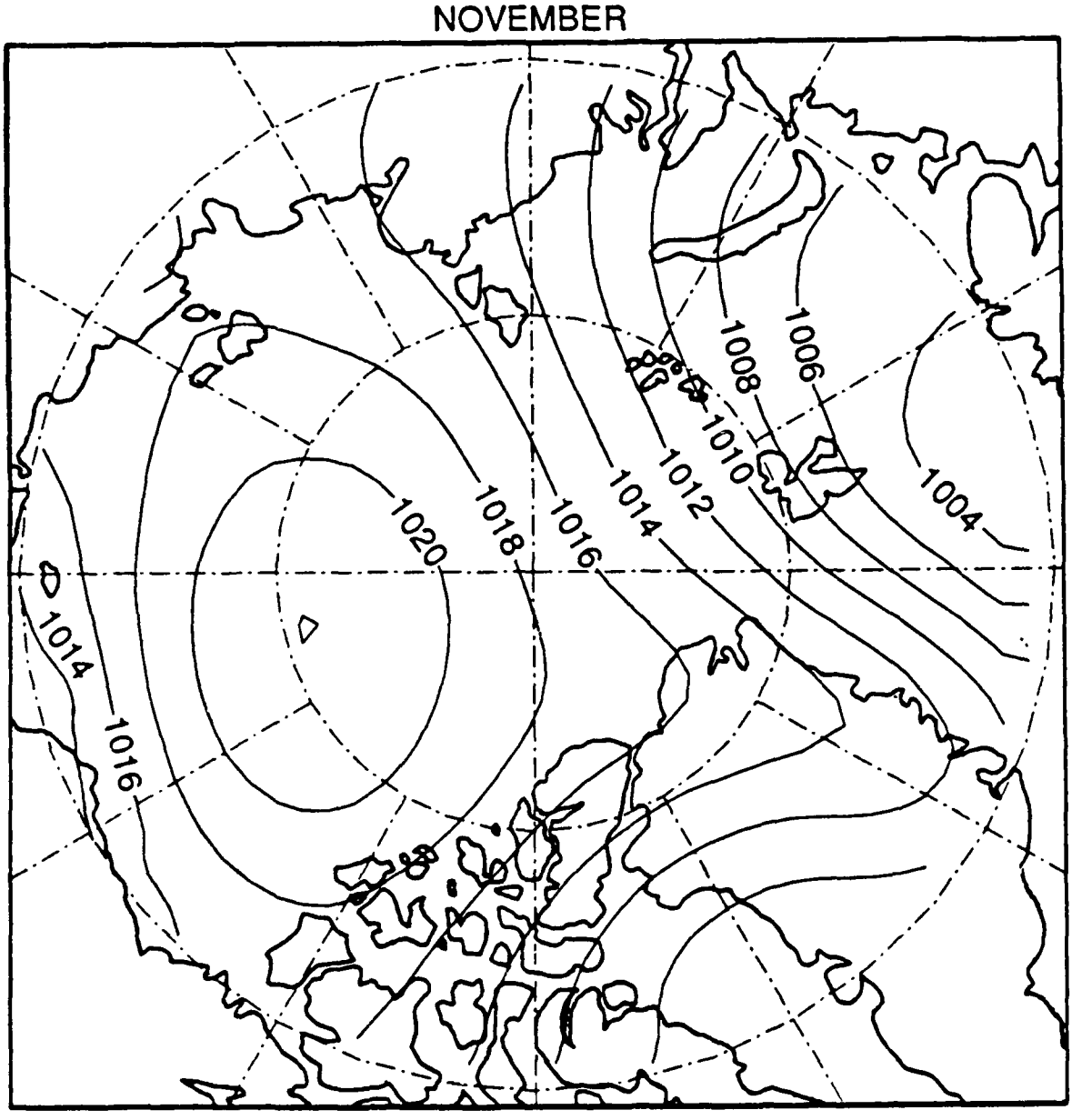

Figure B-11. Mean Sea Level Pressure (mb) for November.

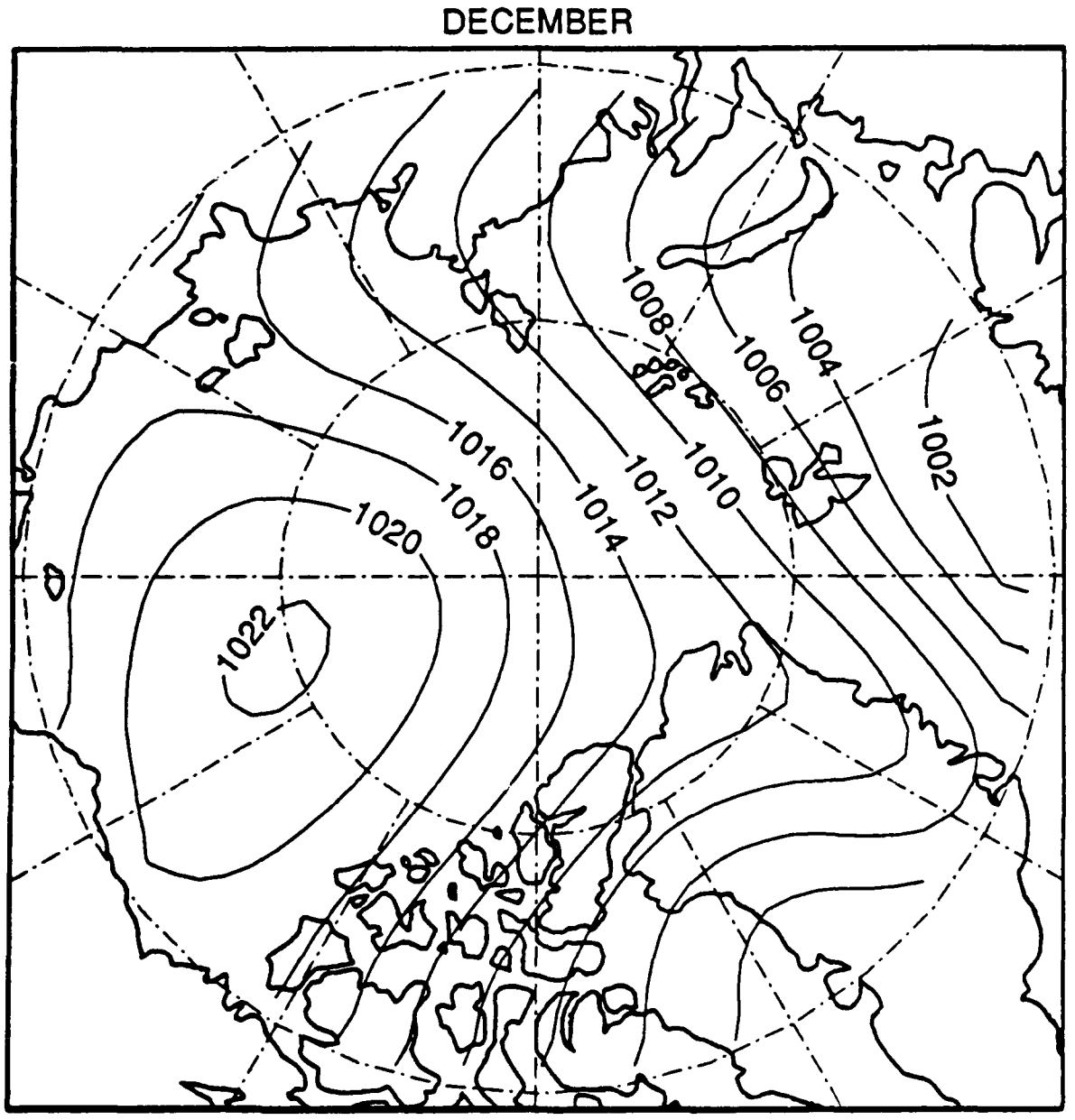

Figure B-12. Mean Sea Level Pressure (mb) for December.

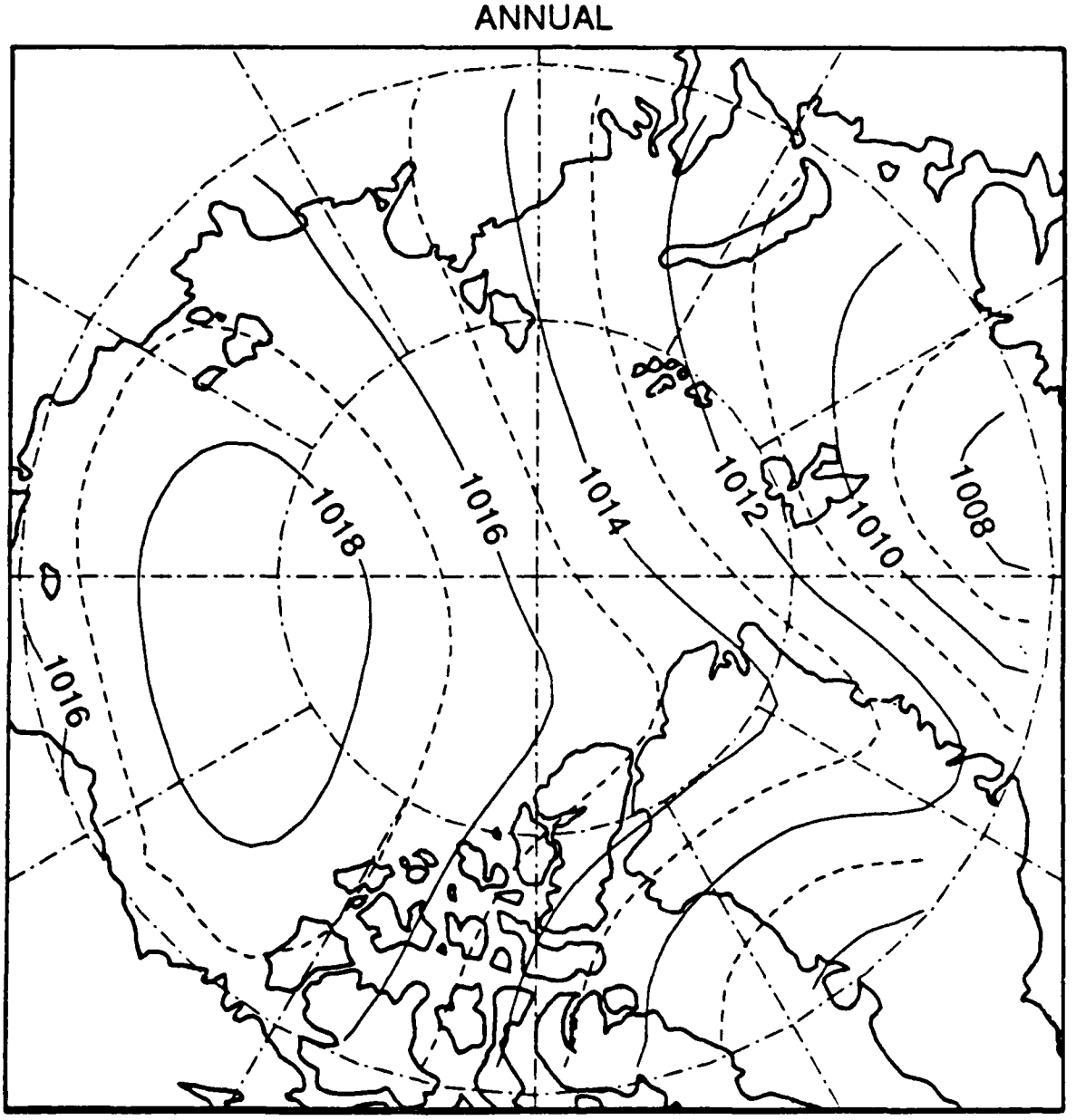

Figure B-13. Annual Mean Sea Level Pressure (mb).

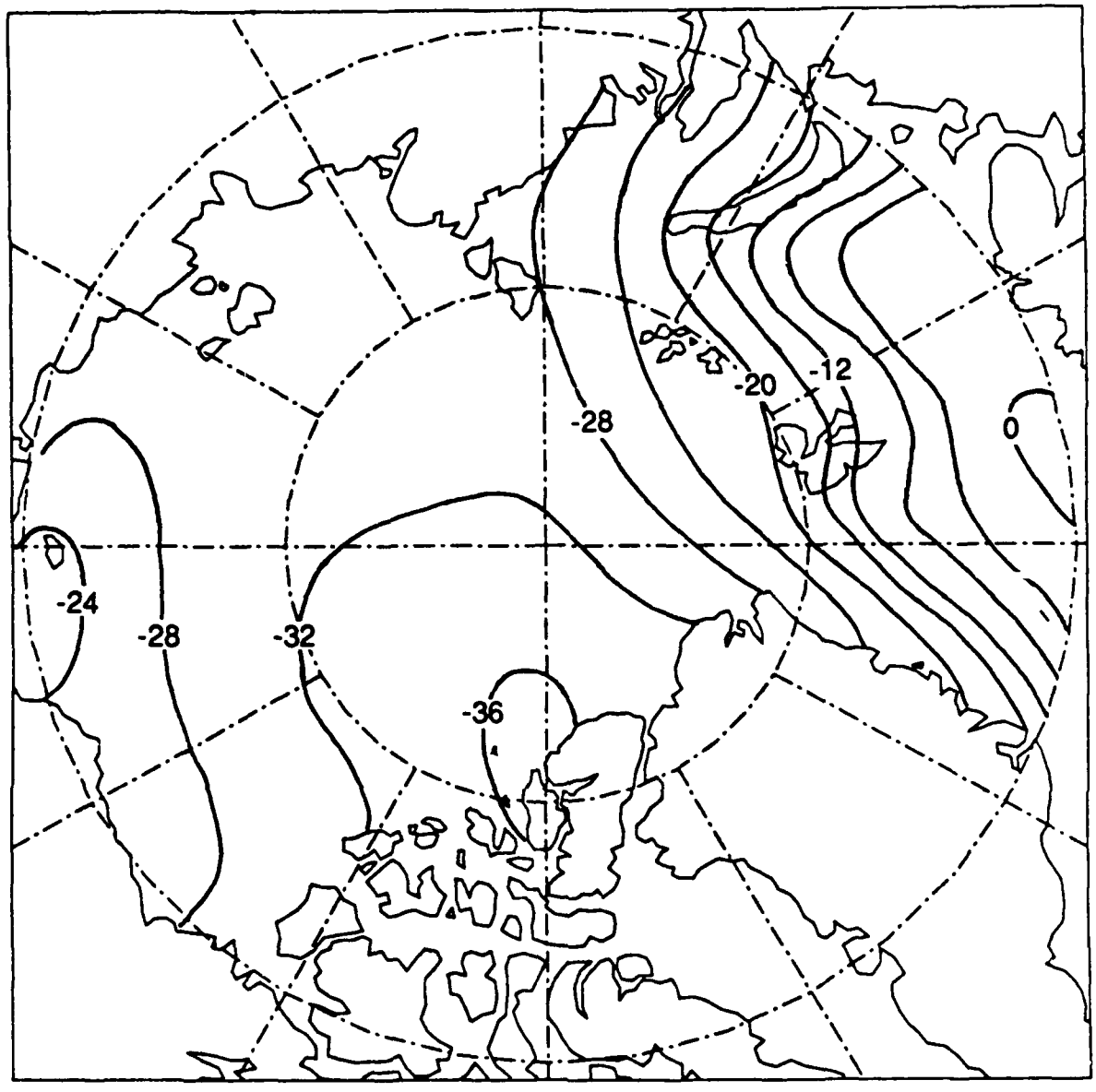

Figure B-14. Mean Surface Air Temperature (°C) for January.

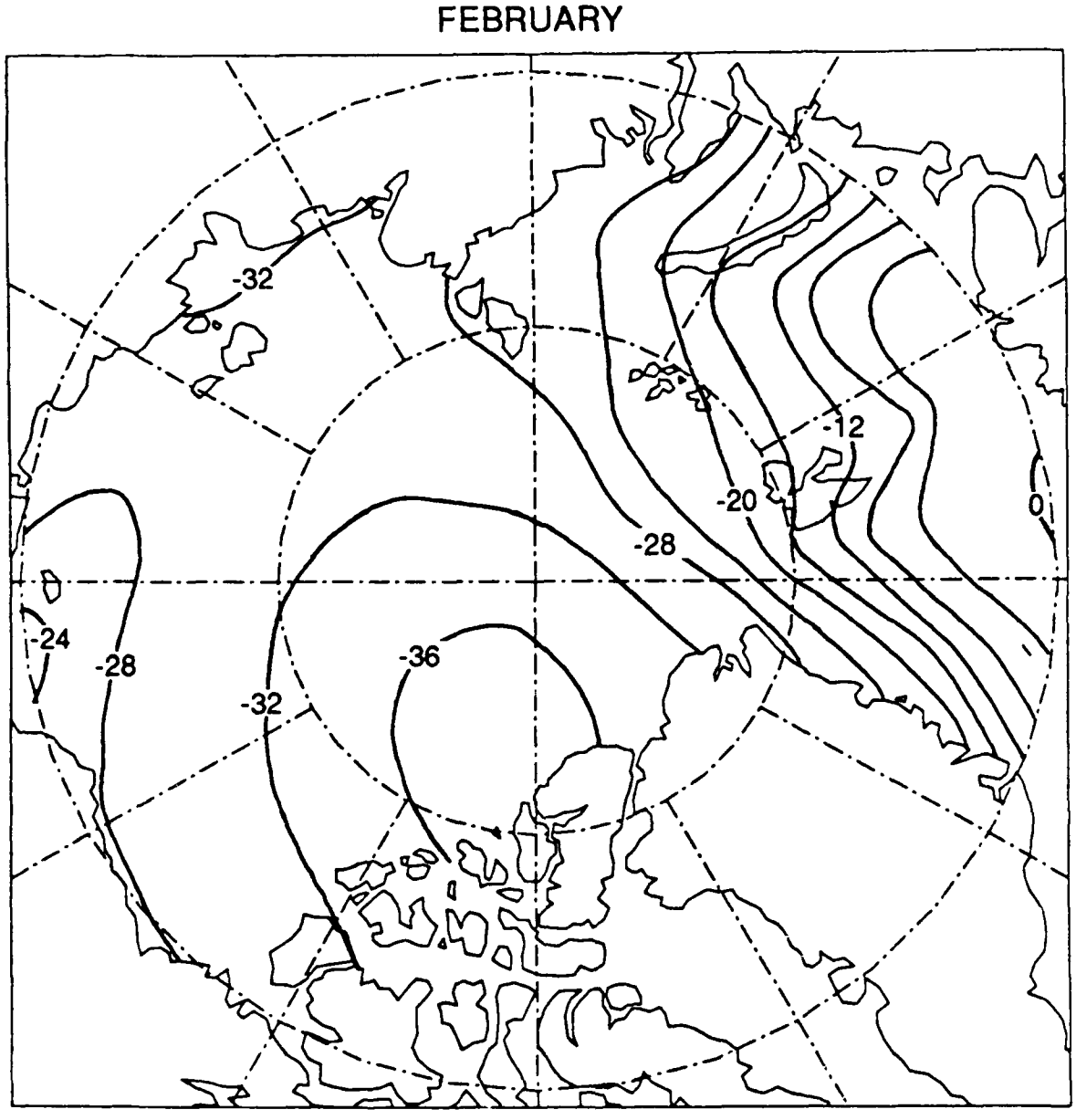

Figure B-15. Mean Surface Air Temperature (°C) for February.

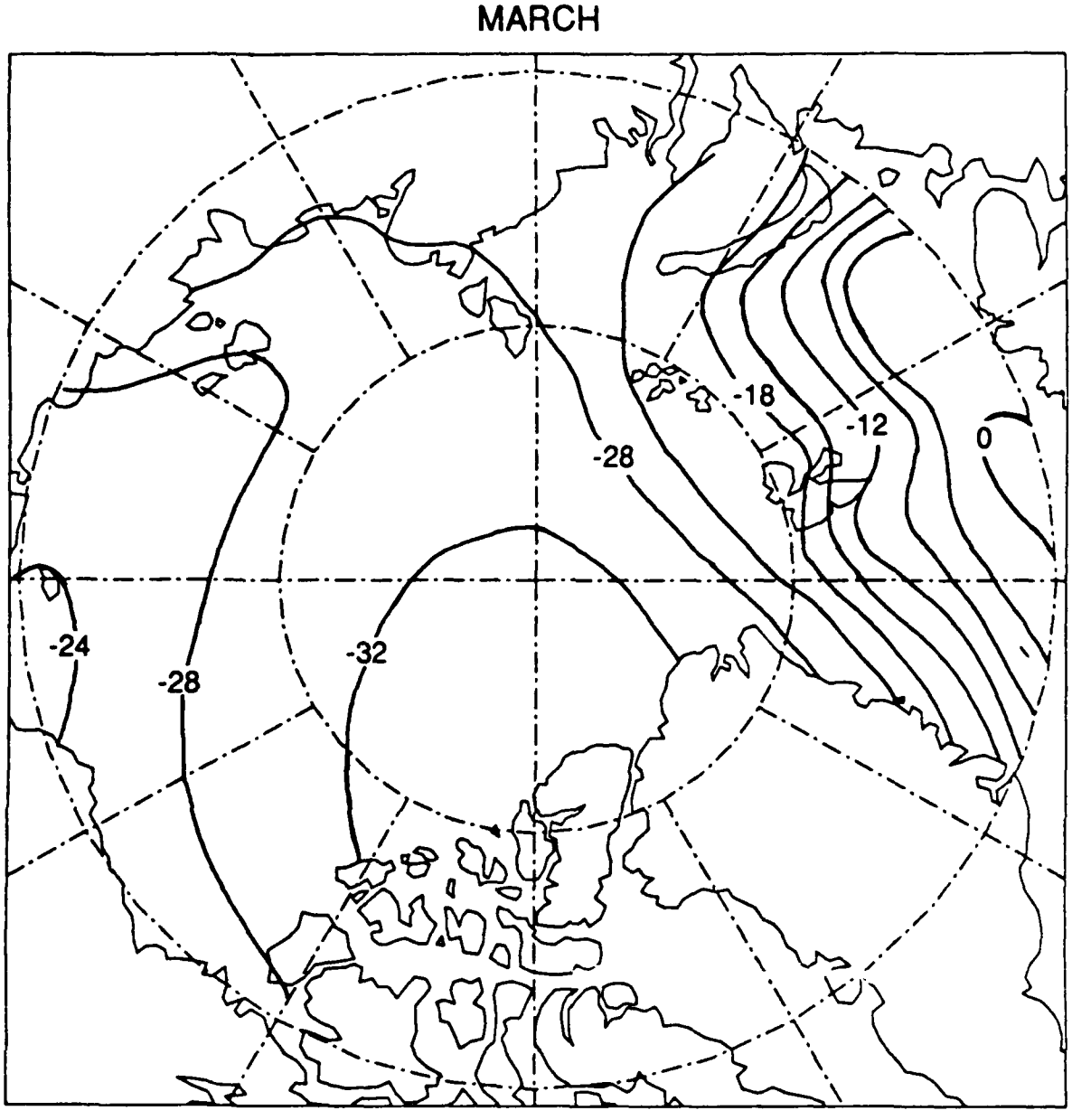

Figure B-16. Mean Surface Air Temperature (°C) for March.

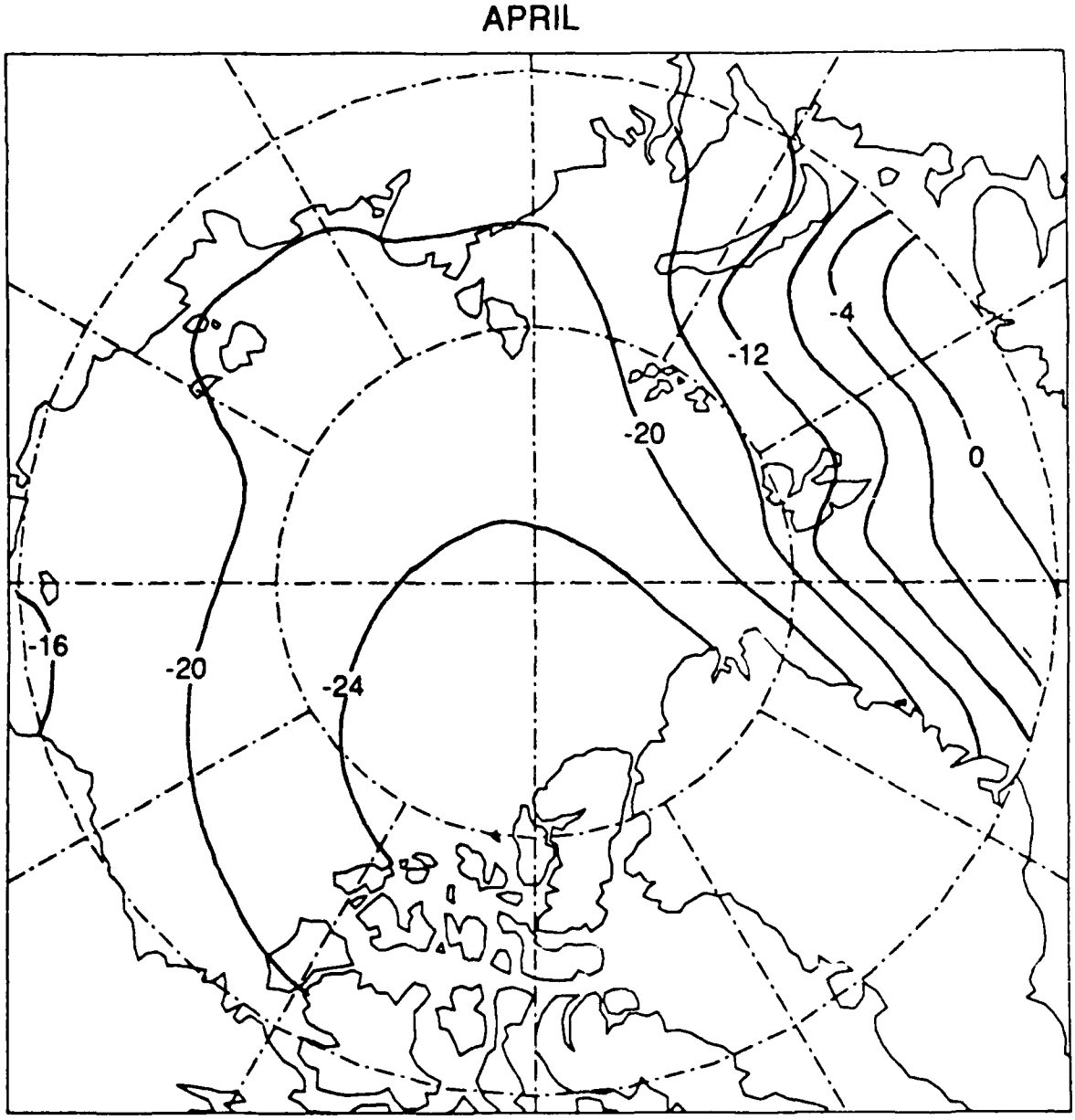

Figure B-17. Mean Surface Air Temperature (°C) for April.

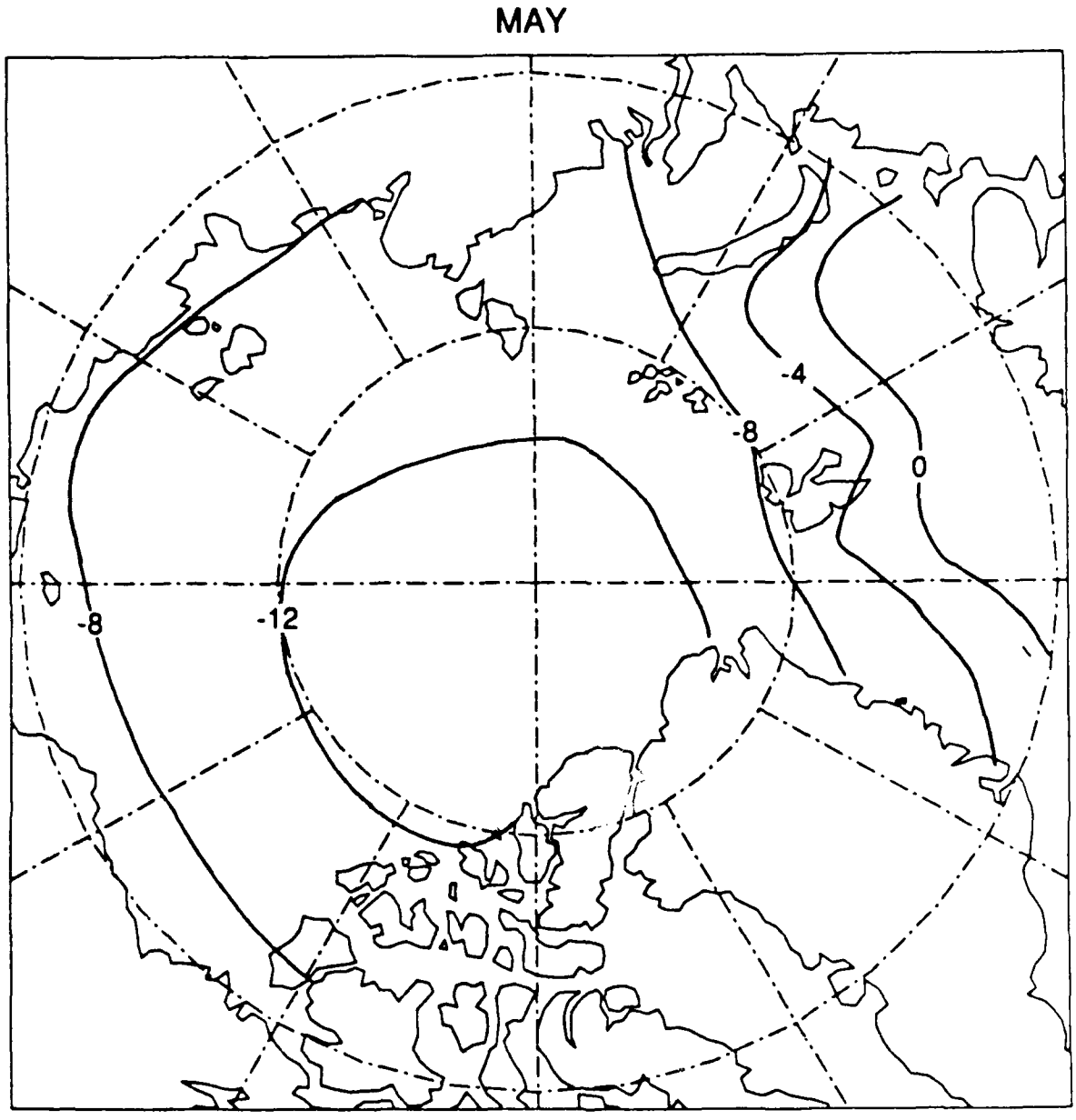

Figure B-18. Mean Surface Air Temperature (°C) for May.

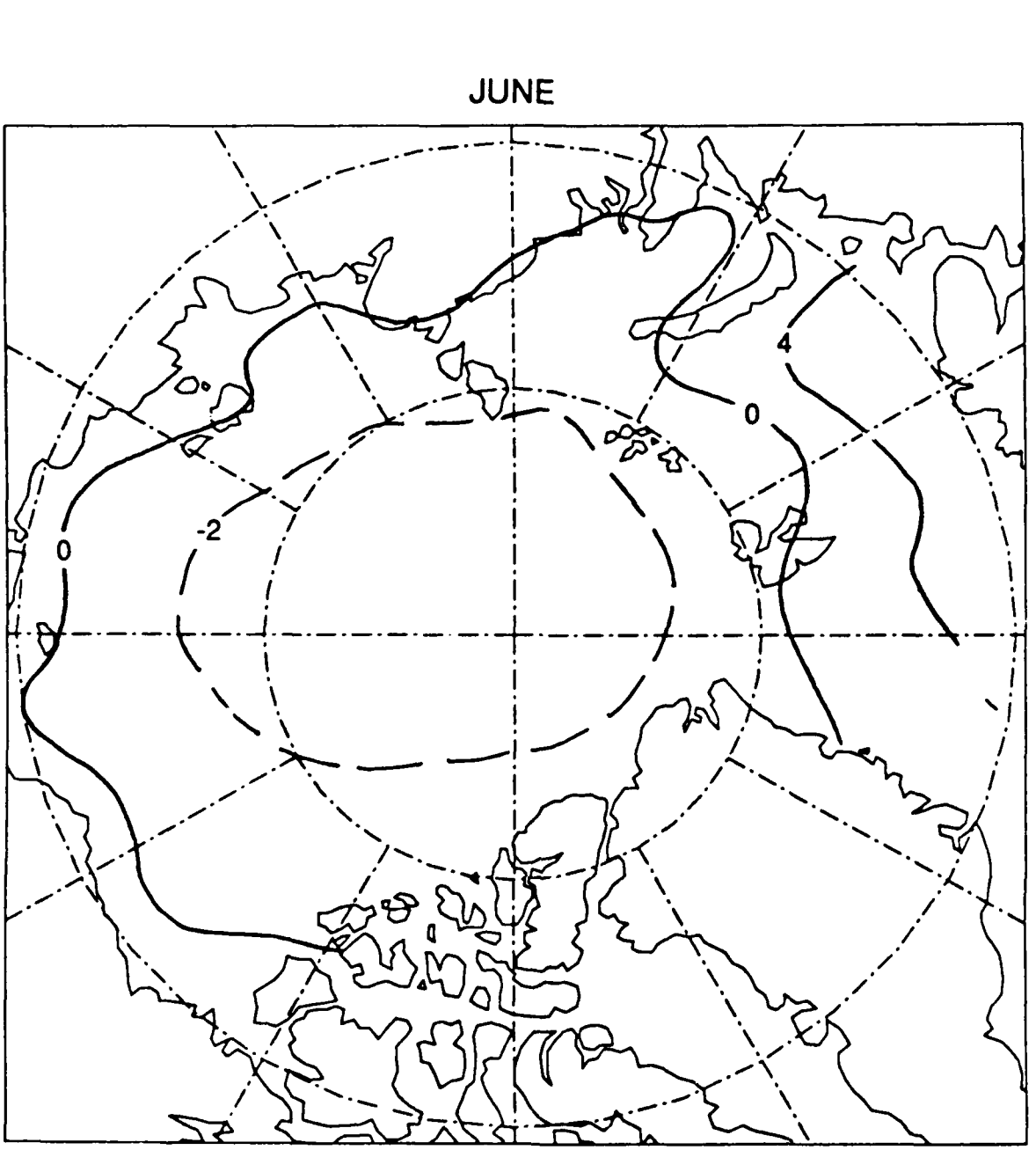

Figure B-19. Mean Surface Air Temperature (°C) for June.

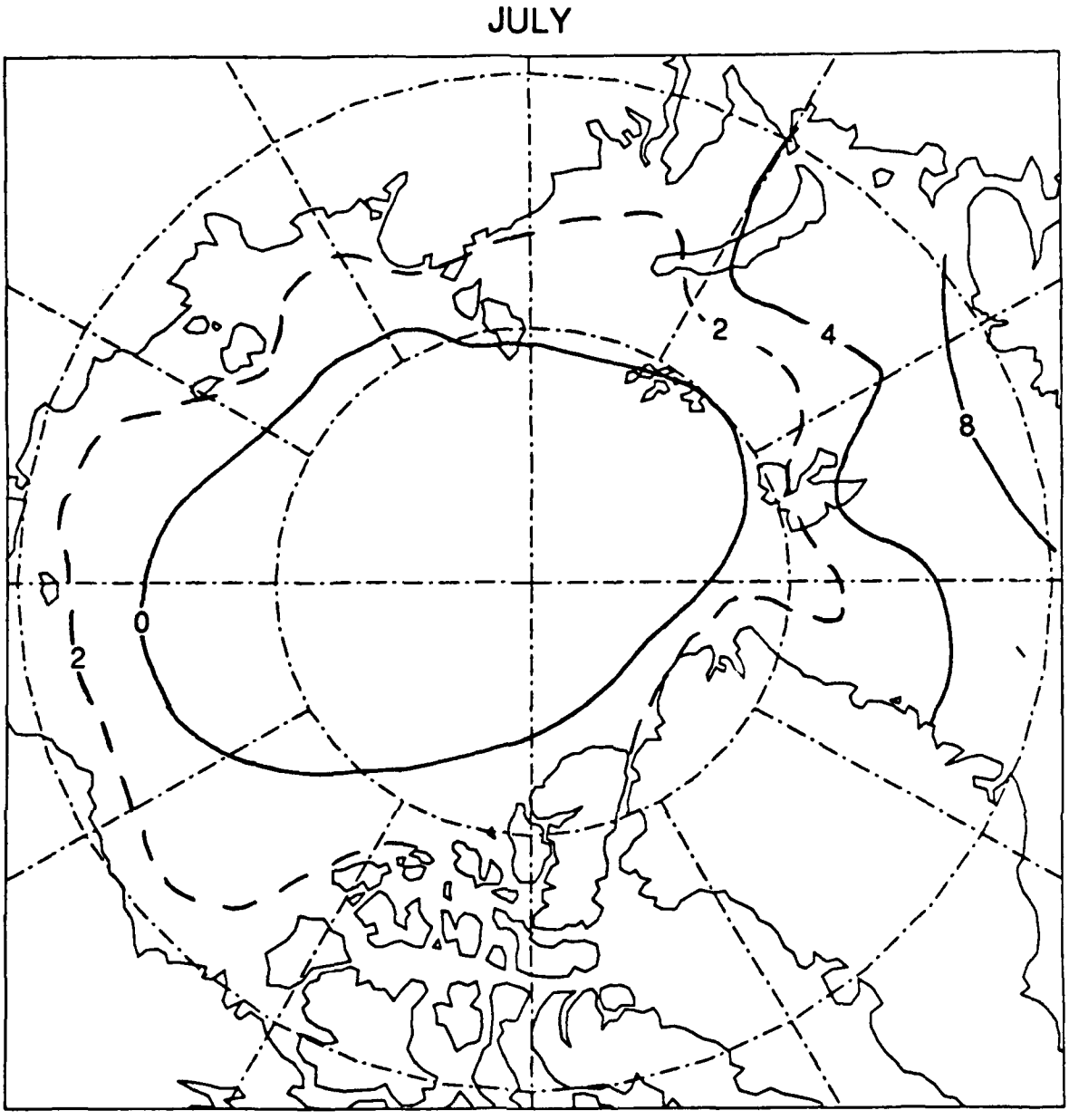

Figure B-20. Mean Surface Air Temperature (°C) for July.

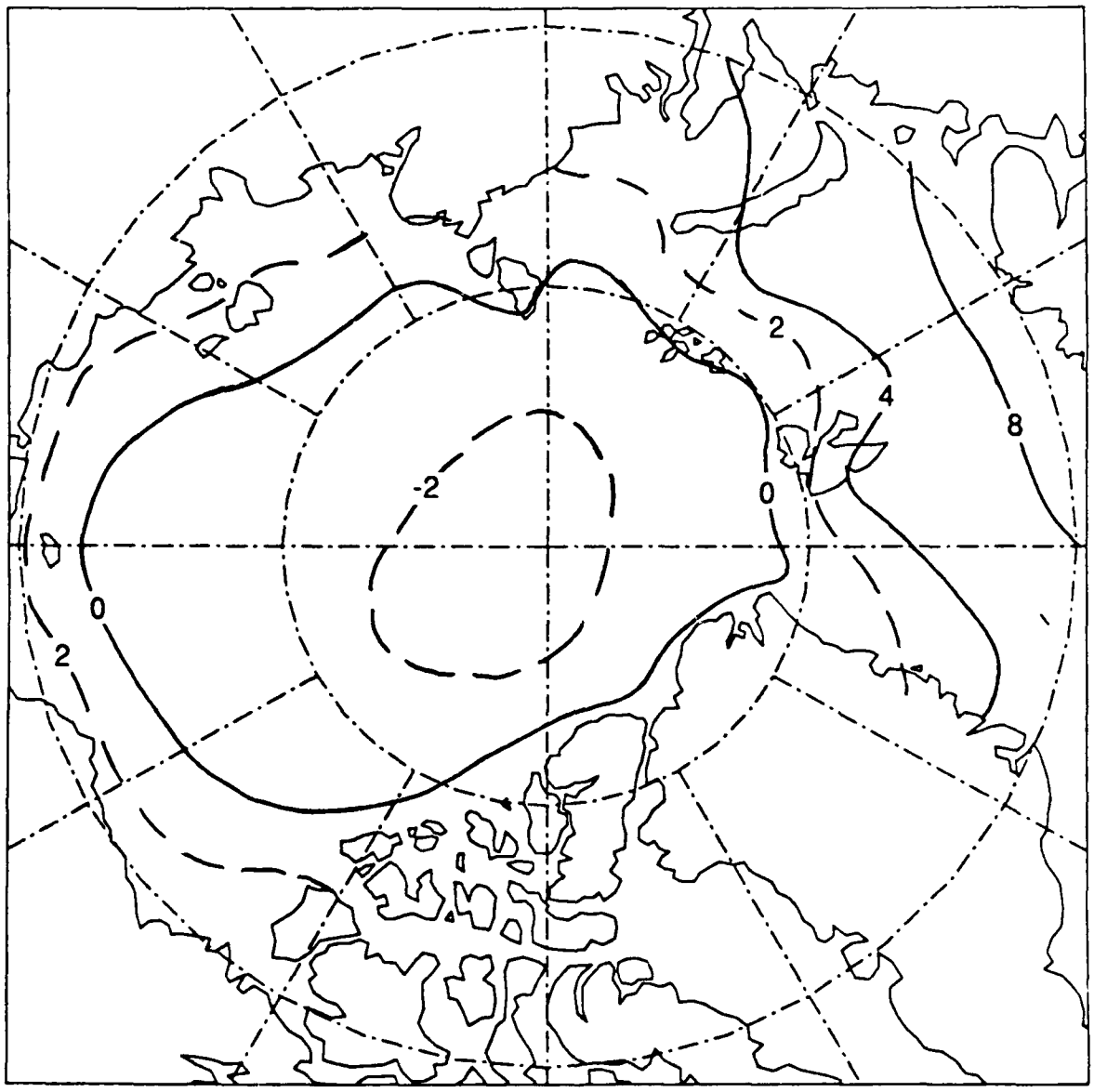

Figure B-21. Mean Surface Air Temperature (°C) for August.

SEPTEMBER

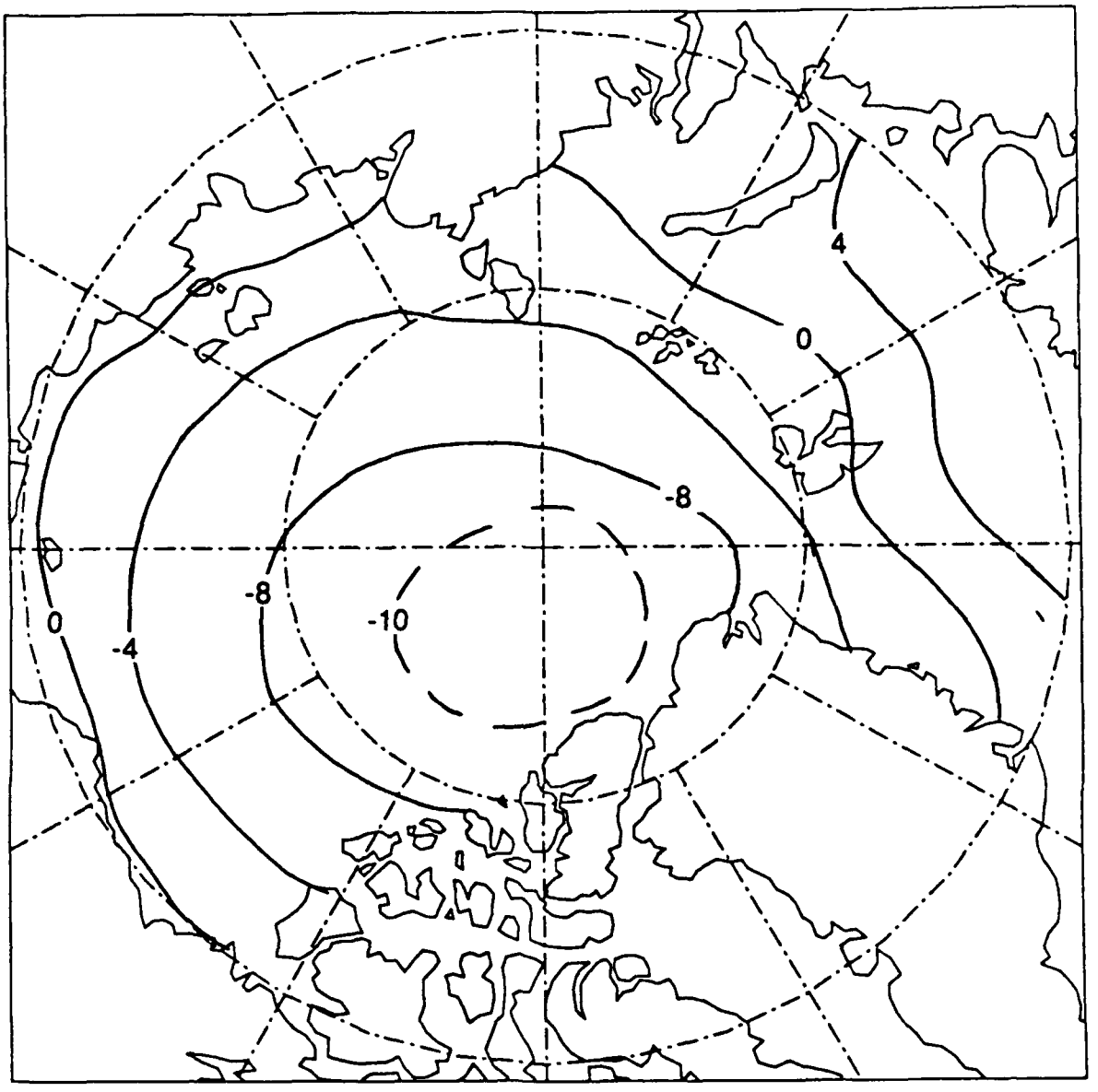

Figure B-22. Mean Surface Air Temperature (°C) for September.

OCTOBER

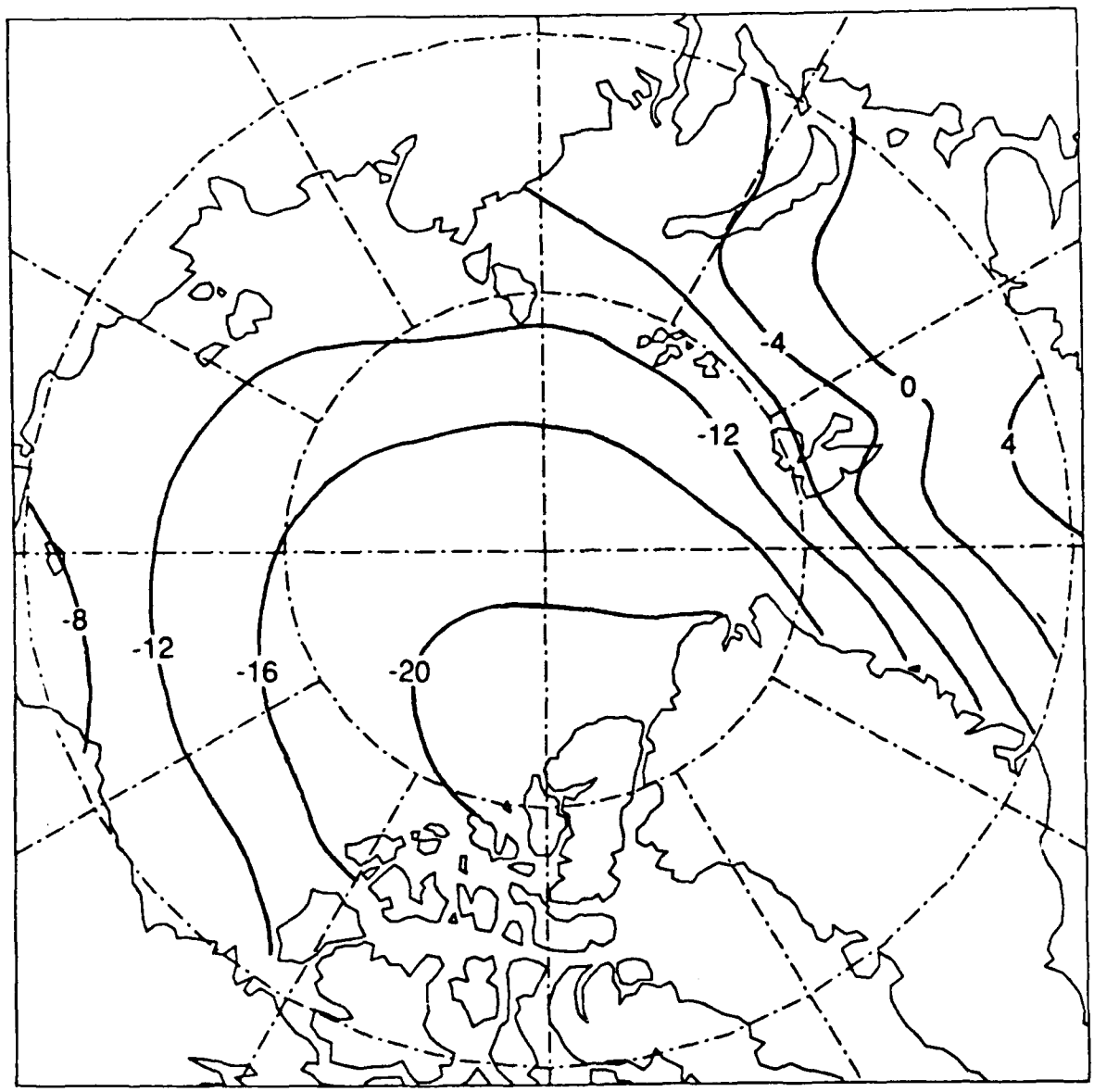

Figure B-23. Mean Surface Air Temperature (°C) for October.

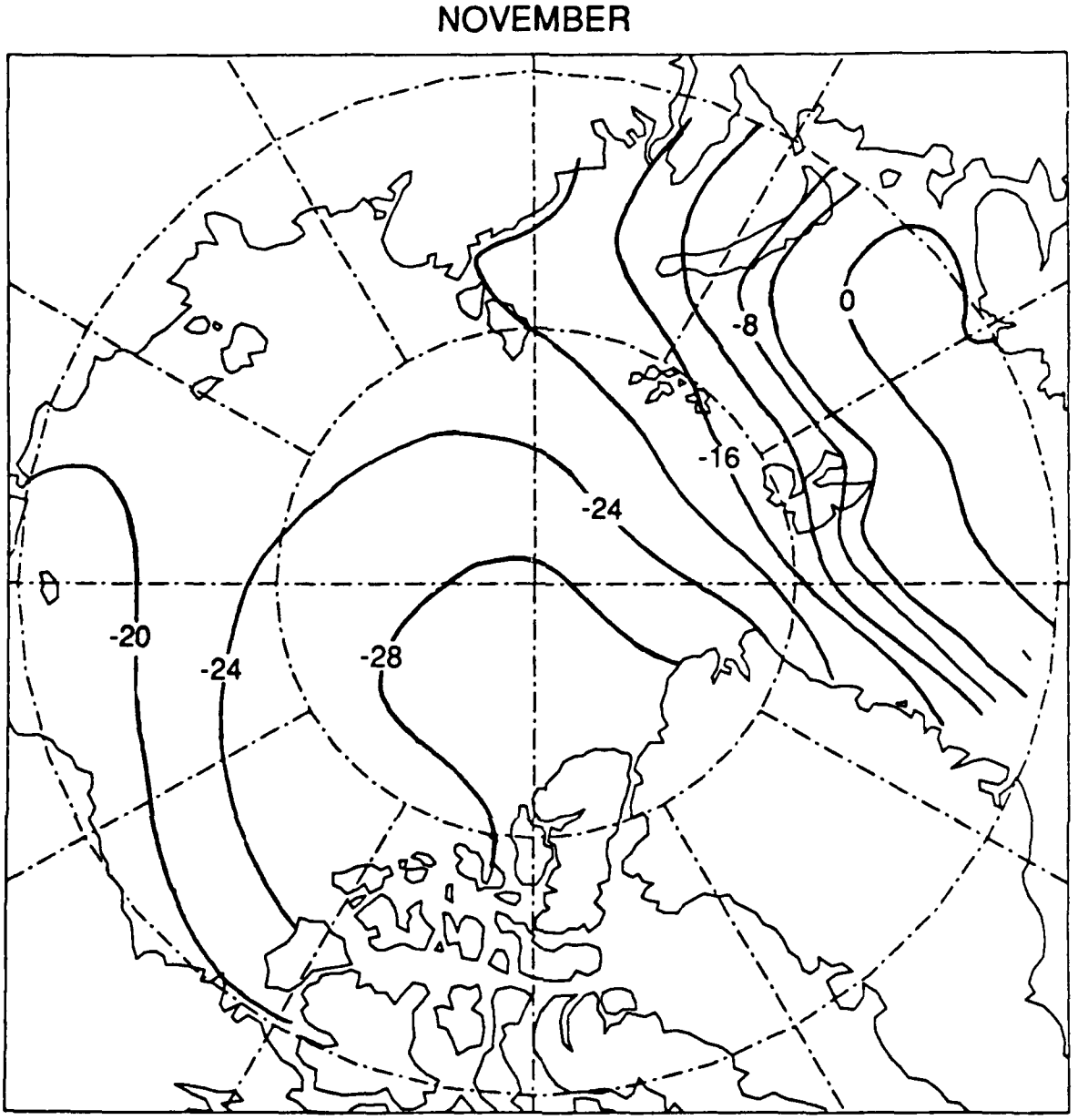

Figure B-24. Mean Surface Air Temperature (°C) for November.

DECEMBER

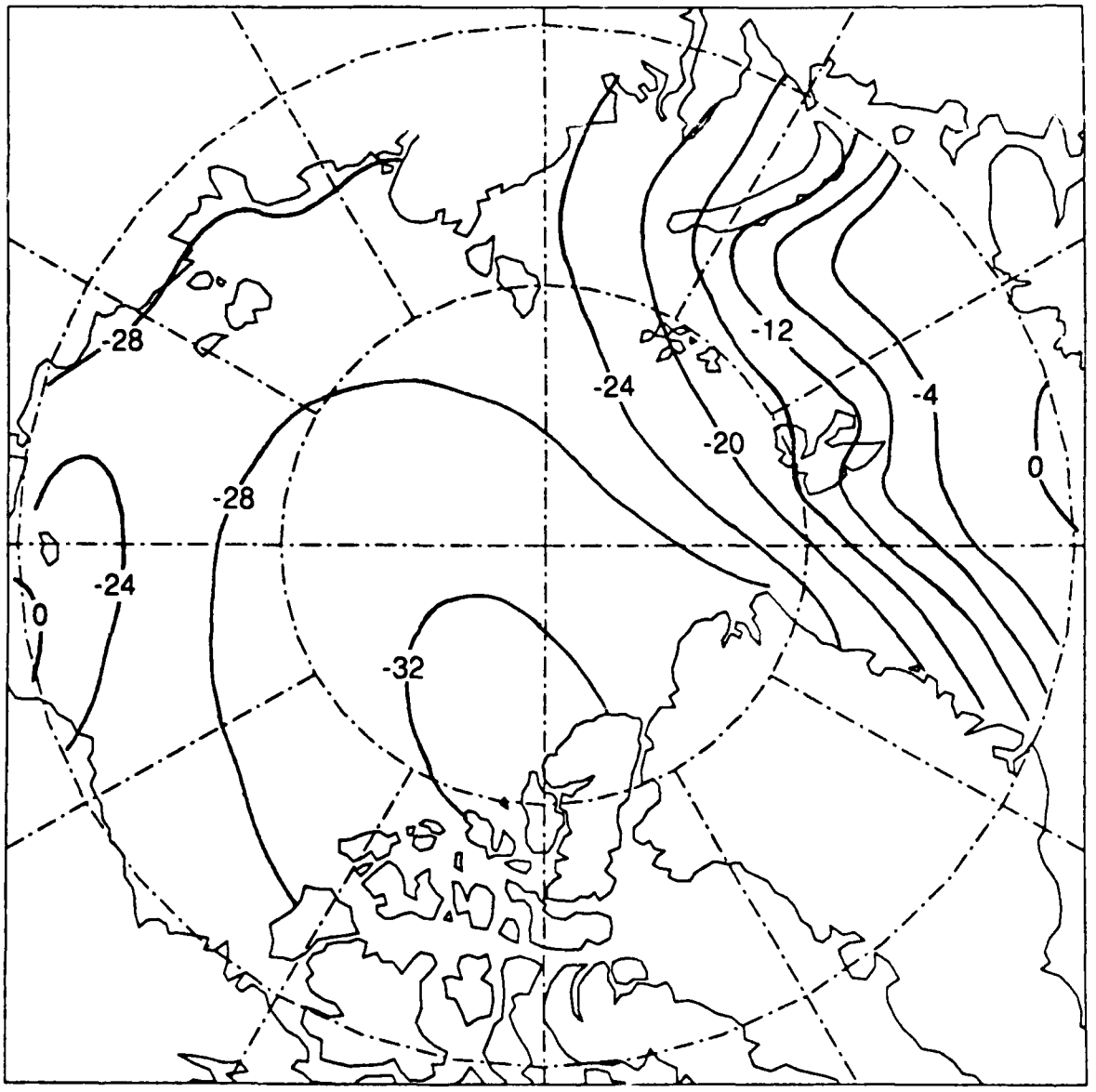

Figure B-25. Mean Surface Air Temperature (°C) for December.

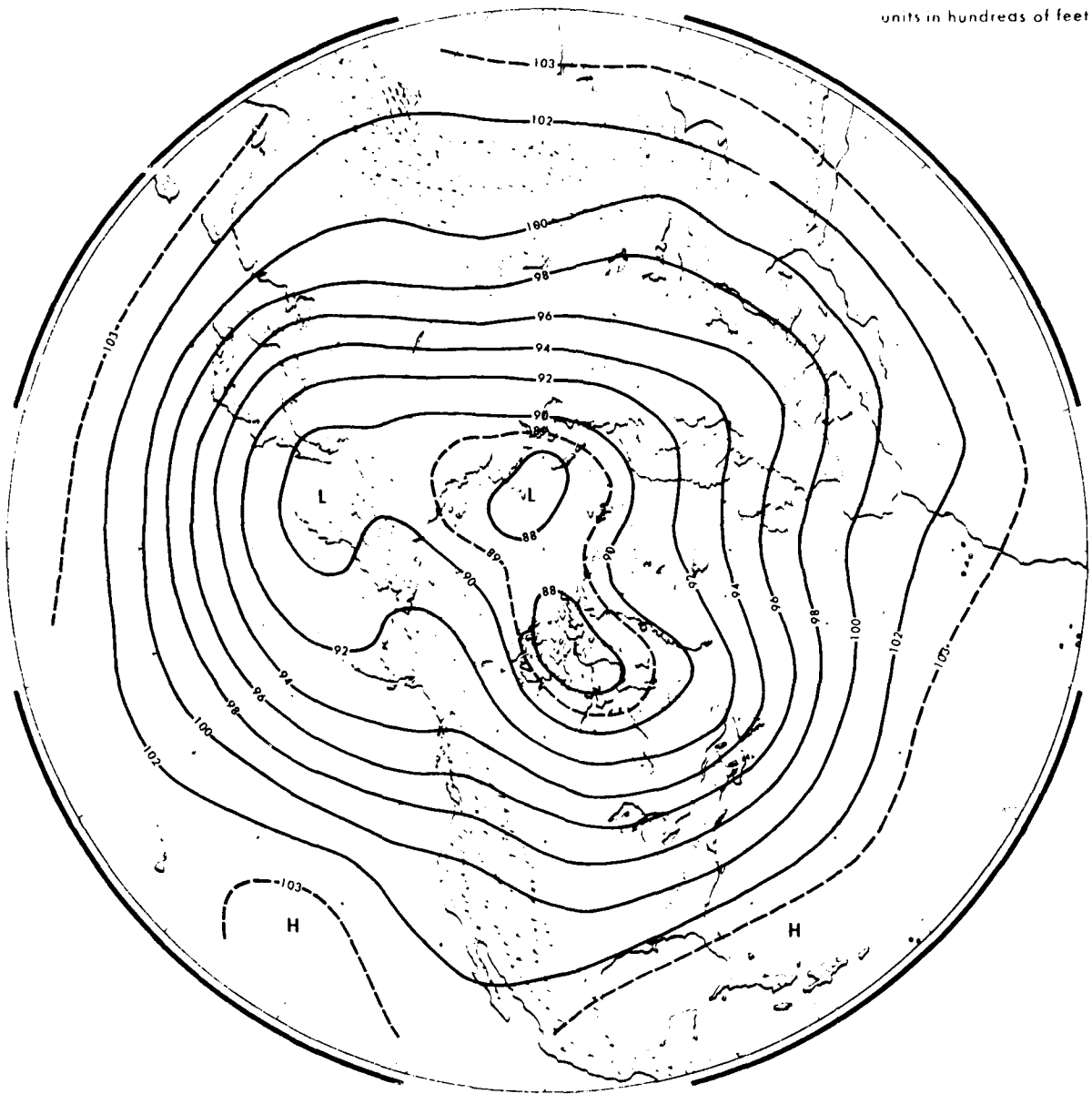

Figure B-26. Mean Height of the 700-mb Pressure Surface for January.

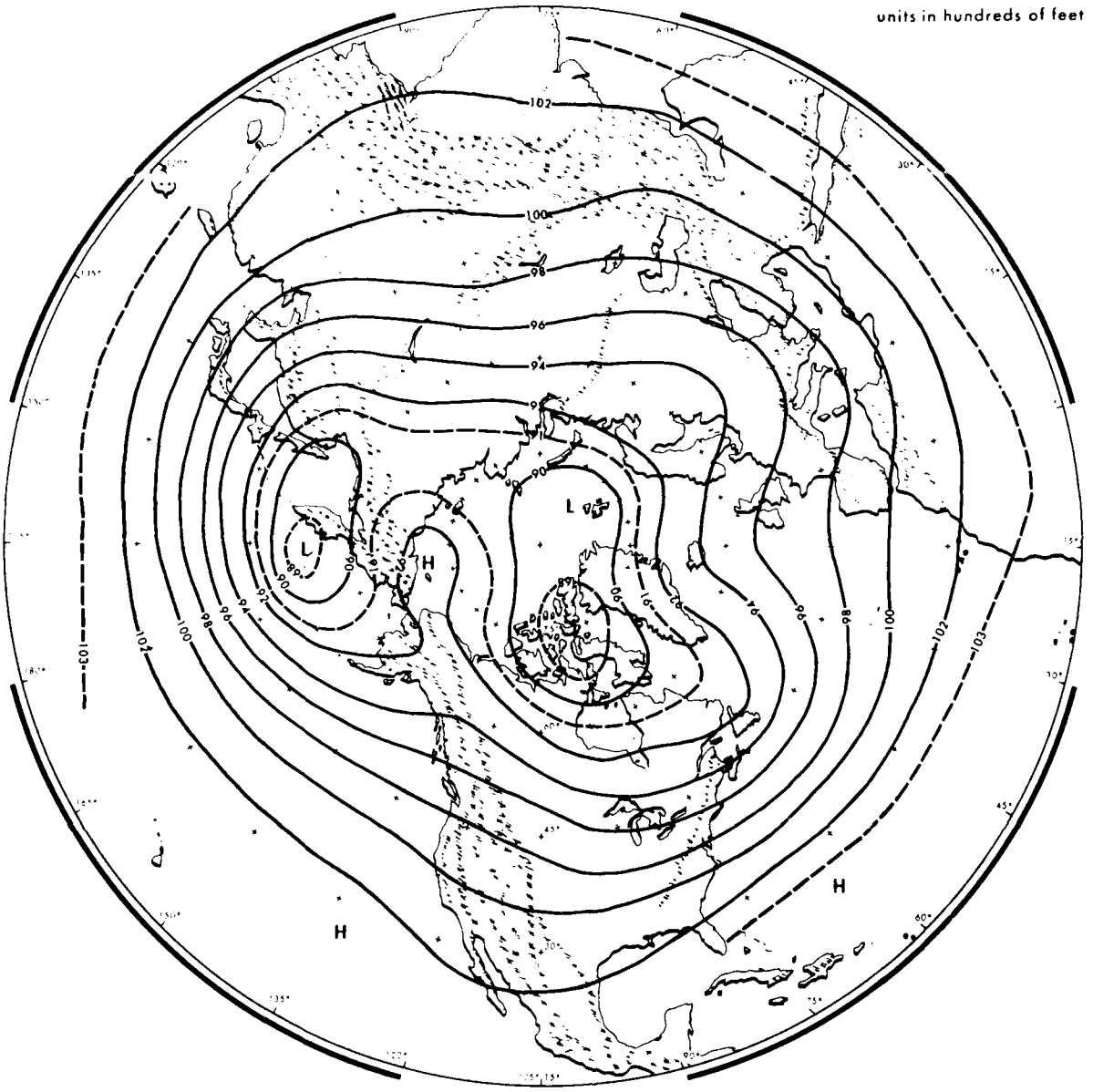

Figure B-27. Mean Height of the 700-mb Pressure Surface for February.

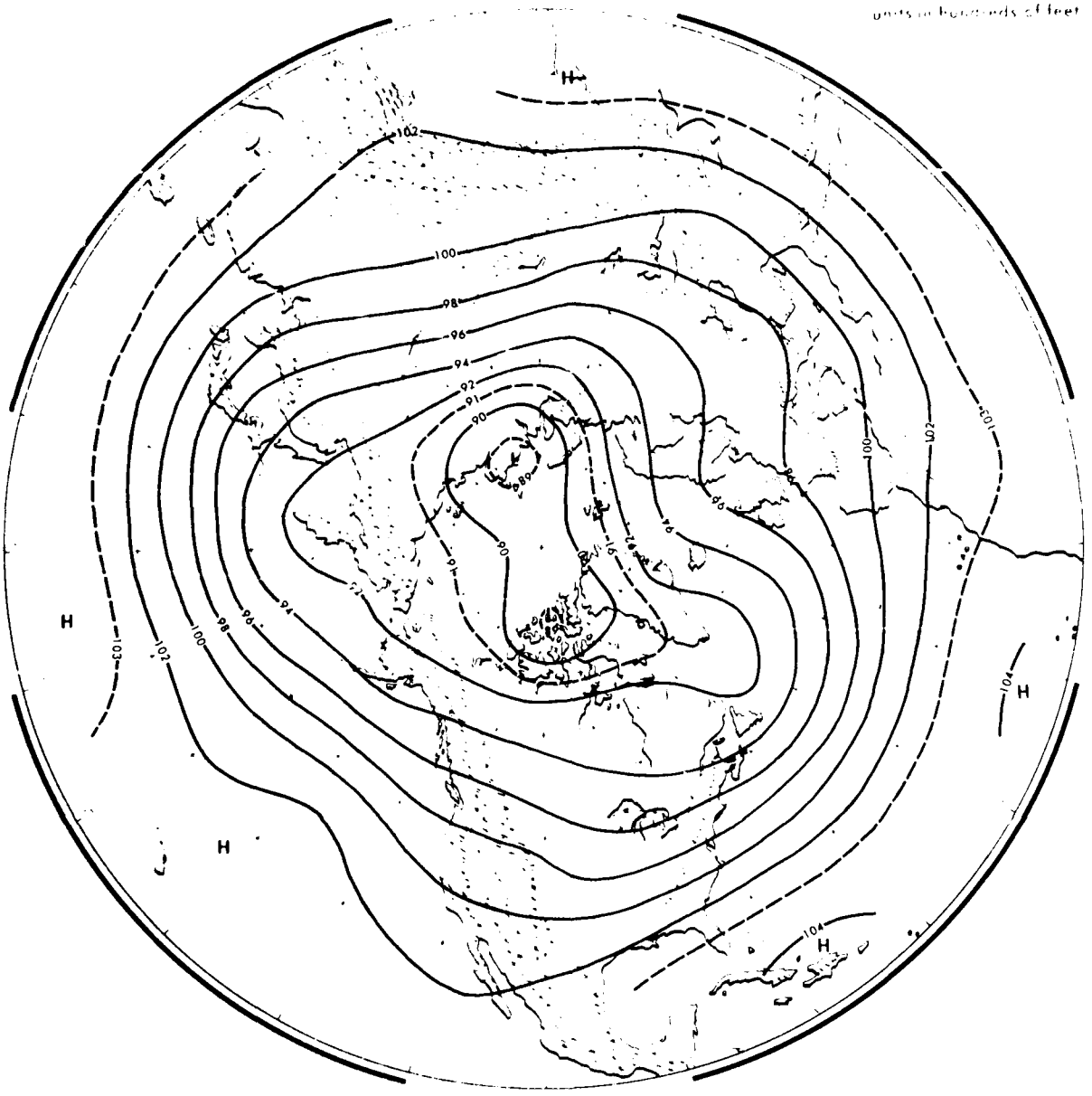

Figure B-28. Mean Height of the 700-mb Pressure Surface for March.

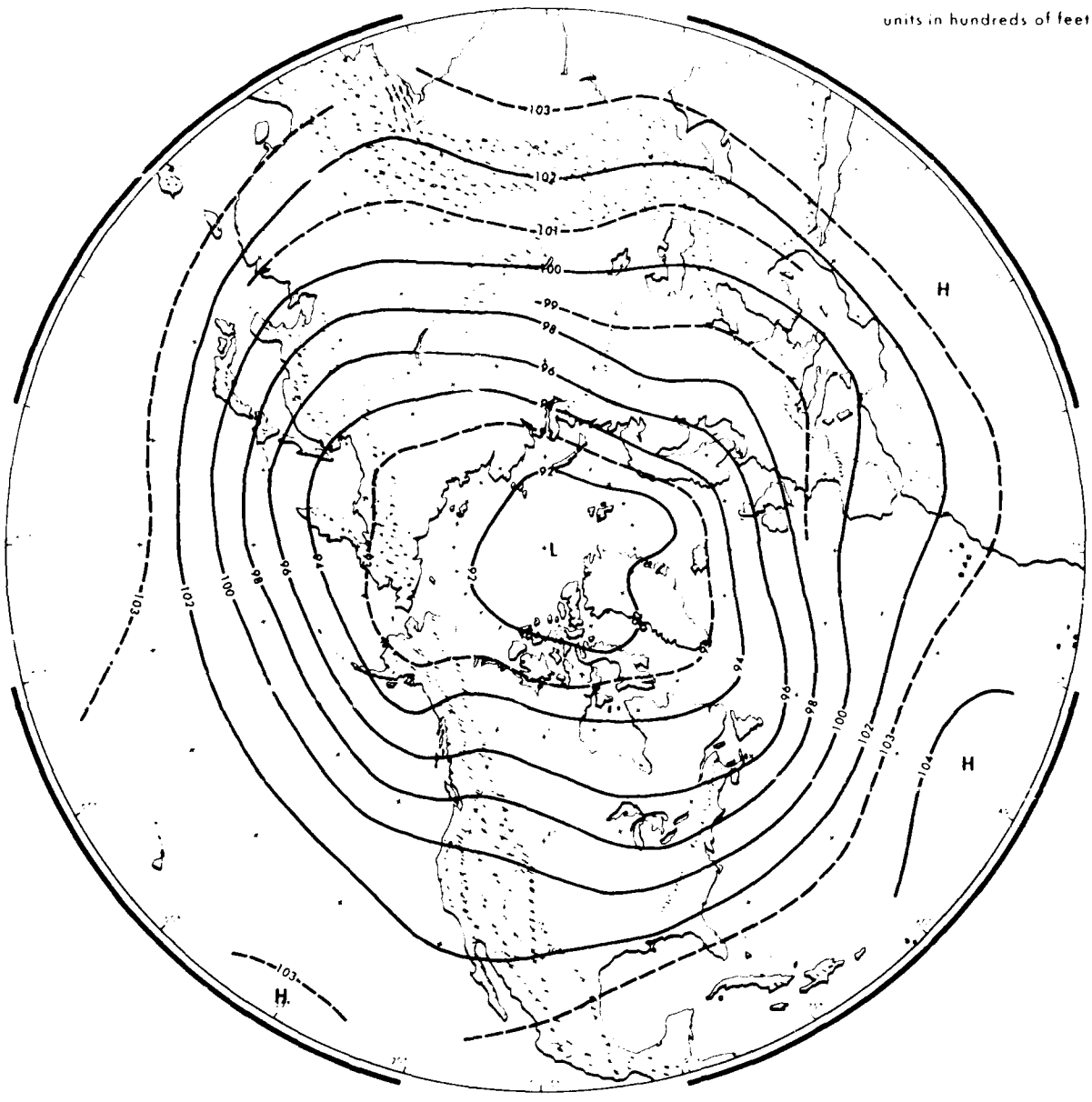

Figure B-29. Mean Height of the 700-mb Pressure Surface for April.

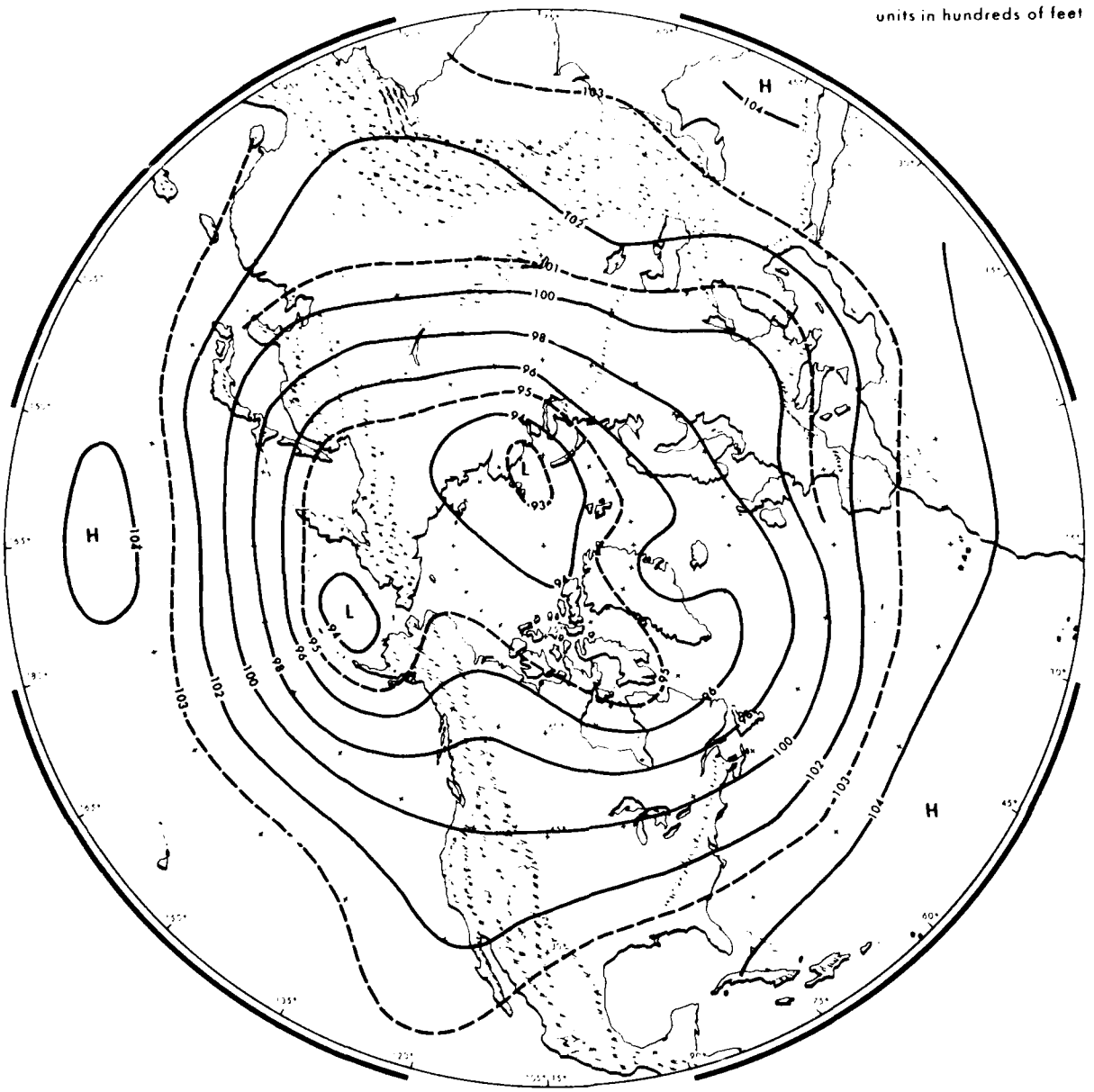

Figure B-30. Mean Height of the 700-mb Pressure Surface for May.

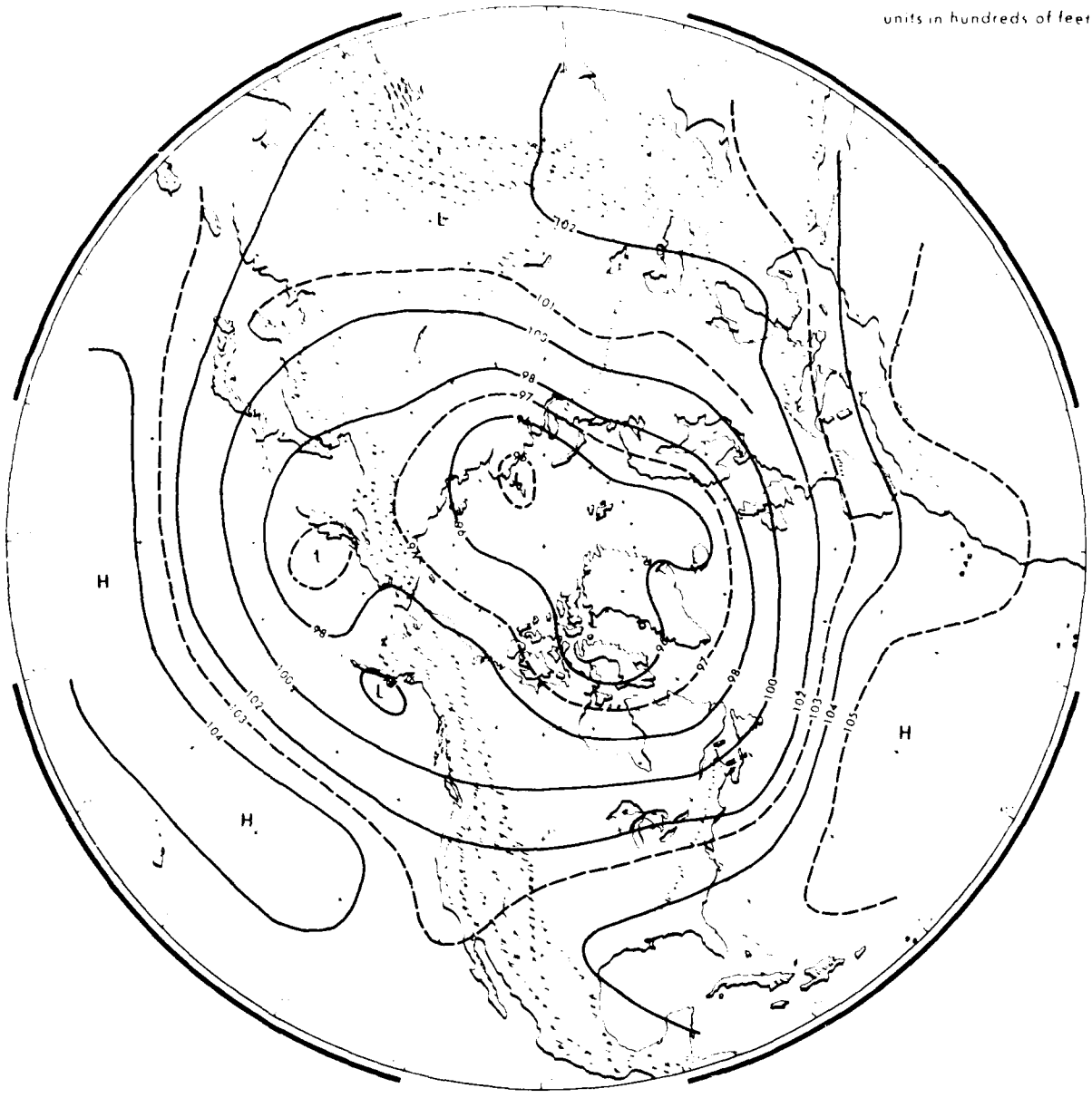

Figure B-31. Mean Height of the 700-mb Pressure Surface for June.

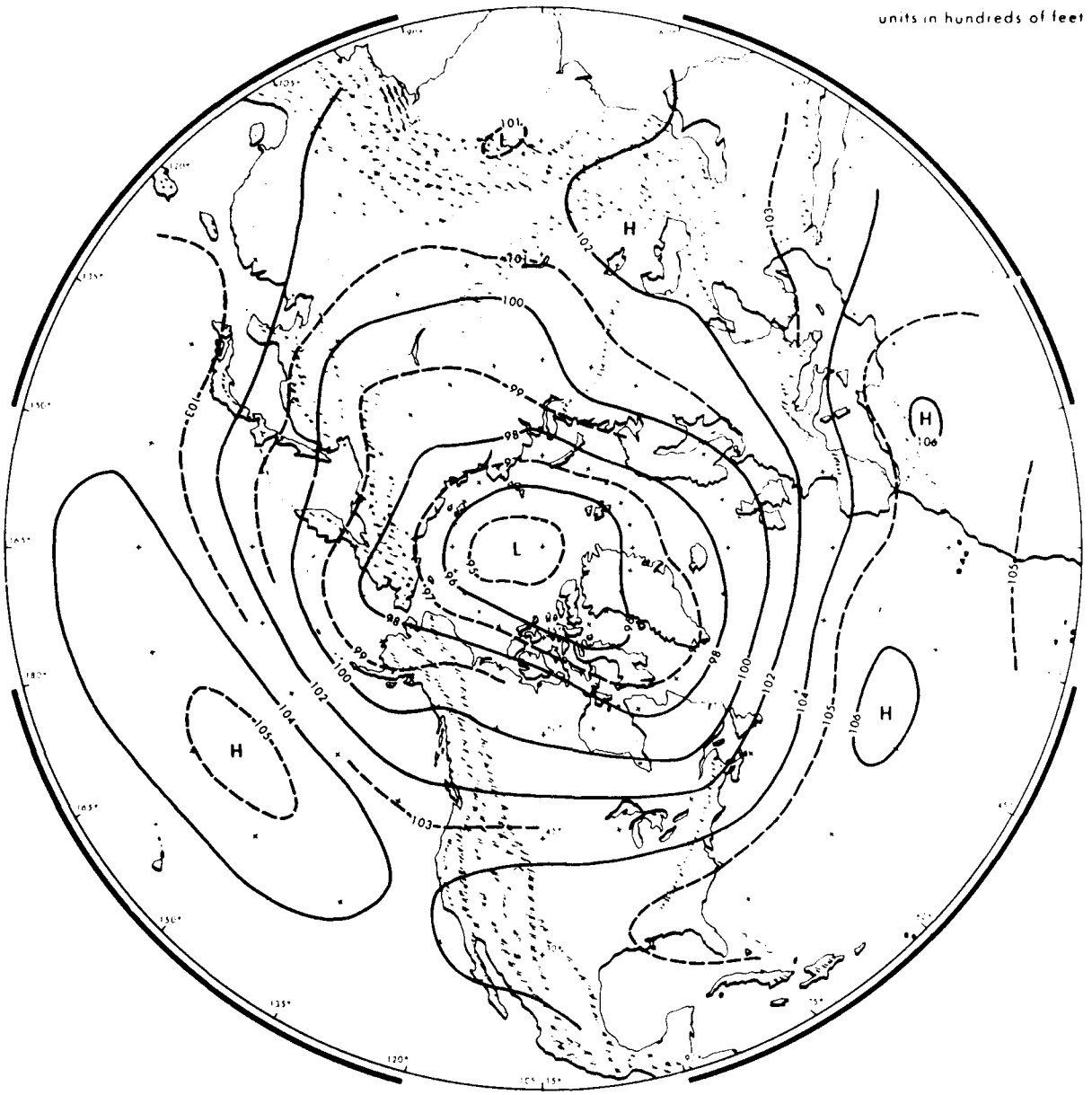

Figure B-32. Mean Height of the 700-mb Pressure Surface for July.

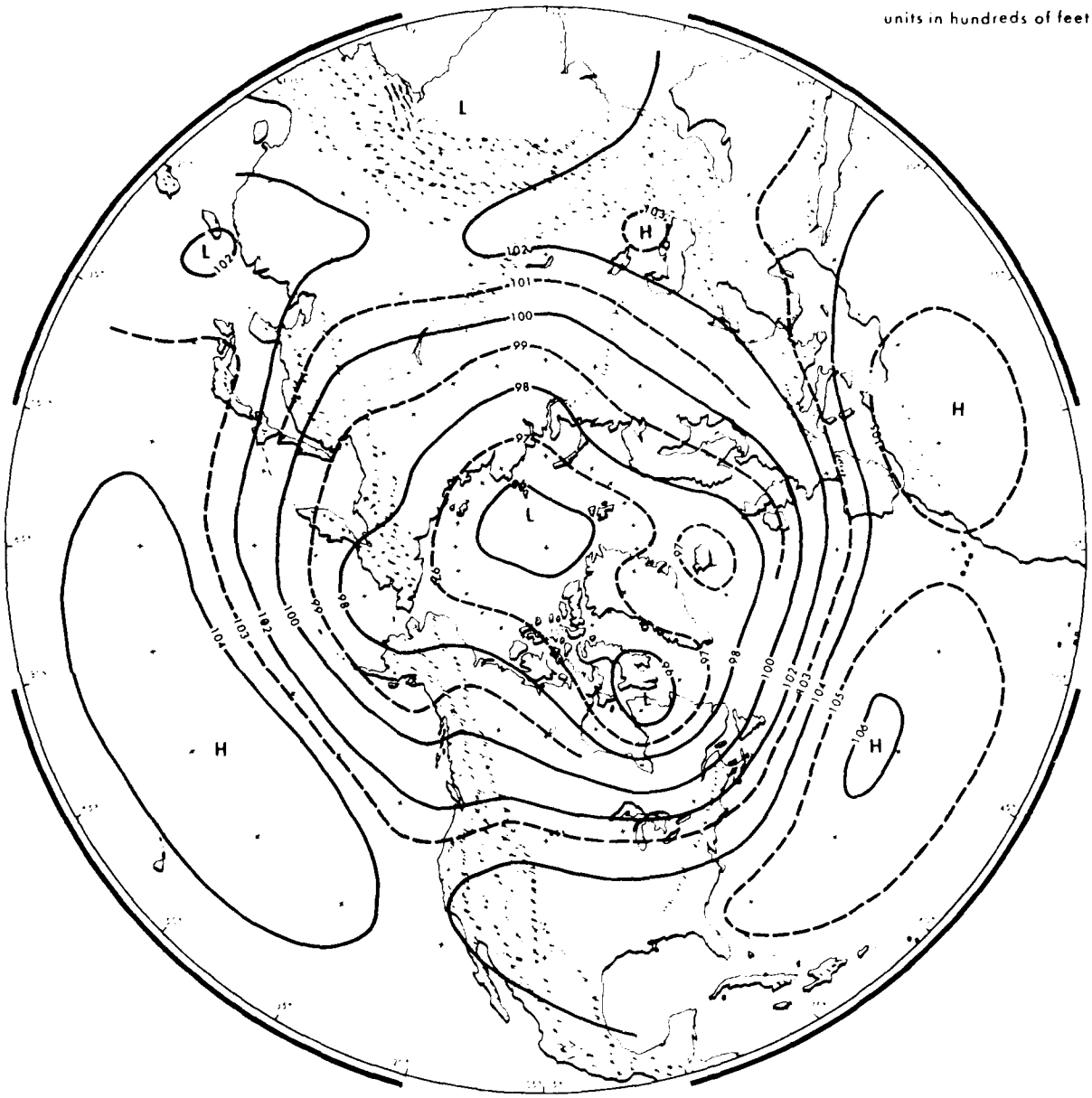

Figure B-33. Mean Height of the 700-mb Pressure Surface for August.

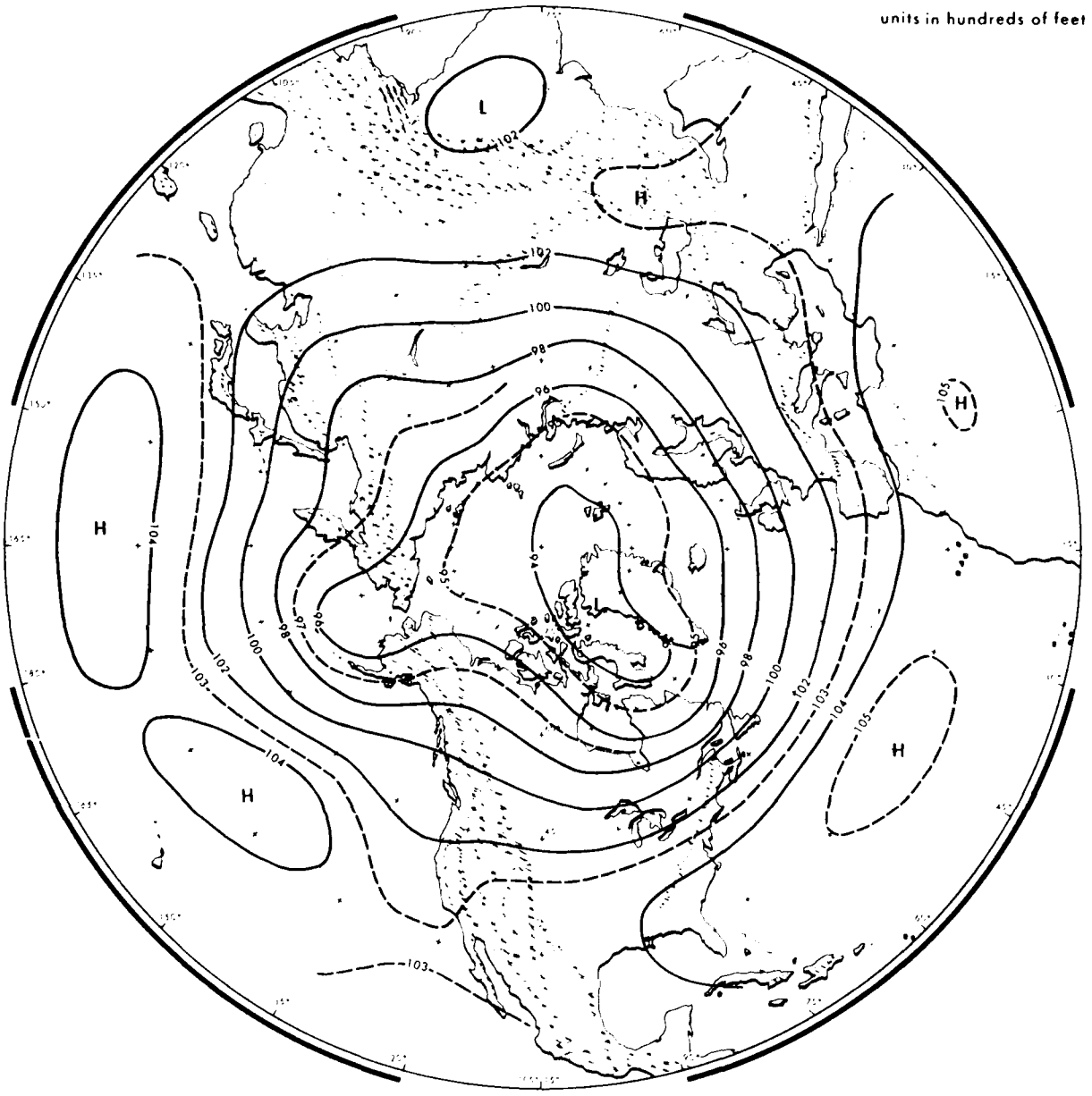

Figure B-34. Mean Height of the 700-mb Pressure Surface for September.

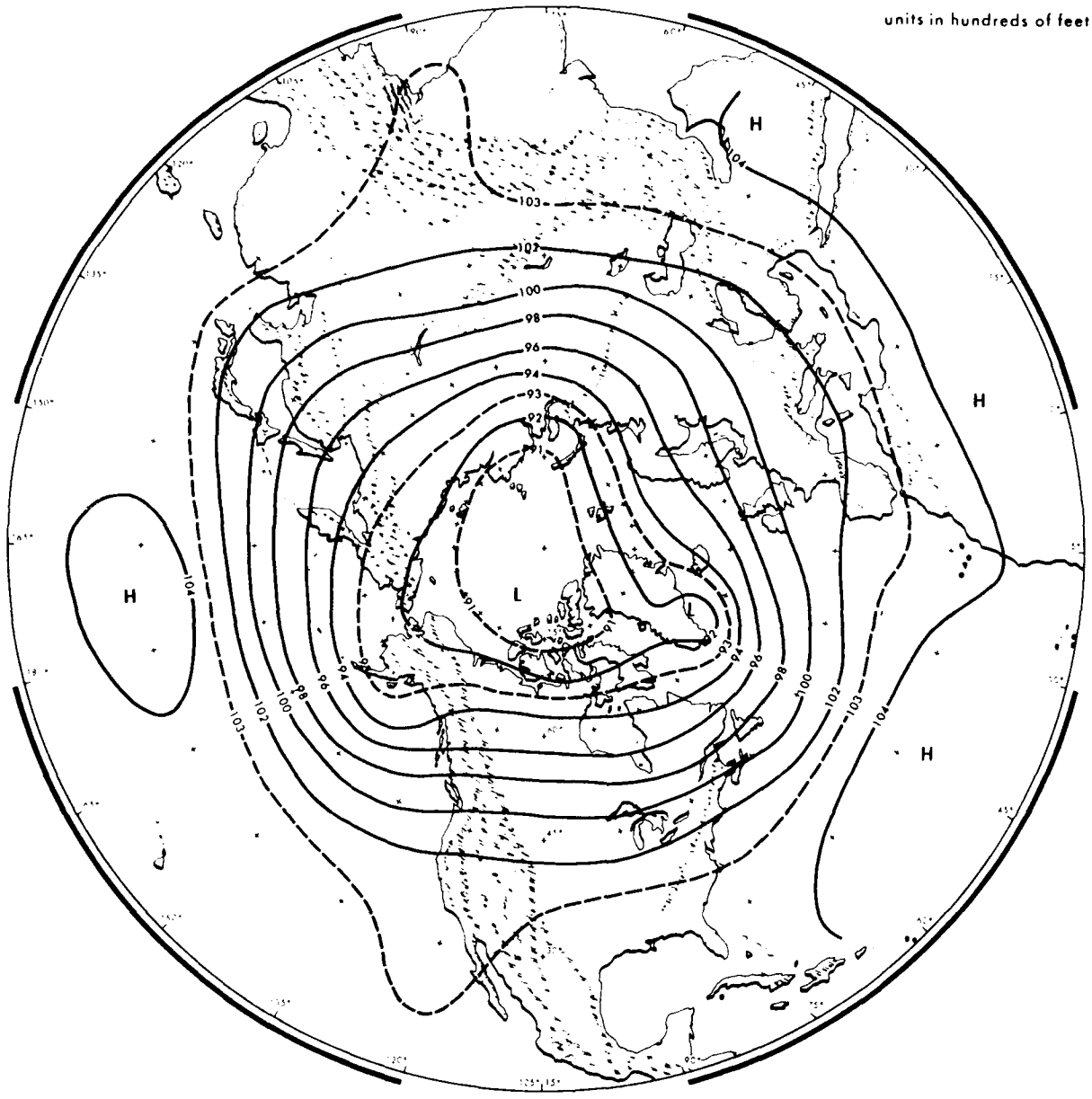

Figure B-35. Mean Height of the 700-mb Pressure Surface for October.

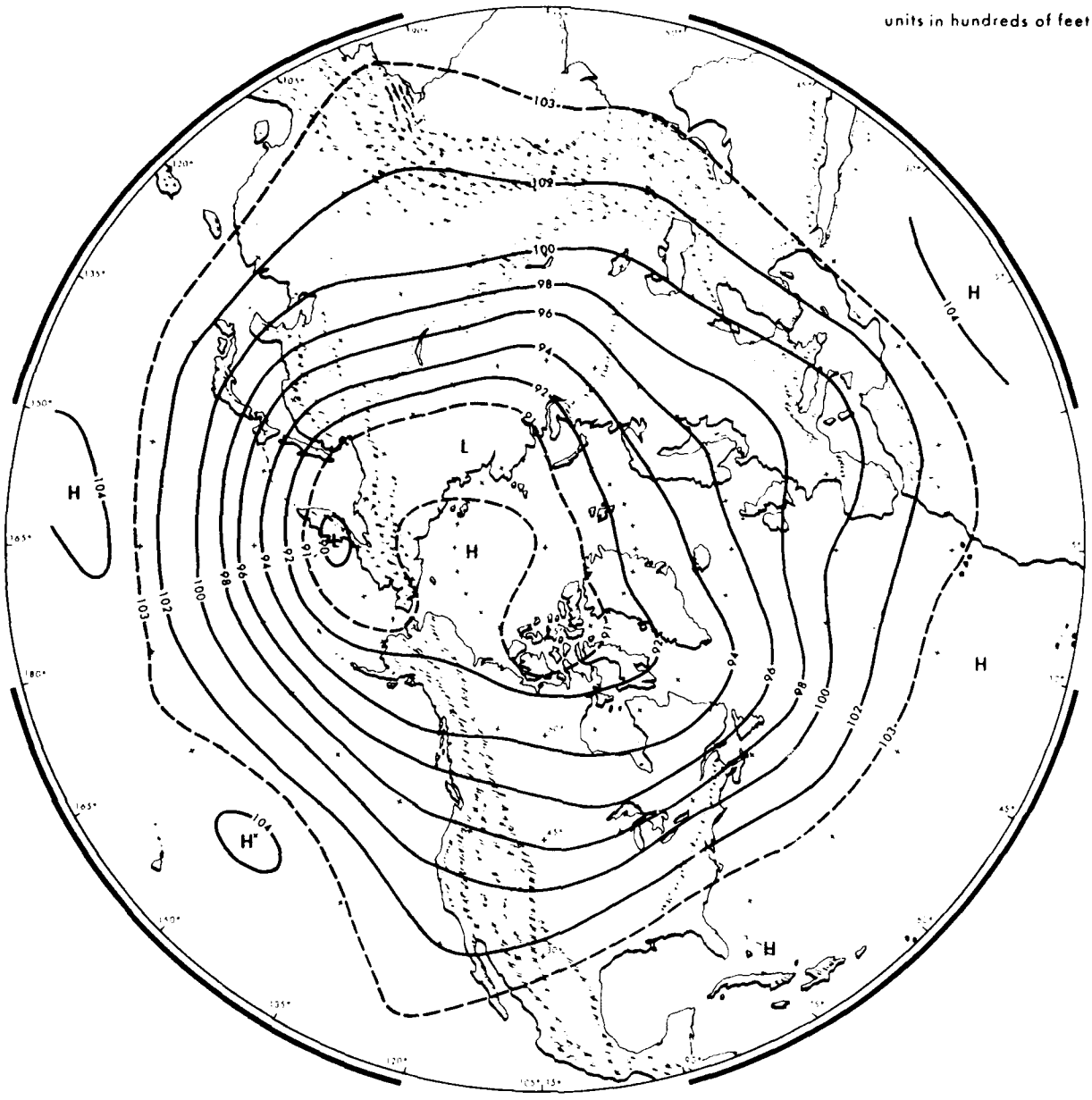

Figure B-36. Mean Height of the 700-mb Pressure Surface for November.

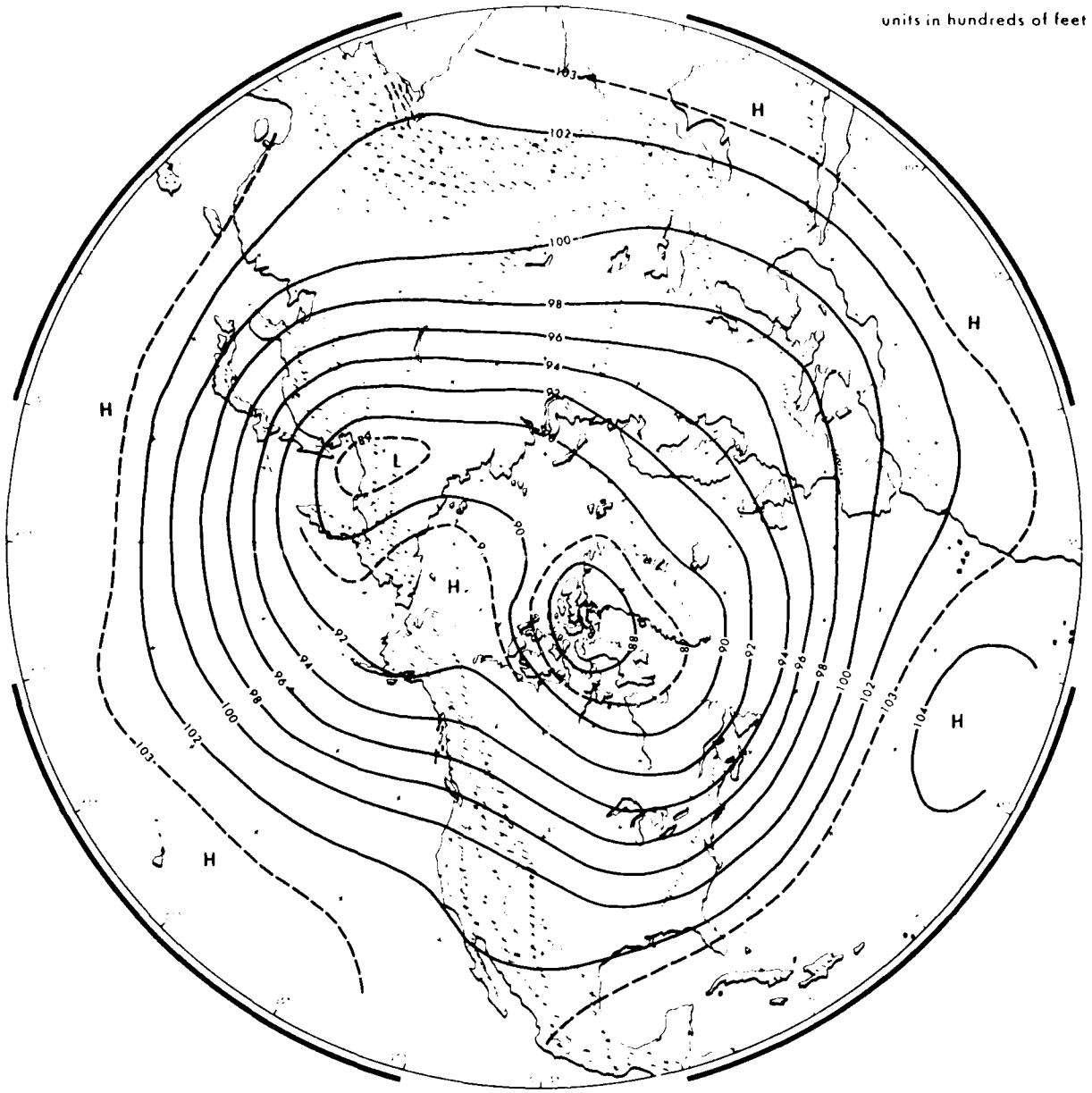

Figure B-37. Mean Height of the 700-mb Pressure Surface for December.

Appendix C

Weather Reporting Stations

The following partial listing of weather reporting stations north of 60 °N contains only those stations consistently appearing on international broadcasts. Other broadcasts, local or regional, will include many more stations but may not always be available in other locales or regions. RAOB reporting stations are noted with an asterisk (*). Also included is a listing and map of current (May 1990) drifting buoys in the Arctic Ocean.

NAME	WMO #	LATITUDE	LONGITUDE
	EUROPE		
NORWAY			
Jan Mayen	*01001	7056N	840E
Svalbard	01008	7815N	1528E
Andoya	01010	6918N	1609E
Bardufoss	01023	6903N	1833E
Tromsø	01025	6941N	1855E
Bjornoya (Bear) Island	*01028	7431N	1901E
Hopen Island	01062	7630N	2504E
Bodo	*01152	6716N	1422E
Orland	*01241	6342N	936E
Trondheim	*01271	6328N	1056E
Bergen	01311	6018N	513E
Oslo	*01384	6012N	1105E
SWEDEN			
Kiruna	02044	6749N	2020E
Gunnarn	02128	6501N	1741E
Kallax/Lulea	*02186	6533N	2208E

NAME	WMO#	LATITUDE	LONGITUDE
SWEDEN (Continued)			
Haparanda	02196	6550N	2409E
Sarna	02316	6141N	1307E
Sundsvall	*02366	6232N	1727E
Soderhamn	02376	6116N	1706E
FINLAND			
Sodankyla	*02836	6722N	2639E
Kuusamo	02869	6558N	2911E
Kajaani	02897	6417N	2741E
Vaasa	02911	6303N	2146E
Jyvaskyla	*02935	6224N	2541E
Jokioinen	*02963	6049N	2330E
Helsinki	02974	6019N	2458E
SHETLAND ISL. (U.K.)			
Lerwick	*03005	6008N	111W
WEATHER SHIP			
C7M	*99006	6600N	200E
ICELAND			
Keflavik	*04018	6359N	2236W
Akureyri	04063	6541N	1805W
Raufarhofn	04077	6627N	1557W
Hjardarnes	04082	6415N	1511W
FAEROE ISL. (Denmark)			
Thorshavn	*06011	6201N	646W
GREENLAND			
Sob Story	04175	6511N	4350W
Thule Air Base	*04202	7632N	6845W
Gullissat	04214	7003N	5251W
Egedesminde	*04220	6842N	5245W
Holsteinborg	04230	6655N	5340W

NAME	WMO #	LATITUDE	LONGITUDE
GREENLAND (Continued)			
Sonders Stromfjord	04231	6700N	5048W
Red River	04235	6638N	5252W
Godthab	04250	6410N	5145W
Frederikshaben	04260	6200N	4943W
Narssarssuaq	*04270	6111N	4525W
Julianehaben	04272	6043N	4603W
Nord	04310	8136N	1640W
Danmarkshaven	*04320	7646N	1840W
Danborg	04330	7418N	2013W
Scoresbysund	*04339	7029N	2158W
Kap Tobin	04340	7025N	2158W
Angmagssalik	*04360	6536N	3738W
Kulusuk	04365	6532N	3711W
U.S.S.R.			
EAST OF 58°E			
Barencburg	*20107	7804N	1413E
Maliye Karmakuli	*20744	7223N	5244E
Murmansk	*22113	6858N	3303E
Kanin Nos	22165	6839N	4318E
Kandalaksa	*22217	6708N	3226E
Krasnoscelye	22235	6722N	3702E
Sojna	*22271	6753N	4408E
Kemi Port	*22522	6459N	3447E
Arhangel'sk	*22550	6435N	4030E
Koynas	*22583	6445N	4739E
Shenkursk	22768	6206N	4254E
Sortovala	*22802	6143N	3043E
Petrozavodsk	*22820	6149N	3416E
Kargopol'	*22845	6130N	3856E
Kotlas	22887	6114N	4638E
Naryan Mar	*23205	6739N	5301E
Pechora	*23418	6507N	5706E
Ust' Shchugor	23518	6416N	5737E
Troitsko Pechorsk	23711	6242N	5612E
Syktyvkar	*23804	6140N	5051E
Cherdin	23914	6024N	5631E
Leningrad	*26063	5958N	3018E

NAME	WMO #	LATITUDE	LONGITUDE

U.S.S.R. (Continued)

WEST OF 58° EAST

Kheysa Ostrov	*20046	8037N	5803E
Vize Ostrov	*20069	7930N	7659E
Golomjanniy Ostrov	20087	7933N	9037E
Uyedineniya Ostrov	*20274	7730N	8214E
Mys Chelyuskin	*20292	7743N	10417E
Mys Zhelaniya	*20353	7657N	6835E
Russkaya Gavan'	20357	7611N	6334E
Beliy Ostrov	*20667	7320N	7002E
Dikson Ostrov	*20674	7330N	8014E
Khatanga	*20891	7159N	10228E
Zhokhova Ostrov	*21358	7609N	15250E
Kotelniy Ostrov	*21432	7600N	13754E
Preobrazheniya Ostrov	*21504	7440N	11256E
Mys Shalaurova	*21647	7311N	14356E
Saskylakh	21802	7158N	11405E
Tiksi	*21824	7135N	12855E
Jubilejnaja	21931	7045N	13613E
Chokurdakh	21946	7037N	14753E
Chetyrekhstolbovoy Ost.	*21965	7038N	16224E
Wrangel Island	21982	7058N	17832W
Amderma	*23022	6946N	6141E
Mare Sale	23032	6943N	6649E
Dudinka	23074	6924N	8610E
Mys Kamenniy	*23146	6828N	7336E
Khoseda Khard	23219	6705N	5923E
Tazovskoye	23256	6728N	7844E
Igarka	23274	6728N	8634E
Salekhard	*23330	6632N	6632E
Agata	23383	6653N	9328E
Turukhansk	*23472	6547N	8757E
Tarko Sale	*23552	6455N	7749E
Berezovo	23631	6356N	6503E
Verkhne Imbatskoye	23678	6309N	8757E
Nyaksimvol	23724	6226N	6052E
Oktyabr'skoye	23734	6227N	6603E
Surgut	23849	6115N	7330E
Podkamennaya Tungus	*23884	6136N	9000E
Baykit	23891	6140N	9622E
Ivdel	*23921	6041N	6026E

NAME	WMO #	LATITUDE	LONGITUDE

U.S.S.R. (Continued)

WEST OF 58° EAST (Continued)

Khanty Mansiysk	*23933	6058N	6904E
Aleksandrovskoye	*23955	6026N	7752E
Vanzhil' Kynak	23966	6021N	8405E
Yessy	24105	6828N	10222E
Olenek	*24125	6830N	11226E
Jarjan	24143	6844N	12400E
Verkhoyansk	*24266	6733N	13323E
Shelagontsi	24329	6615N	11417E
Zhigansk	*24343	6646N	12324E
Ust Moma	24382	6627N	14314E
Tura	*24507	6410N	10004E
Vilyuysk	*24641	6346N	12137E
Tompo	24671	6357N	13552E
Oymyakon	*24688	6316N	14309E
Suntar	24738	6209N	11739E
Yerbogachen	*24817	6116N	10801E
Vanavara	*24908	6020N	10216E
Olekhminsk	*24944	6024N	12025E
Yakutsk	*24959	6205N	12945E
Ust Maya	24966	6023N	13427E
Cherskiy	*25123	6848N	16117E
Mys Shmidta	*25173	6855N	17929W
Ilirney	25248	6720N	16814E
Mys Uelen	*25399	6610N	16950W
Zyryanka	*25400	6544N	15054E
Markovo	*25551	6441N	17025E
Anadir	*25563	6447N	17734E
Provideniya Bay	*25594	6426N	17314W
Kedon	25621	6400N	15855E
Ugolnaya Bay	*25677	6303N	17919E
Seymchan	*25703	6255N	15225E
Nayakhan	25821	6155N	15859E
Korf	*25954	6021N	16600E
Apuka	25956	6027N	16935E

NAME	WMO #	LATITUDE	LONGITUDE
	NORTH AMERICA		
ALASKA			
Barrow	*70026	7118N	15647W
Prudhoe Bay	70063	7015N	14820W
Barter Island	*70086	7008N	14338W
Kotzebue	*70133	6653N	16238W
Nome	*70200	6430N	16526W
McGrath	*70231	6258N	15537W
Fairbanks	*70261	6449N	14752W
Anchorage	*70273	6110N	15001W
CANADA			
Norman Wells	*71043	6517N	12648W
Teslin	71045	6010N	13245W
Sachs Harbour	71051	7200N	12516W
Mould Bay	*71072	7614N	11920W
Fort Reliance	71073	6243N	10910W
Isachsen	*71074	7847N	10332W
Hall Beach	*71081	6847N	8115W
Alert	*71082	8230N	6220W
Clyde	71090	7029N	6831W
Longstaff Bluff	71091	6854N	7509W
Cape Hooper	71093	6826N	6647W
Cape Dyer	71094	6635N	6137W
Pond Inlet	71095	7240N	7800W
Killinek	71098	6025N	6451W
Frobisher	*71909	6345N	6832W
Coral Harbour	*71915	6412N	8322W
Eureka	*71917	7959N	8556W
Pelly Bay	71919	6826N	8943W
Ennadai Lake	71923	6108N	10054W
Resolute	*71924	7443N	9459W
Cambridge Bay	*71925	6906N	10507W
Baker Lake	*71926	6418N	9605W
Gladman Point	71927	6840N	9748W
Byron Bay	71929	6845N	10904W
Fort Smith	*71934	6001N	11157W
Hay River	71935	6050N	11547W
Yellowknife	71936	6228N	11427W
Coppermine	71938	6749N	11509W

NAME	WMO #	LATITUDE	LONGITUDE
NORTH AMERICA (Continued)			
CANADA (Continued)			
Fort Simpson	71946	6145N	12114W
Cape Parry	71948	7010N	12441W
Watson Lake	71953	6007N	12849W
Inuvik	*71957	6818N	13329W
Whitehorse	*71964	6043N	13504W
Dawson	71966	6403N	13908W

DRIFTING BUOYS
(as of May 1990)

ARGOS ID	WMO #	LATITUDE	LONGITUDE
2991	—	86.485N	65.542W
3284	—	85.519N	125.139W
3285	—	87.168N	133.868E
3288	—	86.761N	96.959E
3366	—	80.379N	136.697W
3369	—	81.263N	163.472W
7049	65501	73.691N	67.870W
7406	47504	83.888N	50.962W
7408	48538	71.979N	159.341W
7410	—	82.170N	99.721W
7412	48544	84.129N	89.532W
7425	25526	80.083N	127.592E
8890	—	80.380N	136.694W
8897	—	88.543N	18.295W
8898	—	89.282N	42.580W
8899	—	89.049N	5.491E
12782	48518	73.885N	145.010W
12783	48519	74.863N	129.848W
12784	48520	85.706N	117.442W
12785	47601	82.873N	98.226W
12786	64533	84.712N	42.217W
12787	64539	80.402N	8.086W
12788	64540	88.055N	3.547W
12789	25537	83.287N	169.778E

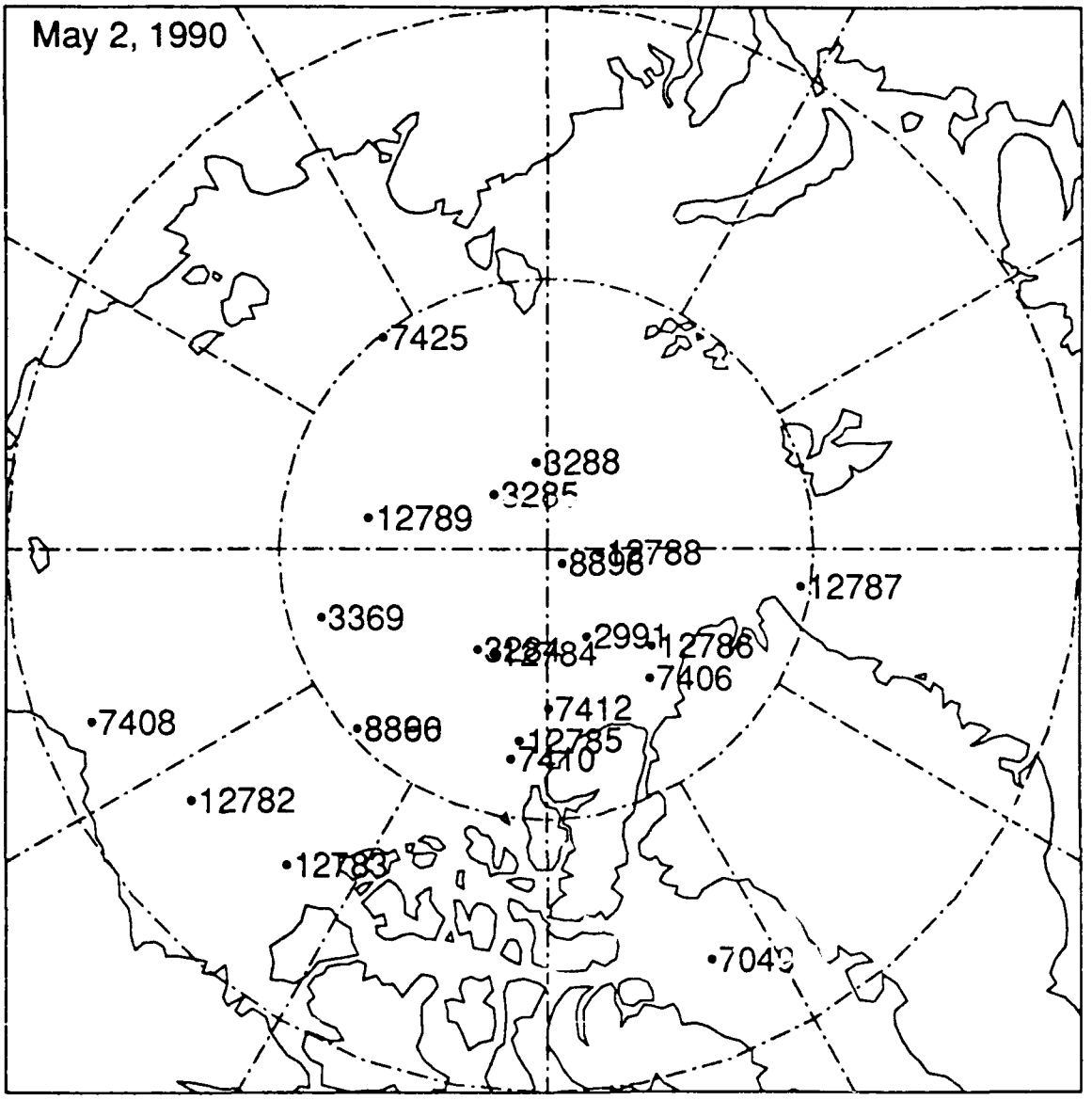

Figure C-1. Locator Map of Arctic Drifting Buovs, 19 May 1990.

Appendix D

Equivalent Wind Chill Temperature

Table 10–1. The cooling power of the wind expressed as "Equivalent Chill Temperature," and the danger of freezing exposed flesh. Courtesy of USAF Air Weather Service (MAC).

Wind Speed		Cooling Power of Wind Expressed as "Equivalent Chill Temperature"																			
Knots	*MPH*	Temperature °F																			
Calm	Calm	40	35	30	25	20	15	10	5	0	-5	-10	-15	-20	-25	-30	-35	-40	-45	-50	-55	-60
		Equivalent Chill Temperature																				
3-6	5	35	30	25	20	15	10	5	0	-5	-10	-15	-20	-25	-30	-35	-40	-45	-50	-55	-65	-70
7-10	10	30	20	15	10	5	0	-10	-15	-20	-25	-35	-40	-45	-50	-60	-65	-70	-75	-80	-90	-95
11-15	15	25	15	10	0	-5	-10	-20	-25	-30	-40	-45	-50	-60	-65	-70	-80	-85	-90	-100	-105	-110
16-19	20	20	10	5	0	-10	-15	-25	-30	-35	-45	-50	-60	-65	-75	-80	-85	-95	-100	-110	-115	-120
20-23	25	15	10	0	-5	-15	-20	-30	-35	-45	-50	-60	-65	-75	-80	-90	-95	-105	-110	-120	-125	-135
24-28	30	10	5	0	-10	-20	-25	-30	-40	-50	-55	-65	-70	-80	-85	-95	-100	-110	-115	-125	-130	-140
29-32	33	10	5	-5	-10	-20	-30	-35	-40	-50	-60	-65	-75	-80	-90	-100	-105	-115	-120	-130	-135	-145
33-36	40	10	0	-5	-15	-20	-30	-35	-45	-55	-60	-70	-75	-85	-95	-100	-110	-115	-125	-130	-140	-150
Winds Above 40 Have Little Additional Effect		Little Danger					Increasing Danger (Flesh may freeze within 1 min.)							Great Danger Flesh may freeze within 30 seconds								
Danger of Freezing Exposed Flesh for Properly Clothed Persons																					

Figure D-1. Equivalent Wind Chill Temperature Chart (Kotsch, 1983).

Appendix E

Inversion Statistics

The information in Appendix E was developed under the guidance of Dr. Russell Schnell of the Environmental Research Laboratory, Boulder, Colorado; Dr. John Kahl, University of Wisconsin/Milwaukee; and Dr. Mark Serreze, University of Colorado, Boulder.

The maps (Figs. E-1 through E-20) are statistical representations of inversions in the North Polar region. The database used to derive the maps contains soundings for 0000 GMT and 1200 GMT for the regularly reporting stations north of 60 °N in Eurasia, Alaska, Canada, and Greenland for the years 1976 to 1987. Some U.S.S.R. drifting station data were also used

The stations were selected to achieve maximum spatial coverage with the most data possible at each station. (A list follows the figures.) Some stations have complete data for the time span while most others have at least 50 percent availability each year for at least 10 of the 12 years of record. Two exceptions were Khatanga and Zyrianka, both in the U.S.S.R.; these stations had the 50 percent criterion for 8 years and 5 years, respectively. They were included to gain better coverage over the Taimyr Peninsula and Eastern Siberia. The drifting station data were obtained from three U.S.S.R. North Pole (NP) series of manned camps (NP-22, NP-26, and NP-28). Data from NP-26 and NP-28 were available intermittently from November 1983 through December 1987, with a nearly complete record for July 1986 through December 1987. Station NP-22 reported data from May 1979 through February 1982.

Quality control checks were made by passing the data through a limits check with loose bounds to identify obviously erroneous values. Soundings were then inspected to ensure that geopotential heights increased and pressures decreased upward. Further errors were eliminated during processing to obtain the inversion statistics. Only $\approx 0.1\%$ of all data were found to contain errors.

The focus here is on low-level inversions, defined as those with a base below the 700-mb level. Inversions are identified using the detection algorithm developed by Kahl (1990). Each temperature profile is scanned upwards from the surface to the 700-mb level to locate the first layer (if any) in which temperature decreases with altitude. Thin (< 100 m) negative-lapse layers are occasionally encountered in the upward scan. If the next layer above shows an increase in temperature with altitude, the thin layer is considered to be embedded within the overall inversion layer. Examples of the technique are given by Kahl.

The statistics are defined as follows:

(1) Frequency of inversions (%): The percentage of all valid soundings in which an inversion was present.

(2) Frequency of elevated inversions (%): The percentage of all valid soundings in which an elevated inversion (i.e., an inversion with a mixed layer below the inversion base) was present.

(3) Median inversion depth (Z): The depth of the inversion layer, defined as the difference (in meters) between the inversion top and inversion base. Both elevated and ground-based inversions are included in this statistic.

(4) Median temperature difference across the inversion layer (T): The median temperature difference from the inversion top to the inversion base. Both elevated and ground-based inversions are included.

(5) Inversion intensity: This statistic, defined as T^2/Z, was originally defined by Belmont (1958) in similar form as T^2/P (P being pressure) as an overall measure of inversion strength. Clearly T itself is a valid measure of inversion strength. However, while two different inversions may have a similar T, their relative importance is increased by weighting T with Z, thus highlighting the greater temperature gradient. Both elevated and ground-based inversions are included in calculating this statistic.

In the maps the seasons are defined as follows: winter (Jan-Mar), spring (Apr-Jun), summer (Jul-Sep) and autumn (Oct-Dec). Drifting station location is defined as the midpoint along the station trajectory for each season of each year. The maps were contoured using a computer graphics package with some subsequent manual adjustments. The location of the fixed stations are shown by dots. Solid contours are used for areas over land and in the marginal seas where the data are fairly extensive, while dashed contours are used for areas within the pack ice north of the land stations where the interpolations are mostly determined by the relatively sparse drifting station data.

Eureka, Northwest Territories and Verkhoyansk, U.S.S.R. are located in valleys where cold-air drainage apparently occurs. Data from these stations showed extremely high intensity inversion values, which resulted in the computer-generated contours depicting "bullseyes." These two stations were eventually eliminated from the data set that produced the contours, and their intensity values are identified on the maps as local maxima.

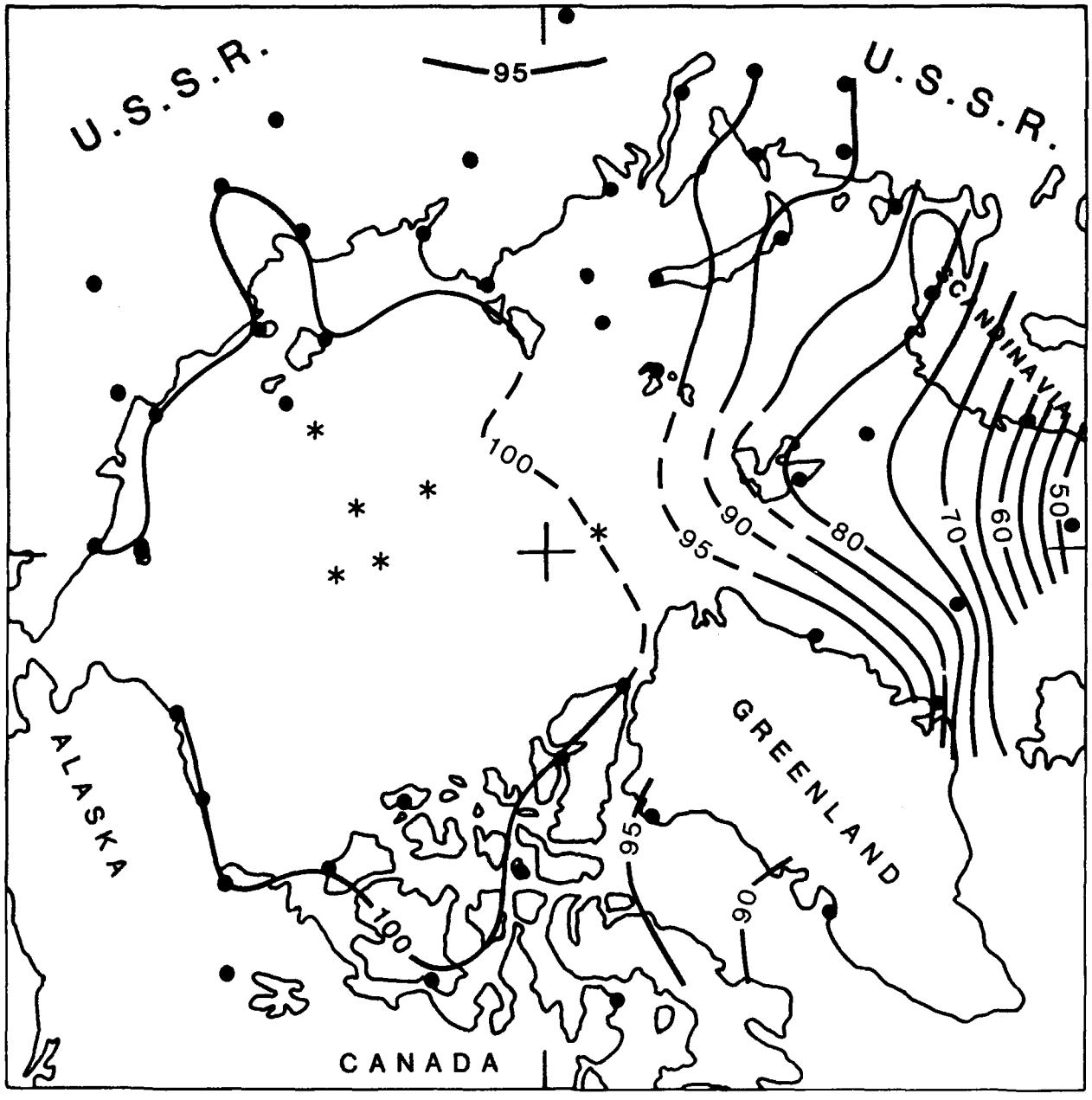

Figure E-1. Frequency of Inversions (%) for Winter.

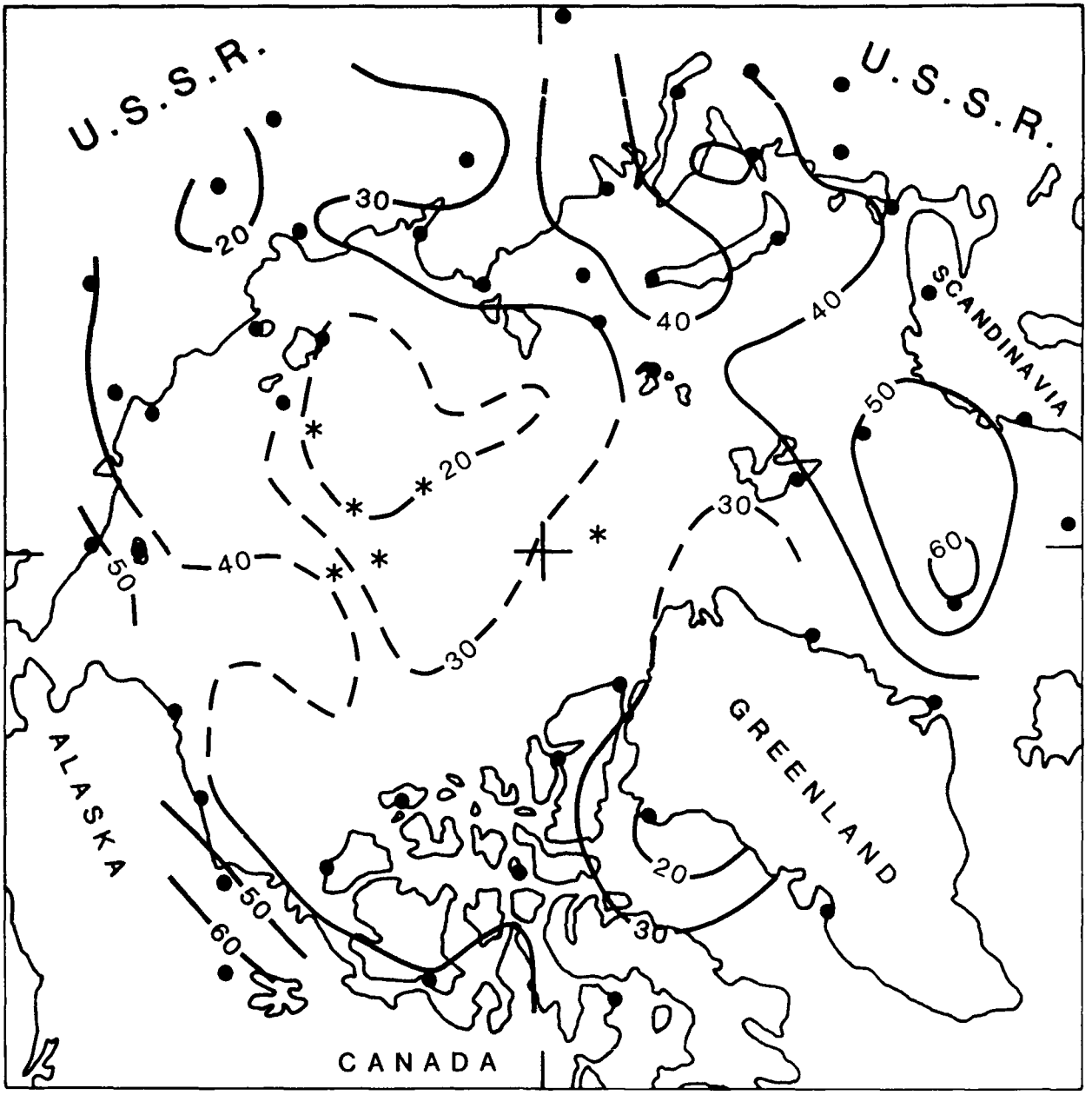

Figure E-2. Frequency of Elevated Inversions (%) for Winter.

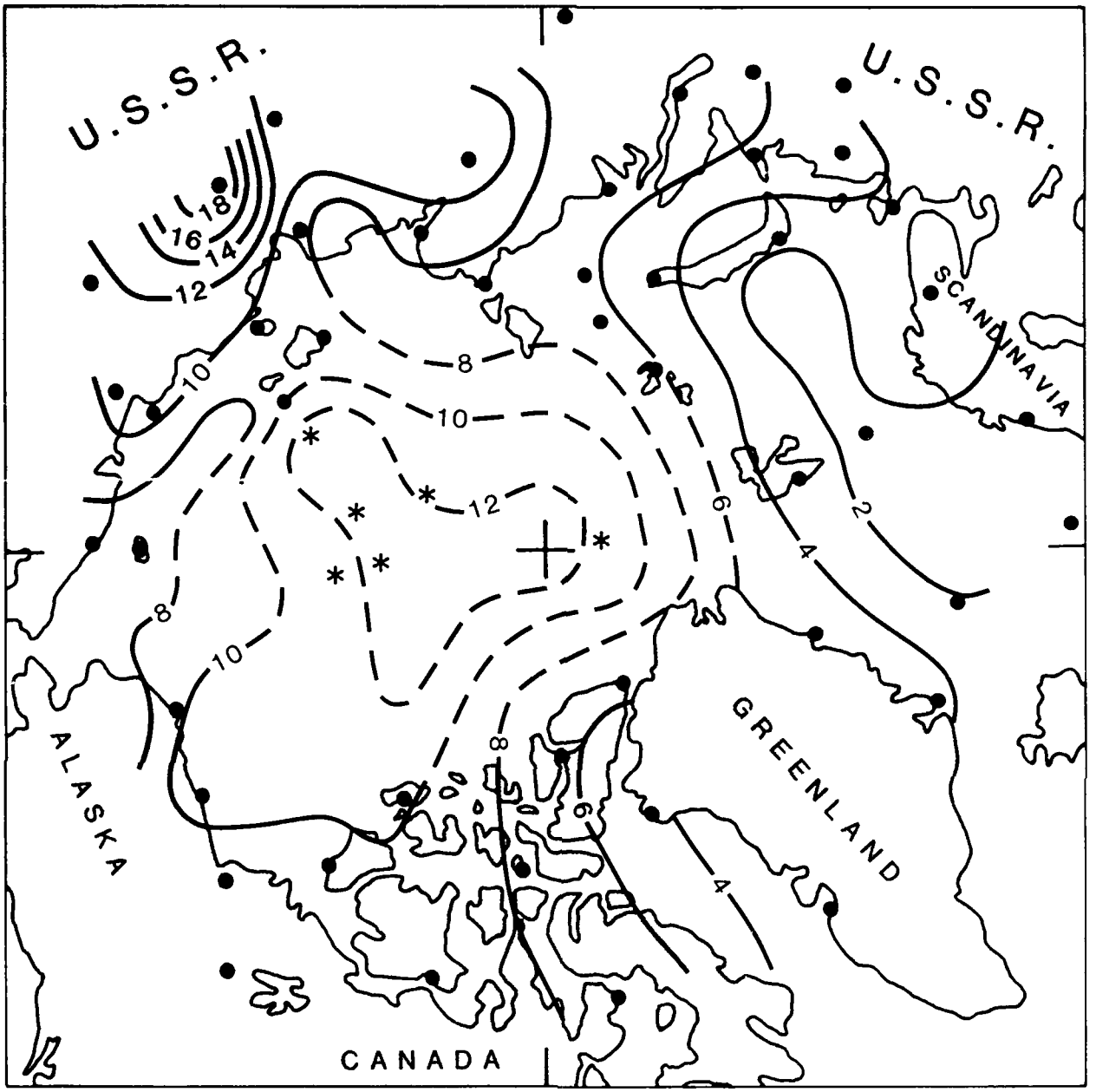

Figure E-3. Median Temperature Difference Across Inversion (°C) for Winter.

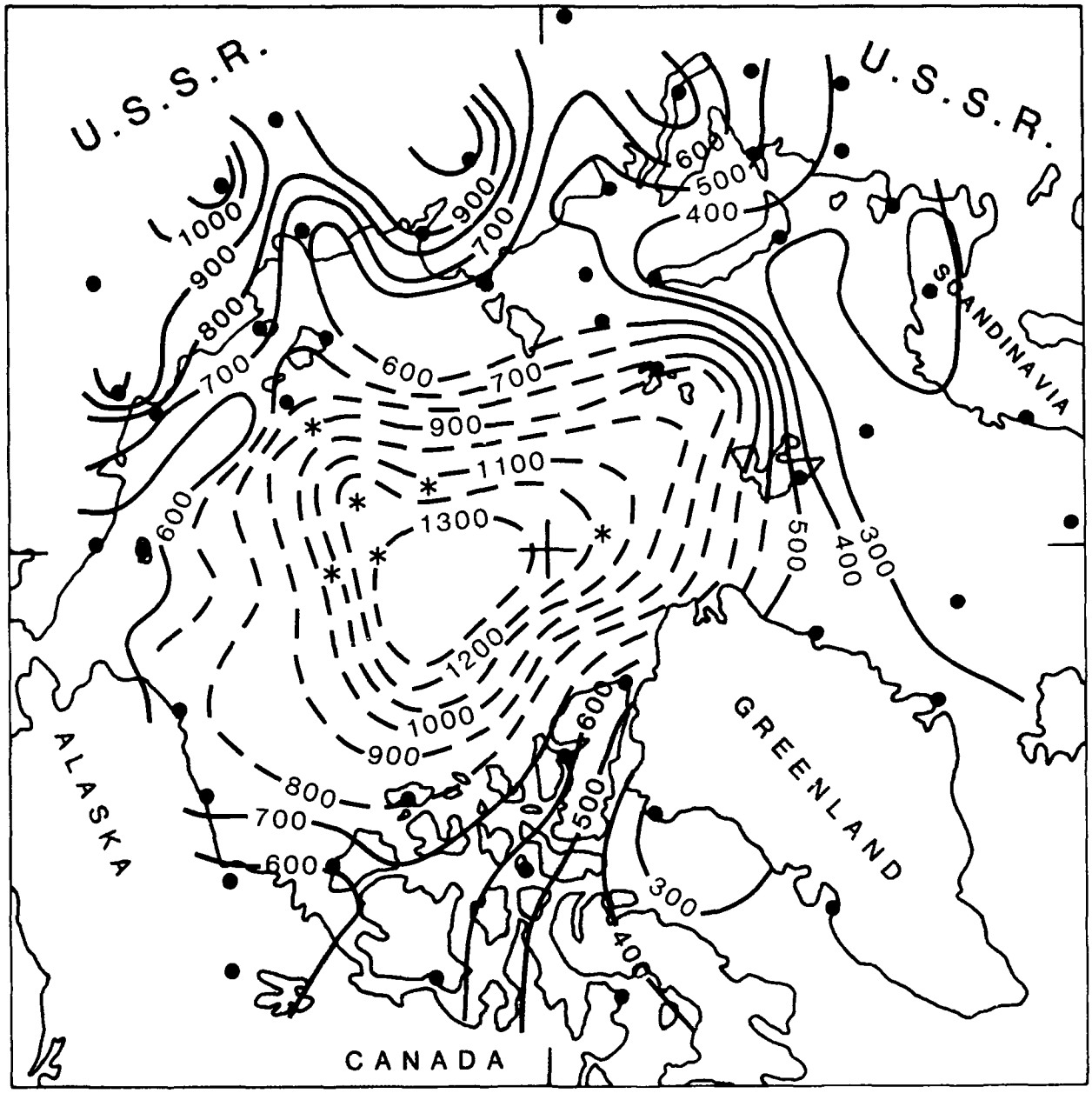

Figure E-4. Median Inversion Depth (m) for Winter.

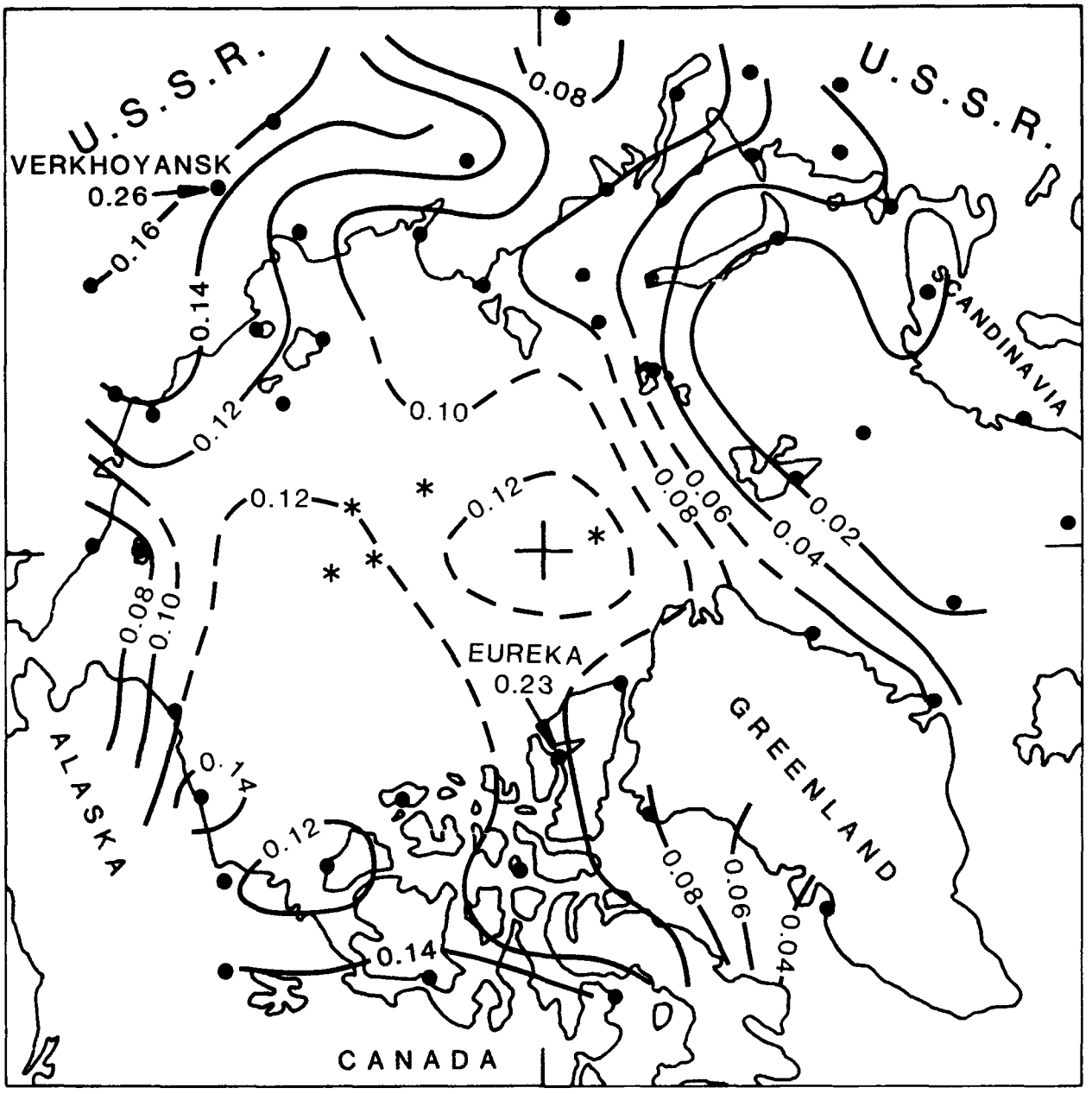

Figure E-5. Median Inversion Intensity ($\Delta T^2/m$) for Winter.

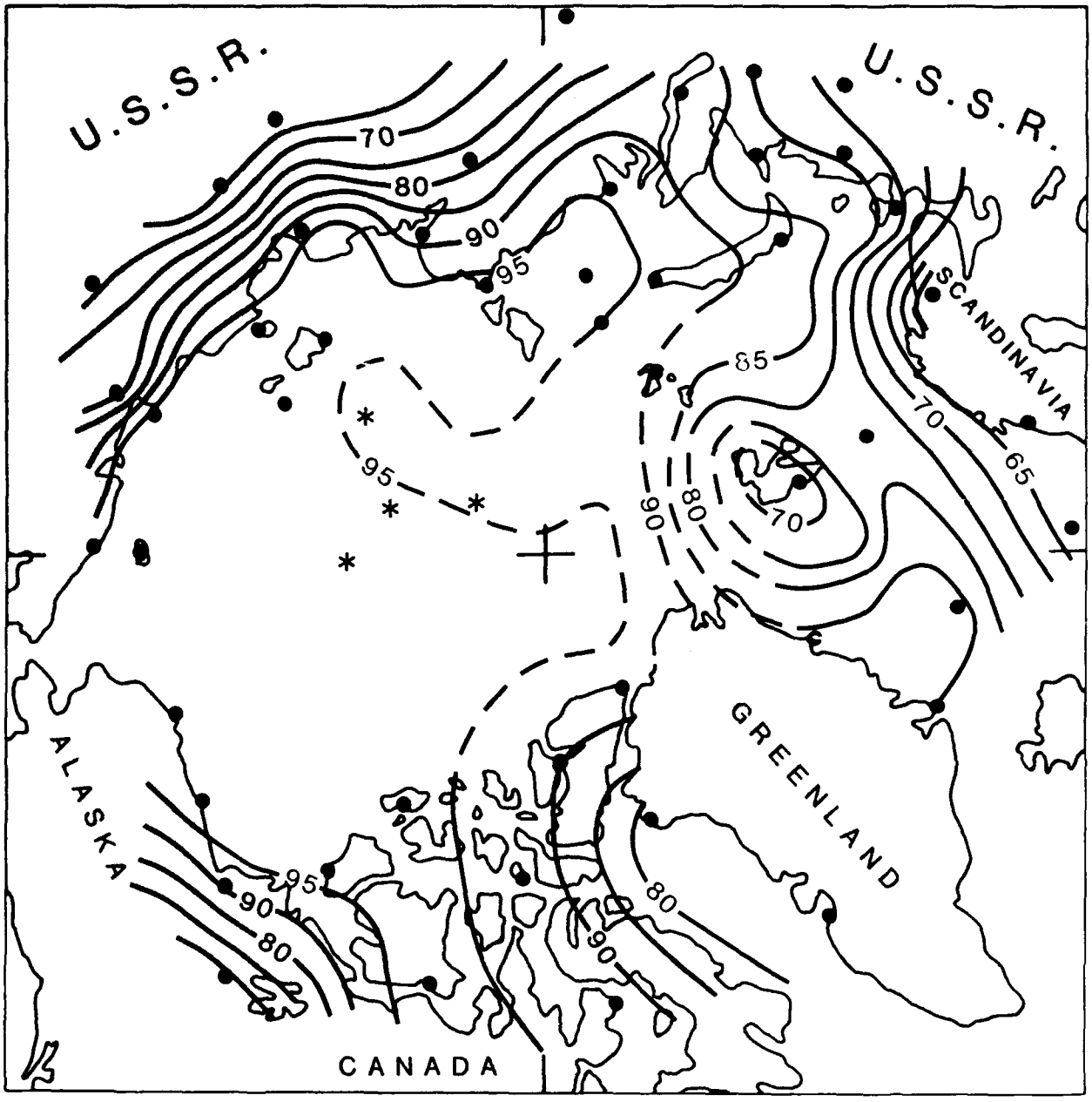

Figure E-6. Frequency of Inversions (%) for Spring.

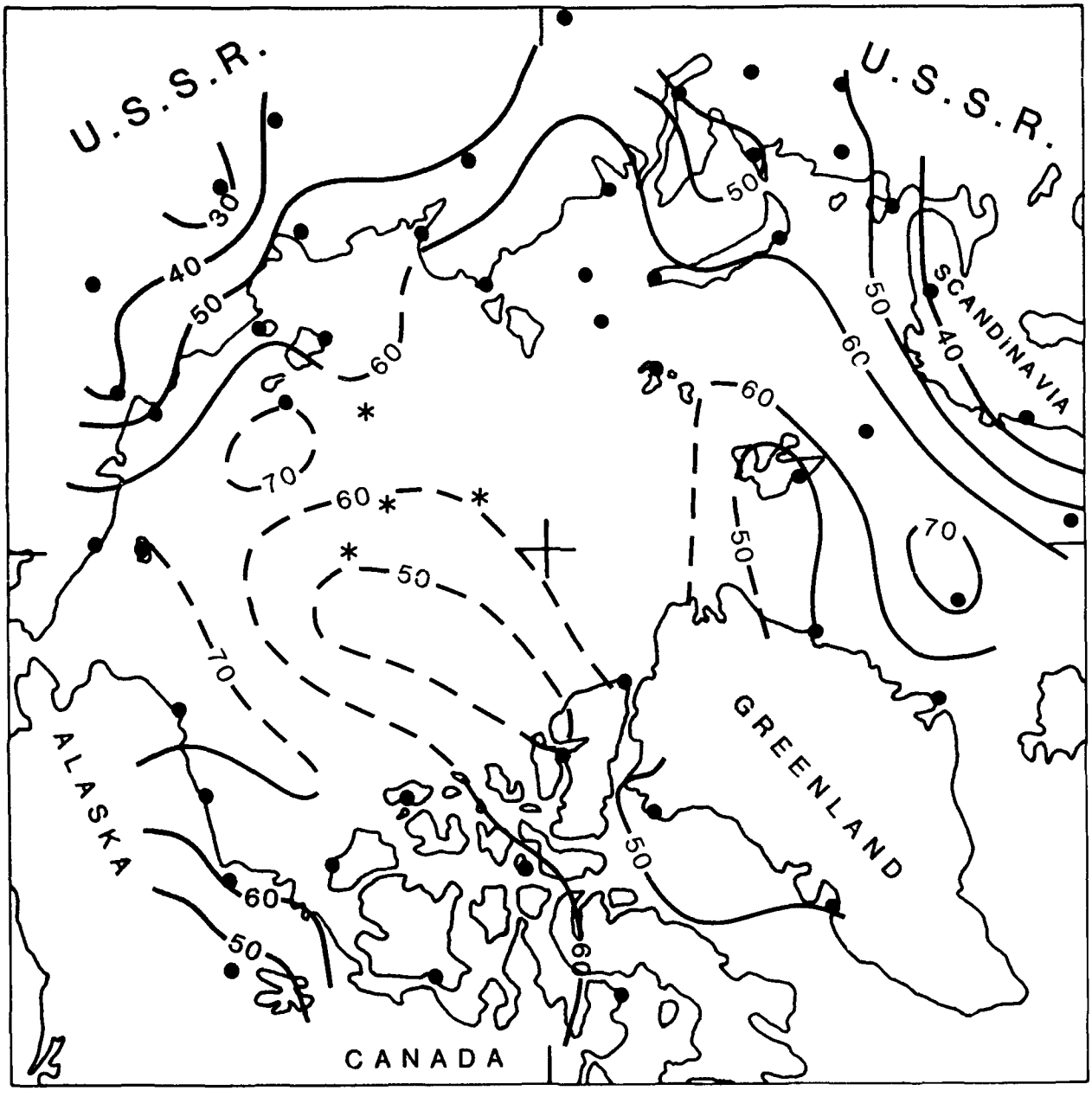

Figure E-7. Frequency of Elevated Inversions (%) for Spring.

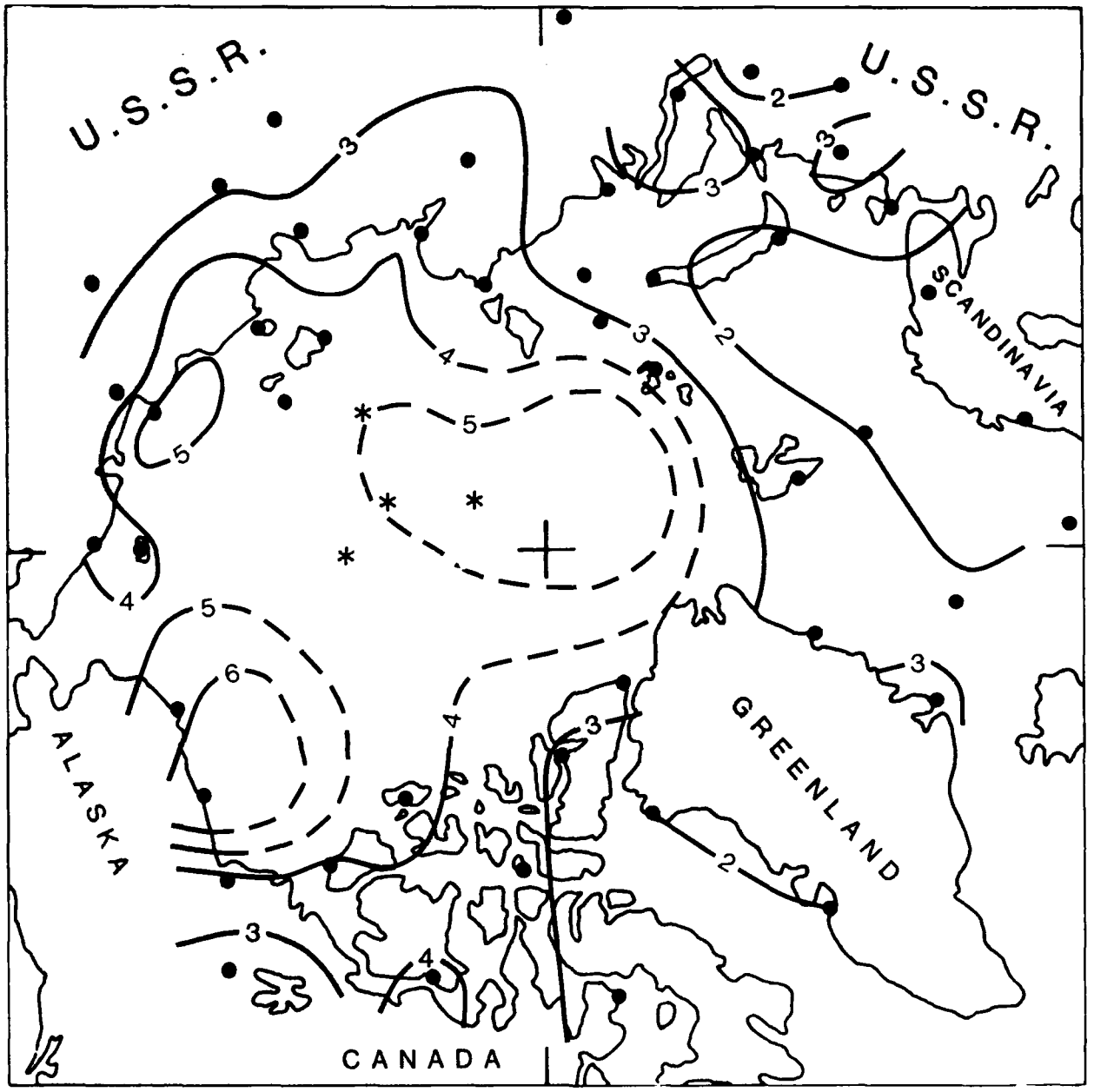

Figure E-8. Median Temperature Difference Across Inversion (°C) for Spring.

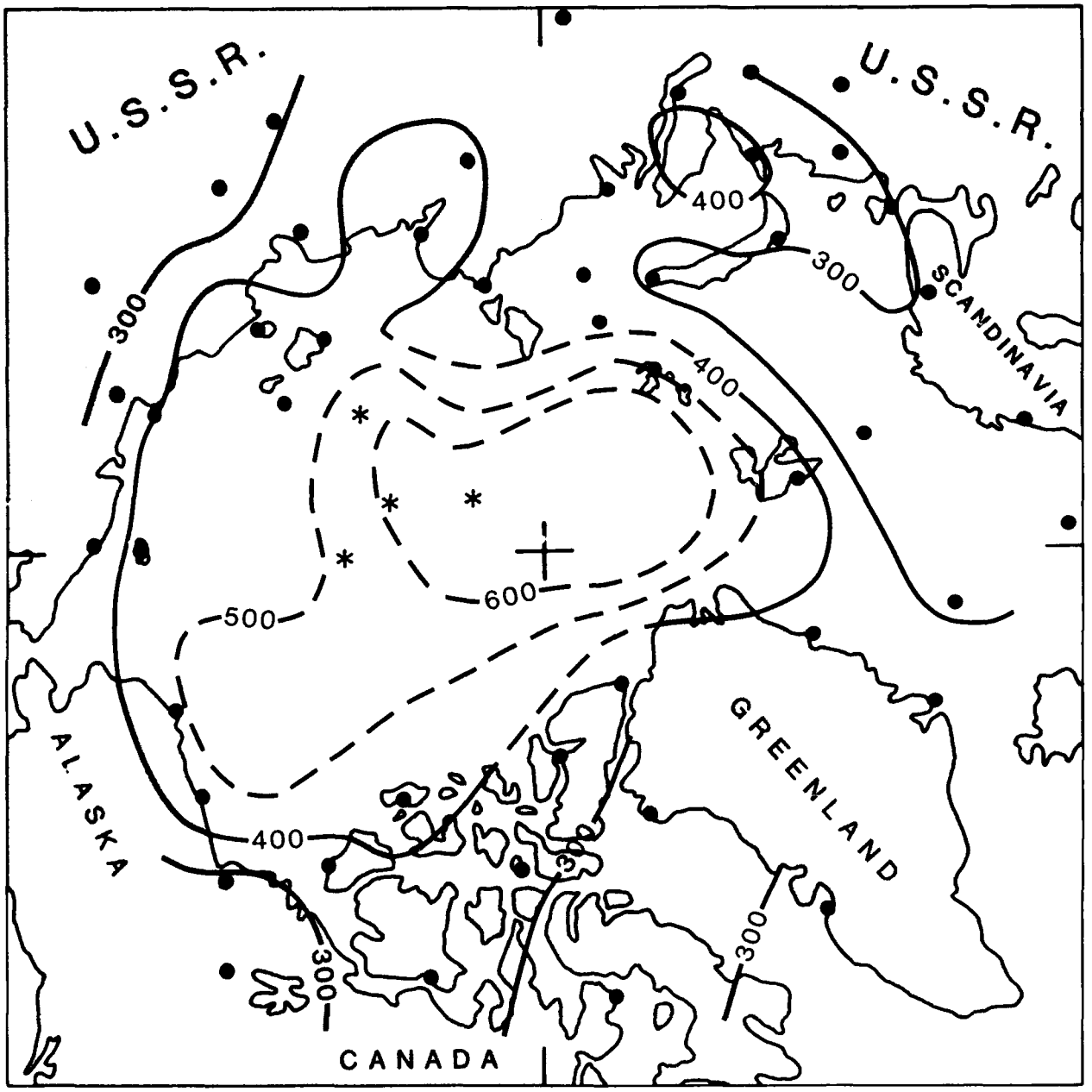

Figure E-9. Median Inversion Depth (m) for Spring.

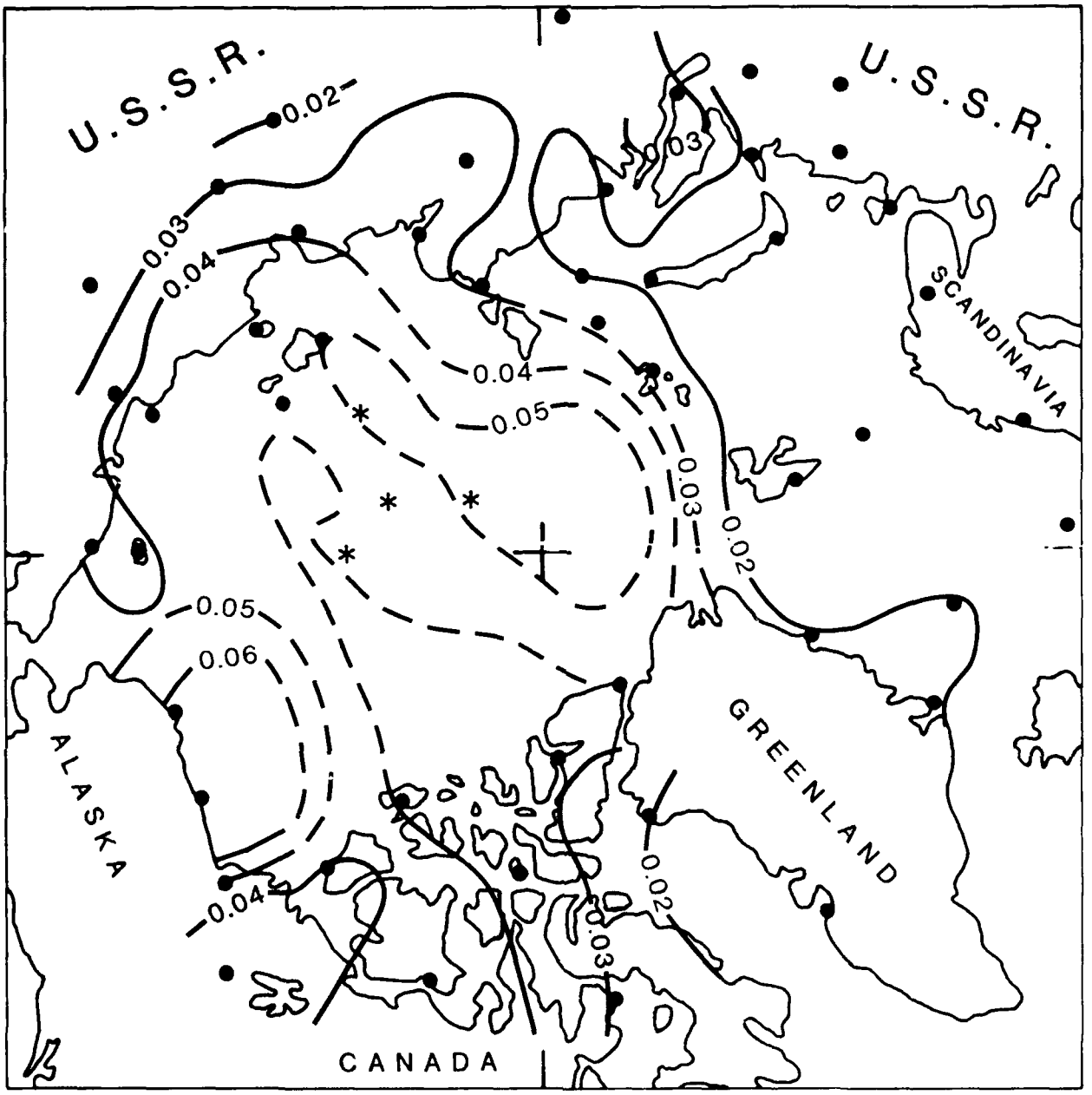

Figure E-10. Median Inversion Intensity ($\Delta T^2/m$) for Spring.

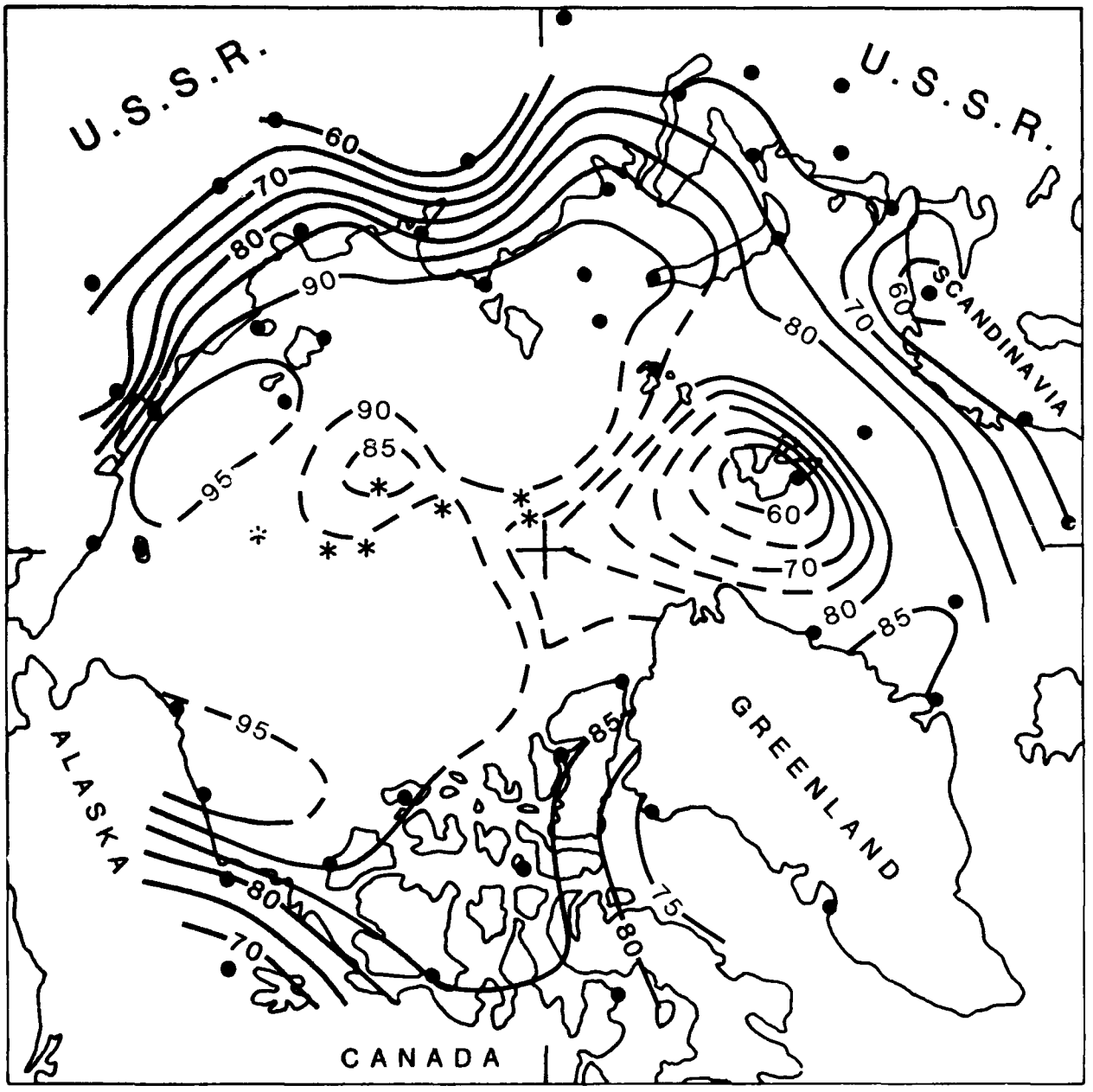

Figure E-11. Frequency of Inversions (%) for Summer.

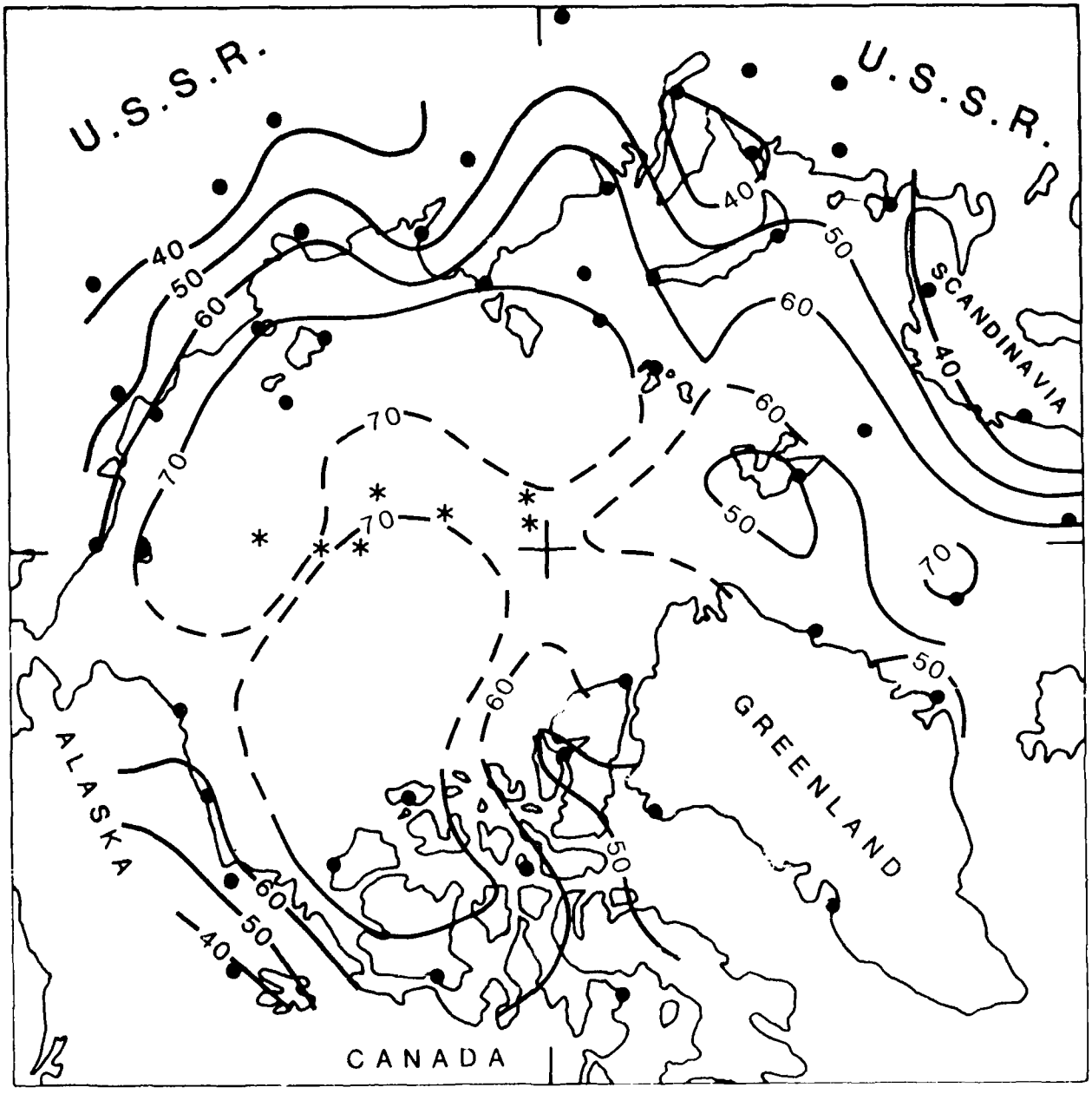

Figure E 12. Frequency of Elevated Inversions (%) for Summer.

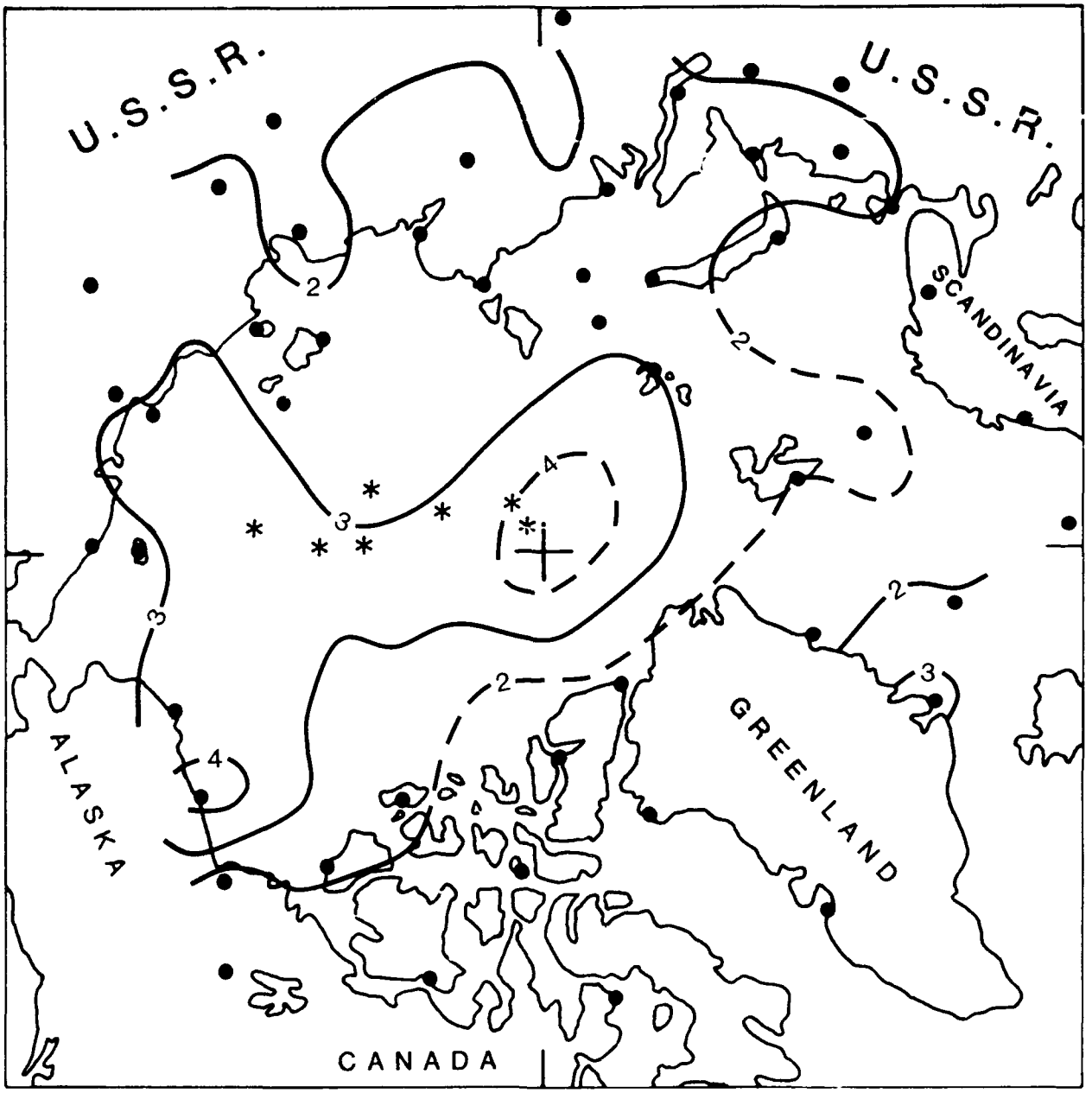

Figure E-13. Median Temperature Difference Across Inversion (°C) for Summer.

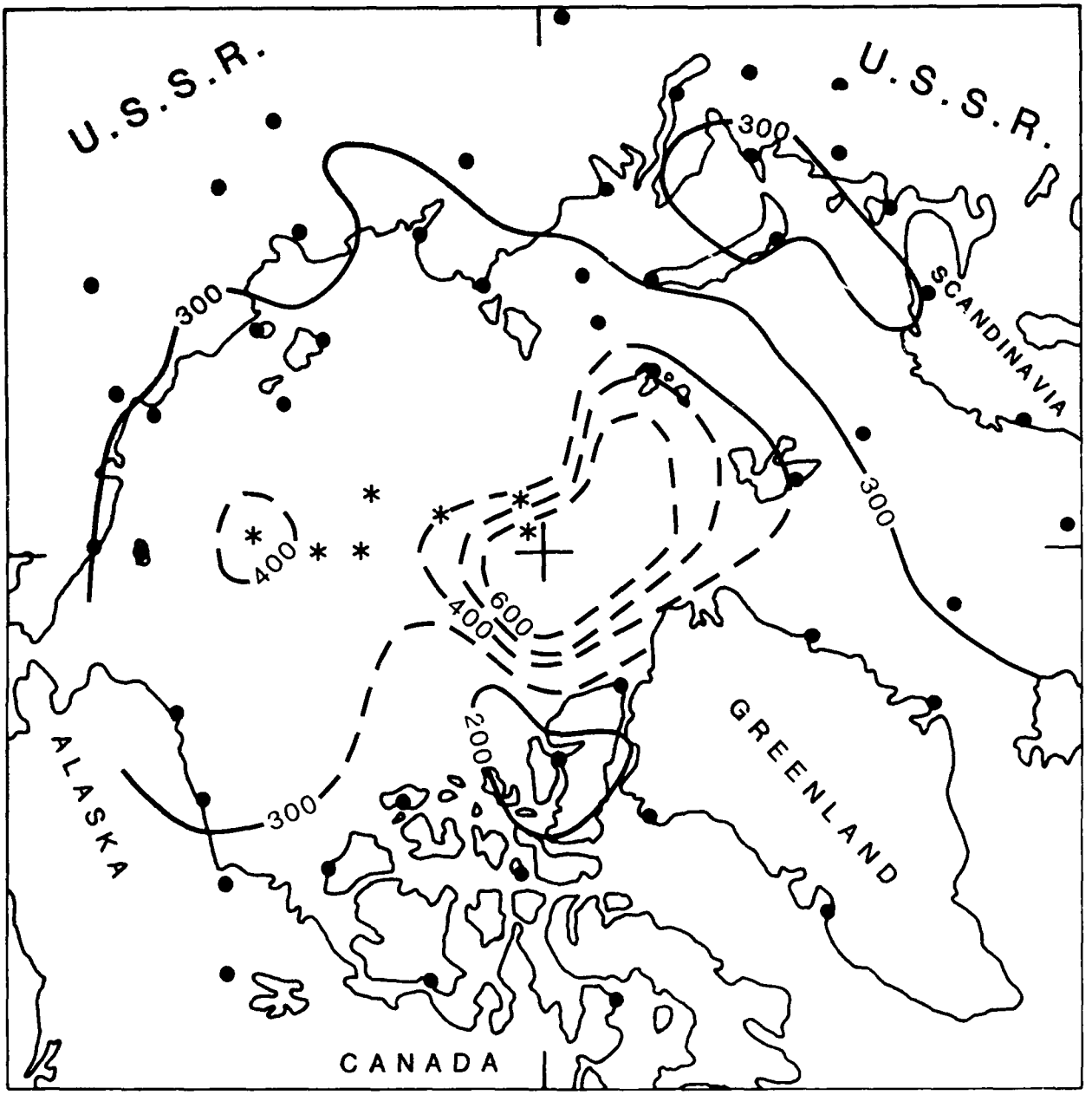

Figure E-14. Median Inversion Depth (m) for Summer.

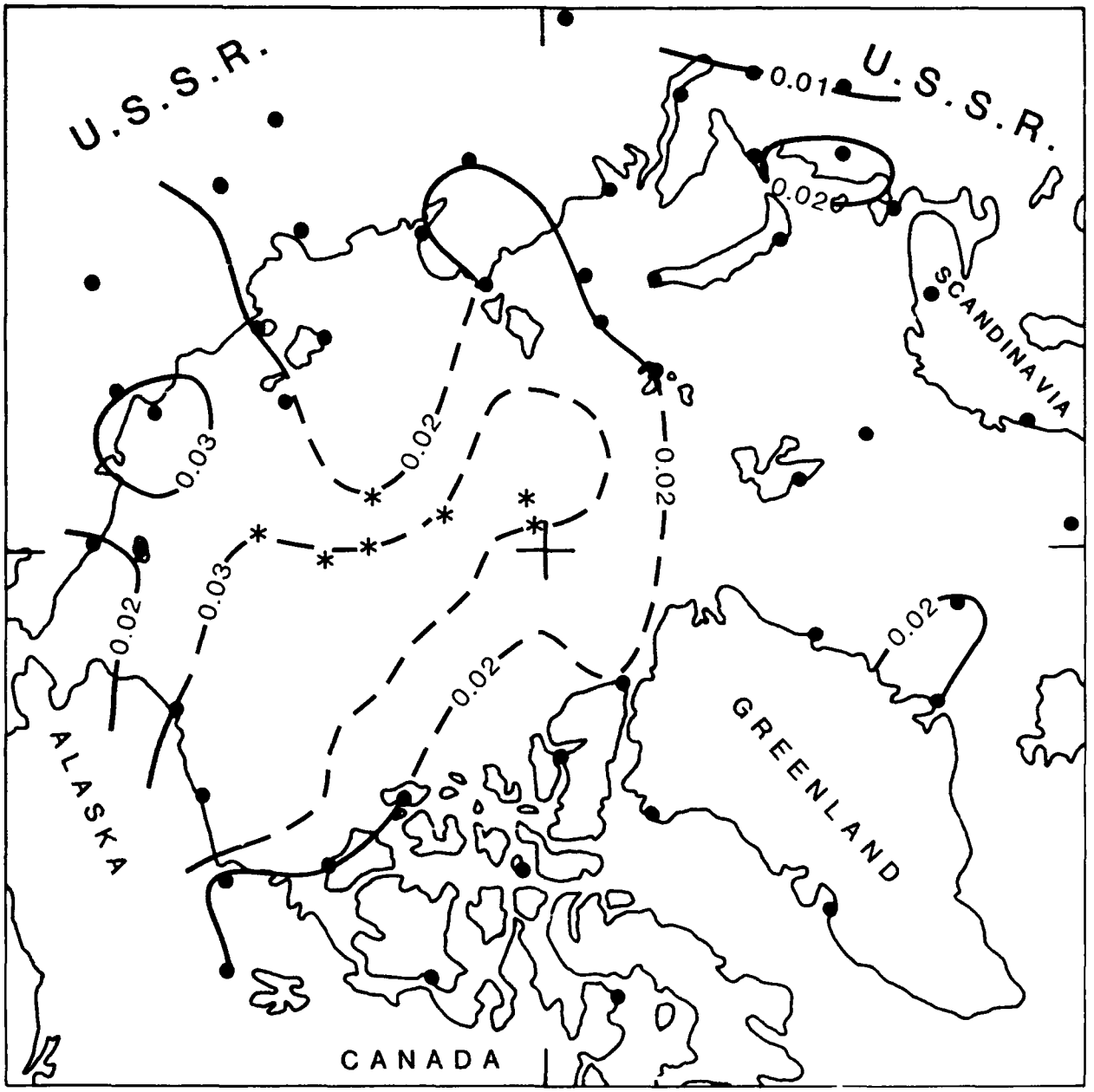

Figure E-15. Median Inversion Intensity ($\Delta T^2/m$) for Summer.

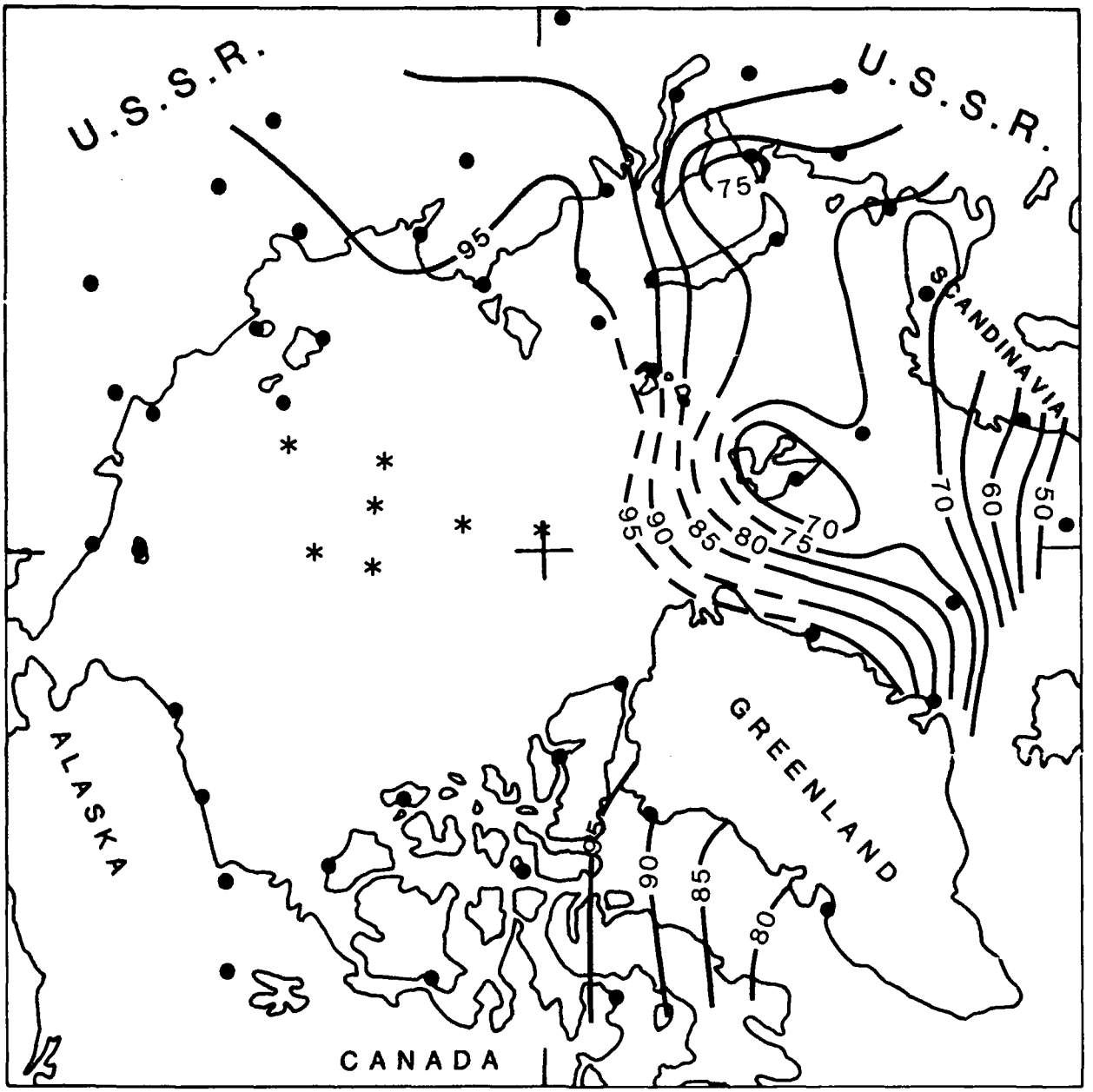

Figure E-16. Frequency of Inversions (%) for Autumn.

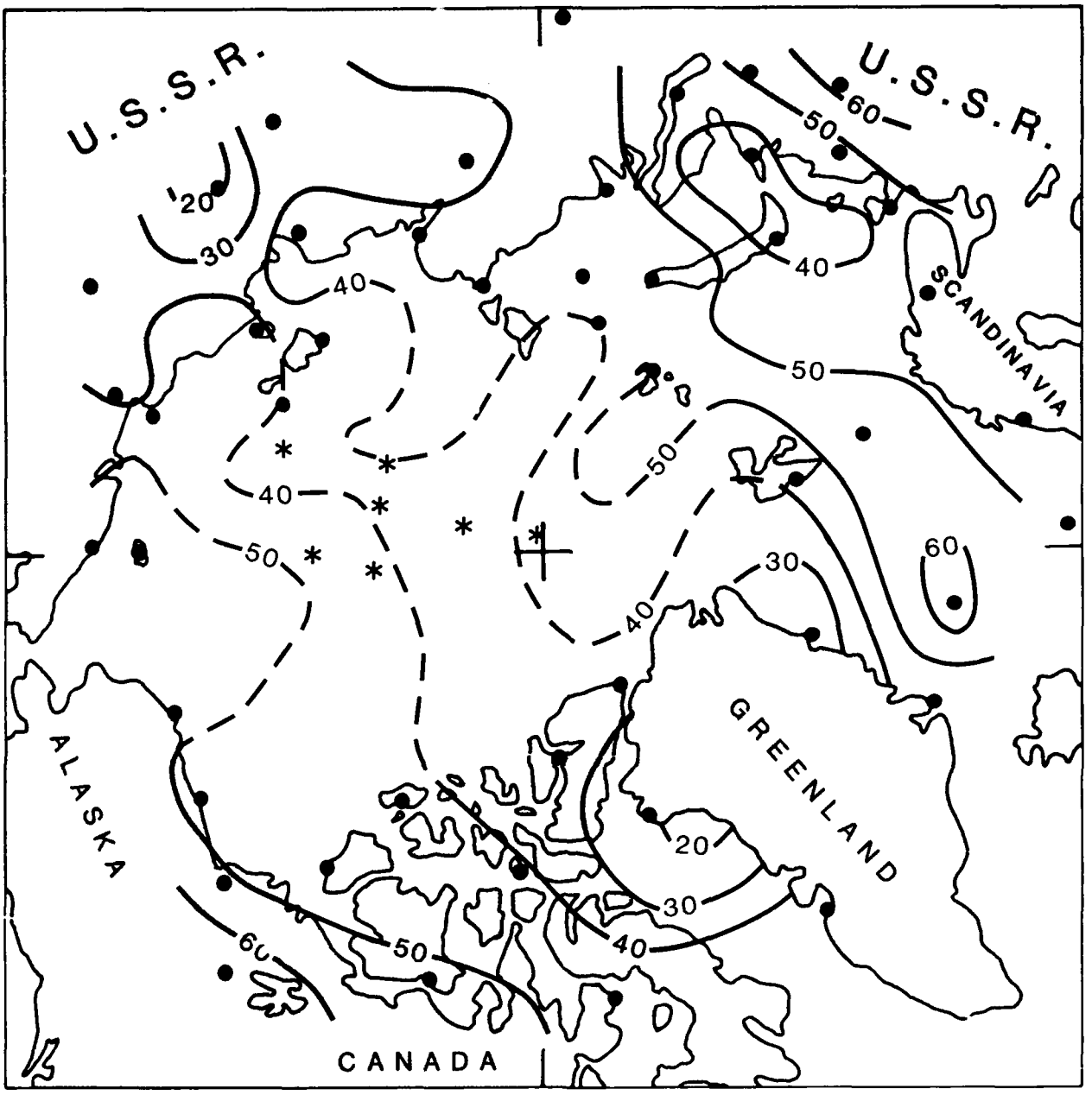

Figure E-17. Frequency of Elevated Inversions (%) for Autumn.

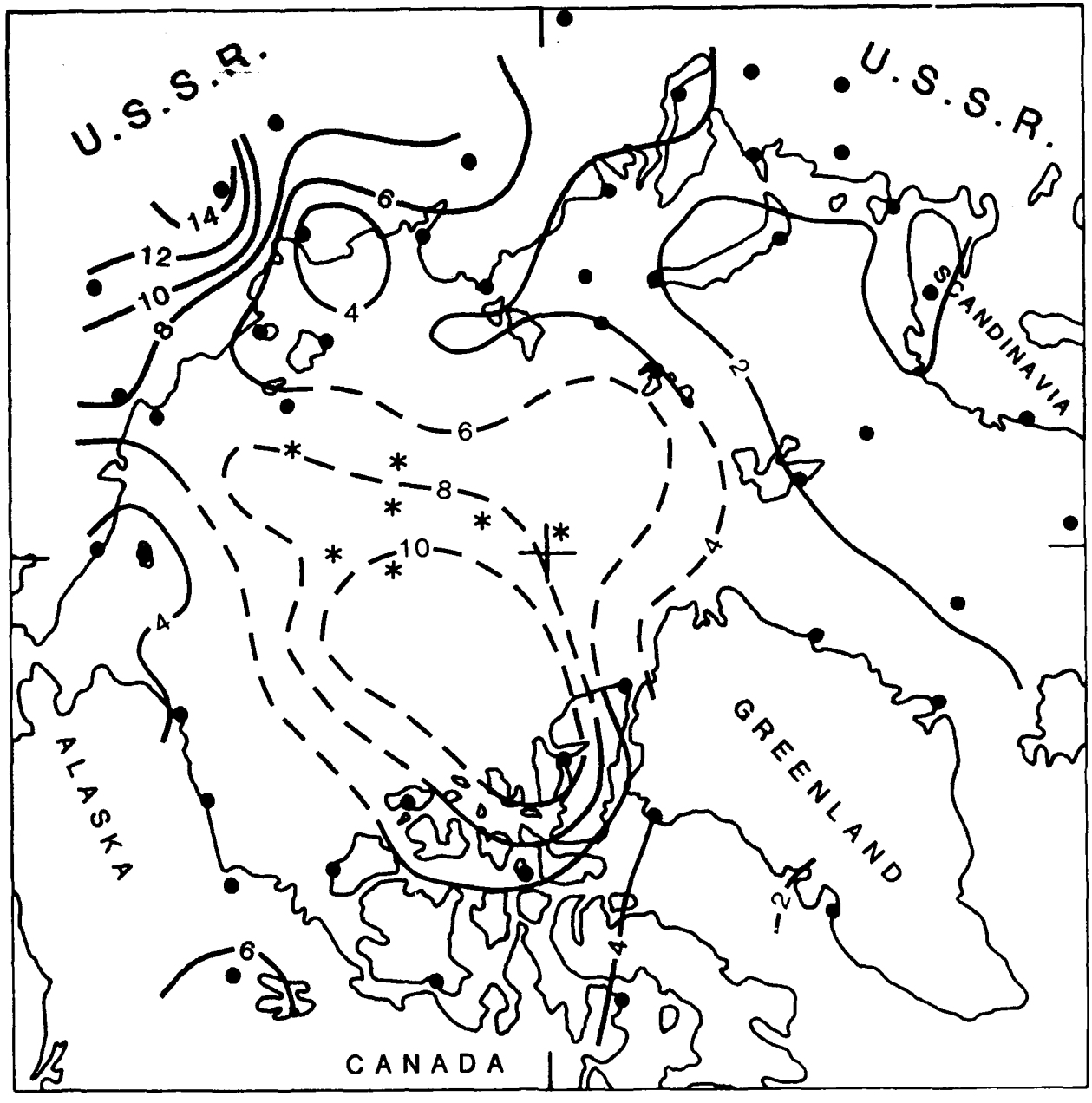

Figure E-18. Median Temperature Difference Across Inversion (°C) for Autumn.

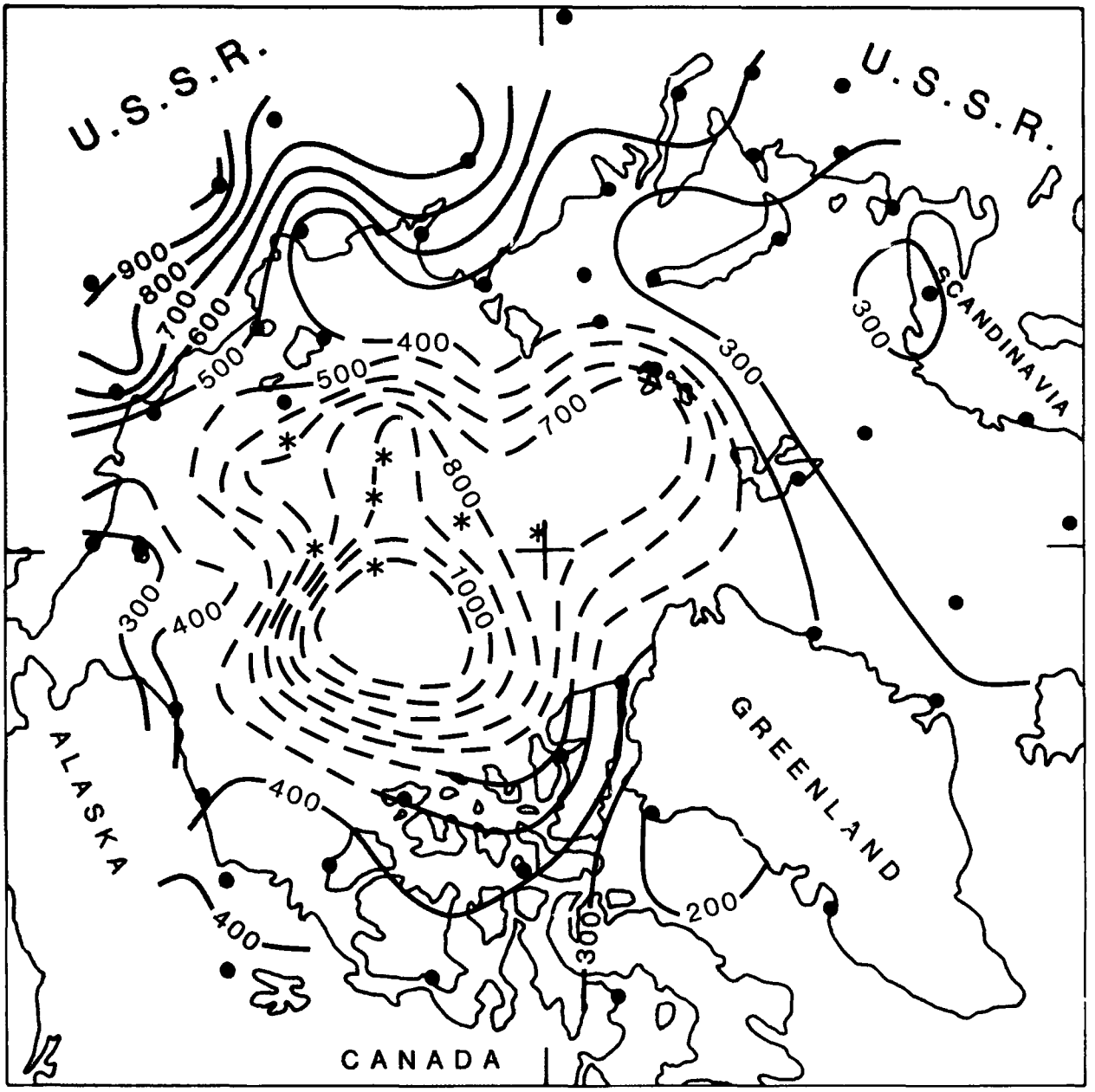

Figure E-19. Median Inversion Depth (m) for Autumn.

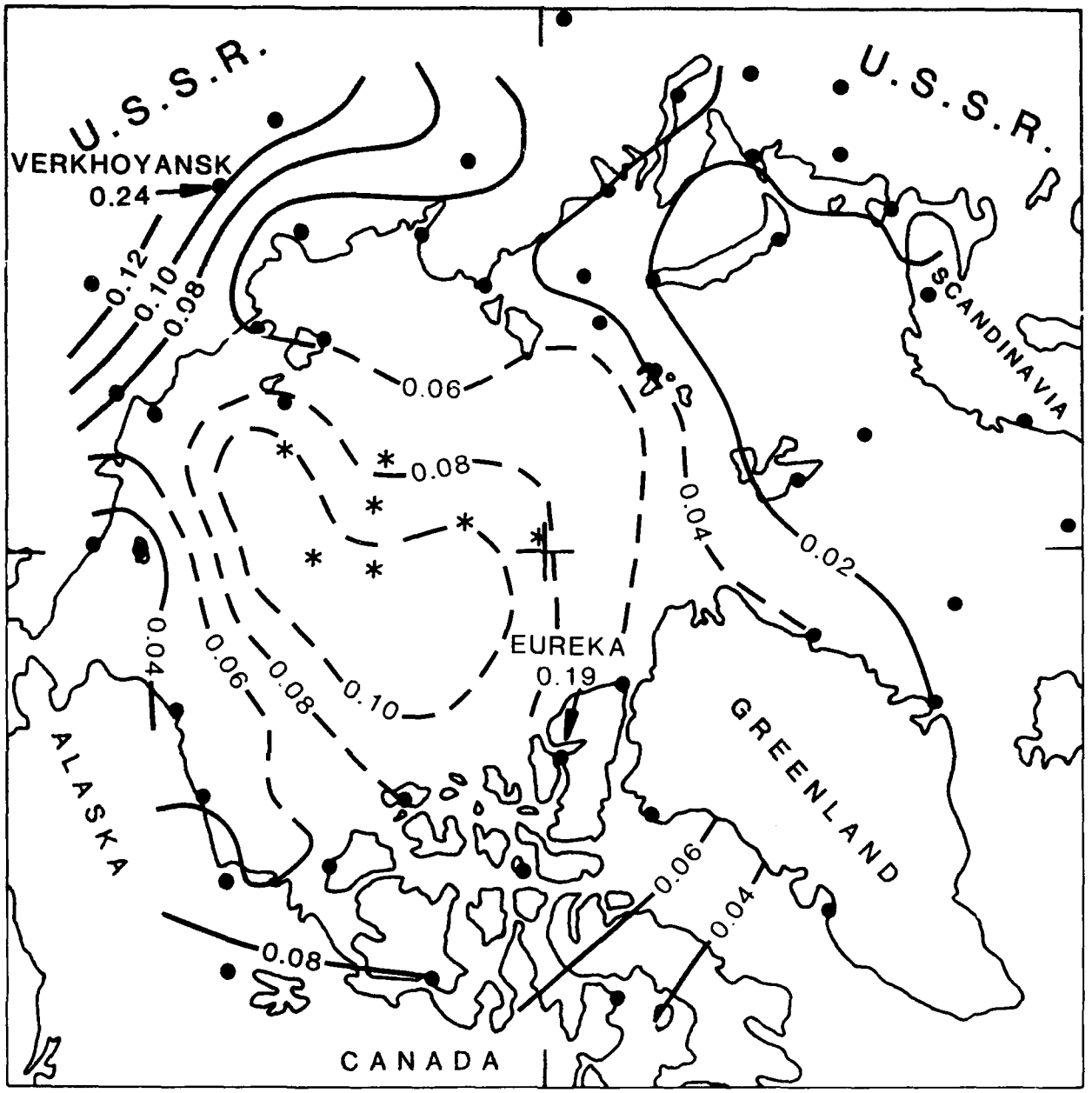

Figure E-20. Median Inversion Intensity ($\Delta T^2/m$) for Autumn.

STATION LISTING

	Lat(N)	Long	Elev(m)	Soundings	Station
Eurasian					
1	69.77	61.68E	53	6005	Amderma
2	78.07	14.22E	18	4991	Barentsburg
3	74.50	19.00E	18	7448	Bjornova
4	67.25	14.48E	8	7347	Bodo
5	71.58	128.92E	2	7200	Bukhta Tiksi
6	71.98	102.47E	32	4384	Khatanga
7	72.38	52.73E	19	4904	Malye Karmakuly
8	68.97	33.05E	57	6395	Murmansk
9	77.72	104.28E	12	6298	Mys Cheliuskin
10	68.47	73.60E	5	5736	Mys Kamenny
11	68.92	179.28W	4	7299	Mys Schmidt
12	73.18	143.93E	23	7068	Mys Shalaurova
13	76.95	68.58E	8	5586	Mys Zhelania
14	67.65	53.02E	7	7068	Narjan Mar
15	68.75	161.30E	23	7400	Nizhnie Krestiy/Cerski
16	70.63	162.40E	38	6881	Ostrov Chetyrekhstolbo
17	73.52	80.33E	45	5473	Ostrov Dikson
18	80.62	58.05E	20	6629	Ostrov Heisa
19	76.00	137.90E	13	7024	Ostrov Kotelny
20	74.67	112.98E	32	6519	Ostrov Preobrazhenia
21	77.60	82.23E	22	5735	Ostrov Uedinenia
22	79.50	76.98E	8	6137	Ostrov Vise
23	70.97	178.55W	2	6502	Ostrov Vrangelya
24	76.15	152.83E	14	6376	Ostrov Zohova
25	65.12	57.22E	54	6530	Pechora
26	66.53	66.55E	18	6031	Sale-Khard (Obdorsk)
27	67.88	44.17E	7	6354	Sojna
28	65.78	87.95E	38	6290	Turukhansk
29	67.55	133.38E	137	5033	Verkhoyansk
30	66.77	123.40E	82	6418	Zhigansk
31	65.73	150.90E	43	1974	Zyrianka
32	70.93	8.67W	9	6143	Jan Mayen
Greenland					
33	76.53	68 75W	77	5437	Thule
34	76.77	18.77W	11	5711	Danmarkshavn
35	70.42	21.97W	42	2772	Kap Tobin
36	68.70	52.75W	47	6677	Egedesminde

STATION LISTING (Concluded)

	Lat(N)	Long	Elev(m)	Soundings	Station
Moored Snip					
37	66.00	2.00E	0	6283	Ship "M"
U.S./Canada					
38	68.78	81.25W	10	6421	Hall Beach
39	74.72	94.98W	67	6371	Resolute
40	82.50	62.33W	63	6488	Alert
41	80.22	86.18W	10	6301	Eureka
42	68.32	133.53W	68	6510	Inuvik
43	69.10	105.13W	27	6559	Cambridge Bay
44	65.28	126.80W	73	6478	Norman Wells
45	76.23	119.33W	20	6351	Mould Bay
46	71.97	124.73W	86	6470	Sachs Harbour
47	71.28	156.77W	7	6864	Barrow Island
48	70.13	143.57W	2	6800	Barter Island

Total land station soundings = 295,671

Drifting Station Data:

NP-22, NP-26, NP-28

Total drifting station soundings = 2,994

References:

Belmont, A. D., 1958: Lower tropospheric inversions at ice island T-3. *Polar Atmospheric Symposium, Part I Meteorology Section*, Pergamon Press, London, 215-284.

Kahl, J. D., 1990: Characteristics of the low-level temperature inversion along the Alaska Arctic coast. *Int. J. Clim., 10*, 537-548.

Appendix F

Seasonal Ice Movement

The information in Appendix F was developed by Dr. R. Colony and Dr. A. Thorndike of the Polar Science Center, University of Washington, Seattle, Washington.

The maps (Figs. F-1 through F-4) on the following pages show mean sea ice movement in the Arctic Ocean and through the Fram and Bering Straits. The movement is summarized for four 3-month periods; February–April, May–July, August–October, and November–January. The maps were derived using navigational data from drifting sea ice buoys for a 10-year period from 1979 to 1989. The vectors show both direction and speed; the speed scale is noted in the upper left-hand corner of each map.

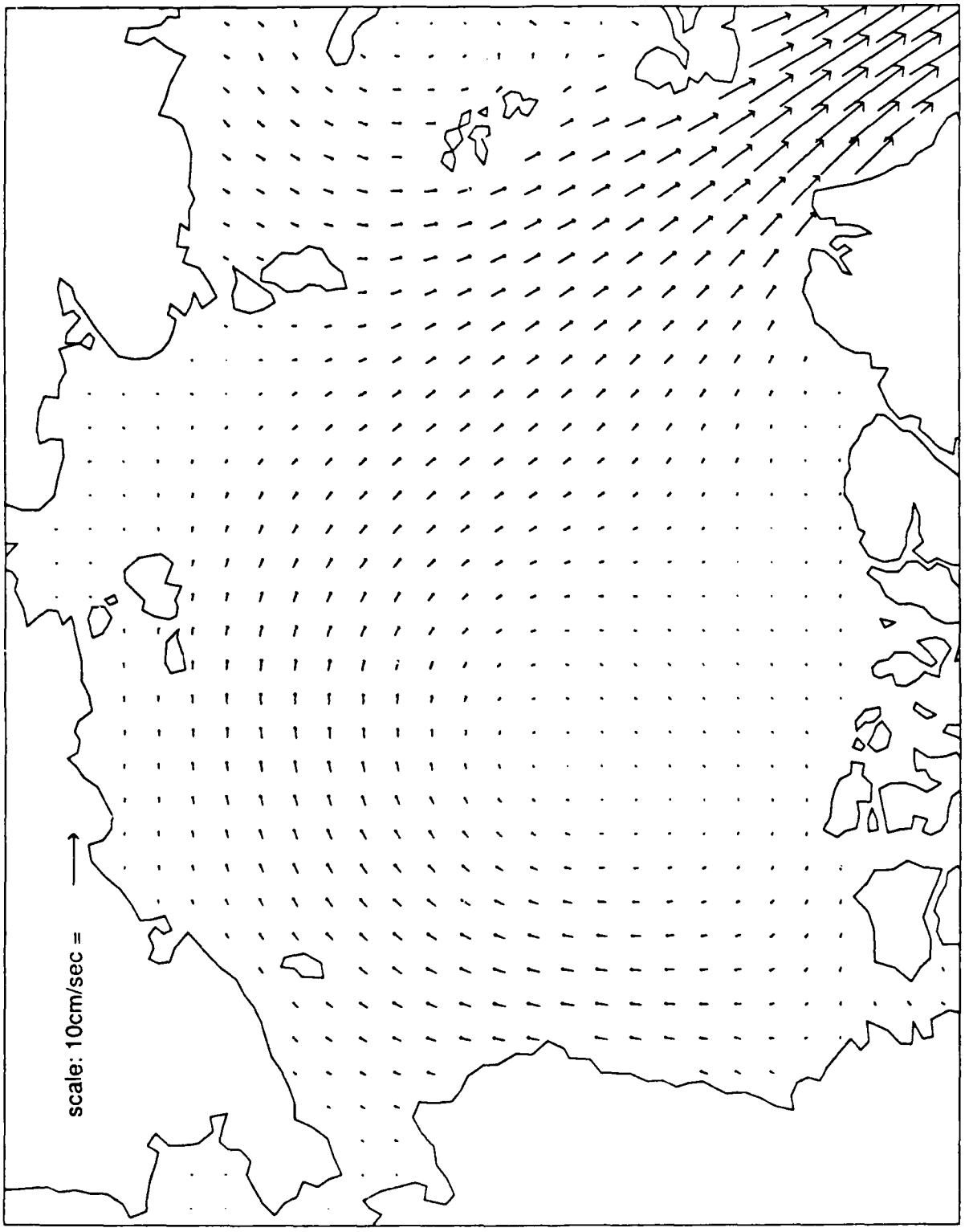

Figure F-1. Arctic Basin—February, March, April.

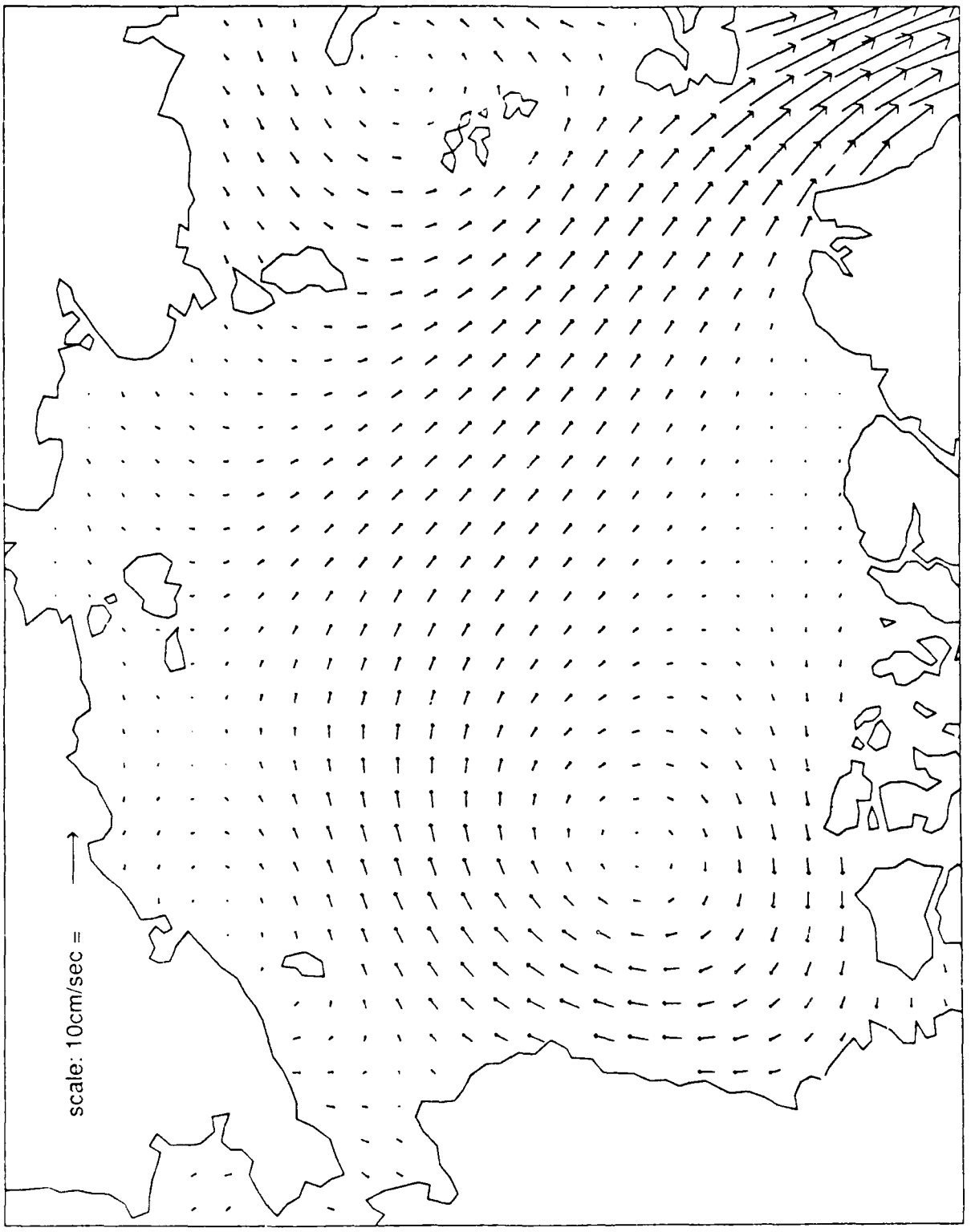

Figure F-2. Arctic Basin—May, June, July.

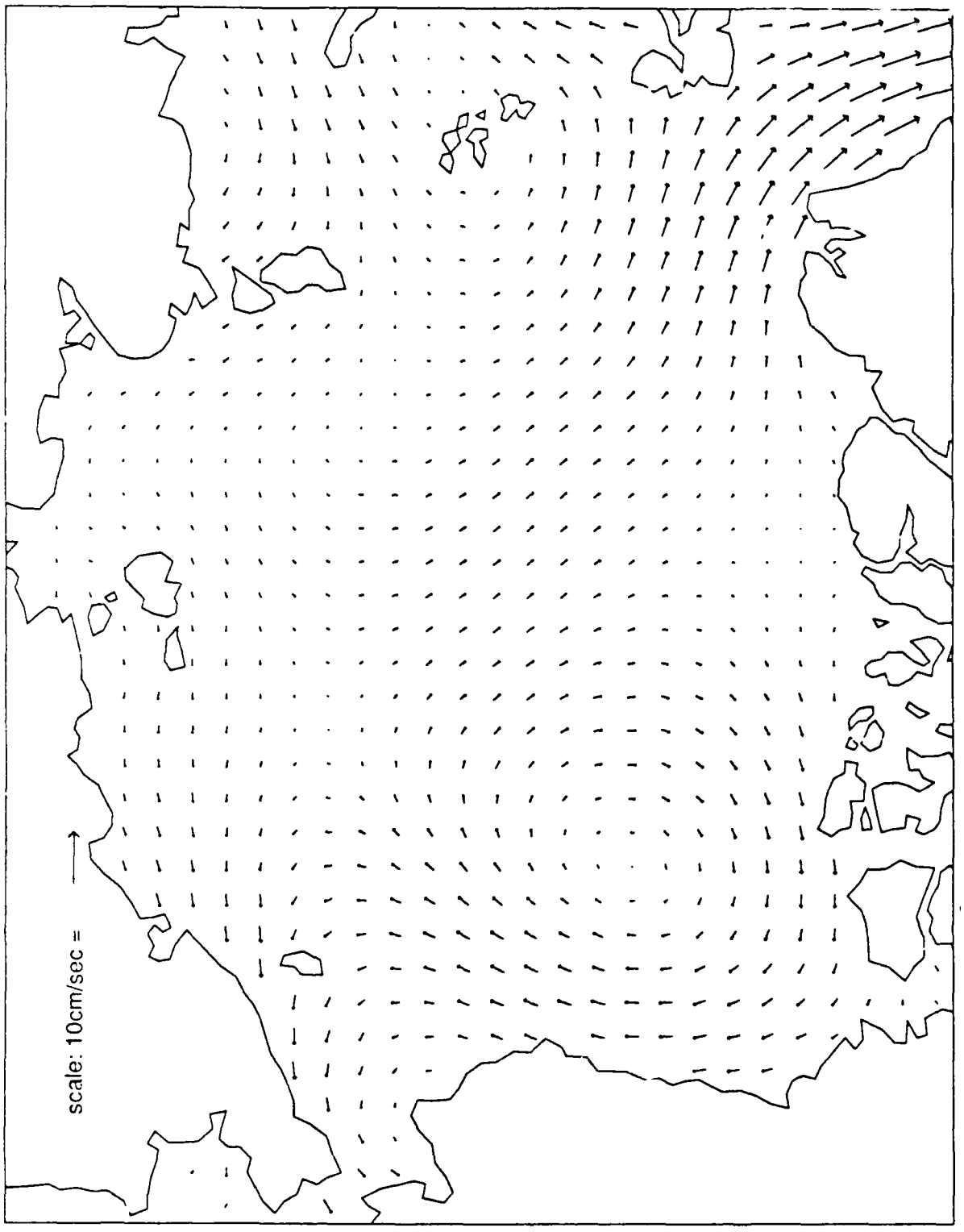

Figure F-3. Arctic Basin—August, September, October.

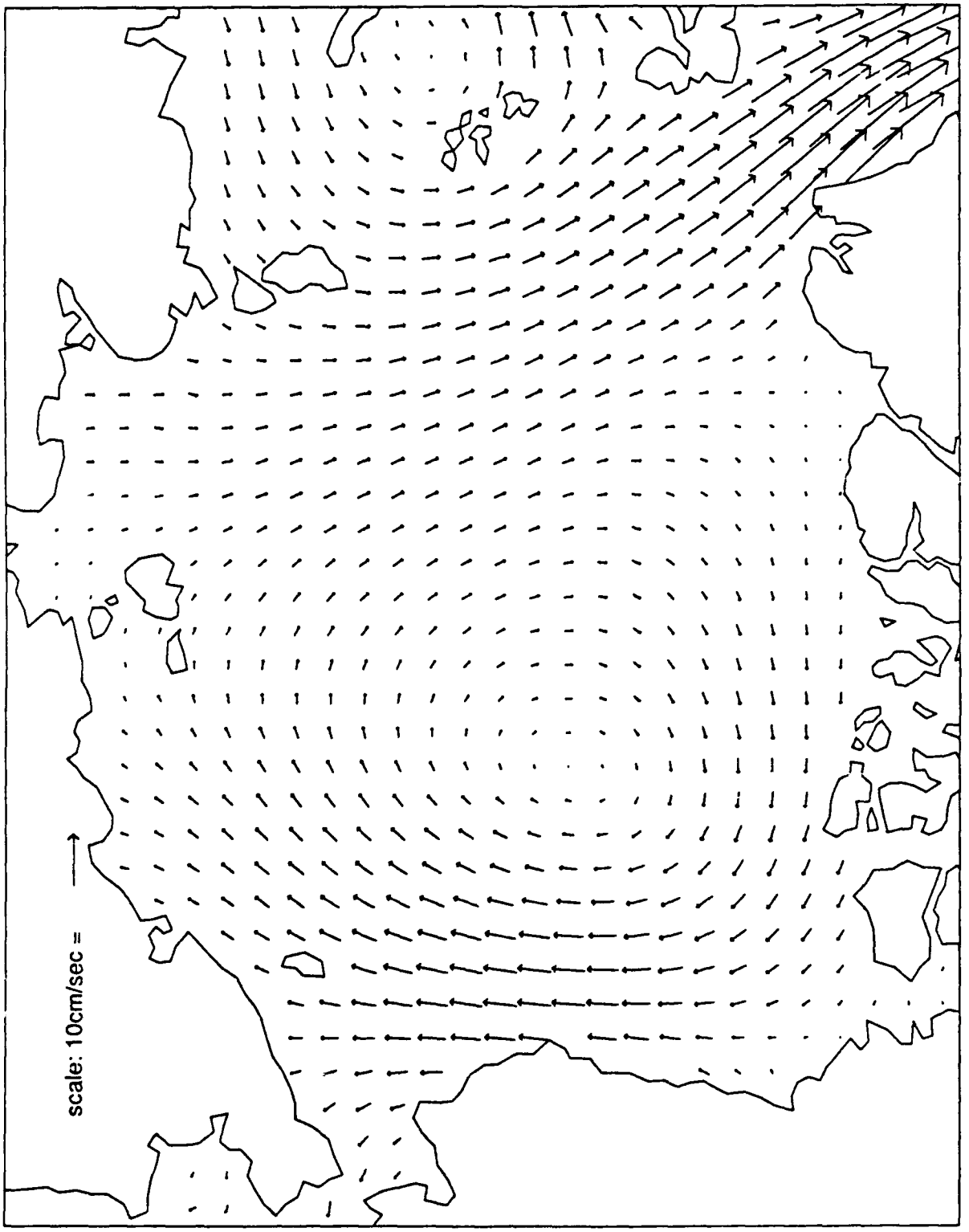

Figure F-4. Arctic Basin—November, December, January.

THIS PAGE INTENTIONALLY LEFT BLANK

Distribution List

NATIONAL OCEAN DATA CENTER
ATTN: G.W. WITHES
6001 EXECUTIVE BLVD. RM 103
ROCKVILLE, MD 20852

COMFLENUMOCEANCEN
MONTEREY, CA 93943-5005

COMMANDER
D.W. TAYLOR NAVAL RSCH. CEN.
BETHESDA, MD 20084-5000

COMMANDING OFFICER
FLEET ANTI SUB WARFARE
TRAINING CENTER
ATLANTIC NAVAL STATION
NORFOLK, VA 23511-6495

COMMANDER IN CHIEF
U.S. ATLANTIC FLEET
ATTN: FLT METEOROLOGIST
NORFOLK, VA 23511-6001

COMMANDER IN CHIEF
SECOND FLEET
ATTN: METEOROLOGICAL OFFICE
FPO NEW YORK 09501-6000

COMSECONDFLT
ATTN: NSAP SCIENCE ADVISOR
FPO NEW YORK 09501-6000

COMTHIRDFLT
ATTN: NSAP SCIENCE ADVISOR
PEARL HARBOR, HI 96860-7500

COMMANDER
U.S. NAVAL FORCES, JAPAN
FPO SEATTLE 98762-0051

COMNAVAIRPAC
ATTN: NSAP SCIENCE ADVISOR
NAS, NORTH ISLAND
SAN DIEGO, CA 92135-5100

CHIEF OF NAVAL OPERATIONS
ATTN: OP-096, OP-0961B
U.S. NAVAL OBSERVATORY
WASHINGTON, DC 20392-1800

COMMANDING OFFICER
NAVAL OCEANOGRAPHIC OFFICE
JCSSC, MS 39522-5001

SUPERINTENDENT
NAVPGSCOL
MONTEREY, CA 93943

OFFICE OF NAVAL TECHNOLOGY
DR. M. BRISCOE, CODE 228
800 N. QUINCY ST.
ARLINGTON, VA 22217-5000

COMMANDER IN CHIEF
U.S. ATLANTIC FLEET
ATTN: NSAP SCIENCE ADVISOR
NORFOLK, VA 23511-6001

CINCUSNAVEUR
U.S. NAVAL FORCES, EUROPE
ATTN: METEOROLOGICAL OFFICER
FPO NEW YORK 09510

COMTHIRDFLT
ATTN: FLT METEOROLOGIST
FPO SAN FRANCISCO 96601-6001

COMSEVENTHFLT
ATTN: NSAP SCIENCE ADVISOR
BOX 167
FPO SEATTLE 98762

COMMANDER
U.S. NAVAL FORCES, KOREA
APO SAN FRANCISCO 96301-0023

COMMANDER
NAVAL SURFACE FORCE
U.S. ATLANTIC FLEET
NORFOLK, VA 23511-6292

COMMANDER
SPAWARSYSCOM
WASHINGTON, DC 20363-5100

COMMANDING OFFICER
ONR BRANCH OFFICE, BOX 39
FPO NEW YORK 09510-0700

OFFICE OF NAVAL RESEARCH
ATTN: CODE 10
800 N. QUINCY ST.
ARLINGTON, VA 22217-5000

UNIVERSITY OF WASHINGTON
APPLIED PHYSICS LABORATORY
1013 NORTHEAST 40TH ST.
SEATTLE, WA 98105

CINCPACFLT
ATTN: CODE 82M
PEARL HARBOR, HI 96860-7000

COMMANDER
BOX N39
FPO NEW YORK 09510-0150

COMSEVENTHFLT
ATTN: FLT METEOROLOGIST
FPO SAN FRANCISCO 96601-6003

COMMANDER
U.S. NAVAL FORCES, ICELAND
FPO NEW YORK 09571

COMMANDER
U.S. ATLANTIC FLEET
ATTN: NSAP SCIENCE ADVISOR
NORFOLK, VA 23511-5188

COMNAVSURFLANT
ATTN: NSAP SCIENCE ADVISOR
NORFOLK, VA 23511

COMSUBFORLANT
ATTN: CODE 014
NORFOLK, VA 23511-6296

COMMANDING OFFICER
USS D. EISENHOWER (CVN 69)
ATTN: MET. OFFICER, OA DIV.
FPO NEW YORK 09532-2830

COMMANDING OFFICER
USS J. F. KENNEDY (CV-67)
ATTN: MET. OFFICER, OA DIV.
FPO NEW YORK 09538-2800

COMMANDING OFFICER
USS T. ROOSEVELT (CVN-71)
ATTN: MET. OFFICER, OA DIV.
FPO NEW YORK 09559-2871

COMMANDING OFFICER
USS ENTERPRISE (CVN-65)
ATTN: MET. OFFICER, OA DIV.
FPO SAN FRANCISCO 96636-2810

COMMANDING OFFICER
USS RANGER (CV-61)
ATTN: MET. OFFICER, OA DIV.
FPO SAN FRANCISCO 96633-2750

COMMANDING OFFICER
USS NEW JERSEY (BB-62)
ATTN: MET. OFFICER, OA DIV.
FPO SAN FRANCISCO 96688-1110

COMMANDING OFFICER
USS BLUERIDGE (LCC-19)
ATTN: MET. OFFICER
FPO SAN FRANCISCO 96628-3300

COMMANDING OFFICER
USS INCHON (LPH-12)
ATTN: MET. OFFICER
FPO NEW YORK 09529-1655

COMMANDING OFFICER
USS SAIPAN (LHA-2)
ATTN: MET. OFFICER
FPO NEW YORK 09549-1605

COMSUBFORPAC
ATTN: CODE NZ16
PEARL HARBOR, HI 96860-6550

COMMANDING OFFICER
USS FORRESTAL (CV-59)
ATTN: MET. OFFICER, OA DIV.
FPO MIAMI 34080-2730

COMMANDING OFFICER
USS NIMITZ (CVN 68)
ATTN: MET. OFFICER, OA DIV.
FPO SEATTLE 98780-2820

COMMANDING OFFICER
USS A. LINCOLN (CVN-72)
ATTN: MET. OFFICER
FPO NEW YORK 09580-2872

COMMANDING OFFICER
USS KITTY HAWK (CV-63)
ATTN: MET. OFFICER, OA DIV.
FPO NEW YORK 09535-2770

COMMANDING OFFICER
USS CARL VINSON (CVN-70)
ATTN: MET. OFFICER, OA DIV.
FPO SAN FRANCISCO 96629-2840

COMMANDING OFFICER
USS WISCONSIN (BB 64)
ATTN: OA DIVISION
FPO NEW YORK 09552-1130

COMMANDING OFFICER
USS GUADALCANAL (LPH-7)
ATTN: MET. OFFICER
FPO NEW YORK 09562-1635

COMMANDING OFFICER
USS IWO JIMA (LPH-2)
ATTN: MET. OFFICER
FPO NEW YORK 09561-1625

COMMANDING OFFICER
USS BELLEAU WOOD (LHA 3)
ATTN: MET. OFFICER
FPO SAN FRANCISCO 96623-1610

COMMANDING OFFICER
USS AMERICA (CV-66)
ATTN: MET. OFFICER, OA DIV.
FPO NEW YORK 09531-2790

COMMANDING OFFICER
USS INDEPENDENCE (CV-62)
ATTN: MET. OFFICER, OA DIV.
FPO SEATTLE 96618-2760

COMMANDING OFFICER
USS SARATOGA (CV-60)
ATTN: MET. OFFICER, OA DIV
FPO MIAMI 34078-2740

COMMANDING OFFICER
USS CONSTELLATION (CV 64)
ATTN: MET. OFFICER, OA DIV
FPO NEW YORK 09558-2780

COMMANDING OFFICER
USS MIDWAY (CV-41)
ATTN: MET. OFFICER, OA DIV.
FPO SAN FRANCISCO 96631-2710

COMMANDING OFFICER
USS IOWA (BB-61)
ATTN: MET. OFFICER, OA DIV.
FPO NEW YORK 09546-1100

COMMANDING OFFICER
USS MOUNT WHITNEY (LCC-20)
ATTN: MET. OFFICER
FPO NEW YORK 09517-3310

COMMANDING OFFICER
USS GUAM (LPH-9)
ATTN: MET. OFFICER
FPO NEW YORK 09563-1640

COMMANDING OFFICER
USS NASSAU (LHA-4)
ATTN: MET. OFFICER
FPO NEW YORK 09557-1615

COMMANDING OFFICER
USS NEW ORLEANS (LPH-11)
ATTN: MET. OFFICER
FPO SAN FRANCISCO 96627-1650

COMMANDING OFFICER
USS OKINAWA (LPH 31)
ATTN: MET. OFFICER
FPO SAN FRANCISCO 96625-1630

COMMANDING OFFICER
USS TRIPOLI (LPH 18)
ATTN: MET. OFFICER
FPO SAN FRANCISCO 96626-1645

COMMANDING OFFICER
31 OCEANO. DEV. SQDN 8-VXN-8
NAVAL AIR STATION
PATUXENT RIVER, MD 20670-5109

DET. 2, HQ, AWS
THE PENTAGON
WASHINGTON, DC 20330

LIBRARY
NAVAL ARCTIC RESEARCH LAB
BARROW, AK 99723

NAVEASTOCEANCEN
ATTN: OPS. OFFICER
MCADIE BLDG. (U-117), NAS
NORFOLK, VA 23511-5399

NAVOCEANCOMFAC
ATTN: OPS. OFFICER
NAVAL AIR STATION
BRUNSWICK, ME 04011-5000

DIRECTOR OF RESEARCH
U.S. NAVAL ACADEMY
ANNAPOLIS, MD 21402

NAVAL POSTGRADUATE SCHOOL
ATTN: LIBRARY
MONTEREY, CA 93943-5002

SUPERINTENDENT
ATTN: USAFA (DEG)
USAF ACADEMY, CO 80840

COMMANDER
AWS/DNXS
SCOTT AFB, IL 62225

COMMANDING OFFICER
USS PELELIU (LHA-5)
ATTN: MET. OFFICER
FPO SAN FRANCISCO 96624-1620

COMMANDING OFFICER
USS PUGET SOUND (AD 38)
ATTN: MET. OFFICER
FPO NEW YORK 09544-2520

USCINCPAC
BOX 13
ATTN: STAFF CINCPAC J37
CAMP SMITH, HI 96861

OFFICER IN CHARGE
NAVOCEANCOMDET
NAVAL STATION
FPO SEATTLE 98791-2943

COMMANDING OFFICER
FLEET INTELLIGENCE CENTER
(EUROPE & ATLANTIC)
NORFOLK, VA 23522

NAVPOLAROCEANCEN
ATTN: OPS. OFFICER
4301 SUITLAND RD
WASHINGTON, DC 20395-5180

U.S. NAVAL ACADEMY
ATTN: LIBRARY REPORTS
ANNAPOLIS, MD 21402

NAVAL POSTGRADUATE SCHOOL
ATTN: CODE 63
MONTEREY, CA 93913-5000

NAVAL WAR COLLEGE
ATTN: GEOPHYS. OFFICER
NAVOPS DEPT.
NEWPORT, RI 02841

AFGL/LY
ATTN: MET. OFFICER
HANSCOM AFB, MA 01731

USAFETAC/TS
ATTN: TECH. LIBRARY
SCOTT AFB, IL 62225

COMMANDING OFFICER
USS TARAWA (LHA-1)
ATTN: MET. OFFICER
FPO SAN FRANCISCO 96622-1600

COMMANDING OFFICER
USS LASALLE (AGF-3)
ATTN: MET. OFFICER
FPO NEW YORK 09577-3320

NATIONAL SECURITY AGENCY
ATTN: LIBRARY (2C029)
FORT MEADE, MD 20755

OFFICER IN CHARGE
NAVOCEANCOMDET
AFGWC
OFFUTT AFB, NE 68113

NAVWESTOCEANCEN
ATTN: OPS. OFFICER
BOX 113
PEARL HARBOR, HI 96860

U.S. NAVOCEANCOMFAC
ATTN: OPS. OFFICER
FPO NEW YORK 09571-0926

U.S. NAVAL ACADEMY
ATTN: OCEANOGRAPHY DEPT.
ANNAPOLIS, MD 21402

NAVAL POSTGRADUATE SCHOOL
ATTN: CODE 68
MONTEREY, CA 93943-5000

SPAWARSYSCOM
ATTN: CODE PMW-141
NAT. CTR. #1
WASHINGTON, DC 20363-5100

COMMANDING OFFICER
NAVAL UNIT
ATTN: LNN/8TOP 62
CHANUTE AFB, IL 61868-5000

3350 TCHTG/TTMV
CHANUTE AFB, IL 61868

U.S. ARMY RESEARCH OFFICE
ATTN: GEOPHYSICS DIV.
P.O. BOX 12211
RSCH TRIANGLE PARK, NC 27709

COMMANDANT
U.S. COAST GUARD
WASHINGTON, DC 20226

DIRECTOR
NATIONAL EARTH SAT. SERV/SEL
FB-4, S321B
SUITLAND, MD 20233

CHIEF, SCIENTIFIC SERVICES
NWW/NOAA, WESTERN REGION
P.O. BOX 11188
FEDERAL BLDG.
SALT LAKE CITY, UT 84111

DIRECTOR, NWS
NOAA, ALASKA REGION
BOX 23, 701 C STREET
ANCHORAGE, AK 99513

SPACE FLIGHT METEORO. GROUP
ATTN: STEVE SOKOL, CODE Z8
JOHNSON SPACE CENTER
HOUSTON, TX 77058

OCEANROUTES, INC.
680 W. MAUDE AVE.
SUNNYVALE, CA 94086-3518

DIRECTOR, METEO. & OCEANO.
NATIONAL DEFENSE HDQ.
OTTAWA, ONTARIO, KIA OK2
CANADA

DIRECTOR, INSTITUTE OF
PHYSICAL OCEANOGRAPHY
HARALDSGADE 6
2200 COPENHAGEN N.
DENMARK

LIBRARY
USA COLD REGION RSCH.
& ENGINEERING LAB
HANOVER, NH 83755

NOAA-NESDIS LIAISON
ATTN: CODE SC2
NASA-JOHNSON SPACE CENTER
HOUSTON, TX 77058

FEDERAL COORD. FOR METEORO.
SERVS. & SUP. RSCH. (OFCM)
11426 ROCKVILLE PIKE
SUITE 300
ROCKVILLE, MD 20852

DIRECTOR
PACIFIC MARINE CENTER
NATIONAL OCEAN SURVEY, NOAA
1801 FAIRVIEW AVE., EAST
SEATTLE, WA 98102

NOAA LIBRARY, E/AI216
7600 SAND POINT WAY N.E.
3IN C15700
SEATTLE, WA 98115-0070

UNIV. OF WASHINGTON
ATMOSPHERIC SCIENCES DEPT.
SEATTLE, WA 98195

CHAIRMAN, METEOROLOGY DEPT.
MCGILL UNIVERSITY
805 SHERBROOKE ST., W.
MONTREAL, QUEBEC
CANADA H3A 2K6

DEPT. OF NATIONAL DEFENCE
DEFENCE RESEARCH BOARD
DRT GEOPHYSICS PROGRAM
SHIRLEY BAY
OTTAWA 13, ONTARIO, CANADA

DIRECTOR OF NAVAL
OCEANO. & METEOROLOGY
MINISTRY OF DEFENCE
LACON HOUSE, THEOBOLD ROAD
LONDON WC 1X8RY, ENGLAND

DIRECTOR
DEFENSE TECH. INFO. CENTER
CAMERON STATION
ALEXANDRIA, VA 22314

DIRECTOR, NMC
NWS, NOAA
WWB, W32, RM 204
WASHINGTON, DC 20233

NATIONAL WEATHER SERVICE
WORLD WEATHER BLDG., RM 307
5200 AUTH ROAD
CAMP SPRINGS, MD 20023

NW OCEAN SERVICE CENTER
7600 SAND POINT WAY N.E.
BNC15700
SEATTLE, WA 98115

EXECUTIVE SECRETARY, CAO
SUBCOMMITTEE ON ATMOS. SCI.
NATIONAL SCIENCE FOUNDATION
RM. 510, 1800 G. STREET, NW
WASHINGTON, DC 20550

SCIENCE APPLICATIONS INTERNATIONAL CORP. (SAIC)
205 MONTECITO AVE.
MONTEREY, CA 93940

LIBRARY/BIBLIOTHEQUE
ATMOSPHERIC ENVIRON. SERV.
4905 DUFFERIN STREET
DOWNSVIEW, ONTARIO CANADA
M3H 5T4

INSTITUT FOR TEORETISK METEOROLOGI
HARALDSGADE 6
DK-2200 KOBEHAVN N
DENMARK

DEPARTMENT OF METEOROLOGY
UNIVERSITY OF READING
2 EARLYGATE, WHITEKNIGHTS
READING RG6 2AUT
ENGLAND

COMMANDER IN CHIEF FLEET
ATTN: STAFF METEOROLOGIST & OCEANOGRAPHY OFFICER
NORTHWOOD, MIDDLESEX HA6 3HP
ENGLAND

ICELANDIC MET. OFFICE
BUSTAOAVEGUR 9
105 REYKJAVIK, ICELAND

EILEEN MATURI-NESDIS
WORLD WEA. BLDG/RM 601
5200 AUTH ROAD
CAMP SPRINGS, MD 20023

NOARL/CRREL, CODE 332
72 LYME RD
HANOVER, NH 03755-1290

CDR L.E. BOUND (ONT-228)
OFFICE OF NAVAL TECHNOLOGY
800 N. QUINCY ST.
ARLINGTON, VA 22217-5000

LIBRARY
FINNISH METEORO. INSTI.
BOX 503
SF-00101 HELSINKI 10
FINLAND

MARITIME METEOROLOGY DIV.
JAPAN METEOROLOGICAL
OTE-MACHI 1-3-4 CHIYODA-KU
TOKYO, JAPAN

NAVPGSCOL **(15)**
ATTN: PROF. F. WILLIAMS, 63WF
DEPT. OF METEOROLOGY
MONTEREY, CA 93943

AWC NEIL PARKER
TWIN ATRIA BLDG/AES
4999 98TH AVE.
EDMONTON, ALBERTA
CANADA TGB 2X3

DIRECTOR, METEOROLOGIE INST
ZENTRALEINRICHTUNG DER
FREIEN UNIVERSITAT BERLIN
BIBLIOTHEK, PODBIELSKIALLE
1000 BERLIN 33
FEDERAL REPUBLIC OF GERMANY

DIRECTOR, SWEDISH METEORO. & HYDROLOGICAL INSTITUTE
P.O. BOX 923
S-601, 19 NORRKOPING
SWEDEN

DENNIS PERRYMAN **(3)**
NOARL WEST
MONTEREY, CA 93943-5006

DR. G. WELLER
DEP DIR/GEOPHYSICS INST.
UNIVERSITY OF ALASKA
FAIRBANKS, AK 99775-0800

CARL BYERS
GEOPHYSICS INSTITUTE
UNIV. OF ALASKA
FAIRBANKS, AK 99775-0800

METEOROLOGIST IN CHARGE
NATIONAL WEATHER SERVICE
101 12th AVE. BOX 21
FAIRBANKS, AK 99701

DIRECTOR, NORWEGIAN METEOROLOGICAL INST.
P.O. BOX 320, BLINDERN, N-0314
OSLO 3, NORWAY

DR. TORGNY VINJE
NORSK POLARINSTITUTT
P.O. BOX 158
N-1330 OSLO LUFTHAVN
NORWAY

HANK BRANDLI
3165 SHARON DR.
MELBOURNE, FL 32904

JERRY EHRHARDT
NAVAL SEA SYSTEMS COMMAND
CODE PMS 377 J-2
WASHINGTON, DC 20362-5101

ARCTIC RESEARCH CENTER
SCRIPPS INSTITUTE
DIV. H-014
ATTN: R. WHRITNER
LA JOLLA, CA 92093

DIRECTOR, NORTH NORWAY
WEATHER CENTRAL
P.O. BOX 2760, ELVERHOY, N-9001
TROMSØ, NORWAY

METEOROLOGIST IN CHARGE
NATIONAL WEATHER SERVICE
222 WEST 7TH AVE., #23
ANCHORAGE, AK 99513-7575

DR. ROGER COLONY
APL, U. OF WASHINGTON
1013 NE 40TH STREET
SEATTLE, WA 98105-6613

U.S. GOVERNMENT PRINTING OFFICE: 1991 - 587 - 146